


Siegfried Siegesmund  
Rolf Snethlage *Editors*

# Stone in Architecture

Properties, Durability

*5th Edition*

 Springer

# Stone in Architecture

Siegfried Siegesmund · Rolf Snethlage  
Editors

# Stone in Architecture

Properties, Durability

Fifth Edition

 Springer

*Editors*

Siegfried Siegesmund  
Geoscience Center  
Universität Göttingen  
Göttingen  
Germany

Rolf Snethlage  
Naturstein, Bauchemie und Bauphysik  
in der Denkmalpflege  
Bamberg  
Germany

ISBN 978-3-642-45154-6      ISBN 978-3-642-45155-3 (eBook)

DOI 10.1007/978-3-642-45155-3

Springer Heidelberg New York Dordrecht London

Library of Congress Control Number: 2014930006

© Springer-Verlag Berlin Heidelberg 2014

This work is subject to copyright. All rights are reserved by the Publisher, whether the whole or part of the material is concerned, specifically the rights of translation, reprinting, reuse of illustrations, recitation, broadcasting, reproduction on microfilms or in any other physical way, and transmission or information storage and retrieval, electronic adaptation, computer software, or by similar or dissimilar methodology now known or hereafter developed. Exempted from this legal reservation are brief excerpts in connection with reviews or scholarly analysis or material supplied specifically for the purpose of being entered and executed on a computer system, for exclusive use by the purchaser of the work. Duplication of this publication or parts thereof is permitted only under the provisions of the Copyright Law of the Publisher's location, in its current version, and permission for use must always be obtained from Springer. Permissions for use may be obtained through RightsLink at the Copyright Clearance Center. Violations are liable to prosecution under the respective Copyright Law. The use of general descriptive names, registered names, trademarks, service marks, etc. in this publication does not imply, even in the absence of a specific statement, that such names are exempt from the relevant protective laws and regulations and therefore free for general use.

While the advice and information in this book are believed to be true and accurate at the date of publication, neither the authors nor the editors nor the publisher can accept any legal responsibility for any errors or omissions that may be made. The publisher makes no warranty, express or implied, with respect to the material contained herein.

Printed on acid-free paper

Springer is part of Springer Science+Business Media ([www.springer.com](http://www.springer.com))



# Preface

Natural stone is a topic of interest to geologists and natural stone producers, as well as for architects, building specialists, conservators, monument curators, and of course, building owners. It is one of the oldest and more durable construction materials. However, its importance for the construction industry has changed over time and so has its perception by society. In the last three decades, a significantly increased demand has been noticed that can be attributed to its use as cladding material. Predictions suggest an even greater growth rate in the demand.

Natural stone is a construction material with a favorable ecological rating compared to manufactured materials such as Portland cement or bricks. In architecture, this material is particularly valued for its design possibilities, especially with regards to color, shape, and surface processing. This gives the building a unique value.

In past centuries, master builders and sculptors used locally available stones, since transport from distant sources was difficult and very expensive. Therefore, whole towns were built with a single type of stone. This resulted in the development of cultural landscapes that are characterized solely by the type of stone used. With globalization, this local type of landscape construction is being valued again, especially since natural stones are in essence a part of the landscape. They reflect tradition and identity and are fundamental to both the local community and tourism.

Although there may be a general belief that natural building stones are durable materials, all rocks undergo weathering and will literally turn to dust. The use of natural stone in buildings requires that the stone type have the required suitability for the intended purpose. Otherwise, their deterioration will occur even after short periods of time. The weathering and deterioration of historical buildings, as well as that of many monuments or sculptures using natural stones is a problem that has been known since antiquity. Although much of the observed world-wide destruction of these monuments can be ascribed to war and vandalism, many other factors contribute significantly to their deterioration, such as neglect and poor maintenance. There has been a significant increase in deteriorating structures during the past two centuries. This prompted Erhard M. Winkler in his book “Stone: Properties, Durability in Man’s Environment” (1973. Springer Verlag) to make a pessimistic prediction, that at the end of the last millennium these structures would largely be destroyed because of predominantly anthropogenic environmental influences.

Erhard M. Winkler's book "Stone: Properties, Durability in Man's Environment" first published in 1973 marks a milestone in the series of publications on the conservation of our cultural heritage. In the year the book was published, science was not yet concerned with conservation and was still at the level of knowledge that had been accumulated by scientists at the turn of the nineteenth and twentieth century and the two decades between the two world wars. Conservation interventions were not widespread at that time and treatment with chemicals was barely in its infancy. Clever restorers used promising chemical products and applied them to stone conservation, but kept their formulas a trade secret.

Winkler was among the first who embraced the ideas of prewar scientists, such as Hirschwald, Schaffer, and Kieslinger. They advanced the idea that stone conservation should be placed into the context of understanding the processes of weathering and deriving remedies against deterioration. Therefore, he stressed the geologists' role in leading conservation interventions that start with the anamnesis of the building, followed by a correct diagnosis of the problem, and then the development of an appropriate therapy. Simultaneously, other relevant disciplines, such as chemistry, biology, and material science took interest in the conservation of architectural and archeological heritage sites. In 1972, the first international meeting on this topic was held in LaRochelle under the name of "International Symposium on the Deterioration and Conservation of Building Stone." Since then, ten more meetings were convened regularly, and the name simplified to Deterioration and Conservation of Stone. Other international conferences were also organized, such as the Conservation of Monuments in the Mediterranean Basin Meeting.

In the 1980s, the forest decline resulting from increased pollution raised the awareness that "acid rain" could accelerate the deterioration of exterior works of art. This induced politicians—mainly in Europe and in North America—to support research into the effects of air pollution on materials. As a result, the volume of knowledge grew exponentially. In conjunction, the advances in instrumental analysis as well as in technology in general, allowed the development of various chemical compounds that could be adapted for the consolidation or the protection of stone. In the last issue of his book published in 1994, E. M. Winkler added a comprehensive chapter on conservation, a topic which had only been slightly touched upon in the previous editions.

The offer from Springer Publishing Company to prepare a new book to address more thoroughly all the acquired knowledge over the past 20 years will serve to follow the trail that Winkler blazed. The book will cover a wider spectrum with significantly more detail in all topics addressed. Therefore, an attempt was made to develop a natural stone nomenclature from a geoscientific point of view. The suitability of a given stone to the considered function it will have in a building or object is extremely important, therefore different structural engineering and relevant petrophysical and rock technical parameters were compiled for the different rock groups. Since negative material properties of a stone may become evident after a long or very long exposure, suitable testing methods are required for a meaningful stone evaluation. The resistance to weathering is extremely important

because every stone at the outcrop or in a building is subjected to the destructive physical, chemical, and biological influences of weathering. Next to these geogenic factors, anthropogenic influences on the material properties and weathering processes are also decisive. These can be deduced from laboratory experiments and also from experience on historical buildings.

Rocks will react to changing environmental conditions; especially when high “multi-pollutant” situations dominate that are caused by various chemical pollutants, suspended particles, and dust. The pollution during the last two centuries has deteriorated many of our cultural assets that may be considered as “contaminated sites.” Moreover, through climatic changes such as more precipitation, higher temperatures, freeze–thaw impacts, etc., the pollutants may react following different paths and new deterioration scenarios will develop.

Changes on the rock surface produced by weathering processes can be described with the aid of a specific terminology to avoid misunderstandings. To overcome this problem and to harmonize all the existing classification approaches, an updated version was produced by the ICOMOS-ISCS. These will help in the mapping of the various deterioration patterns and their intensity.

The objective of the new edition is to address practitioners like architects, civil engineers, stone producers, restorers, etc., as well as students who are interested in qualifying themselves for a career. All these professions require a basic understanding and experience in many disciplines such as geology, chemistry, material science, and biology. In the course of the past 20 years, knowledge has grown to such an extent that a single person can hardly acquire an overview of the field or even write a textbook on the subject. Therefore, the editors decided to elicit the aid of further specialists to create an up-to-date book containing the most recent progress in this field of science: A. Elena Charola for deterioration processes and salt decay, Michael Steiger for salt and weathering processes, Katja Sterflinger for biological deterioration and conservation issues. Peter Brimblecombe contributed to air pollution and climate change, Helmut Dürrast for the rock technical properties, Heiner Siedel for the characterization of stone deterioration on buildings, and Akos Török for the petrographical characterization of building stones. The editors are indebted to these colleagues for their essential and valuable help. Likewise, the editors want to express immense thanks to the following persons: J. Ruedrich, T. Weiss, W.-D. Grimm, B. Fitzner, K. Heinrichs, C. Schneider, G. Hundertmark, M. Reich, B. Siegesmund, M. Siegesmund, and A. Elena Charola and Christian J. Gross, who made great efforts in correcting the linguistic deficiencies of the German speaking authors.

January 2011

Siegfried Siegesmund  
Rolf Snethlage

# Acknowledgments

First of all, we would like to express our gratitude and acknowledge Springer Verlag, who considered and asked us to be authors for the 4th edition of this book, first published in 2011 as an up-to-date and completely rewritten and expanded continuation of the three earlier versions authored by Erhard Winkler. As a result of the sales success of the 4th edition, a revised version is being published including considerable improvements. We are very delighted to see that our book is being well received by technicians and professionals working in the field of monument conservation and preservation, and furthermore, is being used as a textbook in universities in many different countries. Reworking the chapters provided us with the opportunity to introduce more recent results, as well as eliminate some grammatical errors and polish the style of the text. In this context, we are especially grateful to our colleague Dr. George Wheeler from Columbia University in New York, who undertook the enormous task of checking the entire manuscript for scientific correctness and for spelling mistakes. Likewise, we would like to thank Elizabeth McTernan (Berlin) and Christian Gross (Hannover), who undertook the effort of improving the stylistic quality of the book by looking for and eliminating the German phrasing of the authors.

Substantial additions and improvements have been made to most chapters. The quality of many figures and drawings has also been improved by providing better originals and by redrawing the old diagrams. Some chapters, like Chaps. 1 and 7, however, have been left unchanged in the new edition, since the limited amount of time between the 2011 publication and the latest edition was not sufficient for producing new scientific results.

The authors particularly want to thank Springer Verlag and especially Dr. Annett Büttner for offering us the opportunity to produce the 5th edition of the book. We hope that this edition will be as successful as the 2011 edition.

Göttingen, October 2013  
Bamberg

Siegfried Siegesmund  
Rolf Snethlage

# Contents

<b>1</b>	<b>Natural Stones in Architecture: Introduction</b> .....	<b>1</b>
	Rolf Snethlage	
<b>2</b>	<b>Building Stones</b> .....	<b>11</b>
	Siegfried Siegesmund and Ákos Török	
<b>3</b>	<b>Physical and Mechanical Properties of Rocks</b> .....	<b>97</b>
	Siegfried Siegesmund and Helmut Dürrast	
<b>4</b>	<b>Weathering and Deterioration</b> .....	<b>225</b>
	Michael Steiger, A. Elena Charola and Katja Sterflinger	
<b>5</b>	<b>Environment and Architectural Stone</b> .....	<b>317</b>
	Peter Brimblecombe	
<b>6</b>	<b>Characterization of Stone Deterioration on Buildings</b> .....	<b>349</b>
	Heiner Siedel and Siegfried Siegesmund	
<b>7</b>	<b>Stone Conservation</b> .....	<b>415</b>
	Rolf Snethlage	

# Contributors

**Peter Brimblecombe** School of Environmental Sciences, University of East Anglia, Norwich, UK; School of Energy and Environment, City University of Hong Kong, Kowloon, Hong Kong SAR, People's Republic of China, e-mail: pbrimble@cityu.edu.hk

**A. Elena Charola** Museum Conservation Institute, Smithsonian Institution, Washington, DC, USA, e-mail: charola\_ae@yahoo.com

**Helmut Dürrast** Department of Physics, Prince of Songkla University, Kanjanavanich Road 15, HatYai, Thailand

**Heiner Siedel** Institut für Geotechnik, TU Dresden, George-Bähr-Str. 1, 01069 Dresden, Germany, e-mail: Heiner.Siedel@tu-dresden.de

**Siegfried Siegesmund** Geoscience Centre, University of Göttingen, Goldschmidtstrasse 3, 37077 Göttingen, Germany

**Rolf Snethlage** Natural Stone, Building Chemistry and Building Physics for the Conservation of Monuments, Wetzelstraße 24, 96047 Bamberg, Germany, e-mail: rolf@snethlage.net

**Michael Steiger** Department of Chemistry, Inorganic and Applied Chemistry, University of Hamburg, Martin-Luther-King-Platz 6, 20146 Hamburg, Germany, e-mail: michael.steiger@chemie.uni-hamburg.de

**Katja Sterflinger** Institut für Angewandte Mikrobiologie, Universität für Bodenkultur, Muthgasse 18, 1190 Wien, Austria

**Ákos Török** Geoscience Centre, University of Göttingen, Goldschmidtstrasse 3, 37077 Göttingen, Germany, e-mail: ssieges@gwdg.de

# Chapter 1

## Natural Stones in Architecture:

### Introduction

**Rolf Snethlage**

**Abstract** Since the prehistoric age, men have used stone for its unique durability to erect monuments of extraordinary, mostly religious importance. Due to lacking transportation facilities until the 19th century, stones from nearby sources had to be chosen to build churches, castles and towns. Only for exceptional cases were rare and decorative stones like marble transported over long distances when stone of the same color and beauty was not available in the near vicinity. The design of building structures and elements must be adapted to the mineralogical, physical and mechanical properties of stone. The high compressive strength and the low tensile strength of stone require special techniques to overarch gateways and to erect vaults. Mediaeval builders who succeeded in the erection of high and light structures like Gothic church choirs or spires could only stabilize the construction with the help of hidden steel anchors. Only with the emergence of steel and reinforced concrete, the limits that stone properties posed to building structures had been overcome, and a new era of architectural building design began.

## 1.1 Introduction

Wood, mud bricks and stone are the oldest building materials of men. While mud bricks and wood were mostly used for common buildings like residential houses or stables, stone was used to erect important and impressive buildings like temples, which were meant for extremely long service life and should endure for centuries or even thousands of years. Men regarded stone as ever lasting because the phenomenon of enhanced weathering due to environmental pollution did not exist in former times.

---

R. Snethlage (✉)

Natural Stone, Building Chemistry and Building Physics for the Conservation of Monuments, Wetzelstraße 24, 96047 Bamberg, Germany  
e-mail: rolf@snethlage.net

## 1.2 Stone Provenance and Provinces

Up to the beginning of 20th century, the availability of stone resources determined the appearance of whole cities. Transportation was difficult and slow because of the road conditions. Wherever possible, heavy stone blocks were transported by ships, preferably downstream. The Egyptians shipped obelisks quarried and manufactured in Aswan down the Nile to Luxor and even Memphis. In Roman times, valuable decorative marble and limestone from Greece and Turkey were transported into Italy to embellish Roman villas and temples. Likewise, the unique, red Porfido Rosso Antico (Imperial Red) from Mons Claudianus in Egypt was delivered to Italy for the exclusive use of the Roman emperor and for his imperial buildings.

Stone blocks were also used as ballast in sailing ships to give them the necessary weight for safe sailing on the sea. Plenty of Gotland sandstone from Sweden came this way into the towns along the Baltic Sea coast in Germany and further east where it was preferred for buildings, gateways and many tombstones. When sea or river transport was not possible, rare decorative stone blocks had to be pulled over long distances on ox or horse carts. This way, the Romans even brought Carrara marble over the Alps into their German provinces.

Transportation capabilities and capacities rapidly increased in the 19th century through the construction of canal and railroad networks. From then on, it became easy to transport huge stone blocks and even to send them into remote provincial towns. More and more imported stones from other countries entered formerly uniformly designed towns. In Germany, the impact of new stones in the 19th century is evident in nearly all towns.

For about 20 years, a new dimension of import stone has been observed all over Europe and the USA. Because of cheaper production, huge quantities of stones from China, India and Brazil have invaded Europe and America, thus forcing out the local stone industry. As an example, the floor of the new airport terminal in Munich is paved with Chinese granite because, in spite of the far distance, it is still much cheaper than the Bavarian Forest granite quarried just 100 km away.

The uniform appearance of historic town centers is an important part of our cultural heritage that should be preserved and not be altered by strange import stones. There are famous examples of historic town centers of extraordinary value, especially because their buildings consist of one stone type. A few are worth mentioning. Since Roman times, the buildings in the city of Bath, and of course its Roman bath as well, have been erected with a local Cretaceous limestone from the Great Oolite. Parts of Paris are situated over a system of underground cavities where the Tertiary limestone for the Parisian buildings has been quarried. Rome, on the other hand, is famous for the travertine. In Germany, the center of Dresden is an example of the use of two varieties of Elbsandstone, the Postaer and the Cottaer Elbsandstone (see Fig. 1.1), which come from quarries some kilometers up the Elbe river. The castle in Nuremberg sits on a sandstone rock to which the name “Burgsandstone” has consequently been attributed.



**Fig. 1.1** Frauenkirche in Dresden, Germany. Postaer Elbsandstone



### 1.3 Natural Stone Structures

As already mentioned, the physical and mechanical properties of natural stone narrow its use as building material. Stone has high compressive, however, low tensile strength, which is about 10–30 times lower than compressive strength. Therefore stone should only be loaded with compressive forces because stones loaded with bending forces can easily crack and cause a failure of the whole construction. Already in prehistoric times, builders knew about these limitations.

Stonehenge is a good example to elucidate the expertise of Stone Age men. It has been found that the stone blocks come from a granite complex in Wales from where glaciers must have transported the blocks into the area of Stonehenge. Nevertheless, great efforts were necessary to manage the transport over the remaining miles to the building site, whereby the transportation method is now still under debate. In any case, the Stone Age builders must have known about the low bending strength of natural stone because the stone cross-beams bridging the gap between the vertical columns have sufficient thickness to exclude the risk of cracking (see Fig. 1.2).

**Fig. 1.2** View of Stonehenge. Thick cross-beams were used to prevent crack formation



The reputedly biggest coherent stone block ever made by men is the beautiful marble relief on the north side of Baohedian in the Emperor's Palace in Beijing (Hall of Preservation of Harmony). The relief made from Fangshan marble has a length of 16.5 m, a width of 2 m and a thickness of 1.7 m. The Fangshan area is some 50 km away from Beijing. Chinese archives report that transport was done in winter time on an ice track onto which the stone block could be pulled with relatively little power because it was sliding on a film of thawed water between the stone and the ice track.

The Cheops Pyramid is the biggest accumulation of stone made by men. It consists of about 2,300,000 stone blocks, each of them weighing about 2.5 tons. The pyramid has a height of 146 m. Assuming an average rough density of the limestone as  $2,500 \text{ kg/m}^3$ , the compressive force onto the center of the ground plant results 3.65 MPa. This pressure is more than 10 times less than the compressive strength of the limestone. In spite of the enormous height of the Cheops Pyramid, there is no risk that the stone in the undermost layer could break (see Fig. 1.3).

A look at the forest of columns in the Karnak Temple in Luxor in Egypt demonstrates that the builders had a precise knowledge about the limitations the natural stone properties posed to the construction of the temple hall. As shown in Fig. 1.4, the columns stand extremely close to each other because of the low bending strength of the sandstone beams connecting the capitals of the columns. As a general rule, the thickness of a freely hanging stone block resting on both ends should be one third of its length. In the Karnak Temple, the distance of the columns amounts to around 4–5 m so that the thickness of the cross-beams should be around 1.30–1.50 m, which corresponds quite well to the real situation (see Fig. 1.4).

Bending strength of a stone beam also depends on its moisture content. Because moisture strongly reduces bending strength, it has to be made sure that the beams are not wetted by rain or snow. The technical bending strength measured in a laboratory under standardized testing conditions is higher than the value of

**Fig. 1.3** View of the Cheops Pyramid. In spite of the height of 146 m, the pressure at the base is much less than the compressive strength of the limestone



bending strength in practice. In a building, a stone element is exposed to permanent stress, causing cracks to grow under much less force than measured in a laboratory. Moreover, the thickness of stone beds in the quarry limits the height of available stone beams and, thus, may indirectly determine the distance of columns in a building.

It should also be taken into account that Egypt had a lack of appropriate wood for construction purposes. Consequently, there was a need to take recourse to stone as the main building material because the mechanical properties of palm wood, the only tree available in great quantities, were insufficient for construction. This situation is completely different from classical Greece. The architraves resting above the columns of Greek temples normally have a thickness of around 1 m. Their thickness varies with the distance of the columns; however, the rule that the thickness should be around one third of the length is always obeyed. The cella of the temple, however, is too wide to be covered with stone beams. Instead, it was roofed with a wooden construction able to span over the whole distance between the cella walls. This roof construction was only made possible because, in contrast to stone, wood can bear high tensile forces and, of course, due to the availability of high quality wood.

**Fig. 1.4** Columns in the Karnak Temple in Luxor, Egypt. The thickness of the cross-beams on top of the columns takes into account the low bending strength of the sandstone



The first solution builders found to overarch bigger rooms is the so-called “false vault”. In contrast to a real vault, in this case, stone blocks were put upon each other, the upper one always protruding a little over the lower one. In order to avoid the toppling of the layers, heavy stone blocks or earth filling had to be put on the opposite side as counter weight. Examples of false vault constructions are the trulli in Apulia in Italy or the Tomb of Atreus in Mykene in Greece (see Fig. 1.5).

In addition to the counter weight, the construction is stabilized by the fact that the stones of each layer form a closed ring so that they cannot fall out. Thus, within the ring, the stones are loaded only by compressive forces so that the whole construction is very stable.

A progression in architectural design is the capability to build real arches and vaults allowing lighter and material-saving constructions. In the case of a real arch, the stones support each other and rest on strong corner points. Figure 1.6 shows a limestone arch over the tunnel between the sacred area and the stadium in Olympia, Greece. Different from constructing a false vault, scaffolding is needed for erecting a real vault or an arch. The stones of the arch are laid out upon the scaffolding, and only when the arch is closed can the scaffolding be demounted. In this construction, the stones are mainly loaded with compressive forces. The

**Fig. 1.5** View of the false vault in the Tomb of Atræus in Mykène, Greece



Romans were perfectly capable of building arches, as, for example, long aqueducts like Pont du Gard and bridges in all of Europe demonstrate.

Romanesque architecture resumes the building principles of the Romans. Romanesque churches are characterized by thick walls and narrow window openings. Portals and window frames are terminated with round arches. Romanesque architecture takes into account the mechanical properties of natural stone. The stone is not loaded up to its strength limits. Romanesque buildings make an impression of solidity and compactness (Fig. 1.7).

The Gothic style marks a complete change in architectural design. The formerly solid walls become light and open. Through wide windows decorated with delicate traceries, light floods into the interior of the building. Slim spires reach enormous heights. Quatrefoils between their ribs let wind and rain pass through. Flying buttresses span from the walls of the main nave to the supporting pillars. The elongated structures of Gothic cathedrals go to the limits of the mechanical properties of stone. Therefore, the safety of choirs and spires had to be secured by iron ring anchors invisibly imbedded in the stone in order to hold the structural elements together. Without anchors, the whole structure would be endangered by



**Fig. 1.6** View of a Roman arch in the district of Olympia, Greece



**Fig. 1.7** View of Romanesque stonework of Worms Cathedral, Germany



collapse. In some cases, serious damage has been caused because iron bars running through the window openings had not been seen as parts of ring anchors but have been cut to enable easy demounting of the stained glass windows. The choir of St. Lorenz church in Nuremberg demonstrates the light and rising construction principles of Gothic architecture (Fig 1.8).

With Gothic architecture, the final point of building with natural stone is reached, which cannot be surpassed. The low bending strength of stone does not allow more extreme building constructions. Only in the 19th century did new materials and production techniques open the way to new design concepts. With the emergence of steel and concrete, a new era began. What are the reasons for this change? The Industrial Revolution in the 19th century brought forth new methods of generating energy and production techniques. Modern blast furnaces and converters produced steel of until then unknown high and standardized quality. Subsequently, technically innovative steel constructions could be erected, like the

**Fig. 1.8** View of the choir of St. Lorenz Church in Nuremberg, Germany



**Fig. 1.9** Big hall of German Federal Mail in Munich, built 1965–1969. Length 124 m, height 31 m, width of the arch 146 m



impressive halls overarching railway stations in Europe or the USA, or the unique steel framework of the Eiffel Tower in Paris.

In the field of inorganic binding materials, modern furnaces produced temperatures sufficiently high for the production of cement. In 1843, W. Aspdin achieved a patent for the production of Portland Cement, a mixture of limestone and clay burnt at a temperature of 1,400 °C. Soon, reinforced concrete would become the dominant building material, with the means of which engineers built huge bridges and wide halls with no inside supports (see Fig. 1.9). In this era of concrete, natural stone is restricted to a subordinate use as façade tile. Every year, innumerable stone blocks are cut into thousands of square meters of uniform façade claddings. Traditional stone mason techniques are no longer required. A several-thousand-year-old craft is at the risk of vanishing.

# Chapter 2

## Building Stones

Siegfried Siegesmund and Ákos Török

**Abstract** Most historic structures and many of our recent buildings have been constructed from natural stone. This chapter gives an overview of available natural stone resources and trends in building stone extraction. It documents the various uses of stone from an architectural point of view, showing historic and recent examples in more than a hundred color photos depicting construction periods from prehistoric to recent times. Besides describing the uses of stone, the chapter also provides information on the main rock-forming minerals, their properties and classification, which enables an easier identification of the various stones. Richly illustrated sections outline the main rock groups from igneous and metamorphic to sedimentary rocks, allowing the reader to understand their origin, to recognize various rock types and compare their potential use. Fabric differences, colors, shades and tints of stones and their appearance on facades are also illustrated, helping the reader to distinguish between various types of commercially sold “granites” and “marbles”. By providing detailed descriptions of most stone types with an explanation on their origin, mineralogy, fabric and their potential application, the chapter clarifies the misuse of commercial names and the improper use of stone in engineering and architectural practice. This is often derived from the misidentification of available stones and limited knowledge of stone properties.

### 2.1 Building Stones as a Natural Resource

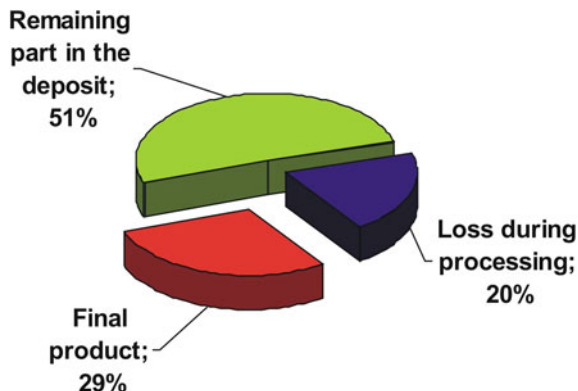
Since time immemorial, natural building stones have been considered a valuable and essential part of the building industry. The constructions and monuments that have been created bear witness to extraordinary technical and artistic achievements.

---

S. Siegesmund (✉) · Á. Török  
Geoscience Centre, University of Göttingen, Goldschmidtstrasse 3,  
37077 Göttingen, Germany  
e-mail: ssiegies@gwdg.de



**Fig. 2.1** Worldwide exploitation of natural building stones and the proportion of finished product versus stone resources (after Montani 2003)



In the last several decades, new technologies have led to considerable advances in the excavation and further processing of natural building stones. The possibilities offered by modern design for creating aesthetic interiors and exterior façades have led to a greater demand in recent years. The forecast for net production has arisen from a continuous production increase, whereby the production volume doubled every 10 years (Montani 2003) until 2008, when economic crises led to a drop in stone production by approximately 40 %. These changes in economic growth bring into question the sustainability of economical stone quarrying and processing. In the future, new deposits have to be developed while older deposits have to be expanded with regard to existing inventories.

The profitability of a deposit is defined by the relationship between the exploitable rock resources (dimension stone) and the non-exploitable rock material (overburden). According to Montani (2003), only a third of the exploited raw material reaches the global market as a finished product, considering the worldwide average in the excavation of natural building stones (Fig. 2.1). From the quarried materials, 51 % occurs as overburden in the deposit as well as 20 % resulting from the loss due to cutting, which is used in the stone industry for further processing. In the future, there will be a great demand for natural building stones. To realize this, more geologic exploration is essential. Detailed surveys and assessments of geological conditions are a necessity in order to utilize a deposit in an optimal way and to ensure sustainable resource protection. In many cases, adequate geological evaluations are missing or non-existent. Indispensable for the development of a deposit is the information on the specific rock formation, its spatial orientation and extent, the depth of the deposit, and characteristics of the overlying rock strata. In addition to large-scale reconnaissance surveys, more precise knowledge is required on factors that can determine the deposit. Knowing these factors has an effect on the respective sizes of the dimension stones and the types of excavation, which, in the final analysis, can determine the quality and quantity of good,

defect-free excavated raw blocks (Mosch 2009). The joint system here plays an important role. The system describes all planar elements that dissect the rock body into individual blocks known as in-situ blocks (Lu and Latham 1999). Disregarding these factors often results in a considerable and avoidable loss during the excavation of dimension stones.

Natural building stones are defined according to EN 12670 (2001) as natural resource rock with use in construction and for the restoration and reconstruction of monuments, where they have a wide range of applications on the international market. They can be used as load bearing elements or for ornamental and decorative elements, e.g. cladding panels or sculptures. The multifaceted possible uses generate a high demand for this resource so that, in the last 30 years, a clear positive balance has been maintained in the production of natural building stones. According to Mosch (2009), three basic quality grades can be differentiated in general for natural building stones: (1) individual blocks, (2) gravestone sector, and (3) building industry (see also Sousa 2010).

The highest requirements are placed on the individual blocks, which are used, for example, in sculptures. A complete homogeneity in color and decor or even special individual needs of the ultimate buyer has to be guaranteed, whereby a very high price is reached in general. In the gravestone sector, a flawless petrography and structural formation of the stone is generally expected. The third grade encompasses all the qualities that are applied in the building industry. A further classification corresponding to the physical and technical construction properties of the materials is possible, which ultimately can be used to determine potential areas of application for the stone (Mosch 2009).

Over the ages, exploitation methods of natural building stones have changed significantly. First, wood edges were watered and the expansion of wood allowed the splitting of larger blocks. This technique is well known from ancient Egypt (Fig. 2.2a). Stone tools were also used, but these were later replaced by metal tools such as chisels and hammers in the exploitation (Shadmon 1989). Handwork and traditional exploitation techniques are still common in the developing world due to low labor costs (Fig. 2.2b). With industrialization, the quarrying techniques have developed significantly, and drilling and cutting equipment is in everyday use (Fig. 2.2c and d). Gang-saw and other techniques allow the exploitation of very large blocks and reducing of block size at quarry level (Fig. 2.2e and f).

The identification of natural stone reserves and the occurrence of stones in nature can be very different in terms of scenery and size (Fig. 2.3a–d). Deposits stretching in small mountains such as the Carrara Marble (Fig. 2.3a) are the most common, but smaller reserves such as boulders are also exploitable (Fig. 2.3b). In contrast, the decorative aspects of stones already become visible at outcrop scale (Fig. 2.3c); however, these are most evident after processing.

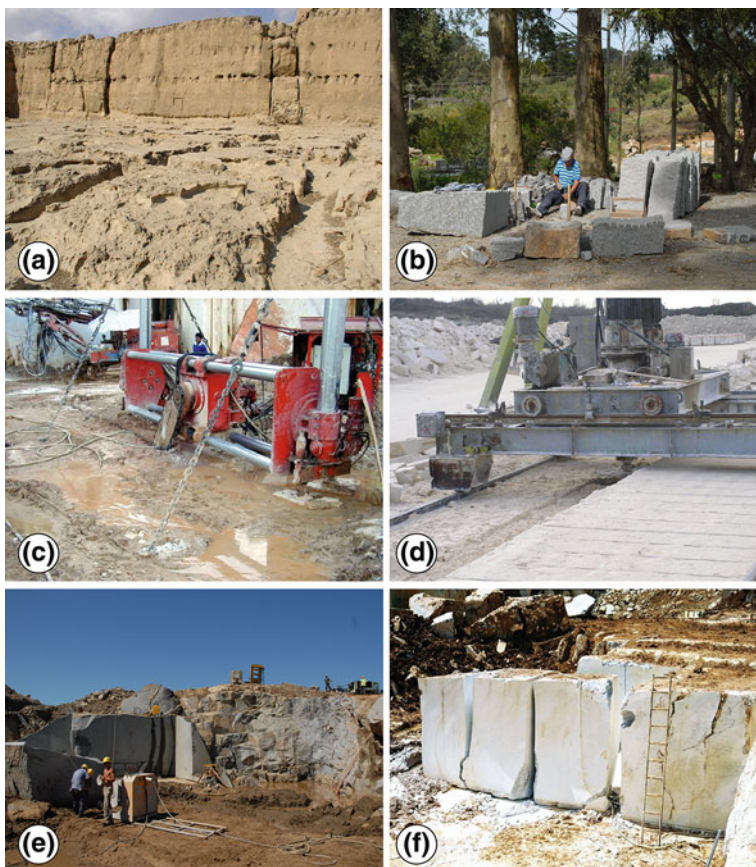


**Fig. 2.2** Methods of stone exploitation from the past to present: **a** Prehistoric traces of the use of wood edges to cut the stone (Egypt, Giza), **b** Manual splitting of granite in Uruguay, **c** Drill hole aided extraction, **d** The use of a saw for the extraction of soft porous limestone (Sóskút, Hungary), **e** In-situ gang-saw cutting for stone extraction in the dolerites in Uruguay, and **f** Reducing of the block size at the quarry level (Thailand)

## 2.2 The Natural Building Stone Market

The building stone industry is part of an important branch in the field of natural resource exploitation in more than 50 countries. Asia and Europe are leaders in the worldwide production of natural building stones (Fig. 2.4).

The European part of dimension stone production amounts to about 38 % and lies behind the Asian states, which manufactured around 50 % of the world production of building stones in 2004 (Montani 2005). The remaining 22 % of world production is distributed across North and South America, Africa, and Oceania. About 75 % of worldwide excavated dimension stones are sustained by 12 countries, which generate a yearly production of >1 Mt of natural building stones.

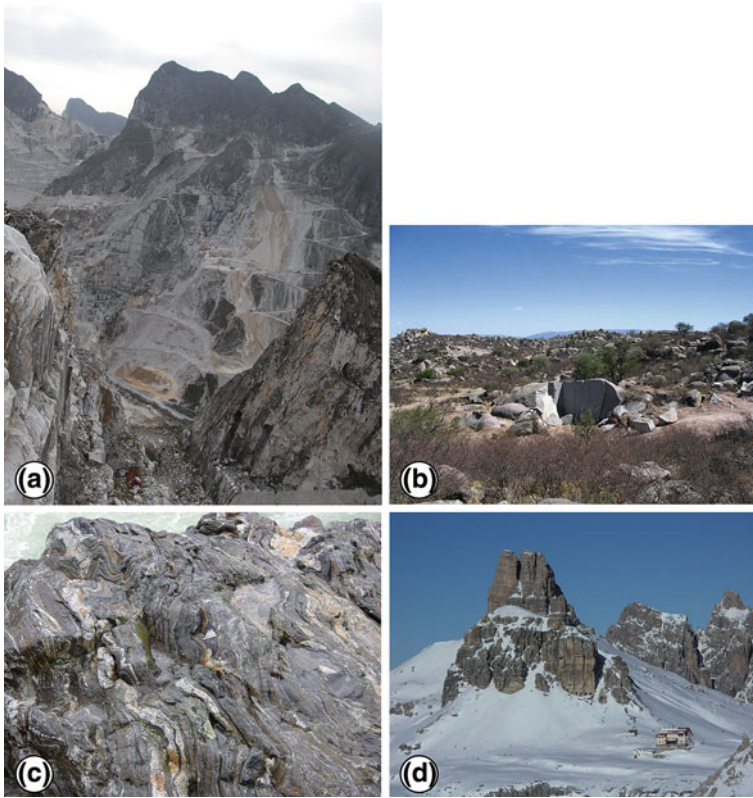
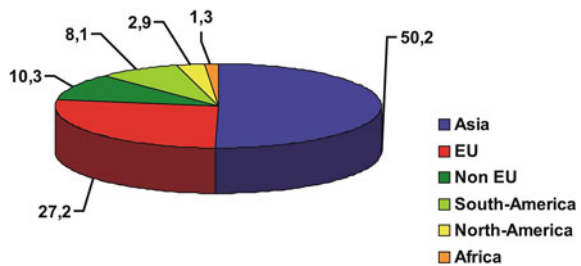


**Fig. 2.3** Occurrence of stones in the field: **a** Marble quarries in the Carrara district, **b** Boulder fields of migmatites due to surface weathering in the Cordoba region (Argentina), **c** Outcrop of migmatites with intense folding in the Ivrea-Zone (Italy), and **d** Steep well bedded and fractured dolomite cliffs (Dolomites, Italy)

**Fig. 2.4** The percentage of stone production with respect to continents in a more general overview (after Montani 2005)



Six of these top producers are European states, with five of them belonging to the European Union (Fig. 2.5). Four producers are in Asia, two are in America, and one is native to Africa. In descending order, export figures of China, Italy, India, Spain, Brazil, and Portugal were able to sell more than 1 Mt of material on the

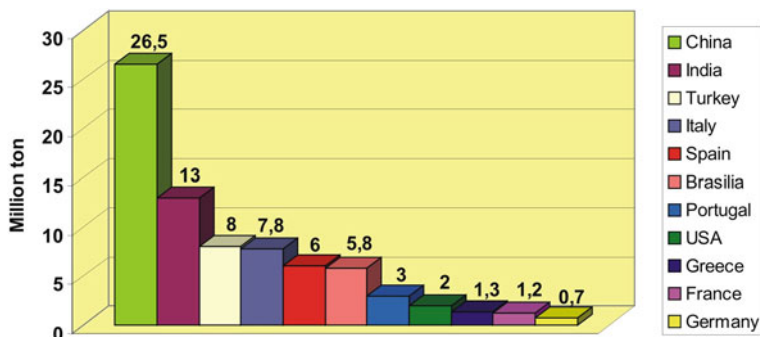


**Fig. 2.5** Leading nations in the production of dimension stones and the amount of stone produced in millions of tons (after Montani 2008)

international market. China is the main stone exporter with 11.8 million tons of export in 2008. The leading position of importing countries includes, among others, Germany, Italy, China, and even Spain. The fact that the three latter countries are also situated as leading exporters clearly demonstrates the dominance they have in the international building stone market. Besides the high production rates, these countries also import large amounts of raw materials and semi-finished products, which is the reason why they can cover the various demands of the market through individual and flexible finished products.

Significant economic regions of the European natural stone industry are located mainly in southern Europe with its direct connection to the Mediterranean Sea. Countries like Italy, Spain, Portugal, and Greece cover around 90 % of EU production (European Commission 1998). This is due to the advantageous conditions of regional geology and the long tradition these countries have in the field of natural stone manufacturing. Besides other traditional natural building stone manufacturers, such as Scandinavian countries, both the Czech Republic and Poland have established themselves in the dimension stone sector (Montani 2003). The European contribution to worldwide natural building stone production has declined in the last several years. The overriding cause of this decline is the high production amount and the current processing capacities in countries such as China, India, Brazil, and South Korea, which are also characterized by distinctly lower labor costs (Terezopoulos 2004). Especially impressive is the growth rate of Asian natural building stone production, which is being continuously introduced into the international market. During the 1990s, China concentrated on increasing the exploitation capacity of its deposits and, furthermore, acquired large amounts of raw material from India, Brazil, South Africa, and Norway for processing. Today, China is in a unique position in the Asian region with regards to the large supply of finished products it has to offer from material acquired abroad and from its own deposits. Due to its favorable geographical position near the Pacific Ocean and other sea routes, China has found stable and profitable markets. These include markets in Europe, the West Coast of the USA, and the Middle East, which only played a subordinate role in



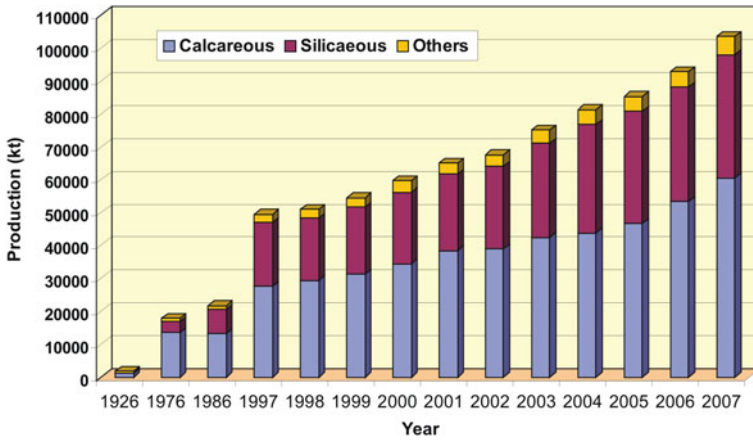
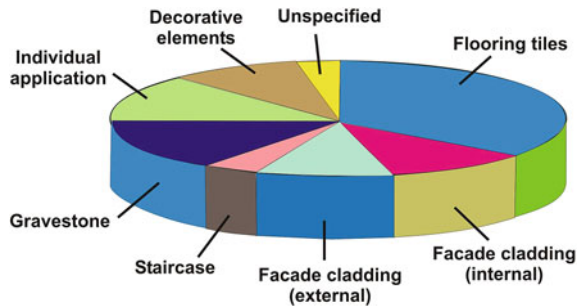


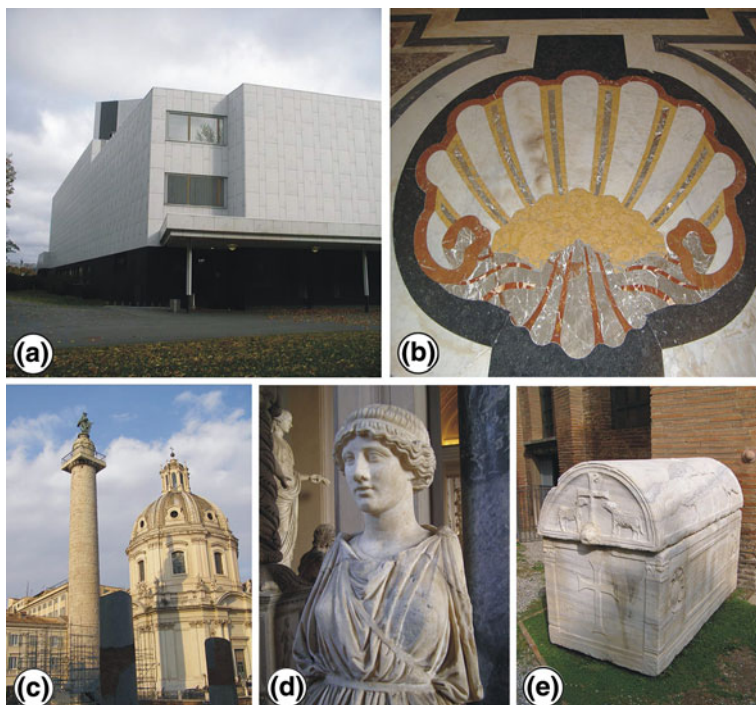
Fig. 2.6 The proportion of major lithotypes in stone production

Fig. 2.7 Different uses of stones and their proportion (modified after Hoffmann 2007)



international trade until a couple of years ago (Bruno and Paspaliaris 2004). The production of ornamental stones was 91.6 million tons in 2007. In terms of various stone types, calcareous stones are the most widely used ones, while other lithologies, such as siliceous stones, are less common in the stone industry (Fig. 2.6).

Natural building stone products range from unfinished raw blocks to semi-finished goods up to polished and refined dimensional stone that can be used for various applications. The building industry processes about 70–75 % (Primavori 1999; Founti 2004) of worldwide exploitable natural resources. These go into the creation of tiles, cladding panels, stairs, or other architectural elements and, thereby, represent the most extensive field for the application of natural stones (Fig. 2.7). Although the construction industry started to replace natural building stones with steel, concrete, glass, artificial stone, and brick over the last three decades, these alternative products could not completely stop the demand for these natural resources. The continuous demand for natural building stones is probably due to the high quality of their appearance, their architectural variability, and their prestigious character, which is evident in many public institutions and representative buildings all over the world (Fig. 2.8).



**Fig. 2.8** Various uses of stones: **a** External cladding with Carrara marble (Finlandia Palace, Helsinki), **b** Interior flooring (St. Stephan's basilica, Vatican-Rome), **c** Roman stone column (Ravenna, Italy), **d** Marble sculpture (Vatican), and **e** Sarcophagus (Roman period, Ravenna, Italy)

Another consumer of relatively large amounts of natural building stone is the gravestone sector, which processes about 15 % of world production. The gravestone industry prefers semi-finished products in the form of small blocks that can be further processed for individual purposes. In the fields of urban development and craftwork, natural building stones essentially fulfill a functional and/or decorative aspect or add to conservation measures within the framework of protection and preservation of the cultural heritage.

The amount of building stones needed cannot be supplied by existing quarries. Therefore, if the current trend of natural stone use continues, it is imperative that the deposits be managed in a more economically efficient way and expanded with regards to existing inventories. In order to meet the current predictions for the demand of natural building stone, it becomes indispensable that new deposits be developed and exploited. For this, sufficient geological assessments and a basis for planning is absolutely necessary. Architects have two choices, either using dimension stones or returning to artificial stones.

## 2.3 Architects Point of View

The oldest manifestations of human civilization are undoubtedly connected to the history of grandiose constructions and monumental depictions in stone, which have fascinated architects and sculptors in all cultures (see [Chap. 1](#)). From a design point of view, natural building stones stand for tradition in contrast to the glass and steel that embodies technical progress. The historical examples, and even the present debate on natural building stones, verify that these structures also stand for a demonstration of power, permanence, and representation ([Fig. 2.9](#)). Many successful examples show that natural stone, one of the oldest construction materials in the world, is still being used in modern architecture and is a popular facing material of the 21st century. There is hardly a bank, insurance company, or headquarters of a large corporation that does not utilize this material to decorate their buildings.

Natural building stones, with their different colors and structural variations that change their appearance with varying weather and light, have always fascinated man. Stones always convey a message of eternity. They are unique materials and are enjoying a surprising renaissance today. Due to globalization, thousands of different kinds of dimensional stones exist on the market, and their numbers are rising because they are being used in most countries in the world. Even in modern architecture, where steel, glass, and pre-cast concrete elements epitomize the dominant materials, it is the decorative stones that will characterize the buildings.

Many architects and building owners are increasingly making the decision to use stone cladding façade elements or stone for interior work. Not to be underestimated is the use of natural building stones in urban planning—for example, in garden and landscape architecture as well as in wellness areas. The choice of the right material represents a major challenge. For the selection of the proper stone from an architectural point of view, aesthetics and fashion are important. These cannot be easily expressed in numerical values or in diagrams. However, certain physical and technical properties of stones need to be assessed or measured to fulfill the requirements of durability and long-term stability of the stone structure. Often, the stone is reduced to its interplay of color, which is without a doubt an important sensory perception in human beings. With regard to the choice of material, building owners and architects focus their vision first on the color. It is for this reason that natural building stone dealers use color as the preference for naming their stones (Verde (Green) Andeer, Azul (Blue) Macauba, Verde (Green) Ubatuba, Rosso (Red) Verona, etc.). There is a great variety of stone types that have the same color or similar shade or hue. Red colored stones are found in sedimentary, igneous, and metamorphic rocks ([Fig. 2.10](#)). The same applies for bluish ([Fig. 2.11](#)) and greenish ones ([Fig. 2.12](#)). The use of stone of different colors can give a very different appearance to the same façade ([Figs. 2.10, 2.11, 2.12](#)). Apart from color, the most important role is also played by structural patterns (i.e. the macroscopic appearance). Color and decor is the result of geologically complex processes. On the basis of the diverse decor properties, the





**Fig. 2.9** Architectural and historical uses of stones: **a** Megalithic temples of Malta (app. 2500–3200 years BP), **b** Pyramids of Giza, **c** The Acropolis (Athens), and **d** Forum Romanum (Rome)

natural stone is also given a sensual quality, which is accentuated by different surface treatments and finishes.

Color, as used in architecture, is one of the most characteristic and visible aspects of natural stones. An almost infinite choice of colors and décors of natural stones exists, which determines the macroscopic appearance of stones. The color may be due to the presence of so-called idiochromatic minerals or natural pigmentation due to organic or inorganic inclusions and particles. Apart from the influence of color, the macroscopic appearance of stones is fundamentally defined by the fabric (i.e. texture) and, finally, by rock-forming geological processes. Moreover, the aesthetic value of stones and their décors are highly variable due to an increasing amount of surface treatment.

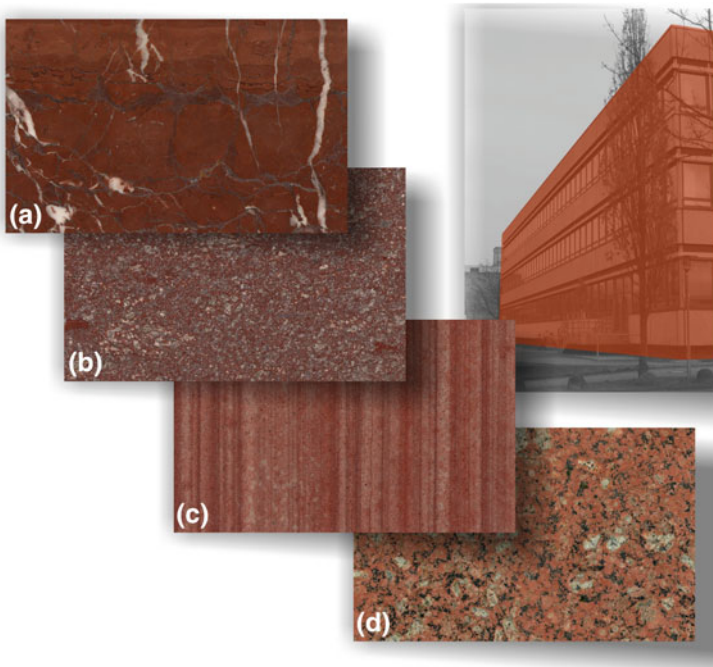


**Fig. 2.10** Collection of red stones compiled exclusively on the basis of color. The different rock types originated under different conditions: **a** Compact limestone, **b** Rhyolite, **c** Sandstone, and **d** Syenite. The rocks are completely different with respect to their technical properties and with respect to their constructional applications (Figure by Natursteinarchiv Wunsiedel)

## 2.4 Confusion Caused by Commercial Names

In the international stone market, a large number of commercial varieties are recognized, whereby a steady increase is observable with progressive globalization. For example, Börner and Hill (2007) collected 13,677 commercial varieties. This large number shows that a great variety of rocks are available on the open market which covers an immense spectrum of colors and decors. The basic problem of this diversity is the arbitrary choice of a commercial or trade name. Therefore, the naming of the stone can result in a complete falsification of the stone's true designation. A good example is the well-known micritic limestone from Belgium, which uses the trade name of Belgian Granite. Sometimes, identical stones are sold under different trade names. Börner and Hill (2007) have shown that the Granite G603 from China is listed on the international market with 67 synonymous terms, e.g. China Sardinia, Padang White, Silverstar, Palace Grey, etc. Some stone introduced internationally astounds with its aesthetic constancy over long periods of time, like the variety Balmoral, which looks the same today as it did before 1900.

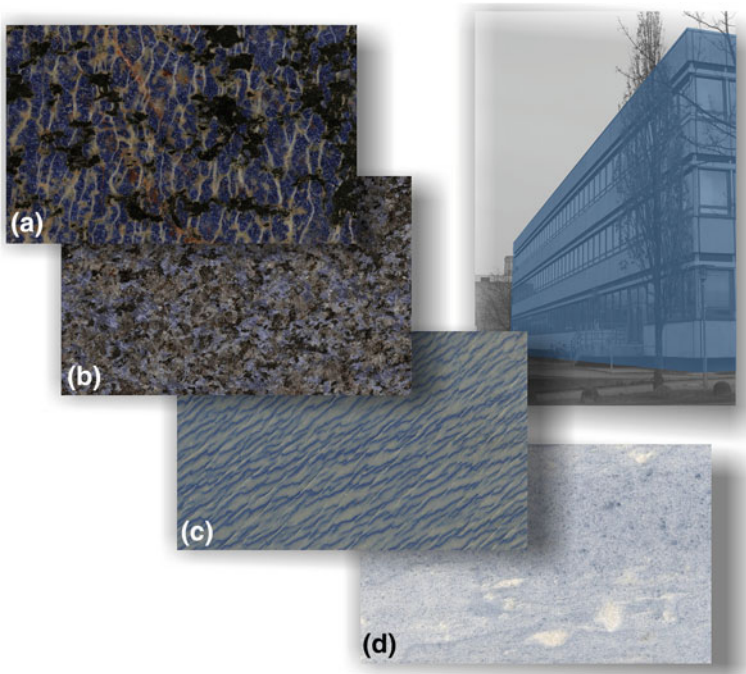


**Fig. 2.11** Bluish stones collected with respect to color: **a** and **b** igneous rocks, **c** and **d** are metamorphic rocks; **c** quartzite and **d** marble (Figure by Natursteinarchiv Wunsiedel)

A rock like Verde Guatemala, which is actually a chlorite schist from Guatemala, is also listed in databases as a serpentinite from India. This situation results from the fact that the original deposit in Guatemala is exhausted and the original trade name has been transferred to the Indian serpentinite. Confusion like this, which may also be intentional, leads to a distortion of the market. When an architect or building owner chooses a pattern for construction, it is not always possible to know whether the stone designation is really valid or corresponds to the true trade name. Architects and planners can become irritated, and competitors can even be eliminated. When a stone is praised and published under the trademark name of Porfido Kern<sup>®</sup> from Trentino (Italy), one comes to the realization that this term is largely unknown in the technical literature. Müller (1996) points out that the naming of natural stones is combined with fantasy names such as Royal, Imperial, Fantastico, Oriental, Oro, Argento, Korall, Christal, and Multicolor, among others. The naming of the stones is done to characterize the material as “noble”, “extraordinary”, “royal”, “unique”, etc. Porfido Kern<sup>®</sup> from Trentino would represent an especially hard and “healthy” stone.

In a strict sense, a Porfido Kern<sup>®</sup> is not a variety or assortment, but basically an internal company designation with specific quality characteristics. The porphyry handbook (Tomio and Filippi 1996) describes the stone as an extrusive ignimbrite

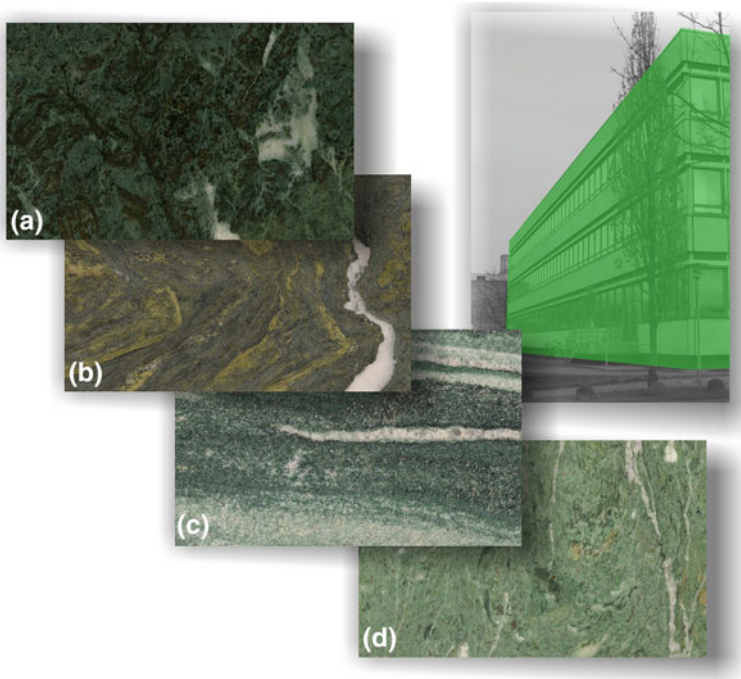


**Fig. 2.12** Greenish stones with a very different origin showing comparable colors (see also Fig. 2.10): **a** Serpentinite, **b** Chlorite schist, **c** Gneiss, and **d** Dolomitic marble (Figure by Natursteinarchiv Wunsiedel)

rock originating from the region of Trentino in Southern Tyrol (Italy). This is, of course, misleading since porphyry occurs worldwide and is found in all geologic time periods. In the EN 12670 titled “Terminology of Natural Stones”, no description of the stone Porfido Kern<sup>®</sup> is listed. The term “porphyry” is defined as the following according to the “Terminology of Natural Stones” No. 3.569: “Designation for all rocks solidified from a melt containing conspicuous phenocrysts in a fine-grained matrix. The resulting fabric is described as porphyritic”. In the European market, a standard for the designation of natural stones already exists. From the EN 12440 titled “Natural Stones: Criteria for the Designation”, the description of natural stones should contain the trade name, the petrographic affiliation, the typical color, the place of origin, and, if possible, the type of surface treatment, the natural properties, the petrographic name, and the geologic age when applicable (Table 2.1).

The term “marble” is also used differently. Ever since antiquity and even today, the natural stone industry has designated most polishable and attractive rocks as marble. Occasionally, even onyx and gypsum rocks (alabaster) are included under the trade name of marble. In the petrographic nomenclature (see this chapter), the term “marble” is restricted to carbonate rocks formed by metamorphic processes.

**Table 2.1** Commercial names of dimensional stones in comparison to their petrographic designation

Commercial name	Petrographic designation
Azul Cielo	Marble
Sankt Nikolaus	Quartzite
Anröchter Dolomite	Calcareous Sandstone
Beola Calvario	Gneiss
Springbok	Quartzite
Verde Orientale	Serpentinite
Petit Granite	Limestone
Pietra Serena	Sandstone
Bardiglio	Marble
Azul Macaubas	Quartzite
Nero Impala	Gabbro
Peperino	Ignimbrite
Naxos	Marble
Halmstad	Migmatite
African Juparana	Migmatite
Verde Serpentino	Chlorite Schist
Anzola	Gabbro
Koesseine	Granite
Blue Pearl	Monzonite
Serizzo Antigorio	Gneiss
Labrador Café	Syenite
Rosso Corallo	Limestone
Rosso Taebri	Travertine
Jaune Imperial	Limestone
Torre Santa Maria	Chlorite Schist
Crema Marfil	Limestone

Within a particular stone assortment, there are varieties true to the normal appearance and ones with different colors. Therefore, Azul Macauba can appear totally white, pale blue, and intense blue. Azul Bahia, one of the most expensive decorative stones, which lies near the petrogenetic field of sodalite-foid syenite to sodalite-foidolite, is frequently traded on the international stone market as granite. Hill (2007) delineated a trade chain that starts with a quarry in Brazil, then moves on to a stone block dealer, and finally reaches Italy for further processing. The processing into untailed slabs and formatting for floors, stairways, or other coverings for export to Germany, e.g. through distributors and sales to craftsmen, creates a very long trade chain. Significant misunderstandings can occur along the trade path because of differences due to language translations. Moreover, complications due to different climatic conditions in the country of origin may cause problems in the country where the material will be used. In the country where the construction site is located, weather conditions can induce freeze/thaw cycles, or the use of corrosive salts for de-icing can lead to negative consequences for the usage properties.



Even the question of color deviations for specific groups of natural stones like “Labrador scuro”, which is sometimes designated a marble, is critical when it is based only on the trade name. According to the EN 12440 (2000), it should be noted that the Labrador scuro is an Emerald Pearl. The number, density, and luminosity of opalescent minerals can vary greatly and, thus, the optical effects connected to them. The trade name is clearly defined and customers who order the Emerald Pearl wish to have a lively stone that is characterized by the luminosity of opalescent feldspars. In Emerald Pearl, the mineral creating the luminous effect is not a labradorite plagioclase, but an anorthoclase. The iridescence is caused by very fine exsolution in feldspar, the so-called cryptoperthite (a hardly recognizable exsolution sub-microstructure in parts of anorthoclase). These exsolution lamellae have thicknesses of about 1,000 Å. For a size comparison, it can be noted that the average thickness of a human hair is about 0.06 mm (600,000 Å). When light encounters these fine exsolution lamellae, it is refracted, reflected, and absorbed. The intensity of the reflected light can vary as a result of the dependency of the composition of the exsolution, the angle of incidence of the light ray, and the thickness of the exsolution lamellae. This then correlates to the color of the minerals or the color play, as in the case above, where it varies between red, blue, and green.

## 2.5 Geology of Building Stones: Terminology

Building stones are defined as those whose origins are igneous, sedimentary, and metamorphic, and which are used for construction and decoration, fill material, crushed stone, and coarse-grained grit material. In practice, these rocks are differentiated into the so-called hard and soft rocks. Hard rocks, e.g. granite, rhyolite, and basalt, are difficult to process mechanically. In contrast, soft rocks, e.g. weakly cemented sandstones, tuffs, porous limestones, and serpentinites, can usually be easily processed. Various properties characterize natural building stones. These are the physical properties, such as compressive strength, porosity, flexural strength, water absorption, and color and décor (see [Chap. 3](#)).

Rocks are composed of minerals. The rock-forming minerals are relatively few in comparison to the overall number of known minerals. Not all of the combinations and proportions of the known minerals are recognized in nature because of restrictions due to physical and chemical laws. Rocks are seldom homogenous materials, in contrast to minerals. Monomineralic rocks contain only one major mineral. Rocks such as marble or quartzite are mostly constituted by calcite/dolomite and quartz, respectively. Many rocks are also polyphase or polymineralic in composition. Granite, for example, consists of the minerals feldspar, quartz, and mica. In any case, a rock is made up of an infinite number of crystals of one or more minerals. The fabric of a rock describes its internal structure. The term “texture” is usually used in the conventional geological manner for spatial relationships between mineral grains in a rock. It includes such features as grain shape

and size and is combined with microscopic structures such as layering, xenoliths, vesicles, and orbs. The structure of a rock describes the size, the shape, and the interactive relationship (intergrowths) of the constituent minerals (e.g. grain size, grain shape, grain size distribution, etc.). Fabric deals with the crystallographic- and shape-preferred orientation, distribution, state and orientation of microfractures, shape and size of grains, their spatial distribution, relations between grains, etc., i.e. the structural elements of a rock.

## 2.6 Rock-Forming Minerals

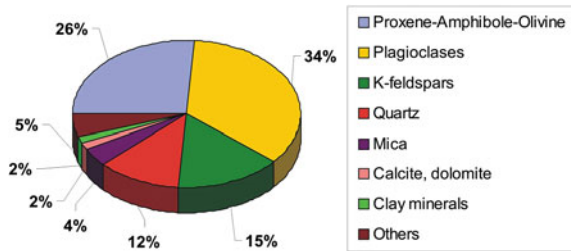
Minerals are solid substances of natural origin. As a rule, minerals have a given chemical composition; therefore, each mineral can be described by a chemical formula. Due to the differences in internal structure, one chemical formula can be attributed to more than one mineral. One example is  $\text{CaCO}_3$ , which can have two very distinct internal structures, and, thus, it is the formula of a mineral called calcite and another mineral named aragonite. In reality, all mineral specimens have individual appearances with some containing impurities. Minerals can be further subdivided according to their internal structure. Crystalline varieties have characteristically regular internal arrangements of atoms, ions, or other compounds and form a structure called the unit cell. In contrast, amorphous mineraloids have no regular internal structure, but they are also solid. Opal is an amorphous form of silica-dioxide. Rock-forming minerals are the most widespread minerals and are the major constituents of rocks. The systematic subdivision of minerals is based on their chemical composition. Accordingly, ten major groups are known (see [Sect. 2.6.1](#)). The most common rock-forming minerals are silicates, which are compounds of silicon, oxygen, and other cations. Additional elements, such as iron, magnesium, calcium, potassium, sodium, aluminum, etc. can also form a part of silicate minerals. Besides chemical composition, minerals can also be subdivided based on their physical properties and external look, or appearance.

### 2.6.1 Mineral Chemistry and Classification

The distribution of minerals is controlled by the chemical composition of the Earth's crust. Only eight elements contribute approximately 99 % of the weight of the Earth's upper zones. These elements, in decreasing abundance, are oxygen (47 %), silicon (31 %), aluminum (8 %), iron (4 %), calcium (3 %), potassium (3 %), sodium (3 %), and magnesium (1 %). It is necessary to note that carbon is not in this list, although, in the processes of life, it plays a key role. The remaining other 90 elements that occur in nature are also found in minerals.

The scientific classification of minerals relies on chemical composition as well as on internal structure. Consequently, mineralogists subdivide all existing

**Fig. 2.13** Frequency of the most important rock-forming minerals of the Earth's crust down to 16 km (data from Peschel 1983)



minerals into 10 groups. Many of these groups are of subordinate importance in terms of their rock-forming ability, since these also include rare or exotic minerals. The 10 groups are as follows:

1. Native elements
2. Sulphides
3. Halogenides
4. Oxides and hydroxides
5. Carbonates and nitrates
6. Borates
7. Sulphates
8. Phosphates
9. Silicates
10. Organic compounds

Of these groups, silicates are by far the most common with contributions of more than 95 % to the Earth's crust. Silicates are the major rock-forming minerals of igneous, metamorphic, and many sedimentary rocks (Fig. 2.13). The native elements are rare, and minerals such as gold or native copper belong to that group. Sulphides are minerals in which sulphur forms the major anion, while mostly metallic and submetallic minerals such as iron, zinc, copper, antimony, and lead provide the cation. Pyrite ( $\text{FeS}_2$ ), galena ( $\text{PbS}$ ), and sphalerite ( $\text{ZnS}$ ) are probably the most common varieties from this group. Halides are minerals containing the halogen anions of chlorine, fluorine, etc. Halite ( $\text{NaCl}$ ) and sylvite ( $\text{KCl}$ ) are well known from this group. Fluorite ( $\text{CaF}_2$ ) also belongs to this group and forms cubic crystals.

Oxides and hydroxides are not rock-forming minerals, but their importance is related to their ability to stain rocks. Iron-oxide (hematite), even if it occurs in ppm (one part per million concentration), can stain rocks red, and the same applies for iron-oxy-hydroxides (goethite, limonite) with their ability to stain rocks brown. Carbonates are key rock-forming minerals for limestones (calcite) and dolomites (dolomite) as well as marbles (calcitic or dolomitic marbles). The carbonate ( $\text{CO}_3^{2-}$ ) anion can form complexes not only with Ca and Mg but also with other elements such as Mn and Fe. Calcium carbonate is known as calcite (trigonal) or aragonite (orthorhombic). Calcite has the greatest number of crystal forms of all existing minerals. Green patinas on copper or bronze structures are also related to a



copper carbonate mineral that is called malachite. For sulphates, gypsum ( $\text{CaSO}_4 \cdot 2\text{H}_2\text{O}$ ) is the most common one, but anhydrite ( $\text{CaSO}_4$ ) and barite ( $\text{BaSO}_4$ ) are also known.

Minerals belonging to silicates contain a basic structural unit cell, which is called the silica tetrahedron. It consists of four oxygen anions on the corners of the tetrahedron and a central silicon cation. The silicates are further subdivided according to the geometric arrangement of silica tetrahedrons. Accordingly, there are isolated tetrahedrons, linked tetrahedrons, ring-silicates, single- and double-chain silicates, sheet silicates, and framework silicates. Framework silicates are the most common ones. Quartz ( $\text{SiO}_2$ ) is an oxide but, due to its structural similarity, is frequently considered together with the true silicates. Rock-forming minerals like feldspars form parts of this latter group. Feldspars are further divided into plagioclases (anorthite  $\text{CaAl}_2\text{Si}_2\text{O}_8$  to albite  $\text{NaAlSi}_3\text{O}_8$ ) and K-feldspars (e.g. orthoclase  $\text{KAlSi}_3\text{O}_8$ ).

## 2.6.2 Mineral Physics

Physical properties play a significant role in the recognition of minerals. The most important ones are shape, color and luster, cleavage or fracture, hardness, specific gravity, and other properties such as magnetic and thermal properties, etc.

The shapes of minerals depend on the internal structure and symmetry of the minerals as well as on the available space where these minerals grow. In most rocks, we can identify idiomorphic and xenomorphic minerals. The first ones have regular shapes, while the latter ones are difficult to identify based on their irregular shapes. When a mineral grows freely, it develops special crystal forms that can be grouped into crystal systems according to their external symmetry. The seven crystal systems, in increasing symmetry, are:

- Triclinic
- Monoclinic
- Orthorhombic
- Trigonal
- Tetragonal
- Hexagonal
- Cubic

Each crystalline mineral belongs to one crystal system and, within the system, one crystal class. Within the system, there can be several morpho-types, whereby one mineral can have different crystal forms of the same symmetry. Pyrite ( $\text{FeS}_2$ ), which belongs to the cubic system, can have tetrahedron, cubic, octahedron, or other crystal forms. The most common rock-forming minerals of igneous rocks are the plagioclases, which belong to the triclinic crystal system, whereas quartz and calcite reside in the trigonal crystal system.

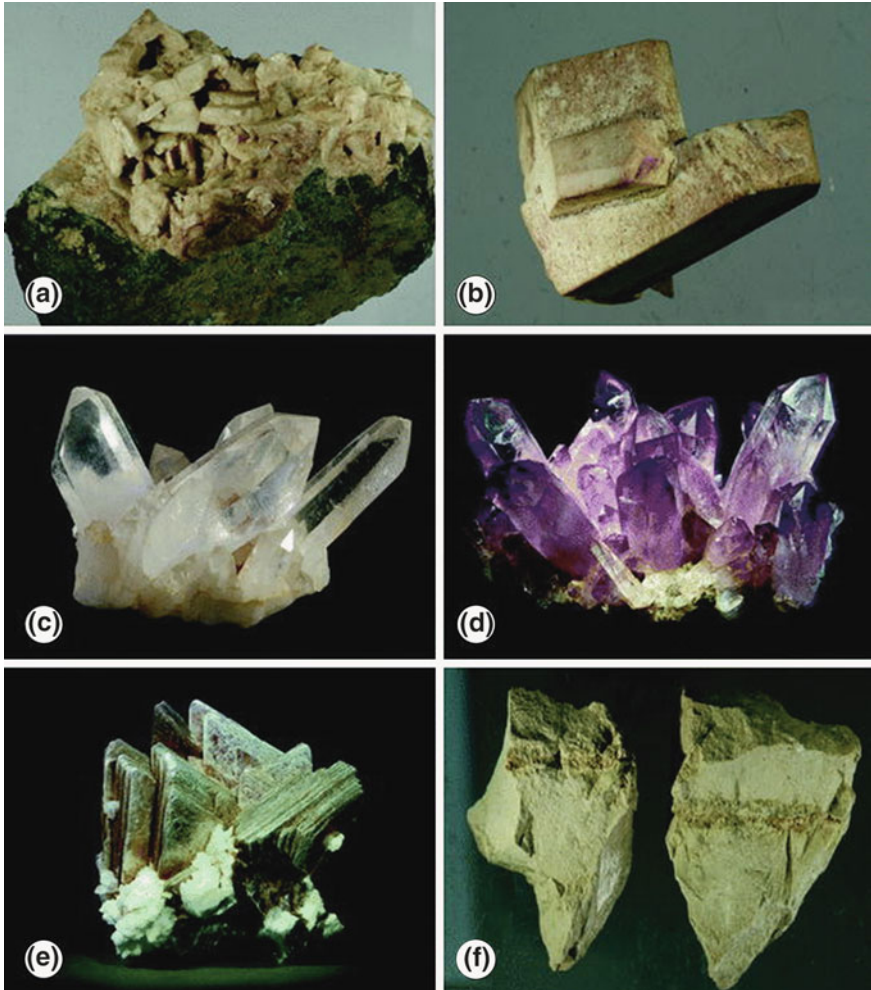


**Fig. 2.14** The most common light-colored rock-forming silicate minerals are **a** Plagioclase (Figure by Geowissenschaftliche Sammlung of GZG Göttingen), **b** K-feldspar (Figure by Geowissenschaftliche Sammlung of GZG Göttingen), **c** Quartz (Figure by Geowissenschaftliche Sammlung of GZG Göttingen), **d** Amethyst, a colored gemstone variety of quartz (Figure by A. Massanek/Geowissenschaftliche Sammlungen of TU Freiberg), **e** Light-colored mica (muscovite) (Figure by A. Massanek/Geowissenschaftliche Sammlungen of TU Freiberg), and **f** Kaolinite (clay mineral) (Figure by Geowissenschaftliche Sammlung of GZG Göttingen)

The color of minerals includes all varieties of the color spectrum, but, for simplicity, minerals are named as light-colored (felsic) (Figs. 2.14 and 2.15) and dark-colored (mafic) (Fig. 2.16). Opaque minerals with a metallic luster generally have a high ability for absorbing light. These are usually ore minerals with industrial importance (Fig. 2.17a–c). Other types of light reflectance (luster)

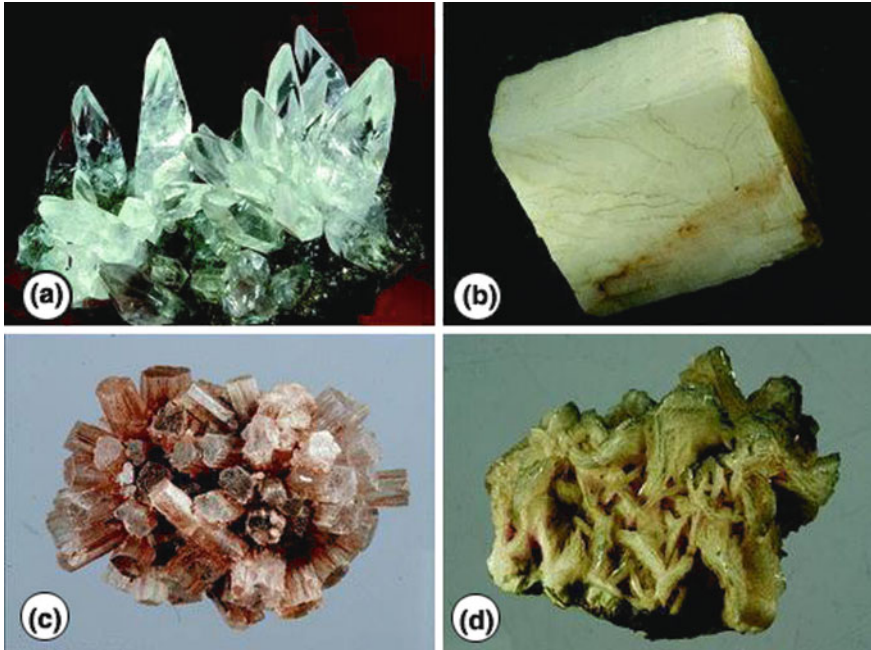


**Fig. 2.15** The most common light-colored rock-forming non-silicate minerals are **a** Calcite (scalenohedral) (Figure by A. Massanek/Geowissenschaftliche Sammlungen of TU Freiberg), **b** Calcite (rhombohedral) (Figure by Geowissenschaftliche Sammlung of GZG Göttingen), **c** Aragonite (Figure by Geowissenschaftliche Sammlung of GZG Göttingen), and **d** Dolomite

includes vitreous, greasy, pearly, earthy, etc. For some minerals, the color of the very fine powder (called streak) is also important; this is different from the color of the bulk specimen. The best example is hematite (iron oxide), which has a reddish streak, whereby the mineral is very commonly metallic black (Fig. 2.17b). A mineral can either break along an irregular surface, which is called a fracture, or it can break along a smooth plane, which is called cleavage. The cleavage plane can be smooth and shiny (perfect cleavage) or less smooth and less light reflecting (moderate cleavage). Micas, such as muscovite, exhibit perfect cleavage, whereas calcite or feldspars have good cleavage. The internal structure of the mineral influences the cleavage, since cleavage planes represent the weakest zones. As a consequence, one crystal can have several cleavage planes depending on the internal structure of the mineral. The fracture surface can also be partly regular—for example, the conchoidal fracture (smooth concentric depressions) in opal.

Hardness of minerals is generally described as scratching hardness. The measure of the scratching hardness is the Mohs scale, which is a relative scale with 10 grades. Minerals that have a Mohs hardness of 1 (e.g. graphite) are the weakest ones, whereas grade 10 (e.g. diamond) is considered to be the strongest. All grades are represented by a common mineral. Grade 2 can be scratched by a fingernail,

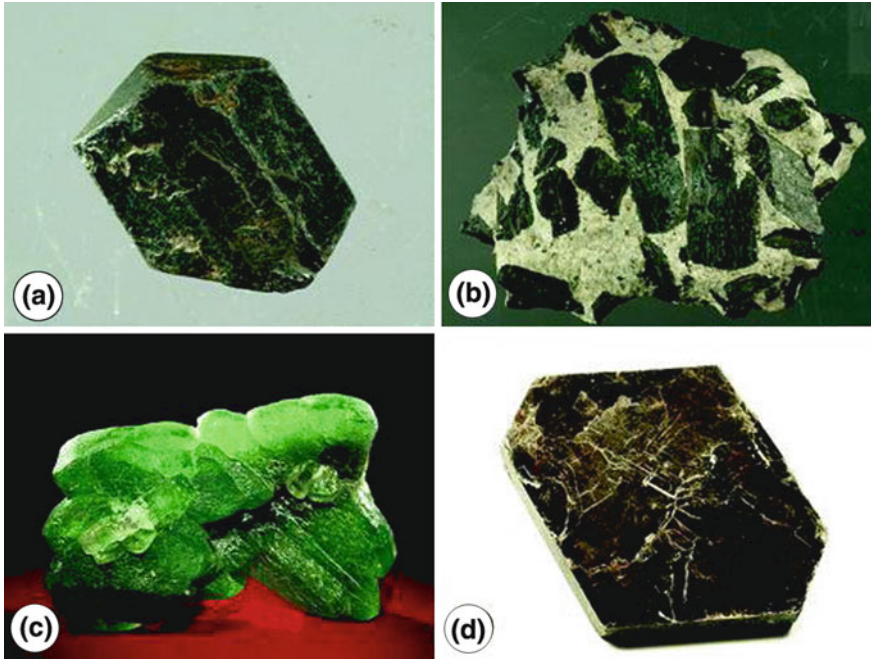


**Fig. 2.16** The most common dark colored rock-forming silicate minerals are **a** Orthopyroxene (Figure by Geowissenschaftliche Sammlung of GZG Göttingen), **b** Amphibole (hornblende) (Figure by Geowissenschaftliche Sammlung of GZG Göttingen), **c** Olivine (Figure by A. Massanek/Geowissenschaftliche Sammlungen of TU Freiberg), and **d** Dark mica (biotite) (Figure by A. Massanek/Geowissenschaftliche Sammlungen of TU Freiberg)

whereas a steel knife has a hardness of 5–6. The minerals that have a Mohs hardness of 7 (e.g. quartz) or more can scratch glass.

Precious minerals are ones which are very rare and have a high aesthetic value. These can be used either in their original forms, such as gemstones (usually with high resistance and scratching hardness), or they need to be extracted and concentrated by metallurgic processing (Fig. 2.18).

The specific gravity or density of minerals is an important parameter, since it determines the weight of the rock. Dark igneous rocks with lots of heavy minerals are much heavier than a quartz sandstone or limestone.

Special properties include the magnetic ability of minerals or thermal or electrical conductivity. The optical properties of minerals are important parameters which are normally studied by using microscopic techniques. The petrographic microscope is the common tool for studying thin sections, whereas ore microscopy utilizes reflected light and can help to distinguish between non-transparent so-called opaque minerals. Transparent minerals have several key optical properties that can be used for identification. Shape, color, birefringence, and cleavage are visible under polarized light and help in the recognition of minerals.



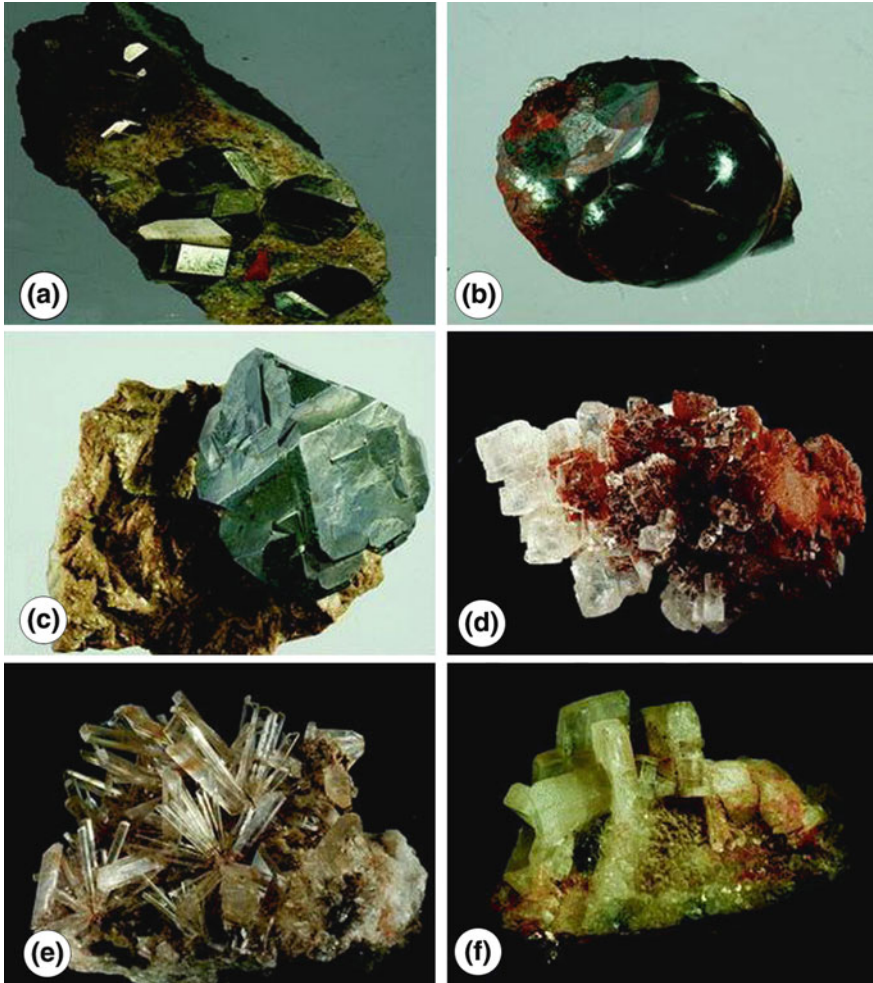


**Fig. 2.17** Ore and industrial minerals. Commonly found iron minerals include **a** Pyrite and **b** Hematite. The main lead mineral is **c** Galena. Industrial use of **d** Rock salt (halite), **e** Gypsum, and **f** Barite is also important (Figure by Geowissenschaftliche Sammlung of GZG Göttingen)

## 2.7 Definition and Origin of Rocks

Three main rock types can be differentiated which develop under different conditions. Igneous rocks form from the cooling and solidification of magma deep in the Earth's crust, in the mantle, or at or near the surface. Thus, igneous rocks can be subdivided into plutonic (intrusive) and volcanic (extrusive) types. Small-scale intrusive bodies like dikes and sills are generally not as relevant in the exploitation of natural building stones as mountain-forming large plutonic bodies.

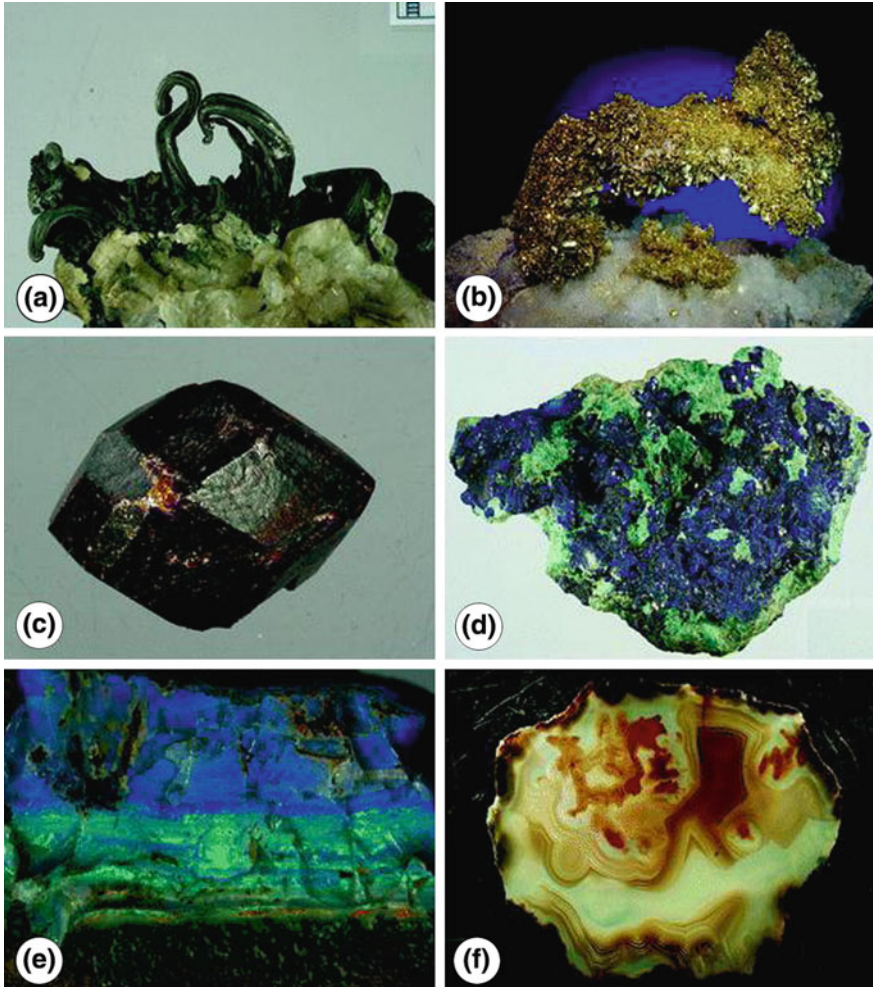
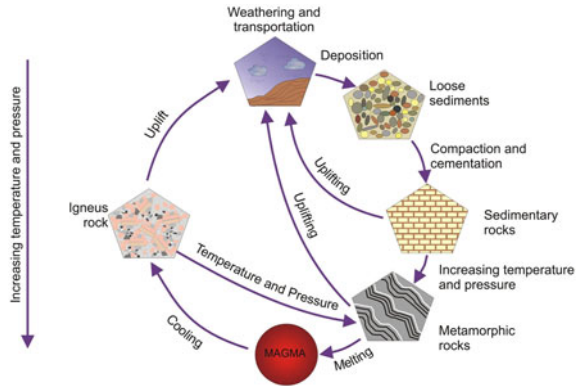


**Fig. 2.18** Precious minerals or gemstones of very high value: **a** Silver (Figure by Geowissenschaftliche Sammlung of GZG Göttingen), **b** Native gold (Figure by A. Massanek/Geowissenschaftliche Sammlungen of TU Freiberg), **c** Garnet (Figure by Geowissenschaftliche Sammlung of GZG Göttingen), **d** Malachite (Figure by Geowissenschaftliche Sammlung of GZG Göttingen), **e** Opal and **f** Agate (Figure by Geowissenschaftliche Sammlung of GZG Göttingen)

Sediments and sedimentary rocks are the product of mechanical and chemical fractionation processes on a large scale. In this case, mechanical weathering or the disintegration of the original rock into smaller fragments is often the prerequisite for a deep and intense chemical segregation. Alternatively, sedimentary rocks can be formed via chemical and biological processes and can be precipitated from water (marine or freshwater, see [Sect. 2.11](#)).

**Fig. 2.19** The geologic rock cycle describes the relationship of the various rock groups to each other and shows the possible pathways of the different rock types



Metamorphic rocks are formed from previously existing rock types under pressure and temperature. Metamorphism is a process whereby the mineralogical and/or structural and/or chemical composition of the rock changes under “solid state” conditions. These changes are caused by physical and/or chemical processes, which differ from weathering, cementation, and diagenesis of sedimentary rocks. Sedimentary, igneous, and even metamorphic rocks can be the source rocks which undergo metamorphism.

Different statistical calculations have been made showing the distribution of the major rock groups. In general, the major rock groups, in decreasing percentage, are: 65 % igneous, 27 % metamorphic, and 8 % sedimentary. These rock types form an interconnected geologic rock cycle (Fig. 2.19). The rocks do not last forever, and there is a cyclical development and transformation between the various rock types. The processes include the uplift of regions and exposure of igneous or metamorphic rocks, which then become prone to surface erosion and provide particles for sediments and sedimentary rocks. When sedimentary rocks are subjected to higher pressures and temperatures, they shift into the metamorphic realm, and mineral transformations begin. At greater depth, melting occurs, and both metamorphic and sedimentary rocks become parts of the magma system and the igneous province.

## 2.8 Rock Fabrics

In surface exposures, rocks show planar and linear structures (different types of foliation, bandings, bedding, lineations, etc.), which are often related to structures ranging from the microscopic to the macroscopic scale.

The anisotropy of rocks is produced by compositional differences as well as structural factors. In sediments, changing layers with different compositions are macroscopically easy to recognize and are generally defined as the bedding (e.g. Fig. 2.20a and b). Other important anisotropic elements are dictated by the

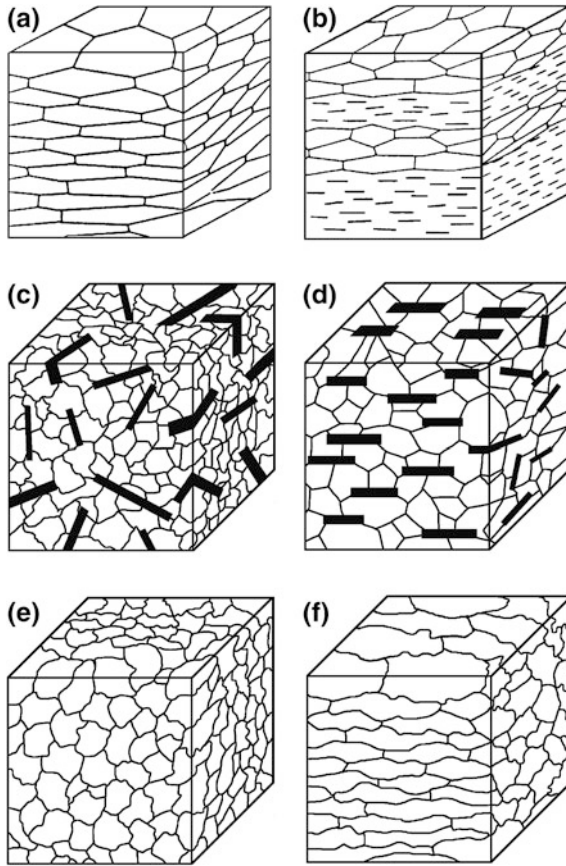


**Fig. 2.20** Schematic representation of various rock fabrics: **a** Planar layering caused by shape-preferred anisotropic minerals, **b** Material-structural fabric anisotropy created by shape-preferred anisotropic minerals connected with the intercalation of different layers, and **c** Polymineralic rocks (e.g. granites) without and **d** With an arrangement of shape-anisotropic minerals (e.g. mica); monomineralic rocks (e.g. marbles) **e** Without and **f** With a shape-preferred orientation. In contrast to the equi-dimensional grains in **(e)**, the grains in **(f)** are distinctly elongated in a cigar-like way (modified from Passchier and Trouw 1996)

microfabric and are only observable in part through microscopic or physical analyses. These include the preferred orientation of mineral grains or their grain boundaries (Fig. 2.20f), in contrast to statistical grain shape orientations (Fig. 2.20e), the arrangement of microcracks, or the crystallographic preferred orientation of mineral grains, known as LPO or texture. Crystallographic preferred orientations are especially important when the arranged crystals themselves show distinct properties of anisotropy. This is the case in many rock-forming minerals.

Borradaile et al. (1982) defined foliation, whether it is spaced or continuous (s-surface in Sander's terminology), based on morphological features such as



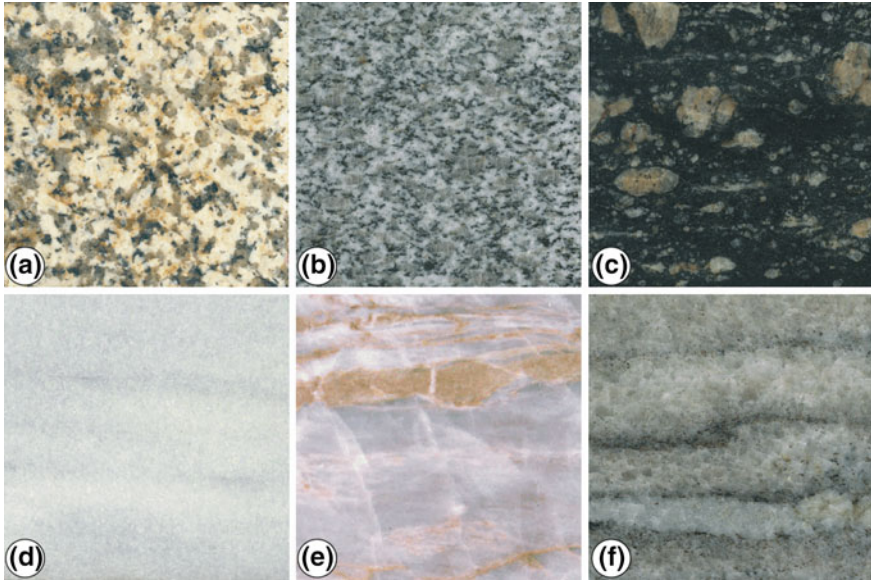


**Fig. 2.21** Macroscopic fabric of various rock types with different anisotropies: **a** Waldstein Granite, **b** Riesenferner Granite, **c** Benin Granite, **d** Laas Marble, **e** Kaufinger Marble, and **f** Grosskunuzendorf Marble (see explanation in text)

elongated or platy grains, compositional layers, or planar discontinuities (Fig. 2.20). A lineation is a homogeneously distributed linear structure (intersection lineation, crenulation lineation, stretching lineation, mineral lineation, groove casts in a bedding plane, etc.).

From the anisotropic elements mentioned above, the following material properties exhibit a distinct directional dependence, which is very important for the practical application of natural building stones. These include the tensile, compressive, and flexural strength, the abrasion strength, thermal properties, susceptibility to weathering, and many more (see Chap. 3).

The causes of anisotropic fabrics are complex rock-forming processes that occur over long geological time periods and are, in part, active in many cycles (Fig. 2.20). In general, this implies that the knowledge of geologic history allows certain predictions to be made in regards to the material behavior of natural building stones. The European standards EN 1341 (2006), EN 1342 (2009), and EN 1343 (2009) require the characterization of the mineral content and the fabric properties of tested natural building stone.

The generation of igneous rocks (formed from a melt) is dictated by the primary melt composition and by the prevailing geological conditions. Low viscosity melts often rise almost to the surface, where they crystallize out very quickly and where they form fine-grained and primarily and relatively weak anisotropic rocks, the most common example being basalt. Highly viscous melts, on the other hand,

remain at great crustal depths, where they can slowly crystallize out and, thus, form coarse-grained fabrics (the most common varieties are granite and similar rocks, see Fig. 2.21). Plutonic rocks show a strong tendency to develop primary anisotropic fabrics. These fabrics can originate when minerals crystallize out early and descend by “sedimentation” in the magma chamber, where cyclical processes can lead to compositional layering. During the deposition of the individual crystals, shaped-preferred orientations and textures can develop simultaneously. However, these granitic rocks often show a macroscopic isotropic fabric, but only by microscopic observation are the distinct anisotropies recognizable.

The erosion of older rocks supplies the materials for sediments (see Sect. 2.11). For almost all sediments, the significant and typical anisotropic element is the bedding (e.g. Fig. 2.20a and b), which develops during the deposition of the supplied material or through changing (and in part cyclical) depositional conditions. In clastic sediments, these changes can be in the types of minerals, grain sizes, and alternating water current velocities at the site of deposition. Another means of generating anisotropies in sediments can take place during diagenesis. In this process, the sediments undergo change with increasing pressure and temperature, which occurs during burial at great depth. Solidification of the sediments takes place essentially through mechanical compaction, dewatering, and mineralization in the pore spaces (cementation). Thus, deposits of sand change into sandstones and calcareous particles, and calcareous muds become limestones. The anisotropy strengthens during compaction, and mineral grains become elongated. Their long axes rotate perpendicularly to the direction of pressure, leading to a shape-preferred orientation. Furthermore, the solution/precipitation of materials can lead to a compositional dissociation, whereby the primary bedding becomes more accentuated and mechanically more significant.

Igneous and sedimentary rocks can be subjected to metamorphism by high pressure and/or temperatures (see Sect. 2.10). In this situation, minerals, some of which are no longer stable in these conditions, become transformed, and a recrystallization of stable minerals can also occur. Moreover, at high temperatures, many rock-forming minerals undergo plastic deformation very easily so that a directed pressure at great crustal depths causes an elongation of the shape, and, thus, a stronger, shape-preferred orientation/anisotropy occurs. Likewise, the newly formed minerals also grow in a preferred way perpendicularly to the main stress direction. Both shape-preferred processes result in an easily recognizable planar fabric (also known as schistosity), which is typical for the important and characteristic metamorphic rocks such as gneisses and mica schists. Through the complex interactions between the plastic deformation and recrystallization that develops during metamorphism, a further anisotropic element arises leading to crystallographic-preferred orientations in the rock-forming minerals.

Rocks that have passed through great depths in the course of their geological history and have essentially received their fabric structure during this period experience extreme stress release and cooling as a result of crustal uplift and the erosion of the overlying rock. This is especially true for plutonic and metamorphic rocks. Through elastic relaxation and thermal shrinkage, these rocks develop large

internal stresses, which, as a rule, lead to pronounced microcrack formation (Vollbrecht et al. 1991, 1993). These microcracks mostly occur in different generations, which show a distinct preferred orientation and, thus, represent a further anisotropic fabric element. When some of these microcracks coalesce, a macroscopic joint pattern often develops. In rock quarries, this jointing pattern is the deciding economic factor for the exploitation of raw blocks, which, for economic reasons, should not be below a certain minimum size (Mosch et al. 2010).

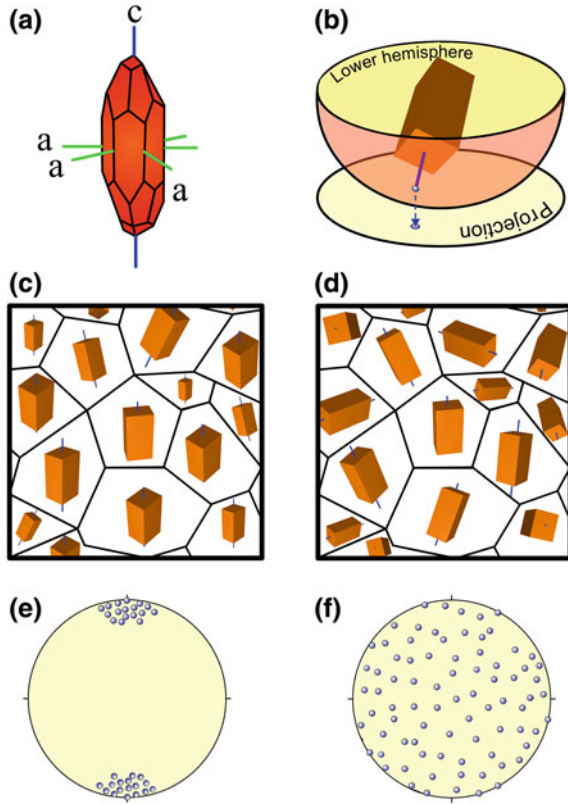
### ***2.8.1 Fabric Parameters***

In the following section, important fabric parameters for selected natural building stones in consideration of the anisotropic elements will be presented in order to demonstrate the possible influences on the rock's mechanical properties. Examples were chosen that mostly consist of monomineralic marbles as well as polymineralic granites and gneisses (see Fig. 2.21). Marbles often exhibit a completely different layering. In contrast, granites are usually characterized as grainy with no oriented fabric. Gneisses show a macroscopic planar fabric caused by metamorphism and deformation and exhibit a mineralogical composition similar to granites.

Different anisotropic rock fabrics can be observed both in granites and in marbles. Even though Waldstein Granite shows a rather isotropic macroscopic fabric, other granitoids display increasingly strong planar fabric anisotropies. This development is schematically illustrated in Fig. 2.20c and d on a cubic rock sample. The result is a distinctly planar (gneissic) fabric with stretched crystals that are oriented parallel to the foliation, which, in strongly deformed rocks, appears mylonitic. Both examples in Fig. 2.21b and c are results of a post-magmatic deformation. Similarly diverse fabrics are also observable in marbles, which gives this rock variety an architecturally interesting decor. The Laas marble (Fig. 2.21d) only shows an indistinct foliation in the form of a gray banding. This banding can be diffusely visible throughout the rock fabric as in, for example, some Carrara Marbles (e.g. Venato). In contrast, the marble in Fig. 2.21e and f shows a distinct compositional banding with changing interbeds of calcitic to dolomitic layers, as well as biotite layers. These recognizable macroscopic features already display distinct, existing fabric anisotropies.

Next to the compositional characteristics, the following section will focus on different fabric factors. Fabric elements are essentially defined as the orientation of grain shapes and the crystal lattice (Lattice Preferred Orientation (LPO)). Under natural conditions, the LPOs in rocks are generated by a directed growth or plastic deformation in which the preferred orientation of the crystal lattice is arranged according to the external main stress directions. As a result, textures are the summation of events of geologic history, which can exhibit locally dependent variations within the rock body (areas of homogenization). When the participating mineral phases show crystal lattice anisotropies, the directionally dependent

**Fig. 2.22** Diagram showing the crystallographic preferred orientation in rocks:  
**a** Representation of a calcite single crystal with corresponding c- and a-axes,  
**b** Schematic representation of the position of the calcite c-axis depicting a specific orientation in a Schmidt Net projection;  
**c** All minerals can have similar orientations or can **d** Exhibit statistical alignment of the crystal axes. Accordingly, the pole points of the crystallographic axes (only the c-axes are shown) lie in a strong texture **e** In a well-defined area or, through a missing texture, is **f** Statically distributed over the entire pole figure (Siegesmund et al. 2002a)



physical and mechanical properties of the rock are essentially determined by the LPOs (next to the preferred orientation). The representation of the rock textures can be depicted in different ways. In geologic fabric analysis, the preferred method for representing the poles to the planes of crystal lattices or crystal lattice axes is using true planar stereo projections (i.e. pole figures). Figure 2.22 schematically depicts a calcite crystal with the main crystallographic axes (c- and a-axes). When the crystal is projected in a stereo net (lower hemisphere), a pole point is generated on the projection plane, which shows its true orientation. The interpretation of the LPO data is usually done with respect to the sample coordinate system, which is defined by macroscopic fabric elements such as bedding, schistosity, foliation, and lineation. In this case, the XY-plane corresponds to the foliation (metamorphic layering), and the Z-direction is the foliation pole. Figure 2.22 shows a schematic representation of a grain mosaic. In the sketch, single crystal orientation is given for each grain. If the orientation of the c-axes in the calcite crystals has been crystallographically and optically measured, the corresponding orientation of the pole figures can be displayed. The texture in a rock can be statistically isotropic, which means the crystallites contain all possible orientations with the same

number, or the crystallites show a more or less similar orientation (Fig. 2.22c and d). In the example on the left, the calcite crystal has more or less the same orientation. Thus, all the c-axes scatter around a very small pole point cluster in the pole figure. The right example shows a strong variation in the orientation, and, naturally, all the measurements in the pole figure are widely scattered over the entire pole figure. In extreme cases, two types of textures can develop: one with a strong preferred-lattice orientation and one that is completely random (Fig. 2.22). This can result in material behaviors wherein the physical and mechanical properties (e.g. Sect. 3.6) can be either isotropic or highly anisotropic.

### ***2.8.2 Shape-Preferred Orientations***

Shape-preferred orientations describe the anisotropic spatial distribution of the long and short axes of shape-anisotropic crystals (see Fig. 2.20a–f). This can be due to different geological processes: sedimentation of anisometric grains, directed longitudinal growth, and deformation. When the shape anisotropy and lattice anisotropy of crystallites are superimposed, a distinct rock fabric will result. In monomineralic polycrystals, the crystal boundaries designate the grain boundaries and are defined by the degree of lattice misorientation in the neighboring crystals. Large misorientations cause relatively high grain-boundary porosities due to the greater width of the dislocation zone. The significance of shape-preferred orientations for material behavior is, first and foremost, that the crystal boundaries represent mechanical and structural discontinuities (compare Fig. 2.20a, e, and f), which delineate the preferred directions of fracture patterns and interconnected networks for material transport (directionally-dependent permeabilities). In dense crystalline rocks, they represent a substantial part of the effective porosity.

### ***2.8.3 Fracture Fabrics***

In the different rock types discussed here, microcracks are a frequently occurring fabric element. They occur either along the grain boundaries (intergranular) or within the mineral grains (intragranular). With increasing density, these types of cracks can form complex networks. With continuous crack growth, macroscopic fractures can also form via the coalescence of these microcracks. Since their formation is due to directed stresses within the Earth's crust, microcracks always show a preferred orientation based on statistical measurements and are a major contributor to the anisotropy in a rock. Microcracks that formed early in the geological process and evolution of the rock often become closed by a later mineralization. Mineralized cracks can be differentiated into “healed” microcracks (filled with the same material as the host grain) or “sealed” microcracks (filled with a foreign material). As a rule, the youngest crack generations are

usually open, which makes them especially important for material behavior (Vollbrecht et al. 1993). They are a major contributor to the porosity and permeability in very dense crystalline rocks (plutonic and metamorphic rocks) and, because of their parallel orientation, often cause anisotropic fracture behavior (see Chap. 3).

In the following section, two rock types, the Waldstein Granite and Wunsiedel Marble, will be used as detailed examples to illustrate the observed rock fabrics.

The Waldstein Granite is yellow in color and shows large feldspar porphyroblasts up to 30 mm in size within a medium to coarse-grained matrix. Compositionally, the mineralogy of the rock consists of 37.5 % quartz, 29.7 % K-feldspar, 21.6 % plagioclase, 6.6 % biotite, 4.5 % muscovite, and accessories comprised of zircon, chlorite, cordierite, apatite, tourmaline, and opaque minerals. These granites were not deformed nor underwent gneissification in the mountain building processes and, thus, still exhibit their primary macroscopic and more or less isotropic fabric. Even the anisotropic processes of a developing preferred orientation, such as those mentioned above, did not occur during the early fractionation of crystals from the magma chamber. However, during the exhumation of the granite, a structural overprinting occurred that is observable in the quarry and represented by the jointing system and faults (Fig. 2.23a). Correspondingly, many microcrack generations can be observed in thin sections as additional anisotropic elements that clearly show a preferred orientation. In general, the macroscopic joints and microcracks in the Waldstein Granite exhibit the same orientation (compare Fig. 2.23a and b), whereby two systems dominate: (1) steep joint surfaces dipping northwest to southeast and (2) horizontal surfaces represented by the maxima in the center of the diagram. In both systems different crack types can be discerned at the microstructural level (Fig. 2.23c–f). For the anisotropy of the rock's mechanical properties, the open cracks shown in Fig. 2.23f are especially significant, because they exhibit a greater dilation and, thus, cut various types of minerals. The Waldstein Granite is a good example of the more or less often described isotropic character of a granite (its grains lacking any distinct orientation), but, as a result of the microcrack fabric, it does show a material behavior of anisotropy. In many cases, the macroscopic joints can give an indication of the orientation of the microcracks. However, some granitic rocks are known in which there is no strong directional relationship between microcracks and joints.

The Wunsiedel Marble shows a distinct banding macroscopically, which is defined by a gray and white fine-, medium-, and coarse-grained layering. Occasionally, local interbeds of thin, dark, graphite-rich layers are observable. Two planar fabric elements or foliation (Fig. 2.24) can be differentiated: (1) The bedding (ss) is recognizable by a change in the grain size and the graphite interbeds, as well as small, quartz grains arranged in layers and (2) a penetrative schistosity that can be discerned by the shape-preferred orientation of calcite crystals. An example of observed shape anisotropies is shown in Fig. 2.24. The Wunsiedler Marble exhibits, in all sections, a more or less strong arrangement of the shape anisotropic grains. Thin section images parallel to the three surfaces of a sample cube show different grain shapes under closer examination. In the upper corners of each



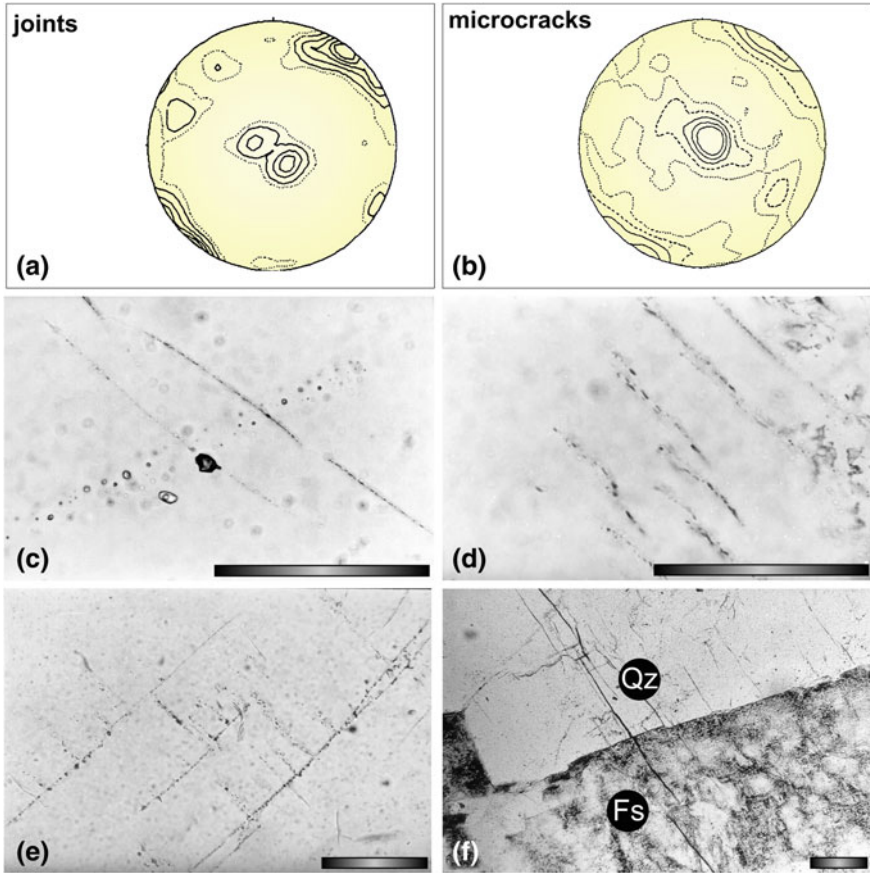


**Fig. 2.23** Fabric anisotropies in granite: **a** Pole diagram of the joints in a quarry and **b** The microcrack orientation in the Waldstein Granite; **c** Healed cracks in quartz defined by fluid inclusions. In areas where younger cracks penetrate the healed ones, the fluid inclusions are empty (see *dark bubble* in the middle of the image); **d** Healed microcracks swarm with the same orientation; **e** Orthogonal crack pattern, where the older generation (*long diagonal cracks*) can be differentiated from the younger generation (*short cracks* perpendicular to the older ones); **f** Opened microcracks in quartz (Qz) grains which migrate into the feldspar (Fs) grains (*intergranular-transgranular cracks*). The scale in all thin section images is 0.1 mm (e.g. Vollbrecht et al. 1991; Siegesmund et al. 2002a)

image, a number of grains have been sketched, with a representative grain shown in color. Essentially, these are arranged as non-equidimensional grains, which can be described as triaxial, “cigar-like” ellipsoids. The larger calcite grains show twinning and are usually surrounded by small recrystallized, untwinned grains. The long axes of the grains do not necessarily dip in a similar direction to the macroscopically visible foliation. When marbles lose strength as a result of weathering along the grain boundaries, which is usually the case, the directional



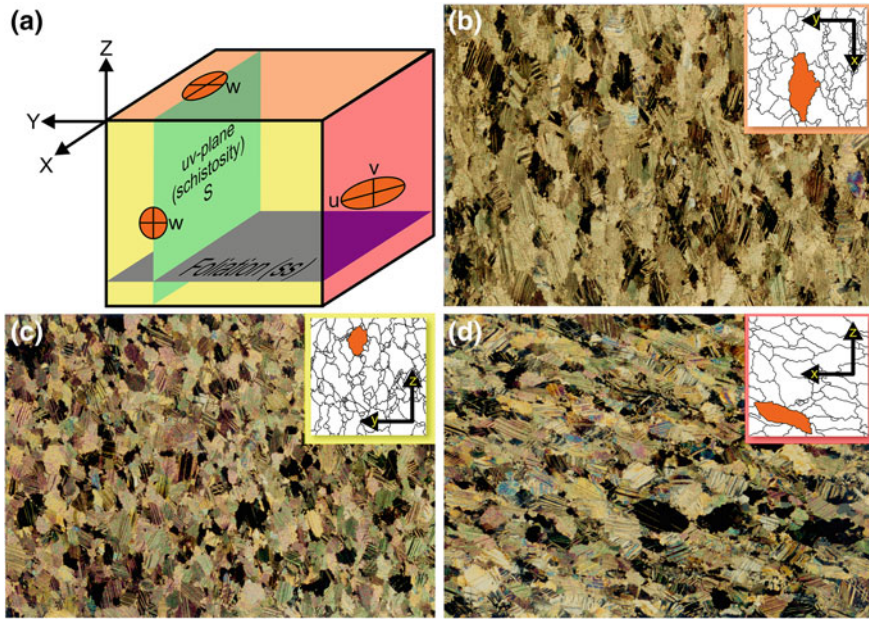
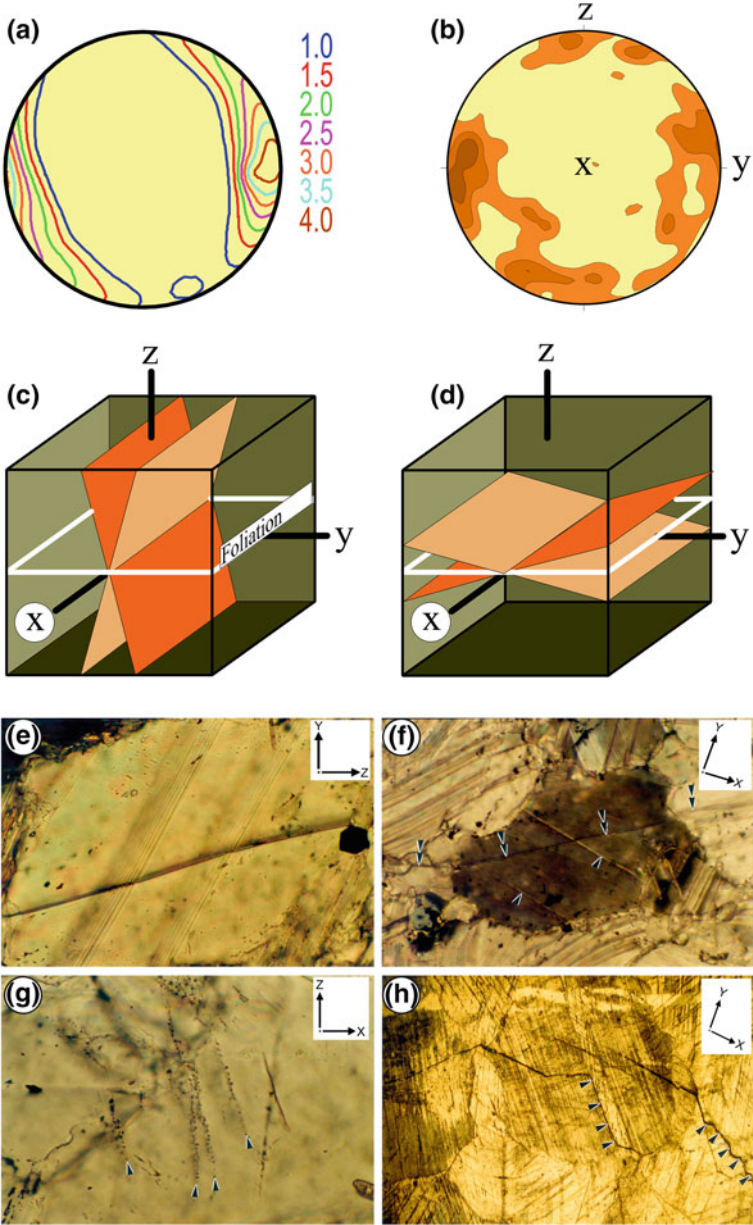


**Fig. 2.24** Shape-preferred orientation in the Wunsiedel Marble: **a** Schematic representation of the grain fabric and its arrangement into subordinate structural characteristics of foliation (ss) and schistosity (s). The total fabric alignment results from the preferred orientation of non-equidimensional grains, which can be described by the triaxial ellipsoids  $u > v > w$  (cigar-like grains). The  $u$  and  $v$  axes stretch the schistosity planes. **b–d** Thin section images of the grain fabric in different sections (photo length = 4 mm). The respective section is specified in the images (**b–d**) in the upper right hand corner of the image, together with a schematic representation of the typical grain shape (Siegesmund et al. 2002a)

relationships have a direct influence on the mechanical rock behavior. In surface exposures, rocks show planar and linear structures (different types of foliation, bandings, bedding, lination, etc.), which are often related to structures ranging from the microscopic to the macroscopic scale (Fig. 2.25).

## 2.9 Igneous Rocks

Igneous rocks are formed by the cooling and solidification of magma, which is a hot, silicate-rich melt containing various compounds and elements. Magma is generated by the partial melting of the Earth's crust or mantle. Based on experimental investigations by Bowen (1928), a characteristic differentiation of minerals with differing composition can be crystallized from a  $\text{SiO}_2$ -poor melt under slow cooling. This differentiation is known as Bowen's Reaction Series and is shown in Fig. 2.26. First, the Si-depleted basic fraction crystallizes from this melt as gabbro.



◀ **Fig. 2.25** Texture and microcracks in the Wunsiedel Marble: **a** Crystallographic preferred orientation of the c-axes with a distinct maximum parallel the Y-direction of the coordinate system; **b** Diagram of all microcracks in the Wunsiedel Marble; **c, d** Schematic representation of two orthogonal microcrack systems, which can be seen in (**b**); (**e–h**) Thin section images of different microcracks in the Wunsiedel Marble; **e** Open intragranular crack (image width = 0.25 mm); **f** An open transgranular crack and an intragranular crack. The directional change of the transgranular crack cutting the grain boundaries is probably due to crystallographic control of the crack orientation (image width = 0.4 mm); **g** Small healed cracks depicted by planes of secondary fluid inclusions (image width = 0.25 mm); **h** Transgranular-intergranular cracks and intergranular segments along the grain boundaries are marked by arrows. Dark coloration due to Fe-oxide staining (image width = 0.4 mm) (Siegesmund et al. 2002a)

Characteristic minerals are olivine, followed by pyroxene, amphibole, and biotite. The crystallization series influences the compositional changes. They determine which components are extracted from the melt. The feldspars that crystallize are the plagioclases that form a continuous solid solution series. First in the series is anorthite (a Ca-rich plagioclase), which crystallizes out in basalts. With continuous differentiation, the plagioclases become more Na-rich. The dark magnesium-iron silicates form a discontinuous reaction series. Continued fractionation in the remaining melt causes a decrease in the amount of Mg, Fe, and Ca, whereas Si, Na, and K increase. According to the model, crystallization ends with the formation of granite that is rich in Si, which means the granitic rock is acidic. Even though Bowen's Reaction Series only describes the fractionation series in an incomplete way, the model does deliver an easy means for understanding the differentiation of important minerals and rocks generated from a melt.

The classification and nomenclature of igneous rocks is typically established by considering the mineralogical and/or geochemical aspects, whereby the modal and normative mineral constituents play an important role. The internationally applied nomenclature for igneous rocks is based on quantitative modal analysis (mineralogical composition). It is used to name a rock with regards to the amount and relationship of the main mineral constituents. This name is further complemented by the secondary minerals (e.g. olivine in an olivine nephelinite or quartz in a quartz-bearing trachyte). The quantitative mineral content is given in volume-percent. According to the proposals of the International Union of Geological Sciences, Subcommittee on the Systematics of Igneous Rocks (Streckeisen 1978, 1980; Le Maitre 1989), the classification follows what is usually known as the Streckeisen Diagram (QAPF double triangle) (Fig. 2.27). The modal composition of volcanic rocks with a micro to crypto-crystalline or glassy or glass-bearing fabric is essentially impossible to determine. In this situation, the chemical composition of the rock is used to calculate the so-called normative minerals, which then helps to determine the normative mineral constituents. Using the normative mineral components, a classification system can be created that is based on the Streckeisen diagram. However, mineralogical compositions based solely on chemical analyses cannot lead to the actual minerals present. For example, the CIPW classification system (Cross et al. 1902) is based on chemical analyses. Along with the chemical composition, rocks are further subdivided into specific

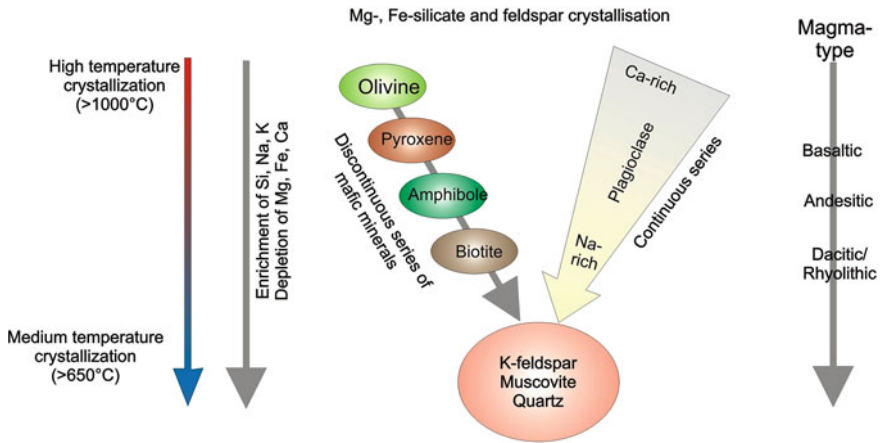
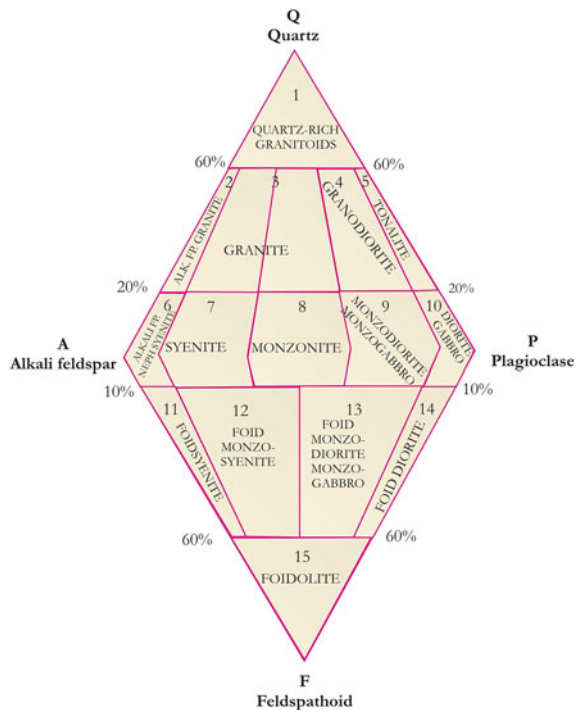


**Fig. 2.26** Bowen’s discontinuous and continuous reaction series for explaining the differentiation of magma and mineral phases that are crystallized from magma at decreasing temperatures

**Fig. 2.27** Simplified classification of the most common plutonic igneous rocks based on the mineralogical content (Streckeisen 1978)



rock types by being based on the SiO<sub>2</sub> content: acid rocks >63 % SiO<sub>2</sub>, intermediate rocks 52–63 % SiO<sub>2</sub>, basic rocks 45–52 % SiO<sub>2</sub>, and ultrabasic rocks <45 % SiO<sub>2</sub>.

Igneous rocks are classified according to the following minerals and mineral groups:

- Q = quartz (and the  $\text{SiO}_2$  varieties tridymite and cristobalite), A = alkali-feldspars (orthoclase, microcline, sanidine, anorthoclase, albite with an anorthite content of  $<5$  mol %),
- P = plagioclase with an anorthite content from  $\text{An}_{05}$  to  $\text{An}_{100}$ ,
- F = feldspar substitutes or feldspathoids (leucite, nepheline, the sodalite group, nosean, hauyne, analcime).

A color index ( $M$ ) is often used for defining plutonic and volcanic rocks. This indicates the percentage of dark minerals (mafic): hololeucocratic plutonic rocks contain 0–10 % mafics, leucocratic (light) plutonics 0–35 %, mesocratic rocks 35–65 %, melanocratic (dark) rocks 65–90 %, and mafic rocks 90–100 %. Mica, amphibole, pyroxene, olivine, garnet, etc. belong to the mafic minerals.

Rocks with an  $M < 90$  vol % are classified according to the amount of light minerals present and are represented in a  $Q-A-P-F$  double triangle (see Fig. 2.27). The procedure is as follows: The parts of light minerals are converted into 100, which means either  $Q + A + P = 100$  or  $A + P = 100$ .

As a rule, the darker constituents are systematically left out of consideration and are used for a rough orientation or for further nomenclature subdivision into specific rock groups.

From the natural stone industry's point of view, a modified Streckeisen diagram may be sufficient. Not only does the diagram depict the correct mineralogical composition, but it also shows the properties of the rock and how they can be applied, which is of the utmost importance. According to the European norm, e.g. the EN 12440 (2000) "Natural Stones: Criteria for the Designation", the description of the natural stone should contain the trade name, the petrographic classification, the typical color, and the location, as well as the type of surface treatment, the natural properties, the petrographic name, and, if necessary, the geologic age of the stone's origin. Thus, in the future, irritation caused by giving the stone fantasy names can be avoided (see Sect. 2.4).

### 2.9.1 Plutonic Igneous Rocks

In the following section, only the most important rocks will be described. According to Wedepohl (1969), the volume relationships of plutonic rocks in the lithosphere can be differentiated as follows: granite and quartz monzonite (44 vol %), granodiorite (34 vol %), diorite and quartz diorite (9 vol %), and peridotite, syenite, and alkaline anorthosite rocks (around 0.5 vol %).

Granites as well as granodiorites are the most commonly used plutonic rocks for building with regard to color, décor, and the wide range of different compositional varieties. The attempt to classify granites according to type, group, and family served the purpose of elucidating the specific conditions of formation and



defining the genetic principles. In the Archean, a very early period in the Earth's history, Na-bearing granites with a tonalitic and trondhjemitic composition occur, whereas, in the Proterozoic Ca-rich, granites are predominant (Kay and Mahlburg Kay 1986). Besides forming from fractionated crystallization (Bowen 1928, see Fig. 2.26), the formation of granites is also possible in the melting of water-saturated metasediments through a process called anatexis (Winkler and von Platen 1961a, b). Today, granites are differentiated into S-type and I-type granites.

S-granites originate from metamorphosed sedimentary rocks, and I-granites form the original rocks of metamorphosed igneous rocks. S-granites are essentially SiO<sub>2</sub>-rich and are felsic rocks consisting of the characteristic paragenesis of biotite ± muscovite ± cordierite ± garnet ± ilmenite. I-type granites contain hornblende ± biotite ± sphene ± magnetite. Even xenoliths (foreign inclusions) are different in both types. In addition, M- and A-type granitoids can be differentiated. A-type granitoids provide most of the dimensional stones (Fig. 2.28).

Granitoid intrusions are often formed in a structurally complex way. The Ardara Pluton in Ireland, which is an example of the ballooning model of emplacement, is a three-phase, normally-zoned pluton (Hutton and Siegesmund 2001). The outer and earliest zone is a feldspar-porphyrific tonalite/quartz diorite, an equi-granular granodiorite forms the intermediate position and age, and the youngest and central position is granodiorite. The fabric of granitic rocks is usually considered to be random and granular. This is the typical criteria used for granites discussed in the literature. Some authors, however, dismiss the observation above by proving that these rocks do show fabric anisotropy. Most of the intrusive rocks may exhibit a macroscopic planar and/or linear fabric by the arrangement of tabular shaped crystals (e.g. biotite and plagioclase). When granites exhibit a fabric with large crystals (phenocrysts) in a relatively fine-grained groundmass, the rock is considered to be porphyritic. Based on microstructural observations, a genetic interpretation may be done. Thus, former flow structures generated during the emplacement of the magma can be verified by the alignment of alkali feldspars. These crystallize out from the magma relatively early and form idiomorphic crystals that are oriented parallel to the direction of magma flow. Fabrics can form during the cooling, whereby the interstitials within the mineral framework are filled with quartz that shows a chessboard pattern, indicating temperatures above the  $\alpha$ - $\beta$  transition. This transition temperature ( $\sim 573$  °C) is used in surface treatment when producing flamed rock surfaces. The absolute size of the individual crystals and their arrangement with each other determines the appearance of the granite. The different grain sizes of granite (e.g. fine, medium, or coarse-grained fabrics) are connected to the cooling period of a granitic melt. Other observations assume that fluid phases lead to an increase in crystal nucleation, which, in turn, is responsible for the large grain size growth.

Optical properties are primarily determined by the feldspars. The quantitative distribution and characterization of the mineral components (see Fig. 2.27) can help in the identification of the various granites. Granites with a constituent fraction of 40–60 % alkali feldspars can range from being coarse-grained to being fabrics with extreme grain sizes. They are mostly vibrant red to reddish or pink,

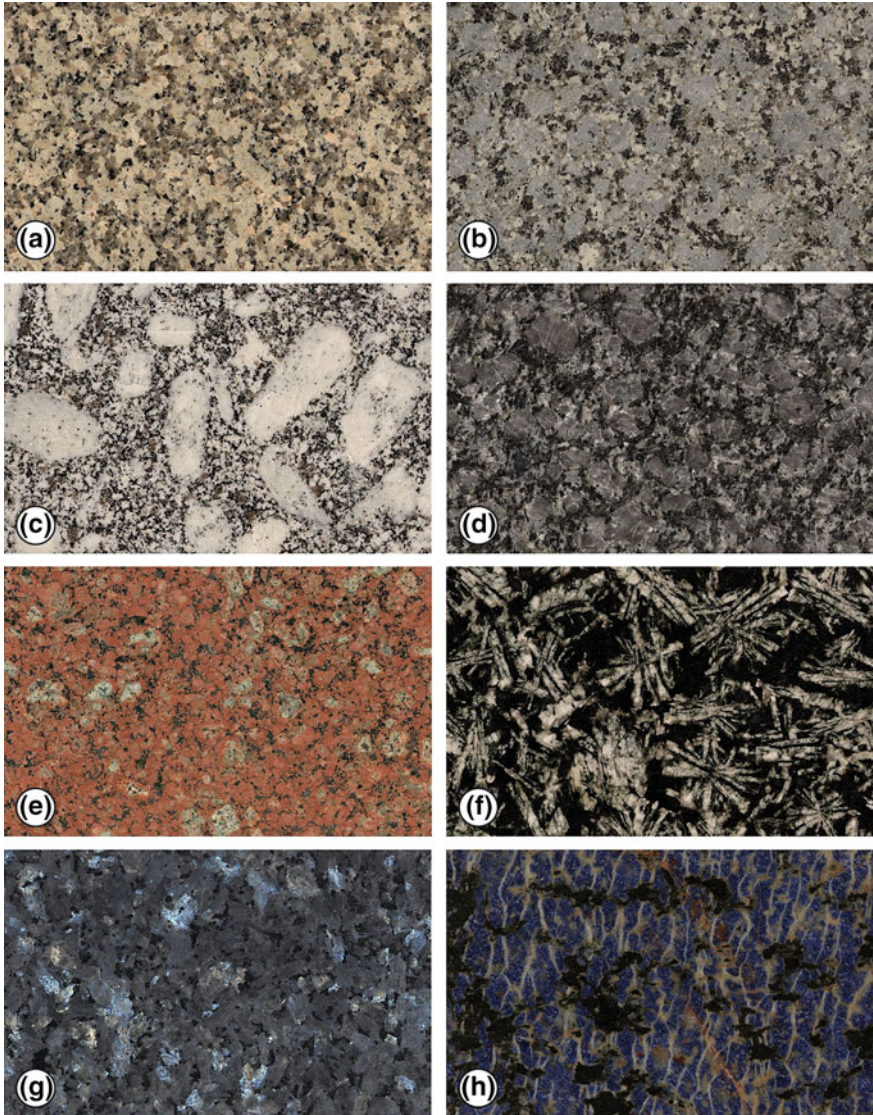


**Fig. 2.28** Commonly used plutonic igneous rocks: **a** Waldstein Granite, **b** Kösseine Granite, **c** Wöllsau Porphyritic Granite, **d** Baltic Blue Monzonite, **e** Salmon Red Syenite, **f** Snowflake Gabbro, **g** Blue Pearl Larvikite, and **h** Namibian Blue Sodalite (Figure by Natursteinarchiv Wunsiedel)

and are seldom bluish, greenish, or gray (Figs. 2.28 and 2.29). When the granites consist of 0–30 % plagioclase, they are either light or white–gray and only seldom show distinct colors. Granites with 20–40 % quartz often show a greasy luster, are mostly colorless to transparent, are seldom gray, blue-gray, or pink, and are



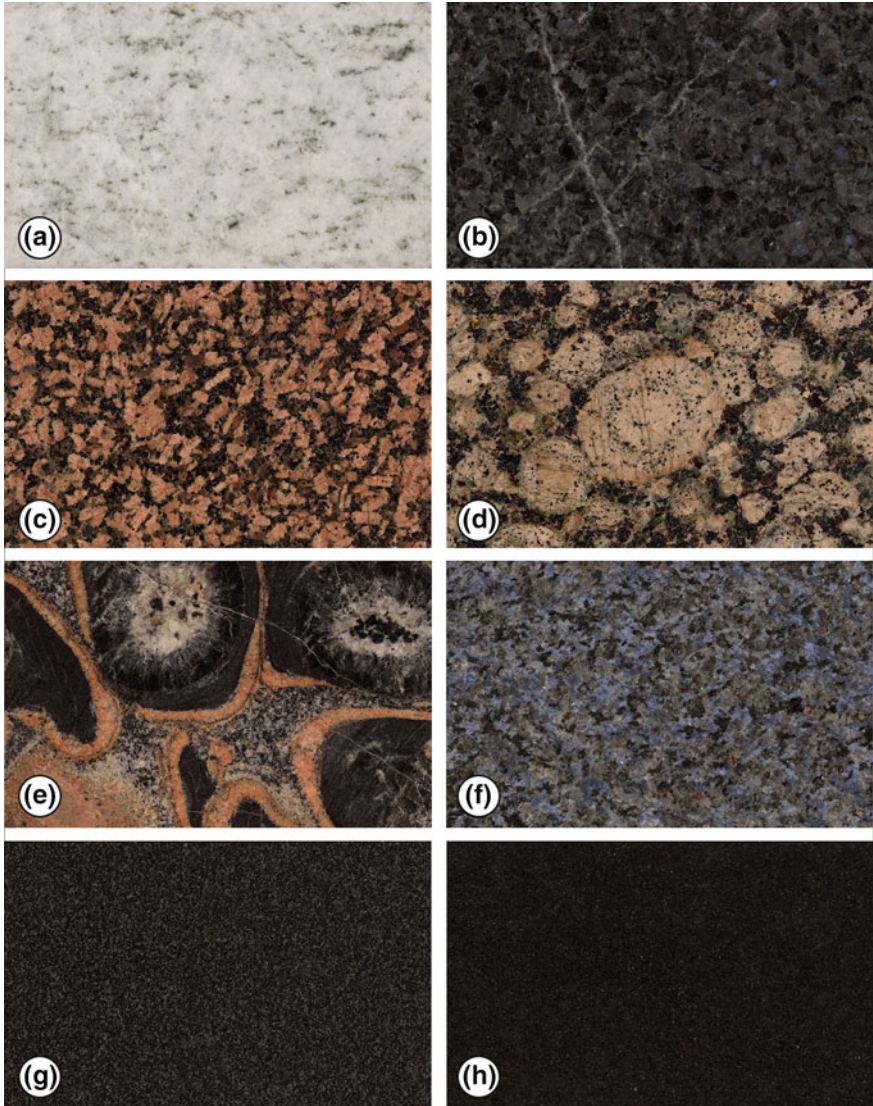


**Fig. 2.29** Commonly used plutonic igneous rocks: **a** Gudvangen Anorthosite, **b** Russlabrador Anorthosite, **c** Balmoral (granite, Finland), **d** Balticosa Rapakivi Granite, **e** Orbicular Granodiorite, **f** Malawi Blue (foyaite), **g** Negro Oriental Dolerite (Uruguay), and **h** Negro Absoluto Black Dolerite (Uruguay) (Figure by Natursteinarchiv Wunsiedel)

irregular on fractured surfaces. Higher amounts of mafic constituents that form interspersed black flakes, like biotite, for example, can impart a darker contrast to lighter colored granites. Both hornblendes and pyroxenes can be present in granites in subordinate amounts. In unweathered rocks, feldspars are more or less

colorful. Orthoclases are often pigmented predominantly by ferrous compounds (hematite), where the color ranges from a subtle to strong pink. Other granites can exhibit conspicuous yellow shading. This rock color results from alteration processes (weathering) in the deposit, which originate during the geological development of the rock. The alteration processes cause the oxidation of the rock-forming minerals like biotite or even ore minerals, e.g. iron hydroxides or pyrite. The greater the alteration, the more intense the yellow shading. Logically, the most intense yellow coloration can be found at the near-surface areas of the deposit. In the core area of the pluton, feldspars show pink coloration, which results from hematite inclusions. Plagioclases appear whitish dull to pale green. The intense white tones are caused by gas and fluid inclusions within the crystal lattice. Even quartz does not always appear colorless or transparent, but can be cloudy or occasionally show a reddish pigmentation. The color of quartz can even adopt different shades of blue. This occurs when the granite has undergone deformation, when it shows an enrichment of fluid inclusions, or when rutile (a titanium mineral) is incorporated into the quartz structure.

Syenite and monzonite are quartz-free to quartz-poor, feldspar-rich, medium to coarse-grained, deep-seated plutonic rocks. They are similar to granites in terms of structure and appearance. When orthoclase dominates the rock composition, the rocks are called syenites, and, if orthoclase and plagioclase are both present in similar amounts or only plagioclase prevails, then the rock is known as a monzonite (Fig. 2.28d, e). Syenitic-monzonitic rocks are generally reddish to red-brown because of the high potash feldspar contents. They are seldom bluish-violet or white, and never dark gray or black. The syenites shown in Fig. 2.28 are gray to pink colored and very coarse-grained. Perthitic orthoclase up to 4 cm, interstitial amphibole, pyroxene, and biotite are the main minerals. Accessory minerals include apatite and zircon. Alkali feldspar exhibits a wide palette of colors in the different intrusions (gray, deep red, brownish red, etc.). In Uruguay (Oyhantcabal et al. 2007), for example, the commercial varieties cover a broad range: Guazubirá (medium-grained and reddish pink), Artigas (coarse-grained, various shades of gray and pink colors), Bodega (medium-grained and deep red), Sara Pink (fine-grained and pink), etc. These rocks have been widely used in the cities of Buenos Aires and Montevideo and in Japan over the last several decades.

The rocks of the diorite-tonalite-trondhjemite group are characterized by the lack of reddish orthoclase, whereas the prevalent mineral is the whitish-gray plagioclase feldspar. Diorite contains plagioclase, hornblende, and biotite as the main mineral constituents. Quartz occurs with less than 5 %. Diorites never appear colored because of this mineralogical composition, but instead are dark green, black-gray, or mottled black and white. Tonalites are diorites that contain over 20 % quartz and, thus, were once designated as quartz diorites. A sub-group of the tonalites is the trondhjemites. They only contain a very small amount of dark colored silicates and appear as light-colored rock. Three types from Norway are processed and used in the natural stone industry.

Gabbros occupy the same field as diorites in the Streckeisen diagram. In gabbros, plagioclase has an anorthite content of over 50 mol percent. This makes it

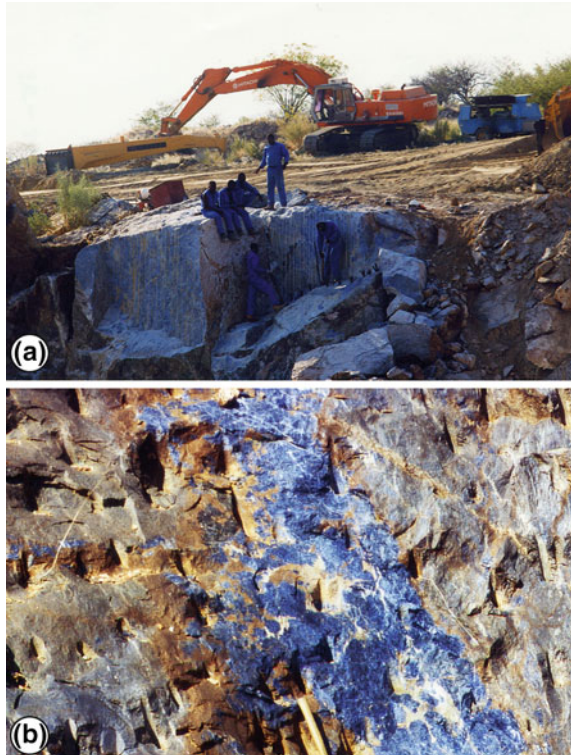
difficult to distinguish the rock from diorite in hand specimens, and mistakes in determinations are absolutely possible. Gabbros are the most frequent plutonic rocks originating from the dark basic magma type. They consist of 50–70 % plagioclase with a black-gray, dark brown, or gray-white coloration, 20–50 % pyroxene colored gray, deep black, or dark green, 0–20 % hornblende showing green to black colors, 0–20 % olivine with a dark green coloration, and 0–15 % ore minerals showing dark bright metallic coloring. From this mineralogical composition, a dark to totally black rock that has a fine to coarse-grained fabric results. Depending on the grain size, the appearance can vary from mottled to a uniform deep black color (Fig. 2.29). For gabbroic rocks, there are complementary composition diagrams which differentiate between plagioclase, pyroxene, and olivine contents, respectively, and plagioclase-olivine-clinopyroxene gabbros, olivine gabbros, gabbro norites, norite anorthosites, etc. These rock groups play a major role in modern architecture, especially because the color and décor offers many design possibilities. Gabbro rocks are designated norites where orthopyroxenes predominate over clinopyroxenes. Almost no difference to normal gabbros exists with regards to the technical and optical properties. Anorthosites are feldspar-rich gabbros where the pyroxenes show a quantitative reduction (Fig. 2.29). Zoned labradorite feldspars forming a mostly coarse crystalline fabric often show spectacular light reflections. The rock fabric also shows an intense blue shimmer. Depending on the viewing direction (incident angle = reflection angle), all the spectral colors can be observed. Its optical appeal has helped to increase the demand for anorthosites (Spectrolite, Blue Eyes, Volga Blue, or Arctic Blue), which are enormously used by building owners and architects.

Feldspathoids form a rare group of plutonic rocks and are known as the feldspathoid rocks or foyaites. They are generally medium to coarse-grained and occur in small rock bodies and veins. Silica poor melts are where they originate, which is why no quartz forms, and only little to no feldspar develops. Instead of feldspar, the so-called foid, which are feldspar substitutes, develop. This is why one refers to feldspathoid rocks as foyaites. Typical feldspar substitutes are nepheline (gray to green), sodalite (blue), leucite (white), and nosean (brown). Feldspathoid rocks have pleasing optical properties (Fig. 2.30).

### ***2.9.2 Volcanic and Subvolcanic Igneous Rocks***

Volcanic rocks not only include the extrusive lava flows but also the volcanoclastics (tuffs). Many volcanic rocks are difficult or inadequately determined macroscopically, because the mineral constituents are generally very fine-grained, whereas they can be clearly distinguished from plutonic rocks. A simplified representation in the TAS diagram (Total-Alkali-Silica) after Le Maitre (1989) is based on the work of Cox et al. (1979). This classification should only be used if the mineral mode of a fine-grained crystalline rock cannot be determined, either due to the presence of glass or to the fine-grained nature of the rock. The classification only requires the

**Fig. 2.30** Photographs of **a** Sodalite opencasting (*Namibia Blue*), which is the only opencasting that is presently mined, and **b** Monomineralic layer or sodalite-rich xenoliths of deep blue sodalite (from Drüppel 2003)



values of  $\text{Na}_2\text{O} + \text{K}_2\text{O}$  and  $\text{SiO}_2$  (Fig. 2.31). Volcanic rocks have a close relationship with their plutonic counterparts, and surface morphology often reflects the origin (Fig. 2.32).

Nearly every plutonic rock can be related to an equivalent effusive rock. The nomenclature can be referenced from the Streckeisen diagram (see Fig. 2.31). Rhyolites (earlier known as porphyry or quartz porphyry) are the volcanic equivalent of granites. When an acid  $\text{SiO}_2$ -rich magma solidifies in the lower crust, granite forms, and, as the lava reaches the Earth's surface, rhyolite develops. Rhyolites are yellowish, reddish, grayish, seldom gray-green, dense, and porous rocks in the upper parts of the flows (Fig. 2.33). The fabric is porphyritic, which means it has a fine-grained groundmass with phenocrysts. In Fig. 2.34, the use of Löbejün Rhyolite is exemplarily illustrated. The rock is characterized by a fine crystalline groundmass (ca. 66 %), where the microgranitic fabric can be recognized with the unaided eye, and phenocrysts up to 30 mm occur. Mineralogically, the rock consists of quartz (27 %), orthoclase (40 %), plagioclase (27 %), and biotite (6 %, Fig. 2.31). Accessories causing the coloration in the groundmass are hematite and magnetite. The groundmass of the rock has a characteristic and distinctive red to coral-red color. Within the groundmass, salmon pink orthoclase, yellow-green plagioclase, and pearl-like quartz occur. Biotite is not observable



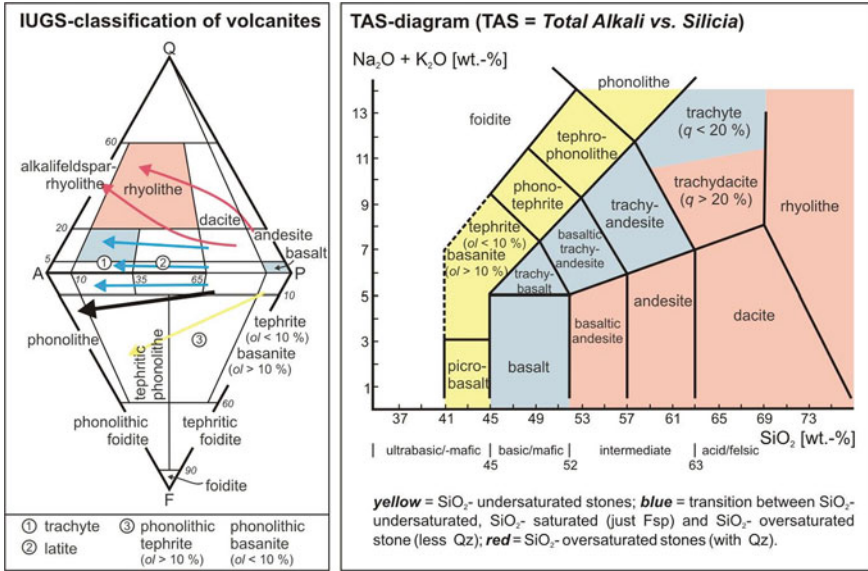


Fig. 2.31 Classification of volcanic igneous rocks according to the IUGS and TAS diagrams (based on Le Maitre et al. 2004)

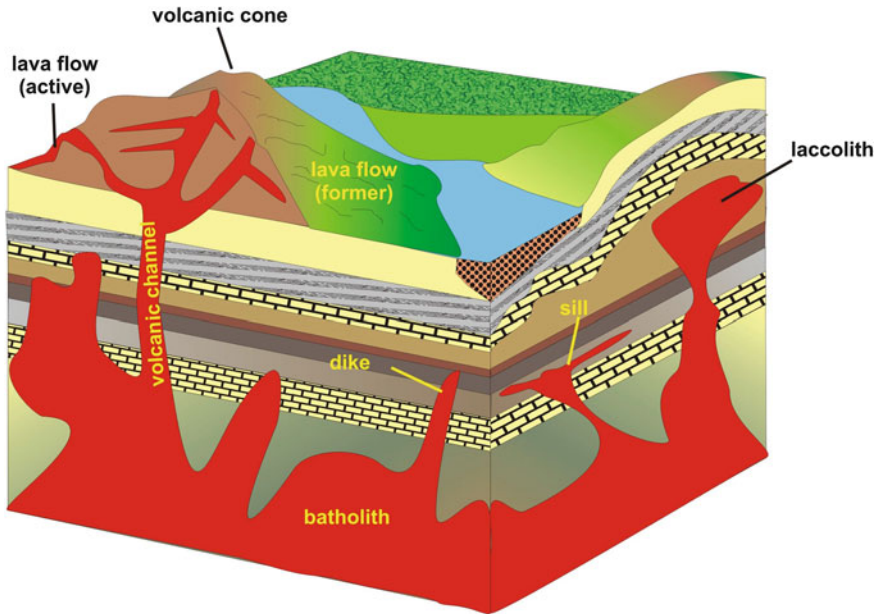
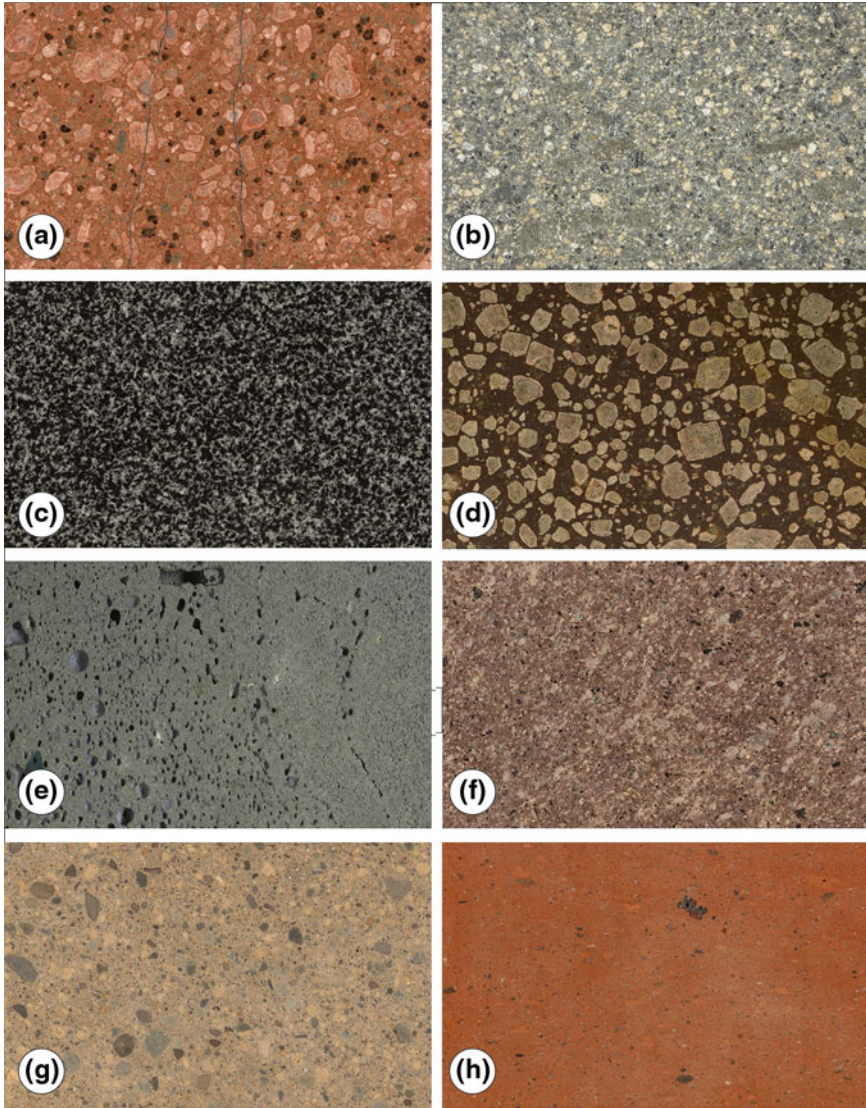


Fig. 2.32 Field occurrences of igneous rocks



**Fig. 2.33** Commonly used volcanic igneous rocks: **a** Löbejün Rhyolite, **b** Porfido Argentino Ryholite, **c** Valtengrund Lamprophyre, **d** Trachyte, **e** Lohndorfer Basaltic Tuff, **f** Ettringen Tuff, **g** Scherwesch Andesitic Tuff, and **h** Dobraniva Andesitic Tuff (Figure by Natursteinarchiv Wunsiedel)

macroscopically. The groundmass as well as the phenocrysts only show a weak alignment, which indicates the rock essentially possesses an almost isotropic fabric property. Frequently, rhyolites show a slight directional orientation, which is represented by the solidified flow movement of the lava. The largest surface

**Fig. 2.34** Dresdner Bank in Halle (Germany) clad with the Löbejün Rhyolite (SH Naturstein, Löbejün in Germany)



exposure of rhyolite deposits in Central Europe is the Bozener Quartz Porphyry in Tyrol, Italy.

Trachytes are the volcanic equivalents of syenites. The chemical composition is intermediate to acidic. According to the Streckeisen diagram (1978, Fig. 2.31), trachytes occupy field 6 (quartz-alkali feldspar trachyte) and field 7 (quartz trachyte and trachyte in the strict sense). These rocks essentially contain little or no quartz. Trachytes frequently contain pyroxene and/or amphibole and sometimes biotite, which can be identified as mostly small, dark phenocrysts. The light phenocrysts in trachytes are predominantly sanidine. Phenocrysts can show a preferred orientation in the matrix and traces a flow fabric, which indicates the former flow direction of the magma. A famous example of where a trachyte (the Drachenfels-Trachyte) has been used is in the Cologne Cathedral. This rock comprises 50 % sanidine, 24 % plagioclase, 13 % quartz, 5 % augite, 5 % biotite, 2 % ore, and 1 % apatite, zircon, and sphene. The fabric of this trachyte is typical for volcanic rock, which is characterized by a fine-grained matrix. Feldspars and quartz comprise the groundmass (Fig. 2.33d). In some places, calcite occurs. Volcanic glass fractions can be altered to montmorillonite. More pyrite occurs in the groundmass than what generally is expected. Furthermore, in some cavities, pyrite and aggregates of pyrite-hematite (limonite?) can be found. Older trachytes frequently contain secondary chlorite, epidote, and calcite.

Basalts are the volcanic equivalents of plutonic rocks like gabbro and norite. They are dark, mostly black, blue-black, and seldom gray with a dense structure. The main mineral constituents are plagioclase, pyroxene, amphibole, olivine and iron ore. In terms of quantity, basalts are the most important volcanic rocks. Basalts are, as a rule, fine-grained and occasionally porphyritic or hyaline. In the wider sense, basaltic rocks can clearly show a distinct flow fabric, which can be applied to the matrix as well as to the phenocrysts. Petrographically, basalts can be understood as consisting of plagioclase, augite, and Fe–Ti oxides. Olivines occur frequently. Feldspar substitutes (like nepheline) are restricted to the alkali basalts. Many deposits show a very well developed columnar jointing (Fig. 2.35a).



**Fig. 2.35** **a** Basalt columns from Giant Causways in Northern Ireland and **b** Use of basaltic rock as a construction material



In an ideal situation, the columns are six-sided so that they connect to each other without gaps. The columns are formed by the contraction of the rock during cooling and perpendicularly to the cooling boundary of the lava flow. Diabases are geologically old basalts from the Devonian and Carboniferous which have turned green due to chemical weathering. Original pyroxenes and amphiboles have undergone serpentinisation or have been altered to chlorite and taken on a dark green color, whereas the former feldspars have taken on shades of gray. For building purposes, basalt generally cannot be considered the most weather-resistant rock, as is often discussed in some textbooks (Fig. 2.35b). Many basaltic rocks show a characteristic gray spot formation that is indicative of the beginning stages of weathering. Later, star-like cracks form between the spots, which eventually lead to the disintegration of the rock. This process can last from many months to years. Rocks with this property are designated as “sunburnt basalt”. The cause of the sunburnt basalt is, in part, the alteration of nepheline into analcime, which leads to a volume increase of about 5.5 %.

Holocrystalline dikes consisting of fine to medium-grained basalts of varying compositions are named dolerites. Dolerites are known as important building stones in different regions of the world. The dolerites of Uruguay (Fig. 2.36) are composed of plagioclase, clinopyroxene, and opaque minerals, and the texture is

**Fig. 2.36** **a** Quarry of black dolerite in Uruguay and **b** Blocks of Negro Absoluto and Oriental

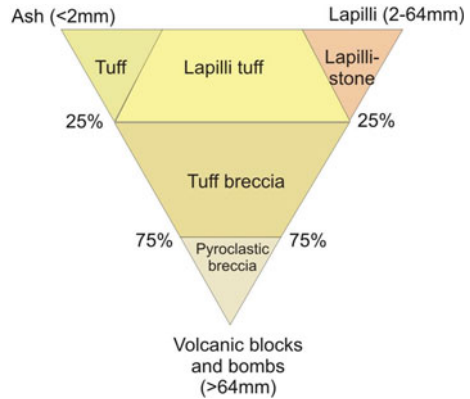


subophitic (Oyhantcabal et al. 2007; Morales et al. 2010). Biotite, apatite, and interstitial intergrowths of quartz and alkali feldspar (micropegmatite) are the main accessory phases. Rims of uralitic amphibole and chlorite are scarce. Two main varieties of dolerite are mined: one is deep black and fine-grained (Negro absoluto), whereas the other is dark gray-black and medium-grained (Negro oriental, see Fig. 2.29). The dikes show chilled margins with different thicknesses that contain a very fine-grained variety, which is highly valued economically on the international stone market. Color inhomogeneities are seldom observed and are associated with pockets of white colored quartz and alkali feldspar intergrowths.

Aplites are fine-grained igneous rocks, commonly of late igneous origin, which are found as veins in granitoid bodies. They are easy to recognize since their difference in color from the host rock is often very clear. Their smaller crystal size is strikingly different from that of granite. Their thickness ranges from the centimeter to meter scale and can even be seen at the block scale.

Pegmatite is just the opposite of aplite, since it contains coarser grained crystals than the host rock. Most pegmatites are granitic in composition and their crystal size ranges from a few centimeters to giant crystals at the meter scale. Most of the world's largest crystals are found in pegmatites (e.g. meter-scale amethysts in

**Fig. 2.37** Classification of polymodal pyroclastic igneous rocks based on the proportions of blocks, lapilli and ash (after Fisher 1961)



Brazil). Aplites and pegmatites do not normally constitute building or dimensional stones, but create heterogeneities in many stones such as granites, gneisses, etc.

### 2.9.3 Pyroclastic Igneous Rocks

Volcaniclastic rocks include the entire spectrum of clastic materials composed in part or entirely of volcanic fragments (Fisher 1961; Fisher and Smith 1991). The designations “tuff” and “tufa” are generally used as a collective term for all the volcaniclastic rocks. The varied fragmentation processes and the type of particles within the volcaniclastic rock groups required a further subdivision into pyroclastic, hyaloclastic, autoclastic, and epiclastic rocks.

The classification of pyroclastic rocks is done by describing the attributes of grain size, composition, and fabric, as well as the origin and depositional environment. A straightforward and easy-to-use classification results from the implementation of granulometric factors (Fig. 2.37). In the strict sense, tuff describes a narrowly defined rock type, wherein the main components show a grain size of less than 64 mm. Characteristic of the rock designation is the prevalent grain size fraction (e.g. tuff). When the rock shows more than one dominant grain size, the subordinate grain size fraction is used to designate the rock type (e.g. lapilli tuff). In the classification of Le Maitre et al. (2004), only those pyroclastic deposits that have been consolidated can be considered to be a rock. Pyroclastics are essentially differentiated according to their average diameter, form, and mode of origin. For example, lapillistones show a grain size of 2–64 mm. They can be differentiated into lapilli tuff, which contains ash and a few blocks or bombs that are larger than 64 mm, and tuff or ash tuff that is dominated by fine (<2 mm) particles. An extremely coarse pyroclastic rock is the agglomerate where blocks or bombs of over 64 mm in diameter dominate. For simplicity in the construction industry and architecture, the term “tuff” is used for the most polymodal pyroclastic rock.



**Fig. 2.38** **a** MUMOK Museum of Modern Art in Vienna (Austria) is clad with basaltic lava (Krings, Schmitz Naturstein GmbH & Co. KG), and **b** Moai from Easter Island in Chile is made from tuff (Figure by B. Fitzner)

Mixed pyroclastic sedimentary rocks are also known; thus, tuffaceous sandstone or tuffaceous mudstone refers to rocks with pyroclastic contents of 25–75 %.

The industrial stone classification of pyroclastic rocks preferentially contains a simplified mineralogical composition; thus, rhyolite tuff, dacite tuff, andesite tuff, and basalt tuff are used as the most common types (Fig. 2.33e–h). Additional pyroclastic rock types include lithologies such as trachite tuff, phonolite tuff, etc.

Rhyolite tuff is buff-beige in color, whereas pumice as lithic clasts frequently occurs. Biotite and quartz are common phenocrysts. Dacite tuff is very similar to rhyolite tuff, but often has higher strength and durability and has a variegated and often darker color than rhyolite tuff. Andesite tuffs have a wide range of color and size, and their fabric can contain lapillis or bombs and frequently forms pyroclastic agglomerates. Basalt tuff is generally somewhat different, more brownish and greenish than andesite tuff (Fig. 2.38a). The common basalt, lapillis, and the presence of olivine crystals allow the identification of this pyroclastic stone.

Most tuffs are easy to cut and work with, and, therefore, they were widely used in masonry structures and stone walls in the past. Especially large structures, such as castles or fortresses, were made of tuffs. Known examples are the Pemian rhyolite tuffs in Germany (Rochlitz) and basaltic tuffs worldwide. Besides their use in building structures, volcanic tuffs were also used in sculptures, and the best known examples are probably the basaltic tuff statues of the Moai on the Easter Islands (Figs. 2.38b).

## 2.10 Metamorphic Rocks

In contrast to the igneous and sedimentary rocks, a large group of metamorphic rocks are only of subordinate importance for use as natural building stones. There are, however, metamorphic rocks that are highly valued because of their exotic composition and very complex rock fabrics. These aspects are a decisive factor for creating the décor, and, thus, they are interesting stones with a high price level and should be included in the natural stone market (see Fig. 2.41).

Metamorphism is a process that leads to changes in the mineralogical and/or structural and/or chemical composition of rocks in the solid state. These changes are caused by physical and/or chemical conditions that deviate from weathering zones—cementation and diagenesis (see Winkler 1967). Metamorphism literally means transformation with respect to the mineral constituents as well as the rock fabric. Metamorphism can also take place isochemically, which means that, during the metamorphism, no chemical changes occur with the exception of introducing H<sub>2</sub>O and CO<sub>2</sub>. Allochemical metamorphism occurs when there is an addition or removal of material that changes the bulk chemical composition of the rock. Sedimentary, igneous, and even metamorphic rocks can be source material for metamorphism. Sometimes, metamorphic rocks can also be designated metagranitoids, metasediments, or metavolcanics. When former igneous or sedimentary rocks are considered where a clear classification to the source rocks can be determined, the rocks can be designated ortho- or para-rocks, respectively. Metamorphic rocks make up about 15–28 vol % of the Earth's crust. With decreasing temperatures, metamorphism is replaced by diagenesis. Experimentally determined melting temperatures of different rocks provide information on the high temperature boundary of metamorphic rocks. Granites begin to melt in the region of the Earth's crust when in the presence of H<sub>2</sub>O at temperatures ranging between 600 and 700 °C. Basalts melt at even higher temperatures. At this boundary, magma formation and metamorphism is dependent on the rock chemistry. The high temperature boundary of metamorphism is estimated to be about 700–900 °C for most rock compositions, with the assumption that a fluid phase is present. Under dry conditions, the boundary can be moved to higher temperatures.

Metamorphic rocks are essentially named after their fabric, because the rock can be characterized by this aspect in hand specimens and at the outcrop (e.g. phyllite, schist, gneiss, hornfels). Other metamorphic rocks, specifically if they are unfoliated and/or monomineralic, are named according to mineralogical criteria (e.g. quartzite, marble, serpentinite, amphibolite). Some metamorphic rocks are named in regards to their mineral constituents and metamorphic grade, e.g. greenschist, amphibolite, eclogite, and granulite (Fig. 2.39).

Metamorphic rocks are subdivided with regards to the grade of metamorphism. The deciding factors are pressure and temperature conditions. In the modern literature, this is characterized as their metamorphic facies. The rocks can be differentiated into greenschist, amphibolite, and granulite facies. The greenschist facies derives its name from metabasites, which were formed as greenschists

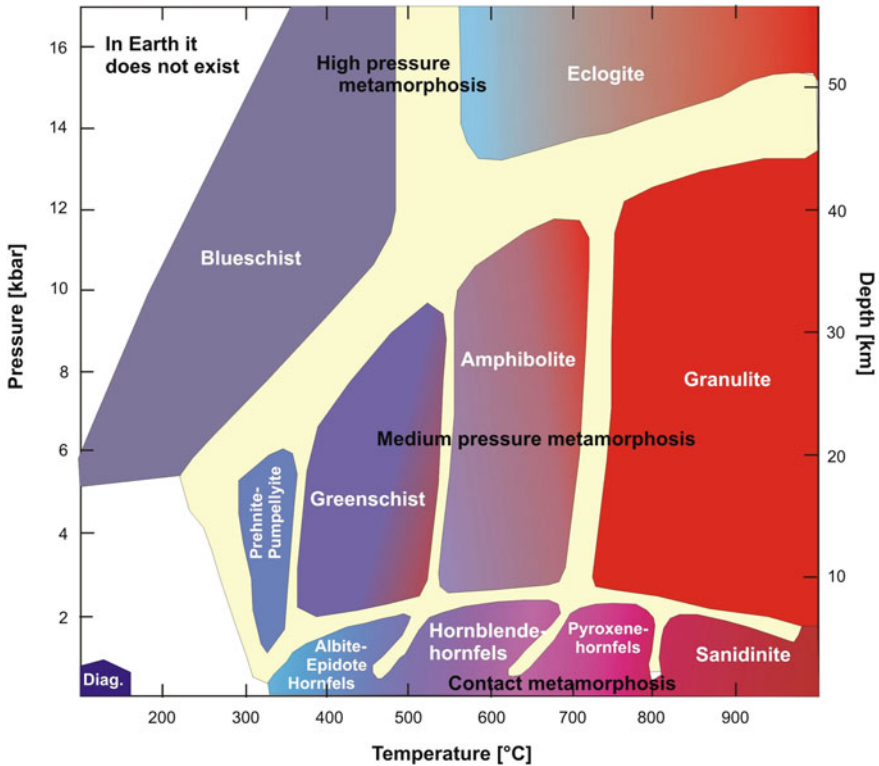


**Fig. 2.39** Various metamorphic phases and the index minerals (after Winkler 1967 and Yardley 1997)

(sometimes known as prasinites) and are comprised of actinolite (a green hornblende), chlorite, epidote, albite, quartz, and sometimes garnet. Kyanite and sillimanite zones are typical for the amphibolite facies. The critical mineral in metabasites, that is, amphibolites, is intermediate-to-basic plagioclase and hornblende. In granulite facies rocks, where water-rich minerals are absent, hornblende is replaced by orthopyroxene and clinopyroxene. Garnet replaces biotite.

Metamorphic rocks that are characterized by very high pressure belong to the glaucophane schist facies or are otherwise known as the blueschist facies. The diagnostic mineral for this facies is the mineral glaucophane, which is an amphibole. The first appearance of eclogites characterizes the eclogite facies. Ocean floor metamorphism is characterized by a high geothermal gradient and material transport through circulating seawater.

Burial metamorphism is defined by Bucher and Frey (2002) as a process directly following diagenesis and, thus, could be viewed as diagenesis under



higher pressure. The zeolite facies and the prehnite-pumpellyite facies characterize this process.

Slates are very low grade metamorphic rocks that originate from fine-grained pelitic and pelitic-psammitic sediments, which are essentially shales and siltstones. The characteristic feature of slates is a well-developed cleavage, where tectonic processes have created a well-developed anisotropy or cleavage parallel to the foliation. Most of the cleavage is caused by the shape-preferred orientation of the sheet silicates (clay minerals or mica). Depending upon the metamorphic grade, the alignment is the result of a passive rotation or a recrystallization and nucleation of the sheet silicates parallel to the foliation. The term “cleavage” is used when the tectonically induced foliation cuts and overprints the bedding (slaty cleavage). Cleavage is a type of foliation consisting of a regular set of parallel or sub-parallel, closely spaced surfaces (on a scale from mineral grain up to several centimeters), which is produced by deformation along a rock body where it will usually preferentially split. More than one cleavage may be present in a rock. Slaty cleavage is used for slates, where they were mostly deformed under greenschist facies conditions. The foliation is perfectly developed and independent of bedding, resulting from the parallel arrangement of phyllosilicates, individual grains which are too small to be seen by the naked eye.

Slates consist predominantly of phyllosilicates like illite, sericite (or fine-grained muscovite), and chlorite, as well as very fine-grained quartz (see discussion in Wagner 2007 or Morales et al. 2013). Wichert (2007) calculated the following contents: muscovite/illite lies between 25 and 55 %, followed by chlorite with 10–20 %, whose proportions may also be 5 % or can be as high as 30 %. Chloritoid can be present in slates where contents generally fluctuate between 2 and 4 %. Paragonite, which represents higher pressures during metamorphism, rarely occurs and shows contents between 1 and 3 %, but some individual analyses have given values ranging from 8 to 16 %. Slates are often used as roofing tiles and wall coverings (Fig. 2.40). As a result of this specific application, roofing and wall slates are not treated as a natural building stone. If, however, slates are used as floor tiles, facades, table and billiard surfaces, or even window sills, then they should be considered a part of the resource group natural building stones. Slate was used earlier as a writing surface (chalk board) in schools. Critical assessment should be made of ore minerals (pyrite, chalcopyrite, etc.) and carbonate contents present in the rock group known as slates.

Phyllites are fine-grained, foliated crystalline schists. They represent the link between non-metamorphosed argillaceous shales and metamorphic mica schists (Fig. 2.41). At relatively small temperature increases, metamorphic minerals such as sericite/phengite and chlorite begin to form, which is also responsible for the silky sheen on the foliation surfaces. Along with these minerals, quartz and even some albite are common in these rocks.

Schist is a metamorphic rock exhibiting schistosity. The term “schistosity” is used when the minerals are coarse enough to be easily seen in hand specimens. By this definition schist is a broad term, and slates and phyllites are also a type of schist. The most frequently occurring parageneses are quartz-biotite, quartz-muscovite,

**Fig. 2.40** Use of slate as cladding material: **a** The slate wall of Lotharheil and **b** Slate flooring tiles (Schieferwerk Lotharheil & Teichmann SchieferZentrum, Geroldsgrün in Germany)



quartz-muscovite-chlorite, quartz-muscovite-biotite, and quartz-biotite-chlorite. Further minerals that occur in mica schists are garnet, albite feldspar, epidote, and others. The typical fabric characterizing mica schists is a well-developed banding. Quartz forms more or less stretched lens-shaped aggregates that lie parallel to the mica and chlorite flakes. Foliation surfaces are mostly uneven in detail, and the thickness of the quartz lenses and mica layers range from a few millimeters to somewhat above that. When other minerals like garnet occur as porphyroblasts, a different fabric develops. The color impression is dependent on the main minerals: muscovite (silver-gray), biotite (dark brown to black), chlorite (green), and the pigment minerals hematite and graphite. Freshly fractured surfaces show an intense brilliance. Over geologic time periods, muscovite schists disintegrate into platy and spiky fragments as a result of weathering.

Chlorite schists consist mostly of 70–90 % chlorite, 10–25 % other silicates, and up to 10 % ore minerals. They are strongly foliated and range in color from dark green to black green (Fig. 2.41). In Italy, chlorite schists are often mistaken for serpentinites because of their similar color, even though serpentinite minerals are either present in subordinate amounts or are not.

Gneiss is a collective term for quartz-feldspar metamorphic rocks that have an acidic to intermediate chemistry, where the fabric and modal constituents can vary

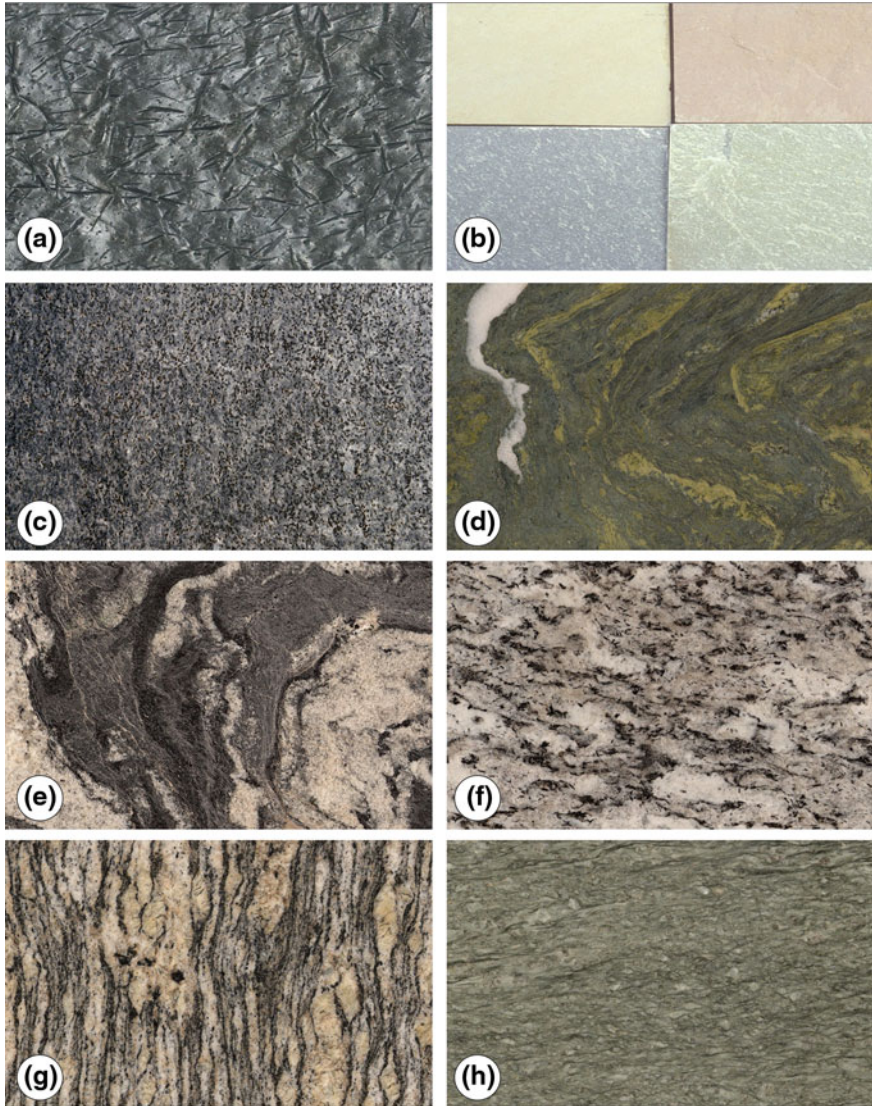


**Fig. 2.41** Commonly used metamorphic rocks: **a** Otta Phyllite, **b** Camine Rufo Slate, **c** Theuma Knotted Slate, **d** Dorfergrün Chlorite Schist, **e** Mähring Biotite Gneiss, **f** Leggiuna Paragneiss, **g** Diodena Gneiss, and **h** Verde Andeer Gneiss (Figure by Natursteinarchiv Wunsiedel)

widely. Accessory minerals include biotite, muscovite, amphibole, cordierite, garnets, sillimanite, kyanite, or graphite, etc. They have a poor rock cleavage and display a gneissose structure. Gneisses are typically layered (also called banded) and often exhibit alternating felsic and darker mineral layers (Fig. 2.42). The rocks may be lineated, but also show segregations of felsic mineral-rich and



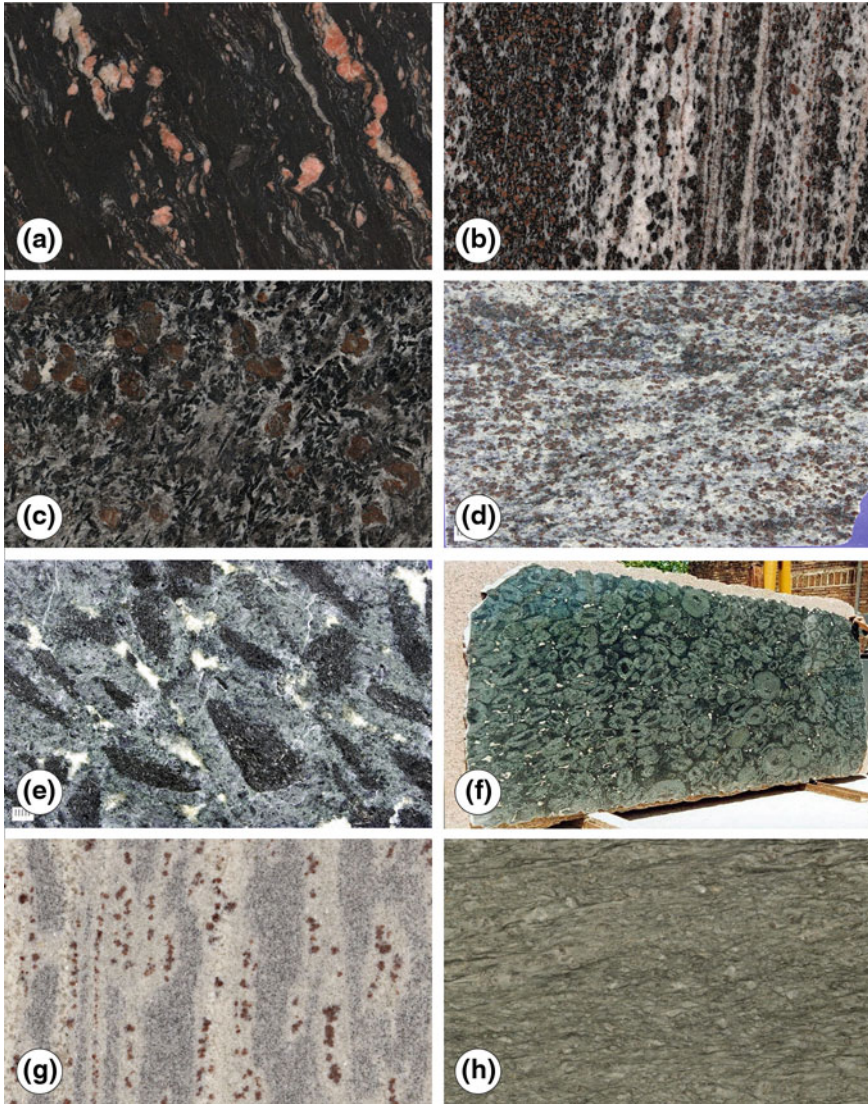


**Fig. 2.42** Commonly used metamorphic rocks: **a** Pontorosa Biotite gneiss, **b** Tundra Gneiss, **c** Kendlbruck Garnet Amphibolite, **d** Azul Tango Cordierite Gneiss, **e** Verde Orcollano, **f** Verde Orcollano, **g** Keralowhite Garnet Gneiss, and **h** Silberbach Eclogite (Figure by Natursteinarchiv Wunsiedel)

dark mineral-rich concentrations (Fig. 2.43). The boundary between mica schists and gneisses is determined by the amount (20 vol %) of feldspar present. Gneisses may also be considered a medium to coarse-grained rock with a poorly developed schistosity where feldspar and quartz are characteristic components

(Brodie et al. 2007). A typical representative of this group is the Beolo Gneiss of the Beura area in Italy, which is widely used as a building stone (Cavallo et al. 2004). This rock is a black and white pencil gneiss that is composed of quartz, plagioclase, K-feldspar, muscovite, and biotite. Chlorite occurs as a retrograde product. The macroscopic appearance is characterized by a strongly developed lineation (stretched Qtz/Fsp aggregates) and rotationally arranged biotite and muscovite. Biotite and muscovite form enriched layers and, next to the flattened Qtz/Fsp aggregates, define the foliation. Since biotite traces the linear fabric, these natural building stones can be split easily. When this gneiss is cut perpendicularly to the layering, the fabric that appears is known as a “augengneiss”, because biotite is rotationally aligned around the quartz and feldspars. Starting as far back as the 12th century, this excellent property, the ability to easily split into thin slabs, has been responsible for the wide use of these stones for buildings, staircases, pavements, and roof coverings.

The term “granulite” was often used in the past to define high grade metamorphic rocks. In the literature, only those rocks which contain the minerals indicative of the granulite facies are considered granulites. In the early petrographic literature, light-colored granulites are described as leptynites. Granulite is a high-grade metamorphic rock in which Fe–Mg-silicates are dominantly hydroxyl-free. The presence of feldspar and the absence of primary muscovite are critical, while cordierite may also be present. The mineral composition is indicated by prefixing the major constituents. The rocks with >30 % mafic minerals (dominantly pyroxene) may be called mafic granulites, and those with <30 % mafic minerals (dominantly pyroxene) may be called felsic granulites. The term should not be applied to ultramafic rocks, calc-silicate rocks, marbles, ironstones, or quartzite (Coutinho et al. 2007). Such rocks are the typical representatives of the lower crust. They consist of feldspar, quartz, garnet, kyanite, sillimanite, and orthopyroxene. The protolith of these rocks are probably rhyolites or rhyolitic tuffs or granitoids. Mafic granulites are also known as pyriclases composed of orthopyroxenes (hypersthene), clinopyroxene, plagioclase, garnet, and ilmenite. The remarkable regions of the Ivrea Zone (Italy) are excellent areas for studying these kinds of high grade metamorphic rocks. In Calabria, a mafic-dominated granulite-pyriclase unit that is composed of pyriclases and mafics, as well as felsic granulites, occurs. The metapelite unit consists of biotite-plagioclase gneisses, metapelitic rocks known as stromalites, and felsic granulites. Sillimanite-garnet gneisses are subordinated. Sometimes coarse-grained granulites are described as granofels. Charnockite granitoids of igneous and metamorphic origin are related to the granulites and carry the orthopyroxene hypersthene.

The upper temperature boundary of metamorphism is defined by the process of migmatization (partial melting). In typical rocks of the continental crust (metapelites, granitoids), the process begins at a temperature of around 650 °C (depending on the composition), under moderate pressure, and at a high H<sub>2</sub>O partial pressure. Migmatites are becoming increasingly popular as a natural building stone. This is because the rock exhibits a lively decor and many different colors, opening the door for various design possibilities (Fig. 2.43). Geologically



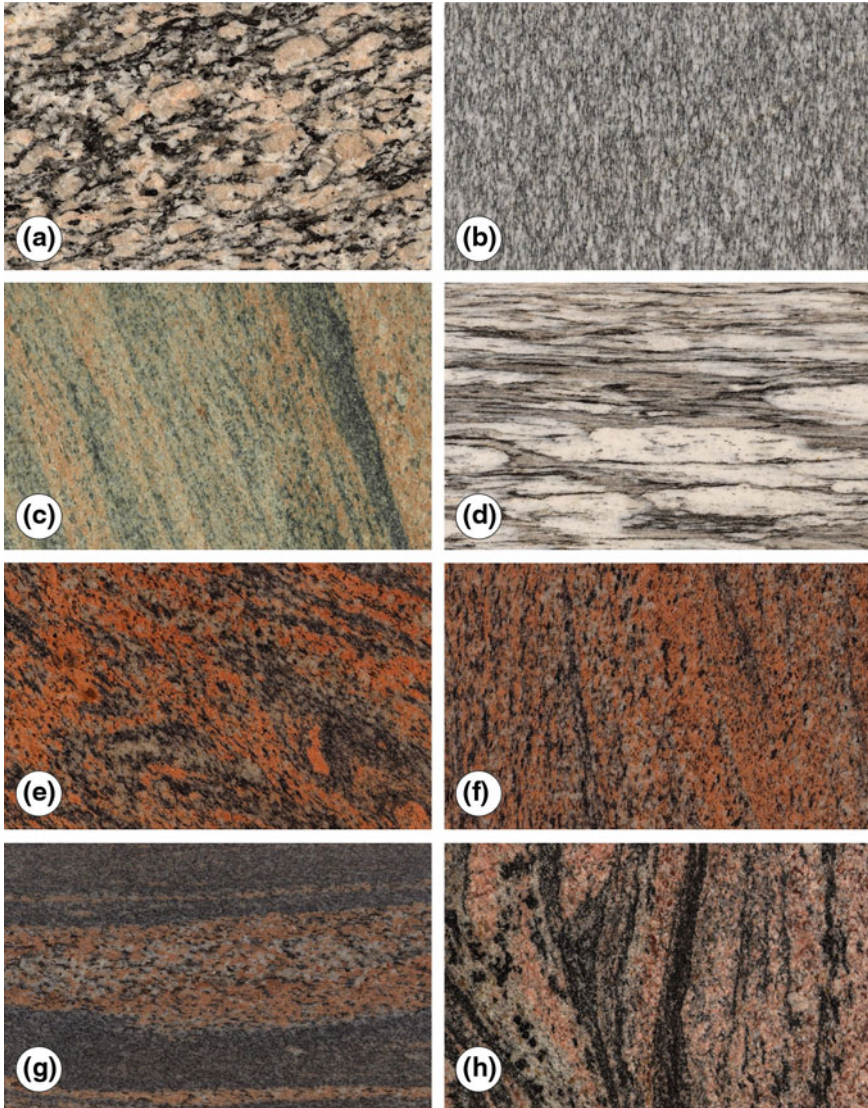


**Fig. 2.43** Commonly used metamorphic rocks: **a** Pekkalan Orthogneiss, **b** Zillertal Paragneiss, **c** Indian Juparana Gneiss, **d** Kapighiandonestriato Orthogneiss, **e** Kinnasöder Migmatite, **f** Vastad Migmatite, **g** Borarp Migmatite, and **h** Rainbow Migmatite (Figure by Natursteinarchiv Wunsiedel)

migmatites can be described as very heterogeneous rocks. Migmatites form under high grade conditions and with various compositions. These aspects lead to the partial melting of the rock material. Magma formation deep in the crust can be studied when these rocks are occasionally exposed at the Earth's surface,



displaying the “frozen” melting process. The rock is characterized by the presence of dark gray to black layers (melanosome), which contain amphibole and/or biotite as the main mineral constituents, and light gray to white layers (leucosome), which are essentially composed of alkali feldspar and quartz ( $\pm$  plagioclase). Unmelted source rocks called restites can also occur. Leucosome and melanosome can also be referred to as neosome, because they both originate from the original source material. Restites can also be termed paleosome. The leucosome is the newly formed partial melt and the melanosome is the part extracted from the melt. At the outcrop scale, migmatites often show a very heterogeneous appearance. Restites can occur as long-sustained layers, or they can form isolated blocks. Migmatites can also show irregular folding of the layers. Mehnert (1968) has established a very useful classification of migmatitic fabrics. The classification utilizes a scale-orientated configurative comparison of the leucosomes and melanosomes without applying the genetic aspects as a basis.

Eclogites are former basalts, basaltic tuffs, or gabbros and, as a result of metamorphism, mainly contain the clinopyroxene omphacite, garnet, and possibly quartz or kyanite, but no plagioclase. The rocks are restricted to smaller deposits and are, therefore, used exclusively for limited building projects and the decorative arts.

Quartzites are metamorphic rocks that are dominated by the mineral quartz. According to Bucher and Frey (2002), quartzites should contain more than 80 % quartz. Associated minerals in quartzites are muscovite, feldspars, and a larger variety of heavy minerals such as magnetite, garnet, ilmenite, etc. In contrast to the orthoquartzites known from sedimentary deposits, the metamorphic ones are characterized by low porosities. Metaquartzites are very hard and stiff and popular building stones, since they are also very weather resistant. They show a widespread distribution, for example, in the Minas District (Brazil). These quartzites are used for exteriors and interiors and widely deployed in the architecture of health resorts. In this type of application, these rocks are resistant to salt damage in saline baths as well as against aggressive cleaning solutions. An interesting phenomenon is the Itacolomites, which are closely associated with the Brazilian quartzites. Itacolomites are very special rocks due to their high flexibility (Siegesmund et al. 2002b). They are composed of quartz (80–95 vol %) and muscovite (2–10 vol %), with kyanite, tourmaline, zircon, feldspar, and ore minerals being the main accessories. The observed bending and its anisotropy can be explained by the rotation of separated quartz grains between layers of mica. These act as flexural slip planes and are also responsible for the observed elastic rebound. This behavior is related to the very thin layers, characteristic higher porosity and a significant change in the pore-radii distribution. Another exotic quartzite is the Azul Macauba and related varieties, which belong to the most expensive dimensional stone in the world (Fig. 2.44a and b). The blue color is related to the mineral dumortierite (an aluminum-iron-boron silicate). The fabric of these quartzites varies strongly, which is also the case for the color. Natural quartzites occur in all colors depending on the proportion of, for example, limonite (yellow and beige varieties) or hematite (red).

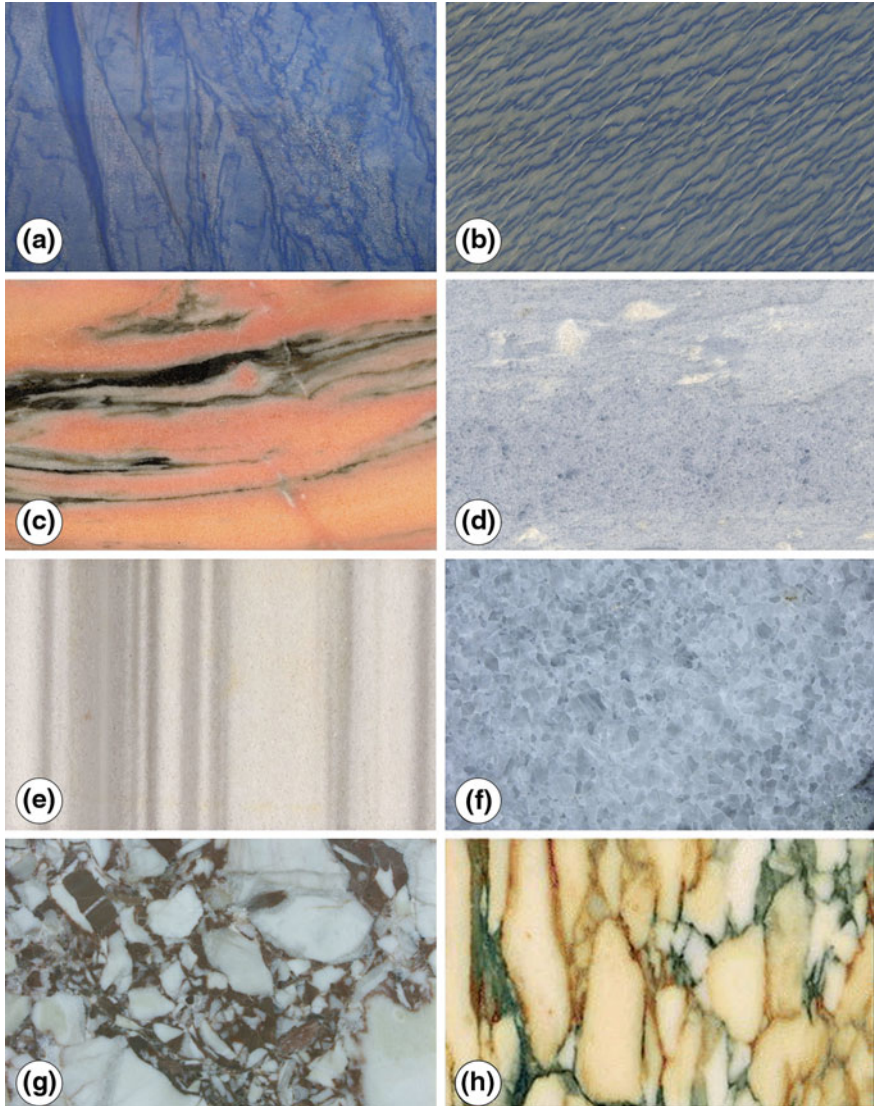


**Fig. 2.44** Color and textural varieties of marbles and selected metamorphic rocks: **a** Azul do Macaubas (quartzite), **b** Azul Macanbas, **c** Artigas (calc-silicate), **d** Celeste Argentina, **e** Bantli (marble), **f** coarse crystalline marble (Thailand), **g** marble breccia, and **h** Carrara Marble (Calacatta) (Figure by Natursteinarchiv Wunsiedel)

In the natural stone industry, all types of polishable limestones are designated as marbles. However, in the petrographic literature, the term “marble” is restricted to those rocks that have undergone metamorphism. Marbles are defined in the strict sense as those rocks containing >90 % calcite or dolomite. Accordingly, the rocks

**Fig. 2.45** The Oslo Opera House where the external facade is covered with Carrara Marble (Vando D'Angiolo, Campolonghi Italia Spa)



are designated as either calcite or dolomite marbles. The presence of siliceous and argillaceous mineral components as well as organic material in the original source rock can lead to the formation of new mineral phases, depending upon the grade of metamorphism (e.g. quartz, muscovite, feldspars, garnets, wollastonite, tremolite, graphite, talc, pyrite, magnetite, etc.). Marbles of this type with a carbonate proportion of 50–90 % are designated as calc-silicate rocks. In many marbles, these mineral phases also form a banding that can, in part, develop an irregularity or, as it is sometimes called, a “marbling” effect (Fig. 2.44). Furthermore, finely disseminated mineral phases can also impart a specific pigmentation, e.g. hematite creates red and chlorite, and serpentine generates green colors. Marbles can essentially be found in many different colors. The most well-known examples are from Greece (Fig. 2.9c) or Italy (Fig. 2.9d).

Grimm (1999) indicates that about 200 marble varieties are economically exploited worldwide (see also Müller 1996). In Carrara (Italy), for example (Fig. 2.3a), there is a vast amount of different marble types that are known under a variety of commercial names, such as Marmo Ordinario, Marmo Venato, Marmo Nulolato, Marmo Arabescato, Marmo Statuario, Marmo Calacata, Marmo Bardiglio, etc. Mecceri et al. (2007) determined three main general fabric types in the Carrara area, i.e. Type A, a granoblastic (polygonal) microstructure, Type B showing sutured grain boundaries, and Type C, which is characterized by a strong shape-preferred orientation including straight to interlobate grain boundaries. Müller (1996) already compiled the above-mentioned Carrara types into an arrangement according to commercial criteria (see Fig. 2.45).

The color variation in marbles shows a wide range: from light white to light yellowish-gray-beige, various shades of pink, red to yellow–brown, and different hues of green. Black and even blue shades are known, although their occurrence is much more rare. An especially impressive variety is the Azul Cielo, where the calcites exhibit a blue color. Next to calcite, a small amount of finely disseminated diopside, wollastonite, apatite, and even quartz occur as accessory minerals. Quartz is mostly recrystallized and forms very fine bands. The impressive blue coloration is probably due to physical defects in calcite. Experiments have shown

that the blue color disappears when the rock is heated to a temperature of over 200 °C (Lamberghini et al. 2000). Marble can also be highly differentiated. Sections of the rock can appear without veins and streaks. Layers can occur with a light streaky fabric and without a clear development of these elements. Other areas are evident where differentiated occurrences of streaks appear with distinct colors of yellow, brown, red, and green. Variations in structure and fabric are possible in deposits where the changes develop over short distances in the quarry. Quarries also rarely produce consistent, uniform, or homogeneous rock material. This is due to the relatively deformable character of marble and the occurrence of frequent fold structures.

Serpentinites are interesting building stones and a very important rock group. They form from peridotites by hydrothermal alteration processes under specific metamorphic conditions. Serpentine minerals predominantly make up the rock. Peridotites represent mantle material directly below the oceanic crust or cumulate rocks formed by the settling of olivine and pyroxene in mafic–ultramafic layered complexes. Protoliths are either lherzolites containing olivine, ortho- and clinopyroxene, or harzburgites consisting of olivine and orthopyroxene. The serpentine minerals are alteration products of olivine and other magnesium-rich silicates and consist of fibrous chrysotile, lamellated antigorite, and sometimes a fine-grained scaly lizardite. Depending on the intensity of serpentinization, olivine, ortho- and clinopyroxene, garnet, chlorite, and talc can occur. During the alteration of olivine, iron is released and is concentrated along the grain boundaries as magnetite, since Fe cannot be incorporated into serpentine minerals. Intense red colorations are due to the alteration of magnetite to hematite.

The purest kind of serpentine generally shows a pale greenish or yellow color, is often variegated and slightly translucent, and breaks with a rather bright conchoidal fracture. Serpentinites exhibit a large spectrum of different rock fabrics. Some form massive bodies. This is seldom the case because serpentinites are easily deformed by tectonic processes. They often show a foliation with sigmoidally developed slip planes, which gives the rock a polished or lineated appearance (Fig. 2.46). Shear planes forming an interconnected system also occur frequently. Serpentinites show brecciated structures that contain more or less large amounts of carbonate in layers or streaks. Included in the carbonate matrix are serpentine fragments. Such rocks are also known as ophicalcites and are a popular building stone because of their conspicuous decor. Occasionally, pronounced talc nests occur together with veins of chlorite. Serpentinites are relatively soft rocks, which are easily polished and have been used over time as gemstones, for monuments and architectural elements, etc. Rock surfaces exposed to the long-term stress of different weathering conditions exhibit a rapid alteration of appearance, and, thus, the use of this stone for exterior applications is not recommended.

Contact metamorphism encompasses the recrystallization of rocks within an aureole around an intrusive body due to the supply of heat, and possibly through the additional transport of materials from the magma (Fig. 2.47). The contact effect is dependent on the temperature of the intruding magma and depth of intrusion. The temperature of an intruding granitic melt ranges from 650 to



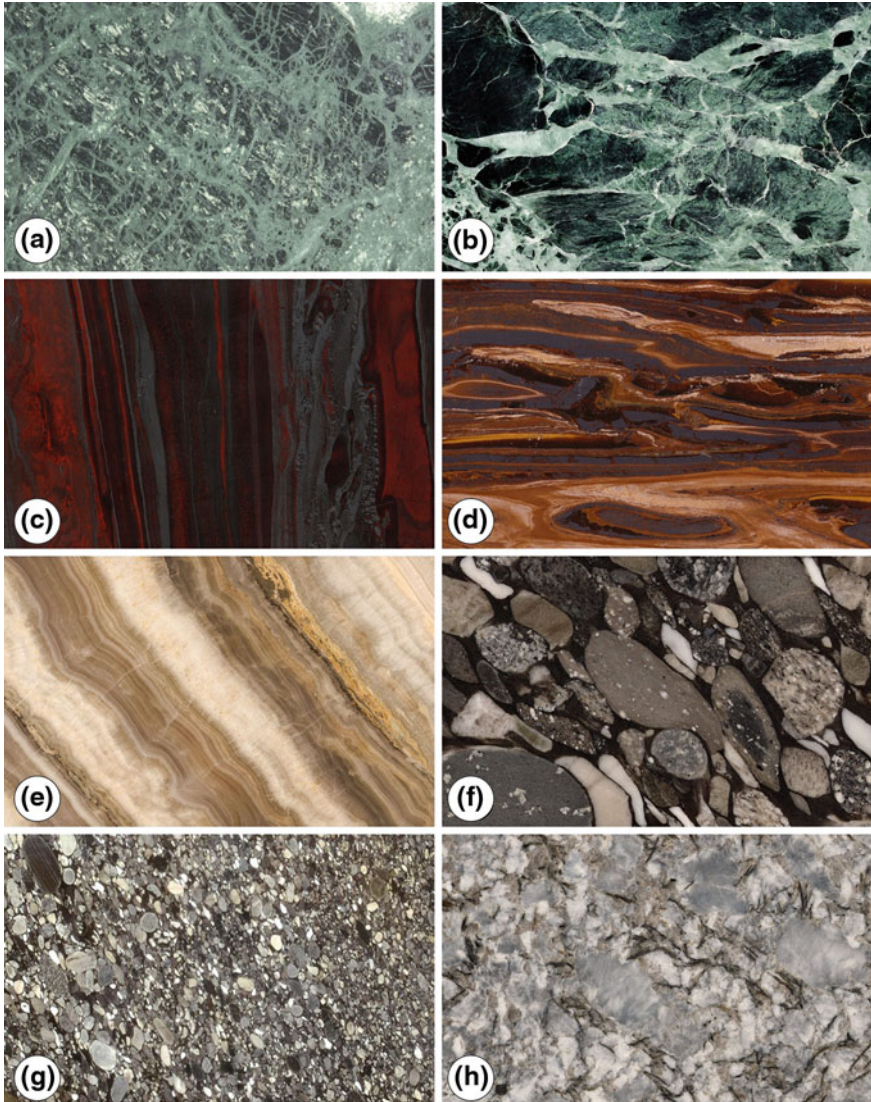


**Fig. 2.46** Commonly used metamorphic rocks: **a** Verde Guatemala (serpentinite), **b** St. Denis (serpentinite), **c** Itabirite (ironstone), **d** Jaspis, **e** Cebrino (onyx), **f** deformed conglomerate, **g** Nero Marinese (deformed conglomerate) and **h** Valdaranzuldarán (pegmatitic gneiss) (Figure by Natursteinarchiv Wunsiedel)

900 °C, whereas a basaltic magma is around 1,200 °C. Country rocks are relatively cold (100–300 °C) when magma intrudes into a region near the surface, which means the temperature difference between the intrusive body and the wall rock reaches a maximum value. In this case, a strong thermal gradient occurs near the intrusive contact.

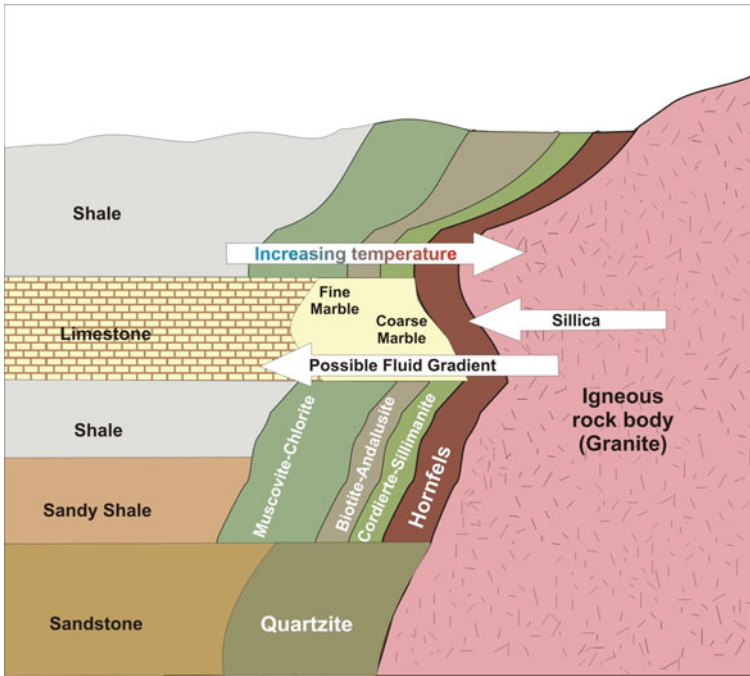


**Fig. 2.47** Contact metamorphism and the most important mineral phases and metamorphic rocks formed from various sedimentary rocks such as limestone, shale and sandstone (modified after Hamblin 1989)

Directly at the contact, completely recrystallized splintered rocks with a dense random fabric, known as hornfels, occur. With increasing distance from the contact, the fabric of the rock hardly shows an overprinting. Only the type and shape of the newly formed minerals (see mineral isograds in Fig. 2.47) indicate the influence of the thermal effect. A good example of this thermal influence is the Knotenschiefer in Theuma (Germany). This schistose rock has a blue-gray, macroscopically homogeneous, and dense groundmass, where dark-gray to black, oriented columnar porphyroblasts up to 5 mm in size occur (Fig. 2.48). The cordierite minerals in the rock are typical for this building stone and give the rock its name, i.e. Knotenschiefer. The porphyroblasts have a shape similar to a seed of grain. The spindle and cigar-shaped cordierite is oriented relatively well to the schistosity, but, within the foliation plane, they lack orientation. Bedding is weakly characterized by a change from light to dark layers. The dark layers consist predominantly of ore (magnetite, ilmenite) (Peschel and Franz 1968). The macroscopic, apparently homogeneous groundmass exhibits a fine, flaky to foliated fabric consisting of sericite, chlorite, and biotite with a grain size of about 15  $\mu\text{m}$  (Peschel and Franz 1968). Limestones grade into marble as a result of grain coarsening in the contact zone. Calc-silicate rocks are formed by the metasomatism between carbonates and silicate-rich rocks or fluids. These rocks are known as scarns.



**Fig. 2.48** Building clad with the Knotenschiefer (knotted slate) of Theuma. The very specific decor is due to the contact metamorphic overprint, which had produced the mineral growth (Natursteinwerk Theuma AG, Theuma in Germany)



## 2.11 Sedimentary Rocks

Sedimentary rocks are the most widespread rock types on the Earth's surface, especially when one considers the present day oceans as the cradle of sedimentary rocks. A continuous formation of sediments of marine origin is well documented from the very beginning of the Earth's history. Vast amounts of sedimentary rocks were produced, from which only parts have been preserved throughout geologic time. Although they represent less than 10 % of the Earth's crust, their contribution to the present day continents are approximately 70 %. The sedimentary rocks can be classified according to their origin into three major groups: (i) detrital sedimentary rocks (clastics), (ii) chemically or biologically precipitated sedimentary rocks, and (iii) organic sedimentary rocks. According to some authors, pyroclastic igneous rocks can also be classified as sedimentary rocks, but, in terms of origin and technical use, these lithotypes should be considered part of the igneous rock system.

Detrital sedimentary rocks are formed from previously existing rocks by subsequent processes, including weathering, transportation, deposition, compaction, and diagenesis. The best known examples are sand or sandstone. Chemically or biologically precipitated rocks are the ones that are mostly formed in aquatic

environments by chemical and/or biological reactions. The formation process also includes compaction and diagenesis. In this group, the most widespread lithotype is limestone. Organic rocks are normally formed from the accumulation of organic carbon-rich fossils via a complex alteration process that produces solid, liquid, or gaseous end products, such as coal, crude oil, or natural gas. This latter group is of limited importance and has no functional use in the design of architectural elements. Therefore, it will not be discussed in detail in this book.

### ***2.11.1 Detrital Sedimentary Rocks***

Detrital sedimentary rocks are formed from the disintegration of formerly existing rocks at or near the Earth's surface by means of weathering. Weathering is a complex process that includes various types of alteration, generating rock fragments or clasts. The other name of detrital sedimentary rocks, "clastic sedimentary rocks", refers to this process. Weathering can be attributed to physical/mechanical, chemical, or even biological processes (see [Chaps. 4 and 6](#)). In most cases, a combination of mechanical, chemical, and biological weathering is responsible for the decomposition of rocks and the formation of rock fragments. The ultimate weathering products of rocks are soils. The best example for chemical weathering is the dissolution of limestone and karstification, but it also includes physical and a limited range of biological decay and alteration. Under a very dry and cold climate, chemical weathering is limited, and physical weathering prevails.

Biological weathering is a combination of physical and chemical processes at the interaction surface of living organisms and stone. Tree roots can also exert pressure on stones and lift up large blocks as they grow, whereas lichens produce acid which can dissolve even the most durable stones.

After the generation of rock fragments of various sizes by weathering, the newly formed particles are transported by means of wind, water, or ice. The transportation can take place on land (by streams, wind or glaciers, etc.) or in the oceanic environment (by waves, currents, etc.). Large masses of sediments are displaced by these processes at every moment, contributing to the sediment budget of land and sea. By scrupulously studying detrital sedimentary rocks, it is possible to identify the transporting medium and the process. Internal structures of rock beds (e.g. cross bedding) and sedimentary features (e.g. grading), as well as fossils, can indicate the origin of the rock. The largest amount of sedimentary rocks are formed in marine or coastal environments ([Fig. 2.49](#)) and as river deposits ([Fig. 2.50](#)), but dry and arid settings such as desert environments also contribute significantly to clastic sedimentary systems. Water and ice can only move particles downward, whereas the wind is able to move dust/sand or, rarely, pebble-sized particles upward.

Transportation is followed by deposition, which presumes changing conditions in water or wind agitation, and, thus, the transporting medium does not have the ability to move the sediments. In terms of depositional mechanisms and environments, a wide range of facies exists both "on land and in the sea".

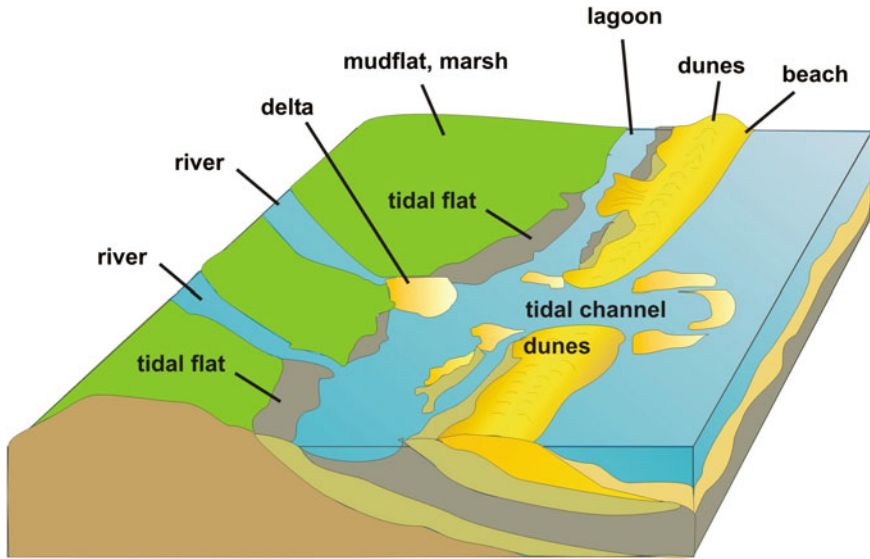
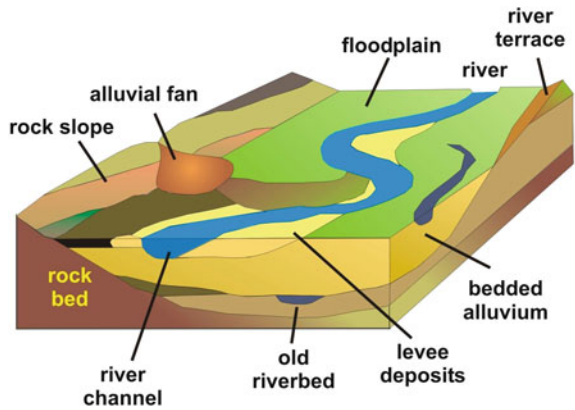


**Fig. 2.49** Detrital sedimentary rock formation in coastal marine settings. Sands and coarser sediments are found at deltaic to coastal environments such as lagoons, beaches, dunes, tidal flats and marshes, etc

**Fig. 2.50** River deposits of detrital sedimentary origin include clay-sized sediments from flood plains to sandy and gravelly deposits from river channels



The deposition could be rapid or slow. When slurries are formed and sediments are deposited, a typical grading is observed. This means that coarse and heavy particles are deposited first, followed by particles of decreasing grain size.

The deposition of clastic sedimentary rock layers on top of each other leads to the compaction of the sediment, which is interpreted as a decrease in volume and a denser packing of grains by the weight of the overlying layers. Cementation can be a simultaneous process with compaction, or, in some cases, it can be coeval with

**Table 2.2** Classification of detrital sedimentary rocks according to grain size and cementation

Sediment	Grain-size (mm)	Consolidated/Cemented
Boulder/cobble (rounded)	63	Conglomerate (rounded)
Rock fragment (angular)		Breccia (angular)
Pebble (rounded)	2–63	Conglomerate (rounded)
Rock fragment (angular)		Breccia (angular)
Sand	2–0.063	Sandstone
Coarse	2–0.63	Coarse sandstone
Medium	0.63–0.2	Medium sandstone
Fine	0.2–0.063	Fine sandstone
Silt (Aleurite, mud)	0.063–0.002	Siltstone (Aleurolite, mudstone)
Clay	<0.002	Claystone

deposition. This causes the binding of the grains/particles by cementing minerals and provides a bridge between particles. By cementation, the loose, so-called unconsolidated sedimentary rock (e.g. sand) becomes a solid rock (e.g. sandstone). The cementation itself is only one part of the diagenesis, which is a term that refers to the processes responsible for the formation of the rock after deposition. Dissolution and the opening of new pores is also a part of the diagenetic process which acts in a way opposite to cementation. This causes a decrease in strength and durability of the rock, whereas compaction and cementation generally increases both.

Detrital sedimentary rocks are classified by two specific aspects: (i) particle size and (ii) rate of cementation. The latter one is difficult to define clearly, but, in general, the sediments that are unconsolidated and do not have any cementing mineral belong to this group (such as gravel, sand, etc.). The classification of detrital sedimentary rocks referring to particle size is a well-defined system, although the numerical values defining one special rock type might change from country to country. In this book, the nomenclatures and grain sizes described by the European Norm (EN 12670, 2001) are used. The most important detrital sedimentary rocks, according to the differences in grain size, are listed in Table 2.2.

### 2.11.1.1 Consolidated Detrital Sedimentary Rocks

The nomenclature of consolidated/cemented detrital sedimentary rocks reflects the differences in grain size and also relies on the visual assessment of grains. From a practical point of view, the cementing mineral is almost as important as the type of grain, since both determine the properties of the rock. Various types of cement are known, including carbonates (calcite, dolomite), iron-oxide or iron-oxi-hydroxide (limonite, goethite), siliceous (crystalline or amorphous silica, such as chalcedony), or even clay cement (e.g. kaolinite). The cementing mineral very often influences not only the mechanical properties but also the color of the detrital

sedimentary rock. Iron-oxide stains red, while iron-oxide-hydroxide gives a brownish color to the stone. Carbonates and clay minerals, as well as silica cement, are often white to colorless and, thus, do not change the visual appearance of the stone. In terms of strength and durability, silica cemented stones have higher load-bearing capacities and resistance against weathering or decay. On the other hand, hard silica-cemented sandstones are difficult to work with, and, therefore, their use for ornaments or statues requires more work.

The rock types that have particles greater than 2 mm are divided into two groups based on the roundness of the particles. Conglomerates are characterized by rounded grains, whereas breccia contains angular particles. In theory, no upper limit for grain size is given, but, in most cases, the size of the larger particles are on the order of tens of centimeters, rarely meters.

Conglomerates contain rounded pebbles of size 2 mm or larger. Some conglomerates resemble concrete, but larger varieties exist due to the differences in the lithology of the pebbles. Most conglomerates are composed of resistant quartz or quartzite pebbles, but limestone or even iron ore can be the dominant pebble type. The types that look like very coarse sandstone and are predominantly composed of quartz are used as ashlars, as cut building blocks, or in the footings of houses. On the other hand, limestone conglomerates are very often used as polished slabs or as polished decorative stones (e.g. columns, pillars, statues), especially in prestigious relics and in churches (see Fig. 2.56h).

Breccia encompasses angular grains of at least 2 mm in size. In conglomerates, quartz pebbles dominate the rock, while most breccias consist of particles other than quartz, very commonly limestone or dolomite. Brecciated marbles are also known (see Fig. 2.44g). Several types of breccias can be easily polished, and, thus, this stone type is commonly used for slabs or ornaments. Stylolitic limestone breccias with their decorative appearance are very often precious stones. The durability of the breccia often depends on the cementation and the compaction and can be determined by the presence of clayey seams. In other words, the clayey seams reduce the strength and durability of the breccia. Breccia can be formed due to tectonic activity, which results in a cataclastic fabric. Dissolution can also generate breccias.

Sandstones are by far the most common detrital sedimentary rocks that are used in architecture and in objects expressing the cultural heritage of a society. In most European countries, historic structures and monuments built from sandstones are still preserved and standing. Scotland, England, and Northern Ireland are characterized by the presence of Carboniferous and Permo-Triassic sandstones. The Permo-Triassic sandstones are generally yellowish-brownish to reddish in color and have been used not only within the UK, but have also been exported to the United States. In Germany, France, and Switzerland, Mesozoic sandstones are very common (Fig. 2.52). Significant amounts of sandstone were formed in the Late Permian to Triassic and Cretaceous periods (see Fig. 2.51). World heritage buildings such as Petra in Jordan (Fig. 6.15 in Chap. 6) are all made of sandstone.

The grain size of sandstones ranges from 0.063 to 2 mm. A further, finer subdivision is also possible according to the grain size. Fine sandstones contain



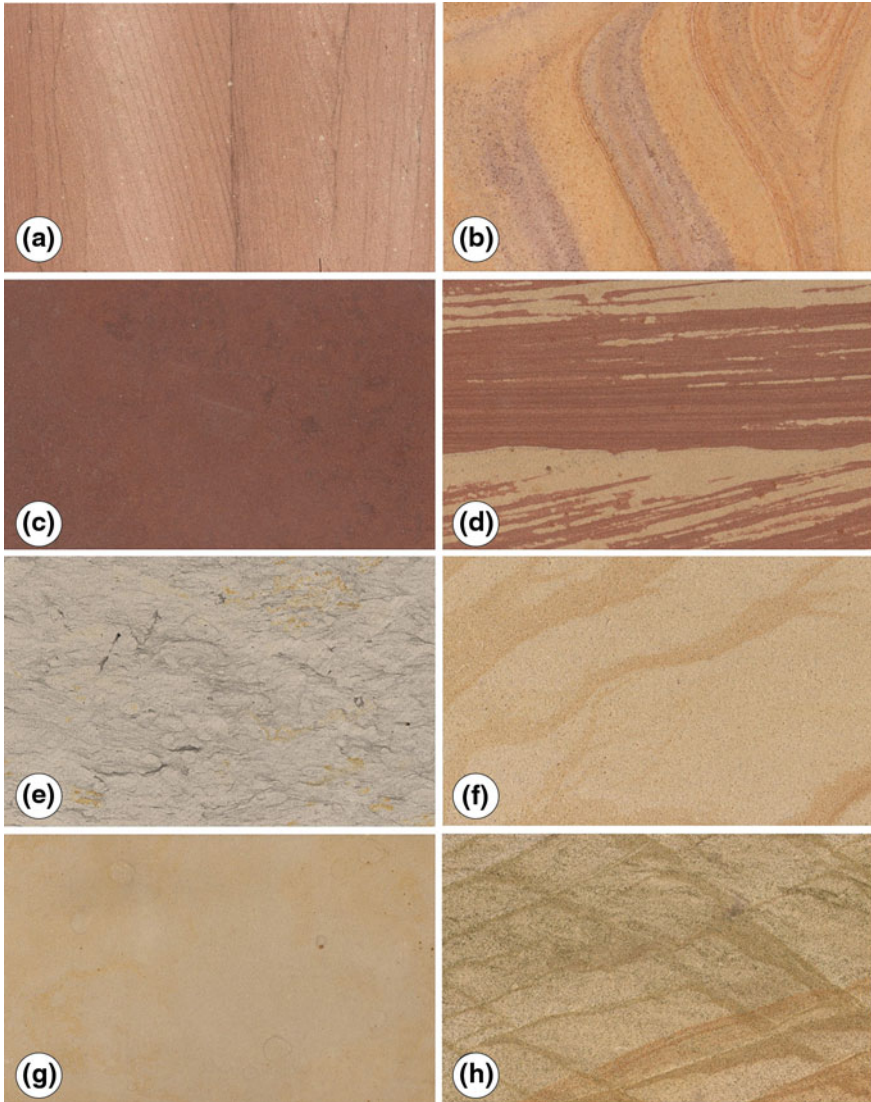


**Fig. 2.51** Color and textural varieties of sandstones: **a** Crossbedded Sandstone, **b** Rainbow Sandstone, **c** Tambach Sandstone, **d** Miltenberg Sandstone, **e** Cotta Sandstone, **f** Posta Sandstone, **g** Obernkirchener Sandstone, and **h** Steinlutter Sandstone (conglomerate) (Figure by Naturstein archiv Wunsiedel)

grains ranging from 0.063 to 0.2 mm; medium-grained sandstones show particle sizes of 0.2–0.63 mm, whereas coarse sandstones with particles ranging 0.2–2 mm form a transition toward conglomerates. Sandstones exhibit great varieties in terms of appearance and properties. The color of sandstone can be white to almost black

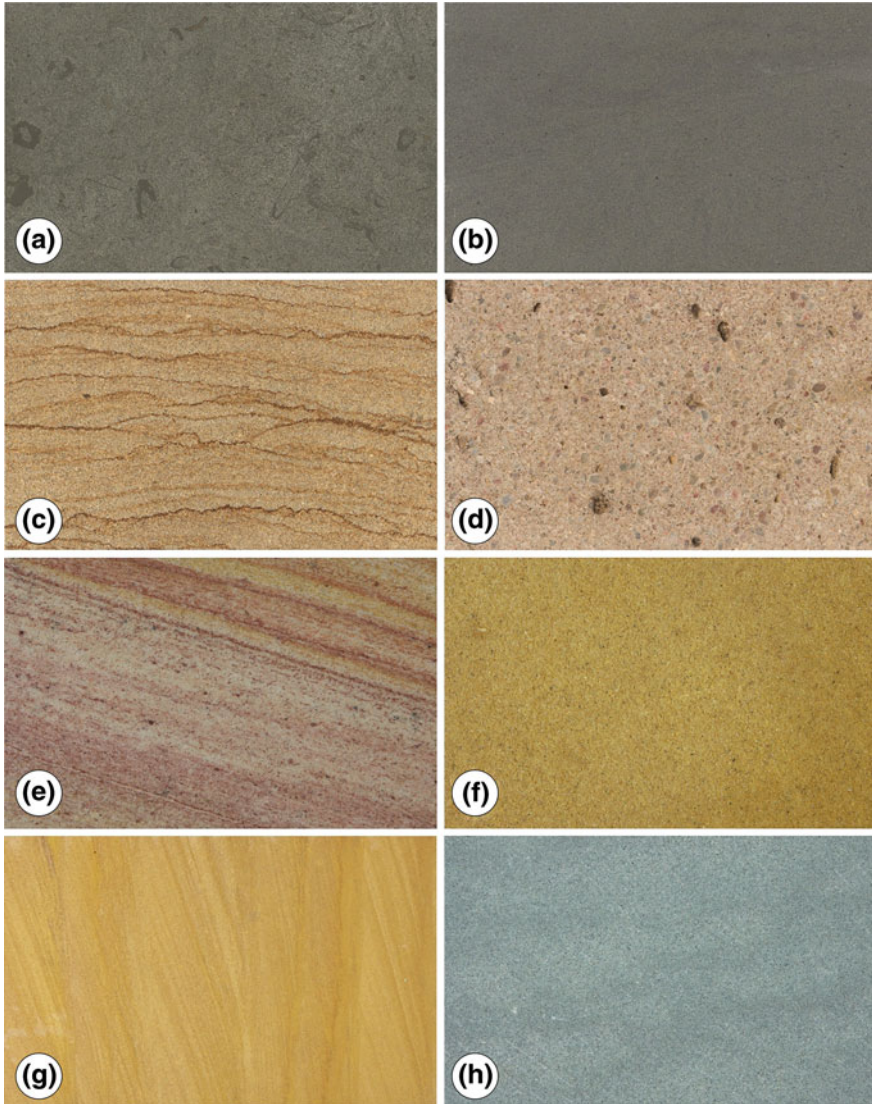


**Fig. 2.52** Color and textural varieties of fine- and coarse-grained sandstones: **a** Anröchter Calcareous Sandstone, **b** Bauermährischer Sandstone, **c** Pietra Dorata Sandstone, **d** Radkow Sandstone, **e** Thailand Red, **f** Thailand Beige, **g** Crossbedded Thailand Beige, and **h** Thailand Green (Figure by Natursteinarchiv Wunsiedel)

(dark gray), but is more commonly light gray, beige, brownish, and reddish, and even greenish varieties are known (Fig. 2.52). The surface of sandstone is always rough and resembles sandpaper. The properties are mostly determined by the mineralogy of the grains, by the mineralogical composition of matrix and cement,

and by the porosity. There is a difference between the framework and the matrix. The former one includes the grains that provide the framework for the rock fabric, whereas the latter one generally includes finer particles less than 30  $\mu\text{m}$ .

The most durable sandstones are the silica cemented quartz sandstones. These varieties often contain smaller amounts of other minerals such as mica or iron oxides. The presence of clay minerals can negatively influence the properties and durability of sandstones. Especially swelling clays, such as montmorillonite, can have an adverse effect on the use and long-term behavior of sandstone (Sect. 3.5). Although quartz sandstones are the most common, there are sandstones which are primarily composed of carbonate grains. This lithotype is also called calcarenite and forms a transition to limestones. In most cases, calcarenitic sandstones are less durable than quartz sandstones, although the workability of these sandstones is much better than their siliceous counterparts. Quartz sandstones often contain feldspars such as orthoclase or plagioclase. The feldspar-rich sandstones (with more than 25 % feldspar) are called arkose. Fragments of other rock types can also occur in sandstones, and these are called lithic fragments. Sandstones are grouped into three main types: quartz arenite, feldspathic arenite, and lithic arenite. With increasing clay and mud content, the stone is called muddy or argillaceous sandstone. These terms are used for sandstones that have a fine matrix consisting of at least 15 % mud and clay. One of the most well-known types is Greywacke, which is a clayey sandstone, with some feldspar content.

The porosity of sandstones shows a wide range from very low (only a few percentage points) to very high values of up to 35–40 %. The pore size is generally less than the grain size, and large open pores are very rare. Important features of sandstones are the sorting and the roundness of grains. Well sorted sandstones contain equi-dimensional grains, whereas, in poorly sorted sandstones, the sand particles show various grain sizes. Sedimentary structures are commonly visible in sandstones. Laminations (parallel to cross-lamination) are small-scale features (less than 10 mm in size), whereas bedding or cross-bedding with layers greater than 10 mm are easily observable at a block scale with the naked eye. A wide range of bedding forms occurs from tabular cross-bedding to trough cross-bedding and symmetrical to asymmetrical forms. In graded sandstones, the whole grain size distribution shows an increasingly fining upward sequence, whereas, in inverse grading or negative grading, the finer particles are found at the bottom of the bed or lamina. Other elements that are commonly seen in sandstones are ripple marks, tracks or trails of fossils, nodules, burrows, etc. Some sandstone may contain fossils that indicate the depositional environment, such as bivalve shells, snails, ammonites, etc. Sandstones are formed in a wide range of environments from marine to terrestrial settings. A large amount of sandstones was formed in fluvial environments or under arid or semi-arid conditions in desert environments. Shallow marine sandstones and sand dunes along the seashore are very common in the present, as they were in the geologic past. These provide excellent environments for the formation of thick sandstone deposits.

Mudrocks are the most widespread rock types from the entire spectrum of sedimentary rocks. They contribute nearly 50 % of all of the existing sediments.

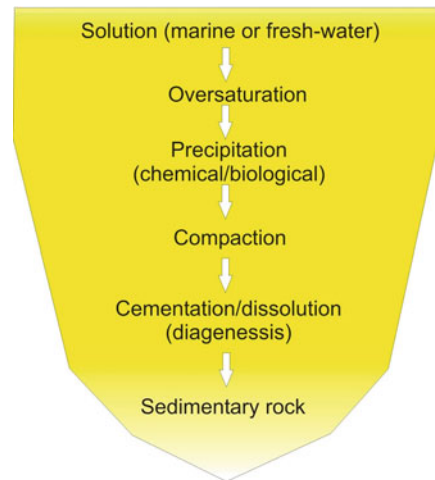
However, due to their low preservation potential and limited use as a building stone, they are under-represented in the architectural heritage of humanity's great monuments and public works. Furthermore, most mudrocks are very prone to weathering and, therefore, when exposed to the elements, very often disintegrate into smaller fragments. The term "mudrock" includes several lithologies under one common term that contains all particles smaller than 0.063 mm ( $<63 \mu\text{m}$ ). Mudrock encompasses names such as mudstone, siltstone, claystone, slightly metamorphosed (or diagenetically overprinted) shale, etc. Mudrocks can be differentiated based on grain size, since silt/mud has a grain size of 63–2  $\mu\text{m}$ , whereas clay generally contains particles smaller than 2  $\mu\text{m}$  (or in some countries, 6  $\mu\text{m}$ ). Due to the very small grain size and the difficulties in identifying the particles in the field or at a building site, the terminology of mudstones is often misleading and used in an incorrect way. From a scientific point of view, two main classifications exist: one is based on the grain size (clay, silt, and sand content), and the other focuses on the mineralogical composition, whereby siliceous compounds, clay minerals, and carbonates are considered. The latter one also includes marls. Marls can also be considered carbonates, since they ideally contain 50 % clay-silt size particles and 50 % carbonates (mostly calcite).

Mudstone is the coarsest mudrock, with a prevailing grain size of 63–2  $\mu\text{m}$ , but it can also contain finer grains of clay or coarser grains consisting of sand or pebbles. It appears in various colors and has a very different consistency, ranging from the soft, non-fissile rock to rigid varieties. Shale is a fissile variety of mudstone that has undergone some deformation and diagenesis. Mudstones and shales range from light gray to black or from yellowish-brown to red, depending on the mineral stain that is present. Black shales are common, and they are often enriched in organic carbon. Both mudstones and shales can show sedimentary features such as laminations or can contain pebbles and fossils. Claystones are characterized by particles of less than 2  $\mu\text{m}$  in size. Due to the very small grain size, the mineralogical composition of mudrocks is difficult to identify, and, thus, laboratory analyses (mostly XRD or DTA-DTG etc.) are needed for exact determination of the minerals present. There is no sharp boundary between the consolidated mudrocks and unconsolidated detrital sedimentary rocks, such as mud, silt, or clay. From an engineering geological point of view, mudrocks are very often considered to be unstable rocks for foundations, because they are commonly subjected to landslides and other slope movements.

### ***2.11.2 Chemically or Biologically Precipitated Sedimentary Rocks***

Chemically or biologically precipitated rocks differ from detrital sedimentary rocks, especially in their genesis. While most detrital rocks are formed from pre-existing rocks by weathering and erosional processes, chemically or biologically

**Fig. 2.53** Formation process of chemically precipitated sedimentary rocks



precipitated sedimentary rocks have no prerequisites in terms of previous rocks, only an over saturation of solution or biological activity is needed. This difference in genesis between detrital and chemically/biologically precipitated sedimentary rocks generates very different properties and behavior.

The prerequisite for the formation of these rocks is the presence of a solution, in most cases either freshwater or seawater. The majority of these sediments are formed from seawater. The initial step is the supersaturation of the solution with respect to any dissolved compound. This could be the result of an increase in temperature or even the mixing of two undersaturated waters that leads to a supersaturated solution. The minerals or chemical compounds precipitated from the supersaturated solution occur by means of biological or chemical activity or both (Fig. 2.53). Moreover, organisms can also precipitate minerals from undersaturated water (e.g. marine snails and corals extract Ca and carbonate ( $\text{CO}_3$ ) from seawater and build their calcite-aragonite shells). The precipitation is coeval with diagenetic processes such as cementation. The pores of the rocks are occluded by cementation or even enlarged by dissolution. Compaction is also a common phenomenon of chemically or biologically precipitated sedimentary rocks.

Unlike detrital sedimentary rocks, chemically or biologically precipitated sedimentary rocks are subdivided by their composition rather than their grain or crystal size. Consequently, four major rock groups of this origin are discussed here: (i) carbonates, (ii) siliceous sediments, (iii) evaporites, (iv) phosphates, and other sediments such as ironstones.

Carbonates are by far the most common chemically and biologically precipitated rocks and represent about one fifth of all sedimentary rocks. For simplicity, carbonates can be divided into two major rock groups, limestones and dolomites. The prevailing mineral of limestones is calcium-carbonate (calcite or aragonite), whereas for dolomites it's calcium-magnesium-carbonate (the dolomite mineral). Although they are very simple in terms of mineralogical composition compared to



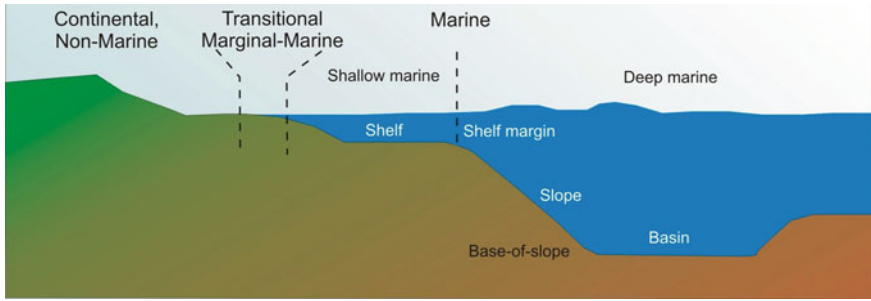


**Fig. 2.54** Major carbonate depositional environments from continental settings such as streams and lakes (travertine) to marginal marine (coastal) and fully marine facies (shallow shelf to deep marine) (modified after Flügel 2004)

igneous or detrital sedimentary rocks, carbonates include very different rock types in terms of appearance and physical properties. One example is the significant difference in color, which ranges from white to black. Furthermore, there are very porous, sponge-like soft carbonates as well as non-porous, very compact and rigid lithotypes.

The formation process of carbonates requires water or biological activity with the presence of moisture. Carbonates as rocks can be either formed by the transportation and deposition of previously existing carbonate particles or in-situ by biogenic and chemical precipitation. These latter ones are often associated with the growth of carbonate skeletons (e.g. reefs, bivalves, etc.) or the trapping or binding of carbonates in organic structures, such as microbial mats. Carbonates are formed in almost all marine environments as well as in freshwater lakes or streams. Carbonate is also precipitated from springs, especially in areas where limestone is present. The greatest portion of the carbonate rocks are formed in marine environments including the coastal, shallow marine to continental slope to deep marine environments (Fig. 2.54). The major carbonate production and the so-called “carbonate factory” are found in shallow and warm marine environments, where light can illuminate the seawater (known as the photic zone), and biological activity is intense. This realm also favors the chemical precipitation from marine waters, which can be over-saturated with respect to calcium and carbonate. The depositional environment has a significant influence on the properties of carbonates, and, therefore, it is more important than in detrital sedimentary rocks. Carbonates are prone to weathering, especially since rainwater is able to dissolve most carbonates. The complex process of weathering and the resulting landforms are called karstification.

The classification of carbonates is very complex, and numerous subdivisions exist. The baseline of classifications can be the grain or crystal size, the main constituents, or the depositional fabric, as well as diagenesis. The old terminology used the grain or crystal size, and, accordingly, fine-grained (calclutite <63  $\mu\text{m}$ ), sand-sized (calcarenite, 63  $\mu\text{m}$ –2 mm), and pebble or larger grain-sized (calcirudite >2 mm) carbonates are known. The other classification system used the major

constituents, lime mud and cement ratio, as well as porosity, for carbonate classification. According to the system of Folk (1962), micrite is a very fine-grained calcite ( $<4 \mu\text{m}$ ) which is found in many limestones either as cement or as a main constituent. Sparite is a coarsely crystalline calcite (aragonite or dolomite) that has a crystal size of greater than  $15 \mu\text{m}$ . Microsparite is in between micrite and sparite in terms of crystal size. The major carbonate grains that are present in the carbonates also play an important role in the designation of these limestones. Ooids are rounded carbonate grains which are formed by successive coatings of thin carbonate films around a nucleus. Ooids have a diameter between 0.2 and 2 mm, but commonly range from 0.5 to 1 mm. Oncoids are very similar to ooids, but generally larger and characterized by non-concentric coatings. Peloids are small, spherical to ovoid-shaped micritic grains that range from 0.02 to 1 mm in size. They are probably formed by biological activity and are polygenetic in origin, but many of them may be faecal in origin. Clasts are common carbonate grains found in limestones which are variable in size and considered to be reworked fragments of consolidated carbonate sediments. Intraclast is a term used for carbonate clasts from the depositional area, while extraclasts are derived from other areas or even from rocks of previous geologic periods. Skeletal grains or bioclasts are very common constituents of limestones. These biogenic grains very often provide key information on the origin of carbonates. The most common types include bivalves, gastropods, ammonoids, coral, calcareous algae, foraminifers, etc. According to one of the first classification schemes of carbonates, Folk (1962) identified various categories where names refer to the main constituent as well as to the type of cement in the rock. Among others, he identified biosparite, which is a bioclastic limestone with sparitic cement or pelmicrite, which is a limestone with peloids that are embedded in micritic cement.

The pioneering classification of carbonates (mostly limestones) according to their depositional environment was published by Dunham (1962). He subdivided limestones based on their depositional fabric, which is called microfacies. This system was later updated and extended by many authors, and it was Wilson (1975) who grouped carbonates into standard microfacies zones. Dunham's classification, which is based on the percentage of very fine (micritic) and coarser (sparitic) calcite as well as the ratio of cement to grain, was later extended by Embry and Klovan (1972), who included other categories that better describe the role of biological activity. Accordingly, there are mud-supported or grain-supported carbonate fabrics. This is probably the most widely used depositional textural classification of limestones. More recently, Tucker and Wright (1990) and Flügel (2004) gave very detailed descriptions of carbonate depositional environments and fabrics.

The porosity of carbonates are of special importance, since connected pores serve as conduits for fluids such as water and oil or provides reaction surfaces for the dissolution of carbonates. The need for a classification of the pore system in carbonates originates from research in the petroleum industry. Choquette and Pray (1970) distinguished fabric selective, non-fabric selective, and a third group that could either be fabric selective or not. This classification considers the genetics of

the pores and does not deal with the size and connectivity of the pores. Smaller sized intergranular or fenestral pores and larger fracture-related or channel-like pores are also one subclass in the pore classification system (Sect. 3.2). In the architecture and construction industry, the effective porosity (the interconnected pores) of carbonates are more important than their genetic origin, since the ratio of open pores determine the mechanical properties and durability of most carbonates.

Carbonate rocks are important, not only because of their wide use as a construction material, but also as reservoirs for hydrocarbons and groundwater. Forty percent of the world's hydrocarbon reserve is stored in carbonates.

Carbonates are divided into limestones, dolomites, and mixed siliciclastic carbonate rocks such as marl. Limestones are primarily composed of calcium-carbonate, which shows two forms according to the composition and crystal system. Calcite is the trigonal form of  $\text{CaCO}_3$ , whereas aragonite has the same chemical composition, but structurally is classified as orthorhombic. Aragonite is commonly precipitated in marine environments and forms the skeletal part of many sea organisms. It is metastable and transforms into calcite. Besides the stoichiometric calcite, other impure calcite forms are also known, and elements such as Mg or Fe can also replace Ca ions in the crystal structure. Thus, it is possible to distinguish the so-called high Mg-calcite, low Mg-calcite, and ferroan calcite. One common method for the determination of limestone is the use of dilute hydrochloric acid, which causes a reaction ( $\text{CO}_2$  degassing) in limestones. When the Ca–Mg ratio in the structure is 50 %, then the mineral is called dolomite (the Mg content is 40–60 % in dolomite).

Although limestones are calcite-bearing rocks, their appearance and technical properties are very different. For practical purposes, a simplified classification is proposed here that focuses on the mechanical properties and the possible uses of limestones. Accordingly, limestones are divided into: (i) non-porous or compact limestone, (ii) porous limestone, and (iii) travertine.

Compact or non-porous limestones have very limited porosity (generally less than a few percentage points) and are very well cemented. Their depositional environment, process of formation, and age show great variation, as well as their composition, but, in most cases, they are of marine origin. The key technical properties include making a sharp broken surface, producing small sharp chip fragments, and the ability to polish the surface of these limestones. In the stone industry, such limestones are very often sold as marbles due to their similarity in surface finish. They show a great range in the color spectrum and can also be pure white to black. The fabric is either micritic or sparitic, and they can contain macrofossils or microfossils. The porosity of these limestones is far less than that of the porous limestones. The compressive strength and modulus of elasticity and other rock mechanical parameters reflect higher strength compared to porous limestone or travertine (Török 2006). Their industrial uses include lime and cement production as well as filler and filter materials. The typical and easily recognizable features in many of these limestones are the stylolites or calcite veins that have different colors than the host rock. Besides their importance as a raw material for industrial processes, their use in architecture as decorative stones,

cladding, and flooring, or as ashlar, is very common (Figs. 2.55 and 2.56). Famous examples are known from all over the world. The “Belgium Granite” is a Paleozoic compact limestone that often contains visible white colored fossils (Fig. 2.55c). The German Muschelkalk is a designation that is used for a geological time period as well as a descriptive term meaning shelly limestone. The rock is also considered a compact limestone. In the United Kingdom, Portland Stone, Great Oolite, and Magnesian Limestone are also various types of compact limestones. In France, the Jaumont Limestone and many limestones in Spain belong to this type. The Istria stone is a famous building stone of Venice, which is a light-colored Mesozoic compact limestone that was quarried on the peninsula of Istria (Amoroso and Fassina 1983). Rosso di Verona is a red variety of compact limestone, as is the Adnet limestone of Austria. The streets in Portugal and most of the pedestrian zones in Lisbon and many other cities are paved with small black and white cubic blocks that are made of compact limestones. Compact or non-porous limestones are commonly used as aggregates in the construction industry, but also in smelters in the steel industry.

Porous limestones are less durable than the non-porous varieties and often are lighter in color. These sediments were formed in marine environments, and their porosity can reach 50 %, but, in most cases, it ranges from 10 to 30 %. Porous limestones are generally younger than the compact ones, and, in Europe, most of them were formed during the Tertiary to Quaternary periods and in the Mesozoic. Common examples are the Oligo-Miocene “soft limestone” that is found throughout the Mediterranean area. The globigerina limestone of Malta, which was the construction material of the prehistoric megalithic temples (Cassar 2002) (Fig. 2.9a), is one type of porous limestone. In Greece and Italy, many other monuments and structures were made of porous limestones. A French variety of porous limestone is called “Tuffeau” with extremely high porosities of nearly 50 % (Beck and Al-Mukhtar 2008). Miocene porous limestones from Central Europe are also known. The representative buildings of Vienna (St. Stephen’s Cathedral) and Budapest (St. Stephen’s Basilica) were all made from nearby quarried porous and very often oolitic limestones (Török 2002, 2004). Compared to compact limestones, porous limestones are less durable and more sensitive to weathering and decay. Many structures that are made of these stones now show severe signs of deterioration. In marine environments such as the Mediterranean, salt weathering occurs (Fitzner et al. 1996; Cassar 2002; Rothert et al. 2007), whereas in urban environments, air pollution-related soiling and blackening are observed on porous limestones (Török 2002). Porous limestones are not used in the cement industry. These stones cannot be polished; therefore, their use in construction and architecture is mainly in the form of rubble, ashlar, facing, or cladding, as well as for ornamental and artistic elements.

Freshwater limestone, or travertine, is a type of limestone that is mainly formed in freshwater aquatic environments. They include the calcareous tufas, calc-sinters from cold streams, and carbonates that are deposited from lacustrine environments or hot water such as springs or geysers. Travertines are very often creamy and beige in color and have large to small but often oriented pore systems. In recent

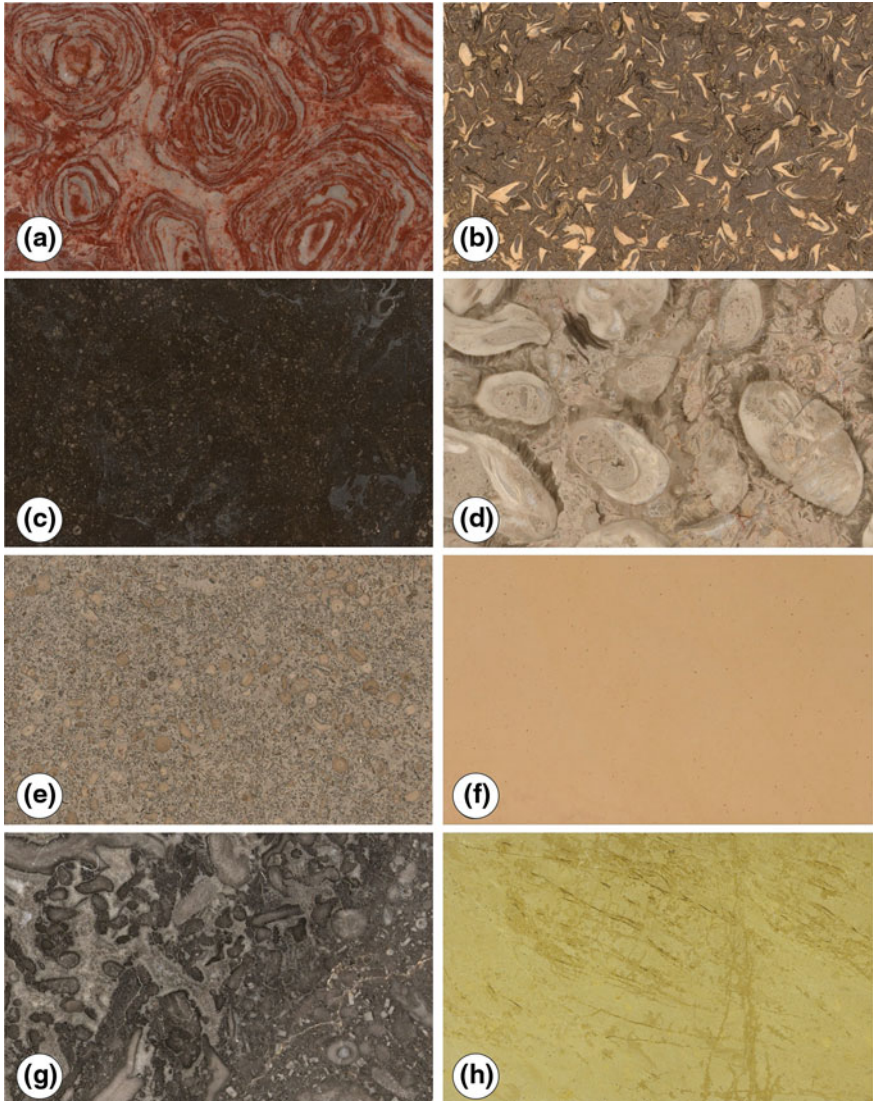


**Fig. 2.55** Color and textural varieties of limestones and dolomite: **a** China (Ustromatolite), **b** Fohndorfer Muschelkalk, **c** Belgisch Granite (black limestone), **d** Fossil Columbia, **e** Crailsheimer Muschelkalk, **f** Solnhofen Limestone, **g** Wirbelau Lahnkalk (limestone), and **h** Dolomita Dorada (Figure by Natursteinarchiv Wunsiedel)

years, more travertines with various colors have been found on the market, such as pink to dark brown varieties. Plant fragments, freshwater snails, and other fossils are commonly found in travertine. Plant leaves of terrestrial origin as well as reeds or even calcified mosses indicate the rapid formation of carbonates and the



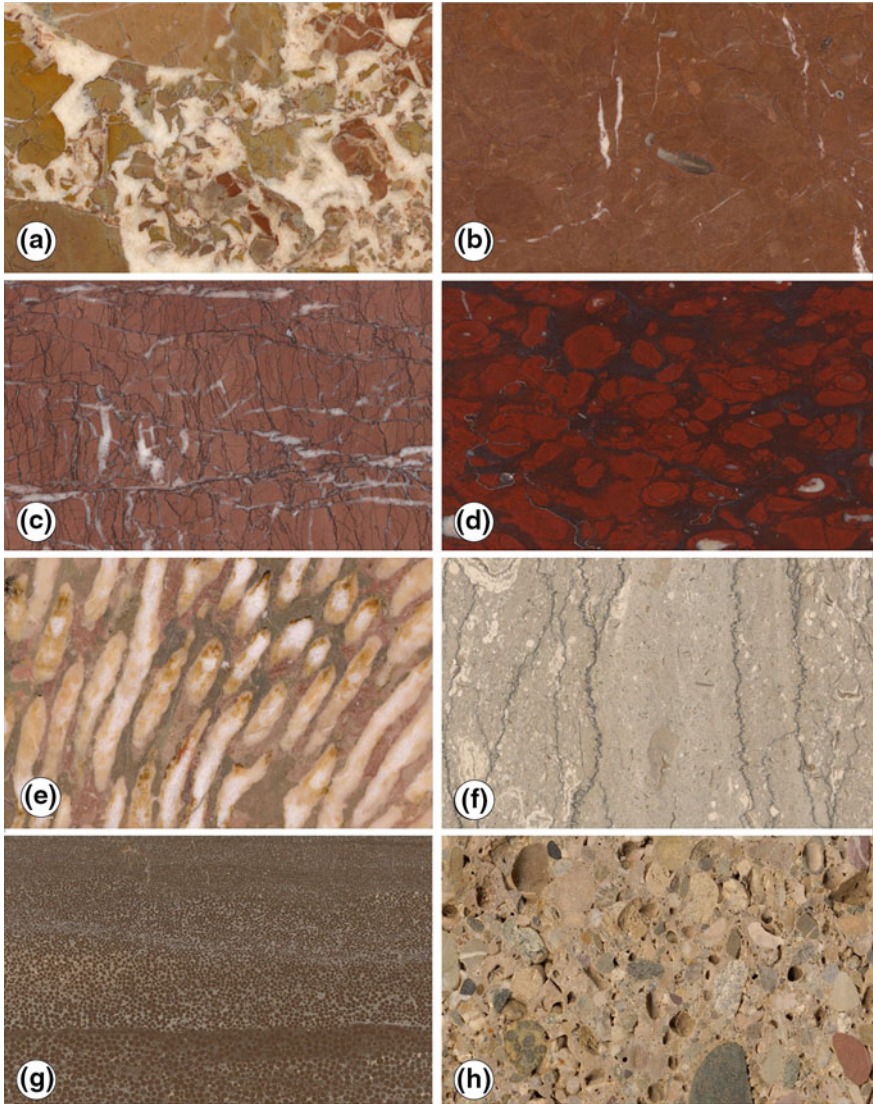


**Fig. 2.56** Compilation of different limestones with different color and decor. **a** Ziller Breccia, **b** Aegea Brown, **c** Troizinarea, **d** Marbreduroi, **e** Adnet, **f** Nagelfluh, **g** Rogenstein, and **h** Perlatoroyal (conglomerate) (Figure by Natursteinarchiv Wunsiedel)

depositional mechanism of travertine (Pentecost 2005). The most durable one is a travertine from a hot or lukewarm water origin. It can be polished and used as cladding stone (Fig. 2.57). The excellent properties of this stone were even recognized by the Romans, who used travertine to build representative structures such as the Coliseum in Rome. The most famous travertine deposit is the one from

**Fig. 2.57** The Parliament Building of Budapest constructed from soft, porous limestone (*gray*) and a successive restoration where this limestone is replaced by travertine (*white*)



Tivoli (near Rome), and other deposits from Turkey are also known. Many countries use travertine as a local building stone. Despite its porosity, travertine is more durable than other porous limestones and shows less severe signs of deterioration in polluted urban environments (Török et al. 2010).

Dolomite or dolostone is a carbonate rock with dolomite as the main mineral constituent. Since limestones are easy to determine by using diluted hydrochloric acid, freshly broken surfaces of dolomites do not show any reaction to HCl, due to their high magnesium content  $\text{CaMg}(\text{CO}_3)_2$ . Dolomite has a trigonal rhombohedral crystal structure that differs slightly from calcite. The different crystal structure also explains why dolomitic rocks have different properties than limestone. Dolomites are white to gray or even black in color, but pink, green, and other color varieties are also known. Very fine crystalline to coarsely crystalline dolomite rocks are known that are called sucrosic or saccaroidal varieties. Dolomite is more brittle than limestone; therefore, many dolomites are intersected by cracks or microcracks. This is the primary reason why it is difficult to exploit large blocks of dolomite, and most dolomites are only used as aggregates rather than ashlars or slabs. Powdered dolomite is an important constituent of many paints and plasters, and, in the past, it was also used in mortars.

Marl is a special sedimentary rock type that contains 50 % calcite and 50 % fine siliciclastic sediments consisting mostly of silt and clay. The composition can be shifted from the ideal 50–50 % content to a greater carbonate portion, (i.e. calcareous marl) and/or a more siliciclastic fraction such as clayey marl. Marl often has a slightly rough, broken surface, and its color is less variable than that of compact limestone. Bedding is a common feature of many types of marl, and the properties and possible use of marl depends on the carbonate content. Calcareous marls are very rigid and similar to compact limestones, whereas clay-rich marls can have a plastic character when they are saturated with water. Marls are formed in marine as well as in lacustrine environments. Due to the presence of carbonate and silica, marls and marly limestones are the preferable raw materials of the cement industry.

Siliceous sediments form in the oceans at great depths, especially below the zone where calcite dissolves. This zone is called the calcite compensation depth (CCD). The composition is primarily determined by the organism that forms the majority of the sediment; accordingly, there is siliceous oozing of radiolarians or diatomaceous origin. Siliceous sediments are also found in some lakes, especially in volcanic areas. Besides these siliceous sediments, silica can be found as isolated

nodules in many limestones. The best known example is flint, which is a black, nodular, very fine crystalline chert that is commonly found in Cretaceous chalk. In architecture, pure siliceous sediments of biological origin are very rare, but chert nodules of different colors are commonly visible in many limestones and marls. Limestones with low silicic content are also found.

Evaporites are sediments that have been chemically precipitated either from marine or non-marine waters and that are supersaturated with respect to one or more salt compounds. During the evaporation of water, various salts can be precipitated, although very few salts are common and occur in great quantities in nature. The most common ones are halite (rock salt), gypsum and anhydrite (two types of Ca-sulphate), and some potassium salts (mostly known as bitter salts). Dolomite may also form from the evaporation of seawater, but biological activity is very important. Evaporites are less commonly used as construction materials than other sedimentary rocks. Alabaster is a form of recrystallized gypsum, is a precious stone of evaporitic origin, and is used mainly in the decorative arts. Furthermore, many limestones of speleogenic origin and travertines are also called alabaster. The role of evaporitic minerals is more important in terms of the salt-related decay of building stones than as a material used for construction purposes. Salt weathering and the occurrence of salt minerals as efflorescence or subflorescence are discussed in detail in [Chaps. 4 and 6](#). Gypsum is a key raw material for plasters and the major constituent of many stuccos and ornaments.

Phosphates are generally formed in marine or terrestrial environments from vertebrate bone fragments, chemical precipitations, or guano. Ironstones of sedimentary origin include a great variety of stones with thick deposits of Precambrian banded iron formation (BIF) and Phanerozoic iron-rich sediments such as the Mesozoic ironoolites of Europe (United Kingdom, France, and Germany). Most ironstones are red to brown in color, depending on the prevailing mineral. Hematite, an iron-oxide mineral, creates a red stain, whereas iron-oxide-hydroxide (goethite) gives the rock a brownish color.

## References

- Amoroso GG, Fassina V (1983) Stone decay and conservation. Elsevier, Amsterdam
- Beck K, Al-Mukhtar M (2008) Formulation and characterization of an appropriate lime-based mortar for use with a porous limestone. *Environ Geol* 56:715–728
- Börner K, Hill D (2007) Große Enzyklopädie der Steine: CD-ROM. Abraxas Verlag, Hasede
- Borradaile GJ, Bayly MB, Powell CMA (1982) Atlas of deformational and metamorphic rock fabrics. Springer, New York
- Bowen NL (1928) The evolution of igneous rocks. Princeton University Press, Princeton
- Brodie K, Fettes D, Harte B et al. (2007) Towards a unified nomenclature in metamorphic rocks. 3. Structural terms including fault rock terms. Recommendations by the IUGS subcommission on the systematics of metamorphic rocks. [http://www.bgs.ac.uk/SCMR/docs/papers/paper\\_3.pdf](http://www.bgs.ac.uk/SCMR/docs/papers/paper_3.pdf). Accessed 20 July 2010
- Bruno R, Paspaliaris I (eds) (2004) Ornamental and dimensional stone market analysis. Osnet edition, Athen

- Bucher K, Frey M (2002) *Petrogenesis of metamorphic rocks*. Springer, Berlin
- Cassar J (2002) Deterioration of the globigerina limestone of the Malteses Island. In: Siegesmund S, Weiss T, Vollbrecht A (eds) *Natural stone, weathering phenomena, conservation strategies and case studies*. Geological Society Special Publication 205, London, pp 33–49
- Cavallo A, Bigioggero B, Colombo A et al (2004) The Beola: a dimension stone from the Ossola Valley (NW Italy). *Per Miner* 73:85–97
- Choquette PW, Pray LC (1970) Geologic nomenclature and classification of porosity in sedimentary carbonates. *AAPG Bull* 54:207–250
- Coutinho J, Krätner H, Sassi F et al. (2007) Towards a unified nomenclature in metamorphic petrology—8. Amphibolite and granulite. Recommendations by the IUGS Subcommittee on the systematics of metamorphic rocks. [http://www.bgs.ac.uk/scmr/docs/papers/paper\\_8.pdf](http://www.bgs.ac.uk/scmr/docs/papers/paper_8.pdf). Accessed 20 July 2010
- Cox KG, Bell JD, Punkhurst RJ (1979) *The interpretation of igneous rocks*. George Allen & Unwin Publishers, London
- Cross W, Iddings JP, Pirsson LV et al (1902) A quantitative chemico–mineralogical classification and nomenclature of igneous rocks. *J Geol* 10:555–690
- Drüppel K (2003) *Petrogenesis of the Mesoproterozoic anorthosite, syenite and carbonatite suites of NW Namibia and their contribution to the metasomatic formation of the Swartbooisdrif sodalite deposits*. Ph.D. thesis University of Würzburg, Würzburg
- Dunham RJ (1962) Classification of carbonate rocks according to depositional texture. In: Ham WE (ed) *Classification of carbonate rocks*. AAPG Memoir 1, Tulsa
- Embry AF, Klovan JE (1972) Absolute water depths limits of late devonian paleoecological zones. *Geol Rundschau* 61:672–686
- EN 12440:2000 Natural stone—denomination criteria
- EN 12670:2001 Natural stone—terminology
- EN 1341:2006 Slabs of natural stone for external paving. Requirements and test methods
- EN 1342:2009 Setts of natural stone for external paving. Requirements and test method
- EN 1343:2009 Kerbs of natural stone for external paving. Requirements and test methods
- European Commission (1998) *European minerals yearbook 1996–1997*. 2nd edn. EU, Luxemburg
- Fisher RV (1961) Proposed classification of volcanoclastic sediments and rocks. *Bull Geol Soc Amer* 72:1409–1414
- Fisher RV, Smith GA (1991) *Volcanism, tectonics and sedimentation*. In: Fischer RV, Smith GA (eds) *Sedimentation in volcanic settings*. Society for Sedimentary Geology Special Publication 45, Tulsa
- Fitzner B, Heinrichs K, Volker M (1996) Stone deterioration of monuments in Malta. In: Pancella R (ed) *Proceedings of the 1995 LCP Congress 'Preservation and restoration of cultural heritage'*. Laboratoire de Conservation de la Pierre, Département des Matériaux, Ecole Polytechnique Fédérale Lausanne, Lausanne
- Flügel E (2004) *Microfacies analysis*. Springer, Berlin
- Folk RL (1962) Spectral subdivision of limestone types. In: Ham WE (ed) *Classification of carbonate rocks*. AAPG Memoir, 1, Tulsa
- Founti M (ed) (2004) *Stone for construction and architecture—from extraction to the final product*. Osnet editions, Athen
- Grimm WD (1999) Beobachtungen und Überlegungen zur Verformung von Marmorobjekten durch Gefügauflockerung. *Z dtsh geol Ges* 150(2):195–235
- Hamblin WK (1989) *The earth's dynamic systems—a textbook in physical geology*. MacMillan, New York
- Hill D (2007) Werkstoff Naturstein aus Sicht der Architekten. *Z dtsh Ges Geowiss* 158/4:701–707
- Hoffmann A (2007) *Naturwerksteine Thailands: Lagerstättenerkundung und Bewertung*. Diss Univ Göttingen, Göttingen
- Hutton DHW, Siegesmund S (2001) The Ardara granite: reinflating the balloon hypothesis. *Z dtsh Geol Ges* 152:309–324

- Kay RW, Mahlburg Kay S (1986) Petrology and geochemistry of the lower continental crust: an overview. In: Dawson JB, Carswell DA, Hall J et al. (eds) *The nature of the lower continental crust*. Geological Society of London, Special Publication 24, London
- Lamberghini A, Fiora L, Alciati L (2000) Il cielo dell' Argentina nel marmo Azul. *L'informatore del marmista*, 464:6–12
- Le Maitre RW (ed) (1989) *A classification of igneous rocks and glossary of terms*. Cambridge University Press, Cambridge
- Le Maitre RW, Streckeisen A, Zanettin B (eds) (2004) *Igneous rocks: a classification and glossary terms*. Cambridge University Press, Cambridge
- Lu P, Latham JP (1999) Developments in the assessment of in-situ block size distributions of rock masses. *Rock Mech Rock Eng* 32(1):29–49
- Mecceri M, Molli G, Conti P et al (2007) The carrara marbles (Alpe Apuane, Italy): a geological and economical updated review. *Z dtsh Ges Geowiss* 158(4):719–735
- Mehnert KR (1968) *Migmatites and the origin of granitic rocks*. Elsevier, Amsterdam
- Montani C (2003) *Stone 2002—world marketing handbook*. Faenza, Gruppo Editoriale Faenza Editrice, Faenza
- Montani C (2005) *Stone 2004—world marketing handbook*. Faenza, Gruppo Editoriale Faenza Editrice, Faenza
- Montani C (2008) *Stone 2008—world marketing handbook*. Faenza, Gruppo Editoriale Faenza Editrice, Faenza
- Morales M, Oyhantcabal P, Stein K-J, Siegesmund S (2010) Black dimensional stones: geology, technical properties and deposit characterization of the dolerites from Uruguay. *Environ Earth Sci* 69(4):1067–1489. doi:[10.1007/s12665-010-0827-5](https://doi.org/10.1007/s12665-010-0827-5)
- Morales M, Oyhantcabal P, Stein K-J, Siegesmund S (2013) Dolomitic states from Uruguay: petrophysical and petromechanical characterization and deposit evaluation. *Environ Earth Sci* 69:1361–1395
- Mosch S (2009) *Optimierung der exploration, gewinnung und materialcharakterisierung von naturwerksteinen*. Diss Univ Göttingen, Göttingen
- Mosch S, Nikolayev D, Ewiak O, Siegesmund S (2010) Optimized extraction of dimension stone blocks. *Environ Earth Sci*. doi:[10.1007/s12665-010-0825-7](https://doi.org/10.1007/s12665-010-0825-7)
- Müller FM (1996) *Gesteinskunde*. Ebner-Verlag, Germany
- Oyhantcabal P, Siegesmund S, Stein K-J (2007) Dimension stones in Uruguay: situation and perspectives. *Z dtsh Ges Geowiss* 158(3):417–428
- Passchier CW, Trouw RAJ (1996) *Microtectonics*. Springer, Berlin
- Pentecost A (2005) *Travertine*. Springer, Berlin
- Peschel A (1983) *Natursteine*. VEB Deutscher Verlag für Grundstoffindustrie, Leipzig
- Peschel A, Franz E (1968) *Der Fruchtschiefer von Theuma (Vogtl.)*. Beziehung zwischen Genese und Verwertbarkeit. *Z Angewandte Geol* 14/9:483–488
- Primavori P (1999) *Planet stone*. Giorgio Zusi Editore S.A.S., Verona
- Rotherth E, Eggers T, Cassar J et al. (2007) Stone properties and weathering by salt crystallisation of Maltese Globigerina limestone. In: Prikryl R, Smith BJ (eds) *Building stone decay: from diagnosis to conservation*. Geological Society of London Special Publication 271, London
- Shadmon A (1989) *Stone: an Introduction*. Intermediate technology publications, London
- Siegesmund S, Vollbrecht A, Weiss T (2002a) Gefügeanisotropien und ihre Bedeutung für Naturwerksteine. *Naturstein* 7:76–81
- Siegesmund S, Vollbrecht A, Hulka C (2002b) The abnormal mechanical behaviour of itacolimites: fabric evidences. Geological Society of London Special Publication 205, London, pp 137–147
- Streckeisen (1978) Classification and nomenclature of volcanic rocks, lamprophyrs, carbonatites and mellilitic rocks. Recommendations and suggestions. *N Jb Mineral Abh* 134:1–14
- Streckeisen A (1980) Classification and nomenclature of igneous rocks. *Geol Rundschau* 69:194–207
- Sousa LMA (2010) Evaluation of joints in granitic outcrops for dimension stone exploitation. *Q J Eng Geol Hydrogeol* 43:85–94



- Terezopoulos N (2004) The challenge for European ornamental stones. Proceedings of the 1st OSNET Workshop. [http://www.osnet.ntua.gr/Sectors/01\\_Quarrying/Publications/The\\_challenge\\_for\\_European\\_Ornamental\\_Stones.pdf](http://www.osnet.ntua.gr/Sectors/01_Quarrying/Publications/The_challenge_for_European_Ornamental_Stones.pdf). Accessed 20 July 2010
- Tomio P, Filippi F (1996) *Das Porphy Handbuch*. e.s.Po, Albiano Trento
- Török Á (2002) Oolitic limestone in polluted atmospheric environment in Budapest: weathering phenomena and alterations in physical properties. In: Siegesmund S, Weiss T, Vollbrecht A (eds) *Natural stones, weathering phenomena, conservation strategies and case studies*. Geological Society of London Special Publication 205, London, pp 363–379
- Török Á (2004) Leithakalk-type limestones in Hungary: an overview of lithologies and weathering features. In: Prikryl R, Siegel P (eds) *Architectural and sculptural stone in cultural landscape*. The Karolinum Press, Prague, pp 89–93
- Török Á (2006) Influence of fabric on the physical properties of limestones. In: Kourkoulis SK (ed) *Fracture and failure of natural building stones*. Springer, Dordrecht, pp 487–495
- Török A, Licha T, Simon K, Siegesmund S (2010) Urban and rural limestone weathering; the contribution of dust to black crust formation. *Environ Earth Sci*. doi:[10.1007/s12665-010-0737-6](https://doi.org/10.1007/s12665-010-0737-6)
- Tucker ME, Wright JP (1990) *Carbonate sedimentology*. Blackwell Scientific Publication, Oxford
- Vollbrecht A, Dürrast H, Weber K (1993) Open microcracks: indicators for in-situ stress directions. *KTB-Report* 93–2:227–230
- Vollbrecht A, Rust S, Weber K (1991) Development of microcracks in granites during cooling and uplift: examples from the Variscan basement in NE Bavaria (FRG). *J Struct Geol* 13(7):787–799
- Wagner W (2007) Grundlagen für die Prüfung von Dach- und Wandschiefern. *Z dtsh Ges Geowiss* 158/4:785–805
- Wedepohl KH (1969) Composition and abundance of common igneous rocks. In: Wedepohl KH (ed) *Handbook of geochemistry*. Springer, Berlin
- Wichert J (2007) *Schieferlexikon*. <http://www.schieferlexikon.de/htm>. Accessed 20 July 2010
- Wilson JL (1975) *Carbonate facies in geologic history*. Springer, Berlin
- Winkler H, von Platen H (1961a) Experimentelle gesteinsmetamorphose IV. *Geochim Cosmochim Acta* 24:48–69
- Winkler H, von Platen H (1961b) Experimentelle gesteinsmetamorphose V. *Geochim Cosmochim Acta* 24:250–259
- Winkler HGF (1967) *Die Genese der metamorphen Gesteine*. Springer, Berlin
- Yardley BWD (1997) *Einführung in die Petrologie metamorpher Gesteine*. Ferdinand Enke Verlag, Stuttgart

# Chapter 3

## Physical and Mechanical Properties of Rocks

Siegfried Siegesmund and Helmut Dürrast

**Abstract** Since early antiquity, dimension stones have been used as building materials due to their natural beauty and availability, and the diversity of their applications has been increasing ever since. As any other building material, dimension stones today have to fulfill the physical and technical requirements demanded by architects. This chapter focuses on the physical and mechanical properties of dimension stones, while emphasizing that stones are an old, yet still modern, building material. Among the parameters discussed here are water absorption, thermal conductivity and expansion, hygric and hydric properties, strength, abrasion, the more modern aspect of breaking load at the dowel hole, and ultrasonic wave velocities. Extensive data sets and a variety of case studies reveal relationships between the physical properties and the internal fabric elements of the dimension stones, such as sedimentary layering, metamorphic foliation, pores, and microcracks. In addition, these fabric elements are often responsible for the weathering behavior of the dimension stones, which not only affects the heritage but also the safety of modern buildings. This is illustrated through laboratory experiments and case studies.

---

S. Siegesmund (✉)  
Geoscience Centre, University of Göttingen, Goldschmidtstrasse 3, 37077 Göttingen,  
Germany  
e-mail: ssieges@gwdg.de

H. Dürrast  
Department of Physics, Prince of Songkla University, Kanjanavanich Road 15, HatYai,  
Thailand

### 3.1 Density, Mean Atomic Weight and Cation Packing Index

The density ( $\rho$ ) of a material can be separated into the matrix density ( $\rho_{\text{Matrix}}$ ) and the bulk density ( $\rho_{\text{Bulk}}$ ). Whereas the value of the bulk density is stated with respect to the porosity of a material, the matrix density only depends on the components and does not take the porosity into account. Therefore, the matrix density provides evidence about the composition of a material. For example, calcitic and dolomitic marbles can be differentiated by the matrix density, as the main constituents, calcite and dolomite, have significantly different mineral densities, 2.710 and 2.866 g/cm<sup>3</sup>.

There are different methods to determine the bulk and matrix density for rock samples. A simple and often promising method is the measurement of the buoyancy acting on a sample immersed in water, the Archimedes method (e.g. Monicard 1980). Cubic samples with an edge length of 60–100 mm are preferable. The parameters to determine the density here are (i) the weight of the sample under dry conditions ( $m_{\text{dry}}$ ), (ii) the weight under fully saturated conditions ( $m_{\text{sat}}$ ), and (iii) the sample weight with the sample fully submerged in water ( $m_{\text{sub}}$ ). For the last two values, demineralized water is used for the saturation of the pore space. Fully saturated conditions are achieved through the excavation of the air in the pores before saturation. The density of the water needs to be known or should be determined. The matrix density can then be determined with the following equation:

$$\rho_{\text{Matrix}} = \rho_{\text{Water}} \cdot (m_{\text{dry}}/m_{\text{dry}} - m_{\text{sub}}) \quad (3.1)$$

The bulk density can then be determined as follows:

$$\rho_{\text{Bulk}} = \rho_{\text{Water}} \cdot (m_{\text{dry}}/m_{\text{sat}} - m_{\text{sub}}) \quad (3.2)$$

This method does not consider the closed pore space that cannot be accessed during the saturation process. As a result, the weight values for the fully saturated and fully submerged states tend to be lower, and therefore, so are the values of the matrix density.

The bulk density values for representative plutonic rocks range between 2.55 and 3.26 g/cm<sup>3</sup> with only a few exceptions (Table 3.1, Fig. 3.1). A further analysis of the box plot reveals that a separation into two groups is possible. Generally, if the central segments of a box plot are not overlapping, the related distributions are significantly different at a 5 % level (Popp 1994). Therefore, all subgroups, except the gabbro/diorite group, can be statistically combined. However, it is clear that the bulk density of the highly compacted rocks mainly depends on the mineralogy.

This can be seen in the comparison between the rock types Kösseine Granite (see Table 3.1) and the Ban Tak Granite (Strohmeyer 2003; Hoffmann and Siegesmund 2007; see Table 3.1). The relatively high bulk density of the Thai variety is the result of the mineral composition—here, a higher amphibole content

**Table 3.1** Modal analysis (vol%), densities, mean atomic weights (M), and cation packing index (K-values) for various dimension stones with commercial name, country of origin, and rock type given (Strohmeyer 2003; Ruedrich and Siegesmund 2007; Hoffmann 2008; Mosch 2009; Morales 2011; and unpublished data)

Commercial name	Country of origin	Rock type	Modal analysis (vol.%)	Matrix density (g/cm <sup>3</sup> )	Bulk density (g/cm <sup>3</sup> )	Mean atomic weight	K-value
Ben Tak Black	Thailand	Granite	6.6qz, 6.6mikr, 40plg, 8.8bio, 24hbl, 8ser, 6chl, acc	2.66	2.64	21.97	5.08
Muang Tak Orange 1	Thailand	Granite	30qz, 34mikr, 27plg, 6ser, 2chl, acc	2.62	2.60	20.90	4.59
Kösseine	Germany	Granite	33qz, 26kspar, 29plg, 10bio, 1chl	2.68	2.67	20.77	4.71
Antrona	Italy	Granite	33qz, 24kspar, 24plg, 15mus, 3bio, acc	2.67	2.65	20.86	4.70
Rojo Dragon	Argentina	Granite	32plg, 27.5mikr, 26.6qz, 13.9phyl	2.63	2.62	20.97	4.72
Padang	China	Granodiorite	19qz, 10kspar, 51plg, 11bio, 7cpx, 2mag, acc	2.80	2.80	20.95	4.98
Ben Tak Blue	Thailand	Quartz-monzonite	16qz, 38mikr, 32plg, 3bio, 2hbl, 2chl, 6ser, acc	2.66	2.64	21.20	4.63
Salmon Red	Uruguay	Syenite	13qz, 53plg, 32mikr, 1hbl, 1chl	2.63	2.62	21.01	5.20
Artigas	Uruguay	Syenite	1qz, 14kspar, 20mikr, 46plg, 1hbl, acc	2.67	2.66	21.34	4.93
Nero Absoluto	Uruguay	Dolerite	15qz, 8kspar, 42plg, 20px, 6hbl, 2ilm, 5bio, acc	2.99	2.99	22.20	5.25
Anzola	Italy	Gabbro	35plg, 44hbl, 16opx, 5cpx	3.06	3.05	21.77	5.59
Nero Impala	South Africa	Gabbro-norite	74plg, 13cpx, 12opx, acc	2.92	2.92	20.69	5.28
Negro Riojano	Argentina	Gabbro	51.4plg, 18.6hbl, 5.2phlo, 4.5bio, 0.8chl	2.91	2.91	21.66	5.07
Balmuccia	Italy	Peridotite	59ol, 26opx, 13cpx, 2spi	3.34	3.34	20.28	6.61
Löbejün	Germany	Rhyolite	27qz, 40kspar, 27plg, 5bio, acc	2.64	2.57	21.68	4.66
Stardust Grey	Argentina	Rhyolite		2.54	2.53	21.51	

(continued)

Table 3.1 (continued)

Commercial name	Country of origin	Rock type	Modal analysis (vol.%)	Matrix density (g/cm <sup>3</sup> )	Bulk density (g/cm <sup>3</sup> )	Mean atomic weight	K-value
Monte Merlo	Italy	Trachyte	53kspar, 15plg, 8qz, 8hbl, 8bio, 7pyr, 4cal	2.53	2.39	21.38	4.92
Drachenfels	Germany	Trachyte	49kspar, 20plg, 9qz, 7hbl, 7bio, 4pyr, 4cal	2.66	2.30	21.67	4.80
Weibern	Germany	Phonolite tuff	30neph, 25leu, 23kspar, 12nos, 9px, acc	2.56	1.43	22.31	
Rochlitz	Germany	Rhyolite tuff	63.9qz, 33.6phyl, 2.5haem	2.66	1.91	19.72	4.66
Phanom Sarakham	Thailand	Gneiss	32qz, 22mikr, 34plg, 7bio, 6ser, acc	2.67	2.65	20.82	4.78
Azul Tango	Argentina	Gneiss	28.3qz, 27.1cord, 24plg, 16.5grt, 1.8ilm, 1.7chl, 0.7phyl	2.96	2.96	21.63	5.34
Calanca	Italy	Gneiss	34qz, 9kspar, 38plg, 18bio, 1chl	2.73	2.71	20.76	4.80
Verde Andeer	Italy	Gneiss	34qz, 19kspar, 21plg, 22mus, 4chl	2.71	2.68	20.94	4.64
Serizzo Monte Rosa	Italy	Gneiss	32qz, 11kspar, 38plg, 4mus, 13bio, 1chl	2.67	2.64	20.81	4.70
Wang Nam Kiew Black	Thailand	Hornblendite	90hbl, 4plg, 4chl, 2 acc	3.17	3.16	22.56	5.57
Franco Veteado	Argentina	Migmatite	46.5qz, 17.5cord, 14.8pla, 14.1bio, 7.1kspar	2.75	2.75	21.12	4.87
Rosa Estremoz	Portugal	Marble	98cal, 2haem	2.72	2.71	20.03	5.44
Carrara	Italy	Marble	96.8cal, 3.2dol			20.04	5.40
Phran Kratai	Thailand	Marble	100cal	2.69	2.68	19.96	5.42
Azul Cielo	Argentina	Marble	100cal	2.73	2.71	19.84	5.42
Azul Imperial	Brazil	Quartzite	87qz, 9mus, 4dum	2.69	2.69	20.31	4.50
Camino Rufo	Uruguay	Slate	32qz, 38dol, 18mus, 2chl, 9ill	2.81	2.81	20.31	4.67
San Luis Slate	Argentina	Slate	30.2qz, 39.3mus, 15.6plg, 14.9chl	2.79	2.79	23.25	4.56

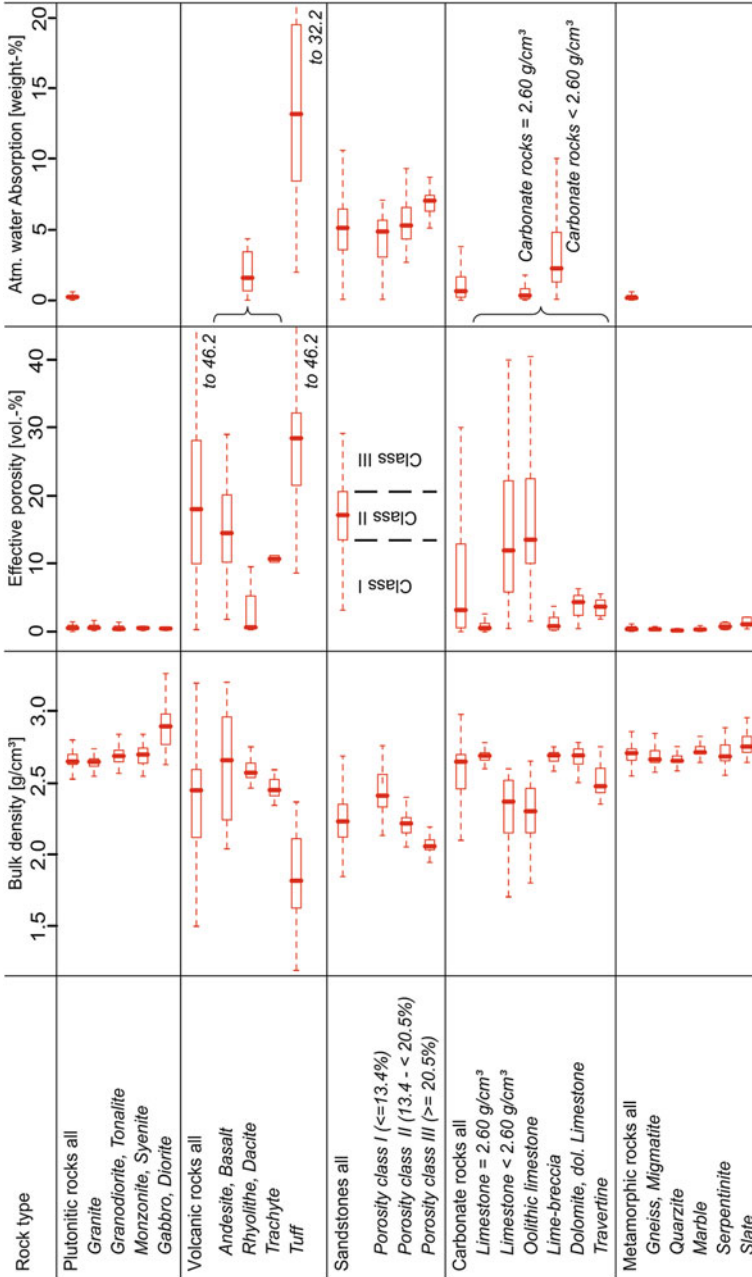
(continued)



Table 3.1 (continued)

Commercial name	Country of origin	Rock type	Modal analysis (vol.%)	Matrix density (g/cm <sup>3</sup> )	Bulk density (g/cm <sup>3</sup> )	Mean atomic weight	K-value
Theuma	Germany	Slate				21.93	
Globegerina	Malta	Limestone	86–99cal, 1–12phyl, 1–8qz, 1kspar	2.63	1.63–1.85	19.97	5.33
Caliza Amarilla	Argentina	Limestone	95.5cal, 4.0qz	2.70	2.39	20.12	5.37
Dolomita Dorada	Argentina	Dolomitic limestone	96dol, 4qz	2.84	2.60	19.16	4.66
Mae Phrik Yellow	Thailand	Limestone	100cal	2.71	2.70	19.95	5.42
Soskut	Hungary	Limestone	82cal, 15qz, 2ser, acc	2.68	2.14	20.14	5.21
Jerusalem	Israel	Limestone	95cal, 3qz, acc	2.68	2.59		5.28
Kuacker	Germany	Limestone		2.75	2.65	19.25	
Thüster	Germany	Limestone	95cal, 5qz	2.68	2.09	20.15	5.37
Bad Langensalza	Germany	Travertine		2.65	2.40	20.64	
Baumberger	Germany	Sandstone-like limestone	55cal, 30qz, 1kspar, 10ill, 2glau, acc	2.68	2.09	20.27	4.91
Anröchte	Germany	Sandstone-like limestone	64cal, 18glau, 17qz, acc	2.74	2.45	20.15	4.87
Bad Bentheim	Germany	Sandstone	98qz, 1rf, acc, kaol	2.65	2.04	20.54	4.42
Schleerither	Germany	Sandstone	80qz, 14rf, 3plg, 2phyl, acc	2.72	2.29	21.50	4.42
Weser	Germany	Sandstone	85qz, 1rf, 19fsp, 2phyl	2.65	2.47	20.93	4.36
Sikhiu Brown	Thailand	Sandstone	93qz, 4kaol, 3ill	2.66	2.38	20.48	4.40
Pakchong Green	Thailand	Sandstone	43qz, 8kspar, 25plg, 16ill, 4chl, 3cal	2.73	2.53	20.93	4.60
Tacuarembó	Uruguay	Sandstone	98qz, 2kspar	2.26	2.03	20.25	4.41

Mineral and rock abbreviations: *acc* accessories, *bio* biotite, *chl* chlorite, *cord* cordierite, *cpx* clinopyroxene, *ctd* chloritoid, *czs* clinozoisite, *diorit* diorite, *dol* dolomite, *dum* dumortierite, *epi* epidote, *glau* glaucinite, *grandior* grandiorite, *grt/lt* garnet, *haem* haematite, *hbl* hornblende, *hyperst* hypersthene, *ill* illite, *ilm* ilmenite, *kaol* kaolinite, *kspar/lf* K-feldspar, *leu* leucite, *metapel* metapelite, *mikr* microcline, *mus/ms* muscovite, *myl* mylonite, *neph* nepheline, *nos* nosean, *ol* olivine, *opx* orthopyroxene, *pend* pendlandite, *phlo* phlogopite, *phyl* phyllite, *plg* plagioclase, *px* pyroxene, *pyr* pyrite, *qz* quartz, *rf* rock fragments, *ser* sericite, *serp* serpentine, *sil* sillimanite, *staur* staurolite, *zoi* zoisite. These abbreviations are used throughout this chapter if not otherwise stated



**Fig. 3.1** Lithology-specific value ranges for bulk density, effective porosity, and water absorption under atmospheric conditions based on a statistical analysis of data from 2,335 dimension stones (Mosch and Siegesmund 2007; Mosch 2009). The *box plots* describe, in each case, the median value, the 25 and 75 %-quartile, and the upper and lower extreme values

of ca. 24 vol.%. The Kösseine Granite, on the other hand, is composed mainly of quartz and feldspar, and additionally, 10 vol.% of biotite. Data from Steindlberger (2004) have shown that volcanic tuff can exhibit a significant range for the matrix density values, from 1.90 to 2.80 g/cm<sup>3</sup>.

In contrast to the plutonic rocks, wherein the bulk density and the matrix density values are often similar due to the very low porosity that can be neglected (see Sect. 3.2), a differentiation between both density values is necessary for the sandstones. The bulk density is significantly affected by the pore space. For a mean porosity of about 15 % and a matrix density of 2.67 g/cm<sup>3</sup>, the bulk density gives a mean value of about 2.27 g/cm<sup>3</sup>. The value for the matrix density (2.67 g/cm<sup>3</sup>) reflects the mineral density of quartz as the main component of sandstones. A clear separation between matrix and bulk density values is also necessary for most of the carbonate rocks, as they can also exhibit significant porosities (see Fig. 3.1; Table 3.1), which is due to the variability in their depositional characteristics and in their mineralogical composition.

The highest median values of the bulk density in the group of sedimentary rocks can be found in the subgroups of dolomite and lime breccias. The limestone group also exhibits a much higher median value, however, with a much larger range and a higher number of outliers. The lowest median values are reported for the subgroup of oolitic limestone, also with a wide range of data, but of uniform distribution. Generally, the values and the distribution of the porosity show a diametrical trend in comparison to the bulk density (see Sect. 3.2), as expected due to the definition of the bulk density.

The group of metamorphic rocks with its subgroups shows no large ranges in the data distribution (see Fig. 3.1, Table 3.1). The highest median value here can be found in the schist group with 2.75 g/cm<sup>3</sup>. For the group of marbles (2.71 g/cm<sup>3</sup>), gneisses/migmatites (2.67 g/cm<sup>3</sup>), and quartzites (2.65 g/cm<sup>3</sup>), the median value of the bulk density reflects the mineral-specific or matrix density of the main mineral phases and, by this, indicate an almost zero percent porosity (see Table 3.1). Since quartzite and many marbles can be assumed to be more or less monomineralic rocks, the matrix density is related to quartz and calcite, respectively. The gneisses can be better compared to the plutonic rocks, as in both groups the main mineral phases are feldspar and quartz. The subgroup serpentinite has a median value of 2.68 g/cm<sup>3</sup> combined with a larger data range. Both can be related to the occurrence of minerals with higher matrix density values remaining from the earlier peridotite stage.

After studying the density and chemical composition (SiO<sub>2</sub>-content), Popp (1994) was able to separate three major rock groups (Fig. 3.2): felsic with  $\rho < 2.8 \text{ g/cm}^3$  and SiO<sub>2</sub>-content > 70 %, intermediate with  $2.8 \text{ g/cm}^3 < \rho < 2.9 \text{ g/cm}^3$  and 55 % < SiO<sub>2</sub>-content < 70 %, and the mafic group with  $\rho > 2.9 \text{ g/cm}^3$  and SiO<sub>2</sub>-content < 55 %.

Classifications like these or others are of importance as several authors have proposed similar empirical relationships in order to estimate certain geotechnical rock properties from the density values alone (Fig. 3.3). Examples are the empirically derived ultrasonic wave velocity-density relationships (Wollard curve,

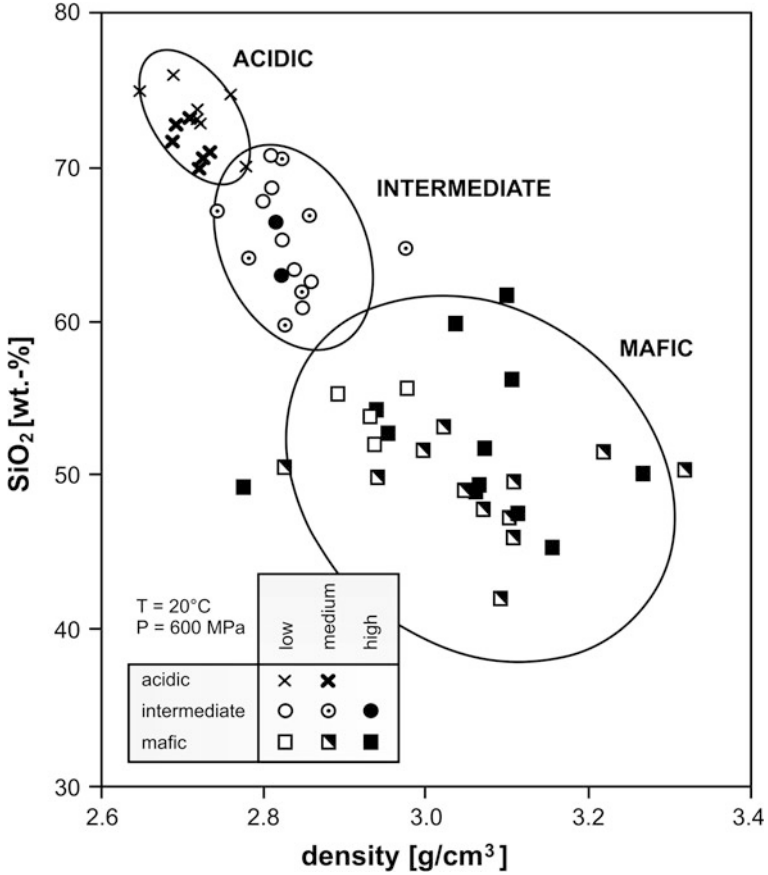


**Fig. 3.2** Correlation of density with the SiO<sub>2</sub> content to differentiate between acid, intermediate, and mafic rocks (after Popp 1994)

Wollard 1959; Nafe-Drake-curve, Nafe and Drake 1963), which attempts to estimate the velocities from the densities and vice versa (see Sects. 3.2 and 3.7).

Birch (1961) developed another velocity-density relationship as follows:

$$V_p = a(M) \cdot b \cdot \rho \tag{3.3}$$

where *a* is a function of the mean atomic weight (*M*), *b* a constant, and  $\rho$  the density. The mean atomic weight can be determined from the chemical analysis of the main element oxides as follows:

$$M = (\sum x_i / M_i) - 1 \tag{3.4}$$

where *M<sub>i</sub>* is the mean atomic weight of the *i*-th oxide of the rock sample, and *x<sub>i</sub>* is the weight percentage of the *i*-th oxide. In general, there is a good correlation between the ultrasonic velocities and the density (Fig. 3.4). The observation that

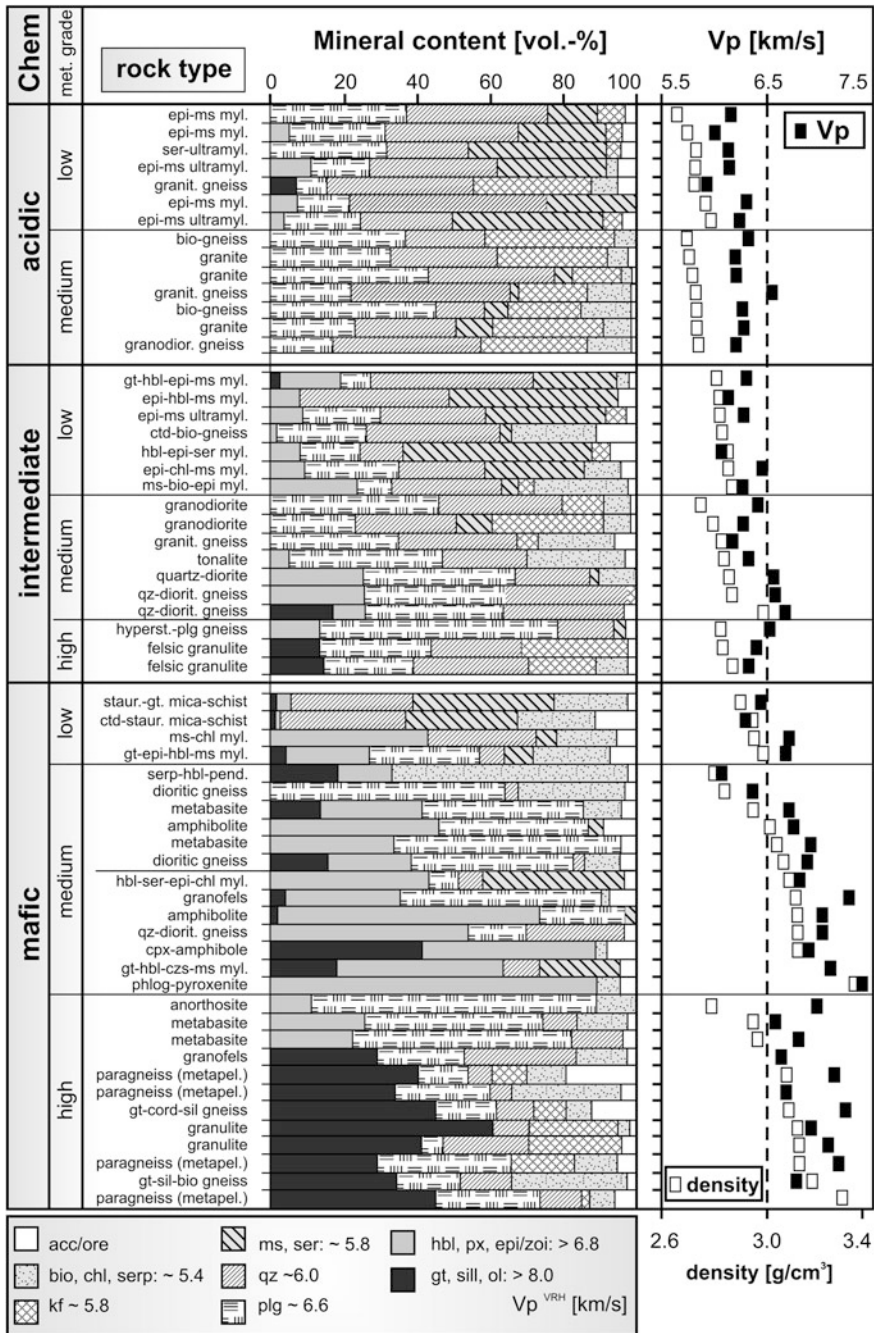


**Fig. 3.3** Correlation of the volume percent of minerals (*left*) with the variation in density ( $g/cm^3$ ) and ultrasonic compressional wave velocity ( $V_p$  in  $km/s$ ; at 600 MPa, 20 °C) (*right*). The samples in each group are arranged based on increasing density. In addition, the Voigt-Reuss-Hill ( $VRH$ ) mean  $V_p$ -values of minerals are given (*bottom*). The influence of the mineralogical composition is clearly visible in the density as well as in the P-wave velocity (after Popp 1994); for mineral and rock abbreviations, see Table 3.1



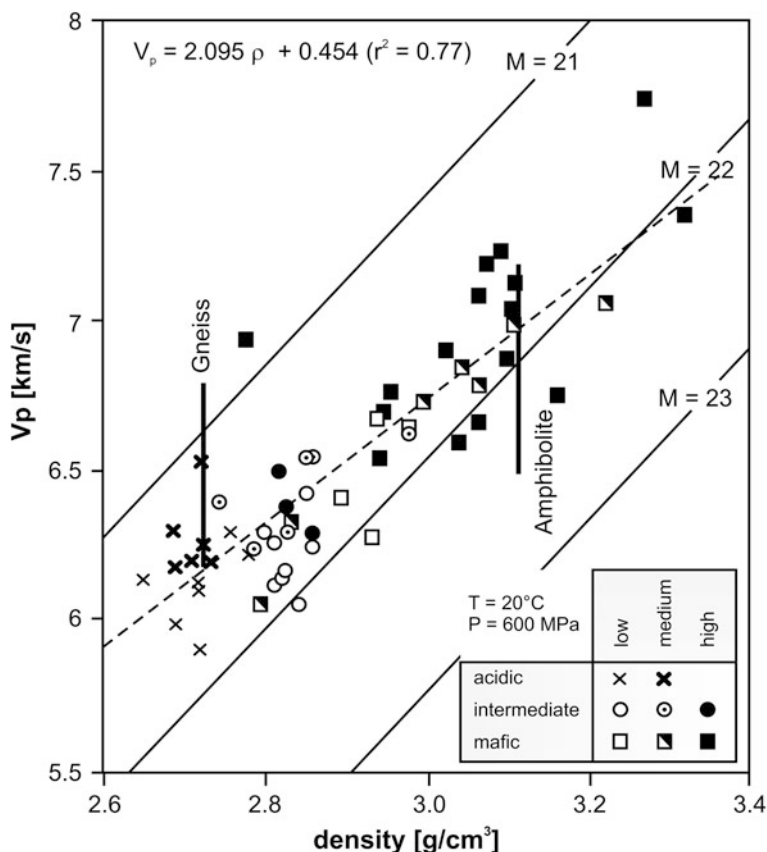


**Fig. 3.4** Velocity-density relationships for  $V_p$  (600 MPa, 20 °C), after Popp (1994). The lines of constant mean atomic weight ( $M$ ) originate from Birch (1961) and Christensen (1968). Additionally shown are the extreme values of the experimentally determined P-wave velocities for a gneiss and an amphibolite sample

velocity-density relationships are more or less parallel to lines of constant mean atomic weight values is well known in the literature, for example, Christensen (1968). The mean atomic weights in Table 3.1 range from 19.70 to 22.31, with the highest values being calculated for the basic/ultrabasic rocks. For these rocks, an increase in the fayalite content in the olivine minerals of 10–25 % comes with a decrease in the seismic velocities of 0.25 km/s and a density increase of 0.2 g/cm<sup>3</sup>. The mean atomic weight, thereby, varies between 20.10 for forsterite (Mg<sub>2</sub>SiO<sub>4</sub>) and 29.70 for fayalite (Fe<sub>2</sub>SiO<sub>4</sub>). The large fluctuation in the mean atomic weight of the olivine varieties comes from the lower atomic weight of the Mg in comparison to the Fe. Higher mean atomic weight values, greater than 21.50, can be related to higher contents of Ca, Ti, and Fe, mainly found in hornblende, garnet, pyroxene, and epidote minerals (see Table 3.1). In general, seismic velocities, densities, and mean atomic weight values can be correlated with each other.

A more promising relationship than using the mean atomic weights was introduced by Buntebarth (1982) and Rybach and Buntebarth (1982) with the use of the cation packing index or k-value, with  $k = (\text{the number of cations per mole}) / (\text{Avogadro's number} \cdot \text{molar volume})$ . The k-value for the whole rock can be determined with the following equation :

$$k = \sum x_i \cdot k_i \quad (3.5)$$

where  $k_i$  is the k-value of the  $i$ -th mineral phase, and  $x_i$  is the amount of the  $i$ -th mineral in the rock determined by modal analysis. However, the empirically derived correlation of Rybach and Buntebarth (1982) with a more or less linear relationship between the P-wave velocities and the densities of various rocks could not be verified by Kern and Siegesmund (1989). On the other hand, the k-value correlates much better with the density values than the mean atomic weight. For further verification, sufficient data sets are needed for statistical analyses.

Ceryan et al. (2008) were able to show that the k-value of granitic rocks decreases with increased weathering. This correlation reflects the observation that, during the weathering process of granitic rocks, for example, feldspar minerals (plagioclase k-values  $4.97\text{--}4.99 \times 10^{-2} \text{ mol/cm}^3$ ) disintegrate and decompose into clay minerals (k-values  $3.997\text{--}4.52 \times 10^{-2} \text{ mol/cm}^3$ ), and biotite ( $4.656 \times 10^{-2} \text{ mol/cm}^3$ ) and hornblende ( $5.309 \times 10^{-2} \text{ mol/cm}^3$ ) change into chlorite ( $4.10 \times 10^{-2} \text{ mol/cm}^3$ ), Fe-oxides, and clay minerals. Since the main cause of the weathering is leaching, the densities and the k-values of the resulting minerals, the weathering products, are lower than those of the original ones. Based on their results, Ceryan et al. (2008) proposed that the k-value has the potential for being applied in investigating the engineering lifetime of building stones.

## 3.2 Porosity

The porosity of a rock is defined by the ratio of the pore volume (e.g. pores, open cracks) to the volume of the whole rock. It can be calculated by applying the same variables used for the determination of the bulk and matrix density. Two different types of porosity can be distinguished: the effective porosity, often called “accessible porosity”, and the total porosity. The first one comprises all the pore spaces in a rock that fluids and gases can access, whereas the latter one includes all pores, even the isolated ones that cannot be accessed (Fig. 3.5). For weathering processes, the effective porosity is of primary interest (e.g. Weiss 1992). For rocks with relatively large pore space values, the effective porosity is assumed to be the dominating type (e.g. Fitzner and Basten 1994). Based on the definition of both porosity types, the effective porosity is either equal to or smaller than the total porosity; however, the difference might be small. Porosity has a direct and indirect effect on most of the physical properties of rocks and is, therefore, considered the most important rock parameter. Increasing porosity has an unfavorable influence

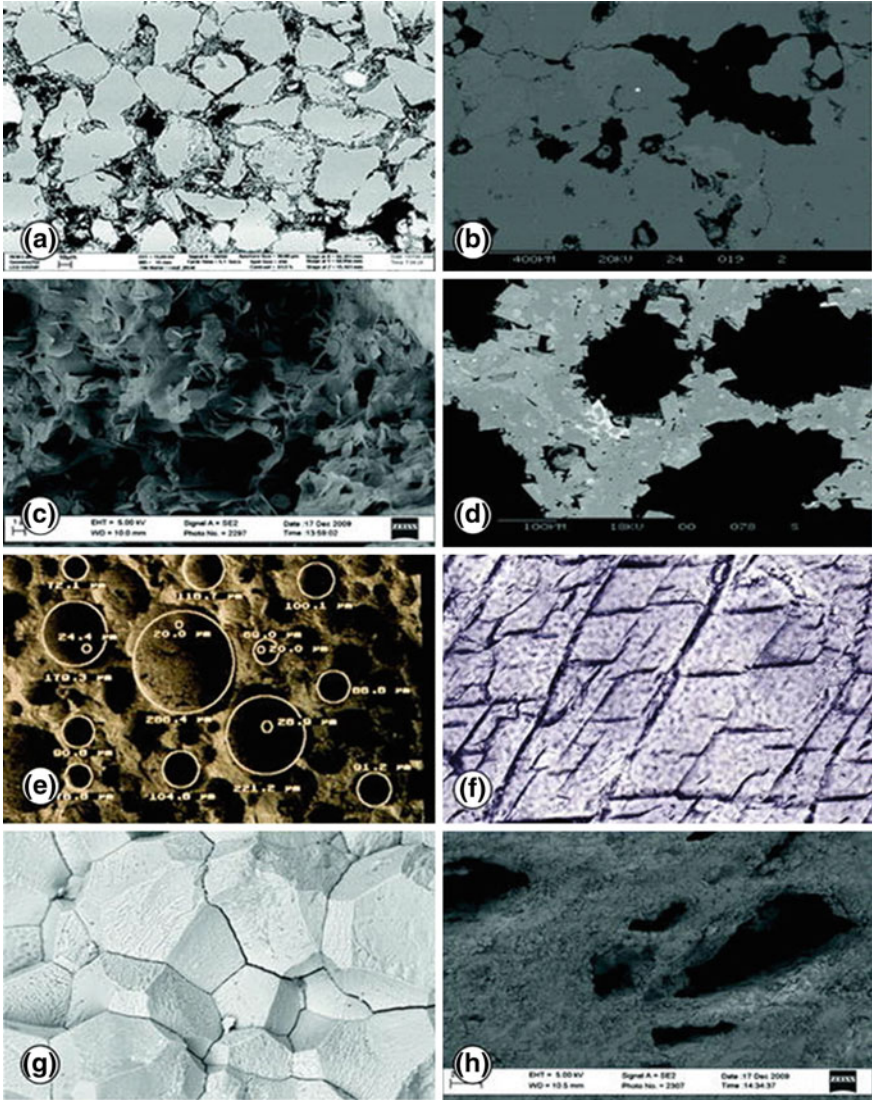


**Fig. 3.5** SEM images showing rocks with their different pore space and porosity: **a** and **b** Sandstone with open pores (*black*) interconnected by open cracks **c** Clay mineral-rich sandstone with very heterogeneous pore sizes ranging from micro to macropores **d** Dolomitic limestone with nearly *spherical pore* shapes and dolomite crystals **e** Volcanic tuff with intraparticle pores of different sizes (Figure by B. Fitzner) **f** Open cleavage cracks and transgranular cracks in hornblende minerals also known as platy pores **g** Open grain boundaries in weathered marbles, and **h** Pores in travertine with a heterogeneous pore size distribution ranging up to several centimeters in size

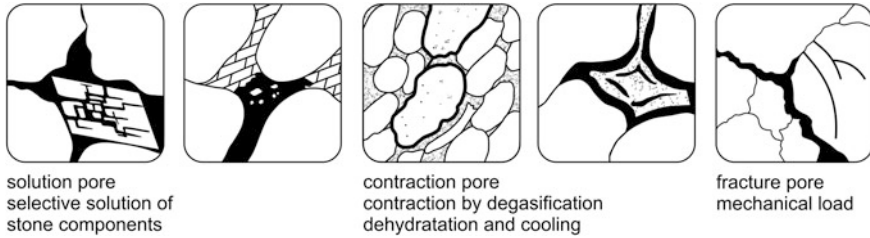


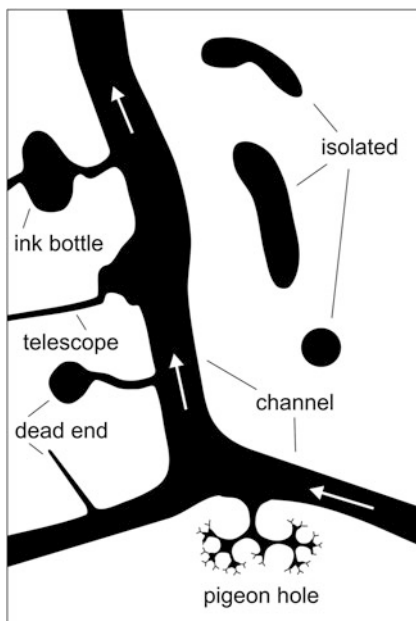
**Fig. 3.6** Pore space types (after Fitzner and Basten 1994)

on weathering characteristics (e.g. Hirschwald 1912; Fitzner 1970; Fitzner and Snehlage 1983; Poschlod 1990; Viles et al. 1997; Ruedrich et al. 2005b, 2010a). All “hollow spaces or cavities” in a rock can be classified under the term “pores”. For the description of the pore space, different classification schemes were developed depending mainly on the application (see e.g. Fitzner and Basten 1994).

- (i) The pore space classification under petrogenetic aspects distinguishes between the primary porosity as the result of sedimentary processes and the secondary porosity as the result of post-sedimentary or diagenetic processes including all processes after the primary sedimentation. The so-called “weathering porosity” of dimension stones is, therefore, a special case of the secondary porosity.
- (ii) Another classification scheme is based on the separation of ideal single pore types by applying pore geometry and the pore genesis—for example, spherical pores, platy pores, cylindrical pores, interstitial pores (near the narrowing area of the grain-to-grain contact), crack pores, dissolution pores, and shrinking pores (see Fig. 3.6).
- (iii) A different pore space classification uses the location of the pore in relation to the solid particles (grains, minerals). Pores between the solid particles comprise “interparticle porosity”, whereas pores in a solid rock particle comprise “intraparticle porosity” or “intercrystalline porosity” at the crystal lattice scale (Fig. 3.5).
- (iv) Another classification scheme applies the criterion of how well fluids or gases can penetrate through the pore system of a rock. Good transmission is provided through a system of interconnected pores with channel pores, ink-bottle pores, and telescope pores, a dead-end transmission by dead end pores and pigeon hole pores. No transmission occurs with isolated pores (see Fig. 3.7).
- (v) Without using other attributes, the pore-size alone is often used for the classification of pores.

Using the effective porosity value, von Moos and De Quervain (1948) developed a classification scheme for rocks, with <1 % compact, 1–2.5 % a few pores, 2.5–5 % slightly porous, 5–10 % significantly porous, 10–20 % many pores, and more than 20 % means a significantly high amount of pore space (Table 3.2).

**Fig. 3.7** Pore space classification using the transmission or penetration criterion (after Fitzner and Basten 1994)



The size of a pore is given by its pore radius, which is determined from the radius of a cylinder representing the ideal form of a pore. However, natural pores usually exhibit a more complex geometrical form than a cylinder. Therefore, the determination of the pore size only reflects the smallest diameter or radius of a pore, which is usually the throat (or entry) of a pore or crack, and thus, it defines the pore-throat radius. Various pore size classifications have been published over time, with some shown in Table 3.2, mainly dividing the pore space into micro-, meso-, and macropores. However, it is quite difficult to get a consistent classification scheme, as the boundaries between the classes vary.

The method for the determination of the pore (throat) radius distribution (see Brakel et al. 1981) is based on the Washburn equation (Washburn 1921), which is derived by combining Poiseuille's Law for viscous flow and the Young–Laplace Equation for capillarity:

$$r_p = -2\gamma \cos \theta / P, \quad (3.6)$$

with  $r_p$  as the pore-throat radius of a capillary pore,  $\gamma$  the surface tension at the liquid interface,  $\theta$  the liquid–solid contact angle, and  $P$  the applied pressure.

The equation is based on the principle that every capillary pore radius is characterized by a certain pressure value that is needed to push a fluid into the pore (Doveton 1987). This relationship holds only for non-wetting fluids with a contact angle of  $\theta > 90^\circ$ , like mercury, which is a non-wetting fluid for almost all substances. Therefore, laboratory work mainly uses the mercury (intrusion) porosimetry technique that allows pore-radius determination for the whole range of possible radii found in rocks. This method is based on pressure-related mercury



**Table 3.2** Comparison of some often used pore size classification schemes exhibiting variations in the ranges according to different authors

	Micropores ( $\mu\text{m}$ )	Mesopores ( $\mu\text{m}$ )	Macropores ( $\mu\text{m}$ )	Large pores ( $\mu\text{m}$ )
De Quervain (1967)	<5	5–200 (fine pores)	200–2,000 (coarse pores)	>2,000
Dubinin (1979)	0.003 to 0.0032–0.0012 to 0.0014	0.2 to 0.4–0.003 to 0.0032	<0.2–0.4	
IUPAC (Gregg and Sing 1982)	<0.002	0.002–0.05	>0.05	
Klopper (1985)	<0.1	0.1–1,000 (capillary pores)	>1,000	
DIN 66131 (1993)	<0.002	0.002–0.05	>0.05	
Kodikara et al. (1999)	1–30		10–1,000	

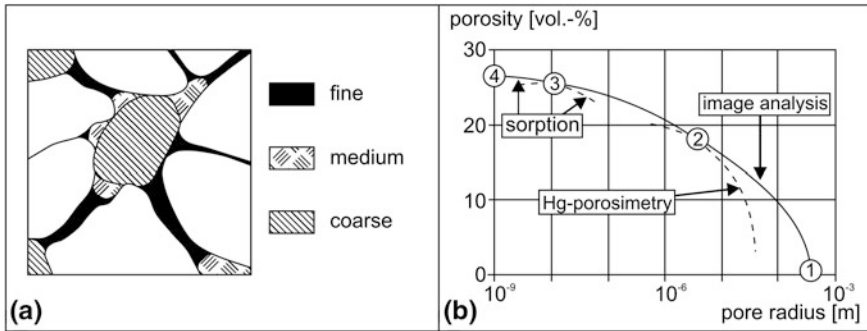
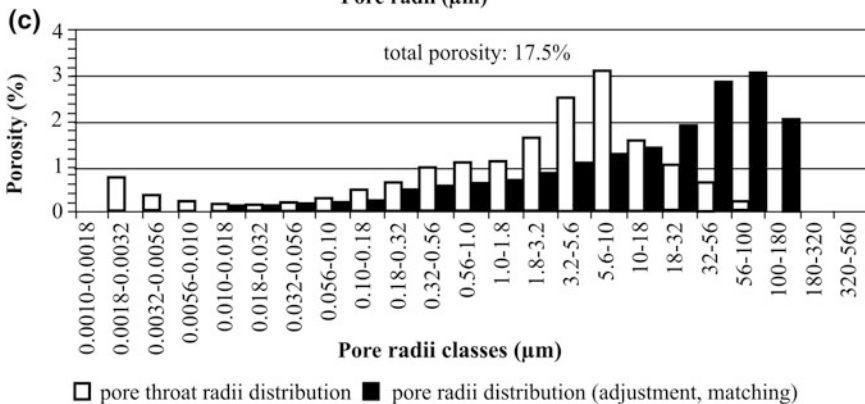
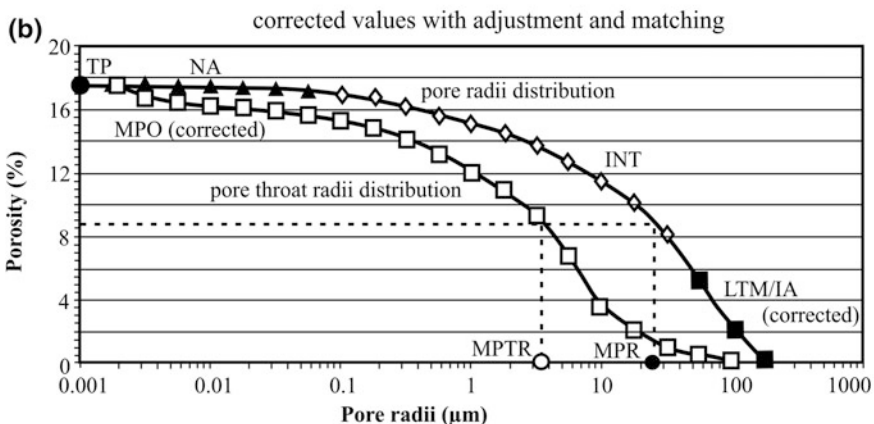
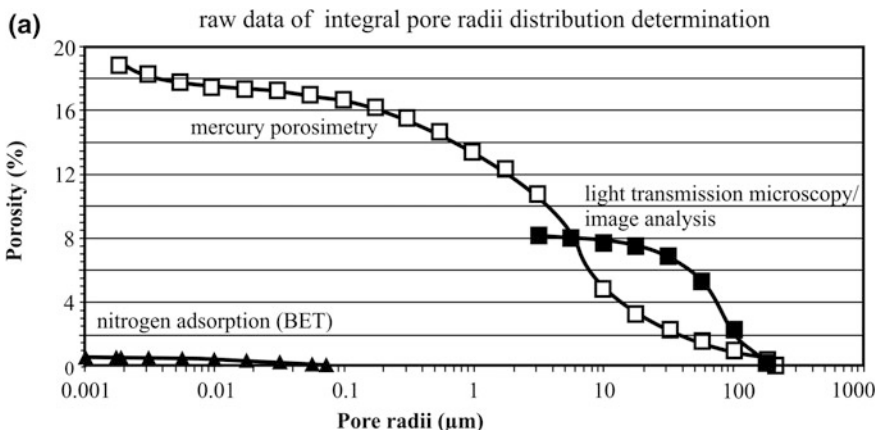


**Fig. 3.8** Pore space in geo-materials: **a** Schematic diagram of the different pore sizes **b** Scale dependency of different methods for pore space characterization (after Meng 1993)

intrusion and extrusion and can be realized with commercial equipment, which allow the measurement of porosity and pore-size-radius distribution values in a range from 0.0020 to 200  $\mu\text{m}$ .

Fitzner and Kownatzki (1991), Fitzner and Basten (1994), Meng (1993), and Heinrichs (2005) showed that with a combination of different methods, a quite realistic image of the pore system can be achieved (e.g. Figs. 3.8 and 3.9). Between ca. 0.001 and 0.1  $\mu\text{m}$ , the pore-radius distribution and pore volume can be determined from the nitrogen sorption method based on the Brunauer-Emmet-Teller (BET) theory (see Brunauer et al. 1938). A pore-radius distribution between 0.1 and 4.0  $\mu\text{m}$  can only be reliably determined with mercury porosimetry, whereas for pores with a radius >4.0  $\mu\text{m}$ , the macropore class, a combination of mercury porosimetry and image analysis based on thin sections has been more successful. The determination of the total porosity can be achieved with different



◀ **Fig. 3.9** Porosity values based on image analysis, mercury porosimetry, and the nitrogen adsorption BET method for the highly porous Petra Sandstone. **a** Raw data **b** Corrected values with adjustment and matching, and **c** Differential distribution of the pore-radius distribution and pore-throat distribution after data correction (after Heinrichs 2005). *NA* porosity part related to the lower radius classes/measurement data from the nitrogen adsorption method (BET), *LTM/IA* (corrected) porosity part related to the upper radius classes/corrected measurement data from light transmission microscopy/image analysis, *INT* interpolated porosity parts of the middle radius classes, *MPO (corrected)* corrected measurement data of mercury porosimetry = corrected pore-throat-radius distribution, *TP* total porosity/data adjustment and matching, *MPTR* mean pore-throat radius/corrected values from mercury porosimetry, *MPR* mean pore radius/data adjustment and matching

methods, the buoyancy method based on the Archimedes principle being a reasonable and efficient one (see Sect. 3.1).

For sandstones (see also Sect. 2.11), for example, the pore space or porosity is developed during sedimentary deposition with the packing density of the grains as one of the main parameters (Tucker 1985). The packing density is mainly influenced by the grain size, the grain shape, and the grain sorting as the result of the depositional environment. During later diagenetic processes, the primary porosity will change through compaction and water loss, through pressure solution at grain boundaries, and through cementation. The alteration of existing minerals and the precipitation of new minerals lead to a progressive decrease in porosity with deeper burial. However, local fluids in the subsurface can also dissolve primary or even secondary minerals, resulting in higher porosity values.

The porosity in each of the main sedimentary rock types can vary significantly (Fig. 3.1 or Table 3.3). Using 360 sandstone varieties, Mosch and Siegesmund (2007) have shown that the porosity values range from 0.1 to 29.0 % (Fig. 3.10). The reason for this lies in the variability of geological processes and variations in the depositional environment leading to the same rock, but to different rock types. For example, beach and barren sands usually exhibit a good sorting with a narrow grain-size distribution, whereas river and delta sands show a much more heterogeneous distribution of the grain sizes, as well as a diversity in the mineralogical composition.

The observed pore-size distributions of sandstones can be classified, according to Ruedrich and Siegesmund (2006), into three types (Fig. 3.10): (A) unimodal distribution over a narrow pore-size range, (B) uneven distribution, and (C) bimodal distribution or a plot showing one sub-maximum. For the capillarity and fluid transport in the pore space, the pores with a radius in the range of <1 mm to ca. 0.1  $\mu\text{m}$  are of great significance. In pores smaller than those, the micropores, the moisture transport is done by surface and solution diffusion processes. Micropores are important for questions related to the drying of rocks and for the penetration of substances with a defined molecule size for conservation and impregnation. In the macropores, however, the water loses its interconnectivity and, thus, can no longer move freely.

During salt crystallization experiments, Fitzner and Snethlage (1983); Fitzner and Basten (1994); and Ruedrich et al. (2005b, 2007) were able to clearly show

**Table 3.3** Porosity, mean pore radius, water uptake in atmospheric conditions, degree of saturation, and vapor diffusion resistance factor for various dimension stones with commercial name, country of origin, and rock type given (Strohmeyer 2003; Ruedrich and Siegesmund 2007; Hoffmann 2008; Mosch 2009; Morales 2011, and unpublished data)

Commercial name	Country of origin	Rock type	Porosity (%)	Mean pore radius ( $\mu\text{m}$ )	Water uptake at atmospheric pressure (weight%)	Degree of saturation (%)	Vapor diffusion resistance factor (-)
Ben Tak White	Thailand	Granite	0.59	0.046		0.83	2,815.8 (5.2)
Muang Tak Orange I	Thailand	Granite	0.76	0.054		0.73	3,869.6 (10.2)
Kösseine	Germany	Granite	0.11	0.02	0.003		
Antrona	Italy	Granite	1.03	0.09	0.19		
Rojo Dragon	Argentina	Granite	0.45	0.088		0.81	1,416.1 (18.6)
Padang	China	Granodiorite	0.25	0.03	0.08		
Ben Tak Blue	Thailand	Quartz-monzonite	0.91	0.065		0.60	3,132.6 (51.1)
Salmon Red	Uruguay	Syenite	0.60	0.042			
Artigas	Uruguay	Syenite	0.72	0.077			
Nero Assolutto	Uruguay	Dolerite	0.05	0.097			
Anzola	Italy	Gabbro	0.31	0.10	0.02		
Nero Impala	South Africa	Gabbro-norite	0.04				
Negro Riojano	Argentina	Gabbro	0.04	0.007		0.53	2,321–5,927
Balmuccia	Italy	Peridotite	0.03				
Löbejün	Germany	Rhyolite	2.30		1.44	0.77	
Stardust Grey	Argentina	Rhyolite	0.60	0.010		0.85	1,187.0 (69.1)
Monte Merlo	Italy	Trachyte	11.76				
Drachenfels	Germany	Trachyte	11.92				
Weibern	Germany	Phonolite tuff	43.08		16.45		
Rochlitz	Germany	Rhyolite tuff	28.27	0.11–0.30	3.54	0.77	8.8–18.2
Eger-Demjen	Hungary	Dacite tuff	34.76		8.54		
Phanom Sarakhram Grey	Thailand	Gneiss	0.71	0.036		0.81	3,132.6 (51.1)

(continued)

Table 3.3 (continued)

Commercial name	Country of origin	Rock type	Porosity (%)	Mean pore radius ( $\mu\text{m}$ )	Water uptake at atmospheric pressure (weight%)	Degree of saturation (%)	Vapor diffusion resistance factor (-)
Azul Tango	Argentina	Gneiss	0.16	0.097		0.95	1,442.9 (15.4)
Calanca	Italy	Gneiss	0.73	0.16			
Verde Andeer	Italy	Gneiss	0.89	0.08			
Serizzo Monte Rosa	Italy	Gneiss	1.01	0.16			
Wang Nam Kiew Black	Thailand	Hornblende	0.55	0.163		0.83	2,813.9 (17.9)
Franco Veteado	Argentina	Migmatite	0.33	0.204		0.51	811.0 (29.4)
Rosa Estremoz	Portugal	Marble	0.14	0.06	0.02		
Carrara	Italy	Marble					
Phran Kratai Grey	Thailand	Marble	0.60	0.013		0.92	
Azul Cielo	Argentina	Marble	0.41	0.658		0.75	1,252.1 (49.0)
Azul Imperial	Brazil	Quartzite	0.18	0.01	0.02		
Camine Rufo	Uruguay	Slate	0.16	0.056			
San Luis Slate	Argentina	Slate	0.13	0.177		0.82	486.3 (73.0)
Theuma	Germany	Slate					
Globegerina	Malta	Limestone	34.59	0.56	14.96	0.76	
Caliza Amarilla	Argentina	Limestone	11.4	0.225	2.02 (40.4)	0.75	156.2 (20.2)
Dolomita Dorada	Argentina	Dolomitic limestone	8.51	0.968	0.95 (31.8)	0.44	1,070.16 (10.2)
Mae Phrik Yellow	Thailand	Limestone	0.52	0.07		0.74	
Soskut	Hungary	Limestone	20.08			0.65	33-40
Jerusalem	Israel	Limestone	3.32			0.92	187-554
Kuacker	Germany	Limestone	3.73	0.37			
Thüster	Germany	Limestone	21.86				
Bad Langensalza	Germany	Travertine	9.12	8.41		0.68	15-28
	Hungary	Travertine					

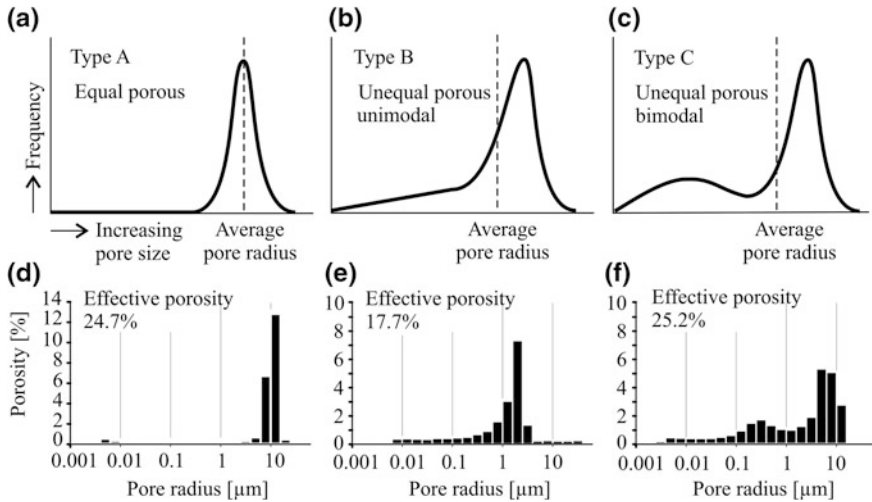
(continued)



Table 3.3 (continued)

Commercial name	Country of origin	Rock type	Porosity (%)	Mean pore radius ( $\mu\text{m}$ )	Water uptake at atmospheric pressure (weight%)	Degree of saturation (%)	Vapor diffusion resistance factor (-)
Baumberger	Germany	Sandstone-like Limestone	21.28	2.16	8.10	0.80	19-27
Rüthener	Germany	Sandstone	25.57	3.2	20.4	0.79	9-11
Bad Bentheim	Germany	Sandstone	23.33	9.15	17.9	0.72	11-13
Schleierther	Germany	Sandstone	14.15	0.105		0.77	22-26
Weser	Germany	Sandstone	6.29	0.06	3.2	0.63	40-45
Sikhiu Brown	Thailand	Sandstone	10.52	0.144	6.56 (73.4)	0.57	
Pakchong Green	Thailand	Sandstone	7.23	0.053	4.12 (15.6)	0.85	
Tacuarembó	Uruguay	Sandstone	22.81	12.09			

Numbers in brackets refer to the determined anisotropy value (in %) based on measurements in different directions



**Fig. 3.10** a–c Schematic representation of ideal pore types and pore-radius distribution in sandstones with Type A equal, Type B unequal unimodal, and Type C unequal bimodal pore-size distribution. Examples of each type are shown below with **d** Bad Bentheimer Sandstone (for A) **e** Obernkirchner Sandstone (for B), and **f** Cottaer Sandstone (for C) (from Ruedrich and Siegesmund 2006)

that sandstones with higher porosity are more sensitive to salt crystallization than sandstones with lower porosity values (see Chap. 4). Also, for lower tensile strength values, a higher sensitivity could be seen here. However, these trends show exceptions that are mainly related to the pore-radius distribution. According to Ruedrich et al. (2005b), sandstone samples with a unimodal pore-size distribution (Type A) and a small percentage of micropores could complete more cycles during the salt crystallization experiment than sandstones with a larger percentage of micropores (Type C).

In carbonate rocks, various pore types can be distinguished (see also Koch and Sobott 2005). All of them are the result of the primary distribution of different components in a matrix influenced by secondary diagenetic processes (e.g. Clemens et al. 1990). During the early water expulsion stage, the mechanical compaction resulting from the overburden pressure is the dominant mechanism for porosity reduction (Schlanger and Douglas 1974; Kim et al. 1985). Archie (1952) was the first one who classified carbonate rocks by using their pore space. Choquette and Pray (1970) presented a fabric-selectivity concept that is based on the differentiation between primary and secondary porosity and, to some extent, on the degree of interconnectivity between the pores. Lucia (1983, 1995, 1999) added a more petrophysical view to the classification of pore space: the pore-size distribution controls the porosity, the permeability, and the saturation, and it is related to the rock fabrics. These considerations and investigations led to two major pore space groups: (a) the interparticle pore space and (b) the vuggy pore space, which is divided into separate-vug pores and touching-vug pores. For the first group,

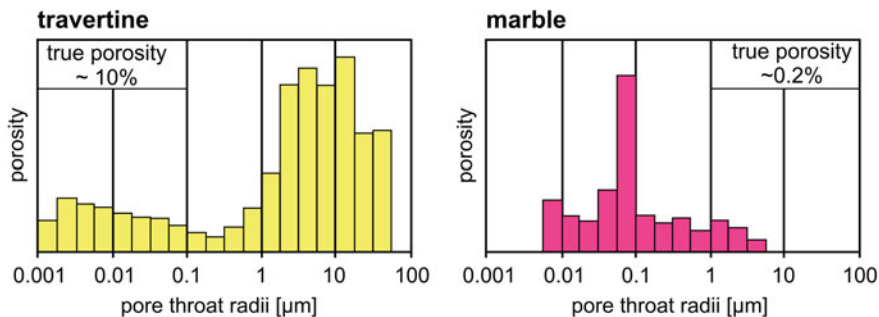


**Fig. 3.11** Pore-radius distribution of a travertine and a marble sample, both quarry-fresh. Note the differences in the true porosity

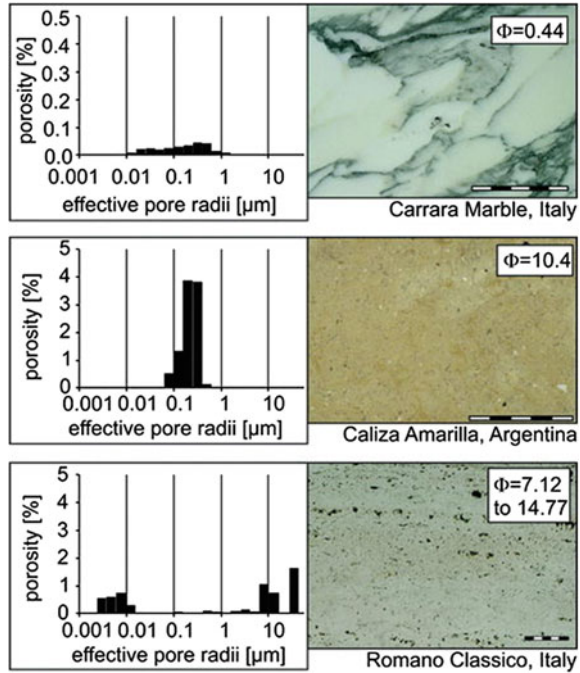
Lucia (1995) characterized three rock fabric/petrophysical classes defined by certain permeability and water saturation fields. In the pore space classification of Lucia (1995), fractures are one type of touching-vug pores. The fractures can be separated from the pore space, because they can contribute to anisotropy as well as to porosity and permeability. The fracture intensity in dolomites is higher than in limy dolomites and in limestones (Stearns 1967; Sinclair 1980), and, with decreasing grain size, the fracture intensity in dolomites increases (Sinclair 1980). For the examination of fractures, van Golf-Racht (1996) presented a descriptive classification scheme defining the following categories: (a) open/closed fractures, (b) macro/micro fractures, and (c) natural/induced fractures.

A study by Mosch and Siegesmund (2007) has shown that carbonate rocks, separated into limestone, oolite, breccia, dolomite, and travertine, cover a large range of porosity values, from very compact rocks with <1 % to highly porous rocks with >20 %, as shown in Tables 3.1 and 3.3 and Fig. 3.2 (e.g. Siegesmund et al. 2010).

The largest variation in the porosity values is recognized in the travertine group. Peschel (1977), for example, presents a value of 60 % as the upper limit for the porosity of travertine, including lime tuff. Furthermore, travertine shows an extreme heterogeneity with respect to porosity and the distribution of the pores within the rock. For example, massive travertine has porosities of <10 %, and laminated travertine can show alternating layers with more and with fewer pores; the phytothermal travertine can contain up to 40 % plant fragments. Porosity measurements of the travertine *Romano Classico* show values between 7 and 15 %, which result from the differences in the pore-space distribution in different layers (Figs. 3.11 and 3.12).

Volcanic rocks, like andesite, basalt, rhyolite, dacite, trachyte, and tuff, also show a larger variability in porosity values, from 1 to ca. 50 % (Fig. 3.1, Table 3.3). This large range in pore-space volume is the result of their geological origin and the environment at the time of deposition. One possible reason is that the degassing of fast flowing magma combined with a rapid cooling might have

**Fig. 3.12** Pore-radius distribution for different carbonate rocks such as marbles, micritic limestone, and a travertine (porosity is given in %). Scale in each photo has 5 cm length



resulted in a pronounced bubble-like structure. Tuff, one of the few volcanic rocks used as a dimension stone, mainly comprises of scoria, ash particles, and rock fragments which were deposited during an explosive eruption and subsequently compacted and welded together (Chap. 2). As a result, the rocks show a greater variation in porosity values, from 8 to nearly 50 %.

Plutonic and metamorphic rocks only exhibit lower porosities due to their geological origins. The values for plutonic rocks range between 0.05 and 1.65 % with some outliers, whereas for metamorphic rocks, the porosity values are not above 1 %, except in a few cases (see Mosch and Siegesmund 2007). The majority of the pore spaces in plutonic and metamorphic rocks can be assumed to be characterized as crack porosity.

Figure 3.13 demonstrates the relationship between the porosity and pore-size distribution and the degree of bowing of marble panels (see Sect. 3.4.2 and Siegesmund et al. 2008b). The indoor exposed marble (sample S0) exhibits an initial porosity of around 0.51 % (Fig. 3.13a). With increasing bowing, i.e. progressive deterioration, the porosity increases up to 2 % (Fig. 3.13). This increase reflects an extreme value compared to porosities usually reported for marbles. Moreover, the pore-size maximum moves towards larger pore radii with an increase in bowing. For example, marble sample S7 (Fig. 3.13b) shows a significant difference in the upper pore-radius range. The maximum pore diameter of this sample is around 1.0 μm and is, therefore, in the range of capillary pores. In contrast, the maximum pores in S0 are smaller than 0.1 μm, which cannot be filled

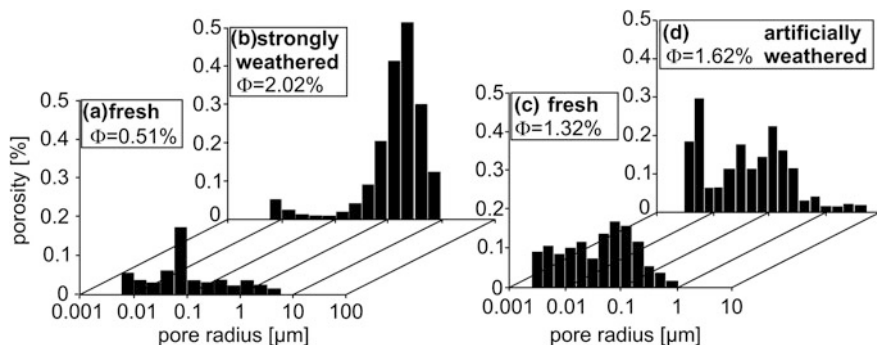


**Fig. 3.13** Pore-size distribution versus bowing of marble panels: **a** Marble sample S0 with a typical porosity of marbles. With increasing deterioration **b**, i.e. bowing of the sample (marble sample S7), the porosity increases, and a shift in the pore-radius distribution can be recognized. The change in the effective porosity is also given for a fresh **c** and artificially weathered **d** Marble sample

by capillary water absorption. This phenomenon is also observed in general when comparing fresh and artificially weathered marble samples.

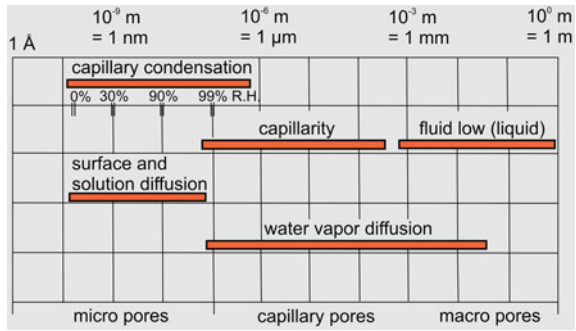
### 3.3 Water Transport and Retention Properties

Water is one of the main factors involved in most of the weathering processes (Snethlage 1984; Weiss 1992; Künzel 1994; Krus 1995; Künzel and Krus 1995; Mirwald 1997). Almost all of the weathering processes taking place in structures and buildings are determined by the presence of water, e.g. frost and salt-related weathering (see Chap. 4); dry-wet cycles; hygric expansion, thermo-hygric processes, and thus, the characteristics of water have an immense impact on the long-term stability of dimension stones. The presence of water also has a significant effect on the petrophysical and mechanical properties of rocks. This is mainly influenced by the moisture content, which, on the other hand, is determined by the pore space of the rock (see Sect. 3.2). The pore space and pore system relate to the amount of water absorption, the nature of water transport, and the size of the surface area available for chemical interactions. The important so-called hygric properties here are adsorption, water vapor permeability, capillary water absorption, total amount of absorbed water, and drying characteristics.

Klopfner (1985) correlated pore sizes with water transport and other mechanisms (see also Sect. 3.2). Three clear regions can be differentiated depending on the mechanism involved. For micropores, i.e. pore diameters  $<0.1 \mu\text{m}$ , water will condense at relative humidity values below 99 % RH (relative humidity) (Fig. 3.14). Capillary suction is practically relevant to materials with pore diameters between  $1 \mu\text{m}$  and  $1 \text{mm}$ , the so-called capillary pores. For macropores, i.e. those with a diameter greater than  $1 \text{mm}$ , fluid flow characteristics emerge.



**Fig. 3.14** Water transport mechanisms and the definition of pore size classes (adapted after Klopfer 1985)



The main moisture transport mechanisms are water vapor diffusion and liquid water capillary absorption. Between these two mechanisms, a surface diffusion of sorbed water has been postulated (Stockhausen 1981; Klopfer 1985; Künzle 1994; Krus 1995). The interaction among these three moisture transport mechanisms is illustrated in Fig. 3.15. The driving force for water vapor diffusion is the equilibrium tendency between a higher water vapor concentration and a lower one. With increasing moisture content in the air, i.e. relative humidity, water vapor sorption increases, leading to surface diffusion at the pore walls. This, in turn, favors the eventual liquid capillary transport.

When all the macropores are filled with water, fluid transport will be the main mechanism for water movement in the rock. Furthermore, if hydrostatic pressure is present, such as when a water puddle some centimeters high collects on a surface so that its weight increases the pressure on the pore system of the stone, then the capillary fluid transport changes into fluid flow processes (Darcy flow, e.g. Snethlage 1984; Klopfer 1985).

Among the different water uptake parameters determined, water absorption by total immersion is that measured under atmospheric pressure or under vacuum conditions. From these specific values, the saturation degree of a rock sample can be obtained. Also important is capillary water absorption, which depends on the capillarity of the sample when only one surface is in contact with liquid water. Complementing the total water absorption and capillary water absorption are the drying mechanisms of a porous rock, which relate to the movement of the fluid water and vapor out of the pore system.

The determination of the water vapor sorption is one of the standard measurements for the characterization of building materials, including dimension stones. For the specification and understanding of the hygric properties, i.e. those related to the transport of water vapor, two aspects are important: first, the properties of the pore space with respect to shape, cross-section, surface area, and three dimensional connectivity of the pores, and second, the interaction between the different phases (air, water vapor, liquid water) in the pore space.

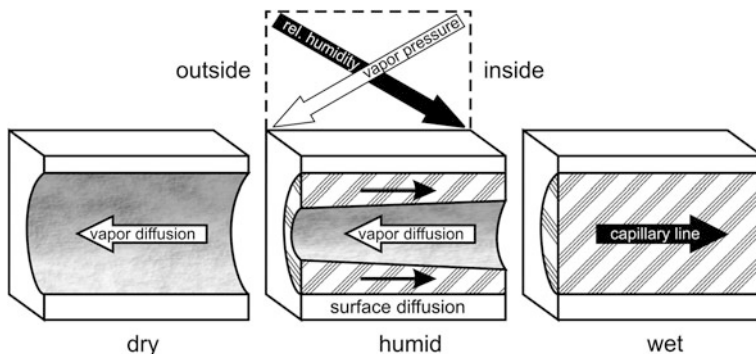


**Fig. 3.15** Schematic illustration of different transport phenomena and their driving forces in porous rocks with different water content (after Holm 2001)

### 3.3.1 Capillary Water Absorption

A porous dimension stone experiences water absorption while exposed to rain as part of building masonry or a cladding, as well as when in contact with groundwater. In general, a porous medium in contact with liquid water will absorb it by capillarity. This is a spontaneous process related to the capillary absorption force originated by the pores in the material between the diameters of 10  $\mu\text{m}$  and 1 mm. It is the result of a balance between the surface tension of the liquid water and the adsorption forces of the pore wall, usually a polar mineral surface. Water at these polar surfaces exhibits a characteristic wetting angle that finally results in the tendency of the water to enter the pore system, the so-called capillary action or capillary suction. The mechanism of capillary water absorption depends mainly on the pore size and the geometry of the pore system.

As shown in Fig. 3.14, capillarity is the main driving force for water absorption by pores between 1  $\mu\text{m}$  and 1 mm.

Water can move upwards against gravity (ascension) in a capillary along hydrophilic surfaces (Fig. 3.16), such as a mineral surface, whereas in the case of a hydrophobic surface, the water descends in the capillary (depression). This is the case when a dimension stone has been treated with a hydrophobization agent as discussed in Sect. 7.9, or when a sample is in contact with mercury during mercury porosimetry, to determine its pore-size distribution. This method as well as others presently used for pore structure analysis is based on idealized shape models of the pores, because the real pore geometry is too difficult to put into an exact mathematical expression.

Both the capillary suction and capillary suction rate depend on the pore diameter, with smaller capillaries having a higher suction power (Fig. 3.16a, b) but a lower capillary suction rate (e.g. Kettenacker 1930; Cammerer 1954; Klopfer 1985). Larger capillaries, on the other hand, have higher suction velocities but a much lower suction power. For a natural pore system with capillaries of different sizes, this will result in generally faster capillary water absorption by larger pores

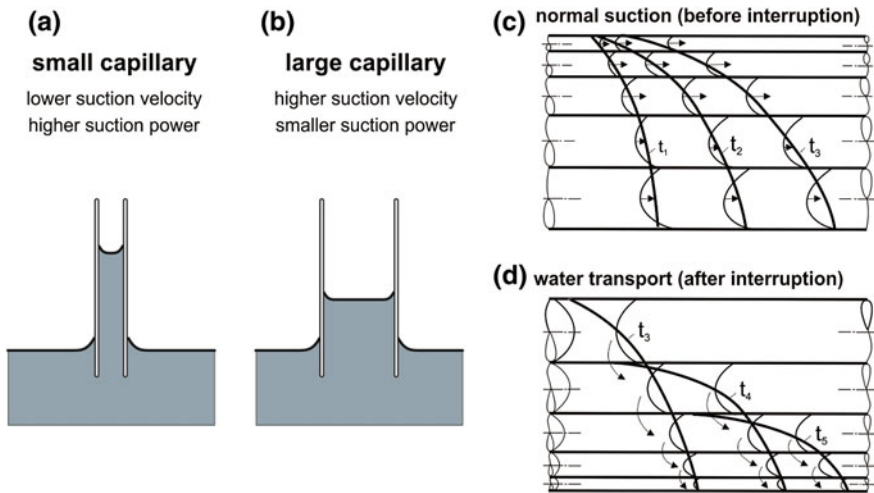


**Fig. 3.16** Rise of the water level for capillaries of different diameters (a, b). The diameter has an influence on the suction behavior and the suction power in general for an uninterrupted suction process (c) and specifically for an interrupted suction process (d). The water front is presented in relation to the diameter of the capillary at different times,  $t_1$ ,  $t_2$ , and  $t_3$ . **d** Rearrangement of the water transport from larger to smaller pores after disruption of the water supply, also over different times,  $t_3$ ,  $t_4$ , and  $t_5$  (after Krus 1995)

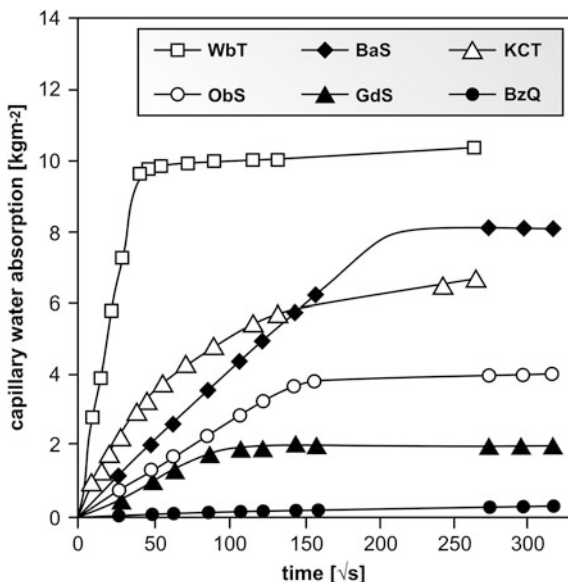
and slower absorption by smaller pores. If the water transport is disrupted or broken at one point, a rearrangement of the processes involved occurs. Smaller pores will then increasingly absorb water from the larger capillary pores due to their higher suction power. This is schematically illustrated in Fig. 3.16c, d for capillary pores with increasing diameter. The water front is presented in relation to the diameter of the capillary over different times,  $t_1$ ,  $t_2$ , and  $t_3$ . Figure 3.16d shows the rearrangement of the water transport from larger to smaller pores following disruption of the water supply, also over different times,  $t_3$ ,  $t_4$ , and  $t_5$ .

The capillary water absorption of porous materials can be described through the water absorption coefficient ( $w$ -value). In the laboratory, this can be determined using a cylindrical or cubic stone specimen placed with only its bottom side in a basin filled with water. The cube for this test usually has a 5 cm side length. Care has to be taken that the water absorption occurs only and constantly through the bottom side. For this purpose, the basin with the water has to be large enough so that no significant change in the water level occurs during the absorption experiment. The relationship between capillary water absorption and time is determined by periodically measuring the change in weight. The  $w$ -value is determined by:

$$w\text{-value} \left[ \text{kg}/(\text{m}^2\text{h}^{0.5}) \right]: w = m_w/\sqrt{t} \tag{3.7}$$

where  $m_w$  is the surface-related water absorption ( $\text{kg}/\text{m}^2$ ), and  $t$  is the absorption time (h).

**Fig. 3.17** Capillary water absorption of some selected rock samples, *Wbt* Weiberner Tuff, *BaS* Baumberger “Sandstone”, a clastic limestone, *ObS* Obernkirchner Sandstone, *GdS* Grödener Sandstone, *KCT* Kufstein Calc-Tufa, and *BzQ* Bozen Quartz Porphyry. The capillary water absorption is given in  $\text{kg}/\text{m}^2$  versus the square root of the time in seconds (after Franzen and Mirwald 2004)



The water absorption per unit area versus the square root of the time initially shows a linear behavior. The slope of this line corresponds with the  $w$ -value, the amount of water per unit area, and the square root of the time taken for capillary absorption into a sample (Fig. 3.17). This relationship only holds for several hours (depending on the rock type) or for dimension stones with good absorption properties until complete penetration (Klopfer 1974; Kraus 1985). According to Meng (1993), three conditions have to be fulfilled for the validity of the  $t$ -relationship: (1) the evaporation has to be low compared to the amount of water absorbed through the absorption process; (2) the material should not have very large pores (over 1 mm in diameter), i.e. where no capillary absorption occurs, nor very small ones (below 1  $\mu\text{m}$  diameter) because the overall absorption rate is low; (3) the  $t$ -relationship only holds for vertical water absorption as long as it is below the theoretical maximum height.

On the other hand, the water permeation coefficient ( $b$ -value) can be calculated by using the following equation:

$$b\text{-value } [\text{m}/\text{h}^{0.5}]: b = z/\sqrt{t} \quad (3.8)$$

where  $z$  is the rise in height, and  $t$  is the absorption time (h).

The  $b$ -value describes the penetration velocity of the water front through a material during the absorption process. Additionally, by dividing  $w/b$ , the water capacity can be determined. Water capacity is generally defined as the water content per unit volume which a rock is capable of absorbing via capillary action (Niesel and Schimmelwitz 1982; Weiss 1992).

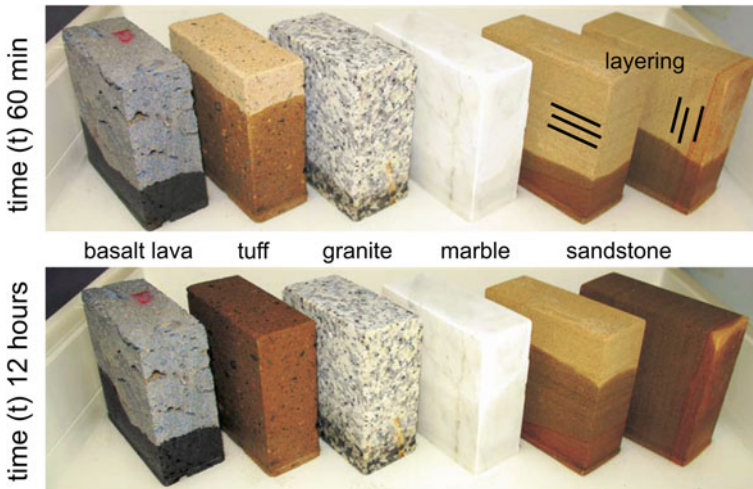


**Fig. 3.18** Photos of the capillary water absorption of different rocks after 60 min ( $t_{60 \text{ min}}$ ) and 12 h ( $t_{12 \text{ h}}$ ). For the sandstone sample, two specimens were used: one with the sedimentary layering parallel and the other perpendicular to the water level

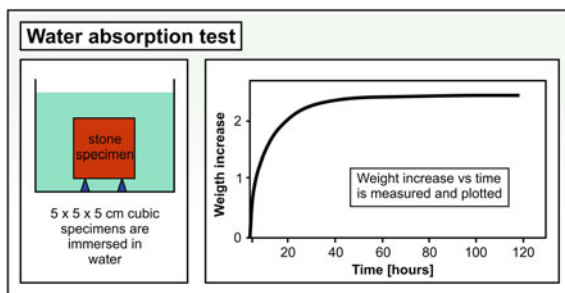
The determination of the capillary water absorption for an outdoor object is usually carried out using the “Karsten” tube (see Chap. 6).

As an example, the capillary water absorption of selected rocks presented in Fig. 3.17 (see also Fig. 3.18) shows the typical trend that can be separated into two parts. The first part shows a linear increase in the capillary water absorption (Kraus 1985). In the second part, the curve exhibits a plateau-style shape with the absorption value increasing only slightly with increasing  $t$ . The  $t$ -relationship can only be used as a first good approximation to describe the time-dependent trend of the initial capillary water absorption. From a large number of experiments, it is known that, for many rock types, a linear relationship of the capillary water absorption versus the square root of the time is valid. Using the  $w$ -value (Snethlage 2005), rocks can be classified into slightly absorbing ( $w < 0.5 \text{ kg/m}^2\text{h}^{0.5}$ ), medium absorbing ( $w < 0.5\text{--}3.0 \text{ kg/m}^2\text{h}^{0.5}$ ), and highly absorbing ( $w > 3.0 \text{ kg/m}^2\text{h}^{0.5}$ ).

For a granite sample, Poschlod (1990) reported a  $w$ -value of  $0.03\text{--}0.41 \text{ kg/m}^2\text{h}^{0.5}$ . A value of  $0.41 \text{ kg/m}^2\text{h}^{0.5}$  means that, during the first hour, the rock absorbed  $0.41 \text{ kg}$  of water per square meter, or  $0.041 \text{ ml}$  of water per square centimeter, accordingly. Marble samples, like Carrara or Laaser Marble, have  $w$ -values of about  $0.10 \text{ kg/m}^2\text{h}^{0.5}$ . For the Globigerina Limestone from Malta, Ruedrich et al. (2005a) determined  $w$ -values in the range of  $7.78\text{--}14.96 \text{ kg/m}^2\text{h}^{0.5}$ . For several often used dimensional building stones from Germany (sandstones and limestone), Szilagyi (1995) reported  $w$ -values between  $0.1 \text{ kg/m}^2\text{h}^{0.5}$  and  $9.4 \text{ kg/m}^2\text{h}^{0.5}$ , which are in accordance with values determined on samples from the Cologne Cathedral (Kraus 1985). In the literature,  $w$ -values of up to  $70 \text{ kg/m}^2\text{h}^{0.5}$  can be found.



**Fig. 3.19** Schematic illustration of the water absorption measurement with the sample totally immersed in water and a schematic curve of the sample's weight increase over time due to the absorption of water until a near weight constancy is reached (after I-Stone 2008)



Capillary absorption also reportedly exhibits a strong directional dependency which can be significant (Poschlod 1990; Weiss 1992; Ruedrich et al. 2005a, 2007, 2010a). Anisotropy values of more than 70 % are found quite often, and it can be assumed that the lowest capillary water absorption values are measured perpendicularly to the sedimentary layering or metamorphic foliation. The b-value is also a critical number, especially when substitution materials have to be identified.

### 3.3.2 Water Absorption by Total Immersion

The water absorption is the difference between the weight of a sample totally immersed in water and its dry weight. In contrast to the capillary water absorption discussed above, the value of the total water absorption can be determined by different methods (Fig. 3.19). The usual methods are the total immersion under atmospheric pressure and under vacuum conditions, although the DIN-standard (DIN EN 1097-6 2005) recommends measuring the water absorption at 150 bar.

The water absorption capacity of a rock is closely related to its porosity. In general, the higher the value of the effective porosity, the higher the total water absorption. However, the total water absorption capacity of a rock is not related to its total porosity, but to the percentage of pores accessible for the water under normal conditions.

The total water absorption value under atmospheric pressure conditions indicates how much water a rock can absorb over 24 h when placed 3–5 cm below the water level. The subsequent weighing of the sample provides the wet weight ( $m_f$ , in g) and the following equation the relationship to the water absorption ( $W_{atm}$  in weight%), where  $m_d$  (in g) is the dry weight of the sample:

$$W_{atm} = \frac{m_w - m_d}{m_d} \cdot 100 \text{ [weight - \%]} \quad (3.9)$$

with  $m_w$  the wet weight at  $t = 48$  h (in g). However, the water absorption  $W_{atm}$  provides a relative value that is only valid for the given experimental conditions (Chitsazian 1985).

The water uptake in relation to the dry weight of the sample is mainly influenced by porosity, pore size distribution, and the mineralogical composition of the rock. Due to the dominance of quartz and feldspar, the mineral density of sandstones is about  $2.64 \text{ g/cm}^3$ , whereas calcitic limestone rocks have a matrix density of around  $2.72 \text{ g/cm}^3$ . From that, a cubic sandstone specimen with a 10 cm edge length and 20 % porosity would show a weight of 2,112 g in the dry state and 2,212 g with 50 % water saturation of the pore space. The related water absorption would be 4.73 weight%. For a limestone specimen with the same dimensions, the dry weight would be 2,176 and 2,276 g with 50 % water saturation of the pore space, with the related water absorption being 4.60 weight%. Although both samples have the same water saturation value, the water absorption varies. This shows the influence of the porosity in relation to the mineral density. For a porosity of 30 %, the water absorption of the sandstone is 8.12 and, for the limestone, 7.88 weight%. These values show that, with increasing porosity, the differences in the water absorption become more pronounced.

Furthermore, the pore size (see Sect. 3.2) has an influence on the total water absorption. A shorter immersion time over hours or days mainly fills the capillary pores to a large extent. Relatively small pores, which are widely found in sandstones, are filled only after a very long immersion time. On the other hand, cavernous mesopores, which are often found in limestone, will drain after taking the specimen out of the water.

Both phenomena are likely to have an influence on the determination of the total water absorption, either related to the volume of the sample or its porosity or to the weight of the sample. Poschlod (1990) compares the total water absorption values of two granite and two marble samples, all measured under atmospheric pressure and water absorption determined in relation to weight% and vol.%; both values obviously differ in their numbers (which is finally due to the effect of the density): Kösseine Granite 0.21 weight% versus 0.56 vol.%; Nammering Granite 0.76 weight% versus 1.97 vol.%; Carrara Marble 0.18 weight% versus 0.50 vol.%; Laas Marble 0.15 weight% versus 0.40 vol.%.

Fitzner (1970) showed that there is a relationship between the water absorption and the size and shape of the sample used in the experiment. The influence of the time period over which a sample is placed underwater on the value of  $W_{\text{atm}}$  was discussed by Weiss (1992). He showed the saturation degree of the pores over the course of time in a logarithmic scale for several sandstones during the full submersion of the samples (see Fig. 3.19). Following Fitzner (1988), the resulting graphs show characteristic distributions depending on the pore-radius distribution of the sample (see Sect. 3.2). If a sample is placed underwater long enough, a “full” or 100 % saturation of the accessible pore space can be assumed, as was demonstrated in a very long, 800-day experiment by Fitzner (1970).

The rocks shown in Fig. 3.20 comprise a granite and three sedimentary rocks (sandstone, limestone, and dolomite). They all show very significant differences in their pore space and, consequently, in their water absorption behavior. Three Hg-porosimetry histograms, total open porosity, and water absorption values are also included in the diagram. The sandstone initially shows, over a short period of time,

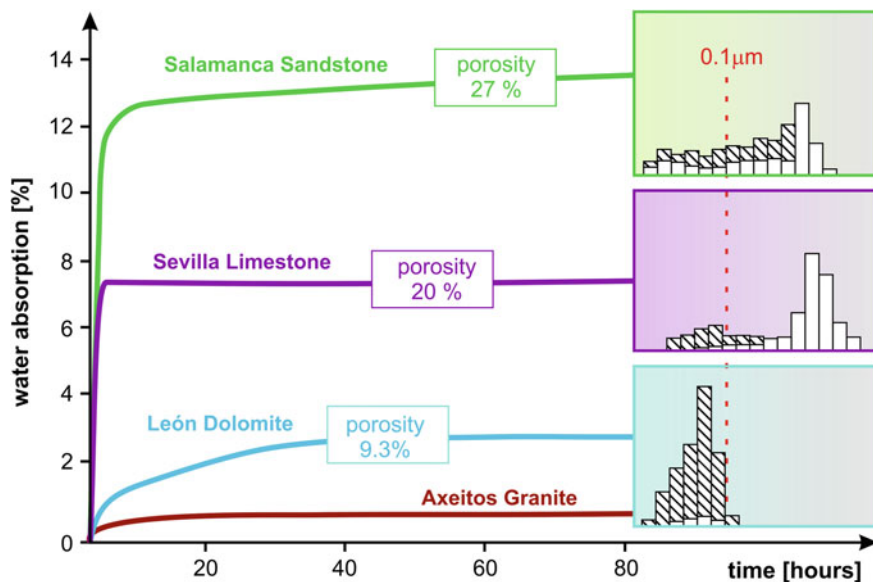


**Fig. 3.20** Water absorption versus time for four different rock types from Spain. The pore-size distribution is also schematically given (after I-Stone 2008)

a very fast water absorption, which is followed by a longer period with far slower absorption. This can be explained by the information provided by its pore-size distribution, i.e. the range of pore sizes that allows water to access the open porosity (27 %). The pore-size distribution is very wide, from less than  $0.01 \mu\text{m}$  to almost  $100 \mu\text{m}$ . In addition, the highest percentage of its total effective porosity is refilled through very wide conduits ( $1\text{--}100 \mu\text{m}$ ). Another small but significant percentage of the pore space is refilled through very narrow conduits (less than  $0.01\text{--}0.1 \mu\text{m}$ ). This explains the initially fast and easy water filling, almost reaching its total water absorption capacity, and the slow and difficult second period. This stone also contains swelling clays (smectites) located in intrapore and in intragranular positions that hinder water movement through the very narrow conduits. The limestone shows an expected behavior in this diagram as its pore space is characterized by very wide conduits ( $1\text{--}100 \mu\text{m}$ ), which give access to almost its total effective porosity (20 %). Consequently, water absorption and water desorption are extremely easy and fast with a clear and short initial period that can be monitored. The behavior of the dolomite is quite interesting. Its total open porosity is 9.3 %, but its increment in weight due to water absorption is only about 3 %. As the Hg-porosimetry histogram shows, only a very small fraction of the open porosity is effective, and this small fraction is only accessed through small conduits in the  $0.01\text{--}0.1 \mu\text{m}$  diameter range. All these observations explain the long period of slow water absorption capacity of this sample. Water movements in crystalline stones are difficult in general, as the granite in Fig. 3.20

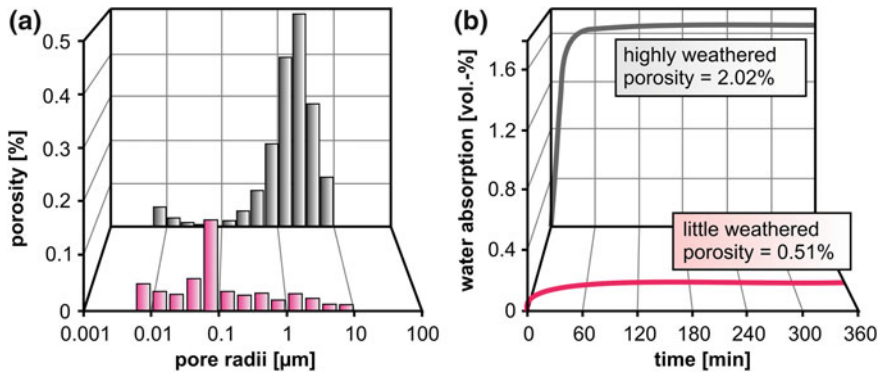


**Fig. 3.21** **a** Porosity and pore-size distribution for fresh and weathered Carrara Marble in comparison to the **b** Water absorption for the same samples

shows. Water movement into the pores of this low porosity sample is entirely channeled through interconnected fissures and microcracks. Figure 3.21 shows the effect of the porosity for a quarry-fresh and strongly weathered marble sample on the water absorption. It can clearly be seen that, with increasing weathering, the pore-radius distribution is moving towards larger pore radii. The weathered marble sample shows spontaneous water absorption in the first minutes and, after that, a longer period of water absorption which does not change with increasing time. As mentioned earlier, the sample has to be placed in the water for 24 or 48 h.

For an evaluation of the water absorption, Mosch and Siegesmund (2007) and Mosch (2009) compiled data from 1,650 dimension stones (Fig. 3.1, Tables 3.3 and 3.4). As shown in Fig. 3.22, there is a clear relationship between the water absorption, the bulk density, and the effective porosity, especially for the group of more porous rocks, like sandstones, carbonate rocks, and volcanic rocks. Despite some outliers, the highest values for the water absorption can be found in the tuffs, which can be related to the relatively low compaction of these rocks during their pyroclastic deposition. This has resulted in relatively high porosity values combined with an effective interconnectivity between the open pores. However, the porosity/ $W_{\text{atm}}$  data pairs overall show a relatively large variation, which is the result of the heterogeneous character of the pore space (see Sect. 3.2). Here, the very large pores do not contribute to the water absorption capacity of these rocks.

For the low porosity rocks, a linear relationship between the water absorption, the porosity, and the bulk density can be established. For plutonic and metamorphic rocks, the correlation coefficient between the water absorption and the porosity is  $R = 0.85$ , whereas the correlation to the bulk density is only  $R = -0.15$ . In some way, the carbonate rock group exhibits a similar picture. Regarding the water absorption, the carbonate rocks with a bulk density of  $\rho_{\text{bulk}} \geq 2.6 \text{ g/cm}^3$  are comparable to the plutonic and metamorphic rocks. With decreasing bulk density and increasing porosity, the values and the distribution of the data pairs are more similar to the sandstone varieties.

**Table 3.4** General values for water absorption

Group	Water absorption [weight-%]		
	Min	Max	Median
Plutonic rocks	0.01	0.60	0.23
Metamorphic rocks	0.01	0.57	0.18
Marbles	0.01	0.38	0.15
Gneisses	0.05	0.54	0.26
Carbonate rocks (all)	0.01	3.75	0.62
Carbonate rocks $\rho \geq 2.6 \text{ g/cm}^3$	0.01	1.75	0.30
Carbonate rocks $\rho < 2.6 \text{ g/cm}^3$	0.05	10.00	2.21
Sandstones (all)	0.04	10.60	5.11
Porosity class I (<13.4 %)	0.07	7.08	4.85
Porosity class II (<20.5 %)	2.64	9.32	5.25
Porosity class III ( $\geq 20.5$ %)	5.12	8.65	7.04
Volcanic rocks (all)	0.05	21.9	3.51
Tuff	2.03	32.20	13.20
Volcanic rocks (without tuff)	0.05	4.40	1.67

The maximum and minimum values are the upper and lower extremes from the box plot data analysis and, therefore, do not give the outlier values (after Mosch and Siegesmund 2007; Mosch 2009)

As shown before, the absolute values of the water absorption are closely correlated to the porosity of a rock. However, the data analysis of the sandstone varieties with respect to the porosity classes (as defined in Sect. 3.2) shows that the porosity is not the only factor that has an influence on water absorption. Even though the median value of the water absorption from the first (porosity < 13.4 %) to the third porosity class (porosity  $\geq 20.5$  %) increases, the central segments of the classes show significant overlaps (Fig. 3.22a).

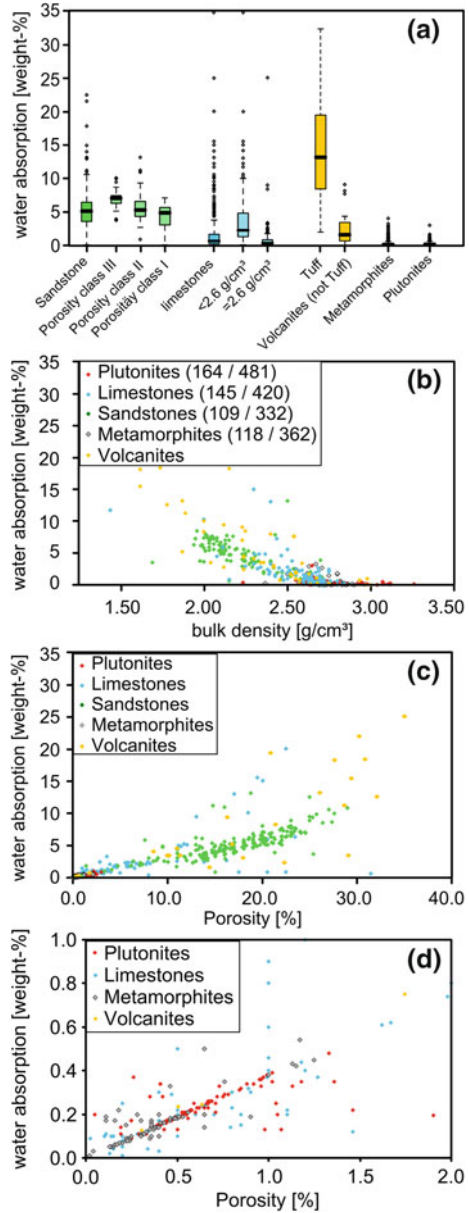
Therefore, the porosity can only be used for a first evaluation of the water absorption capability of a rock. For rocks with a similar porosity value, the pore-radius distribution and the pore shape become increasingly important parameters for water absorption, especially for sandstones, as these parameters are primarily related to the grain and particle size as well as to their sorting. Secondary factors are cementation and related diagenetic processes (see Chap. 2). For plutonic and metamorphic rocks—basically, crystalline rocks—the porosity is mainly due to microcracks, either along grain boundaries or as inter- and intracrystalline cracks (see Fig. 3.5f, g). For capillary water absorption, the important parameters are the states of the grain boundaries, as well as the width and interconnectivity of the existing microcracks.

A data set of 188 sandstones from Germany is shown as an example in Fig. 3.23 to demonstrate the influence of two factors, grain size and sorting, on water absorption. Other factors that might have an influence are not taken into consideration here, e.g. the cement or the sphericity and roundness of the grains.

The rocks are primarily separated according to their grain size (fine-grained sandstones, fS: <0.2 mm; coarse-grained sandstone, mS: 0.2–0.63 mm) and their



**Fig. 3.22** **a** Water absorption for different rock types (see Table 3.4) and some differentiation with respect to bulk density and porosity. Correlation between water absorption and bulk density (**b**) and porosity (**c**). **d** A detailed view of **c** for porosity values  $\Phi < 2\%$  (after Mosch and Siegesmund 2007)



grain sorting (very good, good, good-medium, medium, medium-poor, poor; see Fig. 3.23). Although it is generally assumed that a smaller mean grain size results in a lower porosity (see Chap. 2 and Sect. 3.2), the data here show that the median value of the absorption for rocks with a smaller grain size ( $W_{a_{atm}} = 6.00$  weight%) is slightly higher than for rocks with a larger grain size ( $W_{a_{atm}} = 5.29$  weight%). The data suggest that grain sorting has no direct effect on the rock's

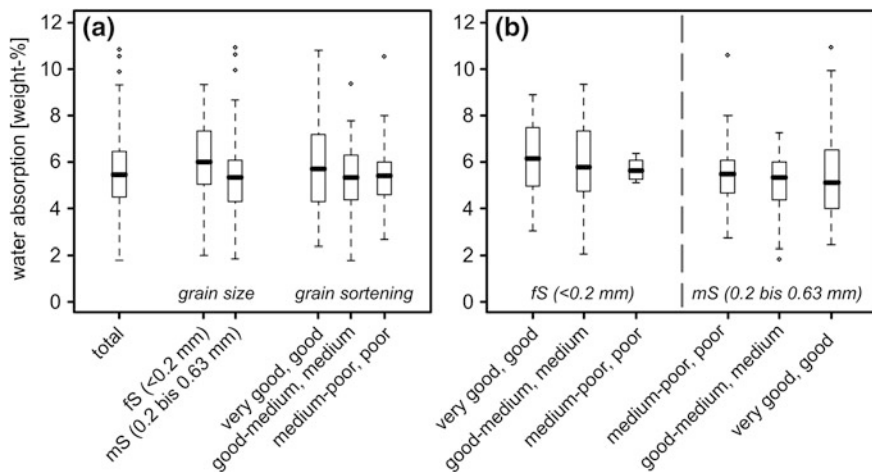


**Fig. 3.23** Data analysis of 188 sandstones from Germany for a correlation between water absorption and (a) grain size and (b) grain sorting (data after Grimm 1990, Wenzel and Häfner 2003, David 2006). The small range for the grain size group “fS”/medium-poor, poor (in b) resulted from the small number of samples,  $n = 4$  (after Mosch and Siegesmund 2007; Mosch 2009)

capacity for capillary water absorption. However, the two data sets, separated by grain size, show some intrinsic trends. The water absorption of fine-grained sandstones (fS) increases with increasing grain size or better sorting, whereas, for coarser grained sandstones (mS), the same correlation shows a decreasing trend. Therefore, the lowest median value of water absorption can be expected for medium-grained sandstones with good to very-good sorting and the highest median value for fine-grained sandstones with very-good to good sorting.

Water absorption is a relatively slow process resulting in the gradual filling of the remaining pore space based on capillary condensation mechanisms (Künzel and Krus 1995; Mirwald 1997). In the laboratory, this state can nearly be achieved by first evacuating the air from the effective pore space until a vacuum is reached and then immersing the sample underwater to saturate the pores. This process creates a significant absorption force or effect. However, Fitzner (1970) has shown that a full saturation with nearly constant values can be achieved only after very long experiments with durations of up to two years.

The calculation of the forced water absorption is as follows:

$$W_{vac} = \frac{m_n - m_t}{m_t} \cdot 100 \quad (3.10)$$

with  $W_{vac}$  as the water absorption under vacuum (weight%),  $m_n$  as the mass of the sample after forced water absorption (g), and  $m_t$  as the dry mass of the sample (g).

For the evaluation of the frost resistance of a dimension stone, the quotient of the freely or unforced water absorption ( $W_{atm}$ ) and the forced water absorption

( $W_{vac}$ ), the so-called saturation degree or saturation coefficient  $S$  (Hirschwald 1912), is of importance. The  $S$ -value is calculated using the following equation:

$$S = \frac{W_{atm}}{W_{vac}} \quad (3.11)$$

The saturation coefficient describes how much of the total pore space is accessible to water absorption, thus providing a value for the frost resistance evaluation (Table 3.3). If the saturation coefficient is smaller than 0.9 or less than 90 % of the pore space, the pores can be filled by capillary absorption, and then the rock should be frost resistant when the volume increase related to the freezing of the water is 9 %. For frost resistance, Hirschwald (1912) proposed the following guideline values using the saturation coefficient: when  $S < 0.75$ , the rock is weather and frost resistant; for values ranging between 0.75 and 0.90, it is uncertain, and further investigations are necessary; when  $S > 0.90$ , the rock is not weather and frost resistant. Hirschwald (1912) himself favored a critical value of  $S = 0.8$ , with some exceptions, for a rock to be frost resistant. In the case of ice formation in a highly saturated pore space, the remaining pore space can hardly compensate for the volume expansion (Hörenbaum 2005). As a consequence, microcracks along the grain boundaries will form, leading to possibly significant damage to the rock, and subsequently, to a decrease in the mechanical stability (e.g. Ondrasina et al. 2002; Ruedrich et al. 2010b).

However, for plutonic and metamorphic rocks as well as for carbonate rocks with a bulk density above  $2.6 \text{ g/cm}^3$ , it is assumed that the saturation coefficient has limited validity and significance. With these rock types, very small values of  $W_{atm}$  and  $W_{vac}$  can sometimes be found, resulting in relatively high values of  $S$  as the quotient of both. In most cases, this is related to the measurement procedure, and the results of the resolution limit are also associated with that. For example, the saturation coefficient of the Lichtenberg diorite, a medium-grained Bt-Hbl-diorite, is  $S = 0.94$  (Grimm 1990); however, its frost resistance should be certain because of the extremely low total porosity.

Sandstones and porous limestones show a higher variability in absorption under atmospheric pressure conditions than in the forced water saturation at comparable porosity values. It becomes evident that the effectiveness of the atmospheric or free water capillary absorption depends on certain pore radii. Here, the variability in the pore size for basalt lava (Chap. 2) can be shown. With porosity values of 22.31 and 29.06 % and atmospheric water absorption values of 2.36 weight% and 3.50 weight%, the saturation coefficient gives values of 0.24 and 0.25 (Grimm 1990). For a possible correlation between the  $S$ -value and the porosity, a relative increase of  $S$  in the porosity range between 10 and 30 % can hardly be seen (Fig. 3.24). However, a general trend based on this data set cannot be determined.

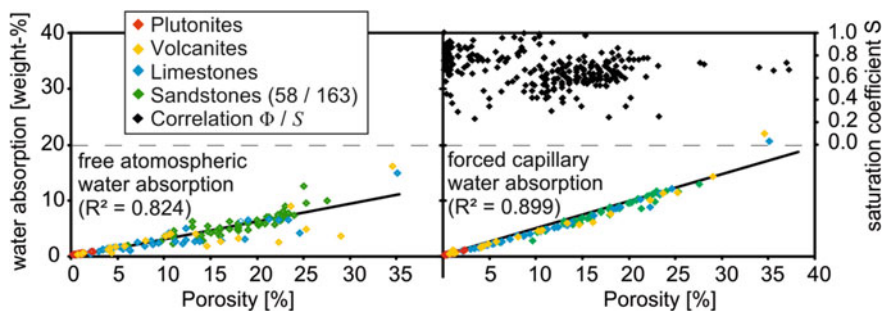


**Fig. 3.24** Group specific point distribution of the correlation between the free atmospheric (*left*) and the forced capillary water absorption (*right*), as well as the saturation coefficient  $S$ . The  $R^2$  for each linear equation is given (after Mosch and Siegesmund 2007; Mosch 2009)

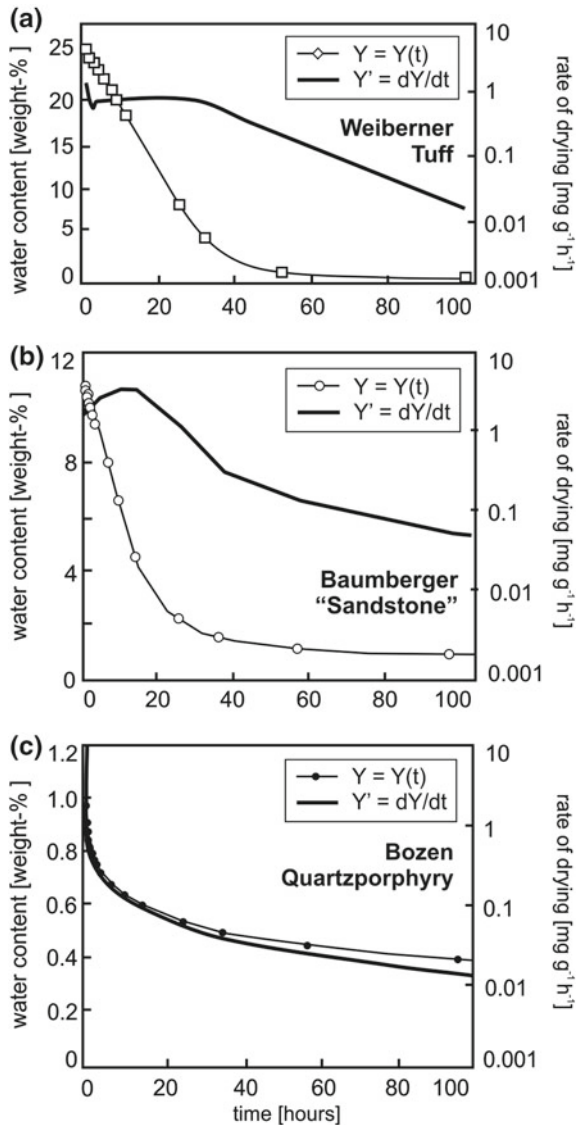
### 3.3.3 Drying Characteristics

The drying characteristic of a dimension stone is a very important factor that clearly determines the weathering resistance. Drying of wet building stones is a multistage process that is mainly governed by air humidity and movement. The faster and the more thoroughly a dimension stone is dried, the lower the probability that the stone will experience frost or salt damage. The theory of the drying of porous building materials is described by Vos (1978), Snethlage (1984), Klopfer (1985), Kraus (1985), and Snethlage et al. (1986), and examples are given in Fig. 3.25. In general, two phases can be distinguished; the first phase is characterized by a rapid decrease in moisture content, which shows a nearly linear trend. This drying path is defined as the capillary moisture transport from the inside of the sample towards the sample surface. After reaching the “critical moisture content” (Vos 1978), the water surface retreats back into the rock sample. During the second phase of the drying process, the capillary moisture transport is completely replaced and determined by water vapor conductivity processes which are related to evaporation mechanisms at the inner surfaces of the pores. The drying process stops when the moisture content in the rock sample and the adjacent air are in equilibrium.

Snethlage (1984) and Tournier et al. (2000) have defined three stages of drying wherein stages 2 and 3 correspond to a level at which the rate first decreases and then levels out at a low evaporation rate, i.e. after evaporation at a high drying rate. Franzen and Mirwald (2004) have subdivided Stage 1 into Stage 1a and Stage 1b: 1a corresponds to a sharp decrease in the drying rate, while 1b shows little change and eventually shows a tendency to increase. Stage 1b coincides with the almost linear decrease in the water content (see Snethlage 1984; Weiss 1992; Tournier et al. 2000).

Figure 3.25 shows the drying curves for different rock types: the Weiberner Tuff, Baumberger “Sandstone”, a clastic limestone, and Bozner Quartz Porphyry (see Franzen and Mirwald 2004; for the Baumberger “Sandstone” also refer to

**Fig. 3.25** Drying curves for the **a** Weiberner Tuff **b** Baumberger “Sandstone”, and **c** Bozner Quartz Porphyry. *Thin lines* with symbols represent water content versus time; *thick lines* indicate drying rates (note: log-scale in right y-axis) (after Franzen and Mirwald 2004)



Kraus 1985). Two curves are shown for each sample, the decrease in water content over time and the drying rate, which is the first derivative of the water content with respect to time. All samples follow the three steps described above. The critical moisture content for different rock types is reached after different time periods. The Baumberger “Sandstone” reaches this point after approximately 14 h and the Weiberner Tuff after about 30 h. The increase in the drying rate for the Baumberger “Sandstone” is quite pronounced, indicating a large, active evaporating surface which is related to the surface roughness of the pore system, expressed by



the specific inner-surface value. The Weiberner Tuff comprises mainly of pores of smaller sizes, likely to be responsible for the almost constant behavior at Stage 1b. The Bozener Quartz Porphyry shows a continuous decrease in the drying rate and water content and reaches a water content after 100 h that is still 40 % of the saturation (see discussion in Franzen and Mirwald 2004).

The drying characteristics are also controlled by the temperature. The samples shown above were dried in an oven at 58 °C, because Krantz (1983) has shown that the critical temperature for granites, for example, is 74 °C, whereby thermally induced microcracks start to form. For marbles, the critical temperature for crack development is much lower, as shown by Battaglia et al. (1993) and Siegesmund et al. (2000a). Vietor (1993) showed that the drying rate of an amphibolite can be very slow, and, even after 1.5 months the sample still continues to lose water, though at a very slow rate. An increase in the drying temperature up to 90 °C does not substantially increase the drying rate. The fact that water remains trapped in the rocks over very long time periods is difficult to explain.

### ***3.3.4 Moisture Adsorption***

Porous media with their specific surface areas are in constant interaction with moisture from the atmosphere surrounding them, as exemplified by the sorption of water molecules at their surface. At the hygroscopic level, the water adsorption of a rock is regulated by the moisture content of the air or humidity (Fig. 3.26), and it is separated into sorption (moisture adsorption) and desorption (moisture release). Here, the water molecules attach or detach themselves to or from the surface of the pore walls through the weak interactions of hydrogen bonds and van der Waals forces. At a given air humidity, a dynamic balance is established between the sorption and desorption of the water molecules—that is, the sorption equilibrium, which, thermodynamically, is a function of the water vapor partial pressure, or the relative humidity of the air at a constant temperature. The sorption moisture or hygroscopic range extends to equilibrium moisture content values of 95 % relative humidity.

Since the processes involved are temperature dependent the determination of the equilibrium moisture content at a given relative humidity, RH, is the basis for determining the adsorption isotherms which are characteristic of and specific to each stone type. Essential conclusions for the material properties of a stone can be drawn from the sorption and desorption isotherm determined over the whole humidity range. The sorption isotherm describes the amount of water adsorbed in relation to the relative humidity of the surrounding air, while the desorption isotherm describes the water released as RH decreases.

Both isotherms can exhibit a hysteresis, which for most stones is not pronounced. Therefore, it is often enough to only determine the sorption isotherm (Künzel 1994). Garrecht (1992) describes the presence of so-called bottleneck pores, large pores connected to a relatively small open pore for entry and access, as

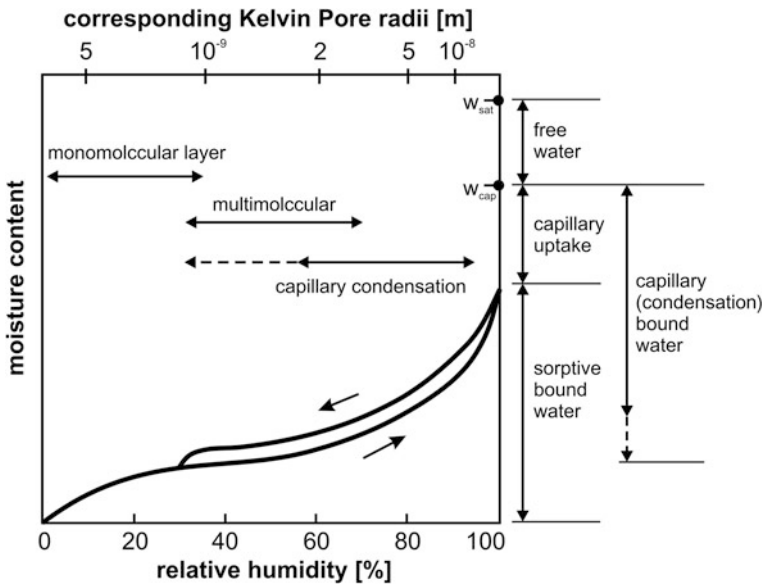


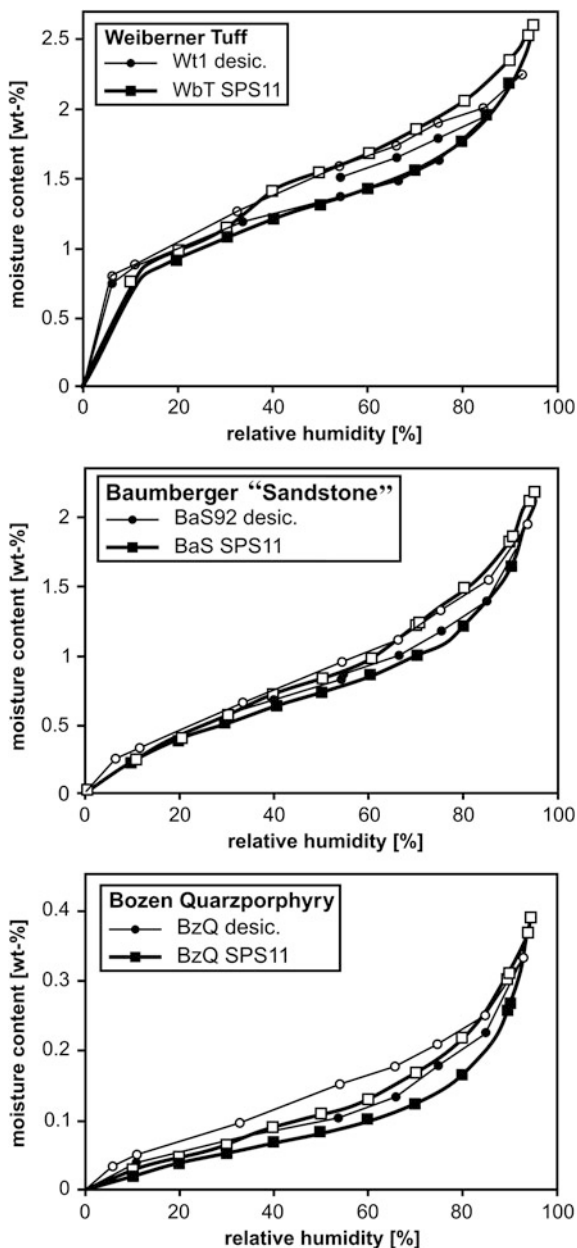
Fig. 3.26 Typical sorption isotherms of materials with small pores (after Kiebl 1983)

one cause of the hysteresis. Here, the partial pressure of the smaller pore determines the moisture condition in the larger pore. The larger pore can only release the water once the partial pressure conditions also allow the small pore to dry.

The often-observed S-shape of the sorption isotherms (Fig. 3.27) reflects different steps in sorption or desorption. For the sorption isotherm, for example, initially one monomolecular layer of water molecules is adsorbed at the pore surface. With increasing relative air humidity, further layers are added, resulting in multimolecular layer adsorption. At relative air humidity levels  $>85\%$ , the sorption isotherm increases significantly due to beginning capillary condensation, resulting in gradual filling of the pores (Krus 1995). In the pores of  $<100\text{ nm}$  ( $10^{-7}\text{ m}$ ) the occurrence of capillary condensation results in more or less full water saturation. The beginning of the capillary condensation varies, starting from 30 to 50 % RH for most of the porous stones. At 95 % RH, the sorption isotherm exhibits a very strong increase (see Fig. 3.26). For this upper range, no measurement methods are known for accurately determining the relative humidity in air humidity. It is the beginning of the capillary water range beyond the hygroscopic level (Krus 1995).

The sorption isotherms can be easily determined in a desiccator. The samples are placed at constant room temperature under different relative air humidity levels established by using different saturated salt solutions as listed in Table 3.5. Depending on their size, the samples need about one month to reach equilibrium between the relative air humidity levels inside the pores and the surrounding air in the desiccator. However, for some stones, it can take up to several weeks or months to reach equilibrium, especially for the determination of the desorption isotherm (Meng 1993). Reaching a stable value for the relative air humidity in the

**Fig. 3.27** Equilibrium moisture sorption isotherms. The filled symbols mark the sorption, and the open symbols mark the desorption data (desiccator method and SPS11 data determined by SPS 11), after Franzen and Mirwald (2004)



desiccator is not enough to assume that equilibrium has been reached (Metz 1992). In general, it is quite difficult to determine the complete water vapor sorption isotherms for stones, because of their heterogeneous composition and their often quite complex pore-space geometry.

**Table 3.5** Saturated salt solutions used for establishing constant relative humidities, their molecular weights, and the relative humidity (RH) they generate in a closed environment (after Meng 1993)

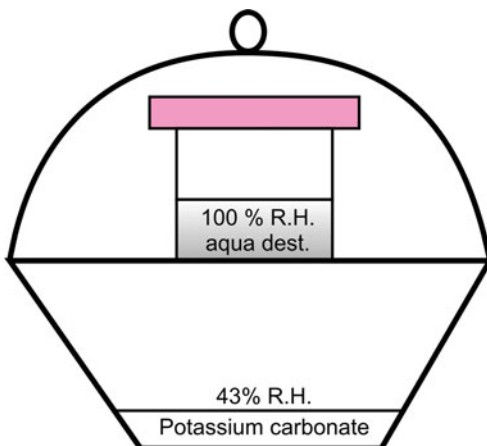
Salt	Mol weight (g)	RH at 21 °C (%)
NaOH	40	6
LiCl	42	11
MgCl <sub>2</sub> ·6 H <sub>2</sub> O	202	33
Mg(NO <sub>3</sub> ) <sub>2</sub>	148	54
NaNO <sub>2</sub>	69	75
NaCl	58	75
KCl	75	85
KNO <sub>3</sub>	102	93
K <sub>2</sub> SO <sub>4</sub>	176	97

Franzen and Mirwald (2004) applied a new, automatic working apparatus for the determination of sorption isotherms which may help to overcome the time-consuming desiccator method (see Griesser and Dillenz 2002). The data from Franzen and Mirwald (2004) further show that the hysteresis effect starts to develop significantly at around 30 % relative air humidity; the level where the monomolecular layer of the initial adsorption is assumed to be completed. All sorption curves in the study exhibit a smooth course, whereas some desorption curves show more non-continuous behavior near the 30 % relative humidity level. All the samples showed hysteresis. For all the samples with non-continuous behavior during desorption (Weiberner Tuff, Baumberger “Sandstone”, and Bozener Quartz Porphyry), the pore-radius distribution mainly comprises pores smaller than 5 μm, whereas the samples with smooth desorption curves have a pore spectrum reaching into the range of macropores. This underscores the importance of the pore-size distribution for the sorption and desorption of porous dimension stones.

### 3.3.5 Water Vapor Diffusion

The gas permeability of a rock is an important property for the drying characteristics of a wet pore surface. At the beginning of the drying process of a completely wet or soaked material, capillarity plays an important role. Further drying is characterized and determined by water vapor diffusion until the equilibrium moisture content, which depends on the environmental conditions at the site, is reached. Therefore, water vapor diffusion is of great importance for the durability of dimension stone (Schuh 1987). The diffusion transport of water vapor from the surrounding air through a porous material is determined by two types of diffusion: (1) water vapor diffusion, based on the motion of water molecules in the gas phase through the pore space and (2) surface diffusion, the fluid transport in the sorbate layer of the hygroscopic porous material. The sorbate layer on two sides of the same pore shows different thicknesses due to differences in the relative humidity. When a water molecule enters the thicker side of the sorbate layer, then on the

**Fig. 3.28** Schematic laboratory setup (wet-cup method) for the determination of the water vapor diffusion resistance factor ( $\mu$ -value). The air moisture content in the desiccator is set at 43 % relative humidity using  $K_2CO_3$ . In this atmosphere, the wet cup is placed, filled with distilled water (aqua dest.) and a relative humidity (RH) of 100 %. A cylindrical core disk is placed tightly on top of the wet cup



thinner side, another water molecule leaves the sorbate layer immediately. This transport is faster than through the gas phase (Klopfer 1985).

The dimensionless figure of water vapor diffusion resistance ( $\mu$ -value) provides information about the diffusion resistance of a porous material towards the moisture of the adjacent air. Besides the capillary water absorption, the  $\mu$ -value is the most important parameter which is used in the evaluation of the effectiveness of the treatment or retreatment of rocks with hydrophobic agents. The  $\mu$ -value is calculated from the quotient between the actual diffusion coefficient of a material and the diffusion coefficient of a static air layer of the same thickness at the same temperature. The figure of water vapor diffusion resistance, therefore, provides a direct numerical value of how much higher the diffusion resistance of a building material is in comparison to a static air layer of the same thickness. The  $\mu$ -value of air is 1. The water vapor diffusion can be determined according to the DIN EN 12572 (2009) using the dry-cup or wet-cup method.

The experimental setup for the wet-cup method is shown in Fig. 3.28. A stone disk of 10 mm thickness is placed on top of a Teflon crucible filled with demineralized water and stored at 20 °C (see Fig. 3.28). Over a period of 14 days, this experimental unit is placed in a desiccator where the relative humidity is set at 43 % by a  $K_2CO_3$  saturated solution. The measurements are carried out at a constant temperature. The water vapor transport follows the concentration gradient through the core disk outwards (wet-cup method). Changes in the weight are determined at regular time intervals. After steady state diffusion flow is reached, the weight change in the glass is proportional to time. From the linear part of the weight change, the water vapor diffusion resistance factor can be determined using the following equation:

$$\mu = \delta L \cdot p_s \cdot \Delta a \cdot A \cdot t / s \cdot \Delta m \quad (3.12)$$

where  $\delta L$  (kg/Pa · m · s) is the water vapor diffusion coefficient of air (at 21 °C:  $1.96 \cdot 10^{-10}$  kg/Pa · m · s),  $p_s$  is the partial pressure of the saturated air ( $2.49 \cdot 10^3$  Pa),  $\Delta a$

the difference of the relative humidity,  $A$  the effective sample area ( $m^2$ ),  $s$  the sample thickness ( $m$ ),  $t$  the diffusion time in  $s$ , and  $\Delta m$  the weight change in  $kg$ .

Typical values for some building stones are given in Table 3.3. From these values, the porosity as well as the pore-radius distribution have a great influence on the  $\mu$ -value because, at elevated air humidity levels, capillary condensation occurs, especially in the small pores of the porous dimension stones.

## 3.4 Thermal Properties

### 3.4.1 Thermal Conductivity

The thermal conductivities of the rocks used for buildings have an effect on the climate of the building and of its interior, especially in cases where the rocks are used as heat insulators. Porous rocks, for example, can delay the heat exchange between the inner and outer environment of a building, and, as a result, the rooms become equally warm inside. Dense rocks with good thermal conductivity often show a tendency towards moisture condensation at their interior surfaces. In general, rocks are poor heat conductors. Their heat conductivity, however, depends on the rock-forming minerals and their specific heat conductivity. Minerals with low heat conductivity values transmit the heat from the rock's surface to the inner part of the rock very slowly. For dimension stones, this is of importance when rocks or some parts of a rock are exposed to direct solar radiation.

Three petrophysical values characterize the thermal properties of rocks: the thermal conductivity  $\lambda$ , the temperature conductivity (thermal diffusivity)  $\kappa$ , and the specific heat  $c$ . The thermal conductivity can be described as the coefficient of the steady state heat transfer, whereas the temperature conductivity is a coefficient that describes the transient heat transport. The latter is an expression of how fast a temperature change spreads through a specific rock or medium. Both physical values are related to the density  $\rho$  and specific heat  $c$  of the medium, with:

$$\lambda = \kappa \rho c \quad (3.13)$$

where  $\lambda$  is given in  $Wm^{-1} K^{-1}$ . The thermal conductivity  $\lambda$  is a basic parameter (along with the heat production) for localizing geothermal fields in the Earth's crust, with application, for example, in developing geothermal energy. In building stones, the exposition is an important extrinsic parameter for conductive heat transfer. The relationship between the temperature gradient ( $grad T$ ) and the heat flow ( $q$ ) with the thermal conductivity ( $\lambda$ ) as a material property is given by the Fourier equation as follows:

$$q = -\lambda grad T \quad (3.14)$$

The two equations above only hold true for an isotropic case which is not realized in nature. However, for a rough estimation, it may be useful. The thermal



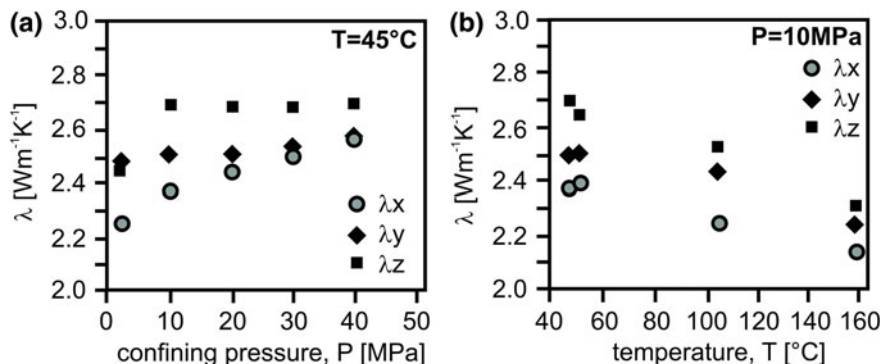


**Fig. 3.29** Directional dependence of the thermal conductivity  $\lambda$  parallel to the x-, y- and z-directions ( $\lambda_x$ ,  $\lambda_y$ , and  $\lambda_z$ ) as a function of **a** Confining pressure up to 40 MPa at a constant temperature ( $T = 45^\circ\text{C}$ ) and **b** As a function of temperature up to 160  $^\circ\text{C}$  at a constant confining pressure (10 MPa) (after Siegesmund et al. 1999)

conductivity can be determined by using stationary and non-stationary methods. Buntebarth (1991) conducted these measurements by using the divided bar technique, while Pribnow et al. (1993) used a line source. Siegesmund (1994) measured the same sample with both methods and observed discrepancies that reached up to 25%. In a strong physical sense, the line source does not allow for anisotropic media (pers. comm. Buntebarth). The in-situ thermal conductivity of rocks mainly depends on the mineralogical composition, rock fabrics, pressure, temperature, type, and degree of fluid saturation.

When considering the rock-forming minerals, a wide distribution of the average thermal conductivity values can be seen, from sillimanite with  $9.10\text{ Wm}^{-1}\text{ K}^{-1}$  over to quartz  $7.67\text{ Wm}^{-1}\text{ K}^{-1}$ , chlorite  $5.14\text{ Wm}^{-1}\text{ K}^{-1}$ , dolomite  $4.50\text{ Wm}^{-1}\text{ K}^{-1}$ , calcite  $3.57\text{ Wm}^{-1}\text{ K}^{-1}$ , and garnet  $3.31\text{ Wm}^{-1}\text{ K}^{-1}$ , down to feldspar  $2.3\text{--}2.5\text{ Wm}^{-1}\text{ K}^{-1}$ , muscovite  $2.32\text{ Wm}^{-1}\text{ K}^{-1}$ , and biotite with  $1.17\text{ Wm}^{-1}\text{ K}^{-1}$ . These values show that quartz-rich rocks should exhibit a higher average thermal conductivity, whereas for rocks with increasing feldspar content, the thermal conductivity values should decrease.

The thermal conductivity of rocks in comparison to metals is about one decimal power smaller, as, for example, copper, which has a value of  $371\text{ Wm}^{-1}\text{ K}^{-1}$  (Landolt-Börnstein 1982). Extensive literature exists on the thermal conductivity data of rock-forming minerals and rocks (e.g. Horai and Simmons 1969; Wenk and Wenk 1969; Horai and Susaki 1989). However, the values cannot really be compared, since they were determined by applying different methods and methodological approaches.

The thermal conductivity of rock samples increases with increasing pressure. The most rapid increase with increasing pressure (Fig. 3.29) has been observed in the low pressure range and has been attributed to the closure of microcracks and voids (e.g. Woodside and Messmer 1961; Buntebarth and Rueff 1987; Horai and

**Table 3.6** Thermal conductivity values of selected rocks together with density and porosity

Rock type	Density (g/cm <sup>3</sup> )	Porosity (%)	Thermal conductivity (W/m <sup>-1</sup> K <sup>-1</sup> )
<i>Sandstone</i>			
Postaer sandstone	2.06	22.7	0.93–1.13
Cottaer sandstone	2.03	24.1	1.54–1.72
Ruhr sandstone	2.53	6.1	0.65–1.40
Obernkirchner sandstone	2.15	18.6	0.81–1.69
Sander Schilf-sandstone	2.30	14.3	0.83–1.29
<i>Limestone</i>			
Muschelkalk Halberstadt	2.18	20.1	0.76–0.83
Krensheimer Muschelkalk	2.60	2.71	0.78–1.23
Schaumkalk Naumburg	1.79	33.3	1.32–1.82
Anröchter “Sandstone” (clastic limestone)	2.51	7.00	1.33–2.04
<i>Volcanic rocks</i>			
Rhyolite	2.46–2.75	0.31–9.98	0.73–3.13
Basalt	2.04–3.20	1.75–29.06	0.51–2.03
Diabase	2.75–3.15	0.20–10.60	2.13–2.90
<i>Plutonic rocks</i>			
Granite	2.55–2.74	0.16–1.65	1.34–3.69
Syenite	2.55–2.84	0.33–0.72	1.74–3.9
Diorite	2.63–3.26	0.24–0.69	1.38–2.89
Gabbro	2.63–3.26	0.24–0.69	1.80–2.83
<i>Metamorphic rocks</i>			
Marble	2.64–2.82	0.02–0.87	1.59–4.00
Serpentinite	2.55–2.89	0.25–1.44	2.31–2.87
Quartzite	2.58–2.75	0.18–0.46	2.68–7.60
Phyllite	2.64–2.88	0.28–1.44	1.67
Schists	2.64–2.88	0.28–1.44	1.03–4.93
Gneisses	2.57–2.88	0.11–0.71	0.94–4.86

From Langheinrich (1983); Schön (1983); Buntebarth and Rueff (1987); Siegesmund (1994); Szilagyí (1995); Peschel (1983); Schön (1996); Mosch and Siegesmund (2007)

Susaki 1989). This phenomenon is less important for dimensional stones, except when the rocks are under loading stress orientations relevant to the statics. The experimental studies, however, show that, above 200 MPa, the thermal conductivity exhibits nearly linear behavior reflecting the intrinsic properties of a rock. The thermal conductivity decreases with increasing temperature. Following a compilation given by Clauser and Huenges (1995) and Buntebarth (1992), it is obvious that the porosity and the pore fluid (air or air–water mixture) may decrease the thermal conductivity due to decreasing bulk density as a result of increasing porosity.

In Table 3.6, a compilation of thermal conductivity values for selected rocks are given. Data for marine basalts from Hawai’i (Fig. 3.30) show a considerable

**Fig. 3.30** Variation of thermal conductivity with porosity for air and water filled basalt samples from Hawaii (after Robertson and Peck 1974)

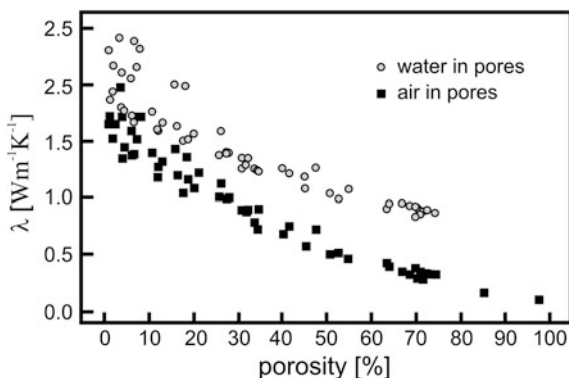
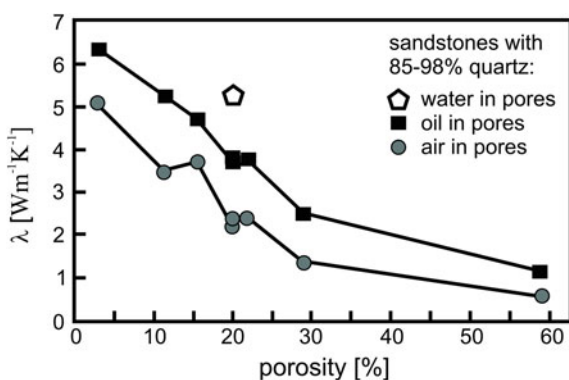


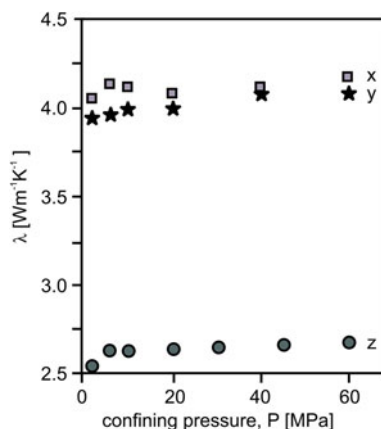
**Fig. 3.31** Variation of thermal conductivity with porosity for water-, oil- and air-filled pores in quartz-rich sandstones (after Messmer 1965)



variation in the thermal conductivity due to changes in porosity (between 5 and 75 %) and due to differences in the pore fluid, either pores filled with water (between 2.5 and 1.0  $\text{Wm}^{-1} \text{K}^{-1}$ ) or air (1.7 and 0.5  $\text{Wm}^{-1} \text{K}^{-1}$ ); see Robertson and Peck (1974). The effect of air-, oil-, and water-saturated conditions on quartz-rich sandstones also shows that the air saturation has a much more pronounced effect on the thermal conductivity than the oil- or water-saturated stones (Fig. 3.31). Transferring these results to the dimension stones, it can be assumed that water retention leads to a significant increase in thermal conductivity. Examining the data in Table 3.6, it stands out that the mineralogical composition has a substantial influence on thermal conductivity.

Different empirical methods exist for the calculation of the thermal conductivity of rocks (e.g. Birch and Clark 1940; Woodside and Messmer 1961; Horai and Baldrige 1972). The basic assumption of these methods is that they used a model of idealized layers arranged in parallel with the number and thickness of each individual component related to the rock-forming minerals and their volume fraction. These relationships correspond to the averaging procedures of Voigt and Reuss in the case of the thermal conductivity parallel and perpendicular to the

**Fig. 3.32** Directional dependence of the thermal conductivity ( $\lambda$ ) of a foliated paragneiss sample as a function of pressure up to 60 MPa (at room temperature) using the divided bar technique (x parallel to the lineation within the foliation plane, y normal to the lineation within the foliation, and z normal to the foliation and lineation), after Siegesmund (1996)



layer boundaries, respectively. Empirically derived averaging schemes, which demonstrate a better fit between the experimentally measured and the calculated thermal conductivities, have been described in the literature (Schön 1983; Siegesmund 1996).

For minerals as well as rocks with a pronounced rock fabric, like gneiss, marble, or schists, the thermal conductivity can be strongly directionally dependent. Langheinrich (1983) found that the thermal conductivity in slates showed considerable differences in different directions. Slates with pronounced fabric anisotropy also show a relatively high anisotropy of the thermal conductivity. Clauser and Huenges (1995) showed, for a gneiss sample and an amphibolite, that the thermal conductivity may vary for the same sample from 100 % parallel to the layering to about 60 % perpendicular to the layering (foliation). Siegesmund (1994) determined values for a comparable paragneiss ranging from around 2.5 to 4.1 Wm<sup>-1</sup> K<sup>-1</sup> (Fig. 3.32).

For all metamorphic rocks investigated, Langheinrich (1983) was able to show that the highest values of the thermal conductivity are observable in the direction parallel to the lineation. The lowest values were measured perpendicular to the foliation. These data are also in accordance with measurements from Wenk and Wenk (1969). The reason for this rock-fabric related anisotropy of the thermal conductivity can be found in the preferred orientation of the mica minerals, mainly muscovite, with their mineralogical (001) planes parallel to the foliation (layering) combined with a strong directional dependence of the thermal conductivity of the mineral itself (Fig. 3.33). The single crystal thermal conductivity for muscovite, for example, is in the range from 0.84 Wm<sup>-1</sup> K<sup>-1</sup> (parallel c-axis) to 5.11 Wm<sup>-1</sup> K<sup>-1</sup> (parallel a- and b-axis) and with an anisotropy of 83 % (Fig. 3.33). This general explanation also holds for metamorphic slates, as here, some of the rock-forming minerals are the phyllosilicates, like illites/muscovites and chlorites. Quartz, which may also show some preferred orientation in these rocks, only plays a subordinate role with respect to the whole-rock anisotropy of thermal conductivity. However, the mineral itself exhibits a significant directional dependence of

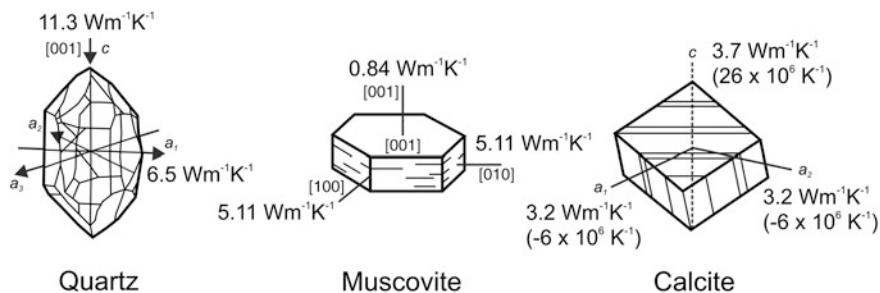


**Fig. 3.33** Thermal conductivity values (in  $\text{Wm}^{-1}\text{K}^{-1}$ ) of quartz, muscovite, and calcite in relation to the crystallographic axis. For calcite, the thermal expansion coefficients are also given (after Siegesmund 1996; Siegesmund et al. 1997)

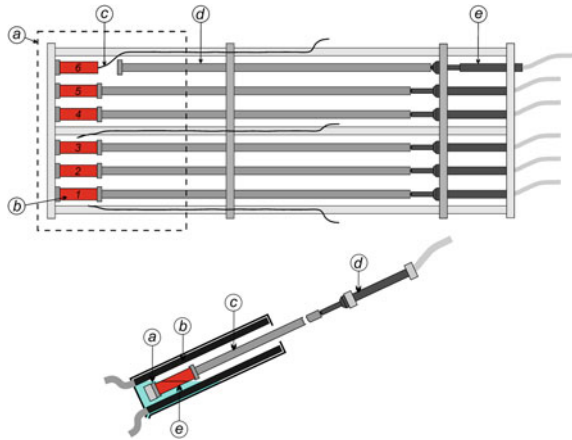
the thermal conductivity, with  $11.3 \text{ Wm}^{-1} \text{ K}^{-1}$  parallel to the c-axis and  $6.5 \text{ Wm}^{-1} \text{ K}^{-1}$  parallel to the a-axes, and with an anisotropy of 42 %. Calcite, as the main mineral in limestone and marbles, only shows a weak anisotropy (13 %), with the highest value parallel to the c-axis ( $3.7 \text{ Wm}^{-1} \text{ K}^{-1}$ ) and the lowest parallel to the a-axes ( $3.22 \text{ Wm}^{-1} \text{ K}^{-1}$ ). However, calcite exhibits a strong directional dependence of the thermal expansion, which is relevant for the application of marbles as dimension stones (see Sect. 3.4.2).

### 3.4.2 Thermal Expansion

Thermal expansion is an important property for characterizing dimension stones, especially for their application and use in structural engineering, e.g. as cladding panels in exterior use or as flooring. For these applications, a standardized evaluation of the expansion behavior during thermal exposure is essential and necessary (e.g. Peschel 1983). This includes the volume expansion of the rock as well as the anisotropy of the thermal expansion and the residual expansion, i.e. permanent length change after thermal treatment (related to thermal crack formation). The knowledge of the thermal expansion together with other petrophysical properties allows conclusions to be drawn concerning the suitability of a given dimension stone for certain applications. Changes in temperature and moisture are supposed to be important factors in stone degradation, as mentioned in Sects. 3.3 and 3.5 and further discussed in Sect. 4.2).

Comparable to other solid media a rock changes its volume when subject to a temperature change. The related thermal properties of a rock can be derived from its mineral content and composition. Most of the minerals show an anisotropic behavior of their linear thermal expansion, similar to many other mechanical properties, and so an anisotropic behavior for the rocks can be assumed. For rock samples with no or less pronounced preferred orientation of rock fabric elements (see Sect. 2.8) the thermal expansion shows more or less similar values in different

**Fig. 3.34** Schematic diagram of a pushrod dilatometer. *Top:* (a) position of the climate chamber (b) sample cylinder 50 mm in length and 15 mm in diameter (c) temperature sensor (d) quartz glass pushrod (e) display sensor. *Bottom:* (a) water level (b) heat exchanger copper plate (c) quartz glass pushrod (d) displacement sensor, and (e) sample cylinder (Strohmeier 2003)



directions. However, the linear thermal expansion coefficient of rock-forming minerals is often only valid for a certain temperature interval. The coefficient should not be extrapolated into other temperature intervals, as the thermal expansion does not linearly increase with increasing temperature. For practical applications it is important to know that after a rock sample experienced a temperature impact the sample length or volume will not be restored to its original value, which means that the temperature impact has resulted in a permanent form change.

Thermal expansion (millimeter/meter or mm/m) expresses the relative length change of a polycrystalline sample with changing temperature (Grüneisen 1926). The connection to the temperature is non-linear, i.e. the thermal expansion coefficient  $\alpha$  ( $\text{K}^{-1}$ ), which describes the specific length change per unit temperature depends on the considered temperature interval. The thermal dilatation coefficient  $\alpha$  is calculated as the ratio between the length change of the samples  $\Delta L$  and the original sample length  $L$  multiplied by the temperature interval  $\Delta T$  in Kelvin ( $\alpha = \Delta L/L \times \Delta T$ ). The residual strain ( $\epsilon_{rs}$  in mm/m) is defined as the ratio between the length change of the sample after cooling down to room temperature  $\Delta L_{rt}$  and the original sample length  $L$  as shown in the following equation:

$$\epsilon_{rs} = \Delta L_{rt}/L \quad (3.15)$$

$\epsilon_{rs}$  can only be related to one temperature level, in this case to room temperature before and after any temperature cycle.

So far no accepted international norm for the measurement and determination of the thermal expansion is available and it is not yet expected for the near future. Thermal expansion can be measured by means of a pushrod dilatometer (Fig. 3.34), which allows the measurement of six cylinders simultaneously (e.g. Strohmeier 2003; Koch and Siegesmund 2004). The dilatometer consists of three main units: the heating unit, the specimen holder in the climate chamber, and the displacement register. Taking room temperature as the basis, heating and cooling



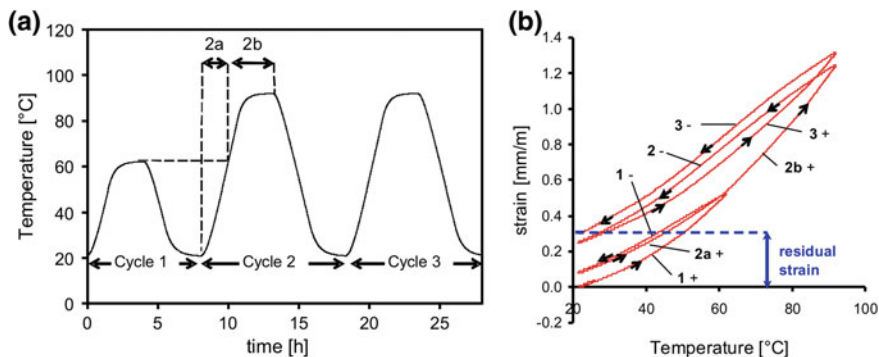


**Fig. 3.35** **a** Temperature course of cycles 1–3 performed in the thermal dilatation measurements under dry conditions. The heating and cooling rate is 0.5 °C/min. The destination temperatures are 60 °C in cycle 1 and 90 °C in cycles 2 and 3. **b** Specific example where the course of the expansion is indicated by arrows and numbers while heating (+) and cooling (–)

are tested at a 0.5 °C/min rate to ensure thermal equilibration of the specimen and to simulate the conditions at a building as closely as possible. After reaching the designated temperature of each cycle, the temperature is kept at that level until the sample length remains stable (Fig. 3.35). This operating sequence allows detection of (a) the thermal dilatation by simulating temperature changes comparable to those observed under natural conditions, (b) the buffering effect of pre-existing microcrack systems due to former thermal degradation or pre-existing microcracks originating from the sample's geological history (Siegesmund et al. 2000b), (c) the effect of the increase in the thermal dilatation coefficients of rock-forming minerals, and (d) the influence of intrinsic properties and thermal degradation (Zeisig et al. 2002).

Temperature changes, especially in thermally sensitive marbles, can cause a pronounced loss of relief structure due to granular decohesion. This weathering phenomenon is also known as “insolation weathering” if the main heat source is the sun (Bland and Rolls 1998). Evidence for this type of weathering is known from many hot rocky deserts (Roth 1955; Goudie 1974; Peel 1974; Ollier 1984). There, diurnal temperature changes on the rock surface of approximately 42 °C may occur (Peel 1974). High temperature changes are also reported from cold environments. Under mid-European climates, however, temperature changes of about 35–40 °C on stone surfaces between day and night can be observed (Weiss 1992). The experimental simulation of this type of degradation has a long tradition. For example, Griggs (1936) heated and cooled coarse-grained granite through a temperature range of 110 °C for a simulated period of 240 years corresponding to 89,400 heating cycles without evidence of any decay phenomena. In contrast, Aires-Barros et al. (1975) observed, for comparable heating cycles, a destruction of the rock fabric and a loss of material up to 4.26 weight%.

Studies from Ide (1937), Richter and Simmons (1974), Simmons and Cooper (1978), Bauer and Johnson (1979), and Glover et al. (1995) investigated the thermal expansion of magmatic rocks, like granite and norite or quartzite (Lu and Jackson 1998). They showed that, for these rocks, the occurrence of thermal cracks can also be expected. However, most of these studies focused on the expansion behavior of these rocks under Earth-crust conditions with temperatures up to 700 °C and higher pressure (Lu and Jackson 1998). Therefore, conclusions about expansion values and behaviors for central-European surface temperature ranges and normal pressure have not been derived. However, very high temperature values can be seen on surface sites where fire impact played a role (see below).

When a stone is heated, it expands and then contracts when it is cooled. While the thermal expansion coefficient characterizes the material's response to heating or cooling, the residual strain after thermal exposure characterizes the thermal sensitivity of a rock. Figure 3.36 depicts very good examples of the thermal behavior of three different marble types. For each marble sample, specimens were prepared, cut in three directions perpendicular to each other in order to identify possible directional dependencies of the thermal properties. The graphs of thermal dilatation as a function of temperature show the following characteristics: both samples of Carrara Marble (CA1 and CA2) have a very similar lattice preferred orientation of the calcite grains and similar grain size (see Chap. 2), but exhibit a completely different magnitude of the residual strain after heat treatment up to 120 °C. Sample CA2 (Fig. 3.36b) exhibits a large residual strain, while the sample CA1 (Fig. 3.36a) has a small one. According to the weak texture of both samples, the directional dependence of the thermal expansion coefficient is small. The corresponding curves are almost linear with the temperature when it is raised for CA1, but for CA2, the slope increases when reaching about 60–70 °C (dotted line in Fig. 3.36b). This indicates that (i) thermally induced cracks are generated at a certain critical crack initiation temperature, or (ii) the total thermal dilatation coefficient is buffered by pre-existing critical crack systems at temperatures lower than the above-mentioned critical temperature. The Kauffung Marble (Poland) is another exceptional example showing a strong directional dependence of the thermal expansion. However, no residual strain, even after heat treatment up to 120 °C, can be observed, and the dilatation increases almost linearly with temperature. Accordingly, the slope of the thermal dilatation curves is quite linear (Siegesmund et al. 2000a; Weiss et al. 2000). Any residual strain left in a stone after heating is the beginning of its deterioration.

For marbles, an average thermal expansion value of around  $11 \times 10^{-6} \text{ K}^{-1}$  was calculated based on a larger sample set (Zeisig et al. 2002). In summary, up to now, all experimentally determined polycrystalline thermal expansion behaviors of marbles as a function of a heating and subsequent cooling cycle can be classified in four main categories: (a) isotropic thermal expansion without residual strain (b) anisotropic thermal expansion without residual strain (c) isotropic thermal expansion with residual strain, and (d) anisotropic thermal expansion with residual strain (Fig. 3.37).

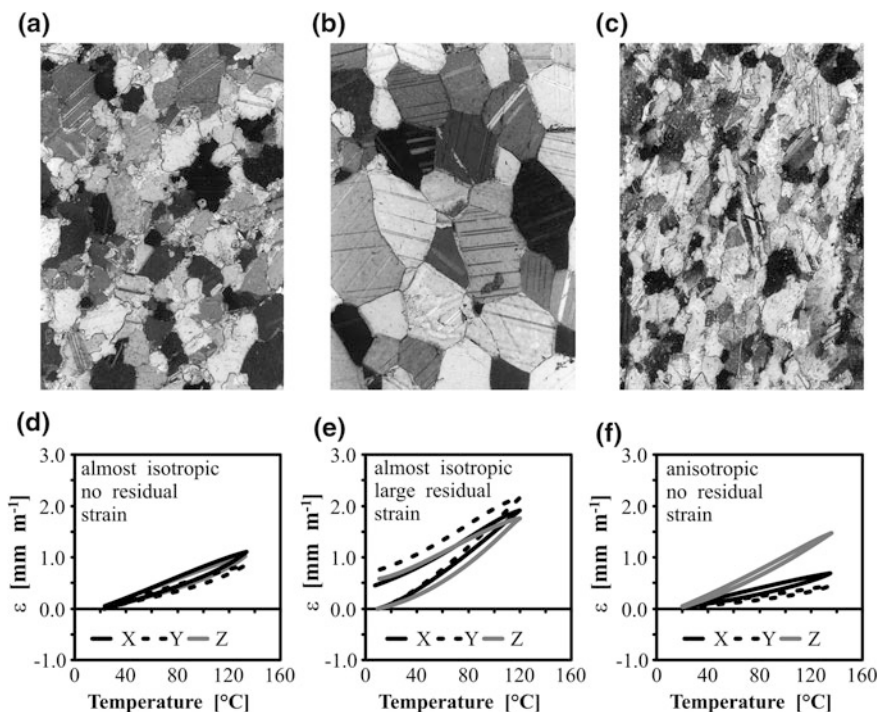
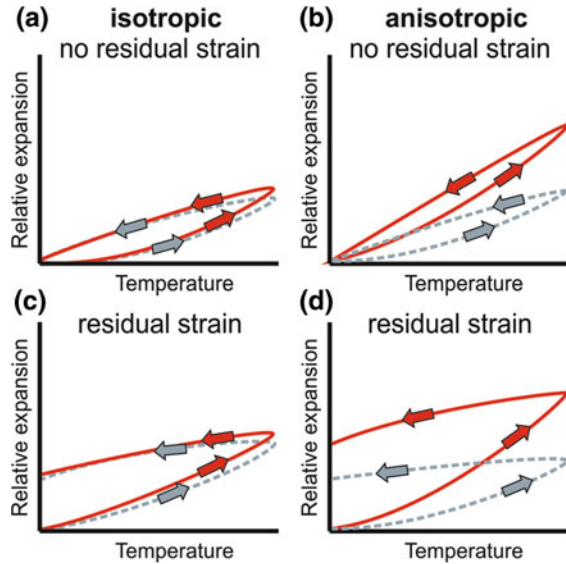


**Fig. 3.36** Microfabrics of different marbles (long side of the photograph corresponds to 700  $\mu\text{m}$ ) with **a** Carrara Marble (CA1) with irregular grain boundaries and a bimodal grain-size distribution with small recrystallized grains and large relic grains **b** Carrara Marble (CA2) with straight grain boundaries (so-called *foam structure*), and **c** Kauffung Marble (KA) with elongated grains showing irregular grain boundaries. The macroscopically visible foliation is parallel to the long side of the photograph. Experimentally determined dilatation as a function of thermal treatment up to 120  $^{\circ}\text{C}$  is shown in **d** Carrara Marble (CA1) **e** Carrara Marble (CA2), and **f** Kauffung Marble (KA). Note the considerable residual strain of the CA2 marble, while no residual strain is observed for the other Carrara Marble. The different curves for each sample correspond to different directions perpendicular to each other of the investigated sample cube (after Weiss et al. 2001)

The thermal expansion coefficients for a number of rocks are compiled in Table 3.7. They have been calculated for the temperature interval between 20 and 90  $^{\circ}\text{C}$ . Since some of the thermal expansion curves are not linear, this approach has to be considered as an approximation (see discussion in Zeisig et al. 2002, and Weiss et al. 2004b).

For magmatic rocks (Table 3.7), the thermal expansion coefficient varies between  $5 \times 10^{-6} \text{ K}^{-1}$  and  $10 \times 10^{-6} \text{ K}^{-1}$ . Samples with extraordinarily low values (like the gabbro-norite) contain a high amount of plagioclase with extremely small volume expansions. Typical expansion curves show a straight increase and decrease in length due to temperature (Weiss et al. 2004b). In some cases, granites may also show a residual strain, which is also evident for those rocks that may show a bowing of thin

**Fig. 3.37** Schematic illustrations of the thermal expansion behavior of marble samples. The arrows indicate directions of temperature change (heating and subsequent cooling) (after Siegesmund et al. 2004a)



slabs. For the Cezlak Granodiorite (Slovenia), the thermal expansion is significantly anisotropic ( $A = 0.25$ ) with  $\alpha = 7.89 \times 10^{-6} \text{ K}^{-1}$  parallel to the  $z$ -direction, i.e. normal with respect to the foliation plane ( $xy$ ), and  $\alpha = 5.89 \times 10^{-6} \text{ K}^{-1}$  parallel to the  $y$ -direction (Fig. 3.38; Siegesmund et al. 2008a).

Gneisses and schists vary between  $6 \times 10^{-6} \text{ K}^{-1}$  and  $9 \times 10^{-6} \text{ K}^{-1}$ . Most gneiss samples show linear expansion behaviors similar to the magmatic rocks. An exception is the Knotenschiefer Slate from Theuma (Germany), which predominantly contains quartz and mica and shows high thermal expansion coefficients (Fig. 3.39). These minerals have a high volume expansion coefficient. Feldspar (with a low volume expansion coefficient) is lacking. The thermal expansion curve of Theuma is also characterized by a dehydration reaction, which is most pronounced in the direction perpendicular to the foliation (residual strain  $-0.3 \text{ mm/m}$  at  $20 \text{ }^\circ\text{C}$ ) and almost negligible parallel to the foliation.

Quartzitic rocks lie within the range of quartz-rich stones. The thermal expansion coefficient for quartz lies between  $9 \times 10^{-6} \text{ K}^{-1}$  and  $14 \times 10^{-6} \text{ K}^{-1}$ . Quartzite shows almost the entire range of this variation as a consequence of the strong lattice preferred orientation of quartz. In general, the thermal expansion coefficient for sandstones is in the range of  $10 \times 10^{-6} \text{ K}^{-1}$ . A rare exception is the Baumberger “Sandstone” (clastic limestone), whose average thermal expansion coefficient is around  $6.5 \times 10^{-6} \text{ K}^{-1}$ . Even if the directional dependence in this rock is weak, its magnitude is directly controlled by the mineral composition—that is, the relative frequency of highly expanding calcite and the lesser expansion in feldspar and quartz.

Its behavior is comparable to that of the Anröchter Limestone. Systematic investigations of limestone are still missing. The sparitic Kuacker Limestone has a

**Table 3.7** Thermal expansion coefficient  $\alpha$  ( $10^{-6} \text{ K}^{-1}$ ) for different directions (x-, y-, and z-directions are perpendicular to each other) for various dimension stones with commercial name, country of origin, and rock type given (Strohmeyer 2003; Weiss et al. 2004a; Ruedrich and Siegesmund 2007; Hoffmann 2008; Mosch 2009; Morales 2011 and unpublished data)

Commercial name	Country of origin	Rock type	Thermal expansion coefficient $\alpha$					Average value ( $10^{-6} \text{ K}^{-1}$ )	Anisotropy (%)
			x-direction ( $10^{-6} \text{ K}^{-1}$ )	y-direction ( $10^{-6} \text{ K}^{-1}$ )	z-direction ( $10^{-6} \text{ K}^{-1}$ )	z-direction ( $10^{-6} \text{ K}^{-1}$ )			
Ben Tak White	Thailand	Granite	7.20	7.99	7.51	7.51		7.57	9.9
Muang Tak Orange I	Thailand	Granite	9.07	8.14	8.60	8.60		8.60	10.3
Kösseine	Germany	Granite	9.37	8.12	10.20	10.20		9.23	20.4
Antrona	Italy	Granite	7.02	6.70	6.68	6.68		6.80	4.8
Rojo Dragon	Argentina	Granite	9.65	9.72	10.00	10.00		9.79	3.5
Padang	China	Granodiorite	6.73	6.99	8.32	8.32		7.35	19.1
Ben Tak Blue	Thailand	Quartz-monzonite	7.97	7.58	7.24	7.24		7.60	9.2
Salmon Red	Uruguay	Syenite	6.50	6.12	7.59	7.59		6.74	19.4
Artigas	Uruguay	Syenite	4.07	7.53	5.96	5.96		5.85	45.9
Blue Pearl	Norway	Larvikite	5.42	3.98	9.63	9.63		6.34	58.7
Nero Assoluto	Uruguay	Dolerite	6.66	6.79	6.68	6.68		6.71	1.9
Anzola	Italy	Gabbro	6.89	7.23	8.02	8.02		7.38	14.1
Nero Impala	South Africa	Gabbro-norite	5.14	4.68	5.23	5.23		5.02	1.7
Negro Riojano	Argentina	Gabbro	7.93	7.85	7.42	7.42		7.73	6.4
Balmuccia	Italy	Peridotite	8.16	8.69	8.74	8.74		8.53	6.6
Löbejün	Germany	Rhyolite	7.27	6.47	6.99	6.99		6.91	11.0
Stardust Grey	Argentina	Rhyolite	7.58	8.00	8.62	8.62		8.07	12.1
Monte Merlo	Italy	Trachyte	7.14		4.03	4.03		5.59	43.6
Drachenfels	Germany	Trachyte	4.66		7.22	7.22		5.94	35.5
Weibern	Germany	Phonolite tuff	5.72	3.23	6.09	6.09		5.01	47.0
Rochlitz	Germany	Rhyolite tuff	8.00	8.28	7.74	7.74		8.01	6.5
Eger-DEMjen	Hungary	Dacite tuff	4.64		4.89	4.89		4.77	5.1

(continued)

Table 3.7 (continued)

Commercial name	Country of origin	Rock type	Thermal expansion coefficient $\alpha$					Anisotropy (%)
			x-direction ( $10^{-6} \text{ K}^{-1}$ )	y-direction ( $10^{-6} \text{ K}^{-1}$ )	z-direction ( $10^{-6} \text{ K}^{-1}$ )	Average value ( $10^{-6} \text{ K}^{-1}$ )		
Phanom Sarakhm Grey	Thailand	Gneiss	8.95	8.82	9.00	8.92	2.0	
Azul Tango	Argentina	Gneiss	7.09	8.35	8.25	7.90	15.1	
Calanca	Italy	Gneiss	6.93	6.54	6.81	6.76	5.6	
Verde Andeer	Italy	Gneiss	7.63	6.41	8.97	7.67	14.9	
Serizzo Monte Roas	Italy	Gneiss	7.65	6.87	7.88	7.47	2.9	
Wang Nam Kiew Black	Thailand	Hornblendite	7.29	7.20	6.64	7.04	8.9	
Franco Veteado	Argentina	Migmatite	9.01	8.88	9.11	9.00	2.5	
Rosa Estremoz	Portugal	Marble	4.37	11.28	10.23	8.63	61.3	
Carrara	Italy	Marbe	9.72	10.34	12.46	10.84	22.0	
Carrara	Italy	Marble	4.81	6.64	6.90	6.12	30.3	
Phran Kratai Grey	Thailand	Marble	-0.60	2.20	11.70	4.43	105.1	
Azul Cielo	Argentina	Marble	1.18	9.70	1.67	4.18	87.8	
Azul Imperial	Brazil	Quartzite	11.40	11.50	11.10	11.33	0.9	
Camine Rufo	Uruguay	Slate	9.99	9.96	1.28	7.08	87.2	
San Luis Slate	Argentina	Slate	9.50	9.89	1.17	6.85	88.2	
Theuma	Germany	Slate	9.84	9.34	12.08	10.42	22.7	
Globegerina	Malta	Limestone	4.72	4.57	4.24	4.51	10.2	
Calizza Amarilla	Argentina	Limestone	5.14	6.89	6.17	6.07	25.4	
Dolomita Dorada	Argentina	Dolomitic limestone	9.20	1.01	9.26	6.49	89.1	
Mae Phrik Yellow	Thailand	Limestone	4.36	4.69	4.18	4.41	10.9	
Soskut	Hungary	Limestone	3.59	4.54	4.39	4.17	20.9	
Jerusalem	Israel	Limestone	3.89	4.61	4.55	4.35	15.6	
Kuacker	Germany	Limestone	4.70	6.62	4.71	5.34	29.0	
Thüster	Germany	Limestone	1.41	3.24	3.89	2.85	63.8	

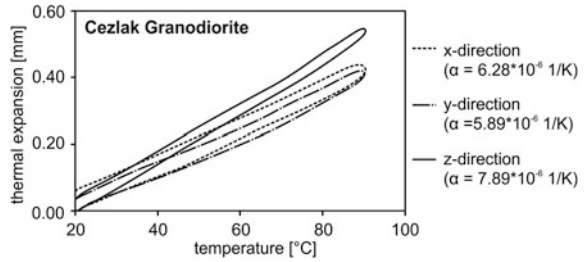
(continued)



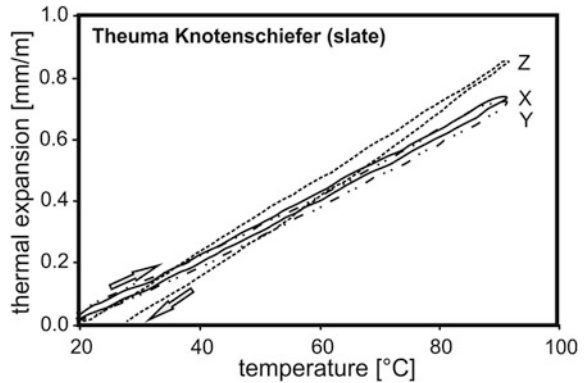
Table 3.7 (continued)

Commercial name	Country of origin	Rock type	Thermal expansion coefficient $\alpha$					Anisotropy (%)
			x-direction ( $10^{-6} \text{ K}^{-1}$ )	y-direction ( $10^{-6} \text{ K}^{-1}$ )	z-direction ( $10^{-6} \text{ K}^{-1}$ )	Average value ( $10^{-6} \text{ K}^{-1}$ )		
Bad Langensalza	Germany	Travertine	5.70	5.92	5.50	5.60	7.1	
Baumberger	Germany	Sandstone-like limestone	5.76	6.46	7.34	6.52	21.5	
Rüthener	Germany	Sandstone	11.10	11.70	11.90	11.57	6.7	
Bad Bentheim	Germany	Sandstone	11.90	12.00	12.50	12.13	4.8	
Schleierther	Germany	Sandstone	10.50	10.50	9.96	10.32	5.1	
Weser	Germany	Sandstone	9.30	7.50	8.40	8.40	19.4	
Sikhiu Brown	Thailand	Sandstone	11.93	12.66	12.50	12.36	5.8	
Pakchong Green	Thailand	Sandstone	8.91	8.25	8.45	8.54	7.4	
Tacuarembó	Uruguay	Sandstone	1.23	1.18	1.24	1.22	4.8	

**Fig. 3.38** Cezlak Granodiorite: experimentally determined thermal dilatation as a function of temperature (after Siegesmund et al. 2008a)



**Fig. 3.39** Thermal expansion behavior for the Theuma Knotenschiefer (slate) that shows high coefficients and a dehydration reaction, which is most pronounced perpendicular to the foliation direction. The thermal expansion path, i.e. heating and cooling, is marked by arrows. Heating was performed from 20 to 90 °C



thermal expansion coefficient of about  $5.5 \times 10^{-6} \text{ K}^{-1}$  and has a residual expansion of 0.07 mm/m, indicating a strong anisotropy (Fig. 3.40, compare x-, y-, and z-directions, Siegesmund et al. 2010).

Besides dehydration effects related to the mineral composition, samples may show different thermal behavior when water is present in the pores. The German Weser Red Sandstone (Buntsandstein) may serve as an example of this behavior. When the sample is heated under dry conditions, the thermal expansion coefficient is quite linear and similar at all sample directions (Fig. 3.41). However, it is remarkably different when water is present in the pores (Fig. 3.41). Then, assumedly, a kind of dehydration reaction occurs which is most pronounced in the z-direction, i.e. the direction perpendicular to the bedding. The second cycle clearly evidences the previous effect of the pore water, since, after the dehydration reaction, the thermal expansion coefficient is the same in the dry condition. This example shows that samples sensitive to hygric/hydric dilatation may also have thermal expansion changes even if this is not the primary reason for these changes.

In summary, most marbles can clearly be considered as thermally sensitive materials (see also discussion in Sect. 4.2) because calcite causes temperature-induced damage at comparably low temperature intervals (about 40 °C; Battaglia et al. 1993).

Even if dolomite marbles are more resistant, the main cause for thermal degradation is the thermal expansion anisotropy of calcite and dolomite and the associated thermal stress generation (Siegesmund et al. 2000a, 2008a; Shushakova

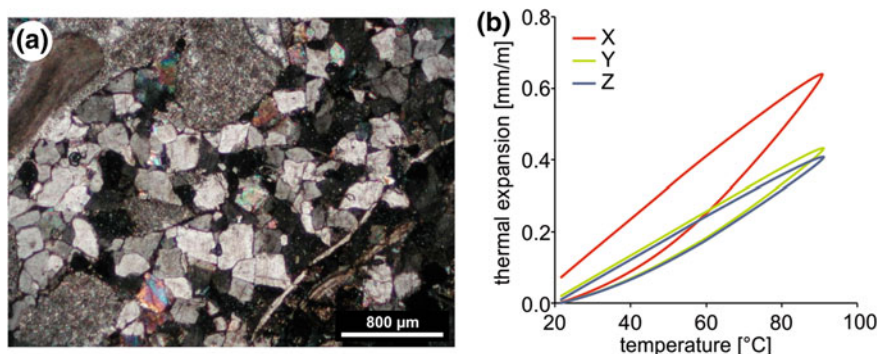


**Fig. 3.40** Thermal expansion for the Kuacker Muschelkalk **a** Microfabrics showing a clear sparitic fabric, and **b** Thermal expansion and its anisotropy as a function of temperature. Note the residual strain values after the heating cycle, corresponding to a permanent length change (after Siegesmund et al. 2010)

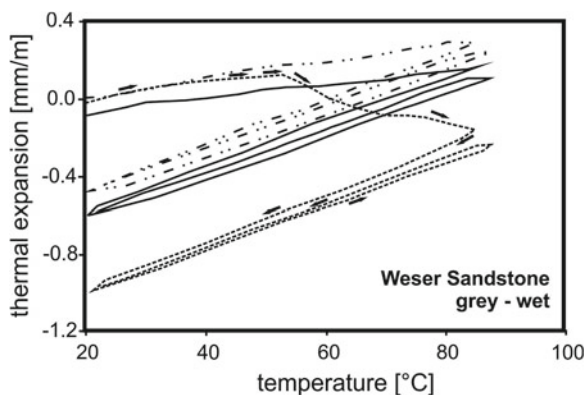


**Fig. 3.41** Thermal expansion curve for a Weser Red Sandstone (Buntsandstein). Heating was performed from 20 to 90 °C in two cycles. The thermal expansion path is indicated by *arrows*. The first cycles clearly indicate a dehydration reaction, i.e. a contraction which is especially pronounced in the direction normal to the bedding. In the following cycles, the Weser Sandstone behaves as expected under dry conditions (after Weiss et al. 2004a, b)

et al. 2010). This effect is much less pronounced but not zero in dolomite marbles (Weiss et al. 2002a, b; Zeisig et al. 2002). Marbles are the only rock types where a preferred orientation of the main constituent minerals can cause certain directional dependencies of the thermal expansion coefficient and of the residual strain. Accordingly, marbles show the highest directional dependence of the thermal expansion coefficient (Shushakova et al. 2010).

Sedimentary rocks show a large variation in thermal properties. In most cases, the thermal expansion curve is quite straight, showing no residual strain after heating. However, a certain alteration of this behavior is to be expected when the

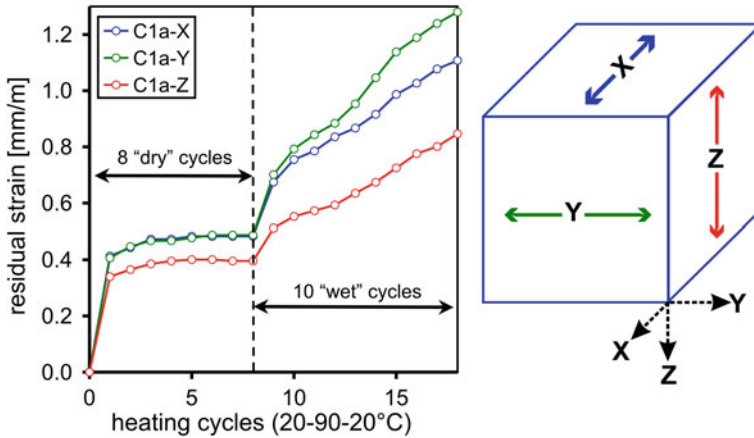


**Fig. 3.42** Progressive increase in residual strain of a calcite marble (Carrara) as a function of 8 dry cycles followed by 10 wet cycles (9–18) in three different directions, perpendicular to each other (from Koch and Siegesmund 2004)

samples are wet. This is particularly the case for rocks with a high porosity, large pore structure, and high phyllosilicate content. Then, only the combination of heating and wetting can cause any remarkable alteration of the thermal expansion behavior (see Sect. 3.5). Even if the directional dependence of the thermal expansion coefficient is weak for sedimentary rocks, its magnitude is directly controlled by the mineral composition, i.e. the relative frequency of highly-expanding calcite and weakly-expanding feldspar and quartz. Very good examples of this behavior are impure sandstones or limestone, such as the Anröchter “Sandstone” (clastic limestone) discussed previously.

### 3.4.2.1 Deformation of Stone Slabs

Many authors (Sage 1988; Koch and Siegesmund 2004; Grell et al. 2004; Siegesmund et al. 2008b) have shown that the increase in residual strain stops after a few heating cycles if moisture is absent. Therefore, Bucher (1956) and Winkler (1996) point out the importance of moisture in the bowing process of stone slabs. To detect the anomalous weathering behavior of rocks, the thermal expansion tests must also be carried out under a combination of dry and wet conditions. For this purpose, the setup shown in Fig. 3.34 can be modified easily by tilting the specimen holder and the climate chamber. To discuss these effects, more detailed measurements of progressive residual strain on a calcite marble were performed. Eight dry cycles up to 90 °C were followed by 25 additional wet cycles, whereby the first six wet cycles were carried out in such a way that, at the end of a heating cycle, the samples in the climate chamber were run until totally dry (Fig. 3.42). The findings from this approach can be summarized in two points. First, under wet

conditions, there is a constant progressive residual strain that increases continuously even after 25 cycles (depending on the marble type). Secondly, the moisture content after heating cycles apparently influences the intensity of the marble deterioration.

The bowing behavior of marble panels can be tested easily in the laboratory (Koch and Siegesmund 2004; Grell et al. 2004; and Siegesmund et al. 2008b). The test was performed on slabs ( $400 \times 100 \times 30$  mm) so that each specimen was exposed to moisture on one side and infrared heating on the reverse side. The applied temperature ranged between 20 and 80 °C, and a total of 40 cycles was performed. The continuous length change and the effect of anisotropic bowing with the applied cycles are shown in Fig. 3.43. The experiment confirmed that the bowing of the marble depends on the temperature and moisture conditions of the mineralogical composition of the marbles, as well as on their fabrics (see discussion in Siegesmund et al. 2008b). Bowing deformation (Figs. 3.63 and 3.78) has also been observed in other rock types, such as granite (Siegesmund et al. 2008b; Vázquez et al. 2010) or the conglomerate Nagelfluh (Grimm 1999).

#### 3.4.2.2 Thermal Behavior at Higher Temperatures

With respect to thermal expansion, most of the rock forming minerals (see Chap. 2) can be seen as anisotropic and, therefore, most of the dimension stones also exhibit anisotropy depending on the degree of preferred orientation of the constituting minerals. As explained above, the thermal expansion coefficient depends strongly on the temperature. However, the relevant temperature range for the evaluation of temperature-related properties for dimension stone is less than 120 °C and may only exceed it for fire impacts. There are few historic and valuable buildings that have not suffered at least one fire during their existence (Sippel et al. 2007).

Thermal expansion measurements up to 1,000 °C reveal that every rock shows a specific expansion behavior. Owing to the transition of low to high quartz, all quartz-bearing rocks experience a sudden and remarkable expansion at temperatures just below 600 °C (Fig. 3.44). The surface finishing of dimensional stones known as “flamed surfaces” uses the effect of higher temperatures to produce rough surfaces. Although the phase transformation of quartz is reversible, a striking positive residual strain can be recognized for the rhyolite and the granite after cooling from maximum temperatures of around 700 °C (Fig. 3.44). Temperatures of 500 °C result in much lower values of residual strain.

Consequently, all quartz-bearing rocks show varying degrees of intragranular microfractures within quartz grains. Fredrich and Wong (1986) refer to intragranular microfractures in the feldspars of heated granites, whereas Hajpal and Török (2004) describe intergranular microfractures in quartzitic sandstones for temperatures below 500 °C (see discussion in Sippel et al. 2007). Residual strains in silicate rocks are significantly higher at temperatures above 700 °C, except for very porous rocks (porosities over 15 %) since the latter can accommodate the expansions.

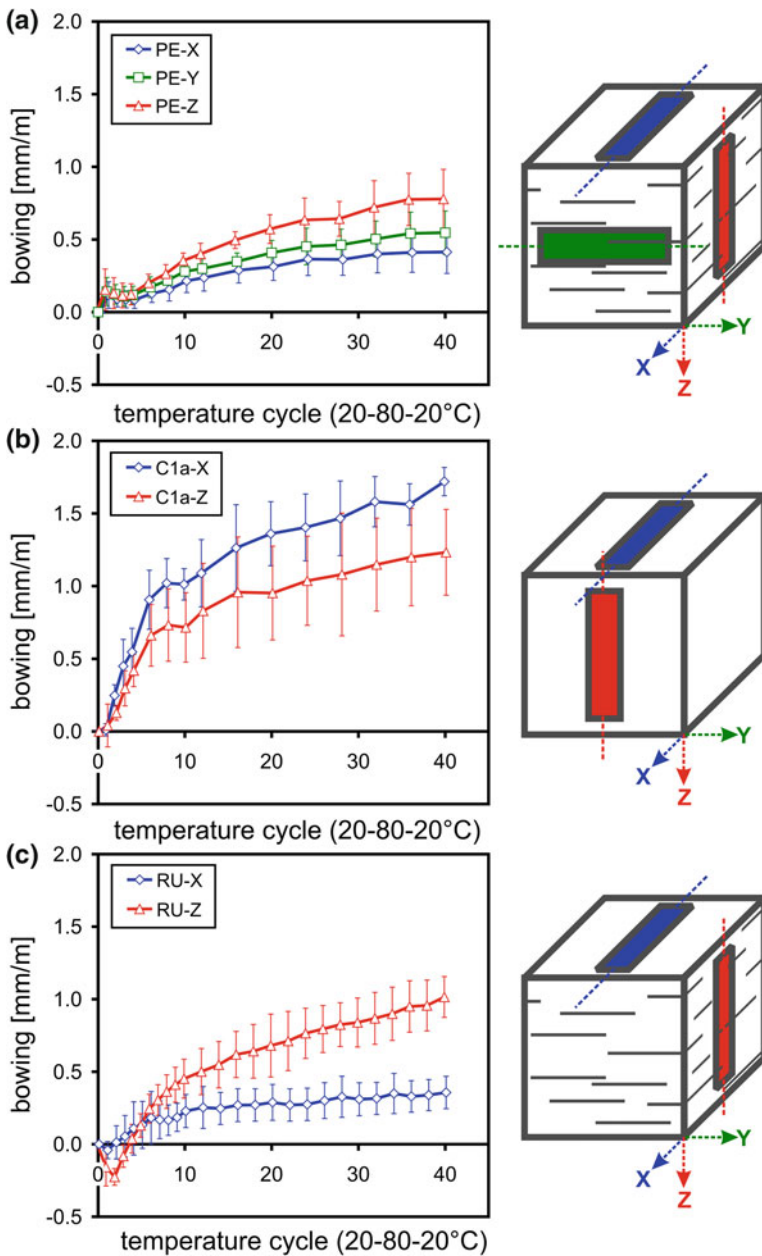
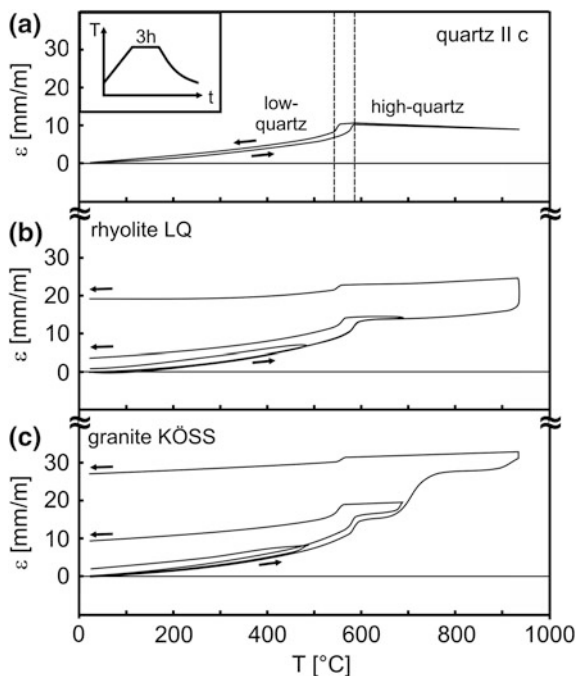


**Fig. 3.43** Bowing of marble slabs versus number of heating cycles (*left*): Peccia (*PE*), Carrara (*CAI*), and Ruviana (*RU*) Marble. Each *curve* represents the mean bowing trend of three slabs (*right*). The colors of the curves are related to the cut direction displayed in the cube sketch (*right*). The colored *rectangles* represent the test pieces. *x*, *y*, and *z* indicate the long axes of the test specimens. Positive values mean convex bowing (towards the heat side) and negative ones mean concave bowing (see also Fig. 6.7a–b in Chap. 6)



**Fig. 3.44** Thermal expansion of quartz parallel to the crystallographic c-axis (a) for comparison to the expansion behavior of the rhyolite from Löbejühn (b) and the granite from Kösseine (c) (after Sippel et al. 2007)

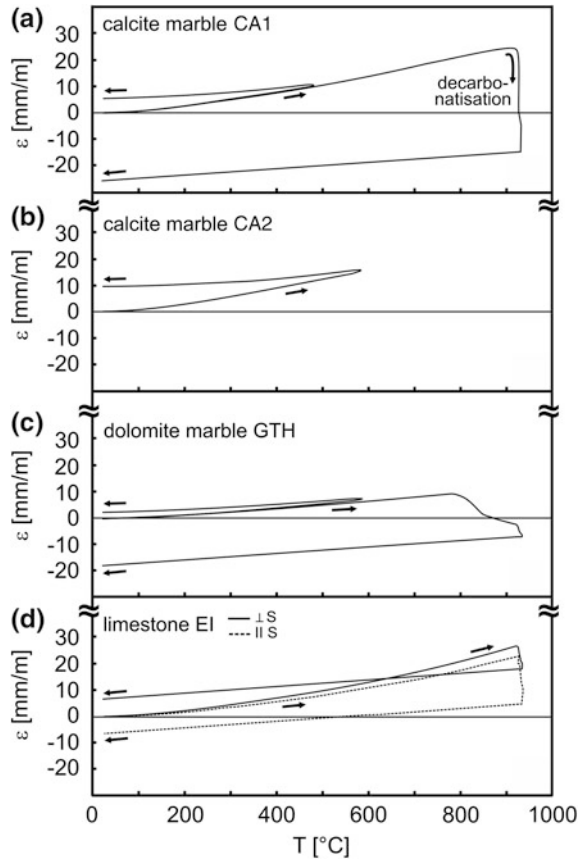


The strong expansion occurring above 700 °C is explained by a progressive crack growth and, finally, a high degree of transgranular microcracking. The impact of temperatures above 500 °C causes an increasing total porosity and a remarkable shift to larger pore radii, whereas, at temperatures below 500 °C, the pore space does not change significantly. Thermal expansion measurements up to 950 °C for silicate rocks generally result in a higher expansion coefficient,  $\alpha$ , associated with a higher residual strain and vice versa (Fig. 3.44).

Calcite marbles (Fig. 3.36) exhibit comparably high expansion coefficients and high residual strains when heated up to 100 °C (Siegesmund et al. 2000a; Zeisig et al. 2002). This thermal sensitivity can also be observed up to 600 °C. For example, the residual strain for the Carrara Marble CA1 (see also Fig. 3.36) is around 5.4 mm/m at 500 °C, while the averaged residual strain for silicate rocks is less than 2 mm/m. The most intense damage is shown by the calcite marble CA2 with a residual strain of 9.5 mm/m (Fig. 3.45). In this case, thermally induced stresses that originated at adjacent grains lead to a total decay, even before decarbonatization starts (Sippel et al. 2007).

In contrast to normal calcite marbles that are translucent, since calcite crystals are transparent to translucent, decarbonatized rocks exhibit a rather dull white appearance. Fracture surfaces of decarbonatized rocks show that the loss of

**Fig. 3.45** Thermal expansion of different carbonate rocks according to the temperature curve shown in Fig. 3.44 (after Sippel et al. 2007)



cohesion after decarbonatization occurs along irregular surfaces and that the shape of calcite crystals survives the partial or total decomposition to CaO. The dolomite marbles appear to be more resistant to heat impacts, even at temperatures up to 600 °C (maximum residual strains of 2.1 mm/m).

For the case of the gypsum bearing rock, two effects are crucial for its thermal behavior: (i) the dehydration of gypsum results in a limited expansion followed by a contraction within the temperature range of 180–300 °C, and (ii) the transformation of CaSO<sub>4</sub> from anhydrite III to anhydrite II, reveals an intense contraction above 800 °C, expressed by a negative residual strain of about 20 mm/m (perpendicular to the bedding) and 35 mm/m (parallel to the bedding). SEM images show that the anhydrite crystals change their habits from prismatic to more isometric shapes when heated.

### 3.5 Hygric/Hydric Properties

The deformation of dimension stones can be related to different processes—mainly changes in the temperature and in the moisture content of the porous rocks. Quite important is the presence of moisture in the case of length or volume changes of dimensional stones (Fig. 3.46). This deformation phenomenon is well known as hygric (in the range between 0 and 95 % RH) and hydric (in contact with water, also immersed) expansion and contraction as a result of moisture changes. An important physical weathering process related to this is the periodic or seasonal hygric dilatation of a rock due to environmental climate factors.

The process of hygric dilatation is related to changes in the relative humidity of the air (Fig. 3.47). For this case, relatively high values of hygric dilatation can also be found, but compared to direct wetting of the surface with liquid water, the values are much lower (Steindlberger 2003; Ruedrich et al. 2005b, 2010a). The hygric expansion of the Schöttmarer Sandstone, shown in Fig. 3.47, reaches a value of 0.84 mm/m perpendicular to the layering at 98 % RH.

The intensity of the hygric dilatation as a function of relative humidity shows large variations depending on the material. Blöchl et al. (1998) found, for three sandstone varieties, values that ranged between 10 % and 28 % for the total hygric dilatation at 95 % RH. Furthermore, the dilatation of a sample is not equally distributed over a certain range of moisture content. There is a clear increase in the rock expansion at higher values of relative air humidity. The dilatation versus time of the Schöttmarer Sandstone shown in Fig. 3.47 can be seen as a representative curve, where the highest expansion occurs above 80 % relative air humidity. At these high relative humidity levels, capillary condensation increases and the expansions measured approximate those obtained when the sample is in contact with liquid water for some time. The absolute hygric dilatation can also exhibit a strong directional dependency, wherein anisotropy values of over 50 % are not uncommon (Fig. 3.47, e.g. Ruedrich et al. 2007, 2010a). These clear directional dependencies are often observed with rocks that have experienced additional deformation or compaction—for example, mudstones, sandstones, or slates.

When samples were exposed to direct contact with liquid water by capillary absorption from one face (mimicking the exposure of stones in buildings), the swelling or hygric/hydric expansion perpendicular to the bedding was 1.13 mm/m (Table 3.8) in the case of the Schöttmarer Sandstone, which is one-third higher than when only exposed to high relative humidity levels (Fig. 3.47).

The combination of hygric or hydric swelling and thermal dilatation processes (see Sect. 3.4.2) is seen as an important factor for the weathering behavior of dimension stones. The result of these processes on dimension stones can be seen in the form of scaling and flaking parallel to the layering (see Chap. 6).

It is well known that the water impact on dimension stones can result in a volume increase in the rock. An overview of the hydric dilatation of different types of dimension stones is given in Table 3.8, while Fig. 3.48 provides hydric dilatation estimates that can be expected for certain rocks and rock types.

**Fig. 3.46** Schematic diagram of the hygric dilatation as a function of time for a sandstone sample. Note that the hygric dilatation gradient changes over time (after Stück et al. 2010)

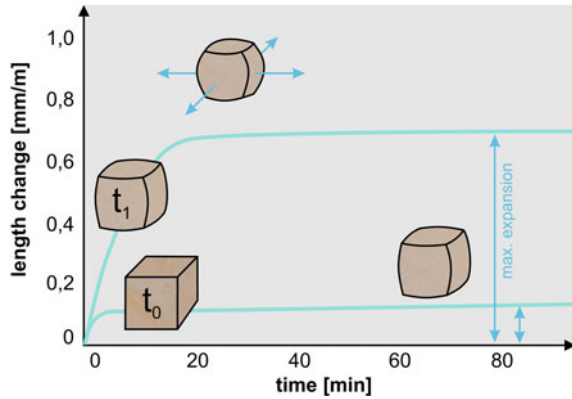
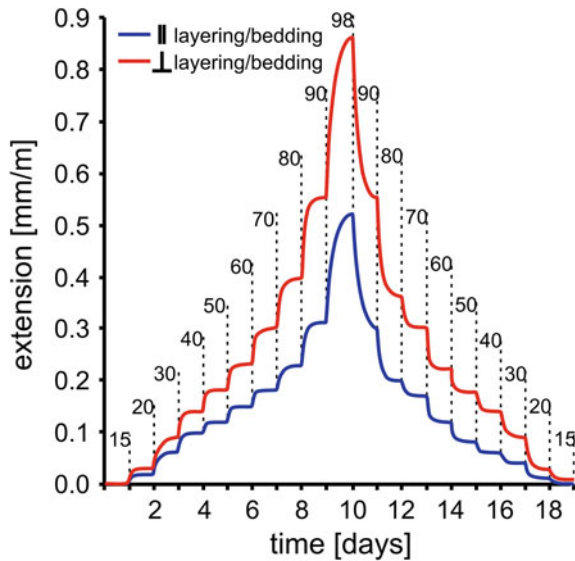


**Fig. 3.47** Hygric expansion of dimension stone shown for the case of the Schöttmarer Sandstone. The dotted lines mark the humidity levels at which the sample equilibrated. A clear increase in the sample length occurs above 80 % relative air humidity (modified after Ruedrich et al. 2005b)



The hygric dilatation values of the three rock groups shown in Fig. 3.48 (Kocher 2005) differ from each other in two orders of magnitude. In the first group, granites, marbles, and carbonate rocks show values of up to 0.1 %. In the second group, sandstone and concrete show dilatation values of almost 1 %, whereas the third group, consisting of mud and mudstones, reaches dilatation values of up to 25 %.

Besides the swelling of clay minerals, hygric dilatation of dimension stones may be the result of other critical processes (see Chap. 4.). This can be seen in the dilatation of rocks that only have a small amount of clay or are even clay free, such as basalt, granite, marble, flint, or chert (Weiss 1992). In these cases, the hygric dilatation has mostly been observed for rocks having a large percentage of micropores, thus, enhancing capillary condensation processes (Stockhausen 1981).

**Table 3.8** Hydric expansion of some selected dimension stones with density and porosity

Rock type	Density (g/cm <sup>3</sup> )	Porosity (%)	Hydric expansion (mm/m)
<i>Sandstone</i>			
Portland brownstone	2.39	8.7	0.45–0.17
Villarlod molasse	2.26–2.67	15.5	1.30–1.73
Tarifa sandstone	2.55	8–11	1.20–2.90
Schöttmarer sandstone	2.45	8.10	0.79–1.13
Meller sandstone	2.30	13.22	0.63–1.18
Obernkirchner sandstone	2.15	18.6	0.09–0.16
Sander Schilfsandstone (sandstone)	2.27	15.4	0.83–1.29
<i>Limestone</i>			
Globigerinen limestone	1.85	34.6	0.17–0.27
Thüste limestone	2.12	21.14	0.02–0.07
Treuchtling limestone	2.60	2.71	0.03–0.07
Travertine	2.40	7.38	0.02
Anröchter “sandstone” (clastic limestone)	2.51	7.00	0.08–0.17
Baumberger “sandstone” (clastic limestone)	2.09	20.00	0.13–0.62
<i>Volcanic rocks</i>			
Löbejün rhyolite	2.52	4.50	0.03
Morshäuser basalt	2.92	1.56	0.10
Niederbrechener diabase	2.71	1.08	0.22
Londorfer basalt lava	2.86	10.88	0.00
Rochlitz rhyolitic tuff	2.01	23.70	0.96
Weibern tuff	1.51	38.50	0.87–1.00
Laubacher tuff	2.71	16.31	3.29
Trachyte Selters	2.32	8.00	0.60–1.10
<i>Plutonic rocks</i>			
Kösseine granite	2.69	0.71	0.08
Padang dark granodiorite	2.80	0.25	0.01
Nero Impala gabbro	2.92	0.04	0.01
Anzola gabbro	3.09	0.13	0.03
<i>Metamorphic rocks</i>			
Calanca paragneiss	2.73	0.73	0.06
Verde Andeer orthogneiss	2.68	0.89	0.01
Prieborn marble	2.70	0.77	0.06
Palissandro marble	2.87	0.33	0.08
Carrara marble	2.71	0.46	0.08
Quartzite	2.69	0.18	0.01
Serpentinite	2.77	0.15	0.00
Theuma Knotenschiefer (Slate)	2.74	0.95	0.15–1.45
Roof slate	2.67	0.70	0.26–4.80

Data from Poschlod 1990; Mirwald 1997; Steindlberger 2003; Jiménez González and Scherer 2004; Weiss et al. 2004a; Ruedrich et al. 2005b; Ruedrich and Siegesmund 2006; Sebastian et al. 2008, Felix (pers. comm.), and Scherer (pers. comm.)

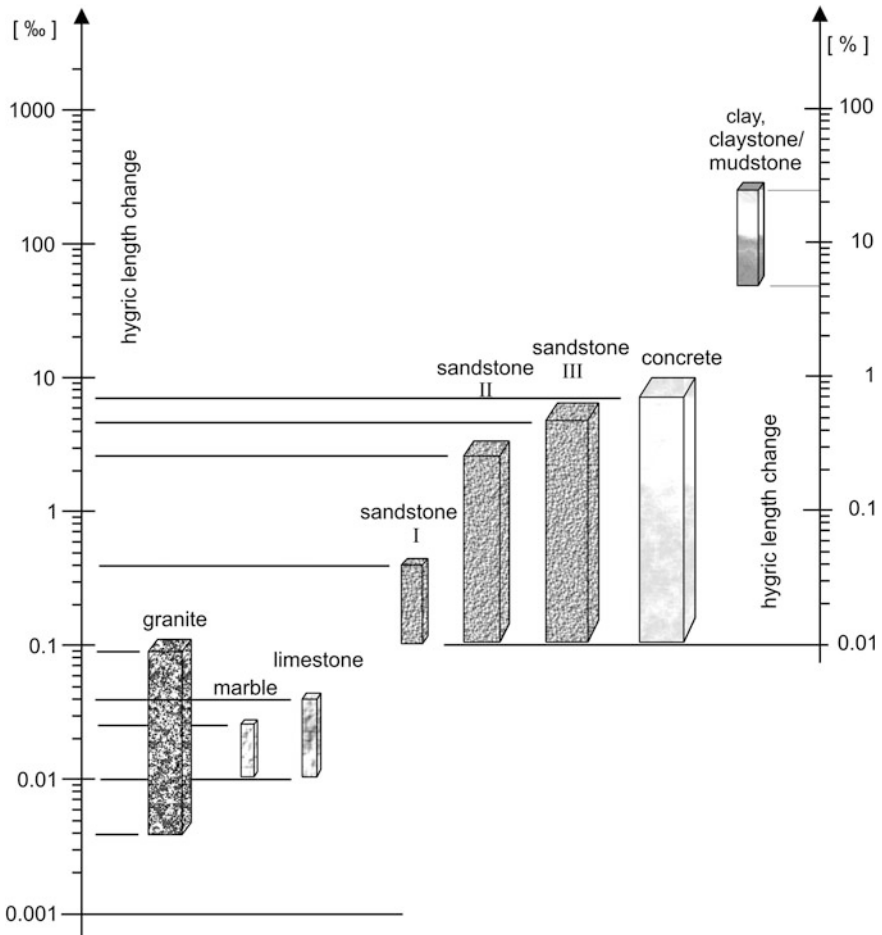


**Fig. 3.48** Hygric dilatation values for different rocks and from different authors: granites, marbles, and sandstones after Hockmann and Kessler (1950), from Snethlage (1984), carbonates after Lukas (1990), Sandstone II after Schuh (1987), Sandstone III after Snethlage and Wendler (1997), concrete after Wesche (1981), clay/mudstones after Madsen (1976), and Madsen and Nüesch (1990). After Kocher (2005)

When clays have been present, pronounced values of hygric dilatation have been measured for mudstone, wherein changes of up to 20 mm/m are not uncommon (Madsen 1976; Madsen and Nüesch 1990). For sandstones, Schuh (1987) and Snethlage and Wendler (1997) reported dilatation values of up to 5 mm/m. However, Ruedrich et al. (2010a) were able to show that some sandstone varieties exhibit a pronounced hygric expansion, although these rocks do not have any swellable clay minerals.

Hygric dilatation is particularly pronounced in clay-bearing sandstones and volcanic tuff. Jiménez González and Scherer (2004) reported, for subarkose



sandstone from the USA, Switzerland, and Spain, hydric expansion values of 0.5 mm/m and up to 2.0 mm/m (Scherer pers. comm., see also Sebastian et al. 2008; Wangler and Scherer 2008; Wangler et al. 2010). Snethlage and Wendler (1997) published hydric dilatation data for a set of sandstones covering a range up to 5 mm/m (for comparison, see the compilation by Ruedrich et al. 2005b and Ruedrich and Siegesmund 2006). For volcanic tuffs, Steindlberger (2003) observed maximum values of up to 3.3 mm/m, while most of them exhibit values of around 0.5 mm/m and up to 1 mm/m, which is in accordance with observations made by Wendler et al. (1996), Ruedrich et al. (2005b), and Stück et al. (2008).

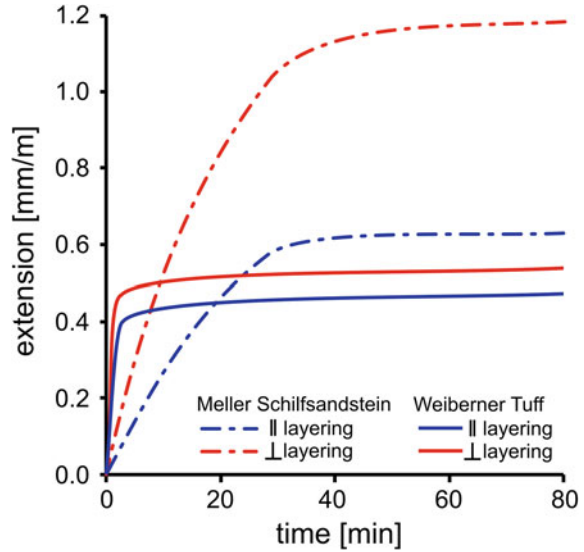
Carbonate rocks usually show low values for hydric dilatation as, in general, these rocks have low clay content. For most of the limestones, hydric expansion is a subordinate factor. The Thüste Limestone (Table 3.8) shows a hydric expansion of 0.02 mm/m parallel to the bedding, while the value perpendicular to the bedding is around 0.07 mm/m (Weiss et al. 2004b). For the travertine of Bad Langensalza, the value is around 0.02 mm/m (Weiss et al. 2004b), whereas Katzschman et al. (2006) reported values of less than 0.01 mm/m. Comparably low values were reported for the limestone of the Unterer Muschelkalk (Terebratelkalk and Schaumkalk), where values between 0.03 mm/m and 0.07 mm/m are given by Katzschman et al. (2006).

In contrast, the Baumberger “Sandstone” as well as the “sandstone” from Anröchter (both are clastic limestones containing 16 and 31 % quartz, respectively; see Table 3.1) have exhibited quite different hydric behavior with different time periods until the maximum expansion was reached, which depends on the direction. The Baumberger “Sandstone” shows a remarkable swelling of 1.5 mm/m parallel to the bedding after 8 min. and of 0.25 mm/m perpendicular to it after 12 min. The Anröchter “Sandstone” exhibits a smaller expansion, about 0.08 mm/m parallel to the bedding and 0.16 mm/m perpendicular to it. The Globigerina Limestone from Malta shows a hydric expansion from 0.17 to 0.27 mm/m with a total anisotropy of around 37 %.

As examples, the hydric dilatation curves of the Meller Sandstone and the Weiberner Tuff are shown in Fig. 3.49. The Meller Sandstone exhibits a relatively large absolute hydric expansion perpendicular to the layering with a value of 1.18 mm/m. Parallel to the layering, the hydric expansion during water uptake is much lower with an absolute value of 0.63 mm/m, which results in an anisotropy of 46.6 %. The Weiberner Tuff displays a similar hydric expansion curve with 0.53 mm/m perpendicular and 0.47 mm/m parallel to the weakly developed layering. The corresponding anisotropy is only 11.3 %.

Another phenomenon of the hydric dilatation is the strong time dependence of the expansion for different rocks. The expansion of the Weiberner Tuff shown in Fig. 3.49 was completed within approximately 5 min. in relation to the sample size, whereas the Meller Sandstone required 40 min. for the main expansion. This time, control mainly depends on the pore space properties of the rocks, so that rocks with a well connected pore network and higher porosities show faster hydric expansion than rocks with less connected pores and lower porosity values.

**Fig. 3.49** Hydric expansion of dimension stones during capillary water uptake for the Meller Schilf Sandstone and Weiberner Tuff parallel and perpendicular to the layering. Note the strong directional dependency associated with the sandstone and the differences in the expansion speed of the samples



Laboratory investigations have shown that the hydric dilatation of dimension stones after a few exposure cycles is more or less a reversible process, where no residual expansion can be measured after the rock sample returns to the original moisture level. Detailed and extensive investigations of the effects of a large number of exposure cycles and long-term exposure to moisture and changes in moisture content have not been carried out so far. However, Morales et al. (2007) discussed the decrease in rock strength induced by the impact of water and found a link between the compressive strength and the magnitude of hydric expansion in sandstones. This connection has been verified for the tensile strength of sandstones in Ruedrich et al. (2010a). The results from Morales et al. (2007) on strength reduction (dependent on the degree of saturation) show that a low degree of saturation for all the sandstones studied led to a strong reduction in the compressive strength. At increasing degrees of saturation, sandstones with a slight hydric expansion and a small proportion of micropores only show a small increase in strength reduction. In contrast, sandstones with a pronounced hydric expansion and a large number of micropores exhibit a progressive strength reduction at increasing saturation levels. This suggests that there is a relationship between the existent pore sizes, the saturation degree, the intensity of hydric swelling, and the strength reduction, i.e. the rock softening of sandstones.

Most of the understanding and relationships related to the hydric and hydric dilation discussed above come from laboratory experiments where demineralized water is usually used. In masonry made from dimension stones, a variation in the salt concentration which has a significant effect on the hydric/hydric dilatation and, therefore, on the swelling pressure being formed, can often be found. In comparison to pure water, the presence of an aqueous solution with a higher

concentration of salt results in a lower swelling capability. However, if salt is present, residual expansion can be observed (e.g. Wendler and Rückert-Thümling 1992; for further explanation, see [Chap. 4](#)).

### 3.6 Strength Properties

The strength of materials is one of the basic parameters used to classify the quality of natural stones. It is one of the most important and reliable methods for classifying rocks and its application for construction purposes. The results can be used directly for the structural requirements considering an acceptable safety margin. However, the mechanical strength is often mainly determined by the heterogeneity of the rock and its fabrics instead of by the individual properties of the rock-forming minerals. The strength values refer to the material's ability to withstand an applied stress without failure. Yield strength refers to the point on the engineering stress–strain curve (as opposed to the true stress–strain curve) beyond which the material begins deformation that cannot be reversed upon removal of the loading. Ultimate strength refers to the point on the engineering stress–strain curve corresponding to the maximum stress. The applied stress may be tensile, compressive, or shear. If the stress limit is reached, material failure occurs.

A material's strength depends on the rock fabric and is influenced by its composition, the shape and size of the material sample, the aging of the material, and its storage conditions. The engineering processes to which a material is subjected can alter these microstructures. The variety of strengthening mechanisms that alter the strength of a material includes work-hardening, solid-solution strengthening, precipitation hardening, and grain-boundary strengthening and can be quantified and qualitatively explained. However, strengthening mechanisms are accompanied by the contradiction that some mechanical properties of the material may degenerate in an attempt to make the material stronger.

Strength is considered in terms of compressive strength, tensile strength, and shear strength—namely, the limit states of compressive stress, tensile stress, and shear stress, respectively. The effects of dynamic loading, especially the problem of fatigue, are probably the most important practical part of the strength of materials. Repeated loading often initiates brittle cracks, which grow slowly until failure occurs.

However, the term strength of materials most often refers to various methods of calculating stresses in structural members, such as beams, columns, and shafts. The methods that can be employed to predict the response of a structure under loading and its susceptibility to various failure modes may take into account various properties of the materials other than material (yield or ultimate) strength. For example, failure in buckling is dependent on material stiffness (Young's modulus).

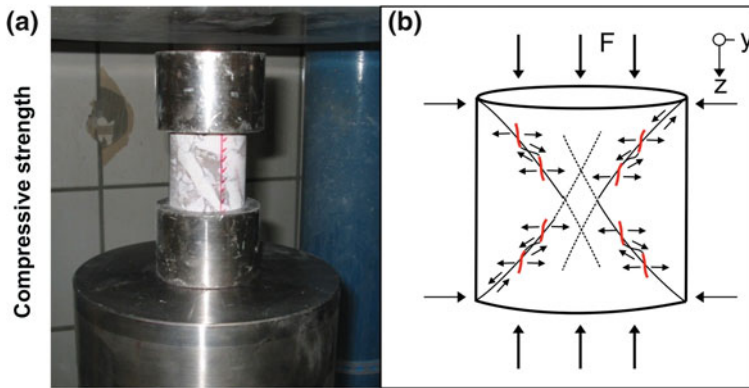


**Fig. 3.50** Experimental setup **a** For determining the uniaxial compressive strength. **b** Rock failures occur through a combination of tensile and shear cracks.  $F$  loading force

### 3.6.1 Compressive Strength

Demands on compressive strength are made in cases where, through a material, a planar load to the subsurface ground has to be ensured. During an unconfined uniaxial pressure experiment, the test specimen that experiences longitudinal stress will be shortened until failure and a final break (Fig. 3.50). The unconfined compressive strength (UCS) of a dry specimen expresses the value wherein the sample experiences total loss of cohesion along the fracture surface. A typical stress–strain curve is shown in Fig. 3.51. At the beginning of the experiment, consolidation of the specimen can usually be observed.

During this phase, open pre-existing microcracks are being closed—preferably those that are oriented perpendicularly to the loading axis. Through this, the test specimen experiences an irreversible shortening but with relatively small values. At about 30–70 % of the compressive strength value, the rock sample shows nearly linear elastic behavior. Beyond that, an increase in microcrack formation occurs that ultimately leads to total material failure. The degree of consolidation depends strongly on the density of the open microcracks, whereas the latter linear elastic behavior is mainly determined by the mineral composition and its elastic properties.

The question of where new microcracks are formed in a test specimen depends, on the one hand, on the geometry and density of the pre-existing microcracks and, on the other hand, on the mechanical stability of the minerals and the fabric-dependent interaction between mechanically weak and strong minerals (Segall and Pollard 1980; Dürrast et al. 2001).

For certain applications of natural dimension stones, minimal values for the compressive strength are requested. This requirement shows that the experimental setups and the specimen involved in the determination of the compressive strength must be comparable and equivalent. The uniaxial compressive strength is the most

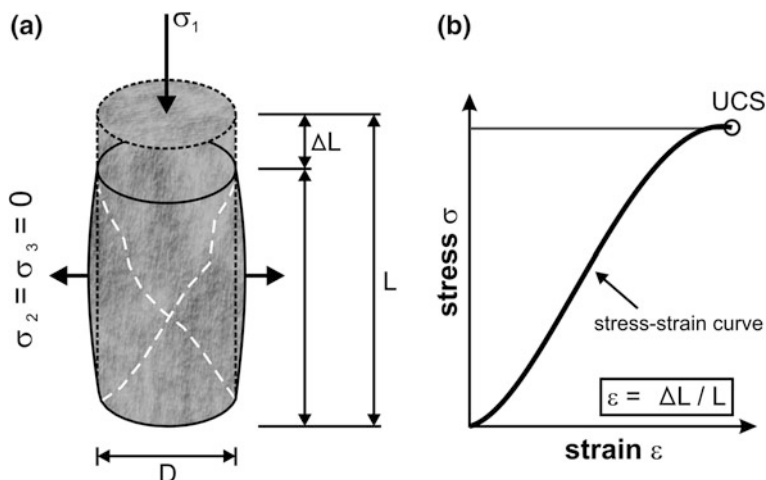
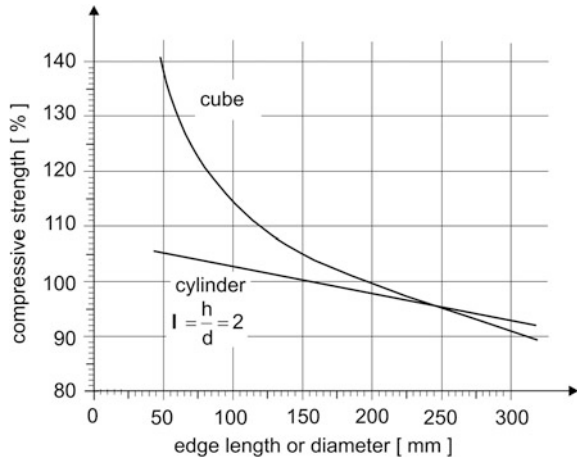


**Fig. 3.51** Unconfined compressive strength (*UCS*) test: **a** A core with failure under unconfined compression **b** A stress–strain curve where the *UCS* marks the failure of the specimen (after Thuro et al. 2001)

common performance measure used by engineers for the quality assessment of rocks. For the experimental compressive strength tests, several countries have standards for these tests (Germany, France, UK, U.S.A., etc.), while, in Europe, the introduction of the European Standards may help to overcome the different approaches in use. Compressive strength is measured by tracking cylindrical, cubic, or prismatic samples in a compression testing machine. Usually, the compressive load is applied by a servo-hydraulic testing machine with a very stiff testing frame and a class 1 load range up to 300 kN. Most critical are the sample preparation, the sample dimension, and the quality of the end-faces, which must be co-planar with an accuracy of 0.1 %. The load is applied to the end-faces of the specimen with a strain rate of  $10^{-5} \text{ s}^{-1}$  until failure. The maximum load is defined as the uniaxial compressive strength. End-faces of lower quality cause local stress and may result in strength loss and low-quality data. The standards allow a large variation with respect to the samples sizes, while, in geotechnical approaches, standard specimens of a ratio  $>2$  (length/diameter) are believed to represent the “true” *UCS* value. Bieniawski (1967) showed that the compressive strength may differ up to 20 % by using a length/diameter ratio of 1.

Following the DIN EN 1926 (1999), it is still possible to determine compressive strength by using cubes with an edge length of 50 mm or cylindrical samples with a diameter and height of 50 mm. The compressive strength determined with cylindrical samples particularly depends on the length-diameter ratio (Fig. 3.52). However, with a length-diameter ratio higher than 2.5–3, the influence of the specimen’s geometry is negligible (Wesche 1981). A still unresolved and discussed issue is the drying of the sample. On the one hand, it could mean that drying is carried out at 70 °C until a constant mass has been reached, and on the

**Fig. 3.52** Effect of the geometric shape of a test specimen (*cylinder* and *cube*) on its compressive strength (after Wesche 1981)



other hand, a not-yet-defined air dry state could be outlined. Rohowski (2001) found that the compressive strength values determined following the DIN EN 1926 (1999) were above and below the values determined by following the DIN 52105 (1988). No systematic trend emerged. Experiments using the European standard showed an increase in the compressive strength values for samples with lower bulk density values and a decrease for samples with higher bulk densities.

A classification of hard rocks in relation to their compressive strength, which is mainly designed for engineering purposes, indicates and separates for dimension stones in five (De Quervain 1967) to eight classes (Peschel 1974). In general, the following discriminations are made: hard rock with more than 110 MPa, medium-hard rocks between 70 MPa and 110 MPa, and weak rocks between 55 MPa and 70 MPa. Explorative data evaluation based on statistical characteristics with the construction of box plots was given by Mosch and Siegesmund (2007). The median value used has an advantage in comparison to the arithmetic mean, as it is more robust towards statistical outliers, which means it is less affected by extreme values (Kürzl 1988). The relative position of the median value in the box also provides an impression about the skewness or symmetry of the distribution based on the data used. The boundaries of the box are the 25 and 75 % quantile values. The box itself is designed to be independent from extreme values and provides a resistant dispersion measure of a given data set. The delineation of the horizontal lines, called “whiskers”, depends on various parameters. Usually, as also applied here, the length of the whiskers has a maximum of 1.5 times the interquartile distance (R Development Core Team 2005), whereas the end values are determined from values of the data set; values below and above the end values are outliers.

Mosch and Siegesmund (2007) found that the uniaxial compressive strength (e.g. Table 3.3 and Fig. 3.53) of plutonic rocks varies between 60 and 292 MPa, a range that covers the majority of the published UCS values for plutonic dimension stones (Peschel 1983; Winkler 1994; Müller 2001). A much higher value of



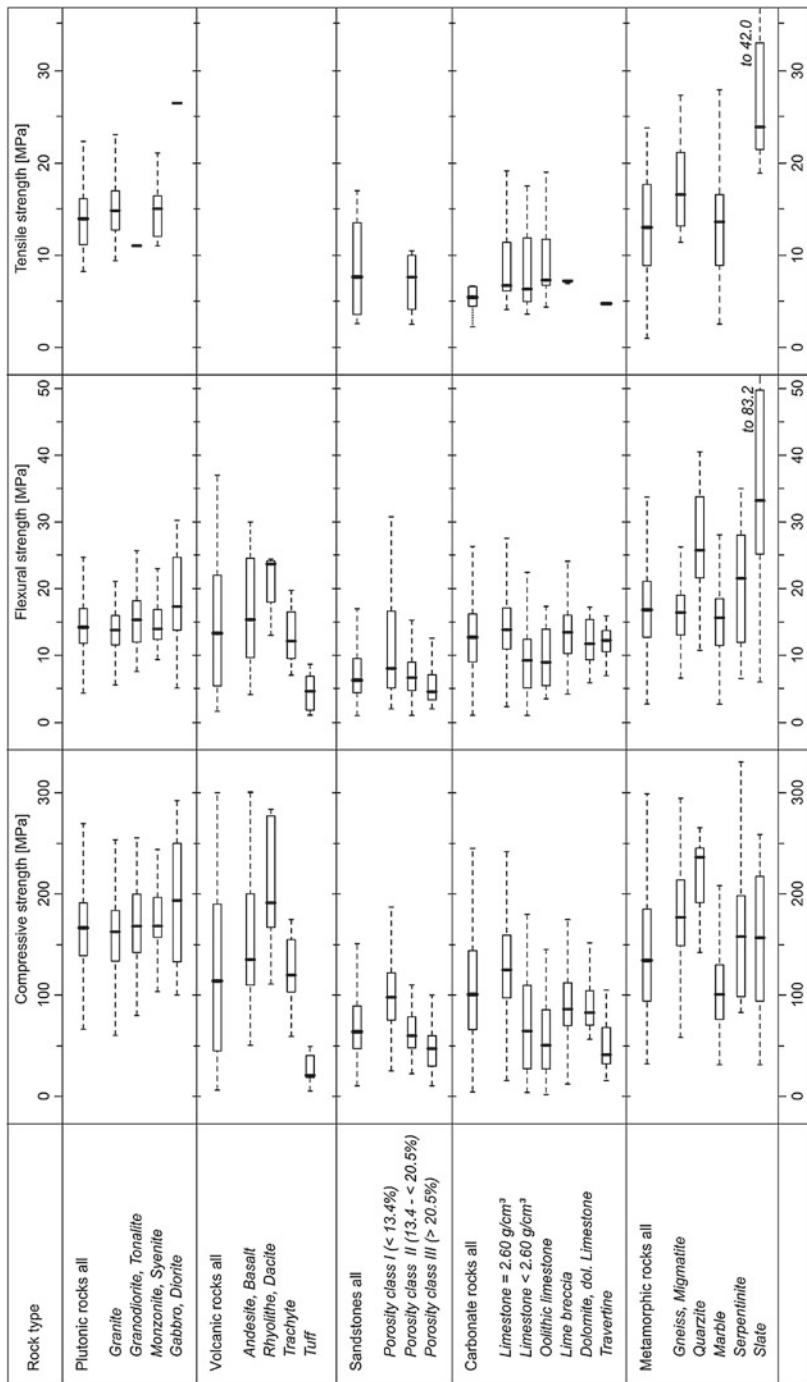


**Fig. 3.53** Typical lithological value ranges with regard to the mechanical strength parameters (e.g. compressive, flexural, and tensile splitting strength) put together on the basis of a statistical analysis of natural stones. The *box plots* describe the corresponding median value, the 25 and 75 % quartile values as well as the upper and lower extreme values (after Mosch and Siegesmund 2007)

427.7 MPa is given for the gabbro “African Blue” from South Africa; this value may be an extreme outlier and needs to be questioned. However, Morales et al. (2010) found, in a more systematic study on dolerites from Uruguay (rocks with commercial names such as Negro Absoluto and Negro Oriental), compressive strength values from 265 to 400 MPa. Volcanic rocks may also show a distinct heterogeneity in regards to the observed compressive strengths. They range between 50 and 300 MPa. Rhyolites, dacites, andesites, and basalts have values that can be comparable. Trachytes and especially tuffs show lower values.

For the group of carbonate rocks, the UCS values vary between 4.4 and 265 MPa. This range also covers the majority of the published UCS values for this rock group. Sandstones show a variation from 10.0 to 257 MPa, while the highest value is related to a conglomerate from Brazil (Marinace Green). Metamorphic rocks show the highest variation with respect to the uniaxial compressive strength (see Fig. 3.53, Table 3.3).

The uniaxial compressive strength can show a strong directional dependence when determined in the different directions of one rock. Moreover, the rock fabric elements, especially the lattice- and shape-preferred orientation of minerals, as well as the degree of grain interlocking (i.e. grain boundary configuration), have been intensively investigated with respect to their influence on petrophysical properties (e.g. Wenk 1985; Howarth and Rowlands 1987; Siegesmund and Dahms 1994; Siegesmund 1996; Brosch et al. 2000). In particular, metamorphic rocks like gneisses show a strong directional dependency of the compressive strength values. Strohmeyer and Siegesmund (2002) carried out a systematic study on a progressively deformed rock sequence, i.e. starting with a more or less undeformed granitoid and ending with a strongly deformed mylonite; this goes along with an increase in the intensity of the foliation. The sample sequence had a more or less similar chemical and mineralogical composition. The uniaxial compressive strength of the samples ranges between 128 and 225 MPa. The development of a tightly spaced mylonitic foliation and, in particular, the preferred orientation of the micas may significantly determine the anisotropic behavior of the compressive strength. Micas show a perfect cleavage parallel to their (001) planes and often exhibit a strong preferred orientation in those deformed rocks. They are the weakest component in the rock with respect to strength (as observed by Mügge 1898). Most importantly, the failure pattern also varies, with regards to the mylonitisation, from a cone-shaped fracture pattern to a roof-shaped form (Fig. 3.54).

A more detailed study on a sample of the Verde Andeer Gneiss was performed wherein different load directions with respect to the foliation were tested (Fig. 3.55). It is well known that, for foliated rocks, the uniaxial compressive strength is highest in the loading direction is normal with respect to the foliation (e.g. de Quervain 1967; Brosch et al. 2000; Strohmeyer and Siegesmund 2002) and lowest at acute angles to these planes. The compressive strength values are determined by the grain size, closely spaced foliation, mineralogical changes with respect to the layering, etc. All these superimposed fabrics (see also Chap. 2), especially the quantity and spatial arrangement of discontinuities forming zones of weakness, characterize the resistance of rock to compressive fracture.

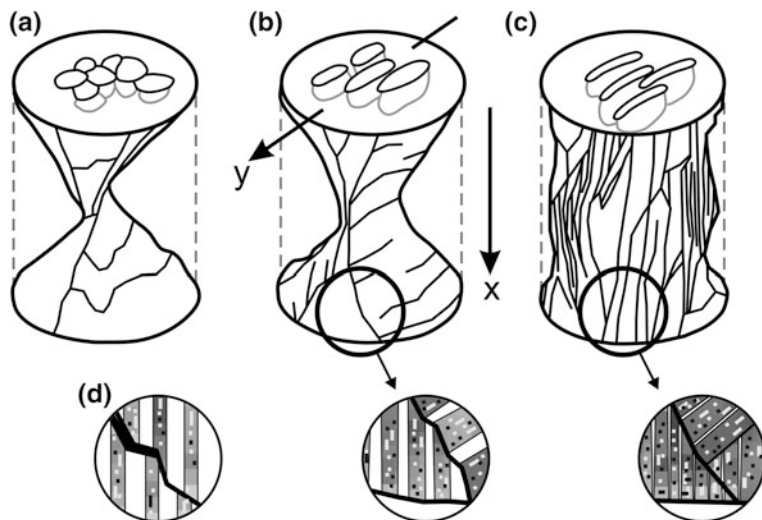


**Fig. 3.54** Crack and failure pattern parallel to the x-direction during the UCS experiments in relation to the rock fabrics: **a** Proto mylonite **b** Mylonite, and **c** Ultramylonite; **d** Shows the crack propagation during the experiment with the *arrows* indicating the displacement (after Strohmeyer and Siegesmund 2002)

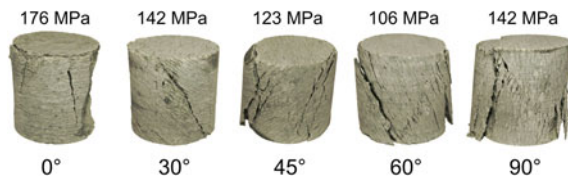


**Fig. 3.55** UCS experiment on rock samples of a foliated gneiss (Verde Andeer) with values given: load perpendicular to the foliation ( $0^\circ = 176$  MPa), load  $30^\circ$  to the foliation (142 MPa), load  $45^\circ$  to the foliation (123 MPa), load  $60^\circ$  to the foliation (106 MPa), and load parallel to the foliation ( $90^\circ$ , 142 MPa)

Hoffmann and Siegesmund (2007) reported an anisotropy value of 47 % for a marble from Thailand (Phran Kratai Gray). The relatively low UCS values of crystalline marbles are related to the almost mono-mineralogical composition of this rock and the grain texture. Compressive strength values of Carrara marbles with polygonal grain boundaries (ca. 109 MPa) can be lower than those of Carrara marbles with stronger interlocked and interlobate grain boundaries (ca. 135 MPa). Strongly weathered marbles with polygonal textures can also show relatively low UCS values of about 40 MPa. Next to metamorphic rocks, dimension stones with pronounced parallel textural elements can also show a directional dependence of the uniaxial compressive strength—for example, sandstones and carbonates with a distinct layering feature (see Fig. 3.53).

Another factor influencing the compressive strength is the so-called “aging” of the testing sample. Peschel (1974) investigated a series of plutonic rocks and found

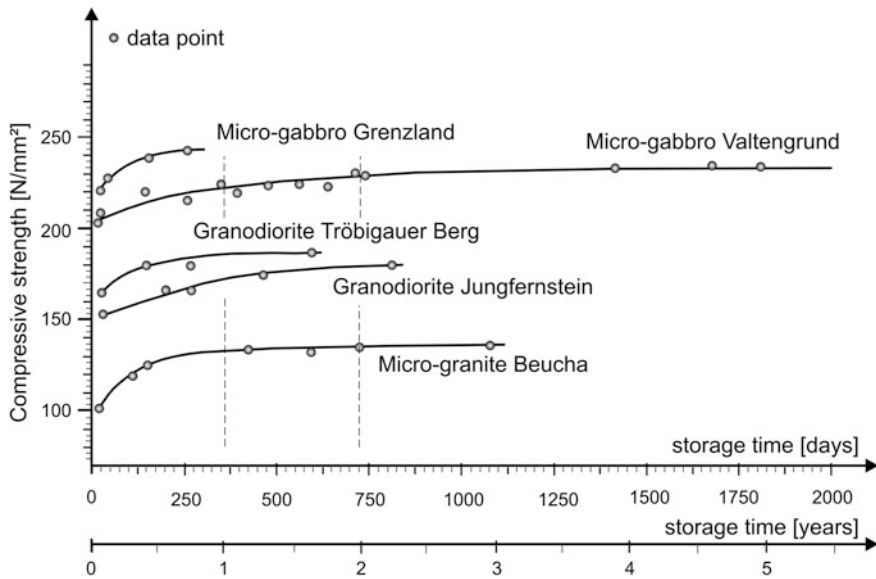
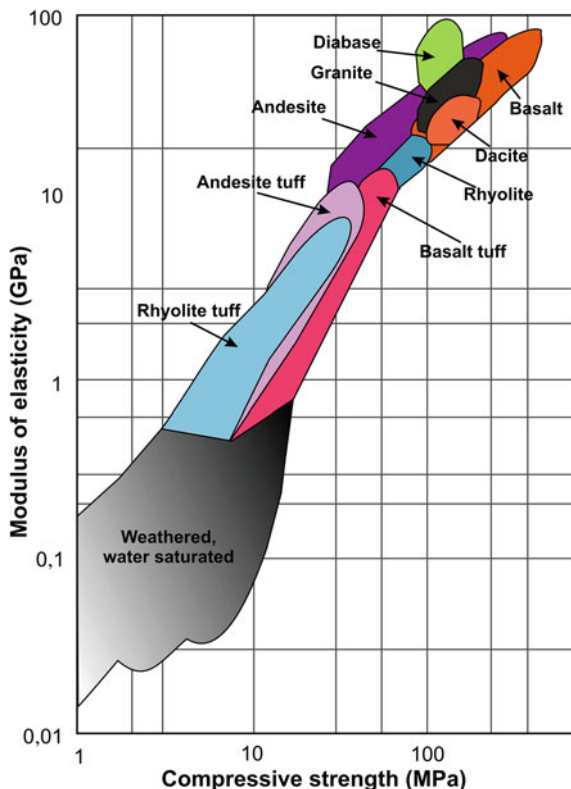


**Fig. 3.56** Change in the compressive strength in relation to the aging of the test specimen (storage time between sample preparation and experiment), after Peschel (1974)

that the compressive strength increases with time (Fig. 3.56). Freshly quarried stones first reached their maximum values in approximately 1.5–2 years and remained relatively constant after that. This can be explained by the relaxation reaction phenomenon of the rocks after they have been removed from the quarry and exposed to changing environmental conditions (pressure, temperature, and moisture). The locked-in stress, which is related to the all-enclosing stress field of a mountain massif, can be lost during aging after the removal of the block from its surrounding.

Another problem is represented by the residual moisture, which is the result of long-term storage and progressive desiccation in the block (Greger 1930). Lentschig (1971) reported that the compressive strength of water-saturated magmatic and metamorphic rocks is lower than for dry samples, ranging 3–15 % depending on the water absorption capacity. For different sandstones, Morales et al. (2007) were able to show that increasing moisture content strongly affects the uniaxial compressive rock strength. However, the degree of rock strength reduction differs over a wide range. Morales et al. (2007) demonstrated that the effect of partial water saturation on rock strength is primarily related to the pore-radius distribution and the matrix mineralogy. A reduction in the strength up to 50 % has been observed. The results are partially in accordance with the conclusion of Hawkins and McConnell (1992), who proposed that the degree of sensitivity to moisture content is primarily determined by the proportion of quartz and clay minerals present and, to a lesser extent, by the rock microfabrics.

**Fig. 3.57** Relationship between the modulus of elasticity and the compressive strength of selected rock types (after Török 2007)



The modulus of elasticity, which is usually quoted as Young's modulus ( $E$ ), is based on the relationship between stress and strain. This value is also known as the static modulus obtained by the tangent, secant, or average method (Schön 1996). The so-called tangent modulus refers to the 50 %-value of the uniaxial strength, the secant modulus is taken as the gradient of the ultimate uniaxial compressive strength on the stress–strain curve from the origin to the 50 %-value, and the average modulus represents an average slope of the straighter portion of the stress–strain curve.

Comparable to the compressive strength (Table 3.3), the main factors that have an influence on the static  $E$ -modulus are the mechanical properties of the minerals and the size of the grains. Török (2007) compiled the modulus of elasticity and the compressive strength for some magmatic rock, which shows the general relationship between these two parameters (Fig. 3.57). However, these parameters do not necessarily correlate with the dynamic  $E$ -modulus. Additionally, open microcracks are an important influential parameter. During a uniaxial pressure experiment, a rock specimen experiences elastic and always experiences plastic deformation. The latter is not expected to occur during the determination of the dynamic  $E$ -modulus, as the time periods for the specimen under loading stress are

relatively short (Schön 1983). Because of this, the value of the dynamic E-modulus should always be higher than the one for the static E-modulus. After Schön (1983), this effect—respectively, the gap between both values—will increase with increasing porosity and fracturing of the rock sample.

### 3.6.2 Tensile Strength

The tensile strength of a material is the maximum amount of tensile stress that it can be subjected to before failure. Because this property does not compare well to other rock mechanical parameters, it is not often measured in natural stones. In addition, its use and relevance is often unclear to many architects and others working with dimension stones. However, its understanding and determination is essential when referring to a complete rock mechanical concept of geological materials.

Tensile-strength testing of rocks can be performed using direct tension tests (i.e. uniaxial or triaxial). The parallel end-faces of a sample cylinder with a defined cross-sectional area are typically glued onto the testing machine pistons. It is then pulled with a controlled, gradually-increasing force until the sample breaks, or indirect tests are applied (e.g. Brazilian test, bending test, fracture toughness test).

The most common testing procedure for the determination of tensile failure strength ( $\sigma_z$ ) is the Brazilian test (or indirect tensile strength test). A disc-shaped rock specimen is subjected to a compressive load in a uniaxial test setup, which results in a largely homogenous tensile stress field. This is a simple, relatively inexpensive, and fully standardized technique, which is well described by several standards, e.g. ASTM and ISRM.

The cylindrical test specimen (typically 20 or 40 mm in length with a diameter of 40 mm, following the recommendations of various standards) is loaded diametrically across the circular cross section, where tensile deformation results perpendicularly to the loading direction (see Fig. 3.58). Tensile failure occurs when the tensile strength of the experiment reaches the value of the rock tensile strength,  $\sigma_z$ . From the vertical load  $F$  and the specimen dimensions (see Fig. 3.58), the tensile strength can be calculated with the following equation:

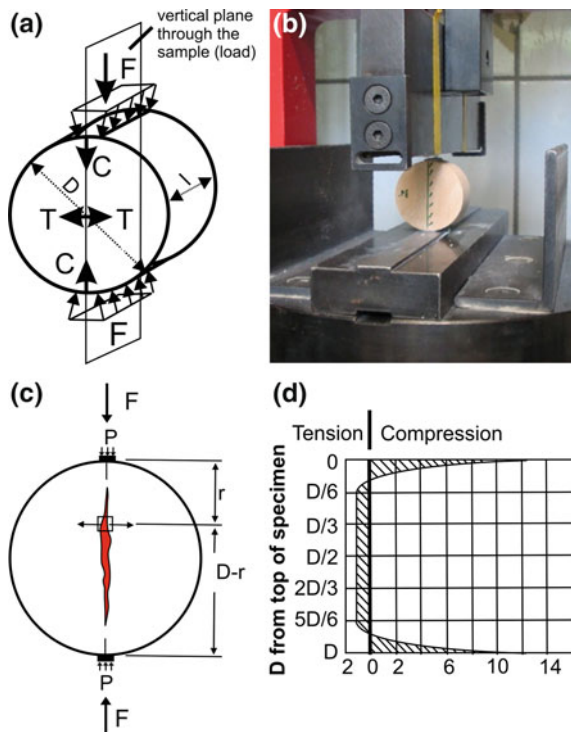
$$\sigma_z = (2 \cdot F) / (d \cdot l \cdot \pi) \quad (3.16)$$

with  $\sigma_z$  the tensile stress at failure (MPa),  $F$  the loading force (N),  $l$  the length of the specimen (mm), and  $d$  the diameter of the specimen (mm).

The tensile strength value of a rock results from the average of at least four tests using specimens close to each other; usually, the standard deviation should be given (e.g. Thuro et al. 2001). However, the tensile stress conditions within the sample are not homogeneously realized. Therefore, the tensile strength values determined via indirect methods such as the Brazilian test method do not reflect “true” tensile values. Peschel (1977) has shown that the Brazilian test and the “true” tensile strength data exhibit an almost constant ratio of 2:1.



**Fig. 3.58** Tensile strength test or Brazil method: **a** Schematic diagram and **b** Photo of the experimental setup **c** Schematic representation of the crack opening due to the tensile force, and **d** Stress distribution inside a cylindrical test specimen under uniaxial load; abbreviations: *C* direction of compression, *T* direction of tension, *P* compressional stress, *F* loading force, *D* diameter, and *l* length



To illustrate the tensile strength for selected lithologies, existing experimental data sets derived from various rocks were compiled. Figure 3.53 and Table 3.9 show the tensile strength data of different rocks with respect to different measuring directions. The tensile strength data show that the median value of the gneiss/migmatite group is at ca. 15 MPa, slightly above the value of the marble data set (median value = ca. 12 MPa), which shows a wider scattering range. Magmatic rocks show tensile strength values of 9 MPa to ca. 27 MPa, which represents the group with the highest strength (Mosch and Siegesmund 2007). The amount of data available for carbonate rocks is quite low, but the known strength range varies between 3.6 and 19.1 MPa. The sandstone group exhibits similar characteristics, also with comparable values. However, the fresh Solling Sandstone shows the highest tensile strength value due to its comparably high density and an interlocked matrix of the rock-forming grains (bulk density 2.34 g/cm<sup>3</sup>); see Tables 3.1 and 3.9 (Ruedrich and Siegesmund 2007).

The samples and data shown in Fig. 3.59 provide a good example to illustrate how rocks assumed to be similar, following their appearance, have significantly different technical properties. The Schilf Sandstone, shown in Fig. 3.59, exhibits a good correlation between porosity and tensile strength values. Choosing a dimension stone only by considering visual and aesthetic aspects might result in having rocks with quite different properties—for example, resulting in different weathering behavior.

**Table 3.9** Compressive, flexural, tensile, and abrasion strength and static Young's modulus for various dimension stones with commercial name, country of origin, and rock type given. Numbers in brackets are the anisotropy values (in %)

Commercial name	Country of origin	Rock type	Compressive strength (MPa)	Flexural strength (MPa)	Tensile strength (MPa)	Abrasion strength (cm <sup>3</sup> /50 cm <sup>2</sup> )	Young's modulus (static) (GPa)
Ben Tak White	Thailand	Granite	183.7 (14.0)	19.7 (19.7)	10.6 (14.4)	4.7 (6.8)	28.0 (17.9)
Muang Tak Orange 1	Thailand	Granite	184.8 (25.8)	16.9 (40.5)	8.9 (29.2)	4.0 (7.2)	28.1 (14.8)
Kösseine	Germany	Granite	195.0 (2.6)	20.1 (20.3)	11.9 (12.7)	5.7 (2.8)	27.5 (17.8)
Antrona	Italy	Granite	208.0 (6.5)		12.4 (20.3)	7.4 (10.7)	15.9
Rojo Dragon	Argentina	Granite	194.4 (1.3)	13.3 (13.3)	6.5 (10.8)	4.2 (4.0)	32.5
Padang	China	Granodiorite	222.0 (6.5)	21.0 (11.9)	12.8 (8.9)	7.1 (3.6)	30.6 (19.3)
Ben Tak Blue	Thailand	Quartz-monzonite	174.5 (4.0)	28.3 (15.0)	13.8 (14.9)	8.4 (11.9)	28.5 (7.2)
Salmon Red	Uruguay	Syenite		14.38 (13.36)	8.9 (3.5)	2.81 (21.4)	
Artigas	Uruguay	Syenite			5.76 (20.6)	3.41 (4.1)	
Nero Assoluto	Uruguay	Dolerite	358.1 (2.9)	49.72 (16.4)	17.87 (15.7)	2.25 (10.6)	27.1 (35.6)
Anzola	Italy	Gabbro	208.0 (16.1)	14.9 (43.1)	9.6 (27.6)	7.8 (20.7)	28.5 (23.6)
Nero Impala	South Africa	Gabbro-norite	235.0 (14.5)	17.1 (5.9)	10.7 (8.0)	6.8 (12.9)	32.8 (35.3)
Negro Riojano	Argentina	Gabbro	200.2 (6.7)	24.6 (3.8)	10.9 (1.7)	3.96 (0.3)	
Balmuccia	Italy	Peridotite	243.0 (9.4)	24.6 (29.7)	13.1 (10.0)	5.7 (10.5)	37.7 (17.4)
Löbejün	Germany	Rhyolite	188.5	19.3 (17.6)	10.3 (31.2)	5.0	
Stardust Grey	Argentina	Rhyolite	207.4 (3.7)	21.5 (29.3)	10.3 (12.9)	7.3 (63.5)	29.6
Monte Merlo	Italy	Trachyte					
Drachenfels	Germany	Trachyte					
Weibern	Germany	Phonolite tuff	11.36		1.6		4.8
Rochlitz	Germany	Rhyolite tuff	23.6	2.7	3.8 (28.9)	11.8	16.7
Phanom Sarakhram Grey	Thailand	Gneiss	194.6 (4.4)	19.1 (20.5)	10.9 (18.9)	4.5 (8.7)	29.2 (5.2)
Azul Tango	Argentina	Gneiss	212.3 (12.2)	23.5 (2.0)	9.7 (29.8)	3.9 (10.5)	36.6
Calanca	Italy	Gneiss	186.0 (22.3)	15.4 (73.4)	9.3 (54.8)	8.1 (15.9)	25.0 (10.8)
Verde Andeer	Italy	Gneiss	176.0 (28.0)	15.3 (72.6)	11.4 (52.8)	7.4 (22.9)	22.1 (7.9)
Serizzo Monte Roas	Italy	Gneiss	169.0 (8.0)		9.8 (54.1)	7.9 (13.7)	20.7 (6.5)

(continued)

Table 3.9 (continued)

Commercial name	Country of origin	Rock type	Compressive strength (MPa)	Flexural strength (MPa)	Tensile strength (MPa)	Abrasion strength (cm <sup>3</sup> /50 cm <sup>2</sup> )	Young's modulus (static) (GPa)
Wang Nam Kiew Black	Thailand	Hornblende	125.5 (8.8)	11.5 (32.5)	6.8 (40.2)	7.1 (14.8)	28.7 (24.6)
Franco Veteado	Argentina	Migmatite	112.1 (16.0)	11.9 (17.3)	8.2 (16.6)		23.3
Rosa Estremoz	Portugal	Marble	81.2 (18.5)	16.4 (31.0)	6.8 (20.0)	24.9 (7.4)	16.4
Carrara	Italy	Marble			4.5 (48.8)		
Carrara	Italy	Marble					
Phran Kratai Grey	Thailand	Marble	122.1 (46.8)	25.3 (59.9)	8.9 (44.4)	15.0 (13.0)	30.4 (9.1)
Azul Cielo	Argentina	Marble	50.2 (2.7)	5.9 (24.7)	3.5 (7.7)		30.8
Azul Imperial	Brazil	Muarzite	281.0 (5.8)	28.4 (41.9)	18.3 (21.9)	4.3 (8.5)	34.2 (14.3)
Camine Rulo	Uruguay	Slate			13.54 (93.1)	11.25 (19.5)	
San Luis Slate	Argentina	Slate	172.4 (33.8)	37.5 (99.3)	13.4 (62.7)	13.8 (67.2)	37.6
Theuma	Germany	Slate	89.7	3.3		31.3	
Globegerina	Malta	Limestone	26.4 (94.4)	1.1–4.7	3.03 (17.5)		21.0
Caliza Amarilla	Argentina	Limestone	84.0 (19.6)	11.4 (13.3)	4.5 (21.0)	24.8 (24.0)	
Dolomita Dorada	Argentina	Dolomitic limestone	194.1 (11.9)	21.3 (22.8)	10.2 (7.6)	21.1 (3.4)	
Mae Phrik Yellow	Thailand	Limestone	125.3 (6.4)	14.7 (11.0)	8.5 (18.9)	9.9 (9.1)	29.3 (23.3)
Soskut	Hungary	Limestone					
Kuacker	Germany	Limestone	82.5	12.6	5.5	23.8	
Thüster	Germany	Limestone	25.0		7.0		
Bad Langensalza	Germany	Travertine	55.0 (52)	7.9 (10.8)	5.6 (34.6)	22.3	47.2 (10.2)
Baumberger	Germany	Sandstone-like limestone	50.0	11.0	4.1	19.1	19
Anröchte	Germany	Sandstone-like limestone	85.0	21.9		19.8	
Bad Bentheim	Germany	Sandstone	50.3	4.2	2.8	16.4	
Schleerther	Germany	Sandstone	76.8 (17.8)		6.8		
Weser	Germany	Sandstone	149.8 (5.5)	21.3	8.4	12.3	
Sikhü Brown	Thailand	Sandstone	147.5 (20.5)	16.7 (35.5)	8.7 (7.7)	9.9 (9.6)	18.4 (5.1)
Pakchong Green	Thailand	Sandstone	103.2 (20.0)	10.7 (39.2)	5.7 (25.2)	12.9 (28.3)	13.5 (19.1)
Tacuarembó	Uruguay	Sandstone	32.7 (28)	4.07 (16.6)	2.4 (56.6)	56.4 (24.2)	5.3 (50)

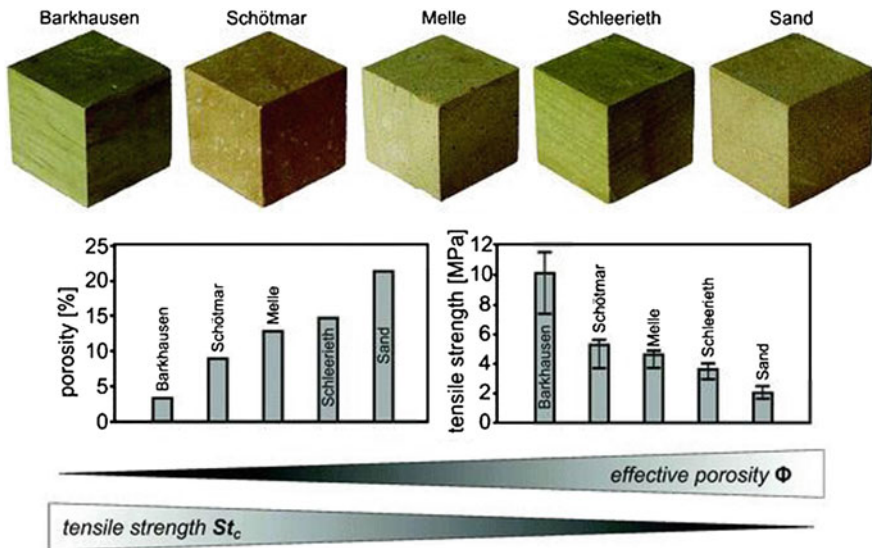


**Fig. 3.59** Five different samples of the Schilf Sandstone (Middle Keuper) shown here are similar in color and structure, but their porosity and tensile strength values vary significantly (Mosch 2009)

One of the main factors affecting tensile strength is the existence and spatial orientation of any foliation or sedimentary layering in the rock sample and the loading direction with respect to these rock fabric elements. In general, many rocks show the lowest tensile strength values perpendicular to the foliation or sedimentary layering. For sandstones, relatively high anisotropy values of up to 40 % related to the occurrence of sedimentary layering have been reported by Koch and Siegesmund (2001, 2005), Hoffmann and Siegesmund (2007), and Ruedrich and Siegesmund (2007).

The geometry of tension cracks and fractures in relation to the pre-existing rock fabric (e.g. intergranular cracks along grain boundaries and intragranular cracks in the rock-forming minerals) are schematically shown as 2D-models in Fig. 3.60. Two different fabric types are compared which have a different angle to the loading direction (indicated by the arrows). (1) The fabric in the upper row (Fig. 3.60d–f) shows a distinct and clear preferred orientation with respect to the grain shape, but no crystallographic preferred orientation. The tensile fracture orientation here is mainly determined by the orientation of the intragranular cracks. (2) In the lower row (Fig. 3.60g–i), the rock has a preferred orientation with respect to the grain shape as in (1), and additionally, a clear and distinct crystallographic preferred orientation of the rock-forming minerals, indicated by two cleavage planes oriented perpendicularly to each other. One of these planes is oriented nearly parallel to the grain boundaries.

The six different test types illustrated in Fig. 3.60 show that the two different fabrics and the three different loading geometries result in extreme differences in

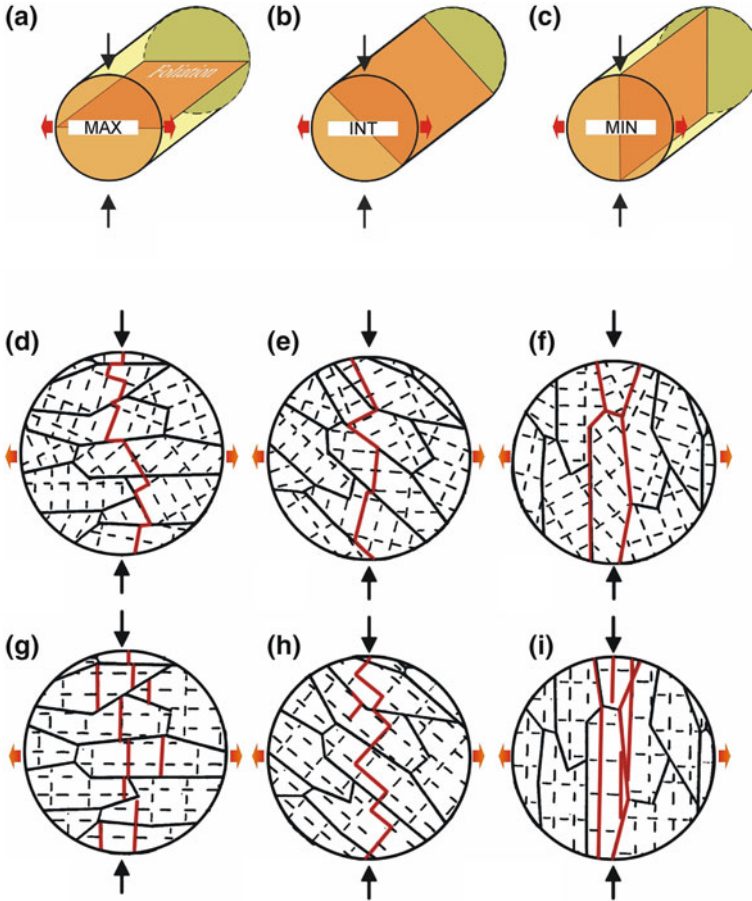


**Fig. 3.60** Anisotropy of the tensile strength in relation to the rock fabric and the orientation of the foliation with **a** Maximum (*MAX*) **b** Intermediate (*INT*), and **c** Minimal (*MIN*) value of the tensile strength. **d–f** Rock fabric without any preferred mineral orientation (schematically shown by the orientation of cleavage planes) but with a clear preferred orientation of the grain shape. Depending on the orientation of the minerals in relation to the loading direction (black arrows), the sample would show higher (**a, d**) and lower (**c, f**) tensile strength values, i.e. the tensile strength is determined by the grain shape. **g–i** Rock fabric with a clear preferred orientation of the minerals (schematically shown by the orientation of cleavage planes) and a clear preferred orientation of the grain shape. The tensile strength is determined by the combination of the orientation of the minerals (cleavage planes) and the orientation of the grain shapes in relation to the loading direction (black arrows) with higher (**a, g**) and lower (**c, i**) tensile strength values. For all possibilities (**d–i**), the crack distribution is shown in red as the result of the tensile forces (red arrows) after Siegesmund et al. (2002)

the values for tensile strength, with the maximum value for the fabric type in the upper left and the minimum value for the fabric type in the lower right. The maximum value results from the situation where the grain boundary cracks do not

have the potential to become tensile cracks, since they are oriented perpendicularly to the loading force. The minimal tensile strength value is the result of a fabric where the grain boundary cracks and the cleavage cracks are oriented parallel to the loading direction, and therefore, both have the potential to become tensile cracks.

For a marble sample, Siegesmund et al. (1999) observed a variation in the tensile strength from 5.5 to 8.3 MPa. Related to this, Ruedrich (2003) has done detailed investigations on the Carrara and Sterzinger Marble. He found that the tensile strength values vary depending on the load direction, between 3.4 and 5.6 MPa and between 4.8 and 7.9 MPa, respectively. His results support the concept of having a superposition of texture and load geometrical effects. As shown in Fig. 3.60, small tensile cracks formed along the grain boundaries in the fine-grained Carrara Marble, which successively connect to each other, thereby forming a growing network. In addition, Peck et al. (1985) and Brosch et al. (2000) were also able to demonstrate that open microcracks in rocks have a significant effect on the rock's tensile strength. For example, the Sterzinger Marble exhibits a clear interlocking of the grain boundaries; however, the tensile forces induced by the uniaxial loading activated the crystallographic, pre-existing intercrystalline microcracks in the rock.

Similar fabric types can be found in many metamorphic rocks as well as magmatic rocks, which are characterized by a distinct magmatic flow direction (see Chap. 2). Strohmeyer and Siegesmund (2002) found a variation of the tensile strength values from ca. 7 to 14 MPa, related to differences in the rock fabrics for a metagabbro from Anzola where the hornblende showed a perfect cleavage. However, it is not clear if this phenomenon is superimposed by the orientation of the grain boundary cracks. On the other hand, the pyroxene (here, a diopside) shows a much less developed cleavage.

Sandstone samples investigated by Koch and Siegesmund (2005) and Ruedrich and Siegesmund (2007) also show a significant directional dependence of the tensile strength related to the loading direction. Figure 3.61 shows several samples with an increasing degree of the preferred orientation of the grains and their tensile strength values in different directions. The anisotropy of the tensile strength increases with an increasing degree of the preferred orientation of the grains, with the Arholzener Sandstone having a value of 33 %. Furthermore, a sample of the Solling Sandstone, which is commonly used as a building stone, revealed a tensile strength parallel to the sedimentary layering (4.5 MPa) 33 % higher than that perpendicular to the layering (3.0 MPa).

Aiming at general correlations between various rock properties, Fig. 3.62 shows the relationship between the uniaxial compressive strength (using cylindrical samples) and the tensile strength for various rocks. Although a clear linear dependency for the various lithologies seems to be obvious, some restrictions have to be considered.

In an extensive experiment, Peschel (1974) tested a large number of specimens from different rock types. Based on these data, he postulated a nearly constant value of 1:10 for the ratio of compressive to tensile strength for the whole



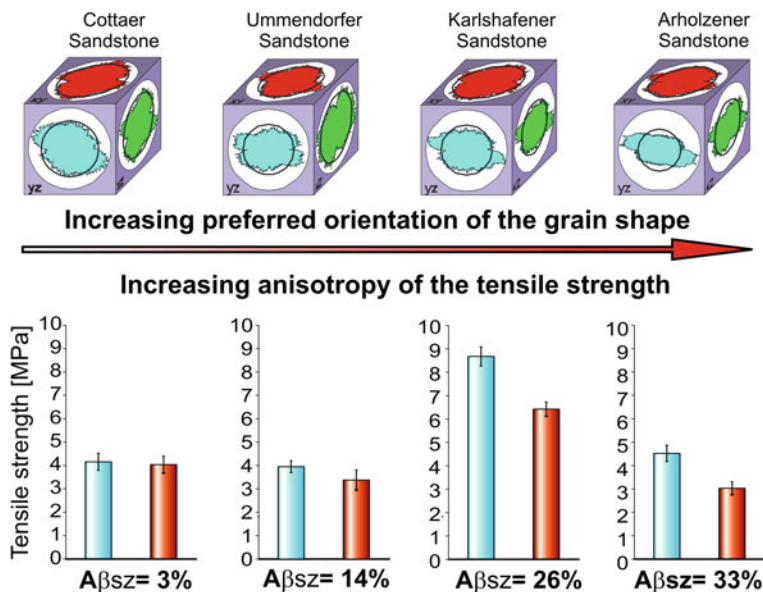


**Fig. 3.61** Relationship between the preferred orientations of the grains related to grain shape and the anisotropy of the tensile strengths ( $A\beta_{sz}$ ) for different sandstones. The Arholzener Sandstone shows a strong preferred orientation of the grain shape and a strong anisotropy (modified after Koch and Siegesmund 2005)

spectrum of dimension stones. However, in 1912, Hirschwald had already published a nearly constant compressive/tensile strength ratio of 1:10–15. Strohmeyer (2003) found that, when using the mean values of the compressive and tensile strength, this ratio might hold. However, when taking anisotropy for both properties into account, the ratio varies significantly. Therefore, on average, the ratio between the compressive and tensile strength is 1:18, for maximum values of extreme anisotropic rocks it is 1:39, and for minimal values it is 1:10.

Finally, taking into account the uncertainties of such empirical relationships, it is strongly suggested that, if tensile strength values are required for any reason, e.g. for mechanical strength calculations, individual experimental investigations on the respective rock material should be performed.

### 3.6.3 Flexural Strength

The flexural strength or bend strength is an important mechanical property of stones (Fig. 3.63). Failures due to bending stresses, both in structural and in decorative stone elements, are more common than those caused by compressive or shear stresses. Typical examples of flexural strength are the effect of the wind suction and wind pressure of rear-ventilated stone facades, the load of stone panels

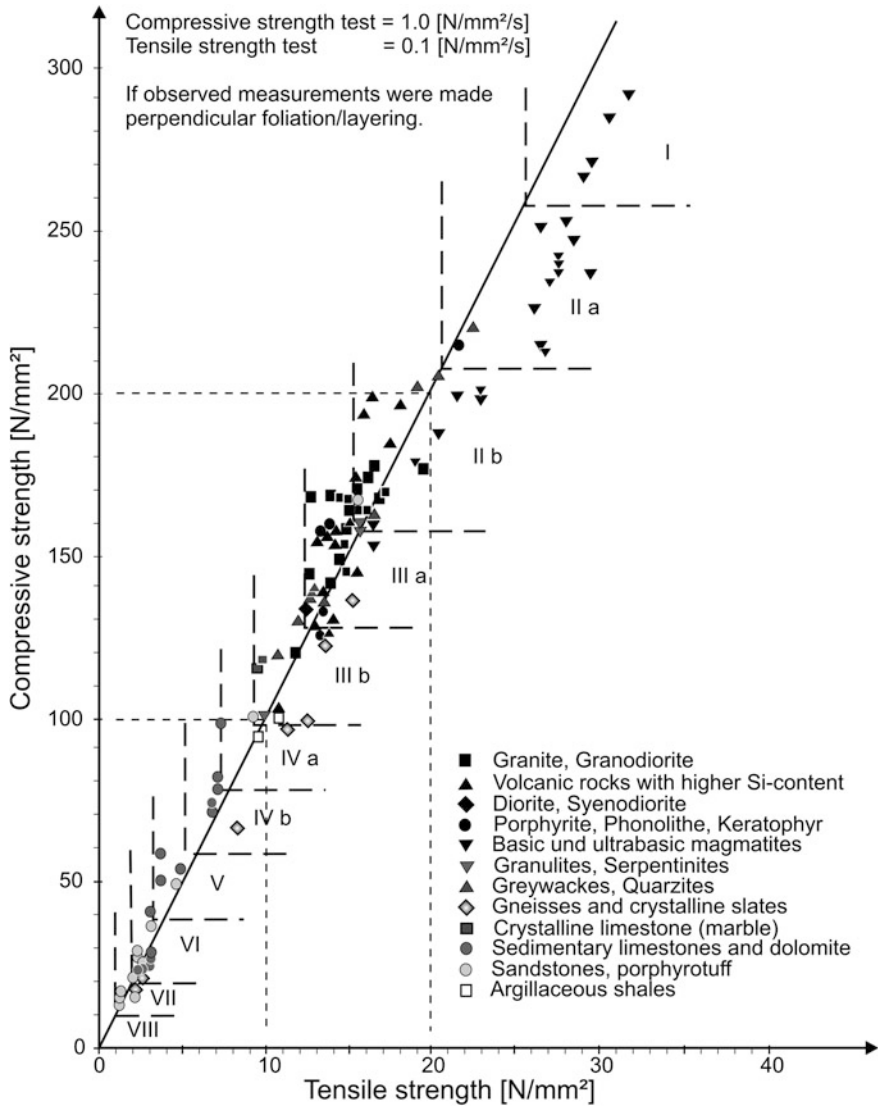


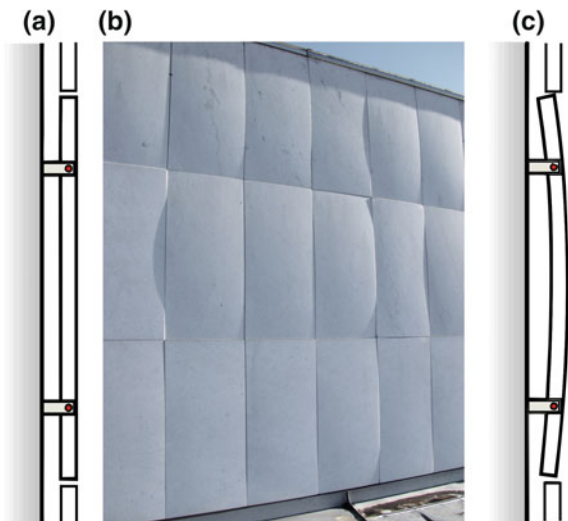
**Fig. 3.62** Relationship between the compressive strength values of cylindrical specimens and tensile strength values of various dimension stones (after Peschel 1977)

built in stairways, and the static force of structurally loaded building parts such as the architrave of a window.

In the rock specimen, the bending load creates tensile stresses (Fig. 3.64). The flexural strength values are usually lower than the tensile strength values for a rock.

The flexural strength is given by

**Fig. 3.63** Testing of the flexural strength is especially important for facade panels (a). For marble facade panels, which frequently show the characteristic bowing phenomenon (b and c), an increase in bowing with a distinct reduction in strength is the typical behavior (Koch and Siegesmund 2004; Siegesmund et al. 2008b)



$$R_{tf} = (3 \cdot F_{\max} \cdot l) / (2 \cdot b \cdot h^2), \quad (3.17)$$

where  $R_{tf}$  is the flexural strength (in MPa),  $F_{\max}$  the applied force at failure (in N),  $l$  the length of the support span (mm),  $b$  the specimen width (in mm), and  $d$  the specimen height (in mm).

The flexural strength can be determined using different methods, i.e. three and four point load tests. There are several test methods according to the standard of the American Society for Testing and Materials (ASTM C880-89 1989) and the two European Standards, DIN EN 12372 (1999) and DIN EN 13161 (2008). The comparability of the flexural strength values determined according to different standards is questionable, because the test after the EN norm requires drying until there is mass constancy, while the specimen dimensions can vary. The drying of the specimen results in slightly higher flexural strength values than determined according to the DIN. Since the EN norm allows variations in the size of the samples tested, a direct comparison of the values or of different rock groups is problematic. For example, in the Italian Standard UNI 9724/5 (1990), the width of the samples could be 30/38 mm with a thickness of 20/25 mm and a span of 100/250 mm. Furthermore, Blasi et al. (2000) were able to show that the four point load test provides somewhat less scattered results than the three point load test based on results from laboratory experiments on 12 selected marble samples.

For plutonic rocks, Mosch and Siegesmund (2007) have published values between 5.1 and 30.2 MPa (see Table 3.9, Fig. 3.53). However, extreme outliers with maximum values up to 40 MPa were reported by Peschel (1983). For volcanic rocks, similar flexural strength values were observed, but with a much wider range, because tuff and tuffitic rocks show relatively low values. Furthermore, carbonate rocks cover nearly the whole range of published flexural strength values

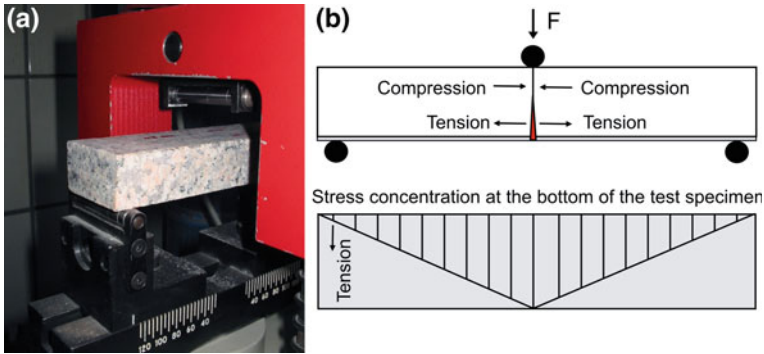


**Fig. 3.64** **a** Photo of the experimental setup for flexural strength determination. **b** Schematic picture of the setup with regions of compression and tension indicated where  $F$  is the loading force direction

for dimension stones, from 1.0 to 34.0 MPa. Sandstones nearly cover the whole data spectrum as well. However, some authors, like Müller (2001), only relate flexural strength values of more than 30 MPa to crystalline schists.

Crystalline marbles can show relatively low values of flexural strength (Brosch et al. 2000). The fabric of the grains shows a great variety throughout the marble (see Chap. 2). The grain boundaries in marbles can be nearly in equilibrium, so that equigranular and polygonal grain fabrics can be observed. As a result, the strength of these marble varieties can be significantly reduced compared to varieties with stronger interconnected and interlobate grain boundaries.

The serpentinite rock group also shows a larger range with respect to flexural strength values. However, this can be related to the heterogeneity and the various fabric patterns associated with this rock group. Many serpentinites contain relic minerals, which often reveal their origin as ultrabasic rocks like peridotites, and additionally, they are often highly deformed.

Metamorphic rocks can especially exhibit a significant directional dependency of the flexural strength (see Fig. 3.65). This anisotropy is pronounced in crystalline schists due to the preferred orientation of various fabric elements. Therefore, the data range of these rocks is quite large, from 5.9 to 82.3 MPa, as given by Mosch and Siegesmund (2007).

The variability in the rock fabric elements is commonly quite pronounced in metamorphic rocks (but this also holds true for magmatic and sedimentary rocks, depending on the rock fabrics; see also Chap. 2), and it is the main reason for the variability in the flexural strength values measured in the different directions of one sample. Because of this, the European Norm (EN) requires laboratory measurements of the flexural strength in different directions for dimension stones, which allows the characterization of the maximum and minimum values for a specific rock type.

The variation in the flexural strength values is also distinct in very heterogeneous rock types, such as migmatites (see Chap. 2). For the migmatite “Franco

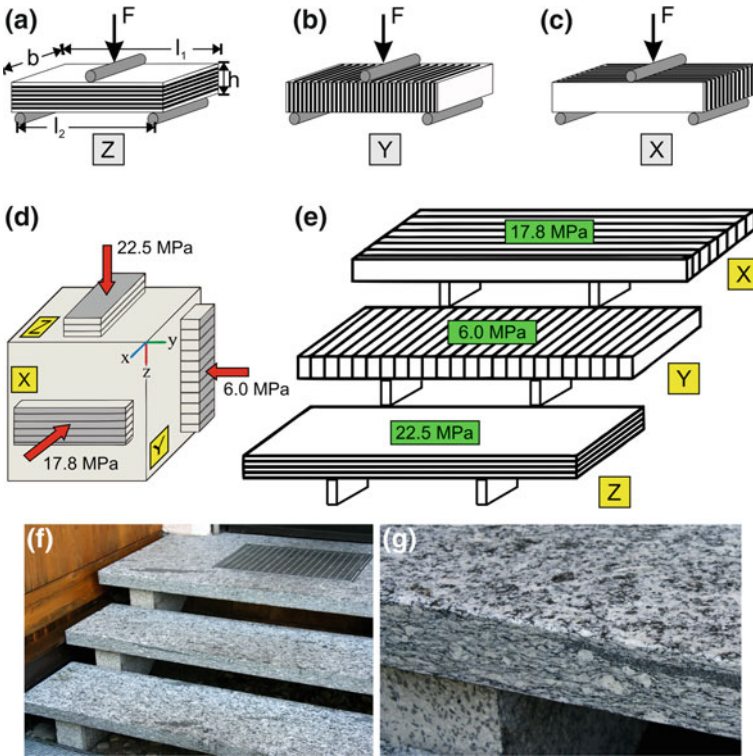


**Fig. 3.65** a–c Schematic diagram illustrating the determination of flexural strength in different directions with respect to a pronounced planar fabric element (layering, foliation), as indicated using three specimens of one rock sample, **d**, with **a** load perpendicular to the planar fabric, **b** load parallel to the planar fabric with the cylindrical axis parallel to the planar fabric, and **c** perpendicular to it. **d** Differences in the measured values exhibit a directional dependency of the flexural strength (anisotropy), with a schematic diagram of a stairway illustrating the use of the different samples in **(e)**. **(f)** shows a real stairway with details of the planar element corresponding to the z-orientation in **(g)**

Veteado” from Argentina, Mosch (2009) reported a maximum anisotropy value of 17.3 %. Figure 3.66 shows how the values can vary due to the occurrence of rock fabric elements, for example, only in the z-direction between 9.2 and 15.6 MPa. The dominating fabric elements in the migmatite are the alternating layers of quartz-feldspar-rich layers (leucosome), layers of original rock material (palaeosome), and layers with biotite minerals. The possible loading pathways for staircase treads should illustrate the problems of anisotropic tensile strength in construction and structural engineering applications.

The directions usually presented are the spatial orientation of the tensile vectors, which are perpendicular to the fracture surface (see Fig. 3.64). The directional dependency of the flexural strength can be relatively complex, which can result in a larger data range, depending on the loading path and fabric elements of

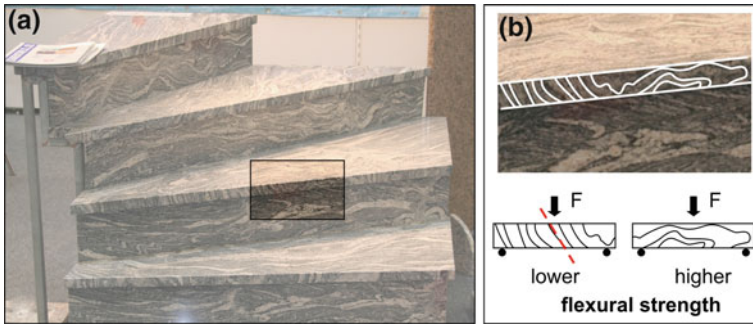


**Fig. 3.66** **a** Variability of the rock fabric in gneisses and migmatites and **b** Their influence on mechanical stability under the conditions of different loading paths (Mosch 2009)

the sample examined. A quite pronounced preferred orientation of fabric elements or the superposition of more than one element can result in significant anisotropy values of the flexural strength. Anisotropy values of more than 70 % for strongly foliated rocks are possible. Sandstones and carbonate rocks exhibiting a strong layering can reach values of around 40 MPa. It comes as no surprise that the loading directions perpendicular to the layering or foliation show the lowest flexural strength values. Koch and Siegesmund (2004) and Siegesmund et al. (2008b) demonstrated that marble facade panels, which showed differences in weathering expressed by their degree of bowing, exhibited flexural strength values varying from around 14–2 MPa (Fig. 3.63). With increasing weathering, which correlates and can be expressed with an increase in the porosity (see Sect. 3.2), the flexural strength decreases. This comes in addition to the possible anisotropy-related lower values of the flexural strength due to the existence of fabric elements in the rock.

### 3.6.4 Hardness and Abrasion Resistance

Rocks are often attributed by laymen with the words hard or soft. However, science and engineering have a more differentiated view on this mechanical property, but it is often derived from and developed for application purposes. In road construction, the compressive strength of the material (see Sect. 3.6.1) or the abrasion of the road construction material itself is used to describe the hardness of a rock. In the dimension stone and stone working industry, a scale for the hardness often reflects and describes the difficulties of rock preparation. An overview of the hardness scales can be found, for example, in Hirschwald (1912), Peschel (1983), and Rösler (1991). A widely used hardness scale, especially in mineralogical and geological investigations, is the scratch resistance, developed in 1812 by the German mineralogist Friedrich Mohs. Further hardness scales in use, for example, are the indentation hardness after Vickers, developed in 1924 by Smith and



Sandland at Vickers Ltd., and after Knoop, developed in the USA in 1939. For polymers, the Shore hardness is mainly used by applying a durometer. The Rosival scale is based on the abrasion hardness, and it is basically an improved Mohs scale mainly used in civil engineering today. For further details on hardness testing, see Franklin and Dusseault (1989). Although hardness is a material property, the different measurement methods provide different values; however, they can often be converted into each other. A direct conversion from the Mohs (MH) to the Vickers (VH) hardness scale is possible using the following equation after Picot and Johan (1977):

$$\text{MH} = 0.7 \cdot \text{VH}^{1/3} \quad (3.18)$$

In general, it can be said that granite is a harder rock than sandstone, for example, as granite consists of minerals with a Mohs hardness of 7 (quartz), 6 (feldspar), and 2–3 (mica), whereas sandstone consists of minerals with a Mohs hardness of 7 (quartz as the matrix) and 2–3 (calcareous or siliceous cement). However, the micro-hardness is a highly variable property due to the heterogeneity of natural stones and the diversity of minerals. Primavori (1999) showed that the micro-hardness based on Knoop could be a useful tool for the characterization of rocks with respect to the wear strength and processing performance, which is finally determined by the hardness of the individual rock-forming minerals in contrast to the average hardness. For granite, this could mean that micro-hardness measurements will produce a data set of extreme variability, because the Knoop micro-hardness is determined by a series of measurements 1 mm apart from each other made by a diamond-tipped penetration device pressed at a given load against the surface.

Attempts have been made to correlate the material hardness directly with other mechanical properties of interest; the Shore hardness related to the compressional strength is one example (Peschel 1983). Materials with higher Shore hardness values also show higher values in compressional strength.

A measure of rock hardness can also be the degree of abrasion, which is the resistance of a rock against a grinding force. The abrasion resistance of a rock depends mainly on the mineralogical composition and the rock fabric. Of further importance is the moisture content in the rock (Hirschwald 1912). The determination of the abrasion resistance basically means how much a rock can resist forces related to footsteps and walking (see Figs. 3.67 and 3.68). This, on the other hand, also depends on the frequency of the footsteps and walking as well as the material hitting the stone on the floor, such as bare feet or shoes. Therefore, places and rooms are classified according to different degrees of exposure. Floors with light exposure are, for example, bedrooms and bathrooms, since these places are commonly entered bare-footed or with house shoes, which, in general, have a soft sole, giving these rooms the classification level “Abrasion Class 1”. This means that the dimension stones used as floor tiles should not produce any sand or dust when stepped on. Interiors with medium exposure are living and dining rooms, since these places are mainly entered with shoes that have soft-to-normal soles; consequently, only light abrasions can be expected in these rooms. Places with



**Fig. 3.67** Carrara Marble stairs in (a) in Montevideo (Uruguay) and (b) in Buenos Aires (Argentina) clearly show differential abrasion

**Fig. 3.68** Staircases in the Geology Department at Princeton University (U.S.A.) showing significant abrasion. The staircases are made of an altered and metamorphosed ultramafic rock. The parts that wear down are talc plus magnesite. The more resistant lines and bumps are chlorite and/or pyroxene



higher exposure levels are kitchens, house entrances, economic areas, foyers, receptions, showrooms, and sales rooms, or, in general, more public places, like airports. These places are highly frequented, and therefore, highly exposed to abrasion and subsequent sand production from the stones used as floor tiles.

For the determination of the abrasion resistance, different methods are applied—for example, the Amsler and Böhme abrasion testing machines basically work with a wheel. Although other methods available apply the same principles, the standardization can be quite difficult. Therefore, a conversion of the data from different methods is not possible at present. For the Böhme test, a rock specimen with a square base is pushed with a defined weight on a grinding wheel and then ground by using a defined grinding medium or abrasive (see Fig. 3.69). At the contact area between the specimen and the grinding wheel, shear and tensional cracks occur, resulting in a drastic softening of the rock fabric (Fig. 3.69). All minerals and fabric elements of the rock contribute to the abrasion resistance (Strohmeyer 2003).

The dimension of the specimens should be  $71 \times 71 \times 25$  mm (length, width, height) because the contact surface between the rock and the grinding wheel has to

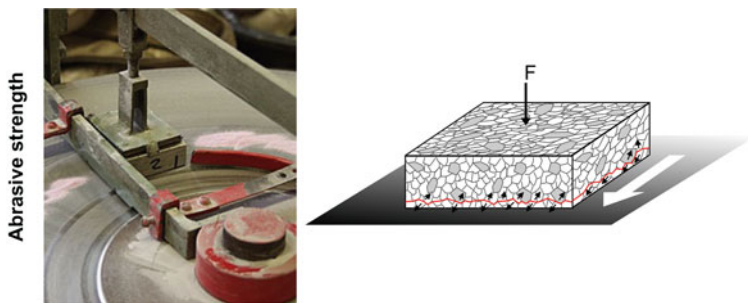


**Fig. 3.69** Measurement of the abrasion resistance: *Left*: Photo of the setup with the cubic sample pushed on the rotating grinding wheel. *Right*: Schematic drawing of the abrasion at the contact area where the rock sample is pushed with a constant force  $F$  onto the moving grinding wheel

**Fig. 3.70** Böhme test abrasion values for different rock types including their range of dispersion (modified after Müller 2001). Note, higher values (from *right* to *left*) indicate a rock having a lower abrasion resistance, lower values indicate a higher abrasion resistance

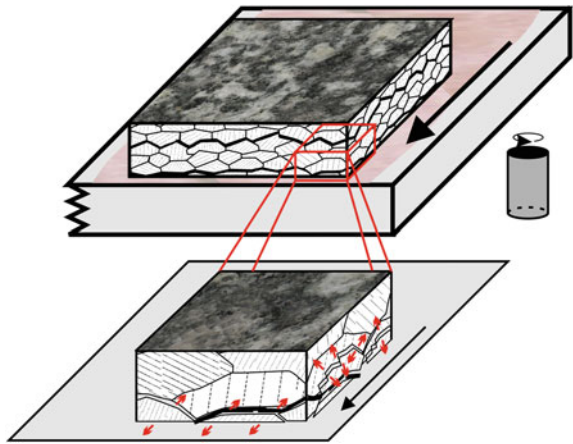
	abrasion resistance					cm <sup>3</sup> /50 cm <sup>2</sup>
	100	80	60	40	20	
Granite + Tonalite						☒
Syenite + Gabbro						☒
Lava					☒	☒
Volcanic tuff			☒	☒	☒	☒
Sandstone					☒	☒
Clay shale	☒	☒	☒	☒	☒	☒
Limestone compact				☒	☒	☒
Limestone porous	☒	☒	☒	☒	☒	☒
Marble				☒	☒	☒
Serpentinite					☒	☒
Paragneiss						☒
Quartzite						☒

be at least 50 cm<sup>2</sup>. The Böhme test value indicates the material loss of a specimen after a certain number of rounds on the grinding wheel. Therefore, higher values represent samples with a lower abrasion resistance, and lower values equate to samples with a higher abrasion resistance.

Table 3.9 summarizes the abrasion resistance values of several rock types, whereas Fig. 3.70 shows the range of dispersion for various rock types. In general, it is desirable to have stone with a lower abrasion resistance value, indicating higher abrasion resistance.

Granites are often seen as very hard rocks and advertised as a robust material that shows almost no abrasion even at higher exposure or wear levels. However, Hoffmann and Siegesmund (2007) and Hoffmann (2008) have observed variations in granites and gneisses with mean values of abrasion of 4.01 cm<sup>3</sup>/50 cm<sup>2</sup> and 4.81 cm<sup>3</sup>/50 cm<sup>2</sup>, respectively. Any directional dependence, or anisotropy, of the abrasion resistance found in rocks is strongly determined by the preferred orientation of the macroscopic fabric elements. However, in comparison to other mechanical strength values, the abrasion resistance seems to be less sensitive to any preferred orientation of macroscopic fabric elements than to other values.

**Fig. 3.71** Schematic illustration of failure mechanisms, which can occur during an abrasion test. The softening of the rock fabric is related to the occurrence of shear and tensile cracks and subsequently leads to the disintegration of the whole mineral assembly



Quartzite shows the highest possible values of the abrasion resistance of rocks compared to other rock types. Because of its hardness, a quartzite can only be processed by saw cutting and machine grinding and polishing. Basalt shares similar values of hardness and abrasion resistance because it is also a relatively hard rock. However, Hoffmann (2008) was able to show that mafic rocks, which mainly consist of scissile minerals like pyroxene and hornblende, experienced higher mass losses during testing, indicating a lower abrasion resistance in these lithologies. For a hornblendite, for example (see Table 3.9), Hoffmann (2008) determined abrasion values of around  $7.10 \text{ cm}^3/50 \text{ cm}^2$ .

Schists are quite softer rocks, but they can also show good abrasion resistance. This higher resistance is the result of a relatively higher quartz content in combination with a very low porosity. Schists exhibit a relatively strong anisotropy in all strength-related properties. For example, the values of the abrasion resistance for a schist sample from Argentina are between  $7$  and  $21 \text{ cm}^3/50 \text{ cm}^2$  (67 % anisotropy). Significantly higher values of abrasion resistance have been found for a schist from Lotharheil, Germany (see Fig. 2.40), due to the sample's high quartz content.

The abrasive material loss values for carbonate rocks show a wide distribution range. Marble and dense limestone can show a similar range of values varying between  $12.5$  and  $32.5 \text{ cm}^3/50 \text{ cm}^2$  (Peschel 1983). Travertine samples as well as porous limestone can exhibit much higher abrasion values.

For sandstones, the hardness and abrasion values mainly depend on the composition of the matrix as well as of the cement. However, frost resistance is always given for this rock type. On the other hand, it is quite difficult or often not really possible to polish sandstones, except some varieties with higher quartz content or siliceous cement, like one rock from Thailand; however, these rocks are rare worldwide.

Detailed investigations of the abrasion surfaces of different stones with a scanning electron microscope by Strohmeyer (2003) and Strohmeyer and Siegesmund (2002) have revealed different mechanisms of failure (Fig. 3.71).

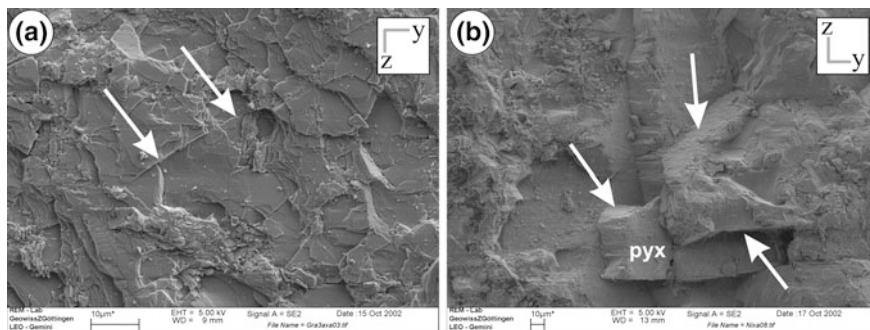


**Fig. 3.72** SEM-figures from Strohmeyer (2003) of rock surfaces after an abrasion test: **a** Granitic ultramylonite with preexisting microcracks (*arrows*) opened during the test. **b** Gabbro norite sample with preexisting microcracks in pyroxene (*pyx*) activated during the abrasion test (*arrows*)

Astonishingly, after the abrasion test, no scratch or stress marks were found on the mineral surfaces in contact with the grinding wheel, respectively, grinding powder. Even the minerals that were weaker than the SiC grinding powder did not produce swarf, but rather experienced smashing and fragmentation of the crystal structure. This results in a softening of the rock fabric, which subsequently leads to disintegration of the whole mineral assembly. Open, pre-existing microcracks parallel to mineral cleavages or along grain boundaries are preferentially activated during this process (Fig. 3.72). Therefore, these fabric elements are mechanically weak links in the rock, so that their frequency of occurrence is an important factor in determining the abrasion resistance.

In general, the mean values of the abrasion resistance are strongly related to the mechanical properties of the rock-forming minerals, especially the mean hardness. For mica-bearing granitic or metagranitic rocks, the content of mica provides some estimate of the abrasion values to be expected. The microcrack density as well as the grain size of the minerals has a relatively smaller effect here compared to other mechanical properties, such as compressive, tensile, and flexural strength. The anisotropy of the abrasion resistance shows a good correlation with the macroscopic fabric elements and the mica content and the distribution and orientation of the mica minerals in the rock (see Sect. 2.8). For rocks with a significant preferred orientation of fabric elements (e.g. sedimentary layering, foliation), the abrasion resistance parallel or perpendicular to these elements can also be significantly different.

### 3.6.5 Breaking Load at the Dowel Hole

In recent years, the breaking load at the dowel hole has increasingly received attention due to new trends in architecture, especially the use of dimension stones for rear-ventilated cladding or lining on buildings. The dowels have two main

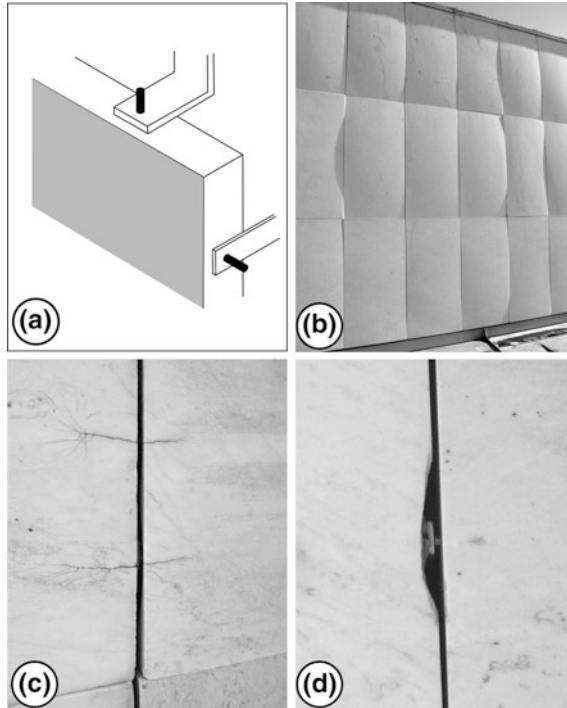


**Fig. 3.73** Restrain fixings, usually ties or cramps with dowels (a), here at the *top* and at the side of a cladding to maintain the stone in position. Observed damages on marble panels: **b** Clearly developed convex bowing of Carrara Marble (university library, Göttingen, Germany) **c** Typical cracks often initiated at the dowels, and **d** The breakout of larger marble fragments at the dowels

functions: first, the load bearing, taking the weight of the cladding or lining units, and second, the restraining, holding the cladding, or lining units in position and resisting the cyclical loads due to wind pressure and suction (see Fig. 3.73a–d). Dimensional stones chosen for such an application have to be tested for the breaking load at the dowel hole according to the DIN EN 13364 (2002). These technical regulations require a square sample with a size of  $200 \times 200 \times 30$  mm, or alternatively, slabs of  $300 \times 300$  mm (Fig. 3.74).

The breaking load at the dowel hole describes the force needed until a dowel breaks out from its dowel hole under vertical loading (Fig. 3.74). The required loading rate according to the DIN EN 13364 (2002) is 50 N/s. Furthermore, the norm requires breaking load tests in different directions in case the dimension stone exhibits any preferred orientation of rock fabric elements, resulting in planar structures like sedimentary layering or metamorphic foliation. Figure 3.75 provides an overview of the different directions, called “types” in the DIN EN 13364 (2002), to be tested in relation to the orientation of the planar elements.



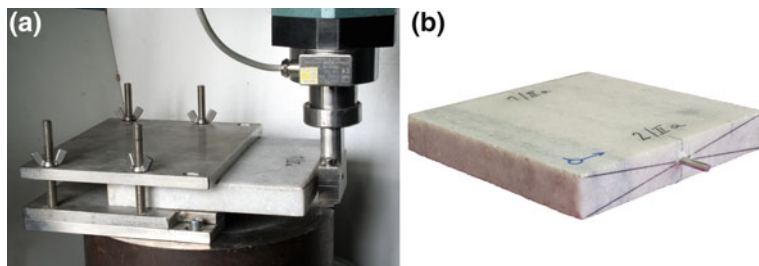


**Fig. 3.74** Experimental setup for testing the breaking load at the dowel hole (a) and a dimension stone sample with the dowel implemented in the center position of the face (b)

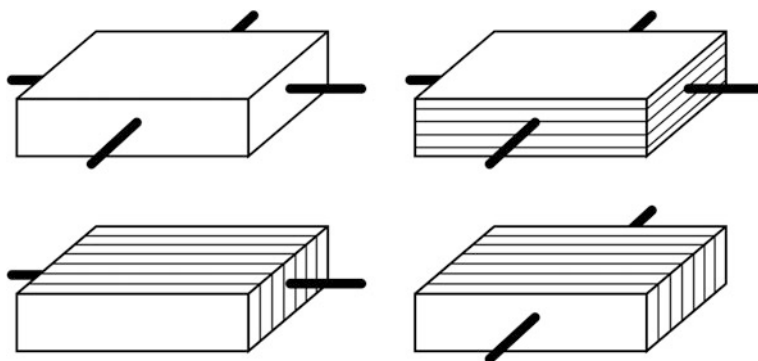


**Fig. 3.75** Orientation of dowels in relation to the spatial orientation and distribution of planar fabric elements in the sample to be tested (after DIN EN 13364 2002)

For the testing, dowel holes have to be drilled into each site of the cubic sample or slab, exactly in the middle and with not more than 2 mm deviation in relation to the shorter margins of the sample face (see Figs. 3.74 and 3.75). Rohowski (2001) compared the values of the breaking load at the dowel hole of 15 different dimension stone types from two different measurements following different norms: the older German norm, LGA (1988), and the 1999 draft version of the European norm DIN EN 13364, which was introduced three years later. With the comparison of the values following both norms, Rohowski (2001) revealed differences of up to 88 %, with higher deviations for the very highly porous rock samples (see Fig. 3.76). Rohowski (2001) suggested there might be a correlation between the breaking load at the dowel hole and the bulk density as shown in Fig. 3.76. However, the mafic rocks and basalt samples, followed by the granite and the gneiss, showed the highest values in both experiments compared to other rock

**Fig. 3.76** Breaking load values at the dowel hole (in N) and density (in 1,000 g/cm<sup>3</sup>) for 15 samples determined after two different norms, the German norm, LGA (1988), and the 1999 draft version of the European norm, DIN EN 13364 (2002). Data from Rohowski (2001)

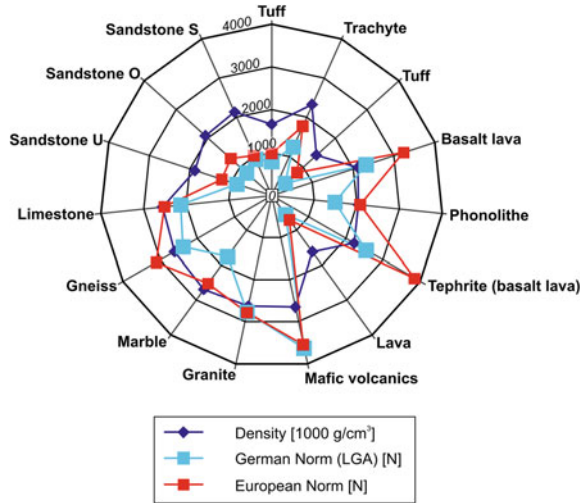
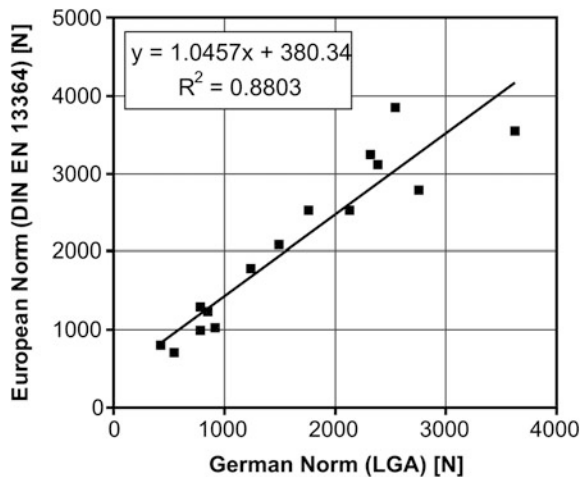


**Fig. 3.77** Comparison of the breaking load values at the dowel hole (in N) for 15 samples determined after two different norms: the German norm, LGA (1988), and the 1999 draft version of the European norm, DIN EN 13364 (2002). Data from Rohowski (2001)

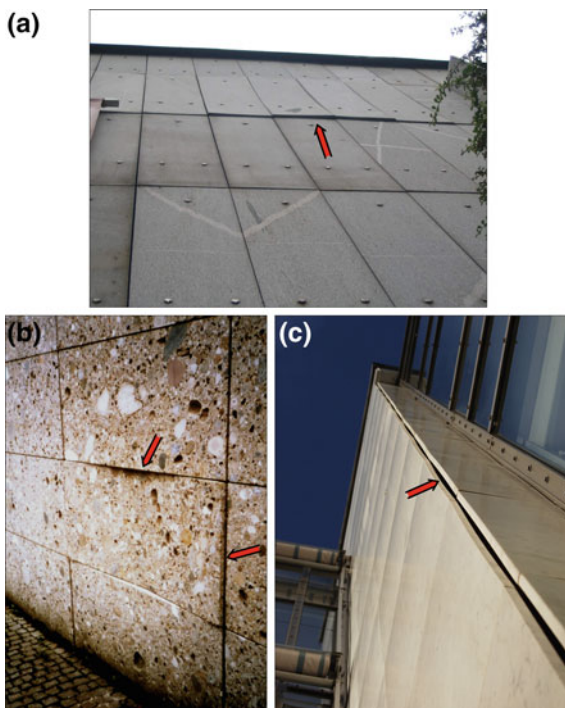


types. These rock types usually have good grain-to-grain contacts, whereas marbles, for example, often have grain boundary cracks.

These differences, a significant amount for some samples, certainly have an effect on the direct comparison between values determined by following different norms, although the data distribution in Fig. 3.77 suggests a systematic difference. However, the sample number is too low, especially for samples with higher breaking load values. Some of the differences may originate from the new rules in sample drying, since the new European norms require drying at 70 °C until mass constancy is reached.

The mean variation coefficient of the experimentally derived values for the breaking load at the dowel hole was 16 % for each of the two data sets following

**Fig. 3.78** Photos of cladding showing bowing: **a** Granite (Siegesmund et al. 2008a) **b** Nagelfluh Conglomerate (after Grimm 1999), and **c** Marble (Siegesmund et al. 2008b)

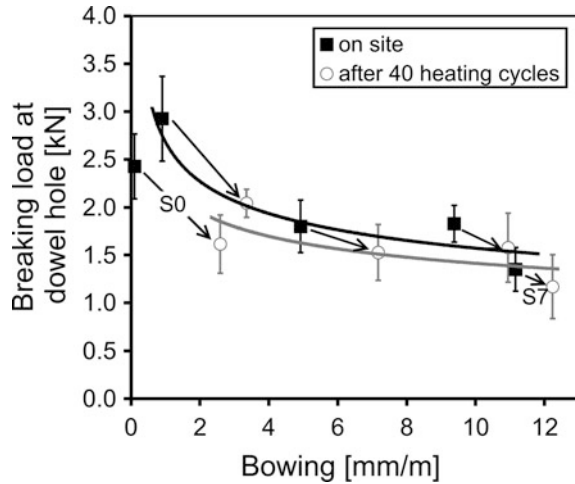


the different norms. The data in Fig. 3.77 also show that, for dimension stones examined under the European norm, higher values of the breaking load at the dowel hole can be assumed. This provides more freedom in the construction of rear-ventilated cladding, especially with respect to the dimension and thickness of the cladding (larger and thinner plates), which subsequently is also a cost-saving factor (Rohowski 2001).

The analysis of the breaking load at the dowel hole is of critical importance for the stability and structural safety of rear-ventilated cladding. The more recently discussed issue of the dimensional stability loss (e.g. bowing) of dimension stones that are used as cladding is actually a very well known phenomenon, especially for marbles, but also for granites, limestone, and conglomerates (Fig. 3.78).

The bowing phenomenon of marble panels on buildings goes along with numerous visible damages like cracks and outbreaks (see Fig. 3.73c, d). Depending on the amplitude of the bowing of the marble slabs, the intensity of damages increases significantly. In a detailed study, Siegesmund et al. (2008b) were able to show that the flexural strength (DIN EN 12372 1999) and the breaking load at the dowel hole (DIN EN 13364 2002) are strongly determined by the bowing, i.e. deterioration of the marble. The decrease in the breaking load at the dowel hole versus bowing for a marble sample is shown in Fig. 3.79. The initial strength of 2.43 kN of Sample S0 with no observed bowing is reduced to 1.35 kN for Sample S7, which showed bowing of 11 mm/m. Consequently, the

**Fig. 3.79** Breaking load at the dowel hole versus bowing of the panels before (*solid lines*) and after 40 heating cycles (*dashed lines*). The standard deviations are indicated by *error bars*



reduction in strength for the breaking load at the dowel hole is around 54 %. Simulating the conditions of marble panels at the building in an extreme way, the bowing potential was tested on marble slabs in the laboratory (see Sect. 3.4.2). The specimens were exposed to moisture on one side, lying on a 1 mm thick film of demineralized water and additionally exposed to cyclical heat from a heating pad 3 cm above the slab surface on the reverse side. A total of 40 cycles were performed (see Koch and Siegesmund 2001, 2004; Grell et al. 2004).

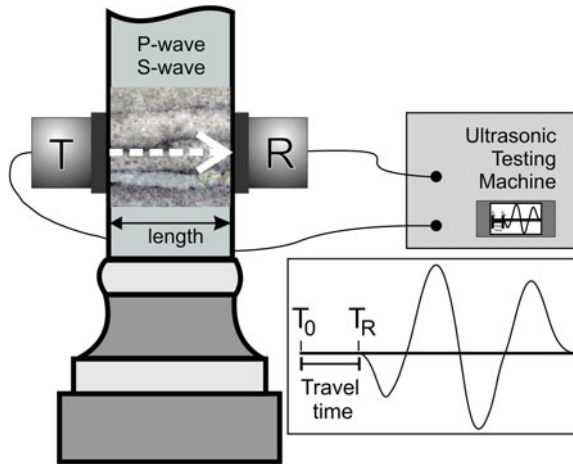
The bowing test was done to demonstrate how the increase in bowing of the panels determines the loss in strength on the breaking load at the dowel hole to constrain any risk management (Fig. 3.79). For example, Sample S7 exhibits the smallest increase in bowing after 40 cycles with 0.75 mm/m. The largest difference (3.62 mm/m) is observed for Sample S1, which corresponds to an irreversible length change of up to 1.1 mm/m. The observed reduction in the breaking load at the dowel hole varies between 13 % (S7) and 33 % (S0). In summary, the evidence clearly shows a loss in rock strength due to the bowing.

However, the general trend observed here also has exceptions. In one case, an existing dowel hole was tested again after the sample was subject to a weathering simulation experiment. The test of the breaking load showed a very critical value, because microcracks that had developed around the dowel hole caused the dowel hole to break immediately after the beginning of the loading.

### 3.7 Ultrasonic Wave Velocities and Young's Modulus

Recently, ultrasonic measurements have been gaining importance as non-destructive tools for evaluating structural damage in historical buildings and artworks. In these methods, P-wave velocity ( $V_p$ ) measurements are correlated with

**Fig. 3.80** Schematic diagram illustrating the ultrasonic measuring technique, with transducer (*T*) and receiver (*R*) in direct contact with the sample of known length (*l* in mm). The P- or S-wave travels the distance in a discrete travel time (*t* in  $\mu$ s) measured with an ultrasonic testing machine. From both pieces of data, the ultrasonic velocity (*V* in km/s) can be calculated with  $V = l/t$



the porosity increase due to fabric damages in rocks. Such correlations provide a method of measuring the degree of structural damage due to weathering and deterioration using indirect measurements. Damage prevention and repair planning can be made on the basis of such a  $V_p$ /structural damage classification.

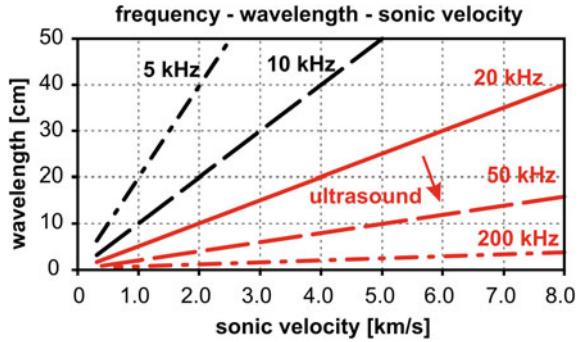
The elastic properties of a solid material and the seismic or acoustic velocities are fully determined by the elastic constants (stiffness). These constants combine stress  $\sigma$  acting in a specified direction to the strain in a specified direction, where both directions are not necessarily the same. Stiffness is described by a fourth rank tensor and written in a  $6 \times 6$  matrix. In case of one dimensional stress,  $\varepsilon$  is proportional to  $\sigma$  through the modulus of elasticity or Young's Modulus  $E$ , described by Hooke's Law as follows:

$$\sigma = E \varepsilon. \quad (3.19)$$

This linear relationship is only valid for small and reversible deformations and as long as the material is below a specific strain. From the elastic properties, the elastic wave velocities may be calculated by solving the Christoffel Equation (Crosson and Lin 1971; Siegesmund 1996).

In general, experimental velocity data are measured in the laboratory using the method of "pulse transmission" through rock samples of a few centimeters in length (Fig. 3.80). This is basically an application that was introduced by Birch (1960) in which an electrical pulse is applied to a transducer at one end of a specimen. The resulting deformation is transmitted through the specimen to a receiving transducer where the mechanical signal is converted into an electrical signal. The velocity is obtained from the travel time and the length of the specimen after correction for the system delay. This method is used in the same way as ultrasonic measurements in the laboratory as well as on-site, indoors and outdoors, when portable equipment is available (see Chap. 6). The transmitter and receiver transducers are then placed on opposite surfaces of the sample to be measured, for example, a column or a sculpture (see Fig. 3.80).

**Fig. 3.81** Relationship between the ultrasound velocities and the frequency as well as the wavelength, which must be considered when using this technique for damage characterization (modified after Köhler 2009)



In order to get reproducible ultrasonic signals and reliable velocity data, it is important to have a solid and smooth coupling between a rock sample and the transmitting and receiving transducers that allows an undisturbed transmission of the acoustic signal. In the laboratory as well as in situ, the velocities are generated and received by piezoceramic transducers with resonance frequencies in a range usually from 0.5 to 2.0 MHz. However, other transducer frequencies can also be used. Köhler (2009) pointed out that, for sample dimensions of less than 20 cm, the ultrasonic frequencies applied should be higher than 20 Hz when the ultrasonic velocities are around 4,000 m/s. The relationships between ultrasonic velocities, applied frequencies, and wavelengths are shown in Fig. 3.81. The waves generated propagate as different wave types; however, in practical use, compressional waves (P-waves) and transversal waves (S-waves) are the most important wave types. Current developments also focus on the use of surface waves. As explained above, the ultrasonic wave velocities are determined from the length of the travel pathway and the travel time. The velocity of the P-wave is always higher than that of the S-wave. As they travel through the rock sample, the different wave types also experience different attenuation. During the experimental measurements, the S-waves are more difficult to handle so that for most applications P-waves are used. However, the determination of the S-wave is essential for the calculation of the modulus of elasticity (E) or Young’s Modulus as shown in the following equations, either directly or through Poisson’s ratio:

$$E = \rho \frac{(3 Vp^2 - 2 Vs^2)}{(Vp^2 - \frac{1}{3}Vs^2)} Vs^2 \quad \text{or} \quad E = \rho \frac{(1 + \mu)(1 - 2\mu)}{(1 - \mu)} Vp^2 \quad (3.20)$$

where Vp is the P-wave velocity, Vs is the S-wave velocity, ρ the density, and μ the Poisson’s ratio. However, to calculate Poisson’s ratio, one has to know the transversal wave velocity. Poissons’s ratio can be calculated by

$$\mu = \frac{Vp^2 - 2 Vs^2}{2(Vp^2 - Vs^2)} \quad (3.21)$$

with Vp as the compressional wave velocity (P-wave) and Vs as the transversal wave velocity (S-wave). Very often, Poisson’s ratio is estimated due to the fact



that most rocks show a value between 0.20 and 0.30. Based on extensive laboratory velocity studies on rocks, it could be suggested that especially quartz-rich rocks show lower Poisson's ratios because most of the important rock-forming minerals exhibit values between 0.24 and 0.30 compared to quartz (0.07) (see discussion in Siegesmund 1996). The direct measurement of the modulus of elasticity or Young's modulus ( $E$ ) is based, as already explained, on the relationship between stress and strain, i.e. expressed as the ratio of stress to the rate of strain (statically measured Young's modulus, see Sect. 3.6.1). However, the dynamic elastic modulus can be measured by a combination of compressional ( $V_p$ ) and shear wave velocities ( $V_s$ ) as well as densities. However, Rentsch and Krompholz (1961) suggested using rod waves, which require a fixed geometry of the sample. By using this approach, the dynamic Young's modulus can be obtained directly. The experimental approach based on Rentsch and Krompholz (1961) has been realized by the Geotron Company (Germany, [www.geotron.de](http://www.geotron.de)) and correlates with a one-dimensional state of stress. However, as already discussed, the dynamically and statically obtained moduli of elasticity are always different from each other. Schön (1983) was able to show that the dynamic Young's modulus is usually higher than the static one; however, Strohmeyer (2003) made a different observation for metamorphic and magmatic rocks.

### ***3.7.1 Ultrasound Velocity and Lithology***

The elastic wave propagation through natural stones is mainly determined by the mineralogical composition, rock fabric, confining pressure, temperature, fluid pressure, pore space, and its distribution and interconnectivity, as well as the pore fluids and their compositions, and the degree of saturation (e.g. Birch 1961; Klima and Kluhanek 1968; Nur and Simmons 1969; Christensen 1979; Gebrande 1982; Siegesmund 1996). However, for practical applications and described here in simple terms, the ultrasonic velocities of a rock sample mainly depend on its water content (degree of saturation), on its density (composition), and on its state of preservation. Therefore, the P-wave velocities are often used as a diagnostic tool for the quality assessment of natural stones. Most of these relationships are empirical, like the P-wave-density relationship, which was already described in the late 1940s by Wollard (1959) and Nafe and Drake (1963), for example. Since their relationships are based mainly on data from sedimentary rocks, Birch (1961) introduced a later relationship based on magmatic and metamorphic rock data (see Figs. 3.3 or 3.4).

The mean P-wave velocity of typical rock-forming minerals varies within a very broad range (e.g. Babuska and Cara 1991; Siegesmund 1996). Mica has acoustic velocities of about 5.5 km/s for  $V_p$  and 3 km/s for  $V_s$ , whereas garnet has values of 8.5 and 5.0 km/s for  $V_p$  and  $V_s$ , respectively. In general, polyphase rocks exhibit a variation in mineral composition so that a unique separation of different rock types using their average P-wave velocities is not possible. For example, an

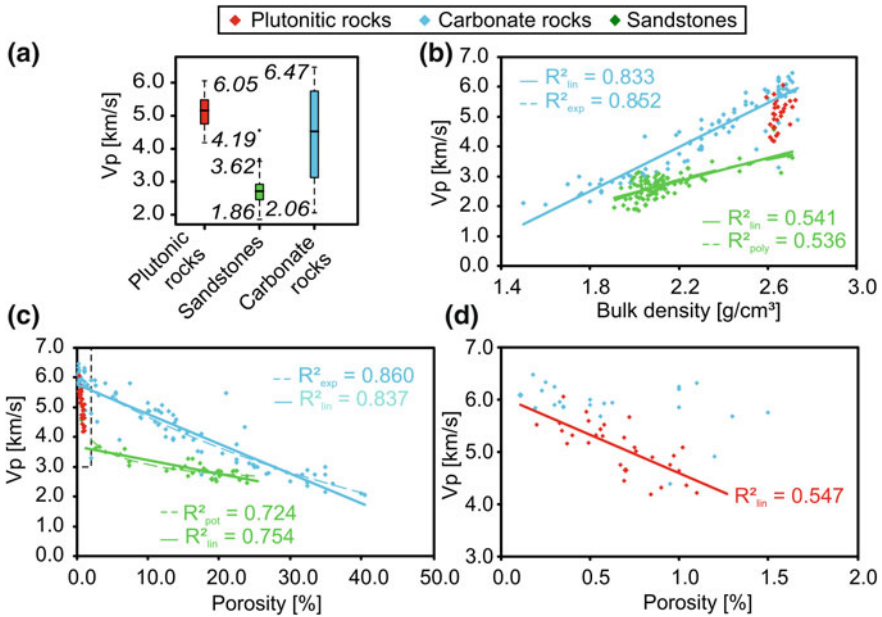
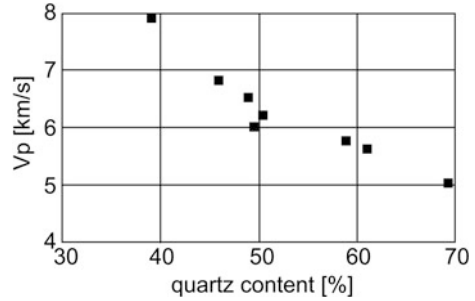


**Fig. 3.82** **a** Ultrasonic wave velocities ( $V_p$ ) of selected samples comprising sedimentary and magmatic rocks. Included are the statistical characteristics of upper and lower extremes. **b–c** Scatter plots for the correlations between the basic parameters of bulk density and porosity and ultrasonic wave velocity as well as the determination coefficients  $R^2$  for each linear ( $R^2_{lin}$ ) and polynomial (quadratic,  $R^2_{poly}$ ) dependency. **d** Detail of **c** for rocks with low porosity (porosities < 2 %)

average P-wave velocity of 5.5 km/s can be found for granite (range 4.18–5.85 km/s), as well as for quartzite (range 2.46–5.56 km/s) or serpentinite (range 4.25–6.23 km/s, after Schön 1996).

In Fig. 3.80, data sets comprising different rock types are shown to include three groups—plutonic rocks, sandstones, and carbonate rocks—with altogether 245 varieties. From the data evaluation, these three groups show clear differences with respect to the absolute acoustic velocities. For the sandstones, Mosch and Siegesmund (2007) documented that the majority of the values were in the range between 1.86 and 3.62 km/s, with only a few outliers. The plutonic group showed much higher values, in the range of 4.19–6.06 km/s, whereas the carbonate group exhibited a much larger range of values, from 2.06 to 6.47 km/s. This separation is seen in the scatter diagrams in Fig. 3.82, although no clear relationship can be established. In fact, a similar trend of the P-wave velocities for rocks with a bulk density up to 2.6 g/cm<sup>3</sup> and a porosity of about 5 % can be seen. But, comparing the carbonate rocks with the sandstone group, it is obvious that, for the same porosity, the sandstones have a lower P-wave velocity than the carbonates. This is due to the mineral-specific acoustic velocities of the main minerals, quartz ( $V_p = 6.05$  km/s)

**Fig. 3.83** P-wave velocities versus quartz content in magmatic rocks (after Schön 1996)



and calcite ( $V_p = 6.54$  km/s) (Gebrande 1982) and the related rock-specific acoustic velocities (see Chap. 6).

Han et al. (1986) has shown that clay minerals exhibit relatively lower P-wave velocities (1.1–2.8 km/s) and that, because of this, sandstones with higher clay content have lower  $V_p$ -values than those with siliceous or carbonate cements. The main reason is the compressibility of the clay minerals, since this contributes significantly to the attenuation of the seismic waves traveling through the rock (Schön 1996). Furthermore, higher clay content in the rock can also lead to variations in the mechanical and elastic properties of the rock due to the change of the mineral specific properties of the clay minerals as the result of changes in the water content. This mineral-specific dependency of the  $V_p$ -values can also be found in the low porosity rocks of the carbonate and plutonic group, since the feldspar minerals (in plutonic rocks) have, in general, lower acoustic velocities than the calcite mineral (in carbonate rocks).

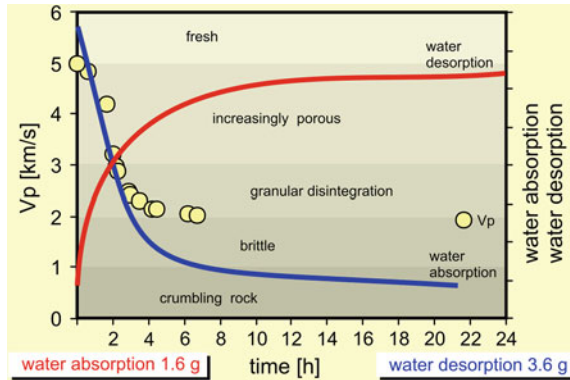
Higher velocity values are only expected for rocks such as peridotites, with a higher olivine content (Olivine  $V_p = 8.42$  km/s, Babuska and Cara 1991; Weiss et al. 1999), or some metamorphic rocks, such as eclogites, metapelites, or high metamorphic gneisses (e.g. Siegesmund et al. 1996), but these rocks are not part of the data set presented in Fig. 3.82. Lower  $\text{SiO}_2$  contents in rocks usually result in higher P-wave velocities (Fig. 3.83; Rudnick and Fountain 1995; Schön 1996). Velocities of metamorphic rocks may cover a broad range.

Velocity–density relations for plutonic, volcanic, and quasi-isotropic metamorphic rocks were reported by Gebrande (1982) based on a quite larger data set. Although the single values may show a large scatter, the obtained mean values of the velocities and densities correlate clearly. The following equations are the result:

$$\begin{aligned} \text{Plutonic rocks} \quad \overline{V_p} &= (-6.73 + 4.36 \bar{\rho} \pm 0.03) \text{ km/s}, \\ \text{Volcanic rocks} \quad \overline{V_p} &= (-2.73 + 2.81 \bar{\rho} \pm 0.18) \text{ km/s}, \\ \text{Metamorphic rocks} \quad \overline{V_p} &= (-6.93 + 4.41 \bar{\rho} \pm 0.37) \text{ km/s}. \end{aligned}$$

The direct correlation between average  $V_p$  and average density is based on the assumption that, for most of the rocks, a variation in the mineralogical composition has an effect on both parameters in the same way (Simmons 1964).

**Fig. 3.84** Drying behavior of Carrara Marble, which has a porosity of 1 %. The blue curve represents the desorption behavior of a completely water-saturated sample with corresponding ultrasonic velocities (*circles*). The dynamics of capillary water absorption are shown for the same marble by the *red curve* (after Weiss et al. 2002a; Siegesmund et al. 2004b)



### 3.7.2 Ultrasound Velocity: Effect of Porosity and Fluids

The acoustic velocities of porous rocks strongly depend on the porosity and the fluid content inside. Rocks in the lower porosity range ( $\Phi < 1.5\%$ ) show a clear linear trend between the porosity and the compressional wave velocities (see Fig. 3.82). The highly compacted carbonate rocks nearly follow the trend of the plutonic rocks. For the carbonate variety Marble Paloma (France,  $\Phi = 0.18\%$ ), a  $V_p$ -value of 6.47 km/s is measured indicating that this rock mostly consists of calcite ( $V_p = 6.54$  km/s) and is more or less comparable to a marble (the average P-wave velocities calculated from 57 different marbles is given by Gebrande 1982 with 5.73 km/s or varying between 5.04 and 6.42 km/s).

The physical influence of fluids on the ultrasonic velocities of a porous rock can be described by the sum of effects related to the elastic properties of the solid matrix in interaction with the compressibility of the fluid phase in the pore space of the rock. In laboratory experiments, Simmons and Nur (1969) observed that an increase in the water saturation corresponds to an increase in the compressional wave velocities, whereas the shear wave velocities remain constant or decrease slightly. This phenomenon is related to the fact that the shear modulus of a rock is less sensitive to changes in the water saturation of the pore space than the effective bulk modulus.

The degree of water uptake as well as the degree of water saturation is mainly related to the pore space itself, with the porosity, the type of pores, the pore geometry, and the interconnectivity of the pores. During the initial stage of deterioration, only very small and flat pores are opened, which do not allow capillary water intake. With increasing deterioration, the individual pore size increases, subsequently the pore connectivity, and finally the overall pore space. The opening of these flat pores along the grain boundaries in marble samples itself results in a drastic reduction in the ultrasonic velocities, as shown in Fig. 3.84. A decrease in the water saturation through a drying procedure for the marble also results in a drastic velocity reduction. The drying of a Carrara Marble in Fig. 3.84

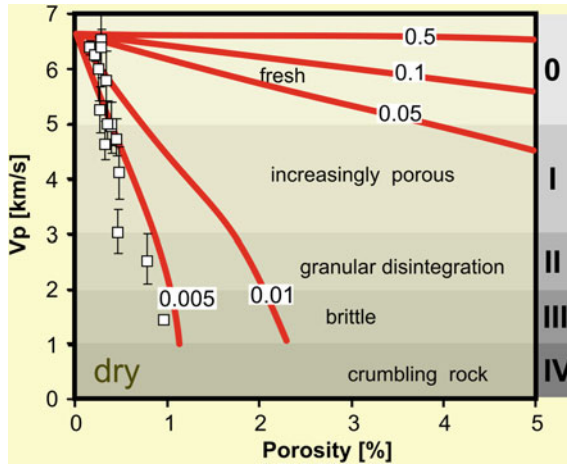
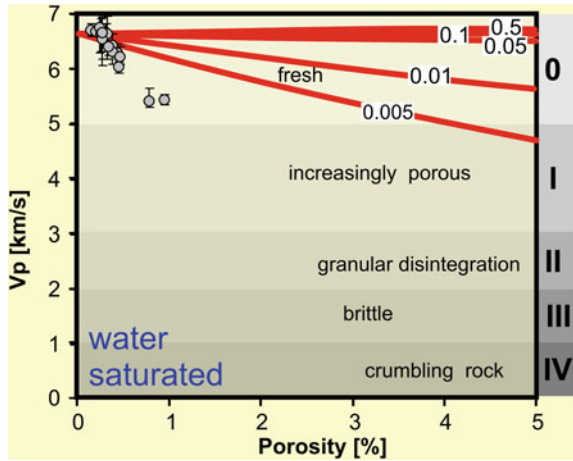


**Fig. 3.85** Experimental versus modeled ultrasonic wave velocities ( $V_p$ ). Velocity reduction due to microcracks with a certain aspect ratio (here: 0.005, 0.01, 0.05, 0.1, and 0.5) for dry sample conditions. The velocity reduction as a function of the porosity acts according to the model of O'Connell and Budiansky (1974). The experimental data (square symbols with standard deviation bars) is clearly shown for the modeled velocity porosity function, which is determined by the aspect ratio of the pores. In addition, the  $V_p$ -structural damage classification (fresh, increasingly porous, granular disintegration, brittle, and crumbling) for marbles (after Köhler 1991) is given (after Weiss et al. 2002a; Siegesmund et al. 2004b)

shows that a decrease in the water content in the pore space corresponds to a significant decrease in the acoustic velocities, as indicated by the blue line. After four hours of drying, the marble sample exhibits ultrasonic P-wave velocities of only about 2 km/s compared to an initial value of 5 km/s.

There are different theoretical approaches describing the elastic behavior of cracked or porous materials. The velocity reduction as a function of crack geometry can be calculated by the well known theoretical prediction (self-consistent model) of O'Connell and Budiansky (1974). The basic principle is that a given porosity is formed by certain types of ellipsoidal cracks. The crack geometry is only defined by the aspect ratio (i.e. the ratio between the small and large axes of the ellipsoid) of the cracks. Spherical cracks have an aspect ratio of 1 and flat cracks of less than 1. The model calculations given by Weiss et al. (2002b) revealed that  $V_p$  strongly decreases as a function of porosity, as observed experimentally (Weiss et al. 2001). The model calculation argues that the observed decrease in  $V_p$  can only be caused by extremely flat cracks with an aspect ratio of about 0.005 (Fig. 3.85). Compared to the same samples under water-saturated conditions, it is obvious that the velocity reduction is less pronounced (Fig. 3.86). Water saturation has an important influence on the magnitude and directional dependence of ultrasonic wave velocities. Popp (1994) also carried out acoustic velocity measurements of samples saturated with fluids. He has shown that water saturation of the pore space results in a significant increase in the P-wave

**Fig. 3.86** Experimental (circles with standard deviation bars) versus modeled velocities (see Fig. 3.85 for further explanation) for water-saturated sample conditions. The same samples were used as given in Fig. 3.85. The effect of deterioration that is clearly documented on the  $V_p$  is less pronounced if the samples are water-saturated (after Weiss et al. 2002a and Siegesmund et al. 2004b)



velocities with a parallel decrease in the crack related anisotropy and more-or-less constant shear wave velocities. Hence, it is essential to gather sufficient information on the state of water saturation of an object under investigation.

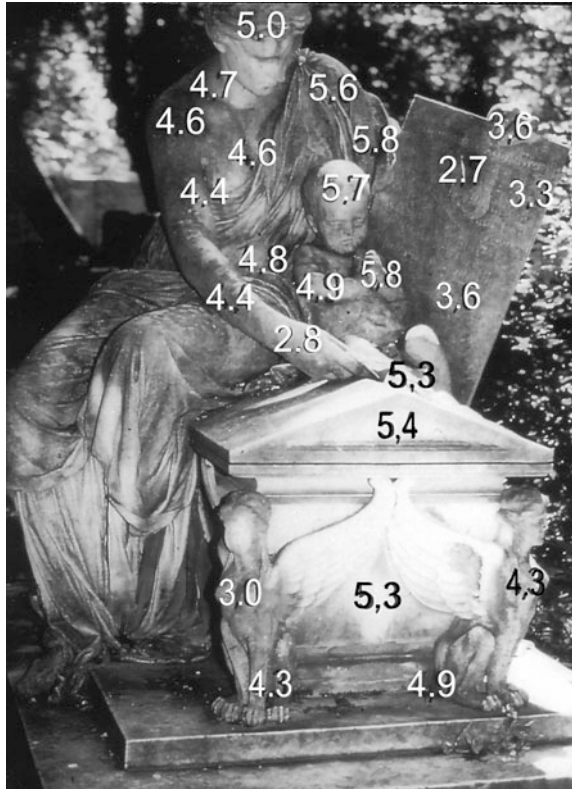
### 3.7.3 Ultrasonic Velocity and Anisotropy

The analysis of the ultrasonic velocities for a tombstone revealed that the velocities can vary significantly depending on the location of measurement. Comparing this data (from the tombstone of Wegmüller) with a statistical evaluation of Gebrande (1982), which used 57 freshly quarried marbles and had a mean P-wave velocity of 5.73 km/s, significant variations can be seen (see Fig. 3.87). Especially the parts of the tomb that have fine and detailed artwork exhibit lower velocity values, down to 2.7 km/s, and these parts also have lower tensile strengths. Other parts are still able to show P-wave velocities of around 5.7–5.8 km/s, which are comparable to the average velocity of the freshly quarried rock samples.

In order to understand a rock’s elastic behavior, it is essential to obtain as much information as possible on the rock’s structure, since there is a complex interaction between the rock fabric and petrophysical properties, as compiled by Siegesmund (1996). The most important fabric elements are the crystallographic preferred orientation of the rock-forming minerals, the microcrack populations, and the shape fabric (grain size, grain aspect ratios, grain-shape preferred orientation; see also Sects. 2.8 and 6.4.2.5). Combined, these fabrics are responsible for the physical anisotropy of rocks, i.e. the directional dependence of the elastic wave velocities. This means, for example, that the P-wave velocity distribution shows different values when measured in different directions for the same rock sample; for the S-waves, it is similar. The spatial dependence of elastic wave velocities ( $V_p$ ,  $V_s$ ), considering anisotropy, has mostly been studied in three perpendicular directions,



**Fig. 3.87** Tombstone of the sculptor Michael von Wagnmüller (after Grimm 1999). Numbers are P-wave velocities in km/s measured at the given locations



which requires the study of different plugs of one stone block if one uses cylindrical samples or velocity measurements on sample cubes. However, the study of anisotropy on spherical samples enables the measurements of compressional wave velocities in more or less any direction with the same accuracy, except the area near the vertical axes of rotation (e.g. Pros and Babuška 1967; Thill et al. 1969).

The complete  $V_p$ -distribution of a strongly foliated gneiss at 0.1 MPa, confining pressure and dry conditions, is shown in Fig. 3.88a (Siegesmund et al. 1993; Siegesmund 1996 and Rasolofosaon et al. 2000), with a minimum velocity of 3.0 km/s and a maximum of 6.6 km/s, giving a real anisotropy value ( $A$ ) of 55 %, following the equation with  $A = 100 \cdot (V_{p\_max} - V_{p\_min}) / V_{p\_max}$  (%). The P-wave velocity distribution shows a distinct pattern, which reflects the orientation of the foliation as shown in Fig. 3.88b and, by this, the orientation of the mica minerals, biotite, and muscovite, with their mineralogical (001) planes parallel to the foliation plane (see Fig. 3.88c). The strong anisotropy is the result of a combination of the single crystal anisotropy of the mica minerals and the orientation of open cleavage cracks parallel to the (001) planes of the mica minerals. Mica minerals have the highest velocities perpendicular to the [001] axis or parallel to the (001) plane, and the lowest ones parallel to the [001] axis. Because of this, a

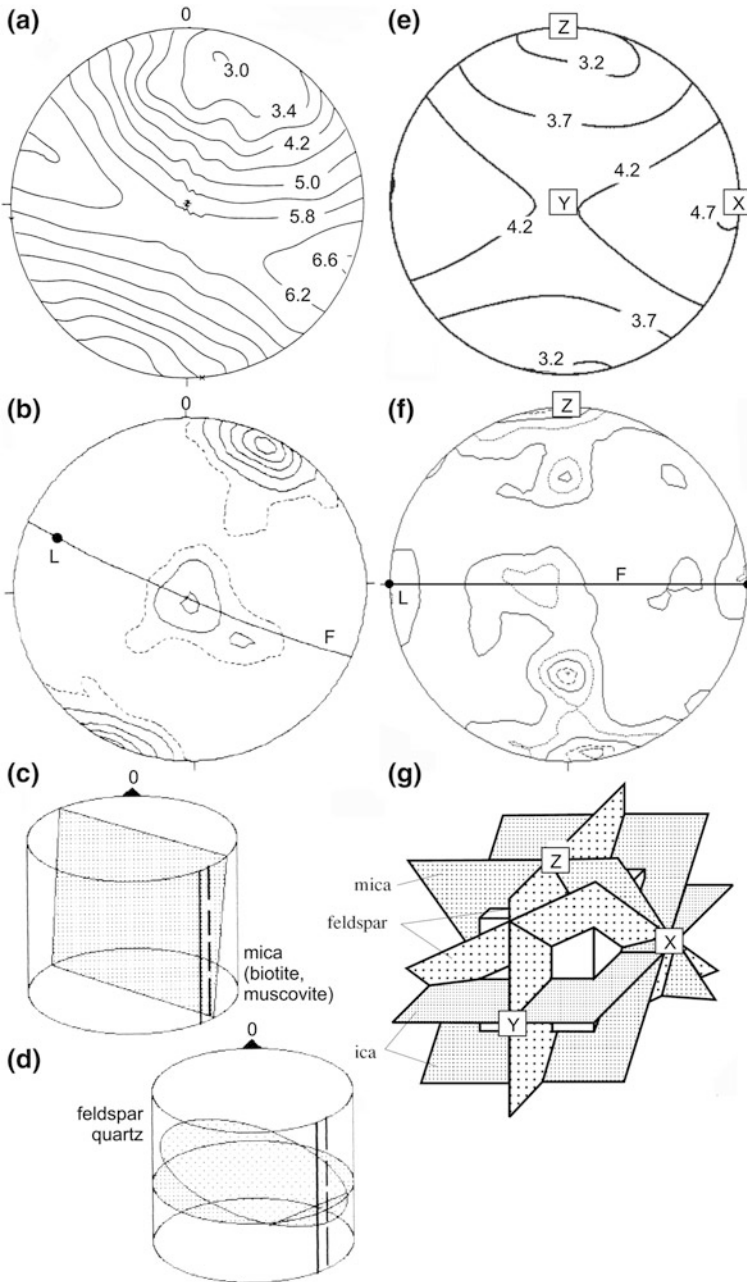


**Fig. 3.88** Anisotropy of the P-wave velocities (in km/s) of strongly foliated gneiss (a–d) after Siegesmund (1996) and Siegesmund et al. (1993) and granodiorite (e–g) after Schild et al. (2001): (a) complete  $V_p$ -distribution at 0.1 MPa confining pressure and (e) atmospheric pressure, Schmidt Net, lower hemisphere; (b, f) pole figures of bulk microcrack population in isolines of multiples of random distribution, Schmidt Net, lower hemisphere, F-foliation, L-lineation; (c, d, g) Schematic illustrations of the microcrack orientations

rock sample with a strong foliation formed by mica minerals would have a perfect transverse isotropic symmetry of the  $V_p$ -distribution. Furthermore, perpendicular to the (001) open cleavage cracks, the P-wave velocity has the lowest values, parallel to them the highest ones. However, a perfect transverse isotropic symmetry of the  $V_p$ -distribution is not achieved due to the existence of nearly horizontal open cracks in quartz and feldspar minerals (see Fig. 3.88b, d), which decrease the P-wave velocities in the vertical direction or the center of the  $V_p$ -distribution. A rather detailed investigation of almost all aspects of the rock fabric of this sample and additional P-wave velocity distributions with increasing confining pressure can be found in Siegesmund (1996).

In Fig. 3.88e, f, the complete  $V_p$ -distribution at atmospheric pressure and the bulk microcrack orientation of a metamorphic overprinted granodiorite are presented (Schild et al. 2001). The main minerals of the foliated rock are K-feldspar, with grain sizes between 100  $\mu\text{m}$  and 2 cm, plagioclase, quartz, and biotite. However, the foliation is not as pronounced as in the previous sample. Features of alteration and brittle deformation can be found. The highest P-wave velocities of more than 4.7 km/s are in the foliation and parallel to the lineation; the lowest ones with less than 3.2 km/s are perpendicular to the foliation as shown in Fig. 3.88e, resulting in an anisotropy of 21.8 %. Comparable to the gneiss sample, the main cause of the anisotropy is the open cleavage cracks parallel to the (001) planes in the mica minerals, which dominate the bulk open crack distribution (Fig. 3.88f). The mica minerals are oriented mainly parallel to the foliation in the xy-plane so that their poles plot perpendicularly to the foliation and parallel to the z-direction. However, the foliation is not as strongly developed as in the gneiss, but the lineation is more pronounced. This means that the mica minerals rotate parallel to the lineation, resulting in a girdle-like orientation of the open cleavage cracks. The schematic diagram in Fig. 3.88 g illustrates the orientations of these different crack populations.

A sandstone sample (porosity 1.8 %) investigated by Dürrast et al. (2002) is shown in Fig. 3.89. The complete  $V_p$ -distribution at 0.1 MPa confining pressure has its highest value at 4.64 km/s almost horizontal and the lowest one at 3.98 km/s almost perpendicular to it, where this reflects the orientation of the nearly horizontal sedimentary layering (ss); the anisotropy is 14.2 %. The sedimentary layering can be identified by small layers of dark clay minerals in the sandstone. Two macroscopically visible cracks ( $r_1$ ,  $r_2$ ), partially open and partially mineralized with semi-vertical orientation, have some but not a significant effect on the P-wave velocity distribution (Fig. 3.89b, c).

Results from ultrasonic laboratory measurements and rock fabric analysis of a dolomitic (94.6 %) carbonate rock sample with a porosity of 9.6 % are shown in Fig. 3.89d–f (Dürrast and Siegesmund 1999). The complete  $V_p$ -distribution at 0.1 MPa confining pressure has the highest velocities of more than 4.7 km/s semi-vertical, and almost parallel to the vertical z-axis. The lowest values of less than 3.8 km/s are, in the horizontal plane, subparallel to the y-direction (Fig. 3.89d). The anisotropy of nearly 25 % is the result of a combination of horizontally-oriented microstructures, stylolites (S) and small layers of accumulated organic

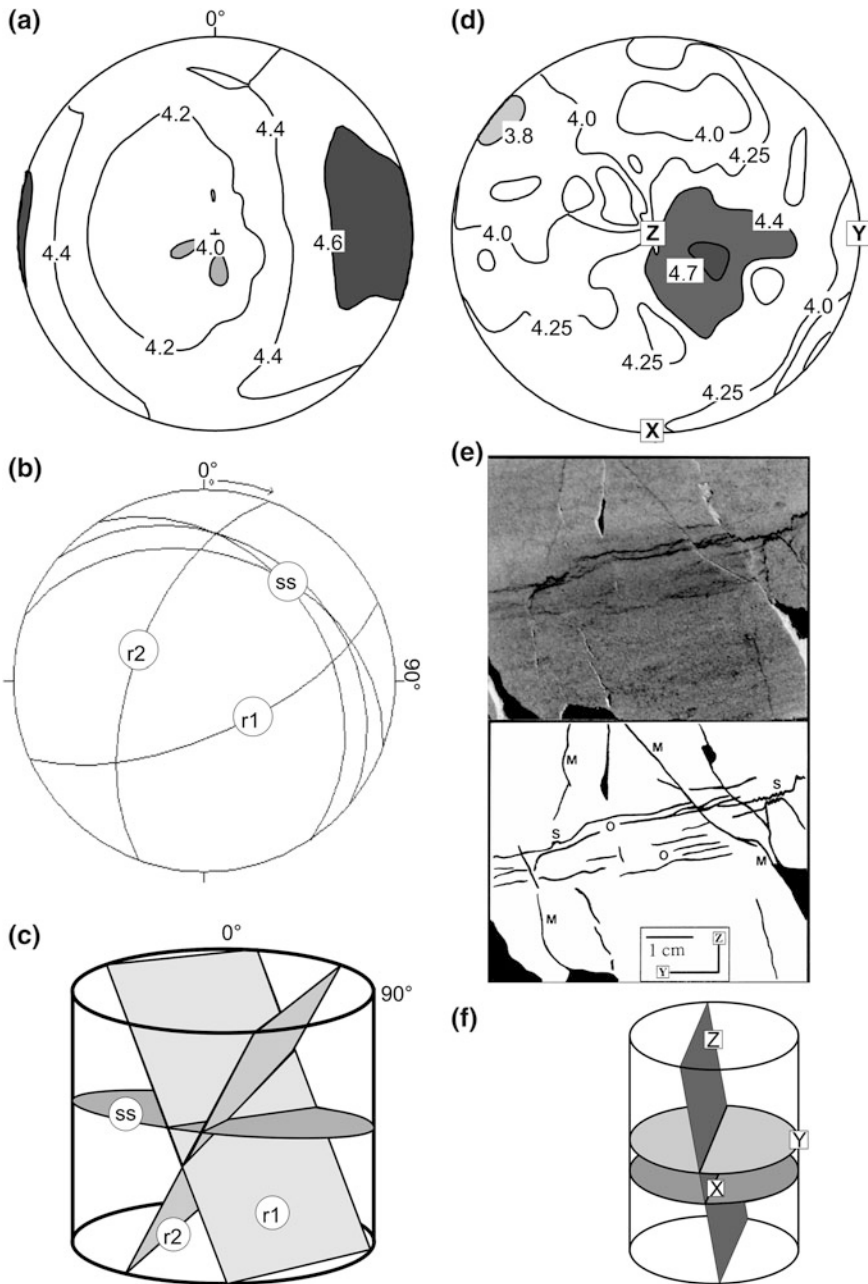


**Fig. 3.89** Anisotropy of the P-wave velocities (in km/s) of a sandstone (a–c) after Dürrast et al. (2002) and a dolomitic limestone (d–f) after Dürrast and Siegesmund (1999): (a, d) complete  $V_p$ -distribution at 0.1 MPa confining pressure, Schmidt Net, lower hemisphere; (b, f) great circle figure of a sedimentary layer (ss) and crack (r1, r2) orientation, Schmidt Net, lower hemisphere; (e) photo and drawing of the main microstructure, *M* mineralized cracks, *S* horizontal stylolites, *O* layers of organic material. (c, f) Schematic illustrations of the microstructure orientations

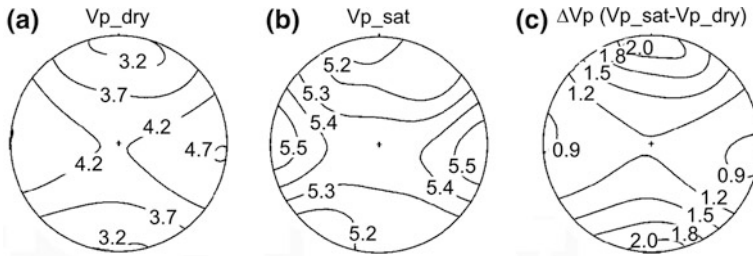


**Fig. 3.90** Anisotropy of the P-wave velocities (in km/s) of a granodiorite under dry (a) and water-saturated (b) conditions at atmospheric pressure (after Schild et al. 2001). (c) Calculated difference in the  $V_p$ -distribution between saturated and dry conditions. All projections are Schmidt Net, lower hemisphere

material (O), and semi-vertical cracks, partially open and partially mineralized (M), as shown in Fig. 3.89e, f. However, here, the influence of the cracks on the  $V_p$ -distribution is much more significant, since the horizontal features at this pressure level only have a minor influence. The highest P-wave velocities are, therefore, more or less parallel to the fracture planes and the lowest perpendicular.

All examples shown here clearly demonstrate that for all rock types, open microcracks—in cases where they are present—have significant effects on the anisotropy of the P-wave velocity distribution at (near) atmospheric conditions. For metamorphic rocks, the preferred orientations of minerals combined with anisotropic minerals have additional effects, whereas, for sedimentary rocks, sedimentary features play an important secondary role.

Water saturation of these samples increases the overall P-wave velocities due to higher density and higher stiffness of the rock samples, and it decreases the anisotropy. However, in most cases, the character of the  $V_p$ -distribution does not change, as shown in Fig. 3.90. The granodiorite from Schild et al. (2001) discussed above was also measured under fully water-saturated conditions and atmospheric pressure. The  $V_p$ -values increase in all directions as the calculated  $\Delta V_p$  diagram ( $= V_{p\_saturated} - V_{p\_dry}$ ) indicates (Fig. 3.90c), but not by the same amount. The highest increase of more than 2.0 km/s is perpendicular to the foliation due to the filling of the open mica cleavage cracks. However, the overall pattern of the  $V_p$ -distribution of the water-saturated samples is still similar to the sample measured under dry conditions, but with anisotropy of about 7 %, compared to 21.8 % under dry conditions (see also Dürrast et al. 2002).

### 3.7.4 Velocity and Degree of Weathering

Based on a number of ultrasonic measurements, Köhler (1991) introduced a decay classification scheme for Carrara marbles that mainly depends on the relationship between the acoustic P-wave velocities and the porosity (see Figs. 3.85 and 3.86,

**Table 3.10** Vp-structural damage classifications for Carrara Marble (Köhler 1991), limestone (Schaumkalk; Fitzner and Heinrichs 1992), and travertine (Akin 2010)

Marble (Köhler 1991)		Limestone (Fitzner and Heinrichs 1992)		Yellow travertine (Akin 2010)	
Rock state	Vp (km/s)	Damage class	Damage of the stone	Vp (km/s)	Weathering degree
Fresh	$5.0 < Vp$	0	None (fresh)	$3.9 < Vp \leq 4.1$	None (fresh)
Increasingly porous	$3.0 < Vp \leq 5.0$	I	Little	$3.0 < Vp \leq 3.9$	Slightly
Granular disintegration	$2.0 < Vp \leq 3.0$	II	Moderately	$2.0 < Vp \leq 3.0$	Moderately
Brittle	$1.5 < Vp \leq 2.0$	III	Heavy	$1.0 < Vp \leq 2.0$	
Crumbling rock	$Vp \leq 1.5$	IV	Very heavy	$Vp \leq 1.0$	$3.66 \leq Vp$ $2.60 < Vp$ $\leq 3.66$ $Vp < 2.60$

**Table 3.11** Vp-structural damage classifications for granite (Illiev 1967), granitoides from Turkey (Ceryan et al. 2008), and acid volcanic rocks from Turkey (Arikan et al. 2007)

Granite (Illiev 1967)			Granitoids (Ceryan et al. 2008)			Acidic volcanic rocks (Arikan et al. 2007)		
Weathering degree	Vp (km/s)	Weathering degree	Vp (km/s) (dry rocks)	Weathering degree	Vp [km/s]			
None (fresh)	$5.0 < Vp$	None (fresh)	$4.111 \pm 0.198$	None (fresh)	$3.35-5.20$			
Slightly	$4.0 < Vp \leq 5.0$	Slightly	$3.553 \pm 0.396$	Slightly	$2.49-4.66$			
Moderately	$3.0 < Vp \leq 4.0$	Moderately	$2.769 \pm 0.553$	Moderately	$2.00-3.44$			
Highly	$2.0 < Vp \leq 3.0$	Highly	$2.158 \pm 0.486$	Highly	$1.39-2.97$			
Completely	$Vp \leq 2.0$	Completely	$0.753 \pm 0.184$					



see also the discussion in Dürrast et al. 1999 and Ruedrich et al. 2001). The initial value of  $V_p = 6.6$  km/s represents a pore-free “quarry-fresh” or “healthy” calcite marble sample. With decreasing  $V_p$ , the degree of deterioration becomes worse and is alarming. At P-wave velocities of 3.0 km/s, an outside exposition is no longer recommended, and a static consolidation should be considered. These low compressional wave velocities can be explained qualitatively by a decrease in the cohesion and a corresponding decrease in the elastic coupling between the calcite crystals of the marble.

A systematic analysis of various marble samples of different origin and decay degree ( $V_p$  range from 6.5 km/s to 1.5 km/s) has shown that, even at very low porosities of around 1 %, the ultrasonic velocities can be reduced drastically (Fig. 3.85). The same sample, a highly deteriorated marble, in contrast, exhibits a  $V_p$ -value of around 5.0 km/s under water-saturated conditions, wrongly suggesting that this marble is not at all deteriorated (Fig. 3.86). This example clearly shows the significant influence of the pore space and the degree of water saturation on the acoustic velocities, as was already discussed in Chap. 6.

The empirically derived  $V_p$ -damage classification developed for Carrara Marble was also incorporated into Table 3.10. In this classification, a damage class of zero (Table 3.10) corresponds to a fresh marble with velocities higher than 5.0 km/s (Köhler 1991). A fragile marble will show  $V_p$ -values between 1.5 km/s and 2.0 km/s (damage class III). Fitzner and Heinrichs (1992) have reported a  $V_p$ -damage classification for the so-called Schaumkalk, the most important limestone used for the construction of the Naumburg Cathedral in Germany: fresh Schaumkalk gives  $V_p$ -values of 3.9–4.1 km/s, while the strongly weathered ones give values below 1.0 km/s.

Comparable values were reported from Iliev (1967) for granitoids ranging between  $>5.0$  km/s (fresh) and  $<2.0$  km/s for strongly weathered ones (Table 3.11). This classification is more or less in agreement with observations from Ceryan et al. (2008) on the Harsit Granitoids (Turkey), where the  $V_p$ -values cover the range from 5.7 km/s (fresh) to 0.76 km/s (completely weathered). The effect of weathering on the compressional wave velocities is also given for volcanic rocks (Arikan et al. 2007) and for travertine (Akin 2010). The basic observation is that, as a consequence of weathering, the state of porosity changes along with the mineralogical and chemical composition.

## References

- Aires-Barros L, Graca RC, Velez A (1975) Dry and wet laboratory tests and the thermal fatigue of rocks. *Eng Geol* 9:249–265
- Akin M (2010) A quantitative weathering classification system for yellow travertines. *Environ Earth Sci*. doi:10.1007/s12665-009-0319-7
- Archie GE (1952) Classification of carbonate reservoir rocks and petrophysical considerations. *AAPG Bull* 36:278–298

- Arikan F, Ulusay R, Aydin N (2007) Characterization of weathered acidic volcanic rocks and a weathering classification based on a rating system. *Bull Eng Geol Environ* 66(4):415–430
- ASTM C 880-89 (1989) Flexural strength of dimension stones. Beuth, Berlin
- Babuska V, Cara M (1991) Seismic anisotropy in the earth. Kluwer Academic Press, Dordrecht
- Battaglia S, Franzini M, Mango F (1993) High sensitivity apparatus for measuring linear thermal expansion: preliminary result on the respond of marbles. *Nuovo Cimento C* 16:453–461
- Bauer SJ, Johnson B (1979) Effects of slow uniform heating on the physical properties of Westerly and Charoocal granites. Proceedings of 20th symposium on rock mechanics, Austin, pp 7–18
- Bieniawski ZT (1967) Mechanism of the fracture of rocks. Pergamon Press, New York
- Birch F (1960) The velocity and compressional waves in rocks to 10 kilobars. Part 1. *J Geophys Res* 65:1083–1102
- Birch F (1961) The velocity and compressional waves in rocks to 10 kilobars. Part 2. *J Geophys Res* 66:2199–2224
- Birch F, Clark H (1940) The thermal conductivities of rocks and its dependence upon temperature and composition. Part I. *Am J Sci* 238:529–558
- Bland W, Rolls D (1998) Weathering. Arnold, London
- Blasi P, Frisa Morandini A, Mancini R, et al (2000) Investigación experimental sobre los ensayos de flexión en los mármoles: confianza de los resultados y efecto escala. *Roc Maquina-Dimension Stone Industry* 36:20–25
- Blöchl B, Kirchner D, Stadlbauer E (1998) Die hygrische Dehnung von Baumberger Kalksandstein-tonmineralogische und gesteinsphysikalische Aspekte. *Arbeitshefte zur Denkmalpflege in Niedersachsen* 15:46–53
- Brakel J, Modry S, Svata M (1981) Mercury porosimetry: state of the art. *Powder Tech* 29:1–12
- Brosch FJ, Schachner K, Bluemel M et al (2000) Preliminary investigation results on fabrics and related mechanical properties of an anisotropic gneiss. *J Struct Geol* 22:1773–1787
- Brunauer S, Emmett PH, Teller E (1938) Adsorption of gases in multimolecular layers. *J Am Chem Soc* 60(2):309–319
- Bucher WH (1956) Role of gravity in orogenesis. *Bull Geol Soc Am* 67:1295–1318
- Buntebarth G (1982) Density and seismic velocity in relation to mineralogical constitution based on an ionic model for minerals. *Earth Planet Sci Lett* 57:358–366
- Buntebarth G (1991) Thermal properties of KTB-Oberpfalz VB core samples at elevated temperature and pressure. *Sci Drill* 2:73–80
- Buntebarth G (1992) Variation of thermal conductivity with structure of rocks. In: Buntebarth G (ed) Thermal properties of crustal materials. *Sitzungsberichte der 22. Sitzung FKPE-Arbeitsgruppe und 92th Seminar of Dr WH Heraeus and E Heraeus-Stiftung*
- Buntebarth G, Rueff P (1987) Laboratory thermal conductivity applied to crustal conditions. *Rev Brasil Geofisica* 5:103–109
- Cammerer JS (1954) Das Verhalten der wichtigsten Baustoffe gegenüber flüssigen und dampfförmigen Wasser. *Tonind Ztg* 78:199–204
- Ceryan S, Tudes S, Ceryan N (2008) Influence of weathering on the engineering properties of Harsit granitic rocks (NE Turkey). *Bull Eng Geo Environ* 67:97–104
- Chitsazian A (1985) Beziehung zwischen Mineralbestand, Gefüge und technologischen Eigenschaften der Niedersächsischen 'Wealden'-Sandsteine (Unterkreide). *Mitt Geol Institut Univ Hannover, Hannover*
- Choquette PW, Pray LC (1970) Geologic nomenclature and classification of porosity in sedimentary carbonates. *Am Assoc Petrol Geol Bull* 54:207–250
- Christensen NI (1968) Chemical changes associated with upper mantle structure. *Tectonophysics* 6:331–342
- Christensen NI (1979) Compressional wave velocities in rocks at high temperatures and pressures, critical thermal gradient, and crustal low-velocity zones. *J Geophys Res* 84:6849–6857

- Clauser C, Huenges E (1995) Thermal conductivity of rocks and minerals. In: Ahrens TJ (ed) *Rock physics and phase relations—a handbook of physical constants*. AGU Ref Shelf. Vol 3. American Geophysical Union, Washington
- Clemens K, Grimm W-D, Poschold K (1990) Zur Kennzeichnung des Korngefüges und des Porenraumes der Naturwerksteine. In: Grimm W-D (ed) *Bildatlas wichtiger Denkmalgesteine der Bundesrepublik Deutschland*. Bayerisches Landesamt für Denkmalpflege, Munich
- Crosson RS, Lin JW (1971) Voigt and Reuss predictions of anisotropic elasticity of olivine. *J Geophys Res* 76:570–578
- David Ch (2006) Buntsandsteine-Bausandsteine, Marburger Bausandsteine unter der Lupe. *Marburger Geowissenschaften* 3:1–129
- De Quervain F (1967) *Technische Gesteinskunde*. Lehrbücher und Monographien aus dem Gebiete der exakten Wissenschaften. Mineralogisch-geotechnische Reihe, Bd 1. Birkhäuser, Basel
- DIN 52 105 (1988) Prüfung von Naturstein. Druckversuch.—2 S. Beuth, Berlin
- DIN 66131 (1993) Bestimmung der spezifischen Oberfläche von Feststoffen durch Gasadsorption nach Brunauer, Emmett und Teller (BET). Beuth, Berlin
- DIN EN 1097–6 (2005) Tests for mechanical and physical properties of aggregates—part 6: determination of particle density and water absorption. German version EN 1097–6 European Committee for Standardization. Beuth, Berlin
- DIN EN 12372 (1999) Natural stone test methods—determination of flexural strength under concentrated load. German version EN 12372 European Committee for Standardization. Beuth, Berlin
- DIN EN 13161 (2008) Natural stone test methods—determination of flexural strength under constant moment. German version EN 13161, European Committee for Standardization. Beuth, Berlin
- DIN EN 13364 (2002) Natural stone test methods—determination of the breaking load at dowel hole. German version EN 13364 European Committee for Standardization. Beuth, Berlin
- DIN EN 1926 (1999) Natural stone test methods—determination of uniaxial compressive strength. German version EN 1926 European Committee for Standardization. Beuth, Berlin
- DIN EN 12572 (2009) Hygrothermal performance of building materials and products—determination of water vapour transmission properties. German version EN 12572, European Committee for Standardization. Beuth, Berlin
- Doveton JH (1987) Log analysis of petrofacies and lithofacies. GFZ Logging Course, Geoforschungszentrum Potsdam, Potsdam
- Dubinin MM (1979) Micropore structures of charcoal adsorbents. 1. A general characterization of micro- and supermicropores in the fissure model. *Proc Acad Sci USSR* 8:1691–1696
- Dürrast H, Jahns E, Tischer A et al (2001) Vorzugsorientierung der Mikrorissbildung im triaxialen Verformungsexperiment am Beispiel des Piesberger Sandsteins. *Z dtsh geol Ges* 152:611–620
- Dürrast H, Rasolofosaon PNJ, Siegesmund S (2002) P-wave velocity and permeability distribution of sandstones from a fractured tight gas reservoir. *Geophysics* 67:241–253
- Dürrast H, Siegesmund S (1999) Correlation between rock physics and physical properties of carbonate reservoir rocks. *Int J Earth Sci* 88:392–408
- Dürrast H, Siegesmund S, Prasad M (1999) Schadensanalyse von Natursteinen mittels Ultraschalldiagnostik: Möglichkeiten und Grenzen. *Z dtsh geol. Ges* 150(2):359–374
- Fitzner B (1970) Die Prüfung der Frostbeständigkeit von Naturbausteinen. *Geol Mitt* 10:205–296
- Fitzner B (1988) Untersuchung der Zusammenhänge zwischen dem Hohlraumgefüge von Natursteinen und physikalischen Verwitterungsvorgängen. *Mitt Ing Geol Hydrogeol* 29:1–217
- Fitzner B, Basten D (1994) Gesteinsporosität—Klassifizierung, meßtechnische Erfassung und Bewertung ihrer Verwitterungsrelevanz—Jahresberichte aus dem Forschungsprogramm “Steinzerfall-Steinkonservierung” 1992, Förderprojekt des Bundesministers für Forschung und Technologie. Verlag Ernst & Sohn, Berlin
- Fitzner B, Heinrichs K (1992) Verwitterungszustand und Materialeigenschaften der Kalksteine des Naumburger Doms—Jahresberichte aus dem Forschungsprogramm “Steinzerfall-

- Steinkonservierung" 1990, Förderprojekt des Bundesministers für Forschung und Technologie. Verlag Ernst & Sohn, Berlin
- Fitzner B, Kownatzki R (1991) Porositätseigenschaften und Verwitterungsverhalten von sedimentären Naturwerksteinen. *Bauphysik* 13(4):111–119
- Fitzner B, Sneath R (1983) Modellvorstellungen zum Kristallisations- und Hydratationsdruck von Salzen im Porenraum von Sandsteinen. Sitzungsbericht des Arbeitskreises 'Naturwissenschaftliche Forschung an Kunstgütern aus Stein', Erlangen
- Franklin JA, Dusseault MB (1989) *Rock engineering*. McGraw Hill Publ, New York
- Franzen C, Mirwald PW (2004) Moisture content of natural stones: static and dynamic equilibrium with atmospheric humidity. *Environ Geol* 46:391–401
- Fredrich JT, Wong TF (1986) Micromechanics of thermally induced cracking in three crustal rocks. *J Geophys Res* 91(B12):12743–12764
- Garrecht H (1992) Porenstrukturmodelle für den Feuchtehaushalt von Baustoffen mit und ohne Salzbefrachtung und rechnerische Anwendung auf Mauerwerk. Dissertation, Schriftenreihe des Instituts für Massivbau und Baustofftechnologie, Karlsruhe
- Gebrande H (1982) Elasticity and inelasticity. In: Augenheister G (ed) *Landolt-Börnstein, Band 1, Physikalische Eigenschaften der Gesteine*. Springer, Berlin
- Glover PW, Baud P, Darot M et al (1995) Alpha/beta phase transition in quartz monitored using acoustic emissions. *Geophys J Int* 120:775–782
- Goudie AS (1974) Further experimental investigations of rock weathering by salt and other mechanical processes. *Z Geomorph* 21:1–12
- Greger O (1930) Druckfestigkeit und Bergfrische beim Granit. *Straßenbau* 21:99–102
- Gregg SJ, Sing KSW (1982) Adsorption, surface area and porosity. Academic, London
- Grelk B, Goltermann P, Schouenborg B et al (2004) The laboratory testing of potential bowing and expansion of marble. In: Prikryl R (ed) *Dimension stone 2004*. Taylor & Francis Group, London
- Griesser UJ, Dillenz J (2002) Neuartiges, vollautomatisches Feuchtesorptionsprüfgerät mit hohem Probendurchsatz. *Conf Proc 9. Feuchtetag, Weimar*
- Griggs DT (1936) The factor of fatigue in rocks exfoliation. *J Geol* 44:781–796
- Grimm W-D (1990) *Bildatlas wichtiger Denkmalgesteine in Deutschland*. Bayerisches Landesamt für Denkmalpflege, München
- Grimm W-D (1999) Beobachtungen und Überlegungen zur Verformung von Marmorobjekten durch Gefügauflockerung. *Z dtsh geol Ges* 150:195–236
- Grüneisen E (1926) Zustand des festen Körpers. In: Geiger H, Scheel K (eds) *Handbuch der Physik*. Vol. 10, Thermische Eigenschaften der Stoffe. Springer, Berlin
- Hajpal LM, Török A (2004) Mineralogical and colour changes of quartz sandstones by heat. *Environ Geol* 46:311–322
- Han D-H, Nur A, Morgan D (1986) Effects of porosity and clay content on wave velocities in sandstones. *Geophysics* 51:2093–2107
- Hawkins AB, McConnell BJ (1992) Sensitivity of sandstone strength and deformability to changes in moisture content. *Quart J Eng Geol* 25:115–130
- Heinrichs K (2005) Diagnose der verwitterungsschäden an den Felsmonumenten der antiken Stadt Petra (Jordanien). *Aachener Geowiss Beiträge* 41:1–144
- Hirschwald J (1912) *Die Prüfung der natürlichen Bausteine auf ihre Verwitterungsbeständigkeit*. Verlag W Ernst & Sohn, Berlin
- Hockmann A, Kessler DW (1950) Thermal and moisture expansion studies of some domestic granites. *US Bur Stand J Res* 44:395–410
- Hoffmann A (2008) *Naturwerksteine Thailands: Lagerstättenerkundung und Bewertung*. <http://webdoc.sub.gwdg.de/diss/2007/hoffmann/hoffmann.pdf>. Accessed 20 July 2010
- Hoffmann A, Siegesmund S (2007) Investigation of dimension stones in Thailand: an approach to a methodology for the assessment of stone deposits. *Z dtsh Ges Geowiss* 158/3:375–416
- Holm A (2001) Ermittlung der Genauigkeit von instationären hygrothermischen Bauteilberechnungen mittels eines stochastischen Konzeptes. *Diss Uni Stuttgart*

- Horai K, Baldrige WS (1972) Thermal conductivity of nineteen igneous rocks, I: application of the needle probe method to the measurement of the thermal conductivity of rock. *Phys Earth Planet Inter* 5:151–156
- Horai K, Simmons G (1969) Thermal conductivity of rock forming minerals. *Earth Planet Sci Lett* 6:259–268
- Horai K, Susaki J (1989) The effect of pressure on the thermal conductivity of silicate rocks up to 12 kbar. *Phys Earth Planet Int* 55:292–305
- Hörenbaum W (2005). *Verwitterungsmechanismen und Dauerhaftigkeit von Sandsteinsichtmauerwerk*. Schriftenreihe des Instituts für Massivbau und Baustofftechnologie, TH Karlsruhe, Karlsruhe
- Howarth DF, Rowlands JC (1987) Quantitative assessment of rock texture and correlation with drillability and strength properties. *Rock Mech Rock Eng* 20:57–85
- I-Stone (2008) Characterization of natural stones and finished products. [http://www.istone.ntua.gr/Training\\_courses/wp1/absorption.html](http://www.istone.ntua.gr/Training_courses/wp1/absorption.html). Accessed 20 July 2010
- Ide JM (1937) The velocity of sound in rocks and glasses as a function of temperature. *J Geol* 45:689–716
- Illiev IG (1967) An attempt to estimate the degree of weathering of intrusive rocks from their physica-mechanical properties. Proceedings of 1st international congress of the International Society of Rock Mechanics, Lisbon. Vol 1, pp 109–114
- Jiménez González I, Scherer GW (2004) Effect of swelling inhibitors on the swelling and stress relaxation of clay bearing stones. *Environ Geol* 46:364–377
- Katzschman L, Aselmeyer G, Auras M (2006) *Natursteinkataster Thüringen*. IFS-Bericht 23:1–196
- Kern H, Siegesmund S (1989) A test of the relationship between seismic velocity and heat production for crustal rocks. *Earth Planet Sci Lett* 92:89–94
- Kettenacker L (1930) Über die Feuchtigkeit in Mauern. *Ges Ing* 53:721–728
- Kießl K (1983) *Kapillarer und dampfförmiger Feuchttransport in mehrschichtigen Bauteilen*. Diss, Univ Essen
- Kim D-C, Manghnani MH, Schlanger SO (1985) The role of diagenesis in the development of physical properties of deep-sea carbonate sediments. *Marine Geol* 69:69–91
- Klima K, Kluhanek O (1968) Quantitative correlation between preferred orientation of grains and elastic anisotropy of marble. *IEEE Geosci Electron GE-* 6:139
- Klopfer H (1974) *Wassertransport durch Diffusion in Feststoffen*. Bauverlag, Wiesbaden
- Klopfer H (1985) *Feuchte*. In: Lutz P, Jenisch R, Klopfer H et al (eds) *Lehrbuch der Bauphysik*. Teubner, Stuttgart
- Koch A, Siegesmund S (2001) Gesteinstechnische Eigenschaften ausgewählter Bausandsteine. *Z dtsh geol Ges* 152:681–700
- Koch A, Siegesmund S (2004) The combined effect of moisture and temperature on the anomalous behavior of marbles. *Environ Geol* 46(3-4):350–363
- Koch A, Siegesmund S (2005) Gesteinstechnische Eigenschaften von Sandsteinen. *Naturstein* 5:84–91
- Koch R, Sobott R (2005) Porosität in Karbonatgesteinen—Genese, Morphologie und Einfluss auf Verwitterung und Konservierungsmaßnahmen. *Z dtsh geol Ges* 156:33–50
- Kocher M (2005) *Quelldruckmessungen und thermische Druckmessungen an ausgewählten Sandsteinen*. PhD thesis, LMU München
- Kodikara J, Barbour SL, Fredlund DG (1999) Changes in clay structure and behavior due to wetting and drying. In: 8th Australian-New Zealand conference on geomechanics, Australian Geomechanics, Hobart
- Köhler W (1991) Untersuchungen zu Verwitterungsvorgängen an Carrara-Marmor in Potsdam-Sanssouci. *Berichte zu Forschung und Praxis der Denkmalpflege in Deutschland*. Steinschäden-Steinkonservierung 2:50–53
- Köhler W (2009) Riss- und Verwitterungsanalytik mit zerstörungsfreien Verfahren. In: Venzmer H (ed) *EU-Sanierungskalender 2009*. Beuth, Berlin
- Krantz RL (1983) Microcracks in rocks: a review. *Tectonophysics* 100(1-3):449–480

- Kraus K (1985) Experimente zur immissionsbedingten Verwitterung der Naturbausteine des Kölner Doms im Vergleich zu deren Verhalten am Bauwerk. University of Cologne
- Krus M (1995) Feuchtetransport- und Speicherkoeffizienten poröser mineralischer Baustoffe. Theoretische Grundlagen und neue Messtechniken. Diss Univ Stuttgart
- Künzel H (1994) Verfahren zur ein- und zweidimensionalen Berechnung des gekoppelten Wärme- und Feuchtetransports in Bauteilen mit einfachen Kennwerten. Diss Univ Stuttgart
- Künzel HM, Krus M (1995) Beurteilung des Feuchteverhaltens von Natursteinfassaden durch Kombination von rechnerischen und experimentellen Untersuchungsmethoden. Intern Z Bauinstandsetzen 1:5–20
- Kürzl H (1988) Exploratory data analysis: recent advances for the interpretation of geochemical data. *J Geochem Explor* 30:309–322
- Landolt-Börnstein (1982) New series, group V(1a): geophysics. Springer, Berlin
- Langheinrich G (1983). Wärmeleitfähigkeiten anisotroper Gesteine. *Geol Rdsch* 72:541–588
- Lentschig E (1971) Qualitätspässe für Werksteine. *Techn Inf Zuschlagstoffe und Natursteine* 3:13–19 and 4:27–32
- LGA (1988) Richtlinie zur Bestimmung der Ausbruchslast am Ankerdornloch in Fassadenplatten aus Naturwerkstein. 1987 ed. with corr. Landesgewerbeanstalt Bavaria, Zweigstelle Würzburg, Würzburg
- Lu C, Jackson I (1998) Seismic-frequency laboratory measurements of shear mode viscoelasticity in crustal rocks: II thermally stressed quartzite and granite. *Pure Appl Geophys* 153(2–4):441–473
- Lucia FJ (1983) Petrophysical parameters estimated from visual description of carbonate rocks: a field classification of carbonate pore space. *J Petrol Tech* 35:626–637
- Lucia FJ (1995) Rock fabric/petrophysical classification of carbonate pore space for reservoir characterization. *Am Assoc Petrol Geol Bull* 79:1275–1300
- Lucia FJ (1999) Carbonate reservoir characterization. Springer, Berlin
- Lukas R (1990) Die Naturwerksteine Baden-Württembergs und ihre Wetterbeständigkeit sowie Verwitterungsprofile ausgewählter Carbonatgesteine. Diss Univ Munich
- Madsen FT (1976) Quelldruckmessungen an Tongesteinen und Berechnung des Quelldrucks nach der DLVO-Theorie. Mitt Institutes für Grundbau und Bodenmechanik, ETH Zürich 108:1–65
- Madsen FT, Nüesch R (1990) Langzeitquellverhalten von Tongesteinen und tonigen Sulfatgesteinen. Mitt Institutes für Grundbau und Bodenmechanik, ETH Zürich 140:1–51
- Meng B (1993) Charakterisierung der Porenstruktur im Hinblick auf die Interpretation von Feuchtetransportvorgängen. *Aachener Beitr Bauforsch* 3:1–71
- Messmer JH (1965) The thermal conductivity of porous media. IV Sandstones. The effect of temperature and saturation. Proceedings of 5th conference on thermal conductivity. Vol 1, pp 1–29
- Metz F (1992) Zur Charakterisierung von Porenraum und ausgewählten Gebrauchseigenschaften verschiedener Natursteine. *Hochschul Sammlung Naturwiss Mineral* 2:1–164
- Mirwald P (1997) Physikalische Eigenschaften der Gesteine. In: Berufsbildungswerk des Steinmetz- und Bildhauerhandwerks e.V. (ed) Ebner, Ulm
- Monicard RP (1980) Properties of Reservoir Rocks: Core Analysis. Edition Technip, Paris
- Morales M (2011) Dimensional stones of Uruguay. PhD thesis, University of Goettingen
- Morales M, Oyhantcabal P, Stein K-J, Siegesmund S (2010) Black dimensional stones: geology, technical properties and deposit characterization of the dolerites from Uruguay. *Environ Earth Sci*. doi:10.1007/s12665-010-0827-5
- Morales Demarco M, Jahns E, Ruedrich J et al (2007) The impact on partial water saturation in rock strength: an experimental study on sandstone. *Z dtsh Ges Geowiss* 158:869–882
- Mosch S (2009) Optimierung der Exploration, Gewinnung und Materialcharakterisierung von Naturwerksteinen. <http://webdoc.sub.gwdg.de/diss/2009/mosch/mosch.pdf>. Accessed 20 July 2010
- Mosch S, Siegesmund S (2007) Statistische Bewertung gesteintechnischer Kenndaten von Natursteinen. *Z dtsh Ges Geowiss* 158(4):821–868



- Mügge O (1898) Über Translationen und verwandte Erscheinungen in Kristallen. *Neues Jahrbuch Miner Geol Palaeont* 1:71–158
- Müller F (2001) *Gesteinskunde*. Ebner, Ulm
- Nafe JE, Drake CL (1963) Physical properties of marine sediments. In: Hill MN (ed) *The earth beneath the sea: history*. Wiley-Interscience, New York
- Niesel K, Schimmelwitz P (1982) Zur quantitativen Kennzeichnung des Verwitterungsverhaltens von Naturwerksteinen anhand ihrer gefügemerkmale. *Bundesamt für Materialprüfung Forsch-Ber* 86:1–100
- Nur A, Simmons G (1969) The effect of saturation on velocity in low porosity rocks. *Earth Planet Sci Lett* 7:183–193
- O’Connell RJ, Budiansky B (1974) Seismic velocities in dry and saturated cracked solids. *J Geophys Res* 79(35):5412–5426
- Ollier C (1984) *Weathering*. Longman, New York
- Ondrasina J, Kirchner D, Siegesmund S (2002) Frost/Thaw cycles and their influence on marble deterioration: a long-term experiment. *Geol Soc Spec Publ* 205:8–17
- Peck L, Barton CC, Gordon RB (1985) Microstructure and resistance of a rock to tensile fracture. *J Geophys Res B* 90:11533–11546
- Peel RF (1974) Insolation weathering: some measurements of diurnal temperature changes in exposed rocks in the Tibesti Region, Central Sahara. *Z Geomorph* 21:19–28
- Peschel A (1974) Zur Ermittlung und Bewertung von Festigkeitseigenschaften bei Natursteinen. *Z Angew Geol* 20:118–128
- Peschel A (1977) *Natursteine*. VEB Deutscher Verlag für Grundstoffindustrie, Leipzig
- Peschel A (1983) *Natursteine*. VEB Deutscher Verlag für Grundstoffindustrie, Leipzig
- Picot P, Johan Z (1977) *Atlas of ore minerals*. Bureau de Recherches Géologiques et Minières, Orleans
- Popp T (1994) Der Einfluß von Gesteinsmatrix, Mikrorißgefügen und intergranularen Fluiden auf die elastischen Wellengeschwindigkeiten und die elektrische Leitfähigkeit krustenrelevanter Gesteine unter PT-Bedingungen. *Diss Univ Kiel*
- Poschold K (1990) *Das Wasser im Porenraum kristalliner Naturwerksteine*. Münchener Geowiss Abh B 7, Verlag Dr. Friedrich Pfeil, Munich
- Pribnow D, Williams CF, Burkhardt H (1993) Well log-derived estimates of thermal conductivity in crystalline rocks penetrated by the 4-km deep KTB Vorbohrung. *Geophys Res Lett* 20(12):1155–1158
- Primavori P (1999) *Planet stone*. Giorgio Zusi Editore S.A.S, Verona
- Pros Z, Babuška V (1967) A method for investigating the elastic anisotropy on spherical rock samples. *Z Geophys* 33:289–291
- R Development Core Team (2005) *R: a language and environment for statistical computing*, R Foundation for Statistical Computing, Vienna. <http://www.R-project.org>. Accessed 20 July 2010
- Rasolofosaon P, Rabbel W, Siegesmund S et al (2000) Characterization of crack distribution: fabric analysis versus ultrasonic inversion. *Geophys J Int* 141:413–424
- Rentsch W, Krompholz G (1961) Zur Bestimmung elastischer Konstanten durch Schallgeschwindigkeitsmessungen. *Fachzeitschrift der Bergakademie Freiberg*. [http://www.geotron.de/tl\\_files/geotron/media/Messverfahren/dynEModul/Quelle2\\_Bestimmung\\_elastischer\\_Konstanten\\_1961.pdf](http://www.geotron.de/tl_files/geotron/media/Messverfahren/dynEModul/Quelle2_Bestimmung_elastischer_Konstanten_1961.pdf). Accessed 20 July 2010
- Richter D, Simmons G (1974) Thermal expansion behavior of igneous rocks. *Int J Rock Mech Min Sci Geomech Abstr* 11:403–411
- Robertson EC, Peck DL (1974) Thermal conductivity of vesicular basalt from Hawaii. *J Geophys Res* 79:4875–4888
- Rohowski H (2001) *Druckfestigkeit und Ausbruchlast neu geregelt*. *Naturstein* 3:88–92
- Rösler HJ (1991) *Lehrbuch der Mineralogie*. Deutscher Verlag für Grundstoffindustrie, Leipzig
- Roth ES (1955) Temperature and water content as factors in desert weathering. *J Geol* 73:454–468

- Rudnick RL, Fountain DM (1995) Nature and composition of the continental crust: a lower crustal perspective. *Rev Geophys* 33:267–309
- Ruedrich J (2003) Gefügekontrollierte Verwitterung natürlicher und konservierter Marmore. Diss Univ Göttingen
- Ruedrich J, Bartelsen T, Dohrmann R, Siegesmund S (2010a) Building sandstone integrity affected by the process of hygric expansion. *Environ Earth Sci*. doi:[10.1007/s12665-010-0767-0](https://doi.org/10.1007/s12665-010-0767-0)
- Ruedrich J, Kirchner D, Siegesmund S (2010b) Physical weathering of building stones induced by freeze thaw action: a laboratory long-term study. *Environ Earth Sci*. doi:[10.1007/s12665-010-0826-6](https://doi.org/10.1007/s12665-010-0826-6)
- Ruedrich J, Rothert E, Fitzner B et al (2005a) Schadensanalyse an Gebäuden aus Kalksteinen auf Malta. In: Siegesmund S, Snethlage R, Auras M (eds) *Stein-Zerfall und Konservierung*. Edition Leipzig, Leipzig
- Ruedrich J, Seidel M, Kirchner D et al (2005b) Salzverwitterung, hygrische und thermische Dehnung als auslösende Schadensquantitäten. *Z dtsh geol Ges* 156(1):59–74
- Ruedrich J, Seidel M, Rothert E et al (2007) Length change behaviour of sandstones induced by salt crystallisation. In: Prikryl R, Smith BJ (eds) *Building stone decay: from diagnosis to conservation*. Geol Soc London Spec Pub, London
- Ruedrich J, Siegesmund S (2006) Fabric dependence of length change behaviour induced by ice crystallization in the pore space of natural building stones. In: Fort A, Alvarez de Buergo M, Gomez-Heras M et al (eds) *Heritage, weathering and conservation*. Taylor & Francis Group, London
- Ruedrich J, Siegesmund S (2007) Salt-induced weathering: an experimental approach. *Environ Geol* 52:225–249
- Ruedrich J, Weiss T, Siegesmund S (2001) Deterioration characteristics of marbles from the Marmorpalais Potsdam (Germany): a compilation. *Z dtsh geol Ges* 152:637–664
- Rybach J, Buntebarth G (1982) Relationship between the petrophysical properties density, seismic velocity, heat production and mineralogical constitution. *Earth Planet Sci Lett* 57:367–376
- Sage JD (1988) Thermal microfracturing of marble. In: Marinos PG, Koukis GC (eds) *Engineering geology of ancient works, monuments and historical sites*. Balkema, Rotterdam
- Schild M, Siegesmund S, Vollbrecht A et al (2001) Characterization of granite matrix porosity and pore-space geometry by in situ and laboratory measurements. *Geophys J Int* 146:111–125
- Schlanger SO, Douglas RG (1974) The pelagic ooze-chalk-limestone transition and its implication for marine stratigraphy. *Spec Pub Int Assoc Sediment* 1:117–148
- Schön J (1983) *Petrophysik*. Akademie, Berlin
- Schön J (1996). *Physical properties of rocks. Handbook of geophysical exploration*. Vol 18. Pergamon, Oxford, New York
- Schuh H (1987) *Physikalische Eigenschaften von Sandsteinen und ihren verwitterten Oberflächen*. Münchner Geowiss Abh (B), Verlag Dr. Friedrich Pfeil, Munich
- Sebastian E, Cultrone G, Benavente D et al (2008) Swelling damage in clay-rich sandstones used in the church of San Mateo in Tarifa (Spain). *J Cult Heritage* 9:66–76
- Segall P, Pollard DD (1980) Mechanics of discontinuous faults. *J Geophys Res* 85:4337–4350
- Shushakova V, Fuller ER Jr, Siegesmund S (2010) Influence of shape fabric and crystal texture on marble degradation phenomena: simulations. *Environ Earth Sci*. doi:[10.1007/s12665-010-0744-7](https://doi.org/10.1007/s12665-010-0744-7)
- Siegesmund S (1994) Modelling of the thermal conductivity observed in paragneisses of the KTB pilot hole. *Sci Drill* 4:207–213
- Siegesmund S (1996) The significance of rock fabrics for the geophysical interpretation of geophysical anisotropies. *Geotekt Forsch* 85:1–123
- Siegesmund S, Dahms M (1994) Fabric-controlled anisotropy of elastic, magnetic and thermal properties. In: Bunge HJ, Siegesmund S, Skrotzki W et al (eds) *Textures of geological materials*. DGM Informationsgesellschaft, Oberursel

- Siegesmund S, Grimm W-D, Dürrast H et al (2010) Limestones in Germany used as building stones: an overview. In: Smith B, Gomez-Heras M, Viles H et al (eds) *Limestone in the built environment: present day challenges to preserve the past*. Geol Soc Spec Pub London, London
- Siegesmund S, Kruhl J, Lüschen E (1996) Petrophysical and seismic features of the exposed lower continental crust in Calabria (Italy): field observation versus modelling. *Geotekt Forschungen* 85:125–163
- Siegesmund S, St Mosch, Scheffzik Ch et al (2008a) The bowing potential of granitic rocks: rock fabrics, thermal properties and residual strain. *Environ Geol* 55:1437–1448
- Siegesmund S, Ruedrich J, Koch A (2008b) Marble bowing: comparative studies of different public building facades. *Environ Geol* 56:473–494
- Siegesmund S, Ruedrich J, Weiss T (2004a) Marble deterioration. In: Prikryl R (ed) *Dimension stone 2004*. Taylor & Francis Group, London
- Siegesmund S, Ullemeyer K, Weiß T et al (2000a) Physical weathering of marbles caused by anisotropic thermal expansion. *Int J Earth Sci* 89:170–182
- Siegesmund S, Vollbrecht A, Chlupac T et al (1993) Fabric-controlled anisotropy of petrophysical properties observed in KTB-core samples. *Sci Drill* 4:31–54
- Siegesmund S, Vollbrecht A, Ullemeyer K et al (1997) Anwendung der geologischen Gefügekunde zur Charakterisierung natürlicher Werksteine—Fallbeispiel: Kauffunger Marmor. *Int J Restor Build Monum* 3:269–292
- Siegesmund S, Vollbrecht A, Weiss T (2002) Gefügeanisotropien und ihre Bedeutung für Naturwerksteine. *Naturstein* 7:76–81
- Siegesmund S, Weiß T, Vollbrecht A et al (1999) Marble as a natural building stone: rock fabrics, physical and mechanical properties. *Z dtsh geol Ges* 150(2):237–258
- Siegesmund S, Weiss T, Ruedrich J (2004b) Schadensmonitoring mittels Ultraschalldiagnostik. *Restauro* 2:98–105
- Siegesmund S, Weiss T, Tschegg EK (2000b) Control of marble weathering by thermal expansion and rock fabrics. *Proceedings of 9th international congress on deterioration and conservation of stone, Venice*. Elsevier, Amsterdam, pp 19–24
- Simmons G (1964) Velocity of compressional waves in various minerals at pressures to 10 kbars. *J Geophys Res* 69:1117–1121
- Simmons G, Cooper HW (1978) Thermal cycling cracks in three igneous rocks. *Int J Rock Mech Min Sci Geomech Abstr* 15:145–148
- Simmons G, Nur A (1969) Properties of granites in situ and their relation to laboratory measurements. *Science* 162:789
- Sinclair SW (1980) Analysis of macroscopic fractures on Teton Anticline, Northwestern Montana. MSc Thesis, Texas A&M University
- Sippel J, Siegesmund S, Weiss T et al (2007) Decay of natural stones caused by fire damage. In: Prikryl R, Smith BJ (eds) *Building stone decay: from diagnosis to conservation*. Geol Soc Spec Pub, London
- Sneathlage R (1984) Steinkonservierung, Forschungsprogramm des Zentrallabors für Denkmalpflege 1979–1983. Bericht für die Stiftung Volkswagenwerk. Arbeitsheft Bayr Landesamt Denkmalpflege 22. Lipp, Munich
- Sneathlage R (2005) Leitfaden zur Steinkonservierung. Fraunhofer IRB, Stuttgart
- Sneathlage R, Hoffmann D, Knöfel D (1986) Simulation der Verwitterung von Naturstein. Teil 2: Physikalisch-chemische Verwitterungsreaktionen. In: Wittmann FH (ed) *2nd Int Kolloquium 'Werkstoffwissenschaften und Bausanierung'*. Technische Akademie, Esslingen
- Sneathlage R, Wendler E (1997) Moisture cycles and sandstone degradation. In: Baer N, Sneathlage R (eds) *Saving our architectural heritage, the conservation of historic stone structures*. Dahlem Workshop Reports ES20. Wiley, Chichester
- Stearns DW (1967) Certain aspects of fracture in naturally deformed rocks. In Ricker RE (ed) *NSF Adv Sci Sem in Rock Mech*, Bedford
- Steindlberger E (2003) Vulkanische Gesteine aus Hessen und ihre Eigenschaften als Naturwerksteine. *Geol. Abhandlungen Hessen* 110:1–67

- Steindlberger E (2004) Volcanic tuffs from Hesse (Germany) and their weathering behaviour. *Environ Geol* 46:378–390
- Stockhausen N (1981) Die Dilatation hochporöser Festkörper bei Wasseraufnahme und Eisbildung. Diss TU Munich
- Strohmeier D (2003) Gefügeabhängigkeit technischer Eigenschaften. PhD thesis, Univ Göttingen
- Strohmeier D, Siegesmund S (2002) Influence of anisotropic fabric properties on the mechanical strength of selected building stones. *Geol Soc Spec Publ* 205:114–135
- Stück H, Fischer C, Siegesmund S (2010) Bausteine der Region Drei Gleichen: Entstehung, Charakterisierung, Verwitterung. In: Siegesmund S, Hoppert M (eds) *Die Drei Gleichen: Baudenkmäler und Naturraum*. Editon Leipzig, Leipzig
- Stück H, Forgó Z, Ruedrich J et al (2008) The behaviour of consolidated volcanic tuffs: weathering mechanisms under simulated laboratory conditions. *Environ Geol* 56:699–713
- Szilaygi J (1995). Leitgesteine für die Denkmalpflege-Untersuchung petrophysikalischer Eigenschaften (key rocks for monument care-investigation into petrophysical properties). Research report TU Dresden [http://www.tu-dresden.de/die\\_tu\\_dresden/fakultaeten/fakultaet\\_bauingenieurwesen/geotechnik/geologie/forschung/geologie/dateien/forschung\\_leitgesteine.pdf](http://www.tu-dresden.de/die_tu_dresden/fakultaeten/fakultaet_bauingenieurwesen/geotechnik/geologie/forschung/geologie/dateien/forschung_leitgesteine.pdf). Accessed 20 July 2009
- Thill RE, Willard RJ, Bur TR (1969) Correlation of longitudinal velocity variation with rock fabric. *J Geophys Res* 74:4897–4909
- Thuro K, Plinninger RJ, Záh S (2001) Scale effects in rock strength properties. Part 1: unconfined compressive test and Brazilian test. In: Särkkä P, Eloranta P (eds) *Rock mechanics—a challenge for society*. Proceedings of ISRM regional symposium on Eurock 2001, Espoo. Taylor and Francis Group, London
- Török A (2007) *Geologia Mernököknek*. Műegyetemi Kladno, Budapest
- Tournier B, Jeannette D, Destrignville C (2000) Stone drying: an approach of the effective evaporation surface area. In: Fassina V (ed) 9th international congress on deterioration and conservation of stone. Elsevier, Amsterdam
- Tucker ME (1985) Einführung in die Sedimentpetrologie. Ferdinand Enke Verlag, Stuttgart
- UNI 9724/5 (1990) Materiali lapidei. determinazione della resistenza a flessione—Norma parte 5a. UNI Ente Nazionale Italiano di Unificazione, Milano
- van Golf-Racht TD (1996) Naturally-fractured carbonate reservoirs. In: Chilingarian GV, Mazullo SJ, Rieke HH (eds) *Carbonate reservoir characterization: a geologic-engineering analysis, part II*. Elsevier, Amsterdam
- Vázquez P, Siegesmund S, Alonso FJ (2010) Bowing of dimensional granitic stones. *Environ Earth Sci*. doi:10.1007/s12665-010-0882-y
- Viator T (1993) Entfestigung von KTB-Gesteinen im Kriechexperiment unter dem Einfluß verschiedener Flüssigkeiten. Diplom Thesis Univ Göttingen
- Viles HA, Camuffo D, Fitz S et al (1997) Group report: what is the state of our knowledge of the mechanisms of deterioration and how good are our estimates of rates of deterioration? In: Baer NS, Snethlage R (eds) *Report of the Dahlem workshop on saving our architectural heritage: the conservation of historic stone structures*. Wiley, Hoboken
- von Moos A, De Quervain F (1948) *Technische Gesteinskunde*. Birkhäuser, Basel
- Vos BH (1978) Hygric methods for the determination of the behaviour of stones. International symposium on deterioration of stone monuments. UNESCO-RILEM, Paris
- Wangler TP, Scherer GW (2008) Clay swelling mechanism in clay-bearing sandstones. *Environ Geol* 56:529–534
- Wangler TP, Stratulat A, Duffus P, Prevost JH, Scherer GW (2010) Flaw propagation and buckling in clay-bearing sandstones. *Environ Earth Sci*. doi:10.1007/s12665-010-0732-y
- Washburn EW (1921) A method of determining the distribution of pore sizes in a porous material. *Proc Nat Acad Sci* 7:115
- Weiss G (1992) Die Eis- und Salzkristallisation im Porenraum von Sandsteinen und ihre Auswirkungen auf das Gefüge unter besonderer Berücksichtigung gesteinspezifischer Parameter. *Münchner Geowiss Abh B* 9, Verlag Dr. Friedrich Pfeil, Munich

- Weiss T, Rasolofosaon PNJ, Siegesmund S (2001) Thermal microcracking in Carrara marble. *Z dtsh geol Ges* 152(2-4):621–636
- Weiss T, Rasolofosaon PNJ, Siegesmund S (2002a) Ultrasonic velocities as a diagnostic tool for the quality assessment of marble. In: Siegesmund S, Weiss T, Vollbrecht A (eds) *Natural stone, weathering phenomena, conservation strategies and case studies*. Geological Society Special Publications, London
- Weiss T, Siegesmund S, Bohlen T (1999) Seismic, structural, and petrological models of the subcrustal lithosphere in southern Germany: a quantitative reevaluation. *Pure Appl Geophys* 156:53–81
- Weiss T, Siegesmund S, Rasolofosaon P (2000) The deterioration velocity-porosity-relation constraint. 9th international congress on deterioration and conservation of stone, Venice 19–24, Elsevier 215–223
- Weiss T, Siegesmund S, Fuller E Jr (2002b) Microstructure-based finite element modeling of microcrack formation in marbles. *Geol Soc Spec Publ* 205:88–101
- Weiss T, Siegesmund S, Kirchner D et al (2004a) Insolation weathering and hygric dilatation as a control on building stone degradation. *Environ Geol* 46(3–4):402–413
- Weiss T, Strohmeyer D, Kirchner D et al (2004b) Weathering of stones caused by thermal expansion, hygric properties and freeze-thaw cycles. In: Kwiatkowski D, Löfvendahl R (eds) *Proceedings of 10th international congress on deterioration and conservation of stone*. ICOMOS, Stockholm
- Wendler E, Charola EA, Fitzner B (1996) Easter Island tuff: laboratory studies for its consolidation. In: Riederer J (ed) *Proceedings of 8th international congress deterioration and conservation of stone*. Möller Druck and Verlag GmbH, Berlin
- Wendler E, Rückert-Thümling R (1992) Gefügezerstörendes Verformungsverhalten bei salz-befrachteten Sandsteinen unter hygrischer Wechselbelastung. In: Wittmann FH (ed) *Materials science and restoration*. Expert, Renningen
- Wenk HR (1985) Preferred orientation in deformed metals and rocks. An introduction to modern texture analysis. Academic, Orlando
- Wenk HR, Wenk E (1969) Physical constants of alpine rocks (density, porosity, specific heat, thermal diffusivity and conductivity). *Schweiz Min Petrogr Mitt* 49:343–357
- Wenzel A, Häfner F (2003) Die roten Werksandsteine der Westpfalz. IFS-Report 15. Institut für Steinkonservierung, Mainz
- Wesche K (1981) *Baustoffe für tragende Bauteile*. 2nd ed., Vol 2. Bauverlag, Wiesbaden
- Winkler EM (1994) *Stone in architecture*. Springer, Berlin
- Winkler EM (1996) Technical note: properties of marble as building veneer. *Int J Rock Mech Min Sci* 33(2):215–218
- Wollard GP (1959) Crustal structure from gravity and seismic measurements. *J Geophys Res* 64:1521–1544
- Woodside W, Messmer J (1961) Thermal conductivity of porous media. II. Consolidated rocks. *J Appl Phys* 32(9):1699–1706
- Zeisig A, Siegesmund S, Weiss T (2002) Thermal expansion and its control on the durability of marbles. *Geol Soc Spec Publ* 205:64–79

# Chapter 4

## Weathering and Deterioration

Michael Steiger, A. Elena Charola and Katja Sterflinger

**Abstract** It is generally assumed that stone is one of the most durable materials because it is compared to weaker building materials, such as wood or mud. But stone can deteriorate, and many factors will affect it. The nature of the stone is critical in determining its resistance to the various deterioration factors. The most important one, salt, was identified by Herodotus, nearly two and a half millennia ago. However, salt by itself is not damaging; it requires the presence of water for its aggressiveness to become evident. And water is needed for biocolonization to occur, for freeze–thaw phenomena, and for wet-dry expansion. Control of this single factor can decrease the deterioration potential of a stone and any structure built from it significantly. This chapter aims to present a review of the most important deterioration processes and their effect on the various types of stones and rocks used by man. Among them are thermal effects, the influence of moisture, both as water vapor and in liquid state, the presence of salts, and the damages that can be expected from biocolonization. This chapter also aims at identifying the areas where more research is needed to understand the actual deterioration mechanism of the various factors.

---

M. Steiger (✉)

Department of Chemistry, Inorganic and Applied Chemistry, University of Hamburg,  
Martin-Luther-King-Platz 6 20146 Hamburg, Germany  
e-mail: michael.steiger@chemie.uni-hamburg.de

A. E. Charola

Museum Conservation Institute, Smithsonian Institution, Washington, DC, USA  
e-mail: charola\_ae@yahoo.com

K. Sterflinger

Institut für Angewandte Mikrobiologie, Universität für Bodenkultur, Muthgasse 18,  
1190 Wien, Austria



## 4.1 Introduction

Stone is generally considered one of the most resistant materials, and so it is when compared to other construction materials such as adobe or wood. Nonetheless, it is also susceptible to deterioration. Herodotus mentioned in his *The History* that the stones of the pyramids in Egypt were already deteriorating when he saw them in the 5th century BC.

Deterioration is a complex process, and, therefore, there are many words that are used to describe it. For example, “weathering” is used for the natural process of rock disintegration by external factors, while “deterioration” implies the impairment of value and use. Thus, rocks weather while stones deteriorate. The difference is that man has intervened in producing and using the stones. Therefore, these two terms are not really equivalent.

On the other hand, “alteration” is defined as a modification of the material; for example, geologists use it to refer to the change in mineral composition of a rock, such as occurs in volcanic rocks. The word does not imply a worsening of its characteristics from a conservation point of view (Grimmer 1984; UNI 11182 2006).

Two other words tend to be used interchangeably with the previously mentioned ones. These are “degradation” and “decay”. Both imply a change for the worse; the former implies disintegration and has specific meanings for chemists, physicists, and geologists. Biologists simply turned it into biodegradation, thus avoiding misunderstandings. On the other hand, decay has the connotation of rotting or decomposition, as reflected in tooth decay. Only some years ago, an online dictionary further described “decay” as “the result of being destroyed... by not being cared for”, a point that always should be kept in mind when considering the conservation of buildings and monuments.

Finally, the last word that needs to be mentioned is “damage”. This is the most general term and needs to be accompanied by a qualifying term, as in “mechanical damage”.

There are many types of damages that stones can undergo (Charola 2004). These may produce particular deterioration patterns that are then described by specific terms. Given the high number of these patterns, and the fact that this problem is being addressed around the world in different languages, it is important to try to come to a consensus about their use (see Chap. 6).

It is important to point out that the same pattern may result from different deterioration mechanisms, while any one specific mechanism may result in different types of patterns, depending on the substrate in question. For example, granular disintegration can be the result of chemical attack, frost damage, or other processes. Hence, in practice, it is generally impossible to deduce the major causes of damage simply by observing the deterioration pattern. Visual observation and documentation serve mainly to attain an overall estimate of the amount and type of damage present. Determining the origin of the damage requires one or more analyses to interpret the observed pattern. In order to assess the relative importance

of different degradation processes and their rates, a detailed understanding of the underlying mechanisms is indispensable.

This chapter describes the various types of damages that can occur as a function of the main process underlying them, such as mechanical, chemical, or biochemical. Specific emphasis is placed on problems introduced by the presence of salts because this is probably the single most relevant deterioration mechanism for building materials.

## 4.2 Deterioration by Mechanical Processes

Mechanical damage results when stone is subjected to a load or a stress that is above the mechanical resistance it has. Many cases of mechanical damage result from poor design of the buildings. For example, the cracks that form around window and door openings are very likely the result of unsymmetrical loads or side thrusts. Other times, differential soil settlement may be the cause of the cracks in structures, while catastrophic events such as earthquakes are responsible for heavy damages in buildings. Binda and Anzani (1997) give a good introduction to this topic that is beyond the scope of this chapter.

The growth of vegetation, starting with grasses and ferns that tend to grow in the mortar joints of masonry, deteriorate the mortar with the mechanical stresses induced by their roots. If maintenance is not regularly performed, this damage will increase with the development of higher vegetation, bushes and even large trees, resulting in the breaking up of the stone masonry itself, as frequently seen in archaeological sites.

Fire is yet another catastrophic event. This can induce stresses because stone is not a good thermal conductor, and, therefore, the surface temperature will be significantly different from that in the underlying stone. The mechanism of this deterioration is described in detail in the previous chapter (Sect. 3.4.2). The expansion suffered during heating to high temperatures will result in the literal shattering of the external layers of the stone blocks, leaving a typical rounded surface behind, known as a conchoidal fracture (Fig. 4.1).

Apart from fissuring, fracturing and spalling, fires may induce discoloration and mineralogical changes in some of the stones' components, modifying their physical properties. For example, the oxidation of iron minerals with the formation of hematite (Dionisio and Aires Barros 2004; Dionisio et al. 2005; Hajpál and Török 2004; Török and Hajpál 2005), the dehydration of clays, the decomposition of calcite or dolomite, the sudden contraction of quartz during transformation of  $\alpha$  to  $\beta$  variety when temperatures increase above 573 °C, and occurrences of partial melting and sintering have also been observed (Kleber 1959; Matthes 1987; Sippel et al. 2007). All of these changes mostly result in an increase of the susceptibility of the material to deterioration. Finally, the damage may be increased by the thermal shock induced during attempts to extinguish the fire with water that rapidly will cool the heated stone surface causing further spalling.

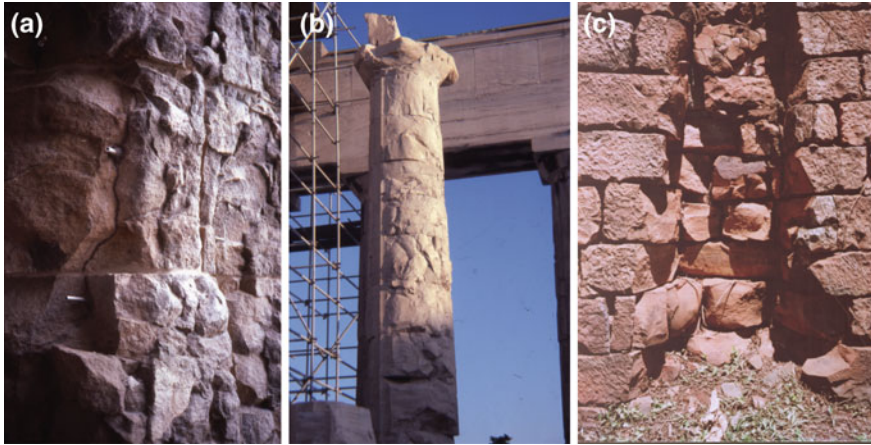


**Fig. 4.1** Detail of the conchoidal fractures resulting from historical fires: **a** Granite pillars in the former custom building, now a market, in Salvador, Bahia, Brazil; **b** Marble columns of the Parthenon, Athens, Greece; **c** Niche for a wooden column in the church wall constructed with argillaceous sandstone in the Jesuit Guaraní Mission of Santa Ana, Misiones, Argentina

Ironically, fire is used to finish some stones, such as the flame-finished granite, which became popular in the 1970s because of its rustic appearance. The applied heat spalls off small scales from the surface and, in this process, opens up many fissures in the stone. As a result, far more moisture is absorbed by the stone than if the surface was just sawn (Grissom et al. 2000). Also, traditional decorative stone finishes used in the past have induced damage to the stone surface, resulting in a deterioration increase (Cecchi et al. 1978; Alessandrini et al. 1979).

Finally, vibrations caused by traffic, including trains and airplanes, and machinery, e.g. air-conditioners, can induce alternating tensile and compressive stresses in building structures. Stone elements may be affected, especially if they are cracked or small and not well connected to the rest of the structure, as smaller elements have higher resonance frequency. Therefore, ceilings, floors, and windows are more likely to suffer from resonance amplification than the building itself. While, in general, vibration may not cause direct damage, it certainly may accelerate the overall deterioration rate, for example, from dust settling into existing open cracks that subsequently cannot return to their previous state.

#### **4.2.1 Thermal Cycling**

Another source for mechanical damage is the dimensional change that stone and other building materials undergo induced by thermal cycling. As discussed in detail in [Chap. 3 \(Sect. 3.4.2\)](#), changes in temperature, either increases or decreases, will result respectively in volume expansion or contraction of stone.

**Table 4.1** Thermal expansion coefficients for magmatic, metamorphic, and sedimentary rocks

Rock class	Rock types	Linear expansion coefficient ( $10^{-6} \times \text{K}^{-1}$ )		
		Average	Max	Min
Magmatic	8 rock types	7.4	10	5
Metamorphic	5 marbles	11	15	8
	1 gneiss, 1schist	7.9	9	6
	2 quartzitic rocks	12.5	14	11
Sedimentary	2 calcareous sandstones	7.5	8	7
	2 limestones	4	6	2
	1 travertine	5	6	4
	5 sandstones	10.8	12	9.5

The data correspond to eight magmatic rock types (granodiorite, granite, gabbro-norite, metagabbro, peridotite, 2 quartz porphyries, and tuff); 12 metamorphic rocks, 5 marbles, and 7 siliceous rocks (slate, serpentinite, 2 paragneiss, orthogneiss, quartzite, and quartz mylonite); 10 sedimentary rocks (2 calcareous sandstones, 2 limestones, travertine, and 5 sandstones)

In general, the volume expansion coefficient for rock varies between 15 and  $33 \times 10^{-6} \text{ K}^{-1}$ . For isotropic rocks, it can be estimated as three times their linear expansion coefficient. It is to be highlighted that expansion coefficients vary with temperature and that the correlation is not necessarily linear. Table 4.1 lists the linear thermal expansion coefficients for some types of rocks (see also Table 3.7).

It should be remembered that, particularly for coarse grained stones, such as granites and marbles, there may be significant differences in the expansion between different varieties of the same rock type. This is a consequence of the various rock textures, e.g. size and orientation of the crystals as well as the type of boundaries between them.

Even if the temperature changes are not particularly large, the repeated heating and cooling of the stone will eventually lead to its deterioration over time. Apart from the expansion that may result from heating, the residual stress that may remain in the stone once it returns to the “normal” temperature, i.e. average temperature, is important since it will accumulate over time.

The expansion coefficients of rocks result from those of the minerals present in them. Thus, granite and sandstone have high expansion values because of the presence of quartz, while marble and limestone reflect that of calcite or dolomite, and slates that of clays and micas, since they are metamorphosed argillaceous rocks such as mudstone. Table 4.2 gives the linear expansion coefficient for some of these minerals, while Fig. 4.2 shows the linear expansion changes they undergo with temperature.

In general, thermal cycling between 20 and 90 °C induces more or less deterioration to most of the stones. However, an equivalent decrease in temperature, down to -40 °C, does not induce damage as long as the sample is dry (Weiss et al. 2004b). Marbles are more susceptible than other stones and are discussed in more detail below.

As can be seen from Table 4.2, calcite is the only mineral that, upon heating, expands in one direction while contracting in the other (Figs. 4.2 and 4.3); upon

**Table 4.2** Linear expansion coefficient  $\alpha$  for some minerals

Mineral	Linear thermal expansion coefficient ( $K^{-1}$ )		Temp range ( $^{\circ}C$ )
	Parallel to c-axis	Perpendicular to c-axis	
Calcite <sup>a</sup>	$25.1 \times 10^{-6}$	$-5.6 \times 10^{-6}$	0–85
Dolomite <sup>b</sup>	$25.8 \times 10^{-6}$	$6.2 \times 10^{-6}$	24–700
Quartz <sup>a</sup>	$7.7 \times 10^{-6}$	$13.3 \times 10^{-6}$	0–80
Albite <sup>c</sup>	$10.5 \times 10^{-6}$	$5.6 \times 10^{-6}$	25–970
Gypsum <sup>d</sup>	$54 \times 10^{-6}$	$*7-117 \times 10^{-6}$	**25–42
Micas <sup>e</sup>	$8.7 \times 10^{-6}$	$17.8 \times 10^{-6}$	
Clays <sup>f</sup>	$6 \times 10^{-6}$	$15 \times 10^{-6}$	25–350

Values from

<sup>a</sup> Hodgman et al. (1963)

<sup>b</sup> Reeder and Markgraf (1986)

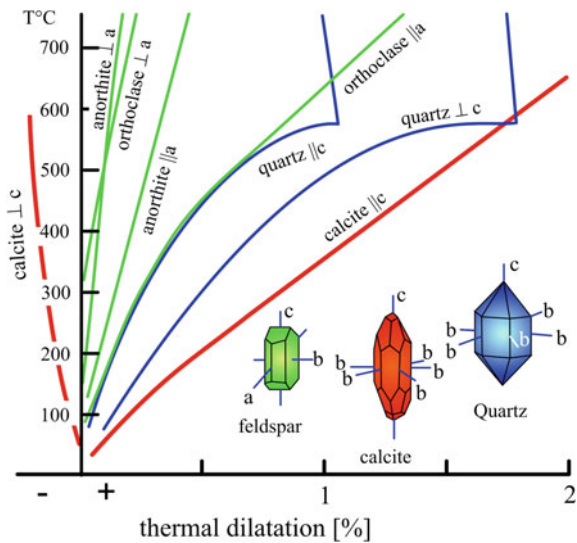
<sup>c</sup> Average of high and low albite (Kleber 1959)

<sup>d</sup> \* or a–b axis, respectively, \*\* calculated average for temperature range (Ballirano and Melis 2009)

<sup>e</sup> Average for muscovite and phlogopite (McKinstry 1965)

<sup>f</sup> Average for kaolinite, dickite, and halloysite (McKinstry 1965)

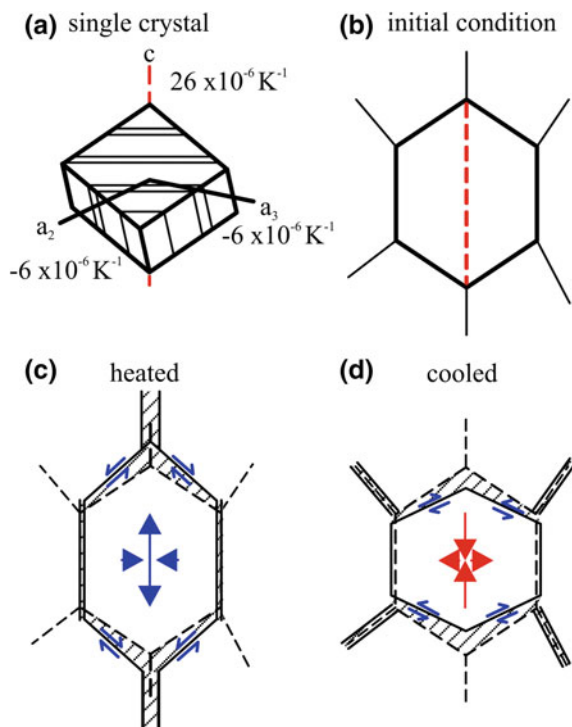
**Fig. 4.2** Linear expansion for some minerals as a function of temperature. Adapted from Winkler (1994)



cooling, it will contract along the c axis while expanding along the other ones. Therefore, calcite marbles are the most susceptible to thermal cycling that leads to granular decohesion of the stone matrix, i.e. the so-called “sugaring” deterioration pattern that has been long known (Kessler 1919; Franzini et al. 1983). This is mostly the result of the thermal stress induced along grain boundaries that leads to their failure and even to grain fissuring (Fig. 4.3).

From the above, it follows that, in principle, dolomite marbles should be more resistant to this deterioration, because their crystals only expand, while calcite

**Fig. 4.3** Diagram illustrating the deterioration mechanism for calcite due to thermal cycling. **a** Anisotropy of individual calcite crystal upon heating, **b** Calcite crystal within an idealized marble matrix, **c** Expansion and contraction suffered upon heating, and **d** Contraction and expansion suffered upon cooling. Adapted from Siegesmund et al. (2004)



expands in one direction and contracts in the other. Mathematical modeling of the thermal expansion behavior of marbles via microstructure-based finite element simulations have been shown to provide good correspondence to real experiments (Weiss et al. 2002b, 2003; Shushakova et al. 2011). Onset and magnitude of thermal microcracking vary for calcite- and dolomite-bearing marbles even when assumed to have exactly the same microstructure and texture; the onset being earlier, and the microcracking greater, for the calcite marbles. Thus, finite element modeling indicates that dolomite marbles may be more resistant against thermal weathering than calcite marbles. Variations in the texture may significantly affect the distribution of thermal stresses within the marble. There is a strong inverse correlation between thermal stresses and degree of texture, i.e. lattice preferred orientation of the minerals, since higher elastic strain energies are associated with weakly textured marbles, and vice versa.

This is the case in general, though specific dolomite marbles may be more susceptible to thermal cycling than specific calcite ones due to their texture and the nature of the residual strain, as exemplified by the Greek Arabella dolomite marble, which is more susceptible to this deterioration than the Portuguese Rosa Estremoz marble (Zeisig et al. 2002).

For the case of marbles, the stress induced by heating leads to fissuring and, eventually, fracturing and results in an increase in porosity (Malaga-Starzec et al. 2002). This may already occur at temperatures around 40–50 °C, a value that is



easily reached by a stone surface on summer days, even in northern countries. But then, the cooling cycles that occur in winter in these countries will also contribute to grain decohesion. This phenomenon has also been observed in marble quarries, and the deteriorated marble is referred to as “marmo cotto” (Bertagnagi et al. 1983).

Although marble weathering by thermal cycling has been studied extensively, the key factors triggering this deterioration have not as yet been quantified (Widhalm et al. 1996; Winkler 1996; Weiss et al. 1999; Ruedrich et al. 2002; Weiss et al. 2002a, b; Zeisig et al. 2002). The deterioration starts with an initial stage of insolation that leads to the progressive loss of cohesion along grain boundaries (Siegesmund et al. 1999, 2000) caused by the different thermal expansion coefficients of the rock-forming minerals during either heating or cooling (Fredrich and Wong 1986). The resulting induced tensile, compressive, or shear stresses along the grain boundaries may be large enough to cause failure along microstructural precursors, such as cracks and cleavage planes (Sage 1988). The grain to grain orientation relationship, frequently called misorientation, and its distribution within the stone is also an important parameter. The magnitude of residual strain may be associated with the grain size, grain shape, and lattice preferred orientation in the marbles (Royer-Carfagni 1999; Weiss et al. 2002a, 2003; Zeisig et al. 2002; Siegesmund et al. 2008b). This suggests a fabric dependence of residual strain after thermal treatment and, consequently, of thermal degradation. Thermally induced microcracks lead to a residual strain after heat treatment and, thus, to the progressive deterioration. However, some authors (e.g. Sage 1988; Koch and Siegesmund 2004) have shown that, after a few heating cycles, there is no further increase of the residual strain as long as moisture is absent.

While marbles show a positive residual strain, rocks containing clays that can dehydrate, such as tuffs, show a significant negative residual strain only during the first cycling that is associated with the shrinking due to dehydration (Weiss et al. 2004b). Some siliceous rocks may also show a directional dependence of the thermal expansion coefficient as a consequence of texture (e.g. quartzites); this observation is rather the exception than the rule and by far not as pronounced as in marbles. The deterioration induced by thermal cycling in granite results in the “sanding disintegration” and is mostly found on weathered granites (Delgado Rodrigues 1996).

In stones, such as granite, that are constituted by different colored minerals, the variations in light absorption or reflection, the latter called albedo, can result in localized deterioration because of temperature differences between lighter and darker colored areas of the same stone. An interesting example has been described by Gómez-Heras et al. (2008) for a 60 year old granite building. The granite was rich in micro-granular (tonalite) enclaves that were darker in comparison to the rest of the stone (monzogranite). These darker areas, with different albedo and thermal conductivity properties compared to the host stone, tended to spall. The study found that the driving factor was the difference in thermal response to insolation and the short term variations in surface temperatures between them.

Another deterioration pattern that can be attributed to thermal cycling is the deformation, i.e. bowing, of stone slabs. In particular, marble slabs suffer it, though granite ones are also prone to this deterioration (Siegesmund et al. 2008a). This has

been a phenomenon long observed on marble tombstones and described in the early literature (Kessler 1919; Fritz 1922), but has become increasingly more evident with new construction technology that uses stone cladding. With improved cutting technology, the thickness of these slabs has decreased from ca. 90 mm down to 20 mm, and, consequently, the bowing of marble has become a growing concern during the past 30 years. As mentioned in the preceding chapter (Sect. 3.4), there is an extensive number of publications dealing with this topic. The deformation of marble panels is a consequence of fissures resulting from thermal expansion. Consequently, porosity increases, and so does the bowing. Therefore, the more bowed the marble, the higher its porosity. However, some studies carried out monitoring this phenomenon have shown that the bowing rate is higher in the first years and decreases in the subsequent ones from ca.  $0.5 \text{ mm m}^{-1}$  per year for the first 9 years to  $0.38 \text{ mm m}^{-1}$  for the subsequent 3 years (Siegesmund et al. 2008b).

However, it should be pointed out that thermal cycling rarely occurs by itself in nature. Even in desert climates, some moisture resulting from condensation is present, especially if temperature differences are high, such as  $40 \text{ }^\circ\text{C}$ , and the change occurs rapidly. Thus, the presence of moisture enhances the deterioration suffered by thermal cycling (Koch and Siegesmund 2004).

Rocks that contain hydrated minerals are also susceptible to thermal cycling because of the loss of the hydration water in these minerals. For example, alabaster, the massive variety of gypsum, was used in historical times for window panes before thin glass sheets became industrially available. These window panes also show deformation that can be attributed to the anisotropic thermal expansion of the constituting gypsum mineral ( $\text{CaSO}_4 \cdot 2\text{H}_2\text{O}$ ) over years of thermal cycling.

Other important hydrated minerals are clays, and many rocks contain them, ranging from marls to sandstones to volcanic tuffs. Heating these rocks results in the dehydration of these minerals and their consequent shrinking. However, this is not the main deterioration problem for these rocks, because clays are far more susceptible to the presence of water, as discussed in the following section.

### ***4.2.2 Hygric and Hydric Swelling***

All porous materials will adsorb water vapor from the atmosphere and expand. Although stone does not suffer this hygric expansion to the degree that wood does, it will still be affected by the inevitable cycling that it is subjected to by the normal changes in relative humidity in the air. Most affected by this process are the stones that contain clays, because their platy structure makes them particularly susceptible to retaining moisture between them.

Water vapor will diffuse into a porous material and be adsorbed onto the pore surface. Initially, a monomolecular water layer will develop that, because of its affinity to the mineral surface, does not behave as “normal” water, generally referred to as “bulk” water. If more water vapor is available, a second layer will form and then a third one. If the pores are very small, they may be totally filled

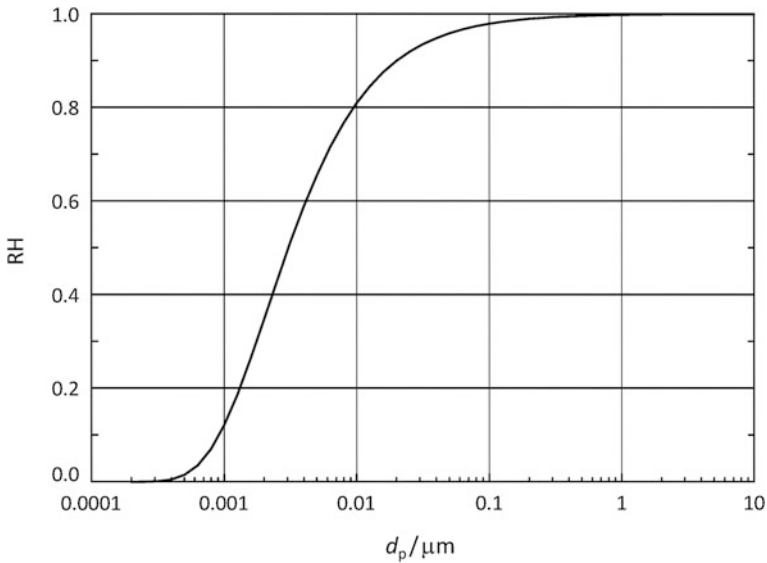


**Fig. 4.4** Capillary condensation for pores with various diameters  $d_p$  as calculated with the Kelvin-Thomson equation

with water by capillary condensation. The Kelvin-Thomson equation gives the relation between RH and the capillary radius and, plotted for cylindrical pores, gives the graph shown in Fig. 4.4.

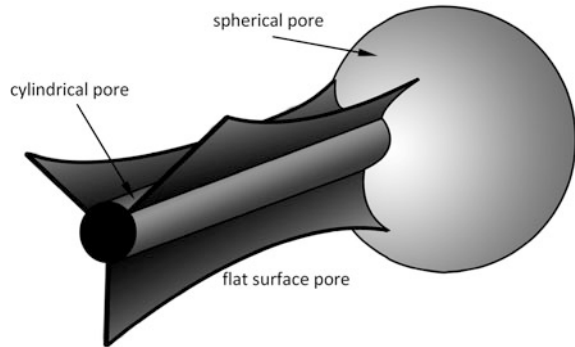
It can be seen that capillary condensation can occur at 10 % RH for pores of 1 nm diameter—for reference, the diameter of a water molecule is about 0.3 nm—while at 80 % RH, condensation occurs in pores one order of magnitude larger, i.e. 0.01  $\mu\text{m}$ . It is in about this range of RH that hygric expansion increases significantly, as illustrated in Fig. 3.47 for the Schöttmarer sandstone (Sect. 3.5). It is important to remember that, in pores  $>0.1 \mu\text{m}$ , water will already behave as bulk water (Stockhausen 1981), and capillary condensation will occur in these pores at 95 % RH. Therefore, hygric expansion will be of practical concern only when water starts to behave as normal water, i.e. bulk water, not adsorbed water.

Figure 4.4 shows a theoretical situation, and it should be remembered that pores in stone have many shapes (Fig. 4.5), and these will influence the behavior of the water in them (Bourgès et al. 2008).

Particularly in flat pores, for example at the boundary between two flat crystal surfaces and especially between thin, platy minerals such as micas, clays, and chlorites, capillary condensation is important. This explains the deterioration suffered by clay bearing stones, either sandstones or limestones, where spalling and delamination parallel to the bedding layer are the characteristic deterioration patterns (Rodríguez-Navarro et al. 1997; Sebastián et al. 2008).

For materials that do not contain clays or other phyllosilicates, the hygric expansion has been attributed to the disjoining pressure and corresponds to the

**Fig. 4.5** Diagram representing basic pore geometries, particularly for sandstones. Adapted from Bernabe (1991)

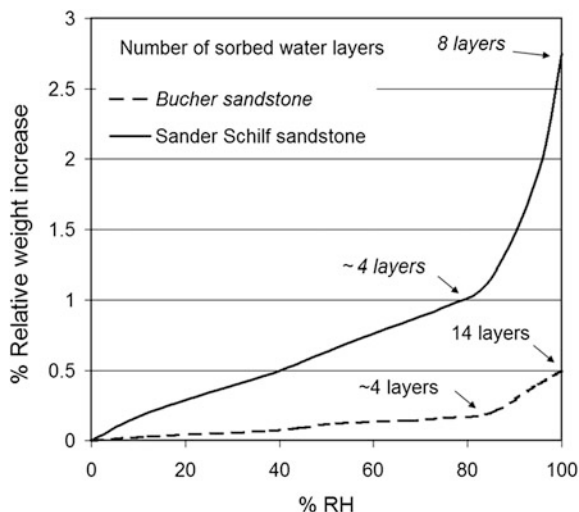


difference in pressure within a water film between two surfaces and the pressure of the bulk phase (Weimann 2001). The expansion has been attributed to the capillary condensation occurring in the micropore region; however, this is a controversial topic that has as yet not been elucidated (Ruedrich et al. 2005, 2011). The hygric behavior has been studied in detail for several German sandstones, many of them containing little or no clay, and a distinct correlation could be established between microporosity and hygric swelling. Hygric swelling increases with decreasing average pore radius and increasing microporosity. Furthermore, there is a distinct influence of the distribution of clays in the sandstones. When the clays are present in lithoclasts, they can transfer the stresses to the rock fabric. If the clays are merely coating quartz grains, their swelling will not be as critical since there is pore space to accommodate this phenomenon (Ruedrich et al. 2011).

Of the phyllosilicates that comprise micas, chlorites, and clays, the latter, because of their mineralogy, shape, and small size, tend to have cations, such as  $K^+$  or  $Na^+$ , adsorbed onto their surfaces to balance isomorphic substitution. The kaolinite group is the least expansive one because it has minimum substitution and a strong bonding between the tetrahedral and the octahedral layers. However, for the other clay groups, the liability of these interlayer exchangeable cations increases from the illite (or hydromica) group of clays to the montmorillonite (or smectite) group, i.e. the expansive clays. Furthermore, these expansive clays can form interstratification with non-swelling clays such as kaolinite and other phyllosilicates such as micas and chlorite, thus leading to significant swelling (Bühmann et al. 1988; Senkayi et al. 1981). Micas can also show interlayer swelling when  $K^+$  ions are replaced by  $Na^+$  (Sánchez Pastor et al. 2010). The expansive behavior of clays can occur via two different regimes: crystalline and osmotic swelling.

Crystalline swelling can occur in all types of clay minerals when they are exposed to changes in relative humidity. It is known to take place in discrete, stepwise formation of adsorbed water layers, and the resulting spacing transitions are thermodynamically analogous to phase transitions (Anderson et al. 2010). The distinct water layers, bonded between the cations and the negative charges of the clay particle surfaces, are more ordered, denser, and viscous than bulk water, being generally referred to as “structured” water (Stockhausen 1981; Madsen and

**Fig. 4.6** Water sorption curves for the coarse-pore Bucher sandstone and the mixed-pore Sander Schilf sandstone which also contains more phyllosilicates. Adapted and simplified from Sneath (1984). The number of sorbed water layers was calculated based on the amount of sorbed moisture that, in turn, reflect the specific surface area of the stones (2.63 and 14.8 m<sup>2</sup>/g, respectively). Note that, at the inflection point of the curve (approx. 80 % RH), both stones adsorbed the same number of water layers



Müller-Vonmoos 1989). A more detailed study of the water adsorption mechanism on swelling clays has found that, below 10 % RH, only the external clay surfaces are hydrated. At RH >10 %, water enters the interlayer space, hydrating the cations while also filling the interparticular porosity that falls into the 2–50 nm range (Salles et al. 2009). At what RH the whole pore system is covered with a water layer depends on the nature of the minerals present. For example, the amount of adsorbed water will vary with the interlayer cation in the order of  $\text{Li}^+ > \text{Cs}^+ > \text{Na}^+ > \text{K}^+ > \text{Ca}^{2+} > \text{Na}^+/\text{Ca}^{2+}$  and does not follow the hydration energy sequence for the cations in solution:  $\text{Li}^+ > \text{Na}^+ > \text{K}^+ > \text{Cs}^+$  (Salles et al. 2009). Crystalline swelling of montmorillonite can lead to a two-fold volume increase of this expansive clay (Madsen and Müller-Vonmoos 1989).

The influence of the presence of clays and of smaller pores is immediately evident in the different hygric water adsorption of sandstones shown in Fig. 4.6. The coarse-pore (most have 100  $\mu\text{m}$  radius) Bucher sandstone (95 % quartz, 5 % kaolinite) adsorbs far less moisture than the mixed-pore Sander Schilf sandstone (55 % quartz, 10 % feldspars, 5 % chlorite, illite, and muscovite, plus 35 % lithic fragments) with fine pores around 0.05  $\mu\text{m}$  and coarse pores around 50  $\mu\text{m}$  radius.

The inflection point of the curves falls around 80 % RH, and, at that point, both stones had only adsorbed approximately 4 water layers; this corresponds to an approximate thickness of 1 nm, indicating that pores of this size are already filled with water. It is at this point that the moisture content in the stone starts to induce hygric swelling as discussed previously for the Schöttmarer sandstone (see Fig. 3.47, Sect. 3.5).

The curves above are not representative of what actually happens in nature as it has been shown that equilibrium is rarely attained. From experiments with the calcareous Baumberger sandstone, it has been found that the stone surface–subsurface quickly changes moisture content upon RH changes (Franzen and Mirwald 2004), but an equilibrium moisture content about 8 cm in depth requires

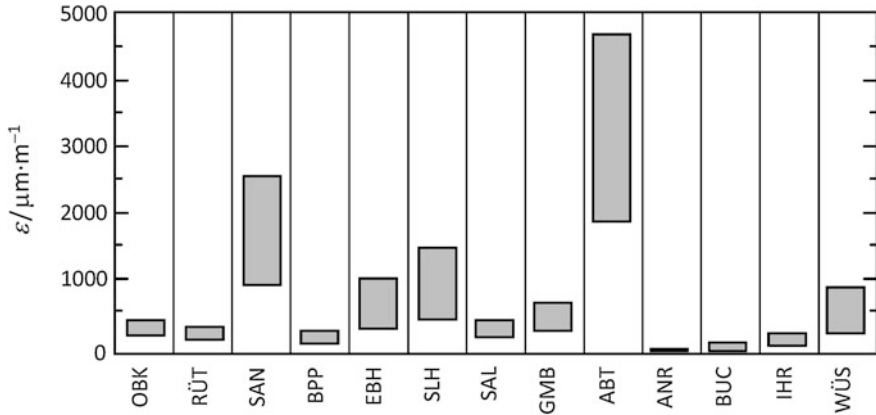


**Fig. 4.7** Hygric dilation  $\epsilon$  of various German sandstones (in parentheses, the binder type): OBK = Obernkirchener (silica); RÜT = Rühthener green (clay and silica with barite); SAN = Sander Schilf (clay); BPP = Burgpreppacher (silica); EBH = Ebenheider (silica and clay); SLH = Schleerither (clay); SAL = Saaler green (calcareous); GMB = Yellow Maulbrunner (clay); ABT = Abtswinder (clay); ANR = Anröchter green (calcareous); BUC = Bucher (silica); IHR = Ihrlersteiner green (calcareous); WÜS = Wüstenzeller (silica and clay). Adapted from Sneathlge and Wendler (1997)

2 weeks to be achieved (Chkirda et al. 1999). Nonetheless, hygric cycling over centuries will contribute to the weakening of the stone matrix.

Osmotic swelling is based on the repulsion between electric double layers and can act over larger distances compared to the 1 nm range of crystalline swelling, and is mostly relevant when liquid water is present. As the name indicates, this process is driven by the difference in concentration of the ions electrostatically held by the clay surface and those in the pore water of the rock. Significantly larger volume increases are observed ( $>2$  to  $\sim 13$  nm). The swelling behavior of clay in rocks depends on the type and amount of clay minerals present, their surface charges, and the cations in the double layer (Madsen and Müller-Vonmoos 1989). For example,  $\text{Na}^+$ -saturated smectites will swell far more than  $\text{K}^+$ -saturated ones (Anderson et al. 2010).

The hygric swelling of various German sandstones, including the ones previously mentioned, is shown in Fig. 4.7. Most of them show an expansion of some  $500 \mu\text{m}/\text{m}$ , except for the clay-bearing ones, where this value can increase tenfold, up to  $5,000 \mu\text{m}/\text{m}$  (Sneathlge and Wendler 1997). Further examples can be found in Chap. 3.

Based on the above, it would appear that wet-dry cycling will induce far more swelling, and, therefore, more deterioration to the stone matrix, than changes in relative humidity. Nonetheless, it has been suggested that crystalline swelling could, for some clay-bearing sandstones such as the Portland brownstone of the northeast US, known for its use in the construction of the typical row-houses in New York City, be the main mechanism for its deterioration (Wangler and Scherer 2008). This sandstone has long been known for its poor performance (Julien 1883)



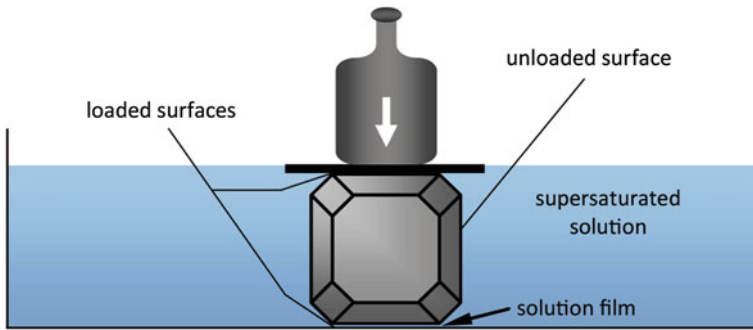


**Fig. 4.8** Growth of a loaded salt crystal

and has a hydric dilation, i.e. strain, perpendicular to its bedding of  $1,000 \mu\text{m m}^{-1}$  (Wangler and Scherer 2008). This result would appear to confirm the statement that the swelling stress from the crystalline process is far higher (ranging from  $400 \text{ N mm}^{-2}$  for the first to about  $30 \text{ N mm}^{-2}$  for the fourth adsorbed water layer) than the osmotic swelling (about  $2 \text{ N mm}^{-2}$ ) for montmorillonite clay (Madsen and Müller-Vonmoos 1989).

### 4.2.3 Crystal Growth

In the case of thermal and moisture cycling, stresses in the stone fabric are induced by expansion of the matrix constituents themselves. In this section, stresses that are induced by the formation and confined growth of new phases within void spaces in the fabric of building stones are considered. The pressure generated by growing crystals is called “crystallization pressure”. Apart from the crystallization of salts, such processes also include the growth of ice crystals upon the freezing of a pore solution.

It is generally accepted that the crystallization of salts is a major damage mechanism in stone. Although experimental evidence that growing crystals can exert pressure in porous materials was provided more than a century ago, until recently, there was no agreement among researchers regarding the nature of the process responsible for the generation of stress (e.g. see reviews of Evans 1970; Ginell 1994). However, in recent years, there has been substantial progress in understanding the thermodynamics of confined crystal growth and the generation of crystallization pressure (e.g. Scherer 1999, 2004; Flatt 2002; Steiger 2005a, b). The following paragraphs present a brief summary of the current state of knowledge.

Evidence that growing crystals can exert pressure was provided by the pioneering experiments of Becker and Day (1905, 1916); Taber (1916) and Correns and Steinborn (1939). The practical setup in these early experiments is illustrated in Fig. 4.8. It was observed that crystals submerged in their solutions and loaded

with additional weights continued to grow against the constraint. Thus, the confined crystals were able to generate stress. Important conclusions were drawn from these experiments. First, in order for a crystal to continue growing on its loaded surface, a solution film must exist, separating the loaded face from its constraint. Otherwise, deposition of matter and growth in this contact region is impossible. The solution film, originating from repulsive forces between the crystal and its constraint, acts as a diffusion path, allowing the exchange of ions between the solution and the crystal (Correns and Steinborn 1939; Scherer 1999).

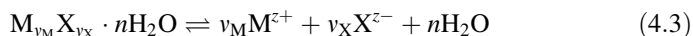
The second important conclusion drawn from the early experiments was that growth upon the loaded face of a crystal can only exert pressure if this face is in contact (via the solution film) with a supersaturated solution. The degree of supersaturation required for growth to occur increases with increasing load (Correns and Steinborn 1939). A thermodynamic treatment of the situation of a growing crystal that is subject to non-hydrostatic, anisotropic stress yields an equation for the pressure that is generated by a crystal confined in void spaces of a rock or any other porous material:

$$\Delta p = \frac{RT}{V_m} \ln S \quad (4.1)$$

Here, the crystallization pressure is defined as the difference between the pressure  $p_c$  upon the loaded face of a confined growing crystal and the liquid phase pressure  $p_l$ , i.e.  $\Delta p = p_c - p_l$ .  $R$  is the gas constant,  $T$  is the absolute temperature,  $V_m$  is the molar volume of the crystalline solid, and  $S$  is the degree of supersaturation in the liquid phase. Equation (4.1) is the most general equation for crystallization pressure. Its application requires an appropriate expression for the degree of supersaturation. For this purpose, the simple situation of a large crystal growing in a large pore where the liquid phase pressure equals the ambient pressure is considered. In this case, the supersaturation  $S = a/a_0$  is defined as the ratio of the activity  $a$  of the dissolved species in the supersaturated solution and the activity  $a_0$  of the saturated solution, thus yielding:

$$\Delta p = \frac{RT}{V_m} \ln(a/a_0) \quad (4.2)$$

For a dissociating solid of general composition



consisting of  $v_M$  positive ions  $M$  of charge  $z_M$ ,  $v_X$  negative ions  $X$  of charge  $z_X$ , and  $n$  molecules of water, the activity of the solid in an aqueous solution is given by the ion activity product:

$$a = a_M^{v_M} a_X^{v_X} a_w^n \quad (4.4)$$

where  $a_M$  and  $a_X$  are the activities of the cation and the anion, respectively, and  $a_w$  is the water activity. It should be noted that  $a_0$ , the activity of the saturated solution, is equal to the thermodynamic solubility product of the respective salt. Several

authors have used Eq. (4.2) to calculate crystallization pressures for different salts. However, many of these calculations contain errors that require further comments to avoid confusion. For example Correns and Steinborn (1939) were the first who recommended the use of Eq. (4.2) for the calculation of crystallization pressure. However, in their own calculations, they replaced activities in Eq. (4.2) with molar concentrations, overlooking the fact that salts are dissociating species and that, in concentrated solutions, molar concentrations differ significantly from the ion activities. This resulted in quite substantial errors (Steiger 2005a, 2006a; Flatt et al. 2007). For example, neglecting dissociation leads to an underestimation of the crystallization pressure by a factor of two in the case of 1–1 salts such as NaCl or KNO<sub>3</sub>. For salts with more complicated stoichiometry, the error is even greater. The influence of the non-ideal behavior in crystallization pressure calculations is discussed in some detail by Steiger (2006a) and Flatt et al. (2007).

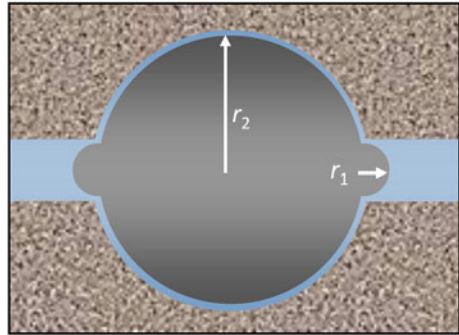
Later Winkler and Singer (1972) and Winkler (1994) presented extensive calculations of crystallization pressures for a number of different salts. However, their calculations are also erroneous for several reasons. First, in their calculations, salts were treated as non-dissociating species, and the non-ideal behavior of their concentrated solutions was neglected. Second, they extended their calculations to entirely unrealistic supersaturation. For example, they list calculated crystallization pressures for supersaturation ranging from 2 to 50 (based on concentration ratios of undissociated solids). Such high supersaturations have no practical relevance and do not even exist for most of the salts listed in their tabulation. For instance, in the case of NaCl, the supersaturation of 50 used by Winkler and Singer (1972) for their calculations refers to a “solution” consisting of about 18 g NaCl per g of water! In contrast, the maximum known concentration that was achieved by evaporation from levitated droplets (Tang 1997) was in the order of 0.8 g NaCl per g H<sub>2</sub>O.

The unrealistic supersaturations in the calculations of Winkler and Singer (1972) caused severe criticism (Lewin 1974; Snethlage and Wendler 1997), and, subsequently, many authors preferred an apparently different damage mechanism previously suggested by Everett (1961). Based on the properties of curved interfaces between crystal and solution and assuming spherical geometry, Everett derived the following equation for the crystallization pressure:

$$\Delta p = 2\gamma_{\text{cl}} \left( \frac{1}{r_1} - \frac{1}{r_2} \right) \quad (4.5)$$

Here,  $r_2 > r_1$  are the radii of two crystals in adjacent pores of different sizes (see Fig. 4.9), and  $\gamma_{\text{cl}}$  is the surface free energy of the crystal-liquid interface. Many researchers preferred this equation, probably because it is apparently more realistic to calculate crystallization pressures on the basis of a measurable quantity such as the pore-size distribution than to estimate the degree of supersaturation in a pore solution. Only a few authors have pointed out that both approaches are entirely equivalent (Scherer 2004; Steiger 2005b). Recently, it has been shown (Steiger 2005b, 2006a) that Eq. (4.5) can be directly derived from Eq. (4.2) by comparison of the different solubilities of crystal surfaces in large and in small

**Fig. 4.9** Large crystal growing in a spherical pore (radius  $r_2$ ) with small cylindrical pore entrances (radius  $r_1$ )



pores (see Fig. 4.9). It has been further shown that Eq. (4.5) is a special case of the more general Eq. (4.2), and equations were also derived for other pore geometries, e.g. cylindrical pores.

The major difference between the more general case of crystallization pressure represented by Eq. (4.2) and the situation in a large pore with small entries as shown in Fig. 4.9 is the fact that the former situation represents a non-equilibrium situation. The crystal shown in Fig. 4.8 can only generate stress as long as the solution is supersaturated. This solution is then just in equilibrium with the crystal face under pressure, but is supersaturated with respect to the unloaded faces of the crystal. Therefore, the crystal continues to grow upon its unloaded faces, and the high concentration required for stress upon the loaded crystal faces to be generated cannot be maintained. As long as unloaded crystal faces are present, the evolution of crystallization pressure in a porous material is a dynamic process that is determined by kinetic influences such as evaporation and cooling rates, the diffusion of ions in the free solution and in the liquid film, the availability of unloaded crystal surface, and the growth rates on unloaded faces. Under such conditions, it is very unlikely that crystallization pressure builds up and remains constant over long periods of time. More likely, high pressures occur as transients if high supersaturation in the pore solution evolves temporarily as a result of sharply dropping temperatures or rapid evaporation. Amplitude and duration of stress maxima are, therefore, dependent on the parameters controlling the degree of supersaturation.

In contrast, the crystal shown in Fig. 4.9 represents an equilibrium situation. Growth of the crystal into the small pore entrances requires a higher concentration of the pore solution due to the greater solubility of the small satellite crystals. At equilibrium under ambient pressure, the concentration in the surrounding solution is just equal to the solubility of the hemispherical crystal of size  $r_1$ . However, this solution is supersaturated with respect to the unloaded large crystal. Therefore, stress is generated due to growth of the confined crystal in the large pore until equilibrium is reestablished. At equilibrium, the solution is saturated with respect to both crystal faces. However, due to their different sizes, the particle in the pore entrance is under ambient pressure, while the large particle must be under enhanced pressure. This is an equilibrium situation, and the result is a static crystallization pressure. However, it should be noted that the equilibrium

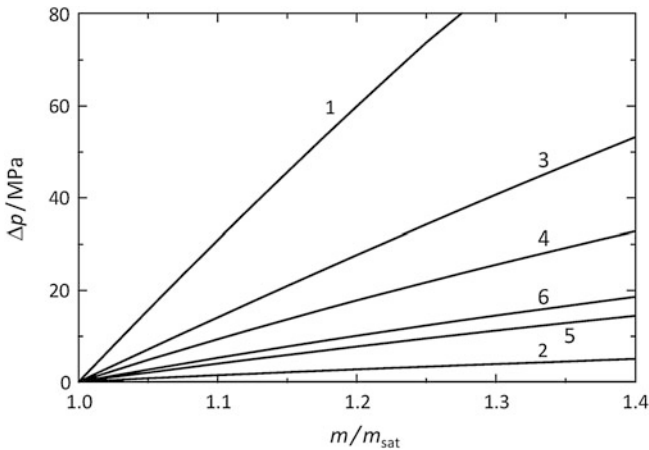


**Fig. 4.10** Crystallization pressures at 25 °C in supersaturated solutions of 1 NaCl (halite), 2  $\text{Na}_2\text{SO}_4 \cdot 10\text{H}_2\text{O}$  (mirabilite), 3  $\text{Na}_2\text{SO}_4$  (thenardite), 4  $\text{NaNO}_3$  (nitratine), 5  $\text{MgSO}_4 \cdot 7\text{H}_2\text{O}$  (epsomite), and 6  $\text{MgSO}_4 \cdot 6\text{H}_2\text{O}$  (hexahydrite). Adapted from Steiger (2005a); supersaturation is expressed as the ratio of the molality  $m$  of the supersaturated solution and the saturation molality  $m_{\text{sat}}$  of the respective salt

crystallization pressure requires the presence of very small pores, preferably with pore radii smaller than about 50 nm.

Crystallization pressures for several salts commonly found in building stone are depicted in Fig. 4.10. They are taken from Steiger (2005a) and were calculated using Eqs. (4.2) and (4.4) together with an electrolyte solution model to account for the non-ideal behavior of highly concentrated solutions. If these pressures are generated in a porous stone, they induce tensile stress within the solid matrix that might eventually exceed the strength of the stone. As a first indicator, the crystallization pressures may be compared to the tensile strengths of natural stones that hardly exceed values of about 3–5 MPa (see Sect. 3.6). Therefore, the pressures shown in Fig. 4.10 may be sufficient to cause damage in nearly every building stone. A more sophisticated treatment is based on the theory of poromechanics (Coussy 2004; Espinosa-Marzal and Scherer 2009). Applying this theory, it has been recently shown that there is reasonable accordance between calculated crystallization pressures using Eq. (4.2) and the crystallization pressure derived from deformation measurements (Espinosa-Marzal and Scherer 2010; Espinosa-Marzal et al. 2011).

Are the high supersaturations required for crystallization stress to be induced likely to occur in the pore solutions of building stones? First of all, according to nucleation theory (Nielsen 1964), a certain degree of supersaturation is always required in order for nucleation and crystal growth to occur. In fact, very high critical supersaturations in sodium sulfate and sodium carbonate pore solutions subject to cooling were determined experimentally (Rijniers et al. 2005; Espinosa-Marzal and Scherer 2008). The observation of both stable and metastable crystalline phases in the same pores during evaporation of sodium sulfate solutions from porous stone

(Rodriguez-Navarro and Doehne 1999; Rodriguez-Navarro et al. 2000) also provides clear evidence of the presence of extremely high supersaturations.

It is also possible to design laboratory salt damage experiments in such a way that crystal growth occurs under conditions of very high supersaturation. One prominent example of this is the classical sodium sulfate durability test for building materials (e.g. RILEM PEM-25 1980) or similar tests as reviewed by Goudie and Viles (1997). Typically, in such tests, a porous material is impregnated with a sodium sulfate solution and dried at an enhanced temperature (e.g. 60–105 °C) such that anhydrous  $\text{Na}_2\text{SO}_4$  is formed. Subsequently, after cooling to room temperature, the specimen is impregnated again with a  $\text{Na}_2\text{SO}_4$  solution leading to the hydration of  $\text{Na}_2\text{SO}_4$ . Repeating this procedure several times, sodium sulfate has been proved to be extremely destructive, and it was observed that most of the damage occurred during the impregnation phase (Schmölzer 1936; de Quervain and Jenny 1951). It is now accepted that the destructive effect is due to the growth of mirabilite crystals from the highly supersaturated solutions originating from the dissolution of anhydrous sodium sulfate during the re-wetting phase (Chatterji and Jensen 1989; Flatt 2002). Under such conditions, a crystallization pressure of 15 MPa at 20 °C can be calculated (Steiger and Asmussen 2008), which is in good accordance with the pressure derived from deformation measurements (Espinosa-Marzal et al. 2011). The crystallization pressure calculations also confirm the strong influence of temperature in the sodium sulfate crystallization test, as observed by several investigators (Price 1978; Chatterji and Jensen 1989; Tsui et al. 2003).

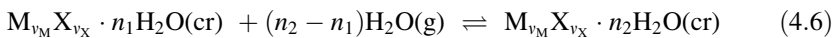
The sodium sulfate crystallization test has been studied extensively to understand the reason for the amount of deterioration it induces. Among these studies, that of Angeli et al. (2008) has been able to provide a clear picture of the induced damage. Through careful analysis of the weathered samples via microscopic observation, both optical and SEM, and mercury intrusion porosimetry, MIP, it has been shown that the porosity after weathering (and after having washed out the salt) is higher than prior to it. From weathered samples that still contain the salt, it was possible to determine in which pore types the sodium sulfate would crystallize, to calculate the pore space occupied by thenardite (since the MIP operates under a vacuum), and to estimate from this the pore space that would have been occupied by mirabilite during the wetting cycle. It was further found that most of the pores were affected by the crystallization of the salt and that a crystal growing in smaller pores (up to several microns) is capable of exerting sufficient pressure to start or propagate a crack. While, in general, stones with smaller pores (up to several microns) are more susceptible to deterioration, there are exceptions when the stone has a high overall porosity, or a low pore connectivity and high tortuosity. Finally, the pre-existing cracks in the stone matrix will accelerate the deterioration if all the other parameters are equal.

Apart from the theories addressing the mechanism that underlies the observed damage in porous materials, it is of practical relevance to find a methodology to quantify and estimate the actual damage that is observed with the standard salt crystallization test using sodium sulfate. For this purpose, a study on various types



of stones was carried out, and the results obtained were carefully analyzed. Three stages were identified during the salt crystallization test: the initial weight increase because of the introduction of salt into the material, the first visual appearance of deterioration including weight variation—a stage that sometimes merges directly with the last one, wherein the weight decrease is continuous as deterioration progresses. These stages reflect the type and degree of deterioration that could be quantified by two indicators: the alteration index (AI) and the alteration velocity (AV). The former correlates the capillary and evaporation coefficient with the lowest mechanical strength, i.e. tensile strength, of the sample. The alteration velocity can be measured via the P-wave velocity, but it has to be taken into account that comparisons can only be made between stones of similar composition given the difference of the P-waves for quartz and calcite. This method allows differentiating stones that have a high AI, but those having a low AV will be more resistant in the long term than others with a low AI and a high AV. Important points to consider are the size and shape of the samples and the fact that these indicators apply only to deterioration by sodium sulfate crystallization (Angeli et al. 2007). Other critical factors in the deterioration induced in a porous material are its characteristics. To determine the most important ones, principal component analysis, PCA, was performed on various rock types, ranging from a quartz sandstone to a calcite or a dolomite sandstone to a calcite quartz conglomerate. Various parameters were measured for them, such as pore size, specific surface, connected porosity, bulk density, and real density. Additionally, mechanical properties and water transport characteristics were determined. Salt crystallization tests were included in the study as well. Through PCA, two principal components were identified that accounted for 86.5 % of the total variance. The first one was linked to mechanical properties, porosity and density, while the second one was associated with water transport and pore structure. Both of them included the dry weight loss (DWL) from standard salt crystallization tests. A multiple regression analysis showed that rock strength has a predominant statistical weight for predicting deterioration induced by salt crystallization, while water transport characteristics and pore structure parameters have a minor influence (Benavente et al. 2007).

Several common salts can exist in different hydrated forms. Hydrated salts that are commonly found in building materials include the series  $\text{Na}_2\text{SO}_4 \cdot n\text{H}_2\text{O}$ ,  $\text{MgSO}_4 \cdot n\text{H}_2\text{O}$ , and  $\text{Na}_2\text{CO}_3 \cdot n\text{H}_2\text{O}$ . The general form of a hydration reaction is given by



The equilibrium constant for this reaction is

$$K = \frac{p_{w,0}}{p_{w,\text{eq}}} = \frac{1}{\text{RH}_{\text{eq}}} \quad (4.7)$$

where  $p_{w,\text{eq}}$  is the equilibrium water vapor partial pressure,  $p_{w,0}$  is the saturation water vapor pressure, and  $\text{RH}_{\text{eq}}$  is the equilibrium relative humidity for the hydration–dehydration equilibrium of the two hydrates with  $n_1$  and  $n_2$  molecules of

water. If the lower hydrated form is confined to void spaces of a porous material, pressure can be generated during the hydration reaction. The maximum hydration pressure  $\Delta p_{\text{hydr}}$  that can be exerted by the growing hydrated crystal is given by

$$\Delta p_{\text{hydr}} = \frac{\Delta n RT}{\Delta V_m} \ln \left( \frac{\text{RH}}{\text{RH}_{\text{eq}}} \right) \quad (4.8)$$

where  $\Delta V_m$  is the difference in the molar volumes of the two solids,  $\Delta n = n_2 - n_1$ , RH is the relative humidity at which the hydration reaction proceeds, and  $\text{RH}_{\text{eq}}$  is the equilibrium value at temperature  $T$  as defined in Eq. (4.7). The hydration pressure is the pressure that would have to be exerted on the hydrated crystal to prevent its growth. In other words, RH is the equilibrium relative humidity of the hydration–dehydration equilibrium if the vapor phase is under ambient pressure  $p_a$  and the solid phases are under the enhanced pressure  $p_c$ ; thus,  $\Delta p_{\text{hydr}} = p_c - p_a$  (Steiger et al. 2008a). It is important to note that the driving force for the hydration pressure is also supersaturation. While the supersaturation of a solution is the driving force for the crystallization pressure, it is the water vapor supersaturation of the ambient air with respect to the equilibrium water vapor pressure of the hydrated salt which is responsible for the generation of hydration pressure.

Equation (4.8) was first derived by Mortensen (1933); later, it was misused by calculating very high hydration pressures at relative humidities close to 100 % (Winkler and Wilhelm 1970; Winkler 1994). In these calculations, the upper limit of the ambient RH due to the deliquescence of both the educt and the product phases, was overlooked (Steiger 2003). If a salt is subjected to a slowly increasing relative humidity, a point will be reached—the deliquescence or saturation humidity—where the solid picks up water vapor forming a saturated solution. Hence, above the deliquescence relative humidity, DRH, of the product phase, i.e. the higher hydrated form, a solid cannot exist anymore and, consequently, there is no hydration pressure at all. On the other hand, if the DRH of the educt phase is exceeded, a solution supersaturated with respect to the product phase is formed, and the hydration reaction follows a two step reaction mechanism including the dissolution of the lower hydrated form ( $n_1$ ) and subsequent crystallization of the hydrate ( $n_2$ ) from a supersaturated solution (Steiger 2003). In this case, the pressure generated by the hydrated crystal is a crystallization pressure, according to Eq. (4.2). The supersaturation is given by the concentration of the solution in the vicinity of the growing hydrated crystal which is determined by the dissolution rate of the anhydrous (or lower hydrated) crystal, the growth rate of the hydrate, and the diffusion rate of the ions to the surface of the hydrated crystal (Steiger et al. 2008a).

#### 4.2.4 Combination of Factors

The previous sections discussed the different processes involved in the deterioration of stone through mechanical stresses. However, in nature, these seldom act alone, and the observed damage is the result of their interaction. One of the difficulties

**Table 4.3** Comparison of thermal and hydric expansion of different rock types

Rock type		Thermal expansion coefficient ( $\mu\text{m} \times \text{m}^{-1}\text{K}^{-1}$ )	Thermal expansion $\Delta T = 40 \text{ K}$ ( $\mu\text{m} \times \text{m}^{-1}$ )	Hydric expansion ( $\mu\text{m} \times \text{m}^{-1}$ )
Magmatic		8	320	49
Metamorphic	Marble	105	420	70
	Siliceous	8.5	340	500
Sedimentary	Limestone	4	160	70
	Travertine	5	200	20
	Sandstones	11	440	1000

Based on data from Weiss et al. (2004a)

Thermal expansion is calculated for a 40 °C temperature change, assuming linear behavior of the thermal expansion coefficient. Hydric expansion values correspond to maximum water absorption by capillarity (ranging between 1 min and 16 h depending on the stone type) and measurements were made perpendicular to foliation (based on data from Weiss et al. 2004a)

faced when trying to find a remedy to a problem is the identification of the key deteriorating factor, or, if there are several, as is more likely, then it is important to know if these act simultaneously or sequentially (Koestler et al. 1994).

To follow the order used previously, the first combination considered will be that of thermal cycling in conjunction with water. For this purpose, it is important to bear in mind the ranges of expansions that can be expected under normal conditions as summarized in Table 4.3.

For the specific case of marbles, wherein thermal expansion is more relevant than the hydric one, the residual strain left in marbles after thermal cycling decreases after the first cycle; however, if moisture is present, there is a progressive increase in the residual strain. Furthermore, there is no correlation between the amount of residual strain remaining after dry and wet cycling (Koch and Siegesmund 2004). However, a correlation could be detected between the bowing tendencies of different marble types with the residual strain measured from the wet thermal cycling experiments mentioned. The amount of deterioration, and of bowing, can be correlated with the marble fabric. Therefore, the type of marble, the presence of moisture, and thermal cycling all interact in the deterioration and, in the case of marble slabs, their deformation tendencies (see Sect. 3.4.2).

The effect of long-term freeze–thaw cycling for marbles has been studied by Ondrasina et al. (2002). The resulting deterioration ranges from a superficial sugaring to a complete loss of cohesion along grain boundaries. The study was carried out on three marbles, Palissandro (a dolomitic marble containing phlogopite and quartz with pronounced foliation), Sterzing (a calcite with some dolomite and muscovite, slightly foliated marble) and Carrara (a fine-grained calcite marble with thin grayish veins). The samples were left for 6 h at  $-20 \text{ }^\circ\text{C}$ . After this, they were stored in a water bath at  $20 \text{ }^\circ\text{C}$  for 2 h. In total, 204 cycles were carried out. The change in their porosity was interesting. While the Sterzing and the Carrara marbles showed a continuous increase in porosity as a function of the number of cycles, the Palissandro marble showed its first increase after 24 cycles

and subsequently did not change significantly. The Carrara marble also showed a significant decrease in the elasticity modulus between the 5th and the 7th cycles, followed by another around the 115th cycle, while the other two marbles did not show such changes, a fact that can be attributed to their dolomite content. The decrease in the elasticity modulus of the Carrara marble correlated to its increase in porosity. This is also a result of the straight grain boundaries of this marble, which results in crack formation along them. The other two marbles, with curved and interlocked grain boundaries, are more resistant to freeze–thaw cycling.

Dolomitic marbles that contain localized inclusions of mica and amphibole minerals, especially prismatic tremolite, are prone to what is called “pock marking”, a larger form of pitting. This minor deterioration pattern has been observed in many historical buildings in the northeast US where it freezes, but not in corresponding buildings in the southeast. The damage could, therefore, be attributed to the preferential moisture retention by the platy mica and the fibrous tremolite, which, upon freezing, leads to their detachment, leaving a rounded pock mark behind (Lewin and Charola 1981).

An important point that has to be taken into account when dealing with stones in historical structures is their microenvironment. This point was studied in detail by Turkington et al. (2002). Experiments were carried out on two blocks of Hollington sandstone, an iron-rich quartz sandstone. These were located in a cabinet, and their moisture and temperature were measured as they were subjected to changes in RH and temperature, attained by heating with an infrared lamp that was turned on and off at 15 min intervals. The experiments were run with the blocks dry and with the blocks saturated in water. Furthermore, the blocks were first set flush so that they both received full light, and then the bottom one was recessed progressively until it was totally in the shade while the top one remained in the light. The depth and steepness of the thermal gradient established in the near-surface of the stone depends on the thermal properties of the stone and the thermal regime applied. If the stone is in the shade, the amplitude between maximum and minimum temperatures decreases. Nonetheless, steep gradients are still created when environmental temperatures fluctuate and may cause significant stress to the stone. When moisture is present, the thermal gradients are enhanced, since the subsurface layers are slower to respond to indirect heating, i.e. when the blocks are in the shade. Thermal stress is not reduced in these cases, but it is limited to the surface layer. This is relevant in the case of the presence of salts, as these will concentrate at the subsurface layer.

For rocks containing phyllosilicates, such as slates and sandstones, the hygric expansion can be twice as high as the thermal expansion. To illustrate this point, the interesting experimental study combined with numerical modeling carried out by Ožbolt et al. (2008) will be summarized. The aim of the study was to determine the location of crack formation in Heilbronner Schilf sandstone quarry samples. The stone is a fine-grained arenite to feldspar arenite with chlorite cement and secondary feldspar to feldspar cement and has a medium–high compressive strength and elasticity modulus. The study considered hygric, hydric, and thermal cycling, including freezing. One of the samples was constantly monitored via

Acoustic Emission Analysis (AEA) during the cycling to determine when cracks were forming. This proved to occur primarily upon heating after a freezing cycle or during freezing of the water-saturated sample. The most critical stresses were induced during fast changes in temperature when the sample was saturated with water. The fast and high water uptake and the consequent swelling of the sample in combination with rapid heating or drying triggered the crack formation in the sample. Cracks developed preferentially in sharp spikes (notches) and corners (acute angles) of the profiled part of the specimen, and stiff but brittle layers, such as diagenetic iron cementations, also served as points for crack initiation. Crack propagation follows the bedding layering of stone; therefore, stone anisotropy is an important factor to be taken into account. The numerical modeling suggests that the thermal cycling alone does not cause any damage, but, coupled with increased water content, it does more damage than hygric-hydric cycling alone. An important factor is the moisture gradient from the surface to the interior, which causes significant damage.

The aforementioned study did not address the formation of ice, and, to understand the deterioration that freezing water can induce in porous buildings, the crystallization of ice is discussed first.

#### 4.2.4.1 Crystallization of Ice

In contrast to widespread belief, crystallization pressure, not the hydraulic pressure that is caused by the volume expansion during freezing of water, is the primary cause of frost damage (Taber 1929; Everett 1961; Walder and Hallet 1986). The mechanisms of frost damage have been recently reviewed by Scherer and Valenza (2004). A strong argument that crystallization pressure is the primary source of stress during freezing comes from experiments with organic liquids that contract upon freezing (Taber 1930; Beaudoin and MacInnis 1974; Litvan 1978). In these experiments, dilation and damage of various porous materials were observed with liquids that were less dense than their respective solid phase. In this case, the damage can only be explained in terms of crystallization pressure.

Just as in the case of salt crystallization, the crystallization pressure that can be exerted by a confined ice crystal requires that the crystal be in contact with a supersaturated solution. However, in the case of a freezing liquid, the supersaturation is usually expressed in terms of the supercooling of the liquid phase, i.e. the temperature difference between the liquid film at the ice crystal-pore wall interface and the equilibrium freezing temperature. The crystallization pressure generated by an ice crystal in contact with supercooled liquid water is given by

$$\Delta p = \frac{S_l - S_{ice}}{V_{m,ice}} (T_f - T) \quad (4.9)$$

where  $S_l$  and  $S_{ice}$  are the entropies of liquid water and ice (respectively),  $V_{m,ice}$  is the molar volume of ice,  $T_f$  is the freezing temperature, and  $T$  is the temperature of

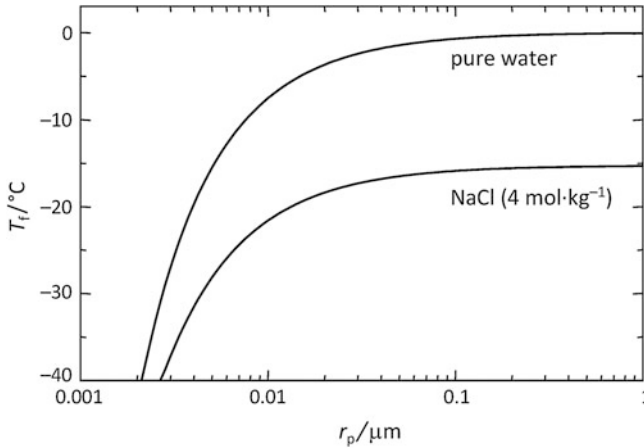


**Fig. 4.11** Freezing temperatures ( $T_f$ ) of water and aqueous NaCl as a function of pore size in a saturated porous material. Adapted from Steiger (2006b)

a supercooled liquid film between the growing ice crystal and the pore wall. It should be noted that the freezing temperature of water is strongly affected by the concentration of dissolved salts, as discussed in more detail below. The supercooling of water in an aqueous solution can also be expressed in terms of supersaturation, i.e. the activity of the water in the supercooled solution. This yields the following equation for the crystallization pressure of a growing ice crystal (Steiger 2004):

$$\Delta p = \frac{RT}{V_{m,\text{ice}}} \ln(a_w/a_{w,0}) \quad (4.10)$$

where  $a_w$  is the water activity in the liquid film, and  $a_{w,0}$  is the water activity of the saturated solution at the same temperature, i.e. the water activity of the solution in equilibrium with ice at its freezing temperature. While for pure water  $a_w = 1$ , in salt solutions the water activity is determined by the dissolved salts. In effect, there is a substantial depression of the freezing temperature with an increasing concentration of dissolved salts (see the following section).

In a porous material, there is no uniform temperature at which the pore water freezes. Apart from the concentration of dissolved salts, the freezing temperature is also affected by pore size. A small ice crystal, i.e. a crystal growing in a small pore, has a higher chemical potential and, therefore, a lower freezing temperature than a large crystal. Figure 4.11 depicts freezing temperatures of pure water and of a NaCl pore solution. It is obvious that there is a strong depression of the freezing temperature with decreasing pore size. Therefore, in a porous stone, pure water starts to freeze in large pores and at temperatures only slightly below 0 °C. In small pores (<0.1  $\mu\text{m}$ ), water only freezes at significantly lower temperatures, as shown by the upper curve in Fig. 4.11. The same effect is also responsible for



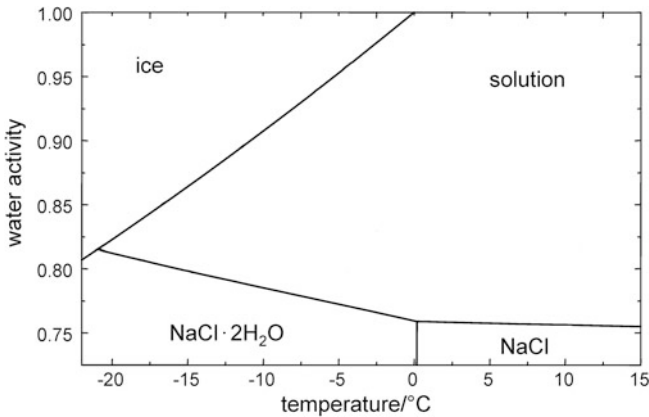


**Fig. 4.12** Phase diagram of a sodium chloride solution. Concentration of sodium chloride increases with decreasing water activity. Adapted from Steiger (2004)

the low freezing temperature of salt solutions in small pores. In contrast, there is a significant depression of the freezing temperature in large pores due to the dissolved NaCl.

Similar to the case of growing salt crystals, the pore size dependence of the freezing temperature can be used to derive an expression for the crystallization pressure in small pores from Eq. (4.10). For example Eq. (4.5) applies to the case of a large spherical pore with small entrances. In fact Eq. (4.5) was first derived by Everett (1961) for the special case of frost damage, i.e. the crystallization of ice in porous materials. Different equations may be derived for other pore geometries, e.g. cylindrical pores (Scherer 1999, 2004; Steiger 2006b).

#### 4.2.4.2 Ice Crystallization in Combination with Clays or Salts

It is well known that a salt solution will freeze at a lower temperature than pure water and that the decrease in temperature is proportional to increasing salt concentration—hence, the use of NaCl or CaCl<sub>2</sub> as deicing salts to keep pavements free of ice. About 50 % of the world's production of NaCl (estimated at 210 million metric tons) is used for this purpose with the unfortunate result that the salt solutions migrate into neighboring buildings with the consequent introduction of these salts into the masonry and its subsequent deterioration.

Figure 4.12 shows the equilibrium diagram for a sodium chloride solution at different relative humidities, reflected by the water activity of the solution and temperature. Sodium chloride crystallizes as such above 0 °C but, as a dihydrate, below that temperature. The  $a_w = 1$  top line corresponds to pure water that freezes at 0 °C. With an increasing sodium chloride concentration, the water activity decreases, and the freezing temperature for ice is shifted below 0 °C.

The graph is valid for a salt-water system. In a porous body, this may vary as a function of the pore diameter. The freezing temperature depression of a salt solution has been calculated to be constant for pore sizes down to 0.1  $\mu\text{m}$  in diameter, i.e. pores that are just at the edge of the capillary pore size (see Fig. 4.11 and Steiger 2006b) so that, for larger pores, the diagram above may be considered valid.

There has been some controversy regarding whether the presence of salts accelerates the damage induced by pure freeze–thaw cycles (Goudie and Viles 1997) since some early laboratory experiments showed that salts could actually reduce the amount of damage (McGreevy 1982). However, subsequent studies have shown that samples from various beds from the same quarry of fine-grained, quartzose sandstone were more damaged when subjected to freeze–thaw cycling where salts, either sodium chloride or sodium sulfate, were present than when only water was present. In general, more deterioration was observed when the samples were vacuum-impregnated with water or the salt solution (Williams and Robinson 1981). Further studies with other salts have confirmed that NaCl is one of the most deteriorating salts under freeze–thaw conditions, and this was attributed to the crystallization of the dihydrate salt (Williams and Robinson 2001). Studies carried out on chalk samples, wherein different salts, such as NaCl,  $\text{MgSO}_4$ ,  $\text{Na}_2\text{SO}_4$ , and mixtures of them were subjected to various freeze–thaw cycles with varying conditions and temperatures (minimums were  $-10$  and  $-30$   $^{\circ}\text{C}$ ), showed that intense freezing conditions caused more damage than milder conditions and that, in general, the presence of salts increased the observed damage, though the amount of damage depended on the type of salt (Jerwood et al. 1990a). These results were confirmed in subsequent studies carried out under non-saturation conditions that proved less damaging (Jerwood et al. 1990b).

Laboratory freeze–thaw tests carried out with various types of sandstones showed that conventional tests provide limited information regarding the deterioration mechanism occurring within the porous matrix. Mostly, the results reflect the presence of weak areas in the stones, such as discontinuities and preexisting microcracks. The study carried out by Ruedrich and Siegesmund (2007) measured the length change of the samples, both dry and saturated in water prior to freeze–thaw cycling. During dry freeze–thaw cycling, the samples show a linear contraction with decreasing temperatures, from 20 to  $-20$   $^{\circ}\text{C}$ . This behavior changes for water-saturated samples that, upon cooling, first show an expansion at about  $-2$   $^{\circ}\text{C}$  that could be attributed to ice crystallization. This was followed by a subsequent contraction at around  $-7$  to  $-12$   $^{\circ}\text{C}$ , depending on the type of sandstone, which was ascribed to the pressure solution and recrystallization of the ice crystals. Upon heating, an expansion occurs at around 3  $^{\circ}\text{C}$ , followed by a contraction that reaches its maximum at 7  $^{\circ}\text{C}$ . This behavior was followed by most of the sandstones containing some clays and with smaller capillary as well as micro-pores. For sandstones with higher clay content, a significant contraction was observed for the subsequent cooling to  $-20$   $^{\circ}\text{C}$  and was attributed to the clay-bound water that does not freeze.

Samples with different water content were also tested. For some stones, a 70 % water content leads to behavior similar to that at full saturation, and strong residual strains were measured in the first cycle that resulted in macrocrack formation.

Furthermore, the water content determined the length change measured on the samples upon freezing. Also investigated was the influence of the cooling rate. One of the effects was the moving of the expansion maxima from  $-4$  to  $-7$  °C when the cooling rate was increased from  $0.05$ – $0.5$  K min<sup>-1</sup>. However, the more slowly cooled samples showed the highest absolute length change.

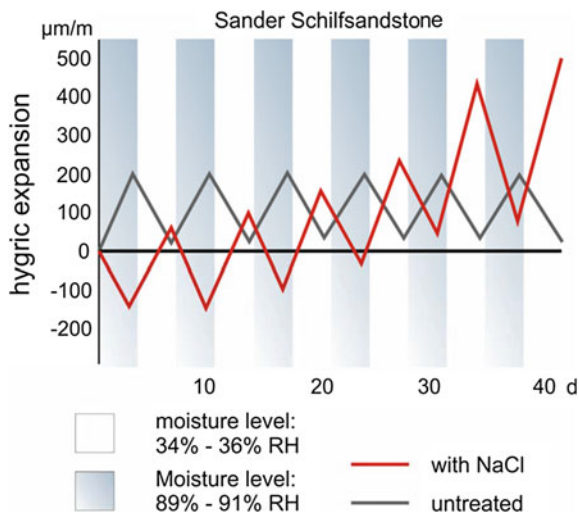
Field experiments were carried out in Antarctica using welded tuff cubic samples that were either pretreated with water or saturated with solutions of halite, thenardite, or gypsum, respectively, for a week (Matzuoka et al. 1996). Then they were exposed on the ledges of rock walls, where there is a limited supply of moisture. Thus, the samples equilibrated within a few days to the ambient conditions. As a reference, the moisture content in the rocks on site was around 35 %. After 4–5 years, little damage had been suffered by the water-pretreated or gypsum solution saturated samples, while those treated with the thenardite solution had cracked and their edges rounded, and the halite-treated ones had disintegrated completely. The limited damage suffered by the two former samples was attributed to the low moisture available on site, since the tuff had suffered severely during laboratory freeze–thaw cycling (Matzuoka et al. 1996). This data is corroborated with laboratory studies of other tuffs where the amount of water in the sample prior to freeze–thawing is critical (Van Hees et al. 2004).

As usual, the situation for stones in outdoor masonry is different. First of all, the distribution of salt is not homogeneous in the stones, with the subsurface, in general, holding a higher concentration of salt. Since the salt in question is most likely sodium chloride from the application of deicing salts, its concentration will be higher at ground level. Secondly, while freezing or below-freezing temperatures will be found at the surface, the interior of the stone may not be at subzero values. However, if the subzero temperature is relatively constant for some days, then this temperature may already be found some distance into the stone. During the day, if the sun is shining, the surface of the stone may thaw, with a resulting expansion, while the subsurface will continue to be frozen and contracted. This will induce stresses at the freezing front that will result in the typical spalling observed. Furthermore, as the solutions in the stone are not likely to be saturated, as ice forms, the solution will concentrate, lowering the freezing temperature of the remaining solution. Therefore, it is difficult to determine which factor is the most relevant for the particular deterioration observed.

#### 4.2.4.3 Salts and Moisture Changes

Hygic expansion is mostly relevant for phyllosilicates, particularly clays, as discussed in Sect. 4.2.2. However, their swelling behavior in the presence of salts changes significantly as already pointed out by McGreevy and Smith (1984). To illustrate this point, the following experiment, similar to that discussed by Snelthage and Wendler (1997), is described using the clay containing Sander Schilf sandstone that was discussed in Sect. 4.2.2. One sample of the stone was first impregnated with NaCl, and a second sample served as a control. Both

**Fig. 4.13** Hygric expansion for a Sander Schilf sandstone sample and for one pre-treated with a NaCl solution. Adapted from Sneathlage and Wendler (1997)



samples were dried to ambient conditions (30 % RH and 20 °C) prior to subjecting them to RH cycling between 35 and 90 % RH. The behavior of these samples is shown in Fig. 4.13.

The graph shows that, while the control sample expands upon moisture absorption and contracts upon its loss, the one containing salt has exactly the opposite behavior. Furthermore, for the control sample, the expansion—contraction is constant and reversible over at least ten cycles, while, for the salt-impregnated sample, it increases with cycling becoming irreversible. Similar results were also obtained by pre-treating the stone with  $\text{MgSO}_4$  and  $\text{Ca}(\text{NO}_3)_2$  solutions (Wendler and Rückert-Thümling 1993). The contraction of the salt-containing sample upon exposure to high RH (above the equilibrium relative humidity of the salt in question) can be the result of the formation of dense hydration layers because of the higher electrolyte content in the stone. Since the expansion of these stones is associated with their clay content, this could be related to the two swelling mechanisms associated with them. The first one corresponds to the crystalline swelling where the incorporation of cations from the salt in the intermediate layers of the clay minerals can result in a reduction of hydration possibilities. The second is associated with the intercrystalline, i.e. osmotic, swelling of these minerals. The thickness of the diffuse electrical double layer at the surface of the clay minerals decreases significantly in the presence of a salt solution as repulsive forces between the clay layers decrease (Scheffer and Schachtschabel 1984).

However, these theories do not take into account the presence of the salts and the role that their crystallization-dissolution plays during the hygric cycling. As has been long known and is discussed in detail in Sect. 4.2.3, when salts crystallize from a saturated solution, there is an expansion in the system, whereas, when they dissolve, there is a contraction. At the beginning of the experiment, both samples

are dry, but the salt-containing sample with the crystallized salt in it will already have been expanded. Subjecting it to high relative humidity, above the DRH of the salt, the salt will deliquesce and go into solution with a net contraction of the system, as shown in the graph.

There is certainly an interaction between the clays and the salts, but it appears that the overall behavior of this system reflects that of the salts rather than that of the clays. However, comparing the salt-induced deterioration of a clay containing stone with that of a similar stone without clays, it is clear that the clays contribute significantly to the overall deterioration.

#### 4.2.4.4 Further Examples

To illustrate the complexity of the problem, a case study is presented that compares two clay-bearing limestones used in the construction of many buildings of historical value in Sicily, Italy (Cultrone et al. 2008). The limestones are the Syracuse limestone (Pietra di Siracusa) and the Melilli limestone (Pietra Bianca di Melilli), both of the Monti Climiti Formation. The Syracuse limestone has been used since Greek and Roman times, while the Melilli one was used for reconstruction of the destroyed eastern part of Sicily after the 1693 earthquake. Quarry samples were characterized through analysis, including mercury porosimetry and ultrasound measurements, the usual tests of water uptake and release, and salt resistance tests. The deterioration patterns were observed in selected monuments and in areas with a comparable environment, such as orientation, height, and rainfall. The Syracuse limestone (SL) showed typical selective weathering where algal nodules were preferentially eroded out—reflecting its nature as a bioclastic packstone—as well as some exfoliation. The Melilli limestone (ML) suffered mostly from differential erosion due to its more homogeneous texture of a bioclastic wackestone.

Both limestones contain over 99.5 % calcite. The main difference is in the acid insoluble residue, which is slightly higher for the ML (0.41 %) than for the SL (0.30 %). Analysis of these fractions showed further differences, the ML having more sand and slightly less clays than the SL. Expansive clays of the smectite group are found in both limestones, but the ML also has kaolinite and illite (hydromica group). Visually, the SL is more compact than the ML.

Their hydric behavior is quite different; ML has a higher capillary water absorption coefficient and absorbs more water than the SL. Furthermore, ML also dries faster than the SL, suggesting a high pore interconnectivity. Their porosity values from forced water absorption are similar (around 27 %), but, for free water absorption, the open porosity of the SL is only 21.6 %, suggesting the presence of bottle necks in the pore system. Similarly, their behavior after 15 cycles of the standard UNI-EN12370 (2001) sodium sulfate salt test was different. The weight loss was nearly 9 % for the SL—mostly by flaking—but only 1 % for the ML. After the tests, the open porosity increased more for the SL than for the ML, reflecting changes in their pore structure. Interestingly, the ultrasound wave

velocities of both stones followed a parallel behavior, decreasing in velocity with an increasing number of salt cycles, but, after 10 cycles, the ultrasound velocity decreased significantly for the SL, indicating higher deterioration, i.e. crack development. This was also confirmed by the pore-size distribution, which had significantly changed.

The laboratory tests could reproduce the observed damage of these stones in the monuments. The apparently more compact SL deteriorates faster than the ML. There is a complex interaction of the mineralogy and texture of the stone that affects the hydric behavior of these stones and, consequently, that of salt crystallization, which, in the present example, was the main deteriorating factor.

Similar deterioration patterns were found for other limestones, such as the French Sébastopol limestone (FSL) and the white tuffeau (WT) (Van et al. 2007). The former contains mainly calcite with some quartz, 80 and 20 %, respectively. The latter has a more complex composition (50 % calcite, 10 % quartz, 30 % opal, 10 % clay and mica). Both stones have a high open porosity, FSL 42 % and WT 48 %. The deterioration patterns observed in monuments constructed with these stones show that, while the FSL tends towards a granular deterioration, the clay containing WT shows delamination.

### 4.3 Deterioration by Chemical Processes

Chemical damage processes refer to the dissolution or alteration of the mineral constituents of a stone material via chemical reactions. This section provides a brief summary of such reactions and will also discuss the resulting damage patterns in building stones and the changes in the appearance of building façades. Mineral dissolution in building stones is closely related to atmospheric pollution and acid deposition. The origin and changes of this pollution are more thoroughly dealt with in Chap. 5. Here, the focus will be on the chemical reactions in the stone and on the behavior of the reaction products.

#### 4.3.1 Mineral Dissolution Reactions

Many minerals present in rocks and building stones are thermodynamically unstable in the Earth's surface conditions. Therefore, these minerals are undersaturated if they are in contact with natural waters, e.g. rainwater. Mineral dissolution reactions in building stones involve the attack of water and its associated acidity. The  $H^+$ -ion attack on the mineral components causes their dissolution and the formation of deterioration products. Some examples of mineral dissolution reactions relevant to stone deterioration are:

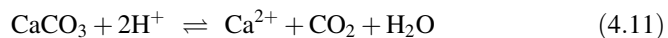
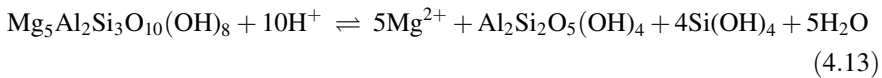
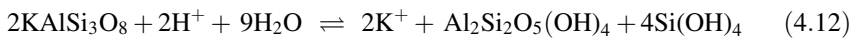




**Table 4.4** Ions released from weathering of some common minerals in building materials (Steiger 2003)

Mineral name	Idealized formula	Ions released
Carbonate minerals:		
–Calcite	$\text{CaCO}_3$	$\text{Ca}^{2+}$
–Dolomite	$\text{CaMg}(\text{CO}_3)_2$	$\text{Ca}^{2+}$ , $\text{Mg}^{2+}$
Feldspars:		
–Plagioclase feldspar	$\text{Na}_x\text{Ca}_{1-x}\text{Al}_{2-x}\text{Si}_{2+x}\text{O}_8$	$\text{Na}^+$ , $\text{Ca}^{2+}$
–Microcline (K-feldspar)	$\text{KAlSi}_3\text{O}_8$	$\text{K}^+$
Clay minerals:		
–Biotite	$\text{K}(\text{Mg},\text{Fe})_3\text{AlSi}_3\text{O}_{10}(\text{OH})_2$	$\text{K}^+$ , $\text{Mg}^{2+}$
–Chlorite	$\text{Mg}_5\text{Al}_2\text{Si}_3\text{O}_{10}(\text{OH})_8$	$\text{Mg}^{2+}$



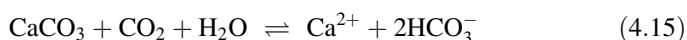
Acid attack generally causes the mobilization of metal cations and dissolved silica,  $\text{Si}(\text{OH})_4$ , from the parent minerals. The weathering of silicates also leads to the formation of new mineral compounds, e.g. iron or aluminum oxyhydroxides and clays such as kaolinite,  $\text{Al}_2\text{Si}_2\text{O}_5(\text{OH})_4$ . Compared to the parent materials, the mineral reaction products are depleted in metal cations relative to Al and Si. Additionally, the product minerals are usually more hydrated. If the parent mineral contains Fe(II), the dissolution reaction usually also involves an oxidation step, as in, for example, Eq. (4.14). Table 4.4 lists the cations released from the weathering of some common mineral constituents of building materials. It can be seen that mineral dissolution reactions lead mainly to the formation of sodium, potassium, magnesium, and calcium salts, i.e. the major cations in natural waters.

The rates of mineral dissolution reactions depend on: (1) the amount and contact time of liquid water available at mineral surfaces; (2) the solubility of the mineral in question; (3) the availability of acidity, i.e. the pH of the aqueous solution in contact with the mineral surface. The major source of liquid water in building stones is precipitation, and damage caused by mineral dissolution reactions often shows a distinct pattern following the exposure to direct rainfall, driving rain, and surface runoff waters, as discussed in more detail below. Most rock-forming minerals exhibit a very low but finite solubility in water. In historical buildings, the amount of rainwater infiltration and the contact times over centuries are sufficiently long enough that mineral dissolution reactions can cause significant damage. The carbonate minerals, i.e. calcite and dolomite, exhibit the highest solubilities, followed by feldspars, clay minerals, and quartz. As a rule of thumb, the solubility increases with decreasing silica content and with an increasing content of calcium and magnesium. According to reactions such as (4.12), (4.13),

and (4.14), the solubility of the rock-forming minerals also increases with decreasing pH, i.e. in acidic solutions. It should be noted that some minerals, such as silicates, also exhibit an increased solubility in alkaline solutions, i.e. at pH above 10. However, in the present context of building stone deterioration, the focus will be limited to the dissolution reactions in acidic solutions, since these are the most common ones.

Carbon dioxide,  $\text{CO}_2$ , is a major source of acidity in natural waters, and it is the acid responsible for most natural rock weathering on a geological time scale.

The solubility of carbonate materials in water is enhanced in the presence of  $\text{CO}_2$  according to the reaction:



The pH value of unpolluted rainwater in equilibrium with atmospheric  $\text{CO}_2$  is about 5.6, i.e. slightly acidic. The equilibrium solubility of calcite in rainwater in equilibrium with atmospheric  $\text{CO}_2$  ( $5.5 \times 10^{-4} \text{ mol L}^{-1}$ ) is about four times higher than in pure water. Thus, even in the absence of other sources of acidity, there is a natural dissolution reaction of carbonate minerals which is commonly referred to as the karst effect. The pH values of natural river, lake, and ground waters are also affected by rainwater infiltration, but the pH varies depending on the composition of surrounding rocks and sediments. Natural waters in contact with carbonate-rich rocks usually have pH values greater than 7, whilst the groundwater will tend to remain acidic if carbonate rocks are absent, i.e. in the presence of sandstones and other silicate rocks. Although the dissolution rates of silicate minerals are far slower than those of carbonate minerals, the former are also subject to natural chemical weathering (Stumm and Wollast 1990; Drever 1994a, b; Lasaga et al. 1994). The same reactions are responsible for the dissolution of quartz and silicate minerals in building stones; however, in this case, the presence of mortars, generally alkaline, will increase their dissolution.

Acid deposition is the major source of  $\text{H}^+$  in building materials and significantly increases the natural rates of mineral dissolution reactions. Here, acid deposition refers to both wet deposition, i.e. acid precipitation, and the dry deposition of gaseous and particulate pollutants into water films on mineral surfaces. In acid rain, the pH values are significantly lower and can reach values of about 4 during the initial rainfall. In acid fog, even lower pH values of about 2–4 can occur, because, there being less water available, the solution is more concentrated. However, in recent years, a continuous increase in the pH of rainwater has been observed at least in North America and Europe.

Atmospheric acidity is closely related to the atmospheric chemistry of sulfur dioxide ( $\text{SO}_2$ ) and the nitrogen oxides ( $\text{NO}$ ,  $\text{NO}_2$ ) which become oxidized to sulfate and nitrate through gas and aqueous phase processes. Most of the nitrates and sulfates of the major cations that are mobilized in mineral dissolution reactions, i.e. the reaction products of acid deposition, are substantially more soluble than the respective parent minerals. Therefore, mineral dissolution reactions cause a substantial loss of cohesion if acid attack and dissolution occur at grain contacts.

Apart from insoluble new minerals such as kaolinite or iron oxyhydroxides, soluble nitrates and sulfates are the major reaction products of acid deposition onto building stones. It is generally not possible to clearly distinguish damage due to the chemical reactions with the rock-forming minerals and subsequent salt stress, as discussed in Sect. 4.4.

A number of studies were carried out to determine the effect of acid deposition on building stones. A useful experimental technique is the collection and analysis of stone runoff solutions (Rönicke and Rönicke 1972; Reddy et al. 1985; Livingston 1986; Cooper 1986; Cooper et al. 1992). Any differences in the concentrations between runoff and incident rainfall must be due to interactions with the stone. For carbonate stones, the excess calcium concentration in runoff solutions provides a direct measure of calcite dissolution. Here, excess calcium concentration refers to a corrected concentration, taking into account contributions from the dry deposition of particles and the calcium concentrations in the incident rainfall itself (Reddy 1988). Data obtained from runoff water experiments were used to determine the relative contributions of the karst effect, the neutralization of acid rain, and the dry deposition of sulfur dioxide (Livingston 1992; Baedeker et al. 1992). It was found that, in urban areas with significant SO<sub>2</sub> pollution, the dry deposition of local sulfur dioxide was dominant (Roekens and van Grieken 1989; Livingston 1992; Steiger et al. 1993; Cardell-Fernández et al. 2002). The mobilization of metal cations as an indicator for the dissolution of silicate minerals, mainly clay minerals and feldspars, was also observed in the runoff from sandstone surfaces (Steiger and Dannecker 1994; Halsey et al. 1995).

Mineral dissolution reactions in sandstone can also be detected by careful analysis of weathered stone samples. Using petrographic analysis of depth profiles in sandstone samples from several buildings in Germany, Mausfeld and Grassegger (1992) obtained distinct profiles of fresh and leached feldspars and a significant increase in the total feldspar content with increasing distance from the exposed stone surface. In a similar study, these authors also found profiles of clay mineral composition in building stones with rather constant compositions in the unweathered interior and distinct profiles close to the surface (Mausfeld and Grassegger 1994). Schäfer and Steiger (2002) measured profiles of cation exchange capacities (CEC) in clay minerals containing sandstones. In all cases, they found distinct profiles with significantly lower CEC close to the exposed stone surfaces, indicating a significant loss of the mineral surface area available to ion exchange processes due to partial dissolution of clay minerals.

While most reaction products of mineral dissolution reactions are very soluble, calcium sulfate is an important exception. Calcium sulfate in the form of gypsum, CaSO<sub>4</sub>·2H<sub>2</sub>O, is the major reaction product of the dissolution of carbonate stone, i.e. limestone and marble, and is a ubiquitous compound found in building materials. The properties of gypsum and its role in the deterioration of building stones have been recently reviewed by Charola et al. (2007). Gypsum crusts are preferentially formed on rain-sheltered surfaces of carbonate building materials. According to Camuffo et al. (1982), gypsum crusts occurring on surfaces not directly exposed to rainfall correspond to the black areas that can be clearly

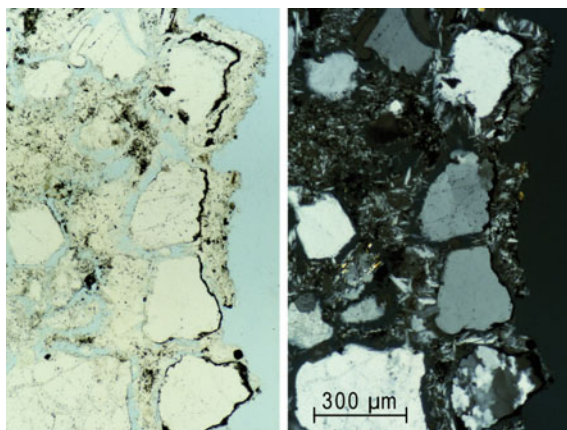
distinguished from the rain-exposed white areas of limestone and marble buildings. In fact, gypsum crusts on buildings in urban environments nearly always appear black. Their black color is caused by the embedding of air pollutant particles originating from a number of different sources, including fly ash, soot, mineral dust, iron oxides or oxyhydroxides, and organic pollutants mostly from combustion reactions, such as combustion engines (e.g. Del Monte et al. 1981; Del Monte and Sabbioni 1984; Nord and Tronner 1991; Whalley et al. 1992; Saiz Jimenez 1993).

There is no doubt that the formation of gypsum crusts on calcareous stones is the result of the preferential dry deposition of sulfur dioxide onto the moist surface of a stone followed by the dissolution of calcite and subsequent precipitation of gypsum. Hence, the major damage mechanism is one of mineral dissolution. The replacement of calcite by gypsum and the growth mechanism of crusts have been studied in detail, both for limestone (Schiavon 1992) and marble (Vergès-Belmin 1994).

Other crusts related to mineral dissolution reactions in calcareous stones are the calcium oxalate films or patinas. Whewellite ( $\text{CaC}_2\text{O}_4 \cdot \text{H}_2\text{O}$ ) and weddellite ( $\text{CaC}_2\text{O}_4 \cdot 2\text{H}_2\text{O}$ ) are commonly found on Italian marble and limestone monuments and natural carbonatic outcrops (Del Monte et al. 1987; Watchman 1991). In this case, the product of the replacement reaction, i.e. calcium oxalate, is even less soluble than the parent mineral calcite such that a crust is also formed on exposed surfaces. There have been controversial discussions about the origin of these films, many of them orange colored, particularly with respect to the patina called “scialbatura” commonly found on Roman imperial marble monuments (Del Monte and Sabbioni 1987; Lazzarini and Salvadori 1989). Their origin has been attributed to various mechanisms, from geological weathering at outcrops to chemical weathering of intentional treatments or to biological weathering of them, or plain biological activity as summarized elsewhere (Del Monte et al. 1987; Charola et al. 2002). However, biological activity may probably be the major source of oxalate crusts as discussed in Sect. 4.5.

The formation of gypsum crusts on sandstone is less obvious. However, gypsum crusts are commonly found on calcite cemented sandstones (e.g. Zehnder 1982) and nearly calcium-free materials such as quartz sandstone and granite (Whalley et al. 1992; Neumann et al. 1993; Smith et al. 1994). In contrast to calcareous stone, the mechanism of crust formation on sandstone is different, because both sulfate and calcium must originate from external sources. Therefore, the formation of gypsum crusts on non-calcareous stones cannot be considered the result of chemical deterioration of the substrate. Nonetheless, the low solubility of gypsum favors its accumulation in the pore space of these materials. Very often, the pore space close to the surface is completely filled with gypsum deposits (Charola et al. 2007). A characteristic feature at a later stage of the damage process is the complete destruction of the original internal fabric, which is replaced by a secondary gypsum supported fabric (Neumann et al. 1993, 1997; Steiger 2003). Figure 4.14 shows an example of these gypsum crusts on quartzitic sandstone.

**Fig. 4.14** Thin section of gypsum crust on a quartz bound sandstone at Leineschloss (Hanover) with//Nicols (*left*) and X Nicols (*right*). Note the loss of cohesion of the surface quartz grains due to secondary gypsum growth. The gypsum crystals growing on the original thin black surface layer resulted from the subsequent development of a leak above this area. Reproduced with permission from Neumann et al. (1993)



In contrast to marble and limestone, black discolorations often appear more evenly distributed on sandstone and granite surfaces. Their occurrence is not restricted to sheltered areas; rather, intensely black thin films are preferentially found on surfaces that are frequently wetted by rainfall or runoff. These discolorations often appear as homogeneous black layers firmly attached to and tracing the stone surface. Following Nord and Ericsson (1993), we prefer the term “thin black layer” for this kind of surface deposits that have to be clearly distinguished from gypsum crusts. A more detailed discussion of their composition and morphology is provided by Steiger (2003).

### 4.3.2 Surface Recession Rates on Calcareous Stone

In contrast to sheltered areas, surfaces on limestone and marble façades that are freely exposed to wind and rain usually appear as white areas. In these areas, rainwater runoff dominates. Hence, there is a significant contribution of the karst and the acid dissolution effects, and the reaction product gypsum is dissolved and removed by the runoff water. The surface recession in such exposed areas is a direct measure of the integral material loss due to acid deposition and dissolution of calcite and the karst weathering effect. Several attempts have been made to determine the resulting surface recession. The lowering of the surface can be measured with a high resolution micrometer, using reference points such as lead plugs (Sharp et al. 1982) or unweathered mineral constituents (Winkler 1987). Using lead plugs as references Sharp et al. (1982) found average recession rates of  $0.078 \text{ mm a}^{-1}$  for the period 1718–1980 measured on a Portland limestone balustrade at St. Paul’s Cathedral. This value was later confirmed by re-measurements of Trudgill et al. (1989). However, both studies revealed substantial spatial variation, making comparisons of different data sets, e.g. for different exposures, difficult. Winkler (1987), using unweathered hornblende as a reference, determined average surface recession rates

of  $0.026 \text{ mm a}^{-1}$  on ribs of Georgia marble columns at the Chicago Field Museum of Natural History. Attewell and Taylor (1990) determined the recession on Carrara marble tombstone surfaces by measuring the lowering with reference to lead-filled letters of the inscriptions. They obtained average recession rates of  $(0.002\text{--}0.014) \text{ mm a}^{-1}$  for exposure periods of about 10–100 years at different sites near Durham, UK. The lowest rates were observed at rural sites, and the highest recession rates were obtained in industrial areas.

Several authors determined the surface recession rates on tombstones by comparing upper and lower slab thicknesses. Using this method Baer and Berman (1983) found marble recession rates of  $0.014 \text{ mm a}^{-1}$  and  $0.018 \text{ mm a}^{-1}$ , respectively, for urban sites in Philadelphia and New York and  $0.008 \text{ mm a}^{-1}$  for a suburban site in Long Island. With the same method Feddema and Meierding (1987) obtained average annual recession rates of  $0.035 \text{ mm a}^{-1}$  for marble tombstones in highly polluted downtown Philadelphia for a period of some 150–200 years exposure. In contrast, they obtained annual rates of  $<0.005 \text{ mm a}^{-1}$  at rural sites and  $(0.014\text{--}0.018) \text{ mm a}^{-1}$  for moderately polluted sites over approximately the same period of time.

Recession rates can also be calculated from weight loss data determined in exposure experiments. Weber (1985) obtained recession rates up to  $0.062 \text{ mm a}^{-1}$  for porous Austrian limestones exposed for one year in Vienna. Jaynes and Cooke (1987) carried out an extensive two-year exposure study at 25 sites in Southeast England. They obtained recession rates for Portland limestone ranging from  $0.010 \text{ mm a}^{-1}$  at rural sites to  $0.016 \text{ mm a}^{-1}$  at central London sites. They also calculated recession rates from the weight loss data of a 10 year (1955–1965) exposure study with Portland limestone carried out by Honeyborne and Price (1977). Their weight data yielded recession rates of  $0.029 \text{ mm a}^{-1}$  in central London and  $0.010 \text{ mm a}^{-1}$  in Garston. Though careful interpretation is required, it appears that the reduced recession rates in central London reflect the decrease in air pollution levels. Baedeker et al. (1992) used weight loss data for samples of Indiana limestone and Vermont marble that were exposed in the United States National Acid Precipitation Assessment Program (NAPAP) to determine recession rates. The recession rates range from  $0.015$  to  $0.024 \text{ mm a}^{-1}$  for marble and from  $0.020$  to  $0.058 \text{ mm a}^{-1}$  for limestone. Similar values were obtained using an interferometric technique to determine the erosion rate. The trend observed by Jaynes and Cooke (1987) is confirmed by more recent data from the UN ECE Program on Effects on Materials (Kucera et al. 2007). In this program, Portland limestone was exposed over a 4-year period at 49 sites, most of them spread all over Europe with additional sites in Russia, Israel, the US, and Canada. The recession rates determined from weight loss data hardly exceeded values of  $0.010 \text{ mm a}^{-1}$  even at the most polluted urban and industrial sites; for rural sites, recession rates were typically  $<0.004 \text{ mm a}^{-1}$ .

Another approach to determining surface recession rates is the collection and analysis of runoff water, as mentioned before (Reddy et al. 1985; Cooper 1986). Extensive runoff water measurements were also carried out at the NAPAP exposure sites (Reddy 1988). Surface recessions were calculated from the excess



calcium concentrations in the runoff water, yielding rates in the range from 0.007 to 0.008 mm a<sup>-1</sup> for marble and from 0.007 to 0.010 mm a<sup>-1</sup> for limestone (Baedeker et al. 1992). These values are less than half of the rates that were determined from weight loss and interferometric data. The reason for the deviation is simply that runoff experiments only measure stone dissolution rates. The calculation of recession rates is based on the assumption that a calcite grain is only lost if it is completely dissolved. However, a much smaller degree of calcite dissolution may be sufficient to weaken the grain contacts, resulting in a loss of cohesion. In this case, the material loss occurs mainly as sanding. In runoff experiments with Portland limestone in Dublin, Cooper et al. (1992) calculated total surface recession rates from both excess calcium concentrations, i.e. reflecting the influence of dissolution, and total particulate matter suspended in the runoff water, i.e. reflecting the recession via particulate loss. The total recession rates they obtained range from 0.013 to 0.039 mm a<sup>-1</sup>.

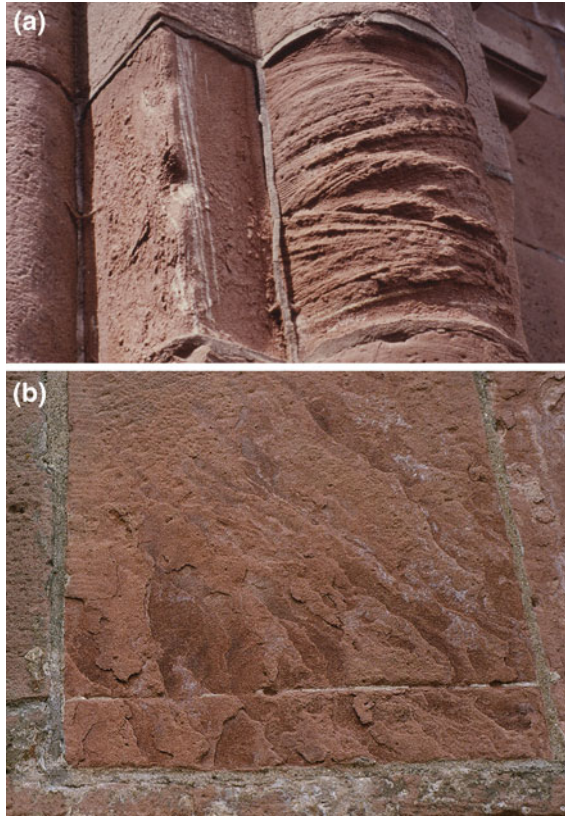
The range of recession rates in the studies mentioned so far shows significant scatter, reflecting the variety of materials, pollutant concentrations, exposure conditions, and times of these studies and, of course, the different experimental approaches used. In several of the studies, substantial scatter also occurred on a point to point basis, again reflecting the complexity of the erosion process due to mineral dissolution involving large variation in local microclimatic conditions, orientation of surfaces, and material inhomogeneities. Considering all these points, the results of the studies appear to be in reasonable accordance and allow an assessment of average recession rates for calcareous materials. One of the major influences appears to be the orientation of the exposed surface, as the incident rainfall intensity is much higher on horizontal than on vertical surfaces.

#### 4.4 Action of Salts

There is no question that salts are probably the single most damaging factor for stone deterioration. Several reviews have been written summarizing this topic (Charola 2000; Doehne 2002), and several conferences on this single topic have taken place over the past 10 years (Leitner et al. 2003; Simon and Drdácý 2006; Ottosen et al. 2008, to name a few).

The deteriorating effect of salts is mostly reflected in the patterns that have been grouped under the detachment category of the ICOMOS-ISCS Glossary (Vergès-Belmin 2008). Within this category, blistering, delamination, scaling, and disintegration are considered, as the glossary focuses on the form of the deterioration, not its origin (Chap. 6, Table 6.1). From practical experience gained over the years, it has been concluded that deterioration induced by salts forms a continuum between the granular disintegration and scaling, delamination, and blistering patterns, as shown in Fig. 4.15 (Snethlage and Wendler 1997). Whether one pattern or the other develops will depend on the type of material, e.g. sandstone or marble, and, more importantly, the conditions under which the salt crystallizes.

**Fig. 4.15** Salt-induced deterioration (by magnesium sulfate) of Bunter sandstone at Kaiserpfalz (Gelnhausen, Germany): **a** Incipient flaking (*left block*) and sanding following the bedding plane (*right block*); **b** Scaling parallel to bedding

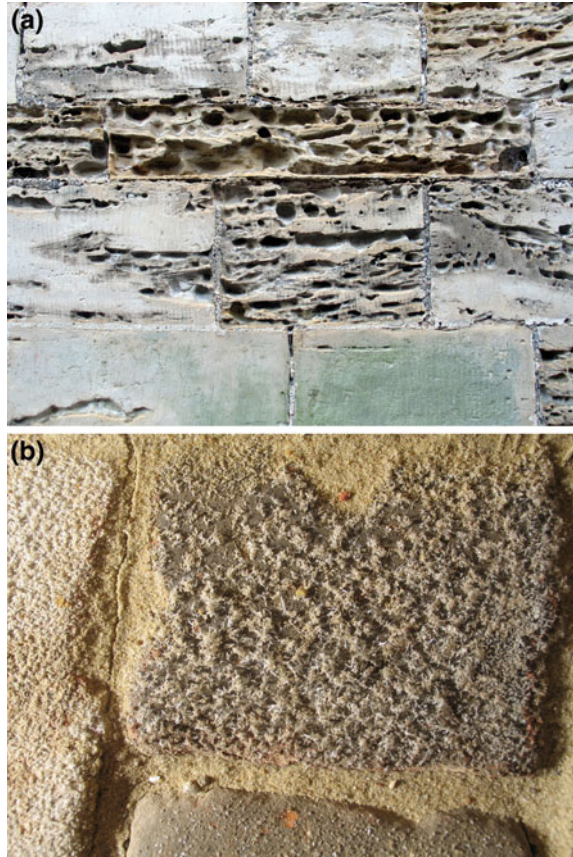


The amount of water available during crystallization, which depends on the porosity of the stone and the environmental conditions, will affect the habit in which the salts crystallize. This topic has been studied extensively by Arnold and Zehnder over many years (Arnold and Küng 1985; Arnold and Zehnder 1985; Zehnder and Arnold 1989; Arnold and Zehnder 1991).

It should be remembered that, when dealing with clay-bearing stones such as some sandstones or marly limestones, the moisture retention of the clays tend to accumulate salts in these layers so that the scaling pattern of a thin surface flake may result in the formation of thicker layers spalling off, i.e., the properly called delamination.

Another pattern is alveolization, or honeycomb formation, which has been found on many different rock types, such as limestones, sandstones, and volcanic stones, among others (see Fig. 4.16). This cavernous-like pattern is most commonly found in coastal areas, but also in other regions, and ranges from smaller cavities to larger ones, referred to as “tafoni” and eventually leading to overhangs. The reason for this characteristic weathering can be attributed to the presence of salts on the stone and wind in the environmental conditions. What role the nature

**Fig. 4.16** Salt-induced deterioration: **a** Alveolization (Kromborg Castle, Copenhagen, Denmark); **b** Salt efflorescences on sandstone flagstones (Marienkirche Salzwedel, Germany); Photos: Hans-Jürgen Schwarz, Ri-Con, Hanover, Germany



and heterogeneity of the stone play is still under study. Pauly (1976) carried out one of the pioneering studies by reproducing this weathering pattern in the laboratory. Many studies have been carried out since then, as summarized by Goudie and Viles (1997).

The formation of efflorescences is yet another important deterioration pattern, though, if their growth occurs only on the surface, it does not cause major damage. The problem is that, since stone is porous, where efflorescences are found, subflorescences will also be present, and these cause damage.

While many studies have been devoted to elucidating why and how salt crystallization causes damage to stone, fewer, or less successful, studies have been carried out in the field, because the number of variables present makes it difficult to determine the leading factors in the observed deterioration. However, an enlightening study was carried out in the Romanesque crypt of the Cathedral of Basel, Switzerland for several months (Zehnder and Schoch 2009). The study was based on an in situ automated monitoring system of the indoor conditions coupled with image-capturing devices. Thus, correlations could be obtained for the

crystallization and deliquescence periods of the salts present in the masonry with changes in temperature and RH in the air as well as on the surface, as will be discussed in detail in the following sections. The actual development of mirabilite, epsomite, and gypsum efflorescence was documented in a degree of detail not previously achieved.

The study confirmed that small changes in RH within the moderate relative humidity range in the crypt triggered the crystallization and dissolution cycles. Consequently, although reducing changes in RH will diminish the intensity of the damage, it does not eliminate it, because keeping RH constant in a large environment where people carry out activities is practically impossible.

#### ***4.4.1 Sources of Salts in Building Materials***

Deposition of acidity from the atmosphere is an important source of salt enrichment in building materials. The major anions associated with atmospheric acid-forming species are sulfate and nitrate. Therefore, the processes described in Sect. 4.4 lead to the enrichment of sulfates and nitrates of calcium for the case of mortars and calcitic stones, as well as those of sodium, potassium, and magnesium in the case of other stone materials. In addition to these salts formed through chemical reaction, there is also a direct input of salts from the atmosphere. For example, in a marine environment, sea salt has an important presence in the local atmosphere. On a global scale, emissions of sea salt droplets ejected from the oceans are considered one of the most important primary sources of the atmospheric aerosol (Blanchard and Woodcock 1980). Sea salt particles will undergo both wet and dry deposition, the major processes leading to their enrichment in building materials.

In contrast to anthropogenic air pollutants whose concentrations have changed dramatically during the last centuries (Brimblecombe and Rohde 1988), the enrichment of sea salt in historical buildings has been progressing continuously for far longer periods of time. Salt accumulations found today represent an integral effect of sea salt deposition, beginning as of the building's construction time. Experience from many monuments located at coastal sites suggests that the deposition and enrichment of sea salt can be a major cause of decay (e.g. Theoulakis and Moropoulou 1988; Zezza and Macri 1995). An example is shown in Fig. 4.17.

Sea salt particles in the atmosphere have a chemical composition very similar to that of bulk seawater. The contribution of the six ions sodium, magnesium, potassium, calcium, chloride, and sulfate amounts to >99 % by mass of the total solids dissolved. The major ions, sodium and chloride, account for 85.6 % of the bulk sea salt. Oceans have a remarkably uniform composition, and it can be assumed that the relative abundances of the major ions have not significantly changed over time. Therefore, the relative abundances of the major constituents can be used as tracers for sea salt deposition (Zappia et al. 1989). It has been



**Fig. 4.17** Sea-salt-induced deterioration at Santa Marija Ta' Cwerra church (Malta); Photo: B. Fitzner, Geological Institute, RWTH Aachen University



shown that the enrichment of sea salt in buildings in coastal environments is considerably variable depending on a number of different influences, including environmental parameters and the geometry and constructional details of a building (Steiger et al. 1997).

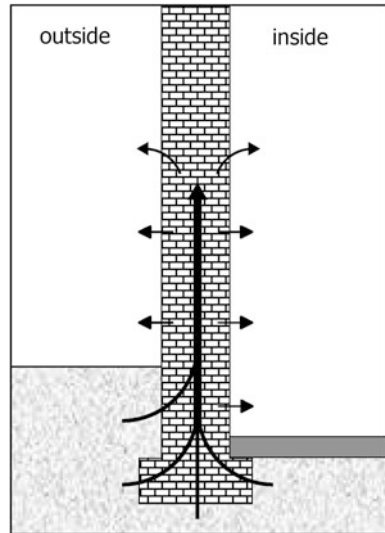
Deicing salts, as they lower the freezing temperature of water, have been used for decades to improve traffic safety on roads and sidewalks and millions of tons of salt have already been applied. The most commonly used deicing salt is NaCl, which is inexpensive and readily available. Sometimes CaCl<sub>2</sub>, MgCl<sub>2</sub>, and carnallite (KMgCl<sub>3</sub>·6H<sub>2</sub>O) are also used. These salts depress the freezing point to lower temperatures and have an additional thermal effect caused by the exothermic dissolution reaction. Transport of deicing salt into the surroundings causes an impact on roadside vegetation, soil, groundwater, and masonry. In fact, the use of deicing salt is a major source of chloride accumulation in masonry near ground level. Figure 4.18 shows efflorescences of deicing salt on a stairway in downtown Basel with an obvious impact on the adjacent masonry (Siedel 2009). Due to the harmful environmental effects of NaCl, alternative deicers such as CMA (calcium magnesium acetate), potassium acetate, and mixtures of potassium and sodium formate are now frequently used. Hence, in the future, there might also be a significant input of these organic anions into building stone.

Another very important source of salts in buildings is ground moisture carried into masonry by rising damp in the absence of damp-proof coursing. Considering a structure in hydraulic contact with the saturated ground, water is absorbed and slowly moves upwards in the wall (Fig. 4.19). Above ground level, the wall is

**Fig. 4.18** Efflorescences of deicing salt on a stairway in downtown Basel. Reproduced with permission from Siedel (2009)



**Fig. 4.19** Moisture transport in masonry affected by rising damp



subject to evaporation, and rising damp is a result of the competition between the rate of capillary absorption and the evaporation rate (Hall and Hoff 2002, 2007).

The composition of groundwater is largely determined by the time of contact and the nature of the geological materials it is moving through. The major constituents of natural ground and surface waters that can penetrate building materials are sodium, potassium, magnesium, calcium, chloride, sulfate, and bicarbonate. Additional constituents may be leached from surface soils. For example, nitrate is an important contaminant in surface soils, originating from the use of fertilizers, animal waste, and the oxidation of organic nitrogen. Therefore, ground moisture penetrating the base of a building that is used as a stable can carry substantial



amounts of nitrates into the masonry. Similarly, a significant input of nitrate into the walls of churches may arise from the use of the surrounding soils as cemeteries.

Initially, ground moisture is a dilute solution of groundwater vertically transported due to capillary rise. However, above ground level, moisture evaporates from the wall, and the solution becomes more and more concentrated while still being subject to capillary rise. As the solution becomes saturated during transport, any further evaporation will cause crystallization and immobilization of the salt. In effect, a zone of salt enrichment evolves some distance above ground level. The height of the accumulation zone is dependent on the rate of evaporation and the solubility of the salt. The maximum height is given as the upper limit of the capillary rise of moisture, i.e. the height at which the evaporation rate equals the supply of moisture from below. It has to be noted, however, that evaporation rates are significantly lower in the presence salts. This is the result of a strong depression of the vapor pressure above concentrated salt solutions (see [Sect. 4.4.3](#)). Therefore, with increasing salt enrichment, the maximum height of capillary rise increases.

In particular, old buildings are very often insufficiently insulated against rising ground moisture. Arnold and Zehnder (1989, 1991) provide a detailed discussion of salt transport and accumulation in walls affected by rising damp based on extensive observations of a number of old buildings that were subjected to ground moisture over long periods of time. During capillary rise and evaporation, the less soluble salts will reach saturation earlier than salts of greater solubility, resulting in a fractionation of the salts according to their solubilities. The composition of the pore solution continuously changes during transport, and only the very soluble salts are transported as concentrated brine solutions to the upper evaporation zone. Arnold and Zehnder (1989, 1991) provide vertical profiles of ion concentrations in the zone affected by rising damp from a number of buildings. Maxima of salt enrichment were observed at heights from 0.5 m to about 3 m above ground level, and the profiles provide evidence of salt fractionation.

The use of alkaline materials, e.g. Portland cement, cleaning products, and consolidation materials, such as water glass, can be an important source of salts in buildings (Arnold and Zehnder 1991). Generally, these materials release sodium and potassium hydroxide and carbonate, which can react with salt mixtures already present in a masonry, forming new, often more damaging salt mixtures.

Sometimes, the present day salt contamination of a building may be directly related to a particular use of the building in a former time. Use as a stable leading to nitrate contamination arising from animal waste has already been mentioned. Other examples include the use of a building or part of it for storage, e.g. for rock salt or gun powder (black powder) etc., thus, leading to direct salt input into masonry. Another example is Angkor Wat in Cambodia (see [Fig. 4.20](#)), which was overgrown by the jungle over a period of about 400 years. The bats inhabiting it roosted in the interior of the temple towers, producing tons of guano. Bat guano is strongly enriched with a number of salts, but mainly contains phosphates and nitrates that were transported into the walls of the temple via uncontrolled water flow through leakages (Hosono et al. 2006; Siedel et al. 2008).

**Fig. 4.20** Salts partially originating from bat guano at Angkor Wat (Cambodia)



#### ***4.4.2 Common Salts in Building Stones***

Depending on the nature of the sources, the salt mixtures that are found in building materials are formed by several different ions. Typically, chlorides, nitrates, sulfates, carbonates, and bicarbonates of sodium, potassium, magnesium, and calcium are the most common. These salts are commonly referred to as “soluble salts”. However, their solubilities differ by orders of magnitude and, consequently, the components of such complex salt mixtures may be either present in dissolved form, i.e. in pore solutions, or as crystallized salts within the pore system. Salts dissolved in a pore solution are subject to capillary transport, for instance, with rising ground moisture or rainwater penetrating the stone. In contrast, crystallized salts are less mobile and may accumulate. Crystalline solids formed during drying may either form efflorescences on the stone surface or they can crystallize as subflorescences within the pore space of the stone. Crystal growth on the stone surface is usually not harmful as long as the growing crystals are not confined. However, during the formation of crystalline deposits in pores, so-called subflorescences, growing crystals may become confined and can then generate substantial stress, as discussed before.

Upon evaporation of water, a pore solution becomes more concentrated and finally reaches saturation with one or more solid phases. From a pore solution containing the above-mentioned ions, a large number of different crystalline salts can be precipitated. In addition to all possible and electrically neutral binary cation–anion combinations, there is also a large number of double salts containing

more than two different ions that can be precipitated from a mixed solution. In addition, several salts can exist in anhydrous and different hydrated forms, e.g. sodium sulfate can exist as the anhydrous  $\text{NaSO}_4$  (thenardite) and as the decahydrate  $\text{Na}_2\text{SO}_4 \cdot 10\text{H}_2\text{O}$  (mirabilite). Only considering solutions of the most common ions in building materials, i.e.  $\text{Na}^+$ ,  $\text{K}^+$ ,  $\text{Mg}^{2+}$ ,  $\text{Ca}^{2+}$ ,  $\text{Cl}^-$ ,  $\text{NO}_3^-$ ,  $\text{SO}_4^{2-}$ ,  $\text{CO}_3^{2-}$ , and  $\text{HCO}_3^-$ , about 70 different evaporite minerals can be precipitated in the temperature range of  $-40$  to  $+40$  °C (see Table 4.5). About half of these minerals have, in fact, been detected in building stones (see compilations by Arnold and Zehnder 1991, Nord and Tronner 1991, Allmann and Kraus 2003).

As discussed in more detail in Sect. 4.4.3, it is difficult to predict the precipitation sequences in mixed salt solutions. However, due to solubility limitations, there are certain restrictions for the composition of brine solutions evolving during transport and evaporation. As Hardie and Eugster (1970) have pointed out, the solubilities of the calcium and magnesium carbonates and of gypsum ( $\text{CaSO}_4 \cdot 2\text{H}_2\text{O}$ ) are so low compared to all other salt minerals of interest that they provide a chemical divide. The major pathways of fractionation and brine evolution from solutions initially containing  $\text{Na}^+$ ,  $\text{K}^+$ ,  $\text{Mg}^{2+}$ ,  $\text{Ca}^{2+}$ ,  $\text{Cl}^-$ ,  $\text{NO}_3^-$ ,  $\text{SO}_4^{2-}$ ,  $\text{CO}_3^{2-}$ , and  $\text{HCO}_3^-$  are summarized in Fig. 4.21. The solubilities of the alkaline earth carbonates is about 2 orders of magnitude lower than that of gypsum and about 4–5 orders of magnitude lower than that of the remaining salts. The evaporation of water from such solutions always leads to the crystallization of the alkaline earth carbonates, i.e. calcite, dolomite, or nesquehonite ( $\text{MgCO}_3 \cdot 3\text{H}_2\text{O}$ ). Thus, concentrated pore solutions cannot contain calcium or magnesium and carbonate ions at the same time (Steiger 2003).

A carbonate-rich salt mixture is typically observed in building stones as the result of the application of alkaline materials such as Portland cement or water glass. These materials release alkalinity, initially in the form of calcium hydroxide that is neutralized by atmospheric acidic gases—mainly carbon dioxide and sulfur dioxide. If there is sufficient excess alkalinity compared to the dissolved alkaline earth elements, the resulting salt system is characterized as a mixture of mainly alkali carbonates, bicarbonates, and sulfates together with chlorides and nitrates originating from other sources (Fig. 4.21). Such a carbonate-rich salt mixture is called a type III mixture (Steiger 2003) and the efflorescences and subflorescences that result from it may contain typical crystalline phases such as trona,  $\text{Na}_3\text{H}(\text{CO}_3)_2 \cdot 2\text{H}_2\text{O}$ , thermonatrite,  $\text{Na}_2\text{CO}_3 \cdot \text{H}_2\text{O}$ , thenardite,  $\text{Na}_2\text{SO}_4$ , darapskite,  $\text{Na}_3(\text{SO}_4)(\text{NO}_3) \cdot \text{H}_2\text{O}$ , and burkeite,  $\text{Na}_6\text{CO}_3(\text{SO}_4)_2$  (e.g. Charola and Lewin 1979; Arnold 1985; Arnold and Zehnder 1991; von Konow 2002; Bionda 2006).

If the sum of the calcium and magnesium concentrations exceeds the total carbonate concentration, a carbonate-poor solution will evolve due to the precipitation of the alkaline earth carbonates. Then, due to its low solubility compared to all other salts, gypsum is precipitated next and acts as a second divide. If the initial calcium concentration exceeds that of sulfate, a sulfate-poor, type I solution evolves. Here, the term “sulfate-poor” only refers to the composition of the pore solution. There might also be a high sulfate concentration in the stone; however, as long as there is more calcium, all sulfate is essentially immobilized as gypsum.

**Table 4.5** Solid phases in the  $\text{Na}^+ - \text{K}^+ - \text{Mg}^{2+} - \text{Ca}^{2+} - \text{Cl}^- - \text{NO}_3^- - \text{SO}_4^{2-} - \text{CO}_3^{2-} - \text{HCO}_3^- - \text{H}_2\text{O}$  system from  $-45^\circ\text{C}$  to about  $50^\circ\text{C}$ 

Formula (name)	Formula (name)
Chlorides	$\text{CaCl}_2 \cdot 6\text{H}_2\text{O}$ (antarcticite)
$\text{NaCl}$ (halite)	$\text{MgCl}_2 \cdot 6\text{H}_2\text{O}$ (bischofite)
$\text{NaCl} \cdot 2\text{H}_2\text{O}$ (hydrohalite)	$\text{MgCl}_2 \cdot 8\text{H}_2\text{O}$ (magnesium chloride octahydrate)
$\text{KCl}$ (sylvite)	$\text{MgCl}_2 \cdot 12\text{H}_2\text{O}$ (magnesium chloride dodecahydrate)
$\text{CaCl}_2 \cdot 2\text{H}_2\text{O}$ (sinjarite)	
$\text{CaCl}_2 \cdot 4\text{H}_2\text{O}$ (calcium chloride tetrahydrate)	
Nitrates	
$\text{NaNO}_3$ (nitratine)	$\text{Ca}(\text{NO}_3)_2 \cdot 4\text{H}_2\text{O}$ (nitrocalcite)
$\text{KNO}_3$ (niter)	$\text{Mg}(\text{NO}_3)_2 \cdot 2\text{H}_2\text{O}$ (magnesium nitrate dihydrate)
$\text{Ca}(\text{NO}_3)_2$ (calcium nitrate)	$\text{Mg}(\text{NO}_3)_2 \cdot 6\text{H}_2\text{O}$ (nitromagnesite)
$\text{Ca}(\text{NO}_3)_2 \cdot 2\text{H}_2\text{O}$ (calcium nitrate dihydrate)	$\text{Mg}(\text{NO}_3)_2 \cdot 9\text{H}_2\text{O}$ (magnesium nitrate nonahydrate)
$\text{Ca}(\text{NO}_3)_2 \cdot 3\text{H}_2\text{O}$ (calcium nitrate trihydrate)	
Sulfates	
$\text{Na}_2\text{SO}_4(\text{V})$ (thenardite)	$\text{MgSO}_4 \cdot 1.25\text{H}_2\text{O}$ (magnesium sulfate 1.25 hydrate)
$\text{Na}_2\text{SO}_4(\text{III})$ (sodium sulfate, phase III)	$\text{MgSO}_4 \cdot 2\text{H}_2\text{O}$ (sanderite)
$\text{Na}_2\text{SO}_4 \cdot 7\text{H}_2\text{O}$ (sodium sulfate heptahydrate)	$\text{MgSO}_4 \cdot 2.5\text{H}_2\text{O}$ (magnesium sulfate 2.5 hydrate)
$\text{Na}_2\text{SO}_4 \cdot 10\text{H}_2\text{O}$ (mirabilite)	$\text{MgSO}_4 \cdot 4\text{H}_2\text{O}$ (starkeyite)
$\text{K}_2\text{SO}_4$ (arcanite)	$\text{MgSO}_4 \cdot 5\text{H}_2\text{O}$ (pentahydrate)
$\text{CaSO}_4$ (anhydrite)	$\text{MgSO}_4 \cdot 6\text{H}_2\text{O}$ (hexahydrate)
$\text{CaSO}_4 \cdot 1/2\text{H}_2\text{O}$ (bassanite)	$\text{MgSO}_4 \cdot 7\text{H}_2\text{O}$ (epsomite)
$\text{CaSO}_4 \cdot 2\text{H}_2\text{O}$ (gypsum)	$\text{MgSO}_4 \cdot 11\text{H}_2\text{O}$ (meridianiite)
$\text{MgSO}_4 \cdot \text{H}_2\text{O}$ (kieserite)	
Carbonates	
$\text{NaHCO}_3$ (nahcolite)	$\text{KHCO}_3$ (kalicinite)
$\text{Na}_2\text{CO}_3 \cdot \text{H}_2\text{O}$ (thermonatrite)	$\text{K}_2\text{CO}_3 \cdot 3/2\text{H}_2\text{O}$ (potassium carbonate hydrate)
$\text{Na}_2\text{CO}_3 \cdot 7\text{H}_2\text{O}$ (sodium carbonate heptahydrate)	$\text{MgCO}_3 \cdot 3\text{H}_2\text{O}$ (nesquehonite)
$\text{Na}_2\text{CO}_3 \cdot 10\text{H}_2\text{O}$ (natron)	$\text{MgCO}_3 \cdot 5\text{H}_2\text{O}$ (lansfordite)
Double salts	
$\text{Na}_3\text{NO}_3\text{SO}_4 \cdot \text{H}_2\text{O}$ (darapskite)	$\text{Na}_6\text{Mg}(\text{SO}_4)_4$ (vanthoffite)
$\text{K}_3\text{Na}(\text{SO}_4)_2$ (glaserite, apthitalite)	$\text{Na}_7\text{K}_3\text{Mg}_2(\text{SO}_4)_6(\text{NO}_3)_2 \cdot 6\text{H}_2\text{O}$ (humberstonite)
$\text{Na}_2\text{Mg}(\text{SO}_4)_2 \cdot 4\text{H}_2\text{O}$ (astrakanite, bloedite)	$\text{KCaCl}_3$ (chlorocalcite)
$\text{Na}_2\text{Mg}(\text{SO}_4)_2 \cdot 5\text{H}_2\text{O}$ (konyaite)	$\text{KCa}(\text{NO}_3)_3 \cdot 3\text{H}_2\text{O}$ (potassium calcium nitrate trihydrate)
$\text{Na}_2\text{Ca}(\text{SO}_4)_2$ (glauberite)	$\text{K}_2\text{Ca}(\text{SO}_4)_2 \cdot \text{H}_2\text{O}$ (syngenite)
$\text{Na}_4\text{Ca}(\text{SO}_4)_3 \cdot 2\text{H}_2\text{O}$ (eugsterite)	$\text{K}_2\text{Ca}_5(\text{SO}_4)_6 \cdot \text{H}_2\text{O}$ (gorgeyite)
$\text{KMgCl}_3 \cdot 6\text{H}_2\text{O}$ (carnallite)	$\text{CaMg}_2\text{Cl}_6 \cdot 12\text{H}_2\text{O}$ (tachyhydrite)
$\text{KMgSO}_4\text{Cl} \cdot 3\text{H}_2\text{O}$ (kainite)	$\text{Na}_3\text{H}(\text{CO}_3)_2 \cdot 2\text{H}_2\text{O}$ (trona)
$\text{K}_2\text{Mg}(\text{SO}_4)_2 \cdot 4\text{H}_2\text{O}$ (leonite)	$\text{Na}_6(\text{SO}_4)_2\text{CO}_3$ (burkeite)
$\text{K}_2\text{Mg}(\text{SO}_4)_2 \cdot 6\text{H}_2\text{O}$ (schoenite, picromerite)	$\text{Mg}_5(\text{CO}_3)_4(\text{OH})_2 \cdot 4\text{H}_2\text{O}$ (hydromagnesite)

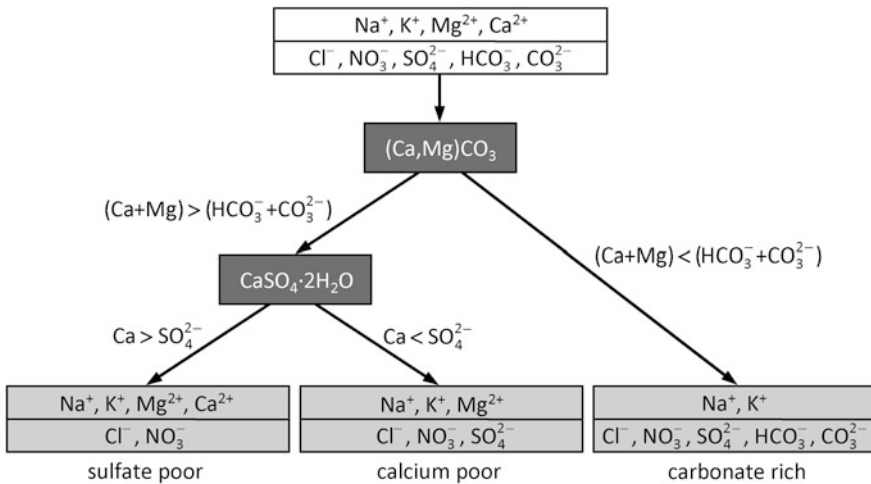


**Fig. 4.21** Evolution of concentrated solutions of major types of hygroscopic salt mixtures. Adapted from Steiger (2003)

Because of its low solubility, calcium sulfate is far less mobile in building stone than any of the remaining salts (Charola et al. 2007).

The mobility of a salt may be conveniently defined as the total amount of salt present in the pore space that could be dissolved in the amount of water filling the pore completely. For example, in a natural stone with a water-accessible porosity of 10 %, the mobility of gypsum is only about  $0.1 \text{ g kg}^{-1}$ , while, in the same material, the mobility of NaCl is  $14 \text{ g kg}^{-1}$  (Steiger 2003). Typically, the concentration of calcium sulfate in historical masonry exceeds its mobility by several orders of magnitude. Hence, only a very small fraction of calcium sulfate present in the pores can be dissolved, even if the pore space is saturated with water. In other words, gypsum, once deposited in the pore space of a building material, tends to continue accumulating over time. Nonetheless, it will also undergo dissolution and crystallization phenomena.

Typically, the solubilities in sulfate-poor (type I) mixtures are very high, particularly if there are significant relative abundances of calcium or magnesium. Type I solutions are very often found in masonry affected by rising damp. Numerous examples can be found in the literature (e.g. Arnold and Zehnder 1991; Zezza et al. 1995; Klenz Larsen 1999, 2004; Schlütter et al. 2003; Sawdy and Price 2005; Weber and Burszán 2008; Brajer and Klenz Larsen 2008; Cooper 2008). The typical fractionation of such mixtures during capillary rise and evaporation of ground moisture has been discussed in detail by Arnold and Zehnder (1991). The least soluble components of type I pore solutions are halite, NaCl, niter,  $\text{KNO}_3$ , and nitratine,  $\text{NaNO}_3$ , which are, therefore, often found in efflorescences of the salt accumulation and damage zones in walls affected by rising damp. In contrast, the very soluble alkaline earth chlorides and nitrates are hardly ever expected to crystallize under normal climatic conditions in buildings. Due to their solubility,

the latter salts often show the strongest enrichment and form a distinct zone above the damage zone in masonry that often appears moist due to their extreme hygroscopicity, as discussed in the following section.

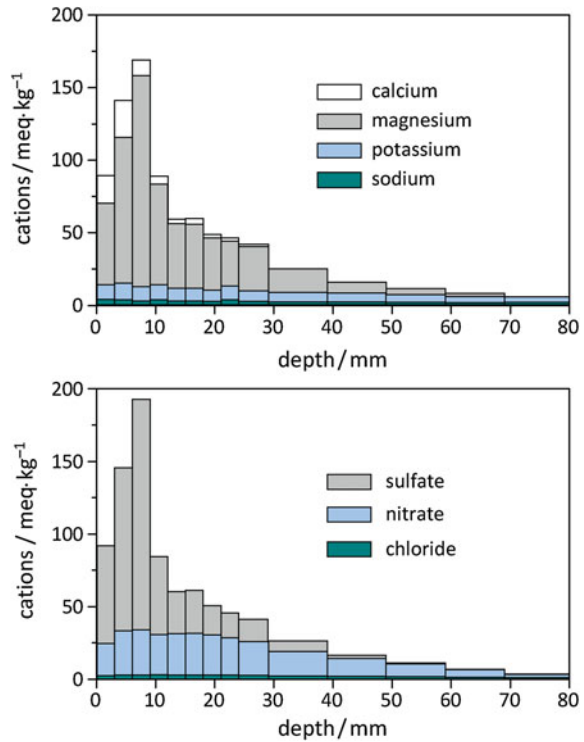
If a pore solution contains more sulfate than calcium, a type II solution evolves upon evaporation. Such a sulfate-rich (or calcium-poor) type of solution composition typically evolves as a result of air pollution attacks to (calcitic) sandstones. In this case, the major reaction products next to gypsum are other sulfates and nitrates listed in Table 4.5. Apart from gypsum, the typical crystalline solids are alkali nitrates, thenardite, magnesium sulfate hydrates, darapskite, and other sulfate-containing double salts such as glaserite (aphthitalite),  $K_3Na(SO_4)_2$ , schoenite,  $K_2Mg(SO_4)_2 \cdot 6H_2O$ , astrakanite,  $Na_2Mg(SO_4)_2 \cdot 4H_2O$ , and syngenite,  $K_2Ca(SO_4)_2 \cdot H_2O$ . Additionally, the evaporation of seawater leads to calcium-poor type salts with halite and carnallite,  $KMgCl_3 \cdot 6H_2O$ , as the major crystalline phases (Braitsch 1971).

In general, it should be noted that salts are not necessarily found where they are formed. For example, salts formed as reaction products of acid deposition are not always found at the stone surface, except for the case of gypsum, which, because of its relatively low solubility, tends to accumulate in the “black crusts” that develop on rain-protected areas. The remaining salts are far more soluble. Their mobilities are one or two orders of magnitude higher than that of gypsum. In effect, unless these salts are present in extremely high concentrations exceeding their mobility, they are usually completely dissolved if the pore space of the stone is filled with water, for example, via the infiltration of rainwater. Therefore, these salts are subject to capillary transport during both the infiltration and the subsequent drying. A similar fractionation mechanism by combined transport and sequential crystallization, which was discussed before for capillary rise and evaporation, is also valid for horizontal transport. This may result from water infiltration as a consequence of roof leaks and broken gutters and downpipes, leading to distinct salt concentration depth profiles in the masonry. For example, Fig. 4.22 depicts a salt profile measured in a sandstone monument. The building is located in a rural environment in Southern Germany where the local air pollution level is low and it is expected that there is a significant contribution of acid rain to the total deposition of acidity.

Magnesium, sulfate, and nitrate are the major constituents of the salt system, whilst the calcium concentration is only of minor importance. The maximum salt concentration (1.1 % w/w total salts) is found at depths of about 6–9 mm. Considering the porosity of the stone and the solubilities in the salt mixture, it can be concluded that, apart from gypsum, all other salts will be completely dissolved if rainwater penetrates the stone. As water evaporates from the stone, salts will crystallize out, resulting in fractionation, as discussed before. For the given salt mixture, it can be simply deduced from available solubility data (see discussion below) that, apart from gypsum, epsomite ( $MgSO_4 \cdot 7H_2O$ ) will be precipitated first. This is in accordance with the profile in Fig. 4.22 showing a strong enrichment of magnesium and sulfate at a distance of 6–9 mm from the surface, whilst the remaining ions are more evenly distributed and are, therefore, probably present in dissolved form. Clearly, the profile shown only reflects an intermediate state.



**Fig. 4.22** Salt profile in sandstone from Schloss Weissenstein, Pommersfelden. Adapted from Steiger (2003)

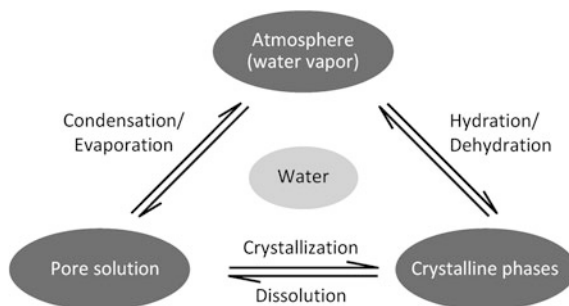


The distribution of the various ions within masonry is only a snapshot in time, as it is the result of a dynamic process affected by continuous transport and phase transformations of the salts. Even if no liquid water reaches the masonry, moisture condensation from changes in temperature and relative humidity as well as the hygroscopicity of materials, including the crystallized salt and its solution, make this system a dynamic one.

#### 4.4.3 Interaction of Salts with the Environment

Salt damage in building stones is the result of confined crystal growth within the pore space. There are various phase changes involving crystal growth, including the crystallization from supersaturated solutions, the change of the state of hydration, and chemical reactions resulting in the growth of new minerals at the expense of previously deposited phases. The dynamics of this process are controlled by the interaction of the salts present in the pore space with the surrounding climatic conditions. Unfavorable climatic conditions result in repeated cycles of crystallization-dissolution or hydration-dehydration. Under such conditions, stone and other building materials are subject to rapid decay.

**Fig. 4.23** Phase transitions of salts in building materials. Adapted from Steiger (2005c)



One obvious climatic influence that can cause cyclic crystallization events is exposure to rainfall. Salts accumulated in the pores are dissolved in rainwater penetrating the stone, and, during the subsequent drying process, the salts crystallize out again and can generate stress. Depending on the amount of salt in the stone, the frequency of rainfall, the exposure of the stone surface to driving rain, and the drying characteristics (largely determined by the properties of the stone and the local microclimatic conditions), such cyclic crystallization processes can cause severe damage to salt-contaminated building stone. However, rainwater is not the only source of liquid water in building materials. In sheltered areas or inside a building, the dynamics of salt damage in porous materials is largely determined by the interaction of the salts present in the pore space and the surrounding atmosphere, i.e. temperature and relative humidity (Arnold and Zehnder 1991). The basic thermodynamics of the underlying phase equilibria have been reviewed by Steiger (2005c). This section provides a brief overview of the crystallization behavior of single salts and salt mixtures.

#### 4.4.3.1 Single Salts

The different interactions between water vapor and crystalline phases are depicted in Fig. 4.23. If a salt is subjected to a slowly increasing relative humidity, the deliquescence or saturation relative humidity (DRH) point will be reached, wherein the solid begins to absorb water vapor, forming a saturated solution. At the deliquescence relative humidity, DRH, three phases can be found in equilibrium: the saturated solution, the solid salt mineral, and water vapor in the ambient air. As the relative humidity is further increased, the solid phase dissolves completely and the solution becomes more dilute. If the dilute salt solution is then subjected to a decreasing relative humidity, water starts to evaporate from the solution until saturation is reached at the saturation or deliquescence humidity DRH. Below this humidity, a solution is not stable, and only a solid phase can coexist with the vapor phase. Therefore, any further decrease in RH will cause the crystallization of the salt and complete evaporation to dryness. It is obvious that fluctuations in the ambient RH across the deliquescence humidity of a salt in a porous stone will cause crystallization-dissolution cycles and rapid decay. The deliquescence humidities of

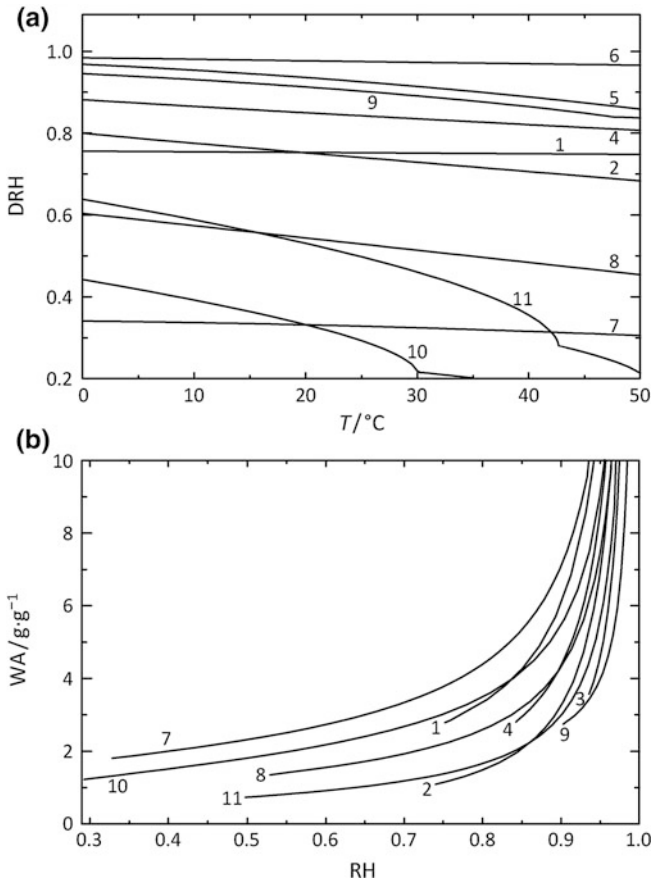


**Fig. 4.24** Deliquescence humidities (a) and hygroscopic moisture uptake (b) of several salts commonly found in building materials: 1 NaCl, 2 NaNO<sub>3</sub>, 3 Na<sub>2</sub>SO<sub>4</sub>, 4 KCl, 5 KNO<sub>3</sub>, 6 K<sub>2</sub>SO<sub>4</sub>, 7 MgCl<sub>2</sub>·6H<sub>2</sub>O, 8 Mg(NO<sub>3</sub>)<sub>2</sub>·6H<sub>2</sub>O, 9 MgSO<sub>4</sub>·7H<sub>2</sub>O, 10 CaCl<sub>2</sub>·6H<sub>2</sub>O, 11 Ca(NO<sub>3</sub>)<sub>2</sub>·4H<sub>2</sub>O

common salts in building materials cover the whole range of typical ambient relative humidities (see Fig. 4.24). For convenience, values of DRH for several important salts are listed at round temperatures in Table 4.6.

Above the deliquescence relative humidity, a salt is dissolved completely and the amount of water uptake is determined by the equilibrium between salt solution and water vapor in the ambient air. At equilibrium, the activity of water,  $a_w$ , in a salt solution equals the relative humidity of the surrounding atmosphere.

$$a_w = \frac{p_w}{p_{w,0}} = \text{RH} \quad (4.16)$$

Here,  $p_w$  and  $p_{w,0}$  are the actual vapor pressure and the saturation vapor pressure of water vapor, respectively. It follows that  $a_w = 1$  for pure water. Any

**Table 4.6** Deliquescence humidities and hydration–dehydration equilibrium humidities of several salts at round temperatures from 0 to 50 °C

	0 °C	10 °C	20 °C	30 °C	40 °C	50 °C
Deliquescence humidities						
NaCl	75.9	75.6	75.4	75.2	75.0	74.8
NaNO <sub>3</sub>	80.1	77.7	75.3	72.8	70.4	68.0
Na <sub>2</sub> SO <sub>4</sub> <sup>a</sup>	98.8 <sup>b</sup>	97.8 <sup>b</sup>	95.6 <sup>b</sup>	90.1 <sup>b</sup>	87.9	88.4
KCl	88.3	86.7	85.0	83.5	82.1	80.7
KNO <sub>3</sub>	97.0	95.5	93.7	91.5	88.9	85.9
MgCl <sub>2</sub> ·6H <sub>2</sub> O	34.1	33.7	33.1	32.4	31.5	30.5
Mg(NO <sub>3</sub> ) <sub>2</sub> ·6H <sub>2</sub> O	61.3	58.6	55.7	52.5	49.2	45.7
MgSO <sub>4</sub> ·7H <sub>2</sub> O	94.5	93.1	91.3	89.1	86.3	83.2 <sup>c</sup>
CaCl <sub>2</sub> ·6H <sub>2</sub> O	44.3	39.4	33.3	21.6 <sup>d</sup>	18.4 <sup>d</sup>	16.3 <sup>e</sup>
Ca(NO <sub>3</sub> ) <sub>2</sub> ·4H <sub>2</sub> O	63.8	58.8	53.1	46.0	35.5	21.3 <sup>f</sup>
Equilibrium humidities						
Na <sub>2</sub> SO <sub>4</sub> (V)–Na <sub>2</sub> SO <sub>4</sub> ·10H <sub>2</sub> O	60.6	68.2	76.4	85.3	–	–
MgSO <sub>4</sub> ·6H <sub>2</sub> O–MgSO <sub>4</sub> ·7H <sub>2</sub> O	30.2 <sup>g</sup>	37.5 <sup>g</sup>	46.7	57.7	70.6	–
MgSO <sub>4</sub> ·H <sub>2</sub> O–MgSO <sub>4</sub> ·7H <sub>2</sub> O	36.1	41.1	46.7	53.0	60.0	67.7 <sup>g</sup>
MgSO <sub>4</sub> ·4H <sub>2</sub> O–MgSO <sub>4</sub> ·6H <sub>2</sub> O	32.0 <sup>g</sup>	35.4 <sup>g</sup>	39.1 <sup>g</sup>	43.3 <sup>g</sup>	48.4 <sup>g</sup>	54.4 <sup>g</sup>

<sup>a</sup> Na<sub>2</sub>SO<sub>4</sub>(V) (thenardite)<sup>b</sup> Na<sub>2</sub>SO<sub>4</sub> · 10H<sub>2</sub>O<sup>c</sup> MgSO<sub>4</sub> · 6H<sub>2</sub>O<sup>d</sup> CaC<sub>12</sub> · 4H<sub>2</sub>O<sup>e</sup> CaC<sub>12</sub> · 2H<sub>2</sub>O<sup>f</sup> Ca(NO<sub>3</sub>)<sub>2</sub> · 3H<sub>2</sub>O<sup>g</sup> metastable

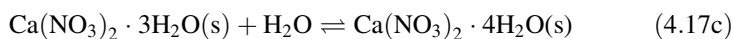
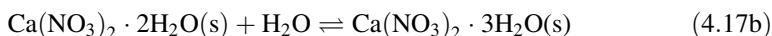
deviation from the equilibrium causes either evaporation of water from the solution (if  $a_w > p_w/p_{w,0}$ ) or condensation of water vapor (if  $a_w < p_w/p_{w,0}$ ). The water activity depends on the composition and concentration of a salt solution and can be experimentally determined by measuring the equilibrium humidity above a salt solution of a given composition. The rate of evaporation is controlled by the difference between the ambient RH and the water activity. Therefore, concentrated salt solutions with low water activity present in the ground moisture zone slow down the evaporation rate significantly and, thus increasing the capillary rise height, as discussed before (see Sect. 4.4.1).

Once a large amount of salt is accumulated in a porous material, the hygroscopic moisture uptake may be the major source of liquid water in the material. This is illustrated in Fig. 4.24 by the hygroscopic water uptake curves for a number of common salts above their respective deliquescence humidities. Above approximately 80 % RH, most salts absorb such a large quantity of water that the water-accessible pore space of the material can be entirely filled with a salt solution if there is sufficient salt enrichment. Considering, for example, a stone material with a total porosity of 15 % that contains 1 % by weight NaCl, the water-accessible pore space is completely filled with a NaCl solution at 91 % RH. Such a solution formed by the hygroscopicity of the salt is subject to capillary

transport, which might be the reason that salts in masonry can be transported to much greater heights than would be expected by simply assuming transport via capillary rise of ground moisture (Klenz Larsen 1999).

The hygroscopicity of a salt is characterized by both the water uptake curves shown in Fig. 4.24 and the deliquescence humidity. In both respects, magnesium and calcium chloride are the most hygroscopic salts. If these salts are enriched in masonry, they will always be responsible for high moisture content in the masonry given their low DRH of about 30 % RH at ambient temperatures. This is also the reason why these salts rarely crystallize out and, therefore, do not induce any crystallization damage. In contrast, other salts have very high deliquescence humidities and will hardly ever go into solution. For example, the deliquescence humidity of  $K_2SO_4$ , arcanite, remains above 97 % at near-ambient temperatures. It is unlikely that this salt dissolves in the absence of another source of liquid water such as rainfall. Finally, gypsum is not hygroscopic at all (DRH > 99.9 %). It is important to remember that water–vapor adsorption is a surface phenomenon. Therefore, the size of the crystals present and their distribution in the masonry will affect the amount of water sorbed.

A number of salts exist in anhydrous and various hydrated forms in which water molecules are part of the crystal lattice of the salt mineral. The most prominent example of that type of equilibrium is the hydration–dehydration equilibrium of anhydrous sodium sulfate (thenardite) and the decahydrate (mirabilite). Many salts found in building materials form different hydrates (see Table 4.5). As already discussed in Sect. 4.2.3, the crystal growth of a hydrated phase can be an important cause of damage. From a thermodynamic point of view, the equilibrium is determined by the relative humidity. If the RH increases above a critical value, the anhydrous or lower hydrated form of a salt picks up moisture from the air, forming a higher hydrated state. For example, in the case of calcium nitrate, several such transitions exist. At 20 °C, the critical RH values for the formation of the di-, tri-, and tetrahydrates are 8.3, 12.4 and 20.5 % RH, respectively. The corresponding phase equilibria are the following:



The tetrahydrate, nitrocalcite, is the highest hydrated form of calcium nitrate. The deliquescence humidity of  $Ca(NO_3)_2 \cdot 4H_2O$  equals 53.1 %. A water uptake curve and the complete phase diagram of the system  $Ca(NO_3)_2$ – $H_2O$  is depicted in Fig. 4.25. Thick solid lines represent deliquescence humidities, i.e. the equilibrium conditions for the coexistence of the various solid phases and a saturated solution. Above these curves, a solution is the stable phase. Thin solid lines are the coexistence curves of two solid phases, i.e. they represent the hydration–dehydration equilibria. At very low temperatures, a solution is not stable, and, hence, the stable phases below  $-28.5$  °C are ice and  $Ca(NO_3)_2 \cdot 4H_2O$ . At temperatures

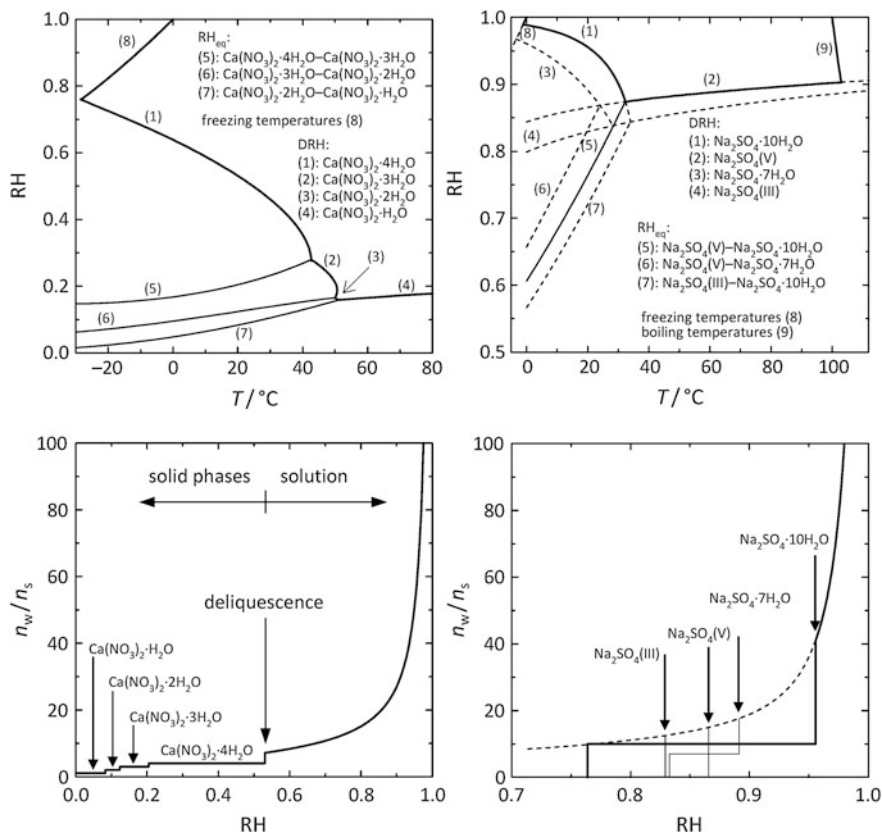


**Fig. 4.25** RH/T phase diagram (*top*) and water uptake curves (*bottom*) of  $\text{Ca}(\text{NO}_3)_2\text{-H}_2\text{O}$  (*left*) and  $\text{Na}_2\text{SO}_4\text{-H}_2\text{O}$  (*right*); dashed curves represent metastable equilibria

between  $-28.5$  and  $0$  °C, two equilibria have to be considered. A solution can either be in equilibrium with ice (line 8) or with  $\text{Ca}(\text{NO}_3)_2\cdot 4\text{H}_2\text{O}$  (line 1). The latter curve represents the deliquescence humidity of the tetrahydrate which is stable from  $-28.5$  to  $42.7$  °C. At a higher temperature, the lower hydrates also have ranges of stable existence.

Calcium nitrate is a very hygroscopic salt with low deliquescence humidity. In effect, the various hydration–dehydration equilibria occur at even lower humidity, and it is unlikely that dehydration of nitrocalcite can occur under typical climatic conditions in buildings. In fact, this is the reason why the lower hydrates have never been identified in building stones. Similarly, the lower hydrated forms of the very hygroscopic salts, bischofite,  $\text{MgCl}_2\cdot 6\text{H}_2\text{O}$ , antarcticite,  $\text{CaCl}_2\cdot 6\text{H}_2\text{O}$ , and nitromagnesite,  $\text{Mg}(\text{NO}_3)_2\cdot 6\text{H}_2\text{O}$ , will hardly crystallize under normal conditions. Due to their hygroscopicity and high solubility, these salts are also most efficient at depressing the freezing temperature of water.



In contrast to the alkaline earth chlorides and nitrates, sodium sulfate is much less hygroscopic, and the formation of  $\text{Na}_2\text{SO}_4$  solutions requires very humid conditions, particularly at temperatures below 25 °C. Therefore, in the absence of other sources of liquid water, typical fluctuations in ambient temperature and relative humidity are such that hydration–dehydration reactions are more likely to occur than deliquescence–crystallization cycles. However, the situation with this salt becomes a lot more complicated due to the formation of metastable phases. Apart from thenardite,  $\text{Na}_2\text{SO}_4(\text{V})$  and mirabilite, there are two additional phases, namely, the heptahydrate  $\text{Na}_2(\text{SO}_4)\cdot 7\text{H}_2\text{O}$  (Rijniers et al. 2005; Hamilton et al. 2008) and the anhydrous polymorph  $\text{Na}_2\text{SO}_4(\text{III})$  (Grossi et al. 1997; Rodriguez-Navarro et al. 2000; Linnow et al. 2006).

The phase diagram of the system  $\text{Na}_2\text{SO}_4\text{--H}_2\text{O}$  and the water uptake curve were recently updated and are also shown in Fig. 4.25 (Steiger and Asmussen 2008). Due to the presence of the metastable phases, the phase diagram is considerably more complicated than previously assumed. However, both metastable phases were identified in experimental studies where, for kinetic reasons, they were formed instead of the stable phases. A more detailed discussion of the phase diagram and the importance of the metastable salts for understanding the damage mechanism of sodium sulfate crystallization in stone can be found in the literature (e.g. Espinosa-Marzal and Scherer 2008; Hamilton et al. 2008; Steiger and Asmussen 2008).

There are also other salts commonly found in building materials whose crystallization behavior is characterized by the formation of metastable phases. In the case of calcium sulfate, gypsum,  $\text{CaSO}_4\cdot 2\text{H}_2\text{O}$ , is the major phase found even at very low relative humidity, although anhydrous  $\text{CaSO}_4$  (anhydrite) is the thermodynamically stable phase under such conditions (Charola et al. 2007). The dehydration of gypsum is hindered for kinetic reasons. Considering the ubiquitous presence of very high gypsum concentrations in building materials, it is beneficial that it is obviously not subject to extensive dehydration–rehydration cycles.

Even more complex is the behavior of the magnesium sulfate hydrates. In the  $\text{MgSO}_4\cdot n\text{H}_2\text{O}$  series, all compounds with  $n = 11, 7, 6, 5, 4, 3, 2.5, 2, 1.25,$  and 1 exist. However, the only thermodynamically stable phases are meridianiite ( $n = 11$ ), epsomite ( $n = 7$ ), hexahydrate ( $n = 6$ ), and kieserite ( $n = 1$ ). An updated phase diagram of the system, considering both stable and metastable phases, was presented recently by Steiger et al. (2011). Meridianiite is only stable at subzero temperatures. In addition, the magnesium sulfate hydrates are only deliquescent at high relative humidities. As changes in the state of hydration require lower relative humidities, they are more likely to occur under typical ambient conditions. Laboratory experiments have shown that, due to sluggish kieserite formation, metastable phases are the major dehydration products of epsomite and hexahydrate (Chipera and Vaniman 2007; Wang et al. 2009; Steiger et al. 2011). In these experiments, the tetrahydrate starkeyite,  $\text{MgSO}_4\cdot 4\text{H}_2\text{O}$ , was found as the most abundant compound under near-ambient conditions (see Table 4.6).

Several common salts do not form hydrated phases, e.g.  $\text{NaNO}_3$ ,  $\text{KNO}_3$ ,  $\text{KCl}$ , and  $\text{K}_2\text{SO}_4$ . Their phase diagrams are particularly simple and are characterized by

their deliquescence humidities (see Fig. 4.24). The hydrated form of sodium chloride is hydrohalite,  $\text{NaCl}\cdot 2\text{H}_2\text{O}$ , which, however, is only formed at subzero temperatures. Similarly, there exist higher hydrated phases of magnesium chloride and nitrate (see Table 4.5) that are only stable at low temperatures.

#### 4.4.3.2 Salt Mixtures

From the phase diagrams discussed so far, the properties of a single salt in porous stone can be easily predicted. Crystallization damage may be avoided by maintaining the relative humidity of the air either permanently below or above the deliquescence humidity. If the RH is kept below the deliquescence humidity, the salt remains in solid form, and, at humidities above the saturation value, the salt remains in solution the whole time. Similar arguments apply to the equilibrium humidity of a hydration reaction. However, contamination with a single salt is extremely uncommon, and, unfortunately, the situation becomes a lot more complicated for mixed systems compared to pure salts as the concept of the saturation humidities of the individual salts no longer applies to mixtures (Price and Brimblecombe 1994; Steiger and Dannecker 1995; Steiger and Zeunert 1996). In fact, salt efflorescences on walls containing complex salt mixtures have been observed at considerably lower relative humidities than would have been expected from the saturation humidities of the respective pure salts (Arnold and Zehnder 1991).

The more complex behavior in salt mixtures can be easily understood considering the influences on solubility equilibria in mixed solutions. The equilibrium constant (the thermodynamic solubility product) of the dissolution reaction [Eq. (4.3), Sect. 4.2.3] is given by

$$\ln K_{\text{MX}} = \nu_{\text{M}} \ln m_{\text{M}} + \nu_{\text{M}} \ln \gamma_{\text{M}} + \nu_{\text{X}} \ln m_{\text{X}} + \nu_{\text{X}} \ln \gamma_{\text{X}} + n \ln a_{\text{w}} \quad (4.18)$$

where  $\gamma_{\text{M}}$  and  $\gamma_{\text{X}}$  are the activity coefficients, and  $m_{\text{M}}$  and  $m_{\text{X}}$  are the molalities of the cation M and the anion X in the saturated solution. It is obvious that the solubility of a salt is strongly affected by the presence of a second salt which might have one ion in common, i.e. increasing either  $m_{\text{M}}$  or  $m_{\text{X}}$ . The second salt will also affect the solubility if it does not have a common ion, as it influences the activity coefficients of the ions M and X. As an example, Fig. 4.26a depicts the solubilities of NaCl and  $\text{NaNO}_3$  in their respective mixed solutions. Due to the common ion effect, the solubilities of both salts decrease with increasing concentration of the respective second salt. The crystallization pathways of mixed solutions upon the evaporation of water can be readily deduced from the solubility diagram. For example, if water evaporates from a solution of initial composition A, the solution becomes more concentrated and the solution composition moves along line AB. Reaching point B, the solution is saturated with respect to  $\text{NaNO}_3$ , and, upon continued evaporation, this salt will start to crystallize out. As  $\text{NaNO}_3$  is removed, the composition of the solution changes; the nitrate concentration decreases while the NaCl concentration still increases due to ongoing evaporation. Therefore, the crystallization of  $\text{NaNO}_3$  continues and the composition of the solution moves

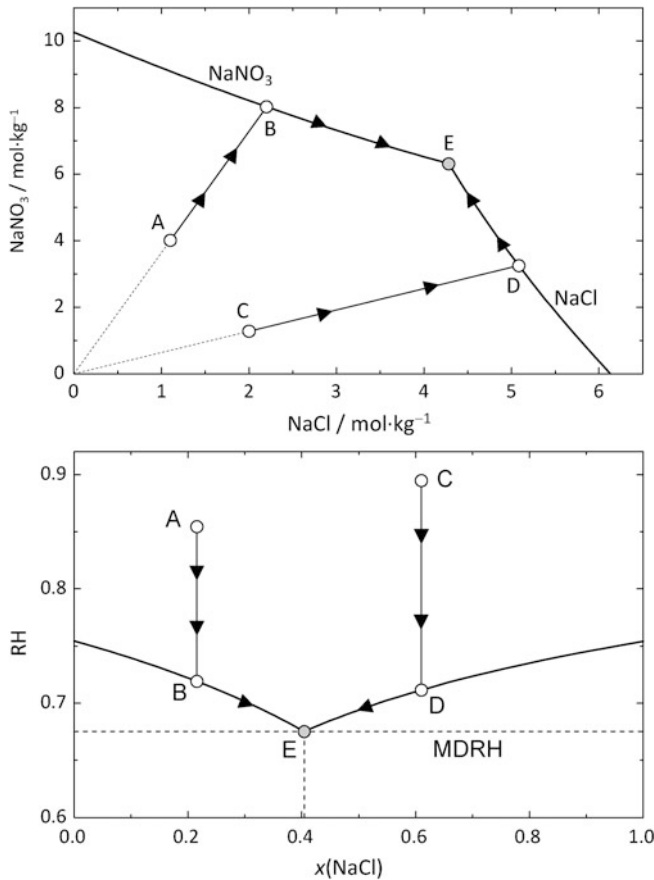


**Fig. 4.26** Solubilities (a) and saturation humidities (b) in the NaCl–NaNO<sub>3</sub>–H<sub>2</sub>O system at 19 °C

along the solubility curve of NaNO<sub>3</sub> until the solution reaches saturation, also with respect to NaCl at point E, which is the drying point of this system. Any further evaporation causes the crystallization of both solids to complete dryness. A solution of initial composition C follows a similar crystallization pathway. In this case, however, the first solid that crystallizes is NaCl, and NaNO<sub>3</sub> is only precipitated at the crystallization end point.

The relative humidities in equilibrium with the respective saturated solutions are depicted in Fig. 4.26b. The mixture composition is expressed in terms of the mole fraction of chloride. It can be seen that the relative humidity in equilibrium with solution A is  $RH_{eq} = 86\%$ . In order to reach saturation with NaNO<sub>3</sub>, the RH has to be decreased to 72.5%, which is the equilibrium or saturation humidity of solution B. NaNO<sub>3</sub> starts to crystallize below this humidity. The crystallization end point is reached at 67.5% RH. In comparison with the two single salts, the crystallization of NaNO<sub>3</sub> starts at a slightly lower RH than for a pure NaNO<sub>3</sub>

solution (72 % instead of 75 %), while the crystallization of NaCl starts at a significantly lower RH (67.5 % instead of 75 %). For the solution with initial composition C ( $RH_{\text{eq}} = 89\%$ ), NaCl starts to crystallize at 71.5 %. Upon further evaporation, more NaCl is precipitated and  $\text{NaNO}_3$  crystallizes at 67.5 %, i.e. far below its single salt DRH. This simple example explains why the formation of efflorescences on walls containing complex salt mixtures occurs at significantly lower RH than implied by the deliquescence humidities of the pure salts.

The behavior of a single salt at a given temperature can be sufficiently characterized by a single value of DRH. If the humidity remains above this RH, the salt remains dissolved; however, if it drops below the DRH, the salt will crystallize. In contrast, a range of relative humidity is required to characterize the crystallization properties of salt mixtures. The upper RH limit depends on mixture composition and is given by the saturation RH curves of the two salts, as shown in Fig. 4.26b for NaCl and  $\text{NaNO}_3$ . Above these saturation humidities, the salt mixture remains in solution the whole time. Thus, these curves define the RH below which the crystallization of a solid phase starts. The lower RH limit is given by the relative humidity in equilibrium with the solution that is saturated in both solids. This relative humidity is called the mutual DRH (MDRH). The MDRH is the lowest RH at which a mixed solution of two or more salts can still exist. The MDRH is also the RH at which the dry salt mixture, provided that the two solids are intimately mixed, first acquires water vapor and forms a saturated solution. The MDRH is always lower than the DRH of any single salt in the mixture. In the range between the MDRH and the crystallization humidities, a salt solution and crystalline deposits coexist. In effect, the crystallization of one salt from a mixed solution does not occur at a specific value but rather across a range of relative humidities (Price and Brimblecombe 1994; Steiger and Dannecker 1995; Steiger and Zeunert 1996).

The simple example of a NaCl– $\text{NaNO}_3$  mixture also provides insight into the process of salt fractionation during transport, as mentioned before. Depending on the initial mixture composition, one of the two solids is first precipitated. If salt crystallization occurs during the transport of the solution, the first salt is immobilized while the solution enriched with the second salt is still subject to transport. Considering evaporation of a mixed solution from a porous stone, one component of the mixture, for example,  $\text{NaNO}_3$  in the case of solution composition A in Fig. 4.26, crystallizes first and might form an efflorescence on the stone surface during the initial drying phase. With ongoing evaporation, the drying front eventually moves into the interior of the stone where the remaining salt mixture continues to crystallize as a subflorescence. It is important to note that the composition of an efflorescence generally is not representative of the salts that are present in the interior.

Fractionation also has important consequences for the deliquescence behavior of salt mixtures. If the dry salts do not form an intimate mixture, the MDRH is not the relative humidity at which the salts pick up moisture again and form a solution. As a result of the fractionation, there are salt deposits consisting of more or less only a single salt. Consequently, deliquescence occurs at the DRH of this single salt. In effect, there is an offset between the drying point of the mixed solution, i.e.

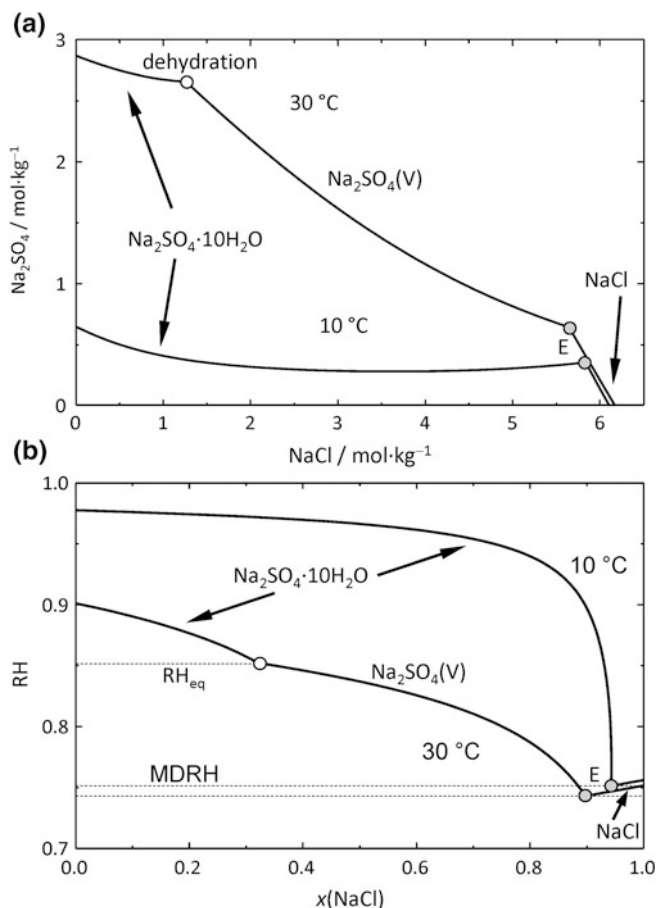


**Fig. 4.27** Solubilities (a) and saturation humidities (b) in the NaCl–Na<sub>2</sub>SO<sub>4</sub>–H<sub>2</sub>O system at 10 and 30 °C

the MDRH of this mixture, and the actual deliquescence humidity, which is the DRH of one of the mixture components.

The discussion so far has only considered a very simple situation, i.e. a mixture with only three different ions and with two crystalline salts that neither form different hydrated states nor double compounds. Moving to different mixture compositions, particularly including sulfate as one of the components, the solubility diagrams become more complicated. Examples including the thenardite-mirabilite equilibrium in the presence of NaCl are shown in Fig. 4.27. According to Eq. (4.18), the solubility of a hydrate salt also depends on the water activity  $a_w$ . In addition to the common ion effect and the influence on the ion activity coefficients, there is also an influence of the components of a mixture on the water activity. With increasing concentration of a salt solution, the water activity decreases, resulting in a solubility increase at high concentrations of the second

salt. This is the reason for the course of the mirabilite solubility curve at 10 °C (Fig. 4.27a). However, according to Eq. (4.7), the dehydration equilibrium is also determined by the water activity. While mirabilite dehydration does not occur at 10 °C (even in saturated NaCl solutions), much lower NaCl concentrations, i.e. far higher water activities are sufficient at 30 °C. The reason for this behavior is the strong temperature dependence of the thenardite-mirabilite equilibrium (see Fig. 4.25). At low temperatures, the dehydration equilibrium humidity is lower than the deliquescence humidity of the salt mixture. At temperatures above 18 °C, the dehydration humidity exceeds the deliquescence humidity and the dehydration or rehydration occurs in the presence of a solution. In the presence of hygroscopic salts such as magnesium chloride, this effect is even more pronounced. This might have important implications, as hydration and dehydration reactions are known to be sluggish in the absence of liquid water (Charola and Weber 1992; Doehne 1994; Steiger et al. 2008a). Therefore, hydration reactions that can cause damage in porous stone can be significantly accelerated in salt mixtures. It is important to note, however, that the presence of other salts does not influence the values of the equilibrium humidity of a hydration–dehydration equilibrium. Hence, the equilibrium curve for the thenardite-mirabilite equilibrium that is shown in Fig. 4.25 also applies to salt mixtures.

Another significant complication in the behavior of salt mixtures arises from the fact that the salts commonly found in building materials form a large number of double salts, i.e. salts that are comprised of three or more different ions. Figure 4.28 shows solubility diagrams including the common double salts astrakanite (bloedite),  $\text{Na}_2\text{Mg}(\text{SO}_4)_2 \cdot 4\text{H}_2\text{O}$ , glaserite (aphthitalite),  $\text{K}_3\text{Na}(\text{SO}_4)_2$ , and darapskite,  $\text{Na}_3\text{NO}_3\text{SO}_4 \cdot \text{H}_2\text{O}$ . Further double salts are listed in Table 4.5. Astrakanite is one of the rare examples of a congruently soluble double salt that is found in building materials. If a compound dissolves congruently, the solution and the solid have the same stoichiometric composition. For example, the dashed line in Fig. 4.28a represents the composition of an equimolar mixture of  $\text{Na}_2\text{SO}_4$  and  $\text{MgSO}_4$ , i.e. a mixture of the same mixing ratio as in the double salt astrakanite. Evaporation of water from a solution of that composition yields first saturation with respect to the double salt which would crystallize out. Since precipitation of astrakanite does not change the solution composition, the equimolar solution behaves just like a single salt. The salt crystallizes out if the ambient RH drops below its saturation humidity, and the dry double salt picks up moisture and forms a solution as the RH is increased to its deliquescence humidity again.

Unfortunately, most of the double salts that are found in building materials are incongruently soluble. For example, the dashed line in Fig. 4.28b represents the stoichiometric composition of aphthitalite, i.e. a 3:1 molar mixture of  $\text{K}_2\text{SO}_4$  and  $\text{Na}_2\text{SO}_4$ , respectively. It is obvious that evaporation of such a solution at 15 °C yields saturation with respect to arcanite ( $\text{K}_2\text{SO}_4$ ) and not aphthitalite. As a consequence, a saturated solution of aphthitalite is supersaturated with respect to arcanite.

Therefore, if the double salt dissolves in a limited amount of water, arcanite would crystallize out instead. It is obvious that the crystallization behavior of



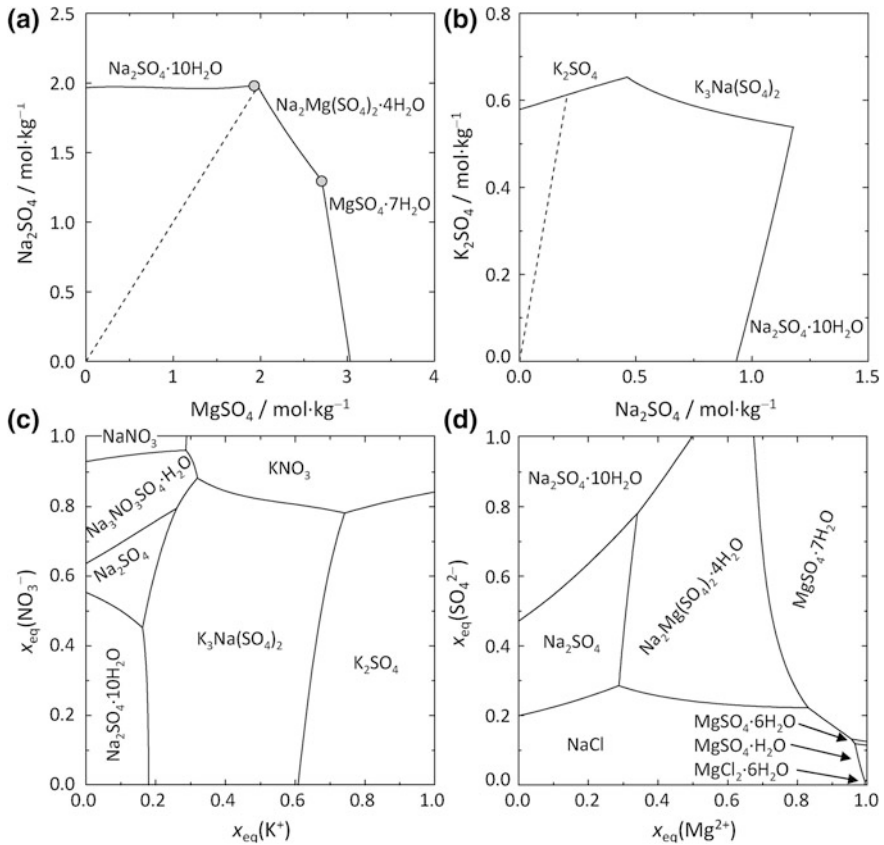


**Fig. 4.28** Solubilities in **a** The  $\text{Na}_2\text{SO}_4$ – $\text{MgSO}_4$ – $\text{H}_2\text{O}$  system at 25 °C, **b** The  $\text{Na}_2\text{SO}_4$ – $\text{K}_2\text{SO}_4$ – $\text{H}_2\text{O}$  at 15 °C, **c** The  $\text{Na}^+$ – $\text{K}^+$ – $\text{NO}_3^-$ – $\text{SO}_4^{2-}$ – $\text{H}_2\text{O}$  system at 25 °C, and **d** The  $\text{Na}^+$ – $\text{Mg}^{2+}$ – $\text{Cl}^-$ – $\text{SO}_4^{2-}$ – $\text{H}_2\text{O}$  system at 25 °C

incongruently soluble double salts is considerably more complicated than that of single salts. Although the formation of double salts has been frequently observed in buildings, only a few laboratory investigations of salt damage in porous stone have been carried with salt mixtures including double salt formation. A recent study of De Clercq (2008) confirms the complex behavior of such mixtures.

The phase diagrams of slightly more complex mixtures that comprise four different ions, two cations and two anions, are also shown in Fig. 4.28. For the sake of simplicity, the solubilities are given as so-called Jänecke projections, i.e. the water content of the saturated solutions is not shown. All possible mixtures of the four ions are represented in terms of charge-equivalent mole fractions of the cations and the anions, respectively, i.e. the fractional contribution of each cation to the total number of positive charges and the contribution of each anion to the total number of negative charges. The corners of the square diagram, therefore,

represent the four pure salts. For example, Fig. 4.28c depicts the solubility diagram of a mixed system containing sodium, potassium, sulfate, and nitrate. Therefore, in this diagram, the corners represent the four salts sodium sulfate, sodium nitrate, potassium sulfate, and potassium nitrate. The lines in the interior of the square are the saturation curves for solutions coexisting with two solid phases. These curves define the crystallization fields of the different mineral phases that would first crystallize out for a given mixture composition. According to the phase rule, a maximum of three different solids can coexist with a mixed solution containing four different ions. The corresponding isothermal invariant points are given as the intersections of the two salt coexistence curves.

In the  $\text{Na}^+ - \text{K}^+ - \text{NO}_3^- - \text{SO}_4^{2-} - \text{H}_2\text{O}$  system, there are seven different crystalline phases that have a range of stable existence at 25 °C. These are anhydrous potassium nitrate (niter), sodium nitrate (nitratine) and potassium sulfate (arcanite), thenardite and mirabilite, and the double salts darapskite and glaserite. A lot of information about the crystallization properties of the four-component system can be readily derived from the diagram. First, it is obvious that the double salts, particularly aphthitalite, have large stability fields and will, therefore, easily form in this four-component system. Second, it can be seen that only certain mineral combinations represent a stable assemblage. For example, niter can coexist with both double salts, with nitratine and arcanite, but with neither thenardite nor mirabilite. Similarly, in the  $\text{Na}^+ - \text{Mg}^{2+} - \text{Cl}^- - \text{SO}_4^{2-} - \text{H}_2\text{O}$  phase diagram (Fig. 4.28d), NaCl (halite) can coexist with the various  $\text{MgSO}_4$  hydrates, but there is no stable assemblage of bischofite,  $\text{MgCl}_2 \cdot 6\text{H}_2\text{O}$ , with either thenardite or mirabilite. Also in this system, there is a large stability field of a double salt (astrakanite), while the very soluble and hygroscopic bischofite only has an extremely small range of stable existence.

#### 4.4.3.3 Modeling of Crystallization Pathways in Salt Mixtures

Phase diagrams as those shown in Fig. 4.28 allow the prediction of complete crystallization pathways as discussed before for the NaCl–NaNO<sub>3</sub> mixture. For practical applications, it is impossible to conduct all the necessary measurements for a huge number of mixture compositions. In order that phase equilibria can be predicted, a model approach is more appropriate (Price 2000; Steiger 2005c). It follows from Eq. (4.7) that calculating solubility equilibria in mixed salt systems requires (a) values of the equilibrium constants,  $K_{\text{MX}}$ , in the temperature range of interest and (b) activity coefficients of the aqueous species as a function of solution composition and temperature. The ion interaction model from Pitzer (1991) has been successfully applied for the prediction of ion activities in complex, mixed electrolyte solutions. The model parameters, including the thermodynamic solubility product, are determined from available experimental data for single salts and simple mixtures (Steiger et al. 2008b). Once the model is parameterized, it can be used to predict crystallization pathways and the critical climatic conditions for complex salt mixtures that are present in building materials.

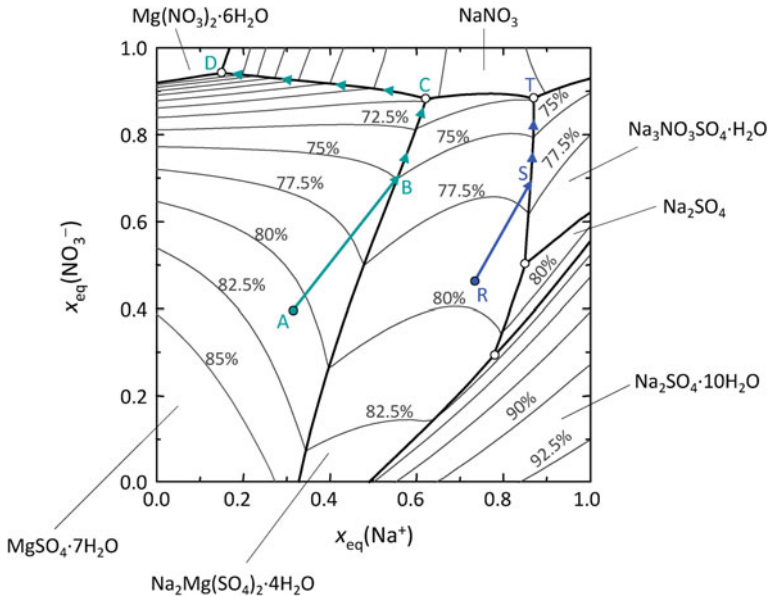


**Fig. 4.29** Solubilities and saturation humidities in the system  $\text{Na}^+ - \text{Mg}^{2+} - \text{NO}_3^- - \text{SO}_4^{2-} - \text{H}_2\text{O}$  at 25 °C. Adapted from Steiger et al. (1998)

The use of such a model approach is illustrated in Fig. 4.29, which represents a calculated phase diagram of the four-component system  $\text{Na}^+ - \text{Mg}^{2+} - \text{NO}_3^- - \text{SO}_4^{2-} - \text{H}_2\text{O}$ . For any solution composition, the crystallization pathway can be readily predicted from the phase diagram. For example, epsomite would crystallize out first from a solution of composition A. Due to the crystallization of epsomite, the solution becomes depleted in magnesium and sulfate. Hence, the solution composition moves along line AB, which is the extension of the straight line connecting point A, the solution composition, with the composition of the solid phase, i.e. the corner representing pure  $\text{MgSO}_4$ . As more water evaporates, epsomite continues to crystallize until the solution is also saturated with respect to astrakanite at point B.

Further removal of water then causes the simultaneous crystallization of epsomite and astrakanite until, at point C, the solution is also saturated with respect to nitratine. The solution is now saturated with respect to three solids. However, point C is not the crystallization end-point for a solution of initial composition A, but C is rather a transformation point. Assuming full equilibrium between the solution and the solids already precipitated, further removal of water would lead to the complete dissolution of astrakanite and the precipitation of nitratine instead. Then, the solution composition moves along the line CD. Finally, point D is the drying point of the solution of initial composition A.

The equilibrium model can also be used to calculate the relative humidity in equilibrium with a solution of any composition. Equilibrium humidities of saturated

solutions are particularly important, as they indicate the critical relative humidities below which a solution of a given composition starts to crystallize. In Fig. 4.29, these critical values are plotted as lines of equal saturation humidity. As in the examples discussed before, it is obvious that there is a considerable decrease in the saturation humidities of the different solids in the presence of other ions.

Such diagrams can be used to obtain critical ranges of relative humidity, within which fluctuations cause crystallization or other phase changes. For example, in a solution of composition A, epsomite starts to crystallize at about 81 % RH, which has to be compared to the saturation humidity of 90.3 % of a pure  $\text{MgSO}_4$  solution at the same temperature. Further decreasing the relative humidity, the solution also becomes saturated with astrakanite at 75 % RH. At about 70 % RH, the double salt redissolves and nitratine starts to precipitate instead. Finally, the crystallization end-point of solution A is reached at a relative humidity of 50 % RH, yielding a mixture of epsomite, niter, and nitromagnesite,  $\text{Mg}(\text{NO}_3)_2 \cdot 6\text{H}_2\text{O}$ .

It is important to note, however, that completely different crystallization pathways result for other solution compositions. For example, the composition of solution R in Fig. 4.29 is in the astrakanite stability and, therefore, follows a different crystallization pathway. Astrakanite starts to crystallize from this solution slightly below 80 % RH, and the remaining solution becomes depleted in sodium, magnesium, and sulfate according to the stoichiometric composition of astrakanite, i.e.  $x_{\text{eq}}(\text{Na}) = 0.5$ ,  $x_{\text{eq}}(\text{NO}_3^-) = 0$ . Hence, the solution composition moves along line RS, reaching saturation with the second double salt darapskite at about 77 % RH (point S). Below this RH, both double salts crystallize simultaneously until the solution composition reaches point T at 75 % RH. Point T is the drying point of solution R, and hence, the dry salt mixture consists of astrakanite, darapskite, and niter. Different pathways are obtained for other solution compositions.

The salt mixtures found in building materials are typically more complex, and it is usually not possible to represent the complete phase diagram of such a mixed system in a simple two-dimensional diagram. However, using a model, it is still possible to calculate the crystallization pathways for any mixture composition. It is possible to predict the critical conditions of climatic conditions that would cause crystallization or hydration processes that could possibly cause material damage. There are several possible applications of thermodynamic models in the conservation of building materials (Steiger 2005c), and a number of very useful applications, using experimentally-determined salt mixture compositions in samples from various building materials as model input data, can be found in the literature (Steiger 1996; Sawdy 2001; Bionda and Storemyr 2002; Schlütter et al. 2003; Sawdy and Price 2005; Bionda 2006; Price 2007; Klenz Larsen 2007; Prokos 2008; Zehnder and Schoch 2009).

In many of these studies, the programs RUNSALT and ECOS (Environmental Control of Salts) were used to calculate the crystallization pathways of salt mixtures from a number of different objects. ECOS was developed in a collaborative project funded by the European Commission (Price 2000). The use of ECOS requires an ionic analysis of a sample taken from the building or the salt-contaminated material in question. The program is then able to predict the crystallization

pathways for specified conditions of RH and temperature. RUNSALT is an improved interface to the fundamental thermodynamic model that was subsequently developed by Bionda (2006).

## 4.5 Biodeterioration of Stone

From the biological point of view, stone is an extreme environment. It is poor in nutrients and suffers large changes in moisture content, with wind and rain wearing away its surface while the sun provides perniciously high UV radiation. Nevertheless, stone is inhabited by microorganisms in all climate regions of the Earth, ranging from the cold Antarctic to temperate and tropical areas to the hot deserts and rocky shores in all places (Warscheid and Braams 2000; Selbmann et al. 2005; Sterflinger 2005). The microorganisms can be epilithic, i.e. living on the rock surface, or endolithic when living within pores and fissures of the stone, and they can grow in both terrestrial as well as aquatic habitats.

Microorganisms, plants, and animals play a considerable role in the formation of rocks. The so-called “banded iron formations” are a result of iron oxidation due to oxygen release by cyanobacteria; carbonate sediments are formed by precipitation resulting from the algal and bacterial CO<sub>2</sub> uptake from seawater at continental edges; massive carbonate rocks were created by the shells of bryozoans, corals, and mollusks; microbes catalyze the diagenesis of crystalline or amorphous components in rock. Finally, they play a major role in the weathering of rock. Geomicrobiologists even postulate that the weathering of rock in the presence of microbes is some ten thousand times faster than without them, the latter being a mere theoretical hypothesis because there are no sterile rock surfaces on Earth. Whereas the alteration of rocks in the natural environment is referred to as bio-weathering, the damage of stone in man-made objects is called biodeterioration (Allsopp et al. 2003; Scheerer et al. 2009).

A biopatina refers to the aesthetic chromatic modification of the material caused by the growth of some organisms but with no visible surface deterioration. On the other hand, the staining that may remain on the stone after the biological organisms have disappeared is called a biogenic discoloration.

The most decisive factor of microbial growth is the availability of water. Therefore, porous stones that are able to retain large amounts of water are easily colonized by a wide variety of bacteria and fungi. Stones with lower porosity or those that easily dry after rain events will not be colonized as easily. Primary colonization requires longer times, and the species diversity of this colonization is generally more restricted.

Bacteria generally need high water activity ( $a_w > 0.98$ ). Fungi and lichen are able to grow at much lower water activity ( $a_w > 0.65$ ) and tolerate periods of complete dryness in a dormant state. However, bacteria are able to tolerate high salt concentrations on and inside of stone (Rivadeneira et al. 2004). For this reason, very humid and salty environments, such as foundations and plinth walls

on exterior facades, are often inhabited by salt-tolerating bacteria but are nearly free of fungal growth. The exception is the growth of some fungal species like *Hortaea werneckii* and *Wallemia ichthyophaga* growing on salty walls in exterior and interior environments (Gunde-Cimerman et al. 2009). Exposed stone surfaces receiving high UV radiation, and with drastic changes in humidity resulting from rain events followed by dry spells, are usually inhabited by black fungi and by cyanobacteria forming dark green and brown crusts on and within natural stone. Algal films are common in extremely damp semi-basements, on pavement, and on terraces.

### 4.5.1 Organisms Involved in Biodeterioration

#### 4.5.1.1 Bacteria

Bacteria are small and mostly single-cell organisms, their size ranging between 1 and 5  $\mu\text{m}$  but up to 100  $\mu\text{m}$  in some special genera. Bacteria are common inhabitants of soil, and their presence is essential for the function of all ecosystems on Earth. In one gram of agricultural soil, there are up to  $10^9$  bacterial cells, while, in a porous stone, there might be up to  $10^6$  cells inhabiting its surface, pores, cracks, and fissures. Because of their remarkable capability of processing materials, ranging from degradation of organic compounds, i.e. hydrocarbons and plastics, to their capability of using carbon monoxide, hydrogen, and minerals as energy sources, bacteria are able to cope with nearly all environmental conditions. However, in arid and semi-arid areas, they are rare, while fungi and lichen, being more tolerant to drier conditions, are predominant. Nonetheless, in extremely dry environments, bacteria can grow as endobionts in the thalli of lichens. Although single bacteria cannot be seen with the naked eye, they can produce visible deterioration phenomena such as discoloration, sanding, and etching of stone.

#### Chemoheterotrophic Bacteria

By definition, chemoheterotrophic bacteria are those that need organic carbon sources for growth. On and in stone, nutrients for heterotrophic bacteria are available from the metabolites of autotrophic bacteria, from airborne organic contamination and dripping water, from animal feces, and from organic compounds that may sometimes be present in the substrate itself.

Chemoheterotrophs can degrade a wide variety of substances, including natural materials from plants and animals, as well as man-made substances such as polycyclic aromatic hydrocarbons (PAHs) derived from traffic; resins or waxes used for the consolidation of stone; and methylcellulose or other organic additives commonly used in slurries and coatings. From this capability, it can be easily deduced that the growth of bacteria on rock can be significantly enhanced by the addition of organic carbon. Chemoheterotrophs produce organic pigments and a



wide range of organics acids. For this reason, they are important deteriorating agents of stone, causing color change and biogenic corrosion. Filamentous bacteria—actinomycetes—inhabit stone more effectively than most of the single-cell bacteria. This can be attributed to their filamentous growth as well as to their effective utilization of various nitrogen and carbon sources (Saarela et al. 2004).

### Chemolithotrophic Bacteria

The chemolithotrophic bacteria—in contrast to the heterotrophs—do not depend on organic carbon sources. Their growth is based on the oxidation of minerals containing iron, sulfur, manganese, or ammonia. Ammonia oxidizers preferentially occur in very damp environments where ammonia is available, e.g. plinths and foundations in the vicinity of animal stables or damaged canalizations. During the process of ammonia oxidation, both nitrite and nitrate ions are released and can lead to the formation of nitrous and nitric acids and the corrosion of natural stone, mortar, and even concrete. On undisturbed stone surfaces, iron and manganese oxidation by bacteria leads to the formation of desert varnish, a dense blackish-brown layer covering the rock surface. Rock varnish occurs on a variety of substrates, including stone and ceramics in diverse environments (O’Grady 2005). Iron and sulfur oxidizing bacteria produce sulfurous and sulfuric acid and are biotechnologically used for the leaching of copper, iron, uranium, and gold from ore-containing rocks.

### Phototrophic Bacteria and Micro-Algae

Phototrophic bacteria occur on all stones if sufficient light and water are available. “Phototrophic” means that these bacteria are able, from the absorption of sunlight, to generate the energy they need for the maintenance of their metabolism, growth, and propagation. This process is called photosynthesis and is also used by higher plants and algae. Phototrophic bacteria build up cell material by incorporating CO<sub>2</sub> and transforming it into carbohydrates such as sugar, using the same biochemical mechanism of higher plants. This is called the Calvin-cycle.

In nature, there are some phototrophic bacteria that need sulphur in addition to water, sunlight, and CO<sub>2</sub>. These do not produce oxygen. They perform an “anoxic” photosynthesis. These bacteria are either pigmented purple “phototrophic purple bacteria” or green “green anoxygen phototrophs”. Both, however, require high  $a_w$  values, and their growth is restricted to aqueous environments. Therefore, the organisms can develop on stones found in small lakes and tarns, where the water might seasonally become anoxic. Only in very rare cases might they affect stone monuments in the vicinity of such aqueous environments. For example, parts of the remnants of the Temple of Artemis in Ephesus (Turkey)—one of the Seven Wonders of the World—are located within and underneath a brackish-water tarn that turns completely red with the bloom of purple bacteria in summer, and that results in the purple coloration of the white calcareous limestone (Fig. 4.30).

The most important and predominant group of phototrophic organisms on rocks and stones are cyanobacteria (Crispim and Gaylarde 2004). Cyanobacteria,



**Fig. 4.30** Ephesus, Turkey: the rosy stain on white calcareous limestone is caused by bacteria-forming blooms in the brackish water of the pond overlaying the subterranean parts of the Artemision

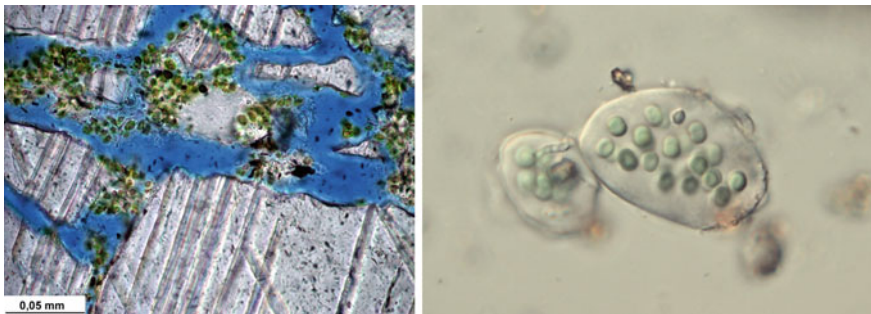


**Fig. 4.31** Gloeocapsalean cyanobacteria with thick, gel-like capsules that protect them against desiccation and chemical attack

formerly called blue-green algae, colonize stone in all climate regions of the Earth. The basic pigment produced by cyanobacteria is the chlorophyll necessary for their photosynthesis. Due to the chlorophyll, cyanobacteria appear as green layers on stone or as parallel subsurface bands inside it. In highly sun-exposed environments, they also produce other pigments for sun protection. Due to the presence of carotenoids and scytonemin pigments in their cells, cyanobacterial layers might also appear orange or dark brown. While dry cyanobacterial layers may appear dark black, this does not mean that they are dead. In fact, they regain full metabolic activity and fresh green color upon wetting.

There are different morphological types of cyanobacteria on stone: The most frequent are the single-cell cyanobacteria with cells encapsulated in a thick layer of slime that helps the bacteria to keep water and that protects them from chemical attack or drying (Fig. 4.31). The genera *Gloeocapsa* and *Chroococcus* are typical representatives. Another morphological type is represented by filamentous cyanobacteria that might even produce a dense sheath around their filaments for protection. Due to their sheath and slime capsules, cyanobacteria are able to live with low amounts of water and to survive long periods of desiccation in a resting state.



**Fig. 4.32** St. Virgil's chapel (Vienna, Austria): halophilic bacteria and archaea cause a rosy stain on the salt-attacked stone surface of the Medieval monument

On stone, cyanobacteria often occur in close association with algae and lichen, the relative abundance of the groups being determined by the climate and exposure to light and other factors in the immediate vicinity. In general, cyanobacteria are regarded as highly resistant to UV-radiation and desiccation. Due to their phototrophic lifestyle, they do not depend on any organic nutrients, although some of them are able to use organic compounds as a dietary supplement. Their ability to adapt to different light qualities, a process called chromatic adaptation, allows cyanobacteria to develop on stone in archeological hypogea with low light intensities, as in the cases of crypts, caves, and catacombs. There, they might be one of the most important deterioration agents for wall paintings and inscriptions. In such subsurface environments, *Eucapsis*, *Leptolyngbya*, *Scytonema*, and *Fischerella* have been the most frequently encountered cyanobacterial taxa (Albertano 2003).

Green layers of micro-algae cannot be distinguished from cyanobacterial layers with the naked eye, and, in fact, most biofilms in humid or wet environments are a complex mixture of both groups. Although the physiology of green micro-algae is similar to that of cyanobacteria—both depend on light and water and are photosynthetic—micro-algae are less stress resistant and need more water. An algal biofilm is a good indicator of a constant water supply. In architectural objects, the presence of green micro-algal films should be regarded as a sign of constructional defects that allow water infiltration.

#### Halophilic Bacteria and Archaea

Archaea are bacteria-like organisms that are supposed to have been among the first organisms to colonize the Earth more than 3 billion years ago. Archaea—formerly called archaeobacteria—tolerate very high temperatures and extreme salt stress. For the latter reason, they are frequently found on stone and mortar with a high load of chlorides, such as NaCl from deicing salt and sulfates or nitrates from agricultural fertilization, and when sufficient humidity is available. The soluble salts migrate



**Fig. 4.33** Side, Turkey: black micro-colonial fungi on a marble surface

into the pore space of the stones, and, as soon as the water evaporates from the stone surface, the salts start crystallizing out forming dense salt crusts. Salt crusts as well as salt efflorescences provide a suitable environment for moderately halotolerant and extremely halophilic (salt-loving) bacteria and archaea. *Salinisphaera*, *Halobacillus*, *Rubrobacter*, and *Bacteroidetes* are common, moderately halophilic bacteria. The most important genera of archaea are *Halococcus* and *Halobacterium*. Many species of the halophilic archaea produce pink or purple pigments, leading to a typical pink stain on stone or mortar surfaces (Fig. 4.32).

#### 4.5.1.2 Fungi

Fungi, in contrast to most bacteria, are multi-cellular organisms forming dense three-dimensional networks of hyphae (cell filaments) on and in stones. Hyphal growth enables fungi to spread over surfaces and to penetrate porous stone. Fungi may be the most important endoliths on building stone because their activity is high and they are extremely corrosive (Sterflinger 2000; Scheerer et al. 2009). Depending on the physical properties of the material, fungi may be found over 1 cm deep in the stone.

There are two major morphological and ecological groups of stone-inhabiting and -dwelling fungi. These are adapted to different environmental conditions. In moderate or humid climates, the fungal communities on rock are dominated by hyphomycetes (mold) that form mycelia (hyphal networks) in the porous space of the stones. Since the settlement of spores from the air is the first step for fungal colonization, the species' diversity of stone fungi is rather similar to the diversity of common airborne spores. *Alternaria*, *Cladosporium*, *Epicoccum*, *Aureobasidium*, and *Phoma* are the most important species. In arid and semi-arid environments, such as those found in the Mediterranean area, the climate conditions are too extreme for most of the hyphomycetes, and, therefore, the communities shift towards the so-called black yeasts and microcolonial fungi. Black fungi belonging to the genera *Hortaea*, *Sarcinomyces*, *Knufia*, *Capnobotryella*, *Exophiala*, and *Trimmatostroma* form small black colonies on and inside the stone and often occur in close association with lichen (Fig. 4.33) (Sterflinger 2005).

Some other genera of black fungi are lichenicolous, i.e. they inhabit not the bare stone but the lichen thallus itself. Black fungi on stone have a remarkable resistance against desiccation and tolerate periods of complete dryness for several months. Their growth is extremely slow because most of their energy is spent in the production of thick cell walls and melanin to shelter them against desiccation, erosion, UV-radiation, and chemical attack. Moreover, they produce large amounts of sugars—trehalose, a disaccharide—and polyols that serve as intracellular protection. Those substances are necessary in order to shelter their cell functions and enzymes against heat, desiccation, and salt stress.

Fungi are especially resistant against heat, and a stone surface exposed to the sunlight might heat up to 80 °C without affecting the fungi. Due to the thick walls they develop, fungi also resist chemical attack and, therefore, resist biocides and other anti-microbial treatments. Black fungi dwell deep inside granite, calcareous limestone, and marble. In addition, they deteriorate those stones both via chemical and mechanical attack. The phenomenon of biopitting—the formation of pits with sizes ranging up to 2 cm in diameter and depth in stone—is caused by black fungi. Biopitting occurs predominantly on marble and limestone. Due to the strong melanization of the cell walls, stones colonized by these fungi show black spots or can be completely covered by a black layer. In addition to outdoor environments, black fungi are also found on the rock surfaces of caves and catacombs (Saarela et al. 2004), especially where the naturally high humidity has been actively decreased in order to suppress algal growth on precious wall paintings.

#### 4.5.1.3 Lichens

Lichens are composed of a pair of symbiotic organisms: an algae or cyanobacteria in close spatial and physiological association with a fungus. Both partners form a physiological and morphological entity called a thallus. There are different kinds of lichen: foliose lichens form a coral-like, scrubby thallus; fruticose lichens form a leaf-like thallus on the bark of trees or on rocks; squamulose lichen form a flat thalli with small lobes on the top. On rocks and stone, crustose lichens are the predominant form (Fig. 4.34).

Crustose lichens are strongly adhered to the surface of the rock. When most of the thallus is formed on the rock and only single hyphae (filaments) penetrate the substrate, the lichens are called epilithic. When most of the thallus is inside the cracks and fissures of the substrate and only the fruiting bodies are visible on the surface, they are called endolithic lichens. The symbiosis between fungi and algae/cyanobacteria enables the lichen to live on nutrient-poor and arid stone surfaces. The algal partner, also called the photobiont, produces sugar through photosynthesis and CO<sub>2</sub> fixation that feeds the fungal partner. This helps the fungus to survive in nutrient-poor conditions. On the other hand, the algae profits from the sheltering action of the fungus that protects it from UV-radiation and desiccation. The fungus forms a dense crust around an inner layer, the latter being composed of loose hyphae associated with the algal cells. For nearly all the lichenized fungi,





**Fig. 4.34** Lichen crusts growing on calcareous sandstone and forming a landscape-like pattern

the symbiotic lifestyle is necessary, while most of the algae and cyanobacteria could live autonomously under suitable environmental conditions. In other words, most lichenized fungi can only live in association with the respective cyanobacterium or algae.

All over the world, lichens are the most common colonizers of calcareous stone. They appear on every stone surface that is not cleaned regularly (Gaylarde and Gaylarde 2005). Lichens are very sensitive to heavy metals and high concentrations of  $\text{SO}_2$ . Therefore, stone monuments in cities in industrialized countries, such as Paris or Munich, had lost most of their lichens by the 1960s and 1970s. In contrast, monuments in rural areas, such as Angkor Wat in Cambodia or the Maya temples in Mexico, are extensively covered by lichen thalli. Today, lichens are re-conquering the urban areas in industrialized western countries because of the decreased  $\text{SO}_2$  concentration and better air quality.

Lichens are colorful, and a surface covered with crustose lichens will appear as a landscape with green, white, gray, black, yellow, and orange areas. Lichens penetrate the rock with their hyphae and with fruiting bodies. This creates a pattern of pitting in calcareous rock. Lichens play an important role in the deterioration of stone, and the pros and cons of removing lichen from a stone surface is discussed in the following section.

## ***4.5.2 Processes of Biodeterioration and Biodegradation***

### **4.5.2.1 Surface Alteration Phenomena and Biogenic Layers**

Bacteria, archaea, fungi, algae, and lichens produce a wide variety of organic pigments that have different functions for the organisms: Chlorophyll is the photosynthetic pigment enabling cyanobacteria and algae to absorb sunlight for energy production. Chlorophyll appears in different shades of green, varying from



light blue-green to deep moss-green and nearly black when the photosynthetic microbial mat becomes dry. In the dry state, the cells of the cyanobacterial biofilm are in a passive state with minimal metabolism. Once water is available again, they regain full metabolic activity within a few minutes and return to their green color.

Carotenoids, orange, yellow, red, brown, and purple pigments, are produced by photosynthetic organisms as supporting pigments for photosynthesis and by many others as a UV absorber and protective agent. Melanin has a dark brown or black color that serves to protect the cells against UV-radiation and some radioactive radiation (Dadachova et al. 2007), as well as desiccation, mechanical destruction, and chemical attack. Moreover, it plays a predominant role in the ability of fungi to attack and penetrate hard substances. Melanin is produced by many fungi and especially by the black microcolonial fungi, such as the *Phaeococcomyces*, *Sarcinomyces*, *Knufia*, and *Capnobotryella* that specialize in colonizing stones. The dark brown scytonemin pigment is incrustated in the cell walls and the sheath of some filamentous cyanobacteria that inhabit bare rock surfaces in very sun-exposed areas (Ortega-Morales et al. 2005), such as the plateaus in the Andes (South America) and Table Mountain of Cape Town (South Africa). The dark biogenic coloration of the stone surfaces increases sunlight absorption, thus amplifying physical stress via temperature cycling.

Organic pigments are located both in the cell walls and in the cell of the organism itself. Some are also excreted by the organisms actively, while others are excreted and liberated into the environment after the death and decomposition of the cells. Especially in calcareous rocks, such as limestone and marble, organic pigments are incorporated into the stone, where they remain stable. For this reason, a biogenic stain may be found many decades after the organisms that produced the pigment have died. This alteration is called a biogenic discoloration.

Organisms may cause an aesthetic, chromatic modification of the material, generally not involving visible destruction or material loss, and the alteration phenomenon is then called a biopatina.

A biofilm is defined as a layer formed by microorganisms that are normally embedded in slime or in a gelatinous capsule composed of extracellular polymers (EPS) (Kemmling et al. 2004). EPS contain mainly anionic sugars accompanied by proteins, lipids, pigments, and nucleic acids. The thickness of a biofilm ranges from several microns up to 5 mm or more. Above this thickness, it is referred to as a biogenic layer. Biogenic layers are formed by crustose epilithic lichens, cyanobacteria, and algae. On exposed stone surfaces, bacterial biofilms are rare because of the low water activity in the environment. However, the inner surfaces of a stone, i.e. pore walls, fissures, and cracks, may well be inhabited by bacterial biofilms. Such inner biofilms are composed of bacterial cells, and their EPS layers can influence the physical properties of the substrate considerably. Biofilms are effective in clogging pores while increasing water uptake and retention within the stone, and they can hamper water diffusion and evaporation (May 2003). As a consequence, chemical weathering processes, such as dissolution, are enhanced. Bacterial slimes are sticky. Therefore, dirt particles, dust, pollen, and fly ash are trapped by the biofilm. This deposition may serve to feed the bacteria and, thus,

increase the biofilm formation, resulting in an increasingly dirty appearance of the surface with the consequent aesthetic damage.

Fungi, due to their special mycelial morphology, do not form biofilms; they either form single clump-like colonies that can merge into a dense fungal crust or they form mycelial networks on the top and inside of the stone. Fungi may also spread over the stone surface with thin “running hyphae” and drill their way into the stone with very thin penetration hyphae. Foot-like penetration pegs and appressoria, hyphal “pressing” organs, help them to induce mechanical stress with the pressure they exert on individual crystals or stone grains.

#### 4.5.2.2 Bio-Chemical and Bio-Mechanical Alterations

Stone micro-organisms not only inhabit the stone surface (called epilithic) but also penetrate the stone to depths of several millimeters and even centimeters. When they inhabit fissures and crevices in the stone, they are called chasmo-endolithic, while, when they invade the pore system, they are called crypto-endolithic. Due to chemical and mechanical actions and processes, the endolithic growth can considerably influence the physical and chemical properties of the stone and lead to accelerated deterioration and weathering.

The deteriorating effect of epi- and endolithic lichens is based upon the induced chemical and mechanical processes and are, therefore, relevant to the conservation of building stone (Lisci et al. 2003). The contraction and expansion of the lichen thallus following wet-dry cycles causes mechanical stress via the disruption of the grain or crystal structure of the stone. Loosened stone particles accumulate within the lower thallus layer but get lost completely upon removal of the lichen from the surface (Gadd 2007).

Lichens, through their release of organic acids or complexing agents, can leach out Mg, Na, K, Ca, Fe, and even Si and other elements from the stone matrix. After a lichen thallus has disappeared or fallen from the substrate, the surface is rougher and, therefore, more vulnerable to chemical and physical processes of weathering. However, an intact lichen crust might well serve to protect the stone surface sheltering it against wind and rain erosion as well as sunlight-induced stresses (Warscheid and Braams 2000). The damage that the lichen crust may induce is smaller than the subsequent deterioration upon its removal. Therefore, it is important to assess whether it is really necessary to remove a lichen crust from stone monuments.

Among the most important alteration phenomena caused by lichens and fungi is the formation of point-like millimetric or submillimetric shallow cavities called biopits. These pits generally have a cylindrical or conical shape and are not interconnected, although transition patterns to interconnected pits can also be observed. The merging of micropits during a proliferating process might even result in macropitting, with sizes ranging up to 2 cm both in depth and diameter. Micropitting is predominantly caused by lichen, whose fruiting bodies and hyphen penetrate the rock through chemical dissolution. Oxalic acid is the most

predominant acid produced by lichens, and its excretion leads to the formation of calcium oxalate crystals through the chemical reaction of the acid with calcareous stones (Monte 2003). Crusts of calcium oxalate, including two main crystal types—whewellite (the monohydrate form) and wheddelite (the dihydrate form)—may be a result of biogenic oxalic acid production. Micropitting is observed in all climatic regions of the Earth where lichens colonize stone surfaces. The phenomenon occurs predominantly on calcareous stones but also on gneiss and granite.

Macropitting is a phenomenon that mainly occurs in arid and semi-arid areas where black microcolonial fungi are common inhabitants of stone. Although black microcolonial fungi also inhabit limestone and granite, the phenomenon of biopitting seems to be restricted to crystalline calcareous rocks, i.e. marbles. Black fungi have been found to penetrate the stone by both mechanical and chemical processes that are not yet fully understood. In fact, the fungi form colonies inside the stone and mechanically loosen and disrupt stone layers and individual crystals. The process is progressive, resulting in large lesions on the stone surface within a time frame of several decades. In addition, cyanobacteria are frequently observed in depressions, lesions, and interiors of stone. The mechanism of their boring activity is not yet understood.

Fungi, heterotrophic bacteria, and cyanobacteria produce various organic acids as products of a very central metabolic pathway, the so-called citric-acid cycle. The production of acids is significantly influenced by the nutrients present and the availability of trace-elements necessary for their metabolism, e.g. Mg, Fe, or Mn. Increasing environmental pollution—by providing nutrients for the microorganisms—can increase acid production and, thus, enhance stone decay (Wright 2002). Organic acids, such as oxalic, gluconic, succinic, malic, fumaric, citric, and acetic are produced by stone-inhabiting organisms and are excreted into the environment. Their chemical action causes carbonate dissolution as well as the etching of quartz crystals and corrosion of other minerals present. Depending on the structure and chemical composition of the stone, acid attack may result in the sugaring of marble, the sanding of limestone and sandstone, and the corrosion of other minerals, i.e. feldspars and micas. The corrosion of mica and feldspar minerals results in their size change and leads to decohesion of the stone matrix. Therefore, granites and volcanic tuffs, the latter through the glassy matrix, can be attacked by fungal and bacterial organic acids (Sterflinger 2000). Especially citric and oxalic acid chelate the ions produced by stone dissolution, enhancing this process by removing one of the reaction products.

Inorganic acids are produced by chemolithotrophic bacteria that derive their energy from the oxidation of ammonium or reduced sulfur compounds, resulting in the formation of nitrous ( $\text{HNO}_2$ ), nitric ( $\text{HNO}_3$ ), sulfurous ( $\text{H}_2\text{SO}_3$ ), and sulfuric ( $\text{H}_2\text{SO}_4$ ) acids. These are highly corrosive to natural stones as well as concrete and cement.

The respiration activity of bacteria and fungi inhabiting the pores and fissures of stone raises the concentration of  $\text{CO}_2$  in the porous spaces. When the pores contain water, the  $\text{CO}_2$  can form carbonic acid that solubilizes calcite in limestone and other stones. Carbonic acid is a weak acid and, therefore, not as aggressive as the

other acids mentioned. Nonetheless, it is corrosive and the resulting deterioration patterns, e.g. sugaring, etching, etc., are similar.

Biom mineralization and especially the biogenic precipitation of calcium carbonate are widespread processes catalyzed by bacteria. Microorganisms from stone surfaces, including most of the common bacteria associated with building stone, have been found to be able to precipitate  $\text{CaCO}_3$  in the form of calcite. Ehrlich (2009) defined microbial mineral formation as either “active”, involving enzymes or metabolic products, or “passive”, where the microorganism serves as a crystallization nucleus for calcium carbonate precipitation. Since organisms are in contact with the available precursors required for crystal formation, new mineral material is produced on the stone.

In summary, biogenic weathering and biodeterioration are the results of various interacting features and abilities of the micro-organisms. The biogenic factors leading to deterioration of stone cannot be clearly distinguished from merely physical and chemical weathering. They are part of it. Therefore, weathering processes must always be regarded as a result of combined factors acting together. Biodeterioration contributes significantly to the overall deterioration of stone and other building materials such as concrete, mortar, slurries and paint coatings, glass, and metals used in architecture (Piñar and Sterflinger 2009).

## 4.6 Final Remarks

The last section of this chapter discusses biodeterioration. However, it limits itself mostly to microorganisms and some of what may be called visually perceptible biocolonization by fungi, algae, and lichens. The deterioration induced by the growth of higher vegetation, especially large trees that can induce severe structural damage with their roots, has already been mentioned in the mechanical processes section. Nonetheless, animals can also contribute to the deterioration of structures and/or their materials. For example, ants (*Camponotus punctulatus*) in the area of northeast Argentina, eastern Paraguay, and southeast Brazil, dig out a lot of earth to build their nearly conical nests above ground, from half a meter to one meter in height and one meter in diameter. The tunnels they dig to obtain the earth, if below a structure, may induce ground subsidence with consequent mechanical damage to the structure above it. Such damage has been identified in some of the structures of the Santísima Trinidad Jesuit Mission in Paraguay (Cedrola and Charola 2009). Birds have been known to selectively pick out grains from limestone and sand grains from mortars, while pigeons present a soiling problem when they roost on buildings. Similarly, bats’ guano is a soluble salt source, particularly for phosphates and nitrates, which may be leached into a structure. Four-legged animals can also contribute to the deterioration of stone: dogs, by their habit of marking objects; cattle and horses, by using monuments as scratching posts.

However, the worst biodeterioration agent is man himself. Not considering catastrophic events such as wars, there are plenty of other examples that condemn

him. To begin with, poor design in buildings, especially detailing, leads to water flowing over walls with the consequent biocolonization of the surface as mentioned in the last section. Then, there is the ubiquitous problem of poor maintenance. Faulty gutters and downspouts allow water penetration into walls, with the resulting problem of hygric expansion of the materials, leading to, if salts are present, their solubilization, mobilization, and eventual recrystallization, or to freeze–thaw damage.

These problems are subsequently followed by the eventual restoration of the building. It is not the aim to criticize those restorations carried out in the past that used some conservation materials that would not be used now, but rather the ones where past experience was not properly applied. This is best illustrated with the by-now classic example of the restoration of the Parthenon by N. Balanos, carried out in the period between the two world wars. Although, in principle, the original method of joining blocks was to be followed, i.e. metal pins or clamps embedded in lead, this was not correctly implemented; poor quality iron was used, and sometimes cement or similar materials were used for filling the holes. Since the condition of the joints between the blocks was not perfect, water penetrated and corroded the iron elements, leading to their expansion with the consequent mechanical damage to the marble blocks, as became evident some 20 years after the intervention.

Another case is given by the structural retrofitting interventions carried out after an earthquake without taking into account the real behavior of the structures, both in the original and the modified condition, which left them more susceptible to subsequent quakes (Binda et al. 1999; Penazzi et al. 2000). Another instance reflects the poor choice in restoration materials that may turn out to be incompatible, depending on their location in the structures, as illustrated by the deterioration the pinnacles of St. Peter's and Paul's Cathedral in Brno (Bayer 2006). In the 19th century, the church suffered a Neogothic reconstruction, wherein two types of stone were used, sandstone and limestone, though the latter was originally also identified as a sandstone with a calcium-dolomite binder. This was used for the more delicately carved elements. Consequently, the limestone finials were set on top of the sandstone blocks of the pinnacles. With increasing air pollution, the limestone was attacked with the resulting formation of gypsum. This salt, being more soluble than the calcite, migrated into the sandstone block, deteriorating it heavily through recrystallization cycles. While the limestone finial was slowly eroded, the sandstone block immediately below it deteriorated heavily. Knowledgeable stone craftspeople would not have made this error.

One last example serves to illustrate the totally irreversible damage that can be inflicted upon an object. The object is the 17th century alabaster sarcophagus of the Duke Melchior von Hatzfeld in Laudenbach, which deteriorated over time and suffered several restorations. Between 1982 and 1984, the sarcophagus underwent a total acrylic impregnation (AVT), a method described in detail in a subsequent chapter (Sect. 7.10) after preliminary tests on sample slabs proved successful. The process involved several steps: drying at 100 °C for several days, vacuum treatment and subsequent flooding with methyl methacrylate monomer, and heating to

80 °C for in situ polymerization. Initially, the sarcophagus showed good superficial strengthening, but warping and cracking became evident some months later and continued to increase with time. The origin of this damage can be attributed to impregnation process, which involved subjecting the object to temperatures of 100 °C and to vacuum, causing the partial dehydration of the gypsum ( $\text{CaSO}_4 \cdot 2\text{H}_2\text{O}$ ). The consequent heterogeneous material was, therefore, not uniformly impregnated. Upon exposure to the humid environment in the church where it is located, rehydration of the gypsum with its accompanying expansion took place, and a new restoration had to be implemented (Grassegger 2002).

As described in this chapter, deterioration of stone is a complex process. Many advances have been made in understanding the mechanisms underlying it, such as salt crystallization—definitely the single-most important deterioration factor—clay swelling, and thermal deformation of marbles. These advances include mathematical modeling that contribute both in identifying the critical factors that act under given conditions and in determining the amount of damage to be expected for a specified material subjected to certain stresses, as exemplified by the study of Derluyn et al. (2008). However, little has been done with regards to applying this knowledge in practice. Otherwise, how can we explain why a pre-deteriorated stone, such as flame-finished granite, is used in new construction instead of a plain sawed one that would last far longer? Why does the repair of faulty gutters take place only after severe damage to the masonry has occurred? This happens not only in the case of private houses but also for buildings of historical and artistic value.

While our understanding of materials and their deterioration increases, the gap between the theoretical understanding of the problem and the application of a solution to the practical situation is widening. Perhaps developing an expert system, similar to the Monument Damage Diagnostic System for the identification of structural patterns via an atlas (Binda et al. 2010; de Vent et al. 2010), could help to put into practice the extensive knowledge that has been gained. For this purpose, mathematical modeling is of fundamental importance.

## References

- Albertano P (2003) Methodological approaches to the study of stone alteration caused by cyanobacterial biofilms in hypogean environments. In: Koestler RJ, Koestler VH, Charola AE, Nieto Fernandez FE (eds) *Art, biology and conservation: biodeterioration of works of art*. The Metropolitan Museum of Art, New York, pp. 302–315
- Alessandrini G, Peruzzi R, Manganeli del Fà C, Vannucci S, Tampone G, Cecchi R (1979) Investigation on the degradation of stones: VIII. The working effects on the Candoglia Marble. In: *Proceedings of the 3rd international congress on stone deterioration and conservation*. Università degli Studi di Padova, Padua, pp. 411–428
- Allmann R, Kraus K (2003) Salze in historischem Mauerwerk. *Ber Dt Min Ges Beih Eur J Mineral* 15:5–6
- Allsopp D, Seal K, Gaylarde CC (2003) *Introduction to Biodeterioration*. Cambridge University Press, Cambridge



- Anderson RL, Ratcliffe I, Greenwell HC, Williams PA, Cliffe S, Coveney PV (2010) Clay swelling—a challenge in the oilfield. *Earth Sci Rev* 90:201–216
- Angeli M, Bigas JP, Benavente D, Menéndez B, Hébert R, David C (2007) Salt crystallization in pores: quantification and estimation of damage. *Environ Geol* 52:205–213
- Angeli M, Benavente D, Bigas JP, Menéndez B, Hébert R, David C (2008) Modification of the porous network by salt crystallization in experimentally weathered sedimentary stones. *Mater Struct* 41:1091–1108
- Arnold A (1985) Moderne alkalische Baustoffe und die probleme bei der Konservierung von Denkmälern. Bayerisches Landesamt für Denkmalpflege. *Arbeitshefte* 31:152–162
- Arnold A, Küng A (1985) Crystallization and habit of salt efflorescences on walls I. In: Félix G (ed) *Proceedings of the 5th international congress on deterioration and conservation of stone*. Presses Romandes, Lausanne, pp 255–267
- Arnold A, Zehnder K (1985) Crystallization and habit of salt efflorescences on walls II. In: Félix G (ed) *Proceedings of the 5th international congress on deterioration and conservation of stone*. Presses Romandes, Lausanne, pp 269–277
- Arnold A, Zehnder K (1989) Salt weathering on monuments. In: Zezza F (ed) *The conservation of monuments in the mediterranean Basin*. Grafo Edizioni, Bari, pp 31–58
- Arnold A, Zehnder K (1991) Monitoring wall paintings affected by soluble salts. In: Cather S (ed) *The conservation of wall paintings*. Getty Conservation Institute, Los Angeles, pp 103–135
- Attewell PB, Taylor D (1990) Time-dependent atmospheric degradation of building stone in a polluting environment. *Environ Geol Water Sci* 16:43–55
- Baedeker PA, Reddy MM, Reimann KJ, Sciammarella CA (1992) Effects of acidic deposition on the erosion of carbonate stone—experimental results from the U.S. National Acid Precipitation Assessment Program (NAPAP). *Atmos Environ* 26B:147–158
- Baer NS, Berman S (1983) Marble tombstones in national cemeteries as indicators of stone damage: General methods. In: Preprints 76th annual meeting of the APCA. Air Pollution Control Association, Atlanta, No. 83–5.7
- Ballirano P, Melis E (2009) Thermal behaviour and kinetics of dehydration of gypsum in air from in situ real-time laboratory parallel-beam X-ray powder diffraction. *Phys Chem Min* 36:391–402
- Bayer K (2006) Gypsum—an overlooked corrosive factor for some silicate sandstones in Czech Republic. In: Simon S and Drácky A (eds) *European research on cultural heritage. State of the art studies*, vol 5. Institute of Theoretical and Applied Mechanics, Prague, pp. 97–108
- Beaudoin JJ, MacInnis C (1974) The mechanism of frost damage in hardened cement paste. *Cem Concr Res* 4:139–147
- Becker GF, Day AL (1905) The linear force of growing crystals. *Proc Wash Acad Sci* 7:283–288
- Becker GF, Day AL (1916) Note on the linear force of growing crystals. *J Geol* 24:313–333
- Benavente D, Cueto N, Martínez Martínez J, García del Cura MA, Cañaveras JC (2007) The influence of petrophysical properties on the salt weathering of porous building rocks. *Environ Geol* 52:215–224
- Bernabe Y (1991) Pore geometry and pressure dependence of the transport properties in sandstones. *Geophysics* 56:436–446
- Bertagnagi A, Franzini M, Gratzu C, Spampinato M (1983) Il marmocotto in natura e nei monumenti. *Rend Soc It Min Petrol* 39:39–46
- Binda L, Anzani A (1997) Structural behavior and durability of stone masonry. In: Baer NS, Sneath R (eds) *Saving our architectural heritage*. Wiley, Chichester, pp 113–150
- Binda L, Gambarotta L, Lagomarsino S, Modena C (1999) A multilevel approach to the damage assessment and seismic improvement of masonry buildings in Italy. In: Bernardini A (ed) *Seismic damage to masonry buildings*. Balkema, Rotterdam, pp 170–195
- Binda L, Saisi A, de Vent IAE, van Hees RPJ, Naldini S (2010) Structural damage in masonry. Description and interpretation of crack patterns: basis for finding the damage causes. *Rest Build Mon* 16:77–98
- Bionda D (2006) Modelling indoor climate and salt behaviour in historical buildings: a case study. Dissertation, Swiss Federal Institute of Technology, Zurich

- Bionda D, Storemyr P (2002) Modelling the behavior of salt mixtures in walls: a case study from Tenaille von Fersen. In: von Konow T (ed) *The study of salt deterioration mechanisms. Decay of brick walls influenced by interior climate changes*. Suomenlinnan hoitokunta, Helsinki, pp 95–101
- Blanchard DC, Woodcock AH (1980) The production, concentration, and vertical distribution of the sea-salt aerosol. *Ann NY Acad Sci* 338:330–347
- Bourgès A, Fehr KT, Simon S, Snelthage R (2008) Correlation between micro-structure and the macroscopic behaviour of sandstones. *Rest Build Monum* 14:157–166
- Braitsch O (1971) *Salt deposits, their origin and composition*. Springer, Berlin
- Brajer I, Klens Larsen P (2008) The salt reduction treatment on the wall paintings in Thirsted Church. In: *Salt weathering on buildings and stone sculptures*. Technical University of Denmark, Lyngby, pp. 219–228
- Brimblecombe P, Rodhe H (1988) Air pollution—historical trends. *Durability Build Mater* 5:291–308
- Bühmann C, DeVilliers JM, Fey MV (1988) The mineralogy of four heaving clays. *Appl Clay Sci* 3:219–236
- Camuffo D, Del Monte M, Sabbioni C, Vittori O (1982) Wetting, deterioration and visual features of stone surfaces in an urban area. *Atmos Environ* 16:2253–2259
- Cardell-Fernández C, Vleugels G, Torfs K, Van Grieken R (2002) The process dominating Ca dissolution of limestone when exposed to ambient atmospheric conditions as determined by comparing dissolution models. *Environ Geol* 43:160–171
- Cecchi R, Tampone G, Vannucci S (1978) Effetti delle tecniche di rifinitura della Pietra Serena fiorentina VII. *Boll Ingegneri* 1:3–22
- Cedrola ML, Charola AE (2009) Biodeterioro de materiales porosos inorgánicos. In: Charola AE, Magadan ML (eds) *Manual Básico de conservación para las Misiones Jesuíticas Guaraníes*. WMF, New York, pp 52–62
- Charola AE (2000) Salt in the deterioration of porous materials. *J Am Inst Conserv* 39:327–343
- Charola AE (2004) Stone deterioration in historic buildings and monuments. In: Kwiatkowski D, Löfvendahl (eds) *Proceedings of the 10th international congress on deterioration and conservation of stone*. ICOMOS Sweden, Stockholm, pp. 3–14
- Charola AE, Lewin SZ (1979) Efflorescence on building stones—SEM in the characterization and elucidation of the mechanism of formation. *Scan Electron Microsc* 79(I):379–387
- Charola AE, Weber J (1992) The hydration–dehydration mechanism of sodium sulfate. In: Delgado Rodrigues J, Henriques F, Telmo Jeremias F (eds) *Proceedings of the 7th international congress on deterioration and conservation of stone*. LNEC, Lisbon, pp. 581–590
- Charola AE, Aires Barros L, Centeno SA, Basto MJ, Koestler RJ (2002) Analysis of colour traces found on the cloister of the Jeronimos monastery in Lisbon. *Restor Build Monum* 8:447–474
- Charola AE, Pühringer J, Steiger M (2007) Gypsum: a review of its role in the deterioration of building materials. *Environ Geol* 52:339–352
- Chatterji S, Jensen AD (1989) Efflorescence and breakdown of building materials. *Nordic Concr Res* 8:56–61
- Chipera SJ, Vaniman DT (2007) Experimental stability of magnesium sulfate hydrates that may be present on Mars. *Geochim Cosmochim Acta* 71:241–250
- Chkirda S, Kintrup H, Müller-Rochholz J (1999) Sorptionsmessungen von Baumberger Kalksandstein mit kapazitiven Feuchtefühlern. *Berichtsband 69*, 10. Feuchtetagung, Berlin, p. 18
- Cooper TP (1986) Saving buildings from the weather. *Technol Irel* 32–35
- Cooper BD (2008) Prevention of deterioration from salt contamination in heritage artefacts. In: *Salt weathering on buildings and stone sculptures*. Technical University of Denmark, Lyngby
- Cooper TP, O'Brien PF, Jeffrey DW (1992) Rates of deterioration of Portland limestone in an urban environment. *Stud Conserv* 37:228–238
- Correns CW, Steinborn W (1939) Experimente zur Messung und Erklärung der sogenannten Kristallisationskraft. *Z Krist A101*:117–135
- Coussy O (2004) *Poromechanics*. Wiley, Chichester

- Crispim CA, Gaylarde CC (2004) Cyanobacteria and biodeterioration of cultural heritage: a review. *Microb Ecol* 49:1–9. doi:[10/s0024800310525](https://doi.org/10/s0024800310525)
- Cultrone G, Russo LG, Calabrò C, Urošević M, Pezzino A (2008) Influence of pore system characteristics on limestone vulnerability: a laboratory study. *Environ Geol* 54:1271–1281
- Dadachova E, Bryan RA, Huang X, Moadel T, Schweizer AD (2007) Ionizing radiation changes the electronic properties of melanin and enhances the growth of melanized fungi. *PLoS ONE* 2:e457
- De Clercq H (2008) The effect of other salts on the crystallization damage to stone caused by sodium sulphate. In: Salt weathering on buildings and stone sculptures. Technical University of Denmark, Lyngby, pp 307–315
- de Quervain F, Jenny V (1951) Verhalten der Bausteine gegen Witterungseinflüsse in der Schweiz. In: Schweizerische Geotechnische Kommission (ed) Beiträge zur Geologie der Schweiz, Geotechnische Serie, vol 30. Lieferung, Kümmerly and Frey, Geographischer Verlag, Berlin, pp 1–66
- de Vent IAE, Naldini S, van Hees RPJ, Binda L, Saisi A (2010) Definition of structural damage patterns: a structural damage atlas. *Rest Build Mon* 13:167–186
- Del Monte M, Sabbioni C (1984) Gypsum crusts and fly ash particles on carbonatic outcrops. *Arch Meteorol Geophys Bioclimatol B* 35:105–111
- Del Monte M, Sabbioni C (1987) A study of the patina called ‘scialbatura’ on imperial Roman marbles. *Stud Conserv* 32:114–121
- Del Monte M, Sabbioni C, Vittori O (1981) Airborne carbon particles and marble deterioration. *Atmos Environ* 15:645–652
- Del Monte M, Sabbioni C, Zappia G (1987) The origin of calcium oxalates on historical buildings, monuments and natural outcrops. *Sci Total Environ* 67:17–39
- Delgado Rodrigues J (1996) Conservation of granitic rocks with application to the megalithic monuments. Conclusion report project STEP CT90-110. In: Vicente MA, Delgado Rodrigues J, Acevedo J (eds) Degradation and conservation of granitic rocks in monuments. Protection and conservation of European cultural heritage research report No. 5. European Commission Directorate General XII. Brussels, pp 178–189
- Derluyn H, Poupeleer AS, Van Gemert D, Carmeliet J (2008) Salt crystallization in hydrophobic porous materials. In: De Clercq H, Charola AE (eds) Hydrophobe V. Water repellent treatment of building materials. Aedificatio, Freiburg, pp 97–108
- Dionisio A, Aires Barros L (2004) Fire effects on stone materials. The case of Lisbon’s Cathedral. In: Proceedings of the 6th international symposium. Conservation of monuments in the mediterranean Basin, (CD) Lisbon, pp 143–147
- Dionisio A, Rodrigues M, Sequeira Braga MA, Andre H, Waerenburgh JC, Rojas DP, Basto MJ, Matias MJ, Aires Barros L (2005) Study of heat induced colour modifications in limestone used in monuments. *Rest Build Mon* 11:199–210
- Doehne E (1994) In situ dynamics of sodium sulfate hydration and dehydration in stone pores: observations at high magnification using the environmental SEM. In: Zezza F, Ott H, Fassina V (eds) Conservation of monuments in the Mediterranean Basin, Proceedings of the 3rd international symposium, Venice, pp 143–150
- Doehne E (2002) Salt weathering: a selective review. In: Siegesmund S, Weiss T, Vollbrecht A (eds) Natural stones, weathering phenomena, conservation strategies, and case studies, Special publication 205. Geological Society, London, pp 51–64
- Drever JI (1994a) Durability of stone: mineralogical and textural perspectives. In: Krumbein WE, Brimblecombe P, Cosgrove DE, Staniforth S (eds) Durability and change. Wiley, Chichester, pp 27–39
- Drever JI (1994b) The effect of land plants on weathering rates of silicate minerals. *Geochim Cosmochim Acta* 58:2325–2332
- Ehrlich HL (2009) *Geomicrobiology*, 5th edn. CRC, Boca Raton 606p
- Espinosa-Marzal RM, Scherer GW (2008) Crystallization of sodium sulfate salts in limestones. *Environ Geol* 56:605–621

- Espinosa-Marzal RM, Scherer GW (2009) Crystallization pressure exerted by in-pore confined crystals. In: Ling HI, Smyth A, Betti R (eds) *Poromechanics IV, Proceedings of the 4th Biot conference on poromechanics*. DE-Stech Publications, Lancaster, pp 1013–1018
- Espinosa-Marzal RM, Scherer GW (2010) Mechanisms of damage by salt. In: Smith BJ, Gomez-Heras M, Viles HA, Cassar J (eds) *Limestone in the built environment: present-day challenges for the preservation of the past*. Geological Society, London, Special Publications 331, pp 61–77
- Espinosa-Marzal RM, Hamilton A, McNall M, Whitaker K, Scherer GW (2011) The chemomechanics of crystallization during rewetting of limestone impregnated with sodium sulfate. *J Mater Res* 26:1472–1481
- Evans IS (1970) Salt crystallization and rock weathering: a review. *Rev Geomorph Dyn* 19:153–177
- Everett DH (1961) The thermodynamics of frost damage to porous solids. *Trans Faraday Soc* 57:1541–1551
- Feddema JJ, Meierding TC (1987) Marble weathering and air pollution in Philadelphia. *Atmos Environ* 21:143–157
- Flatt RJ (2002) Salt damage in porous materials: how high supersaturations are generated. *J Cryst Growth* 242:435–454
- Flatt RJ, Steiger M, Scherer GW (2007) A commented translation of the paper by C.W. Correns and W. Steinborn on crystallization pressure. *Environ Geol* 52:187–203
- Franzen C, Mirwald PW (2004) Moisture content of natural stone: static and dynamic equilibrium with atmospheric humidity. *Environ Geol* 46:391–401
- Franzini M, Gratzu C, Spampinato M (1983) Degradazione del marmo per effetto di variazione di temperatura. *Rend Soc It Min Petrol* 39:47–58
- Fredrich JT, Wong TE (1986) Micromechanics of thermally induced cracking in three crustal rocks. *J Geophys Res* 91:12743–12764
- Fritz (1922) Steinverbiegungen als Verwitterungserscheinungen. *Die Denkmalpflege* 24(7):53–55
- Gadd GM (2007) Geomycology: biogeochemical transformations of rocks, minerals and radionuclides by fungi, bioweathering and bioremediation. *Mycol Res* 111:3–49
- Gaylarde CC, Gaylarde PM (2005) A comparative study of the major microbial biomass of biofilms on exteriors of buildings in Europe and Latin America. *Int Biodeterior Biodegradation* 55:131–139
- Ginell WS (1994) The nature of changes caused by physical factors. In: Krumbein WE, Brimblecombe P, Cosgrove DE, Staniforth S (eds) *Durability and change*. Wiley, Chichester, pp 81–94
- Gómez-Heras M, Smith BJ, Fort R (2008) Influence of surface heterogeneities of building granite on its thermal response and its potential for the generation of thermoplasticity. *Environ Geol* 56:547–560
- Goudie A, Viles H (1997) *Salt weathering hazards*. Wiley, Chichester
- Grassegger G (2002) Restorations of the sarcophagus of Duke Melchior von Hatzfeld-the accompanying scientific and technical investigations. *Otto Graf J* 13:141–154
- Grimmer AE (1984) A glossary of historic masonry deterioration problems and preservation treatments. Department of the interior. National Park Service Preservation Assistance Division, Washington, DC
- Grissom CA, Charola AE, Wachowiak MJ (2000) Measuring surface roughness: back to basics. *Stud Conserv* 45:73–84
- Grossi CM, Esbert RM, Suárez del Rio LM, Montato M, Laurenzi-Tabasso M (1997) Acoustic emission monitoring to study sodium sulphate crystallization in monumental porous carbonate stones. *Stud Conserv* 42:115–125
- Gunde-Cimerman N, Ramos J, Plemenitas A (2009) Halotolerant and halophilic fungi. *Mycol Res* 113:1231–1241
- Hajpál M, Török A (2004) Mineralogical and color changes of quartz sandstones by heat. *Environ Geol* 46:311–322
- Hall C, Hoff WD (2002) *Water transport in brick, stone and concrete*. Taylor and Francis, London

- Hall C, Hoff WD (2007) Rising damp: capillary rise dynamics in walls. *Proc Roy Soc A* 463: 1871–1884
- Halsey DP, Dews SJ, Mitchell DJ, Harris FC (1995) Real time measurements of sandstone deterioration: a microcatchment study. *Build Environ* 30:411–417
- Hamilton A, Hall C, Pel L (2008) Sodium sulfate heptahydrate: direct observation of crystallization in a porous material. *J Phys D* 41:212002
- Hardie LA, Eugster HP (1970) The evolution of closed-basin brines. *Mineral Soc Am Spec Pap* 3:273–290
- Hodgman CD, Weast RC, Shankland RS, Selby SM (eds) (1963) *Handbook of chemistry and physics*. The Chemical Rubber Publishing Co, Cleveland
- Honeyborne DB, Price CA (1977) Air pollution and the decay of limestones. Building Research Establishment. Garston, BRE Note 117/77
- Hosono T, Uchida E, Suda C, Ueno A, Nakagawa T (2006) Salt weathering of sandstone at the Ankor monuments, Cambodia: identification of the origin of salts using sulfur and strontium isotopes. *J Archaeol Sci* 33:1541–1551
- Jaynes SM, Cooke RU (1987) Stone weathering in Southeast England. *Atmos Environ* 21:1601–1622
- Jerwood LC, Robinson DA, Williams RBG (1990a) Experimental frost and salt weathering of chalk I. *Earth Surf Proc Land* 15:611–624
- Jerwood LC, Robinson DA, Williams RBG (1990b) Experimental frost and salt weathering of chalk II. *Earth Surf Proc Land* 15:699–708
- Julien A (1883) The decay of building stones in New York City. *Am Arch Build News* 13:76–77
- Kemmling A, Kamper M, Flies C, Schieweck O, Hoppert M (2004) Biofilms and extracellular matrices on geomaterials. *Environ Geol* 46:429–435
- Kessler DW (1919) Physical and chemical tests on the commercial marbles of the US. NBS Technologic Paper 123. Government Printing Office, Washington, DC
- Kleber W (1959) *Einführung in die Kristallographie*. VEB Verlag Technik, Berlin
- Klenz Larsen P (1999) Desalination of painted brick vaults. Ph.D. thesis, The National Museum of Denmark, The Technical University of Denmark, Lyngby
- Klenz Larsen P (2004) Moisture measurements in Thirsted Church. *J Architect Conserv* 10:22–35
- Klenz Larsen P (2007) The salt decay of medieval bricks at a vault in Brarup Church, Denmark. *Environ Geol* 52:375–383
- Koch A, Siegesmund S (2004) The combined effect of moisture and temperature on the anomalous expansion behaviour of marble. *Environ Geol* 46:350–363
- Koestler RJ, Brimblecombe P, Camuffo D, Ginell WS, Graedel TE, Leavengood P, Petushkova J, Steiger M, Urzì C, Vergès-Belmin V, Warscheid T (1994) How do external environmental factors accelerate change? In: Krumbein WE, Brimblecombe P, Cosgrove DE, Staniforth S (ed) *Durability and change. The science, responsibility, and cost of sustaining cultural heritage*. Dahlem workshop reports. Wiley, Chichester, pp 149–163
- Kucera V, Tidblad J, Kreislova K, Knotkova D, Faller M, Reiss D, Snelthage R, Yates T, Henriksen J, Schreiner M, Melcher M, Ferm M, Lefèvre RA, Kobus J (2007) UN/ECE ICP Materials dose-response functions for the multi-pollutant situation. *Water Air Soil Pollut Focus* 7:249–258
- Lasaga AC, Soler JM, Ganor J, Burch TE, Nagy KL (1994) Chemical weathering rate laws and global geochemical cycles. *Geochim Cosmochim Acta* 58:2361–2386
- Lazzarini L, Salvadori O (1989) A reassessment of the formation of the patina called ‘scialbatura’. *Stud Conserv* 34:20–26
- Leitner H, Laue S, Siedel H (eds) (2003) *Mauersalze und Architekturoberflächen*. Hochschule für Bildende Künste, Dresden
- Lewin SZ (1974) Book review. *Stud Conserv* 19:249–252
- Lewin SZ, Charola AE (1981) Stone decay due to foreign inclusions. In: *The conservation of stone II. Part A. Centro per la conservazione delle sculture all’aperto*, Bologna, pp 205–217

- Linnow K, Zeunert A, Steiger M (2006) Investigation of sodium sulfate phase transitions in a porous material using humidity and temperature controlled X-ray diffraction. *Anal Chem* 78:4683–4689
- Lisci L, Monte M, Pacini E (2003) Lichens and higher plants on stone: a review. *Int Biodeterior Biodegr* 51:1–17
- Litvan GG (1978) Adsorption systems at temperatures below the freezing point of the adsorptive. *Adv Colloid Interface Sci* 9:253–302
- Livingston RA (1986) Evaluation of building deterioration by water runoff. In: Davis G (ed) *Building performance: function, preservation, and rehabilitation*. ASTM, Philadelphia, pp 181–188
- Livingston RA (1992) Graphical methods for examining the effects of acid rain and sulfur dioxide on carbonate stones. In: Delgado Rodrigues J, Henriques F, Telmo Jeremias F (ed) *Proceedings of the 7th international congress on deterioration and conservation of stone*. Laboratorio Nacional de Engenharia Civil, Lisbon, pp 375–386
- Madsen FT, Müller-Vonmoos M (1989) The swelling behaviour of clays. *Appl Clay Sci* 4:143–156
- Malaga-Starzec K, Lindquist JE, Björn S (2002) Experimental study on the variation in porosity of marble as function of temperature. In: Siegesmund S, Weiss, T, Vollbrecht A (eds) *Natural stone, weathering phenomena, conservation strategies and case studies*. Geol Soc Special Publication No. 205. The Geological Society, London, pp 81–88
- Matthes S (1987) *Mineralogie*. Springer, Heidelberg, p 417
- Matzuoka N, Moriwaki K, Hirakawa K (1996) Field experiments on physical weathering and wind erosion in an Antarctic cold desert. *Earth Surf Proc Land* 21:687–699
- Mausfeld SA, Grassegger G (1992) Abbauprozesse an Feldspäten und Tonmineralen unter den Bedingungen der Bauwerksverwitterung. *Z dt geol Ges* 143:23–39
- Mausfeld SA, Grassegger G (1994) The changing environment of pore solutions in natural building stones during immission accelerated weathering processes. In: Zezza F, Ott H, Fassina V (eds) *Proceedings of the 3rd international symposium conservation of monuments in the Mediterranean Basin, Venice*, pp 129–135
- Selbmann L, Hoog GS De, Mazzaglia, A, Friedmann EI, Onofri S (2005) Fungi at the edge of life: cryptoendolithic black fungi from the Antarctic desert. In: de Hogg GS (ed) *Fungi of the Antarctic: evolution under extreme conditions*. *Stud Mycol* 51:1–32
- McGreevy JP (1982) ‘Frost and salt’ weathering: further experimental results. *Earth Surf Proc Land* 7:475–488
- McGreevy JP, Smith BJ (1984) The possible role of clay minerals in salt weathering. *Catena* 11:169–175
- McKinstry HA (1965) Thermal expansion of clay minerals. *Amer Mineral* 50:212–222
- Monte M (2003) Oxalate film formation on marble specimens caused by fungus. *J Cult Herit* 4:255–258
- Mortensen H (1933) Die “Salzsprengrung” und ihre Bedeutung für die regionalklimatische Gliederung der Wüsten. *Petermans Mitteilungen aus Justus Perthes geographischer Anstalt* 79:130–135
- Neumann H–H, Steiger M, Wassmann A, Dannecker W (1993) Aufbau und Ausbildung schwarzer Gipskrusten und damit zusammenhängender Gefügeschäden von Naturwerksteinen am Beispiel des Leineschlösses (Hannover). In: Sneath R (ed) *Jahresberichte steinzerfallsteinkonservierung band 3–1991*. Verlag Ernst and Sohn, Berlin, pp 151–167
- Neumann H–H, Lork A, Steiger M, Juling H (1997) Decay patterns of weathered quartz sandstones: evidence for gypsum induced structural changes. In: Sveinsdóttir EL (ed) *Proceedings of the 6th euro seminars on microscopy applied to building materials*. Icelandic Building Research Institute, Reykjavik, pp 238–249
- Nielsen AE (1964) *Kinetics of precipitation*. Pergamon, Oxford
- Nord AG, Ericsson T (1993) Chemical analysis of thin black layers on building stone. *Stud Conserv* 38:25–35



- Nord AG, Tronner K (1991) Stone weathering. Conservation Institute of National Antiquities, Stockholm, pp 24–44
- O'Grady C (2005) The occurrence of rock varnish on stone and ceramic artifacts. *Rev Conserv* 5:35–42
- Ondrasina J, Kirchner D, Siegesmund S (2002) Freeze-thaw cycles and their influence on marble deterioration: a long term experiment. In: Siegesmund S, Weiss T, Vollbrecht A (eds) Natural stones, weathering phenomena, conservation strategies, and case studies, Special Publication 205. Geological Society, London, pp 9–18
- Ortega-Morales BO, Gaylarde CC, Englert GE, Gaylarde PM (2005) Analysis of salt-containing biofilms on limestone buildings of the Mayan culture at Edzna, Mexico. *Geomicrobiol J* 22:261–268
- Ottosen LM, Rørig-Dalgaard I, Klenz Larsen P, Brajer I, Bøllingstoft P, Marciniak M, Svane M (eds) (2008) Salt weathering on buildings and stone sculptures. Technical University of Denmark, Copenhagen
- Ožbolt J, Grassegger G, Van der Beken P, Periškic G, Reinhard HW (2008) Experimental and numerical study of hygro-thermo-mechanical properties of “Schilfsandstein” from Baden/Württemberg. *Env Geol* 56:535–546
- Pauly JP (1976) Maladie alvéolaire. Conditions de formation et d'évolution. In: Rossi Manaresi R (ed) The conservation of stone I. centro per la conservazione delle sculture all'aperto. Bologna, pp 55–80
- Penazzi D, Valluzzi MR, Cardani G, Binda L, Baronio G, Modena C (2000) Behaviour of historic masonry buildings in seismic areas: lessons learned from the Umbria-March earthquake. Proceedings of the 12th international conference of IBBMac, vol 1. Universidad Politécnica, Madrid, pp 217–235
- Piñar U, Sterflinger K (2009) Microbes and building materials. In: Cornejo DN, Haro JL (eds) Building materials: properties, performance and applications. Nova Publishers, New York, pp 163–188
- Pitzer KS (1991) Ion interaction approach: theory and data correlation. In: Pitzer KS (ed) Activity coefficients in electrolyte solutions. CRC Press, Boca Raton, pp 75–153
- Price CA (1978) The use of the sodium sulphate crystallisation test for determining the weathering resistance of untreated stone. In: UNESCO/RILEM international symposium, Paris, vol 3.6, pp 1–23
- Price CA (ed) (2000) An expert chemical model for determining the environmental conditions needed to prevent salt damage in porous materials. Protection and conservation of the European cultural heritage research report No. 11. Archetype Publications, London
- Price CA (2007) Predicting environmental conditions to minimise salt damage at the Tower of London: a comparison. *Environ Geol* 52:369–374
- Price CA, Brimblecombe P (1994) Preventing salt damage in porous materials. In: Preventive conservation: practice, theory and research. International Institute for Conservation, London, pp 90–93
- Prokos P (2008) Equilibrium conditions of marine originated salt mixtures: an ECOS application at the archaeological site of Delos, Greece. Salt weathering on buildings and stone sculptures. Technical University of Denmark, Lyngby, pp 139–148
- Reddy MM (1988) Acid rain damage to carbonate stone: a quantitative assessment based on the aqueous geochemistry of rainfall runoff from stone. *Earth Surf Proc Land* 13:335–354
- Reddy MM, Sherwood S, Doe B (1985) Limestone and marble dissolution by acid rain. In: Félix G (ed) Proceedings of the 5th international congress on deterioration and conservation of stone. Presses Polytechniques Romandes, Lausanne, pp 517–526
- Reeder R, Markgraf SA (1986) High temperature crystal chemistry of dolomite. *Am Mineral* 71:795–804
- Rijniers LA, Huinink HP, Pel L, Kopinga K (2005) Experimental evidence of crystallization pressure inside porous media. *Phys Rev Lett* 94:075503
- RILEM PEM-25 (1980) Recommended tests to measure the deterioration of stone and to assess the effectiveness of treatment methods. *Mater Struct* 13:175–253

- Rivadeneira MA, Párraga J, Delgado R, Ramos-Cormenzana A, Delgado G (2004) Biomineralization of carbonates by *Halobacillus trueperi* in solid and liquid media with different salinities. *FEMS Microbiol Ecol* 48:39–46
- Rodriguez-Navarro C, Doehne E (1999) Salt weathering: influence of evaporation rate, supersaturation and crystallization pattern. *Earth Surf Proc Land* 24:191–209
- Rodriguez-Navarro C, Hansen E, Sebastián E, Ginell W (1997) The role of clays in the decay of ancient Egyptian limestone sculptures. *J Am Inst Cons* 36:151–163
- Rodriguez-Navarro C, Doehne E, Sebastian E (2000) How does sodium sulfate crystallize? Implications for the decay and testing of building materials. *Cem Concr Res* 30:1527–1534
- Roekens E, van Grieken R (1989) Rates of air pollution induced surface recession and material loss for a cathedral in Belgium. *Atmos Environ* 23:271–277
- Rönicke G, Rönicke R (1972) Über den Mechanismus der zerstörenden Wirkung der Luftverunreinigung am Freiburger Münster. *Dt Kunst- Denkmalpfl* 30:57–64
- Royer-Carfagni GF (1999) On the thermal degradation of marble. *Int J Rock Mech Min Sci* 36:119–126
- Ruedrich J, Siegesmund S (2007) Salt and ice crystallization in porous sandstones. *Environ Geol* 52:225–249
- Ruedrich J, Weiss T, Siegesmund S (2002) Weathering of treated marbles. *Geol Soc Spec Publ* 205:254–272
- Ruedrich J, Kirchner D, Seidel M, Siegesmund S (2005) Beanspruchungen von Naturwerksteinen durch Salz- und Eiskristallisation im Porenraum sowie hygri sche Dehnungsvorgänge. *Z Dt Ges Geowiss* 156:58–73
- Ruedrich J, Bartelsen T, Dohrmann R, Siegesmund S (2011) Moisture expansion as a deterioration factor for sandstone used in buildings. *Environ Earth Sci* 63:1545–1564
- Saarela M, Alakomi HL, Suihko ML, Maunuksela L, Raaska L, Mattila-Sandholm T (2004) Heterotrophic microorganisms in air and biofilm samples from Roman catacombs, with special emphasis on actinobacteria and fungi. *Int Biodet Biodegr* 54:27–37
- Sage JD (1988) Thermal microfracturing of marble. In: Marinos PG, Kouis GC (eds) *Engineering geology of ancient works, monuments and historic sites*. Balkema, Rotterdam, pp 1013–1018
- Saiz Jimenez C (1993) Deposition of airborne organic pollutants on historic buildings. *Atmos Environ* 27B:77–85
- Salles F, Douillard JM, Denoyel R, Bildstein O, Julien M, Beurroies I, Van Damme H (2009) Hydration sequence of swelling clays: evolution of specific surface area and hydration energy. *J Colloid Interface Sci* 333:510–522
- Sánchez Pastor N, Aldushin K, Jordan G, Schmahl WW (2010)  $K^+$ - $Na^+$  exchange in phlogopite on the scale of a single layer. *Geochim Cosmochim Acta* 74:1954–1962
- Sawdy A (2001) The kinetics of salt weathering of porous materials: stone monuments and wall paintings. Ph.D thesis, Institute of Archaeology, University College, London
- Sawdy A, Price CA (2005) Salt damage at Cleeve Abbey, England. Part I: a comparison of theoretical predictions and practical observations. *J Cult Heritage* 6:125–135
- Schäfer M, Steiger M (2002) A rapid method for the determination of cation exchange capacities of sandstone: preliminary data. In: Siegesmund S, Weiss T, Vollbrecht A (eds) *Natural stone, weathering phenomena, conservation strategies and case studies*. Geological Society London, Special Publications 205:431–439
- Scheerer S, Ortega-Morales O, Gaylarde C (2009) Microbial deterioration of stone monuments— an updated overview. *Adv Microbiol* 66:97–139
- Scheffer F, Schachtschabel P (1984) *Lehrbuch der bodenkunde*, 11th edn. Enke Verlag, Stuttgart
- Scherer GW (1999) Crystallization in pores. *Cem Concr Res* 29:1347–1358
- Scherer GW (2004) Stress from crystallization of salt. *Cem Concr Res* 34:1613–1624
- Scherer GW, Valenza JJ (2004) Mechanisms of frost damage. In: Young F, Skalny J (eds) *Materials science of concrete VII*. The American Ceramic Society, Westerville, pp 209–246
- Schiavon N (1992) Decay mechanism of oolitic limestones in an urban environment: King's College Chapel, Cambridge and St Luke's Church, London. In: Webster RGM (ed) *Stone*

- cleaning and the nature, soiling and decay mechanisms of stone. Donhead, London, pp 258–267
- Schlütter F, Juling H, Steiger M (2003) Schädigung von chlorid- und nitratbelastetem Ziegelmauerwerk: Kryo-REM-Untersuchungen zur Wirkungsweise eines Salzgemisches. In: Leitner H, Laue S, Siedel H (eds) *Mauersalze und architektureoberflächen*. Hochschule f, Bildende Künste, pp 72–78
- Schmölzer A (1936) Zur entstehung der verwitterungsskulpturen an bausteinen. *Chem Erde* 10:479–520
- Sebastián E, Cultrone G, Benavente D, Linares Fernández L, Elert K, Rodriguez-Navarro C (2008) Swelling damage in clay-rich sandstones used in the church of San Mateo in Tarifa (Spain). *J Cult Heritage* 9:66–76
- Senkayi AL, Dixon JB, Hossner RL (1981) Transformation of chlorite to smectite through regularly in stratified intermediates. *Soil Sci Soc Am J* 45:650–656
- Sharp AD, Trudgill ST, Cooke RU, Price CA, Crabtree RW, Pickles AM, Smith DI (1982) Weathering of the balustrade on St. Paul's Cathedral, London. *Earth Surf Proc Land* 7:387–389
- Shushakova V, Fuller ER Jr, Siegesmund S (2011) Influence of shape fabric and crystal texture on marble degradation phenomena: simulations. *Environ Earth Sci* 63:1587–1601. doi:10.1007/s12665-010-0744-7
- Siedel H (2009) Zur herkunft von salzen an bauwerken. In: Schwarz H-J, Steiger M (eds) *Salzschäden an kulturgütern*. Ri-Con, Hanover, pp 22–29
- Siedel H, von Plehwe-Leisen E, Leisen H (2008) Salt load and deterioration of sandstone at the temple of Angkor Wat, Cambodia. *Proceedings of the 11th international congress on deterioration and conservation of stone*. Nicolaus Copernicus University Press, Torun, pp 267–274
- Siegesmund S, Weiss T, Vollbrecht A, Ullemeyer K (1999) Marble as a natural building show: rock fabrics, physical and mechanical properties. *Z Dt Geol Ges* 150:237–257
- Siegesmund S, Ullemeyer K, Weiss T, Tschegg EK (2000) Physical weathering of marbles. *Int J Earth Sci* 89:170–182
- Siegesmund S, Ruedrich J, Weiss T (2004) Marble deterioration. In: Prikryl R (ed) *Dimension Stone 2004*. Taylor and Francis Group, London, pp 211–217
- Siegesmund S, Mosch S, Scheffchük C, Nikolayev DI (2008a) The bowing potential of granitic rocks: rock fabric, thermal properties and residual strain. *Environ Geol* 55:1437–1448
- Siegesmund S, Ruedrich J, Koch A (2008b) Marble bowing: comparative studies of three different public building facades. *Environ Geol* 56:473–494
- Simon S, Drdácky M (eds) (2006) *Problems of salts in masonry-SALTeXPert*. European research on cultural heritage. State-of-art studies, vol 5. Institute of Theoretical and Applied Mechanics, Academy of Sciences, Prague
- Sippel J, Siegesmund S, Weiss T, Nitsch KH, Korsen M (2007) Decay of natural stones caused by fire damage. In: Prikryl R and Smith BJ (eds) *Building stone decay: from diagnosis to conservation*. geological society special publication 271. The Geological Society, London, pp 139–151
- Smith BJ, Magee RW, Whalley WB (1994) Breakdown patterns of quartz sandstone in a polluted urban environment, Belfast, Northern Ireland. In: Robinson DA, Williams RBG (eds) *Rock Weathering and landform evolution*. Wiley, Chichester, pp 131–150, 139–151
- Sneathlge R (1984) *Steinkonservierung 1979–1983*. Arbeitsheft 22. Bayerisches Landesamt für Denkmalpflege, Munich
- Sneathlge R, Wendler E (1997) Moisture cycles and sandstone degradation. In: Baer NS, Sneathlge R (eds) *Saving our architectural heritage: conservation of historic stone structures*. Wiley, Chichester, pp 7–24
- Steiger M (1996) Distribution of salt mixtures in a sandstone monument: Sources, transport and crystallization properties. In: Zezza F (ed) *Origin, mechanisms and effects of salts on degradation of monuments in marine and continental environments*. Protection and conservation of the European cultural heritage research report no. 4, pp 241–246

- Steiger M (2003) Salts and crusts. In: Brimblecombe P (ed) *Air pollution reviews*, vol 2. The effects of air pollution on the built environment. Imperial College Press, London, pp 133–181
- Steiger M (2004) Influence of salts on the freezing temperature of water: implications on frost damage to porous materials. In: Kwiatkowski D, Löfvendahl R (eds) *Proceedings of the 10th international congress on deterioration and conservation of stone*. ICOMOS, Stockholm, pp 179–186
- Steiger M (2005a) Crystal growth in porous materials—I: the crystallization pressure of large crystals. *J Cryst Growth* 282:455–469
- Steiger M (2005b) Crystal growth in porous materials—II: influence of crystal size on the crystallization pressure. *J Cryst Growth* 282:470–481
- Steiger M (2005c) Salts in porous materials: thermodynamics of phase transitions, modeling and preventive conservation. *Restor Build Monum* 11:419–432
- Steiger M (2006a) Crystal Growth in porous materials: influence of supersaturation and crystal size. In: Fort R, Alvarez de Buergo M, Gomez-Heras M, Vazquez-Calvo C (eds) *Heritage, weathering and conservation*, vol 1. Taylor and Francis, London, pp 245–251
- Steiger M (2006b) Freezing of salt solutions in small pores. In: Konsta-Gdoutos MS (ed) *Measuring, monitoring and modeling concrete properties*. Springer, Dordrecht, pp 661–668
- Steiger M, Asmussen S (2008) Crystallization of sodium sulfate phases in porous materials: the phase diagram  $\text{Na}_2\text{SO}_4\text{-H}_2\text{O}$  and the generation of stress. *Geochim Cosmochim Acta* 72:4291–4306
- Steiger M, Dannecker W (1994) Determination of wet and dry deposition of atmospheric pollutants on building stones by field exposure experiments. In: Zezza F, Ott H, Fassina V (eds) *Conservation of monuments in the Mediterranean Basin*. Proceedings of the 3rd international symposium, Venice, pp 171–178
- Steiger M, Dannecker W (1995) Hygroskopische eigenschaften und kristallisationsverhalten von salzgemischen. In: Snelthage R (ed) *Jahresberichte aus dem forschungsprogramm steinzerfall—steinkonservierung*. Band 5–1993. Verlag Ernst and Sohn, Berlin, pp 115–128
- Steiger M, Zeunert A (1996) Crystallization properties of salt mixtures—comparison of experimental results and model calculations. In: Riederer J (ed) *International congress on deterioration and conservation of stone—proceedings*. Möller Druck und Verlag GmbH, Berlin, pp 535–544
- Steiger M, Wolf F, Dannecker W (1993) Deposition and enrichment of atmospheric pollutants on building stones as determined by field exposure experiments. In: Thiel M-J (ed) *Conservation of stone and other materials*. E&FN SPON, London, pp 35–42
- Steiger M, Behlen A, Neumann H-H, Willers U, Wittenburg C (1997) Sea salt in historic buildings: deposition, transport and accumulation. In: Moropoulou A, Zezza F, Kollias E, Papachristodoulou I (eds) *Proceedings of the 4th international symposium on the conservation of monuments in the mediterranean*, vol 1. Rhodes, pp 325–335
- Steiger M, Neumann HH, Grodten T, Wittenburg C, Dannecker W (1998) Salze in natursteinmauerwerk—probenahme, messung und interpretation. In: Snelthage R (ed) *Handbuch Naturwissenschaft und Denkmalpflege: Natursteinkonservierung II*. Fraunhofer IRB Verlag, Stuttgart, pp 61–91
- Steiger M, Kiebusch J, Nicolai A (2008a) An improved model incorporating Pitzer's equations for calculation of thermodynamic properties of pore solutions implemented into an efficient program code. *Constr Build Mater* 22:1841–1850
- Steiger M, Linnow K, Juling H, Gülker G, El Jarad A, Brüggerhoff S, Kirchner D (2008b) Hydration of  $\text{MgSO}_4\text{-H}_2\text{O}$  and generation of stress in porous materials. *Cryst Growth Des* 8:336–343
- Steiger M, Linnow K, Ehrhardt D, Rohde M (2011) Decomposition reactions of magnesium sulfate hydrates and phase equilibria in the  $\text{MgSO}_4\text{-H}_2\text{O}$  and  $\text{Na}^+\text{-Mg}^{2+}\text{-Cl}^-\text{-SO}_4^{2-}\text{-H}_2\text{O}$  systems with implications for Mars. *Geochim Cosmochim Acta* 75:3600–3626
- Sterflinger K (2000) Fungi as geologic agents. *Geomicrobiol J* 17:97–124

- Sterflinger K (2005) Black yeasts and meristematic fungi: ecology, diversity and identification. In: Rosa C, Gabor P (eds) *Yeast handbook*, vol 1. Biodiversity and ecophysiology of yeasts. Springer, New York
- Stockhausen N (1981) Die dilatation hochporöser festkörper bei wasseraufnahme und eisbildung, thesis. Technical University, Munich
- Stumm W, Wollast R (1990) Coordination chemistry of weathering: kinetics of the surface controlled dissolution of oxide minerals. *Rev Geophys* 28:53–69
- Taber S (1916) The growth of crystals under external pressure. *Am J Sci* 41:532–556
- Taber S (1929) Frost heaving. *J Geol* 37:428–461
- Taber S (1930) The mechanics of frost heaving. *J Geol* 38:303–317
- Tang IN (1997) Thermodynamic and optical properties of mixed-salt aerosols of atmospheric importance. *J Geophys Res* 102:1883–1893
- Theoulakis P, Moropoulou T (1988) Mechanisms of deterioration of the sandstone of the medieval city of Rhodes. In: Ciabach J (ed) *Proceedings of the 6th international congress on deterioration and conservation OF Stone*. Nicholas Copernicus University, Torun, pp 86–96
- Török A, Hajpál M (2005) Effect of temperature changes on the mineralogy and physical properties of sandstones. A laboratory study. *Rest Build Mon* 11:211–218
- Trudgill ST, Viles HA, Inkpen RJ, Cooke RU (1989) Remeasurement of weathering rates, St. Paul's Cathedral, London. *Earth Surf Proc Land* 14:175–196
- Tsui N, Flatt RJ, Scherer GW (2003) Crystallization damage by sodium sulfate. *J Cult Heritage* 4:109–115
- Turkington AV, Smith BJ, Basheer PAM (2002) The effect of block retreat on subsurface temperature and moisture conditions in sandstone. In: Přikryl R, Viles H (eds) *Understanding and managing stone decay*. The Karolinum Press, Prague, pp 113–126
- UNI 11182 (2006) Beni culturali. materiali lapidei naturali ed artificiali. Descrizione della forma di alterazione—termini e definizioni. UNI, Milano
- Hees RPJ Van, Brendle S, Nijland TG, Haas GJLM De, Tolboom HJ (2004) Decay of Rhenish tuff in Dutch monuments. In: Kwiatkowski D, Löfvendahl (eds) *Proceedings of the 10th international congress on deterioration and conservation of stone*. ICOMOS Sweden, Stockholm, pp 91–98
- Van TT, Beck K, Al'Mukhtar M (2007) Accelerated weathering tests on two highly porous limestones. *Env Geol* 52:282–292
- Vergès-Belmin V (1994) Pseudomorphism of gypsum after calcite, a new textural feature accounting for the marble sulphation mechanism. *Atmos Environ* 28:295–304
- Vergès-Belmin V (ed) (2008) *Illustrated glossary on stone deterioration patterns*. Monuments and Sites XV. ICOMOS, Paris
- Von Konow T (2002) Test results. In: von Konow T (ed) *The study of salt deterioration mechanisms. Decay of brick walls influenced by interior climate changes*. Suomenlinnan Hoitokunta, Helsinki, pp 57–79
- Walder JS, Hallet B (1986) The physical basis of frost weathering: toward a more fundamental and unified perspective. *Arct Alp Res* 18:27–32
- Wang A, Freeman JJ, Jolliff BL (2009) Phase transition pathways of the hydrates of magnesium sulfate in the temperature range 50–5 °C: implications for sulfates on Mars. *J Geophys Res* 114:E04010
- Wangler T, Scherer GW (2008) Clay swelling mechanism in clay-bearing sandstones. *Env Geol* 56:529–534
- Warscheid T, Braams J (2000) Biodeterioration of stone: a review. *Int Biodeterior Biodegr* 46:343–368
- Watchman AL (1991) Age and composition of oxalate-rich crusts in the northern territory, Australia. *Stud Conserv* 36:24–32
- Weber J (1985) Natural and artificial weathering of Austrian building stones due to air pollution. In: Félix G (ed) *Proceedings of the 5th international congress on deterioration and conservation of stone*. Presses Polytechniques Romandes, Lausanne, pp 527–535

- Weber J, Burszán R (2008) Salt-induced decay of interior walls and climate control. The case study of Virgil's chapel. In: Salt weathering on buildings and stone sculptures. Technical University of Denmark, Lyngby, pp 257–267
- Weimann MB (2001) Hygrische eigenschaften von polymerbeton im vergleich zu porösen mineralischen werkstoffen im bauwesen, thesis. Technical University, Zurich, p 149
- Weiss T, Leiss B, Oppermann H, Siegesmund S (1999) Microfabric of fresh and weathered marbles: implications and consequences for the reconstruction of the Marmorpalais Potsdam. *Z Dt geol Ges* 150:313–332
- Weiss T, Rasolofosaon PNJ, Siegesmund S (2002a) Ultrasonic wave velocities as a diagnostic tool for the quality assessment of marble. In: Siegesmund S, Weiss T, Vollbrecht A (eds) Natural stones, weathering phenomena, conservation strategies, and case studies, Special Publication 205. Geological Society, London, pp 149–164
- Weiss T, Siegesmund S, Fuller ER (2002b) Thermal stresses via finite element modeling. In: Siegesmund S, Weiss T, Vollbrecht A (eds) Natural stones, weathering phenomena, conservation strategies, and case studies, Special Publication 205. Geological Society, London, pp 89–102
- Weiss T, Siegesmund S, Fuller E (2003) Thermal degradation of marbles: indications from finite element modelling. *Build Environ* 38:1251–1260
- Weiss T, Siegesmund S, Kirchner D, Sippel J (2004a) Insolation weathering and hygric dilatation: two competitive factors in stone degradation. *Environ Geol* 46:402–413
- Weiss T, Strohmeyer D, Kirchner D, Sippel J, Siegesmund S (2004b) Weathering of stones caused by thermal expansion, hygric properties and freeze-thaw cycles. In: Kwiatkowski D, Löfvendahl (eds) Proceedings of the 10th international congress on deterioration and conservation of stone. ICOMOS Sweden, Stockholm, pp 83–90
- Wendler E, Rückert-Thümling R (1993) Gefügezerstörendes verformungsverhalten bei salzbefrachteten sandsteinen unter hygrischer wechselbeanspruchung. In: Witmann FH (ed) Werkstoffwissenschaften und bausanierung, kontakt und studium 420, vol 3. Expert Verlag, Ehningen bei Böblingen, pp 11818–11830
- Whalley B, Smith B, Magee R (1992) Effects of particulate air pollutants on materials: Investigation of surface crust formation. In: Webster RGM (ed) Stone cleaning and the nature, soiling and decay mechanisms of stone: proceedings of the international conference held in Edinburg. Donhead, London, pp 227–234
- Widhalm C, Tschegg E, Eppensteiner W (1996) Anisotropic thermal expansion causes deformation of marble cladding. *Perf Constr Facil ASCE* 10:5–10
- Williams RBG, Robinson DA (1981) Weathering of sandstone by the combined action of frost and salt. *Earth Surf Proc Land* 6:1–9
- Williams RBG, Robinson DA (2001) Experimental frost weathering of sandstone by various combinations of salts. *Earth Surf Proc Land* 26:811–818
- Winkler EM (1987) Weathering and weathering rates of natural stone. *Environ Geol Water Sci* 9:85–92
- Winkler EM (1994) *Stone in architecture*, 3rd edn. Springer, Berlin
- Winkler EM (1996) Technical note: properties of marble as building veneer. *Int J Rock Mech* 32:215–218
- Winkler EM, Wilhelm EJ (1970) Salt burst by hydration pressures in architectural stone in urban atmosphere. *Geol Soc Am Bull* 81:567–572
- Winkler EM, Singer PC (1972) Crystallization pressure of salts in stone and concrete. *Bull Geol Soc Am* 83:3509–3514
- Wright JS (2002) Geomorphology and stone conservation: sandstone decay in Stoke-on-Trent. *Struct Surv* 20:50–61
- Zappia G, Sabbioni C, Gobbi G (1989) Weathering layers on stone monuments in maritime localities of northern and central Italy. In: Zezza F (ed) The conservation of monuments in the mediterranean Basin. Grafo, Brescia, pp 79–82
- Zehnder K (1982) Verwitterung von molassesandsteinen an bauwerken und in naturaufschlüssen. *Beitr Geol Schweiz, Geotechn Ser* 61. Kümmerly and Frey, Bern



- Zehnder K, Arnold A (1989) Crystal growth in salt efflorescence. *J Crystal Growth* 97:513–521
- Zehnder K, Schoch O (2009) Efflorescence of mirabilite, epsomite and gypsum traced by automated monitoring on-site. *J Cult Heritage* 10:319–330
- Zeisig A, Siegesmund S, Weiss T (2002) Thermal expansion and its control on the durability of marbles. In: Siegesmund S, Weiss, T, Vollbrecht A (eds) *Natural stone, weathering phenomena, conservation strategies and case studies*. Geological society special publication No. 205. The Geological Society, London, pp 65–80
- Zeza F, Macri F (1995) Marine aerosol and stone decay. *Sci Total Environ* 167:123–143
- Zeza F, Pascua NG, Macri F (1995) Rising damp and soluble salts in the weathering processes of biocalcarenes. Case study of cathedrals, churches and buildings of Lecce baroque. In: *Preservation and restoration of cultural heritage, Proceedings of the 1995 LCP congress*. Montreux, pp 161–176

# Chapter 5

## Environment and Architectural Stone

Peter Brimblecombe

**Abstract** It has long been recognized that the environment exerts a wide range of pressures on building stone. These can be loosely thought of in terms of the physical pressures of climate, particularly water and temperature issues and the chemical attack by pollutants. Twentieth century concern was especially focused on attack by acid rain, but, on longer time scales, weathering is likely to be the most important mechanism of degradation. For normal meteorological variables of temperature and precipitation, while valuable in parameterizing climate impacts on stone, it is advantageous to combine or accumulate simple meteorological data when assessing the effect of weather on building stone. Classic maps of climate offer some guidance about the geographic variability of pressures on stone, but these neglect air pollution, wind, and relative humidity. Climate maps need to be tuned to the impacts on heritage issues. Air pollution has been present in cities for thousands of years, but the extensive use of coal and the sulfur dioxide produced when it is burnt has been particularly aggressive towards stone. This sulfur is oxidized to sulphate and responsible for disfiguring gypsum crusts that characterized stone buildings in the 20th century. Contemporary urban atmospheres have lower concentrations of sulfur dioxide, but nitrogen oxides and ozone are increasingly found. Along with these, there is a range of organic acids and polycyclic aromatic compounds that potentially damage and discolor urban facades of the future. Climate change may also impose new threats to architectural stone.

---

P. Brimblecombe (✉)

School of Environmental Sciences, University of East Anglia, Norwich, UK  
e-mail: pbrimble@cityu.edu.hk

P. Brimblecombe

School of Energy and Environment, City University of Hong Kong, Kowloon, Hong Kong SAR, People's Republic of China

## 5.1 Nature of Environmental Exposure

Exposure to the environment poses a threat to building stone. Monumental works of architecture are built to last, so they become exposed for very long times to a changing world. The millennia write upon the stone of our great buildings, and a record of change accumulates on their surfaces. This may be seen as damage or patina, dependent on how it is viewed.

The weathering of architectural stone was recognized by the Roman writer Vitruvius in the chapter on stone in his ten books on architecture (*De architectura* 2:VII:2). He writes of soft stone: “that in open and exposed situations, the frost and rime make them crumble, and they go to pieces. On the seacoast, too, the salt eats away and dissolves them...” A sense of the damaging influence of frost in northern climates is also found in the non-classical world, where, for example, the 8th century Anglo-Saxon wrote of ruins, perhaps those of Roman Bath (*Aquae Sulis*):

This masonry is wondrous; fates broke it courtyard  
pavements were smashed; the work of giants is  
decaying. Roofs are fallen, ruinous towers the frosty  
gate with frost on cement is ravaged chipped roofs  
are torn, fallen, undermined by old age.

Wrætlíc is þes wealstan, wyrde gebræcon; burgstede  
burston, broснаð enta geweorc. Hrofas sind gehrorene,  
hreorge torras, hrungeat berofen, hrim on  
lime, scearde scurbeorge.

Thus, the importance of time and weather as disruptive factors were readily understood. This was significant in the case of stone buildings which were meant to last, so architects wanted their creations to survive long periods. Nicholas Hawksmoor wrote after his early 18th century restoration of Westminster Abbey: “I am of the opinion, if violence does not happen, this fabrick will stand 1000 years” (Hawksmoor 1934).

Although early architects recognized the importance of weather, they were also mindful of air pollutants. At first, this was simply seen as the disfiguration caused by smoke. Horace complained of the smoke begrimed temples in ancient Rome: “Your fathers’ guilt you still must pay, Till, Roman, you restore each shrine, Each temple, mouldering in decay, And smoke-grimed statue, scarce divine” or “*Delicta maiorum, immeritus lues, eomane, donec templa refeceris, aedisque labentis deorum et foeda nigro simulacra fumo*”. The effects of smoke were even more pronounced with the use of coal in cities, which had the potential to create acids that damaged building stone. This caused extensive and accelerated deterioration of buildings over much of Europe by the end of the 19th century and extended elsewhere by the early 20th century. Damage by coal smoke was so serious that it became an important element of R.J. Schaffer’s classic *The Weathering of Natural Building Stones* (1932), which contained chapters on both “air pollution” and “chemical phenomena associated with weathering” and an appendix on air pollution.

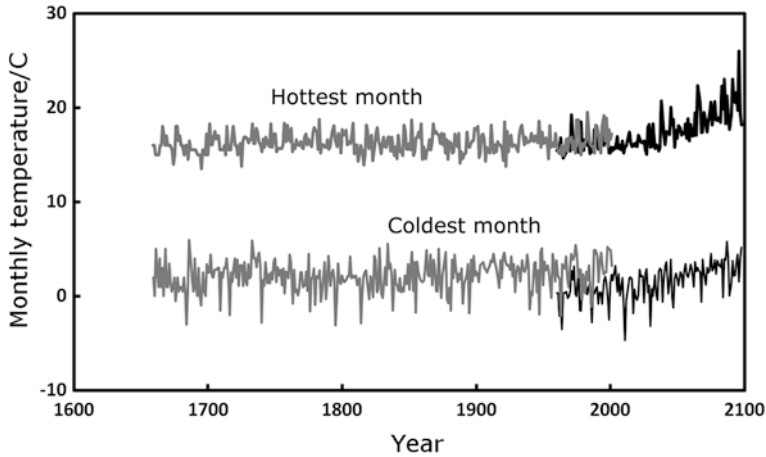


**Fig. 5.1** Annual temperature range in central England showing the temperature of the hottest and coldest months from the central England temperature record (*to* 2000) and predicted values from HadCM3A2 (from 1960)

Schaffer argues that the defects in building stone are responsible for weathering as the seams of different compositions, with the softer parts, eroding more rapidly. These are coupled with vents and shakes, small fissures in the stone that also enhance weathering. All this is compounded by poor craftsmanship and inappropriate choice of stone—for example, the wrong orientation of stone in relation to its bedding. The resilience of stone can also be dependent on seasoning; its aging after removal from the quarry, e.g. some stone, such as travertine, hardens as it dries out.

### 5.1.1 Heritage Climates

Although there has long been an understanding of the role of weather in damaging stone, the nature of these processes is not always appreciated. Simple meteorological parameters are not always adequate in assessing the weathering of many building stones. Very high temperatures damage stone, and some cannot resist fire, so this widely measured meteorological parameter is not very informative by itself. However, fluctuation of simple observed parameters, such as temperature or humidity, can be related to the deterioration of buildings. For example, the annual temperature range can be taken as an indicator of the extent to which a larger building has to change or “breathe” over the year (Fig. 5.1). Thus, when considering the weathering of architectural stone, we often need to consider novel representations of climate.

Climate is frequently defined as weather averaged over time. Its study, climatology, was developed by Wladimir Peter Köppen at the end of the 19th century. He saw the strong relationship between plants and the climates, so he developed a

classification that is relevant to vegetation. Other specialized climatologies have been proposed more recently: (i) ecological climatology has come from an integration of ecology and climatology that enables a better understanding of how terrestrial ecosystems function (ii) bioclimatology deals with the relationship between climate and life, and (iii) building climatology looks at achieving a comfortable climate within buildings together with energy-saving structural designs.

Recent interest in the impact of climate change and cultural heritage has invoked the need for heritage climatology (Brimblecombe 2010a). This can be allied with the suggestions of material climate found in Brischke et al. (2008). Such climatologies are tuned to the built environment (Brimblecombe 2010b) and express classical meteorological parameters in a way that links them with impacts on building materials and heritage (Brimblecombe et al. 2006).

### 5.1.1.1 Key Climate Parameters

Meteorologists think of climate in terms of a number of key variables: temperature, precipitation, wind speed and direction, radiation, relative humidity, etc. There are, additionally, a number of observation parameters less commonly measured, such as pan evaporation and soil moisture, which may, nevertheless, be relevant to the effects of weather on buildings and building stone. Meteorological data are collected by government-run agencies, often with a high spatial resolution. At some sites, the data is available for more than a hundred years, and some special data sets (mostly from Europe) are available that give a limited number of daily measurements for a number of centuries. Although this presents us with a wealth of detail, when considering damage to stone, it is not always well tuned to this purpose.

The temperature of the air is probably, as already suggested, not a key driver of stone deterioration given the limited range experienced at the Earth's surface. Despite this, much greater extremes in temperature can be found at stone surfaces exposed to intense sunlight, which can exceed 50 °C. Such intense exposure to solar radiation can exert stress on some stones, such as granites, where different minerals can absorb different amounts of radiation and differential expansion can place stress on the stone (Bonazza et al. 2009b). When temperatures change rapidly—2° per minute—this can produce thermal shock damage (Hall and André 2003). The interest in rock temperature means that this rather special parameter is sometimes measured in studies of stone degradation.

Temperature can be combined with other meteorological parameters to create new parameters to describe stone weathering. If temperature drops below zero, then water within the pores of the stone can freeze and expand such that the change in phase causes mechanical stresses that leads to frost shattering. This mechanism of damage is widely known in relationship to both building stone and the natural environment (e.g. Matsuoka 2008). Thus, even relatively small changes in temperature can cause significant change in the number of freeze–thaw cycles (Grossi et al. 2007a). This amplification can be seen when changes in humidity cause the

brines within pores to crystallize (or change in crystalline form), exerting pressure within the stone that leads to salt weathering. Once again, the frequency of these phase changes, dissolution-crystallization cycles, can be sensitive to small changes in relative humidity (Benavente et al. 2008).

Precipitation is an important parameter because the dissolution of stone is strongly dependent on precipitation quantity (Lipfert 1989). It can also act along with other meteorological parameters, such as wind speed, to create wind-driven rain. This can force water deep into porous building materials or wash pollutant crusts off building surfaces in disfiguring patterns. Wind-driven sand is also possible in arid regions, where it can abrade friable rocks or earthen building materials.

These combinations of parameters can be quite subtle and not necessarily contemporaneous. For example, the impact of frost weathering can be enhanced if the stone is saturated with water before the freezing event occurs; a combination of a rainy day before a day of freezing weather has an enhanced potential to damage porous stone. Thus, estimating the impact of climate on building stone can require quite thoughtful uses of classical meteorological parameters, combining them or demining the amplitude or frequency of cyclic variation so they become relevant to the weathering of building materials.

The relationship between environmental pressures and the rate of alteration to materials is often described in terms of damage or dose-response functions. These have been widely used to describe the effects of air pollution, but are also available for climate variables. Thermoclastic stress imposed on rocks and frost weathering are typical examples. The maximum thermal stress ( $\sigma_T$ [MPa]) for a uniform elastic medium confined in the horizontal directions and unconstrained in the vertical directions is given by:  $\sigma_T = E \cdot \alpha \cdot \Delta T / (1 - \nu)$ , where  $E$  is Young's modulus (GPa),  $\alpha$  is the thermal expansion coefficient ( $K^{-1}$ ),  $\Delta T$  is the actual amplitude of the periodic surface temperature variation, and  $\nu$  is Poisson's ratio (Bonazza et al. 2009b). Grossi et al. (2007b) suggest a range of parameters, largely involving differences between 1 day and the next, yet setting minimum temperatures, below which damage does not occur.

Such functions can also be useful to make estimates of risk, but we probably need a wider variety, and they need to be understood better in terms of the variety of stones. The functions may work well for isolated stone, but there are always questions about how well these might represent the situation in a wall or a projecting stone element.

### 5.1.1.2 Types of Climate

Despite the need to go beyond classical meteorological parameters when considering weathering to buildings, there is some benefit in considering broad geographical climate regimes, as they have been so frequently mapped. The geography of climate was studied by Köppen in the 19th century. His ideas were tuned to an interest in vegetation, but they can be adapted to understanding the relationship between material heritage and climate and are useful because they



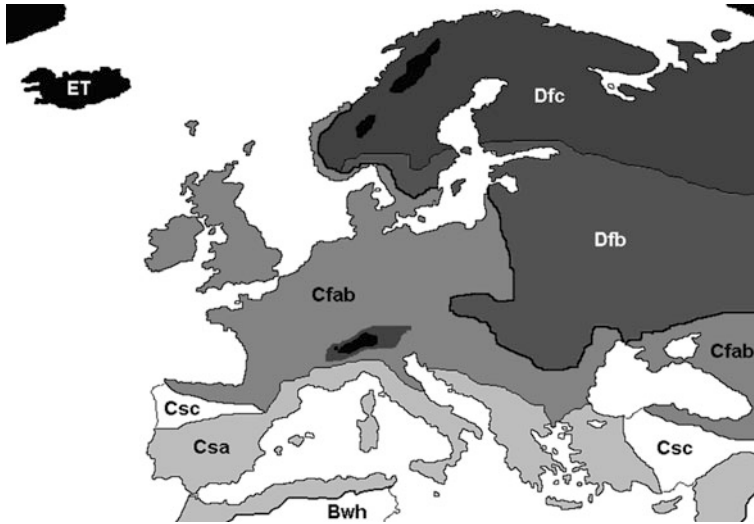


**Fig. 5.2** European climate regions following the Köppen-Geiger scheme as applied by Kottek et al. (2006)

are easily expressed as climate maps of the kind found in many atlases. It may seem surprising to relate maps based on vegetation-climate interactions to building damage, but the potential for correspondence is not entirely unexpected: e.g. stone and vegetation are both sensitive to the frequency of frost.

The classical approach of Köppen has been updated by Kottek et al. (2006) to allow ready digitization. A simplified Köppen-Geiger climate map of Europe is shown in Fig. 5.2. The number of Köppen-Geiger climate types has been reduced so it shows only the broadest changes to simplify our discussion.

The Köppen-Geiger scheme describes climates in terms of codes. The first letter describes the broad groups of climate: A through to E. These can be subdivided into further types. An adaptation of the Köppen-Geiger scheme that describes climates of relevance to the weathering of architectural stone in Europe might be given as (Brimblecombe 2010a, b):

- *Bwh—hot arid climate*: dry ground with little vegetation so there is a chance of wind-blown sand and extreme thermal stress. Earthen buildings are frequent in this climate, and the materials are friable and additionally sensitive to the rare but heavy rainfall.
- *Csa—warm climate with hot summer*: thermal stress on materials exposed to strong insolation. Dry conditions in the summer may limit surface wetness and attack by air pollutants that need water to cause recession.
- *Csb—warm fully humid climate with dry warm summers*: drier conditions and lower variation in humidity leads to less salt damage and some potential for frost weathering. Some potential for thermal stress on materials exposed to strong insolation.

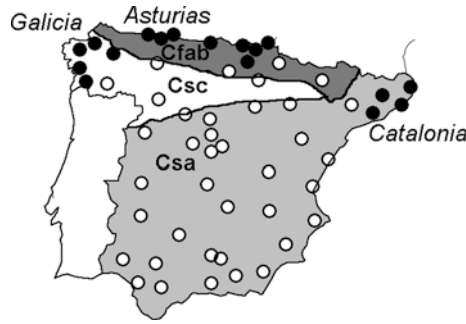


**Fig. 5.3** Salt transitions in the sodium chloride system in contemporary Spain (Grossi et al. 2011), showing the distribution of sites with climates imposing a higher annual frequency of sodium chloride transitions as *filled circles*. Sites with a lower frequency of transitions and dry summers, causing these to occur mainly in winter, are shown as *open circles*. The superimposed climate types are taken from the coarse resolution map of Fig. 5.2

- *Cfab*—warm fully humid climate with warm to hot summers: damp conditions and variation in humidity that cause salt damage, occasional freezing events present the potential for frost weathering. Warm and damp conditions lead to the potential for uptake and reaction of air pollutants on stone.
- *Dfb*—fully humid snow climate with warm summers: lower variation in humidity leads to less salt damage, but a potential for frost weathering.
- *Dfc*—fully humid snow climate with cool summers: lower variation in humidity leads to less salt damage, but cold winter conditions mean a high potential for frost weathering in the spring and autumn.
- *E*—polar or montane climate: conditions so cold that ground may remain frozen. However, processes such as frost heave can disrupt building support.

This Köppen classification is essentially thermohyetal (i.e. it is constructed using seasonal temperature and precipitation). It ignores relative humidity, which is such an important variable in salt weathering. Yet, despite this, it seems that rainfall may act as something of a surrogate for humidity in such broad climate classifications of climate related to materials. Grossi et al. (2011) have mapped the potential for salt damage in Spain. The map in Fig. 5.3 shows the broad agreement between climate groups and the frequency and seasonality of sodium chloride transitions. It captures the differences of Asturias (and Galicia) very well, in addition to the high frequency of transitions in the sodium chloride system that arises in the fluctuating oceanic climate along the northern coast. This region is separated from inland Spain by the Cantabrian Mountains. However, there are subtle differences in the east. In Catalonia, the Mediterranean climate also induces a higher potential for salt weathering.

The Köppen-Geiger maps often lack local detail, but the focus on temperature and precipitation limits their use even though the map of Spain suggests that some elements of humidity have been captured. However, wind, for example, is entirely absent, so coastal regions where wind-blown salt might be important cannot be

illustrated. Similarly, although the maps pick out dry areas where low vegetation might allow sand and dust to be blown about, the intensity and frequency of the wind is not captured by the classification system. Often, more critical for any damage to stone is the lack of information about air pollution, which has been such an important driver of damage in 20th century cities. Even if it were to be added, air pollution damage is often difficult to map because the spatial gradients can be very steep. Vehicle-generated pollution falls off rapidly with distance from the curbside, so, for example, the blackening of buildings is most noticeable very close to busy roads (Brimblecombe and Grossi 2005). Furthermore, climate which is represented in such maps is average weather, although some seasonal information is built into Köppen-Geiger climate maps. Low temporal resolution again limits this as an approach to heritage climatology. It may be best to see these classical climatologies as a starting point for a mapping that is better tuned to describing geographic variation in stone weathering.

### **5.1.2 Pollutants**

This section covers the formation and presence of pollutants in the atmosphere, and, although it will mention their role in inflicting damage on materials, much of the detail of many of these processes will be left to [Chap. 3](#). The impacts of climate and pollutants accumulate on building surfaces over long time periods. The surfaces reveal these for long exposures, so climate and pollution history is relevant to understanding the changing pressures and adds to an ability to predict future impacts.

#### **5.1.2.1 Primary Pollutant History**

Air pollutants were known in ancient cities where the problems arose because of fuel use in the densely populated communities. This led to smoky atmospheres. Sextus Julius Frontinus, once Roman Governor of Britain (~AD75–78) and later Curator Aquarum with responsibility for supplying Rome's water supply, noted the cities' "infamis aer" and "gravioris caeli" in his *De Aquaeductu* (II, 88). Although smoke defaced buildings, this did not raise extreme concern until it was coal, rather than wood smoke, that filled the urban atmosphere. This newer form of urban air pollution, high in sulfur dioxide, was first seen in medieval London after the depletion of convenient nearby wood supplies. Large building operations around London required the production of lime as mortar, and, starting in 1253, the use of oak brushwood as a fuel changed to coal by 1264. Major activities could require a thousand tons of lime, so, when large quantities of coal were used, it is understandable that citizens complained about the sharp smell of the less familiar coal smoke. They worried about its effect on their health. Although industries of the distant past were often small, mineral operations could nevertheless involve large quantities of fuel.

In ancient Rome, the technical control of air pollution from these early industries was difficult and required activities such as tile-, glass-, and brick-making to be moved to the suburbs. In English cities, such as medieval York, there was similar pressure to move smoky activities to the outskirts and downwind (Bowler and Brimblecombe 1990). The nature of the fuel could also be regulated, so, in medieval London, there were attempts to ban coal and pressure artisans to return to wood (Brimblecombe 1987). Even where coal was not used, large wood-burning industrial activities could create pollution problems. A notable example was salt-making in Lüneburg during the medieval and early modern period, where some 48,000–72,000 m<sup>3</sup> of wood were used each year in the 15th and 16th centuries (Lamschus 1993).

Throughout 17th century Europe, there was a growing interest in science. In England, this also brought improved understanding of air pollution, and it was discussed by early scientists within the Royal Society (e.g. Brimblecombe 1978). John Evelyn, in particular, was noted for his pamphlet *Fumifugium* of 1661, which explored the causes and effects of air pollution in a coal burning city. He is often seen as an early environmentalist, but, for economic reasons, he was unable to get industry moved downwind of London. Another fellow of the Royal Society, Sir Kenelm Digby, developed an atomic view of the corrosive effects of coal smoke in his book *Discourse on Sympathetic Powder* (1658), although these ideas can be traced earlier to *Poems and Fancies* (1653) by Margaret Cavendish (Brimblecombe 1987), the first English woman to write extensively on science. She wrote, “If, atomes sharpe are in that coale entire, being strong armed with points, do quite pierce through; those flat dull atoms, and their forms undo.” This uses atoms in an explanation of the corrosiveness of coal smoke.

The growing industrialization of late 18th century Europe, most particularly, the wide adoption of the steam engine, meant that administrators had to consider a more formal approach to controlling air pollutants. Early regulations can be found in France and England from the beginning of the 1800s, but these tended to relate largely to health, despite the growing impacts of aggressive smoke and sulfur dioxide on building facades, such as the newly constructed neo-gothic Houses of Parliament in London.

### 5.1.2.2 Development of Photochemical Smog

A completely new form of air pollution emerged in southern California during the Second World War. Severe air pollution episodes developed in Los Angeles, and, although these contained neither smoke nor fog (i.e. SMOke + fOG), they were called smogs. Their origin lay in the increasing use of liquid fuels, especially by automobiles. Despite the lack of understanding of the chemistry which drove the formation of smog, as early as the 1940s, there was an awareness of its “peculiar nature” (Krier and Ursin 1977). In the mid-1940s in Los Angeles, the smog was seen as a temporary problem that might be easily solved.

This proved not to be the case, and, by the 1950s, the complex nature of the smog and its regulation began to become clear through the work of Arie Haagen-Smit, who, as a biochemist, studied damage to crops by the air pollution. He became aware that smog arose through reactions of automobile exhaust vapors in sunlight. It was notably rich in oxidizing substances and ozone. The mechanism of ozone formation gradually emerged through the work of various groups, including the photochemist Philip Leighton, who wrote the classic book *Photochemistry of Air Pollution* (1961). Although not fully developed, this book laid the foundations of our understanding of smog. It came to be realized that the hydroxyl radical was pivotal to smog chemistry, initiating the photochemistry and producing the peroxide radicals that create the brown nitrogen dioxide that drive the increase in ozone in the polluted atmosphere. The situation found in Los Angeles in the 1940s was gradually found more widely as the number of automobiles grew in the second half of the century. In this way, photochemical smog became a global problem.

### 5.1.2.3 Carbon Compounds as Air Pollutants

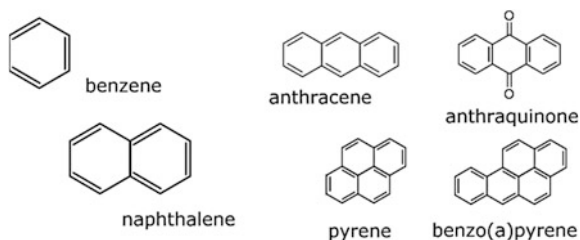
The combustion of hydrocarbons, typically fossil fuels, produces large quantities of carbon dioxide, carbon monoxide, soot, and volatile organic compounds (Brimblecombe 1996). On a global scale, these represent vast fluxes in the atmosphere. Carbon dioxide is a radiatively active gas, so it is much discussed in terms of greenhouse warming. Increasing concentrations of carbon dioxide in the atmosphere are seen as responsible for much of the global temperature increase over recent decades. These climate changes have a role to play in stone weathering, but the carbon dioxide increase will also cause slight changes in the solubility of carbonate stone, which is likely to enhance weathering rates (Bonazza et al. 2009a). Carbon dioxide can be found at enhanced concentrations in urban areas and, most particularly, in crowded interiors.

Incomplete combustion of fossil fuels yields carbon monoxide, and automobiles, which operate using fuel rich mixtures, represent a particularly important urban source. The gas is toxic, and the concentrations may be high enough in busy streets to have health effects on people, as the gas binds strongly with hemoglobin in the blood. This means it is carefully monitored in cities, but it is also of concern indoors as poor ventilation from cooking or heating sources is responsible for a large number of poisonings each year. Quite by contrast, it causes no damage to building stone.

The incomplete combustion of fuel also leads to elemental carbon or soot. This can have concentrations in the  $10 \mu\text{g m}^{-3}$  range in busy urban areas, where diesel vehicles are a contemporary source. The soot deposits on facades cause the blackening that characterizes urban buildings. In the past, this soot arose from coal, but this is less important now as coal is more rarely burnt in cities, although it is still common in some countries, e.g. China.

Additionally, incomplete combustion of fuel also produces organic compounds that often form in the cooler parts of an engine or in wood stoves operating with

**Fig. 5.4** Structural formulae of benzene and some selected polycyclic aromatic compounds



limited oxygen supply. Organic material in the fuel is transformed or pyrolyzed. These may be small molecules, such as acetylene (ethyne) characteristic of automobiles, through to larger organic molecules that can have many benzene rings. Unburnt fuel itself may also be found in exhaust gas and liquid fuels, such as petrol evaporation from a hot engine or when spilt during refueling represents an additional source.

These smaller hydrocarbon molecules, when reacting with the OH radical, play an important role in the formation of photochemical smog. However, compounds such as acetylene, ethylene, and simple alkanes have no direct impact on architectural stone. A potentially more significant problem is likely to be the larger organic molecules formed in the combustion process. These more typically arise from the combustion in diesel engines or, in earlier times, coal combustion. Polycyclic aromatic hydrocarbons are common products of these processes, and a number of these are shown in Fig. 5.4.

Polycyclic aromatic hydrocarbons (PAH) are of concern in urban atmospheres because some, such as benzo(a)pyrene, are extremely carcinogenic. Their actions on building stone are more subtle. These large organic molecules have low volatility and become associated with particles in the atmosphere, such as diesel-derived soot which readily deposits on building surfaces. There is a range of other potential interactions with surfaces. The compounds may help soot particles adhere to buildings or, in some cases, even act as nutrients for micro-organisms. Some of these compounds, such as anthracene, are photosensitizers and promote chemical reactions. If these polycyclic compounds oxidize, they can change from colorless substances (although, of course, the deposits appear black since they are associated with soot) to yellow compounds, e.g. an oxidation product of anthracene would be the yellow anthraquinone (Fig. 5.4).

Oxidation in the atmosphere can transform organic gases in photochemical smog. Aldehydes and ketones are found along with carboxylic acids as products. These irritants have potential health impacts, but it is likely that the acids have the most significant role to play in building damage. Simple organic acids, such as formic and acetic acids, are found in the crusts of buildings along with oxalic acid. Although oxalic acid is readily produced as particles in photochemical smog, some of these acids are likely to originate from biological metabolism on the stone surface (e.g. Bonazza et al. 2007).

#### 5.1.2.4 Nitrogen Compounds as Air Pollutants

Fuels are burnt in air, with the exception of situations such as rockets wherein the oxidant is carried along with the fuel (Brimblecombe 1996). At high temperatures, nitrogen atoms are produced in the flame, and this reacts through a process known as the Zeldovic Cycle:



Additionally, nitrogen oxide can be produced during combustion via HCN or nitrogen present in the fuel. Some nitrogen dioxide ( $\text{NO}_2$ ) is also produced during combustion, especially in some modern diesel engines. More usually, nitrogen dioxide is produced through the oxidation of NO by ozone in the atmosphere. Subsequent chemistry converts the nitrogen dioxide to nitric acid, which can be present either in the gas phase or dissolve in water to form acid rain.



There are ranges of nitrogen-containing organic compounds that are found in air pollution: peroxyacetyl nitrates and nitrated aromatic compounds. These are important from the health perspective and mediate the chemistry of the atmosphere, but they seem to be of little importance in damage to building stone.

#### 5.1.2.5 Sulfur Compounds as Air Pollutants

Sulfur is an abundant impurity in fossil fuels such as coal and oil (Brimblecombe 1996). The concentration can be as much as 5 % in some coals, so combustion and release of large quantities as sulfur dioxide into the air of cities has presented a problem for as long as coal has been used. Large power plants can now desulfurize their emissions and reduce them considerably. Declining use of coal in many cities during the latter half of the 20th century meant that concentrations of sulfur dioxide declined substantially. In some cities, such as London, Berlin, and Pittsburgh, which had used coal extensively in the 19th century, the sulfur dioxide concentrations began to show declines in the first half of the 20th century. These were probably due to the increasing area covered as cities developed efficient transport networks and ensured that the pollution was effectively diluted. Sulfur dioxide in modern cities may be one or two orders of magnitude lower than in the past, which has greatly changed the way in which deposited sulfur alters the stone facades. The black gypsum crusts that dominated buildings of the past can still be produced in modern cities, but they are no longer ubiquitous.

Sulfur dioxide is oxidized to sulfuric acid in the gas phase via a series of reactions initiated by the OH radical. The gas is additionally soluble in water, so it



can be oxidized by oxidants such as oxygen, ozone, and hydrogen peroxide that dissolve in water droplets to make solutions of sulfuric acid. Oxidation by oxygen requires the presence of catalysts, such as traces of dissolved iron or manganese. The production of sulfuric acid means that water droplets can become extremely acidic. Although urban rain can be acidic, it is equally possible to find acid rain in remote areas. The slow oxidation of sulfur dioxide to sulfuric acid allows air masses to accumulate sulfuric acid during long-range transport. The affinity of this acid for water means that strongly acidified rainfall can be found in remote areas. Fortunately, in many regions of Europe and North America, the total amount of sulfur emitted has been in decline for some decades. This contrasts with the developing world, most notably China, where the rising use of coal in a period of rapid industrialization has meant an increase in sulfur emissions. The impacts of sulfuric acid deposition in China may well have been somewhat lessened by the presence of airborne alkaline dusts blown from the western deserts.

Sulfur gases in low oxidation states can also be found in the atmosphere as sulfides. These can exist as hydrogen sulfide or organo-sulfides, both from natural (the oceans are an especially strong source of dimethylsulfide) and anthropogenic sources. The most concentrated of these sulfides in the global atmosphere is carbonyl sulfide. While they have little impact on stone, the sulfides can be important in tarnishing metals, most notably copper and silver.

Volcanoes are also sources of sulfur gases, and, some years, large eruptions can mean an input of  $100 \text{ Tg(S) a}^{-1}$ , rivaling human emissions. These volcanic fluxes are highly variable so, most years, the flux is an order of magnitude smaller. Some of the sulfur from explosive volcanism is forced into the stratosphere where it can persist, lower global temperatures, and alter the ozone layer. Gentler releases remain in the lower atmosphere, and, in some places, such as Hawaii, the clouds of pollutant gas, known as vog, have local impacts. In other places, Rotorua, New Zealand, for example, the sulfur is gently released from fissures as hydrogen sulfide.

#### 5.1.2.6 Halogens as Air Pollutants

Much as with sulfur, halogens are present as trace constituents of fuels and released as pollutants during combustion and high temperature industrial activities (Brimblecombe 1996). Hydrogen chloride is produced in the combustion of wood and high chlorine coals. It is extremely soluble, so it dissolves in clouds and rainwater. This generally takes place close to the source, so it has its greatest impact locally. Britain has high-chlorine coals, and Victorian scientists believed that the attack of hydrochloric acid on building stone was a major element in the decay observed in cities. However, this attack would produce calcium chloride upon reaction with carbonate stone. Calcium chloride is very soluble, so it is lost from buildings and would not form crusts in the same way as attack by sulfuric acid.

Hydrogen fluoride can also be released from high temperature industrial processes (Brimblecombe 1996), notably brick-making or, to some extent, aluminum

smelting. The dispersal of hydrogen fluoride in the vicinity can lead to fluorosis (i.e. bone damage) in grazing animals. Although hydrofluoric acid is extremely corrosive and will even attack glass, the concentrations are typically not high enough to cause noticeable damage to materials. As with sulfur dioxide, there are important volcanic sources for both hydrogen chloride and fluoride.

#### 5.1.2.7 Oxidants in the Air Pollutants

Haagen-Smit and Leighton showed that the atmosphere of the modern photochemical smog is highly oxidizing. We now understand the importance of the hydroxyl radical and, subsequently, the hydroperoxy and organoperoxy radicals in this process. Ozone is the archetypical oxidant in smog. It has a role to play in oxidizing sulfur dioxide to sulfuric acid. It can also oxidize organic matter deposited on building facades, but does not attack stone directly. It may be involved in enhancing the corrosion of some non-ferrous metals.

#### 5.1.2.8 Aerosols

Suspended solids or liquids in the air are called aerosols. These particles have to be less than  $20\ \mu$  in diameter to remain suspended for sufficiently long to be relevant to atmospheric processes. However, larger particles may contribute a substantial flux of material to urban surfaces over short distances or even longer distances under high winds. Large particles and fibers sometimes as great  $100\ \mu$  in length can be important indoors. Here, they are shed from clothing and can soil the walls of rooms or caves on public display (this is known as cave lint). Particle size is relevant to the behavior of particles and their reactivity and capture by surfaces.

Combustion-derived particles in cities contain a significant amount of carbon, dependent on their source. Along with the carbon is a range of organic matter, often as high molecular weight materials such as PAH, which can end up being deposited onto building surfaces. Some of the carbon can be oxidized into high molecular weight materials that resemble the humic acids of soil. This material is called humic-like substance (HULIS) and is typically brown in color. There are also other particles found in air. Sea salt is characteristic of marine locations, but it can be driven inland. If the environment is acidic, the chloride in sea salt may be replaced, so we can find sodium sulfates or nitrates. Sulfuric and nitric acid displace the chloride as hydrogen chloride. Sulfuric acid can react with ammonia in the atmosphere, largely present from the degradation of protein, and produce ammonium bisulfate and ammonium sulfate particles. Ammonium nitrate is also found, but is semi-volatile and may move into the gas phase as ammonia and nitric acid. Mineral dusts can also be transported long distances if the particles are small. They often provide alkaline materials to building surfaces and, in other cases, catalysts for oxidation reactions.

## 5.2 Wind-Driven Processes and Architectural Stone

Storms cause enormous damage to buildings. There is currently much discussion about the potential change in storm frequency as a result of climate change. This is an important debate, both in terms of the direct damage to buildings and flood frequency. Storms have a small spatial scale and so are often difficult to predict, while flooding involves the interaction between the rain that has fallen and the catchment area. It is a measure of the difficulty in predicting these changes that there is still disagreement over the trends in flooding in European cities. However, on a smaller scale, it seems that heavier summer rainfall is likely to lead to more surface water lying around buildings in the future. Heavy rain can also overwhelm the capacity of guttering and cause damage as water flows over building surfaces.

Wind-driven rain (WDR) or driving rain is a key aspect of the way climate affects buildings. This is the component of rain that has a horizontal velocity and falls obliquely onto surfaces. Driving rain is the most important moisture source affecting the hygrothermal performance and durability of building facades. The precipitating water is mainly driven into defect joints of stone structures and can lead to water penetrating into the building, exacerbate frost damage, induce moisture-controlled salt migration, and promote discoloring efflorescences (Blocken and Carmeliet 2004). The runoff that drains over buildings is also responsible for erosion and the changing appearance of soiled facades. This latter process has been the subject of much interest, as it changes the appearance of soiled facades and affects the patterns of blackening.

Wind-driven rain is also important for impelling water onto different elements of the building and is a relevant factor in the dry and wet deposition of atmospheric pollutants to facades. A range of methods is available to calculate the deposit of wind-driven rain on building facades. These have been developed and progressively improved over time to include the semi-empirical models as in the ISO Standard for WDR assessment and CFD models, as compared by Blocken et al. (2010).

The process of wetting and changes in the visual appearance has been widely investigated. Camuffo et al. (1982) argue that the way rain interacts with the surface controls the type of weathering observed: at one extreme, there is a complete washout of the surface, while, at the other, the surface is only very slightly wetted. Rain is important since the wetted surfaces that arise from moisture condensation on the stone surface play only a very minor role compared with that due to rainfall on surfaces in an urban area.

The details of the removal of soiling from the strongly blackened Cathedral of Learning at the University of Pittsburgh have been investigated by the group of Davidson (Davidson et al. 2000; Tang and Davidson 2004; Tang et al. 2004). Archival photographs show that the building became soiled while it was still under construction (completion 1937) since Pittsburgh was heavily polluted. The last half century saw great improvements in air quality in the city, so blackened areas of the stone have been slowly washed by rain, leaving white, eroded surfaces. This cleaning is most extensive at the highest elevations, where there is sufficient rain to

wash off flat areas of stone but not enough to wash irregular surfaces. There are frequent winds through the SW to NW sectors, where there are also greater wind speeds and rainfall intensities. A comparison of soiling patterns and volumes of wind-driven rain suggest that soiling remains on walls at relatively low volumes. The rain streaking that characterizes this removal can be much affected by local irregularities in the architecture. Many of the soiling patterns that develop are annoying and can offend the interested visitor (Grossi and Brimblecombe 2004).

Not only wind drives rain, but sand can also be a problem in arid regions. The Great Sphinx was buried by sand, and it was cleared several times throughout its history. Similar problems are encountered with the monumental mud architecture of Mali in the southern Sahara, where sand accumulates against the buildings and requires continual effort to clear it. The sand is also abrasive, and this causes further deterioration of statues such as the Great Sphinx (Hussein and El-Shishiny 2009) and buildings such as the friable stone of the Temple of Concordia in Agrigento, Sicily.

### 5.3 Air Pollution and Architectural Stone

As we have seen in previous sections, there was an early awareness of the corrosive nature of the urban atmosphere. The English diarist John Evelyn was interested in architecture and concerned about the impact of pollutants. In *Fumifugium* (1661), he wrote of “this horrid Smoke which obscures our Churches, and makes our Palaces look old...” A few decades later, Keepe (1682) described the north side of London’s Westminster Abbey: “... she stands exposed, as also the continual smokes of the sea-coal which are of a corroding and fretting quality...” Sir Christopher Wren, Surveyor of the Abbey from 1698, wrote of extensive damage from weathering and sulfation in a report (Wren 1713): “... the unhappy choice of materials: the stone is much decayed four inches (~ 10 cm) deep and falls off perpetually in great scales.” Such rapid weathering by coal smoke necessitated restoration from the mid-18th century (Brimblecombe et al. 1992), and the corrosion layers were termed *scurff* (Drake 1736), an archaic word to describe saline or sulfurous encrustations. Thus, there is a developing understanding of the nature of the corrosive materials.

#### 5.3.1 Sulfur Dioxide and Acid Rain

##### 5.3.1.1 Coal-Smoke-Laden Atmospheres

When Schaffer (1932) wrote his classic book, he was writing at a time when coal smoke filled the urban air. He confronted this issue by devoting much attention to aggressive pollutants. Although some early research promoted hydrochloric acid

as a source of severe damage to building stone, ultimately, sulfuric acid was seen as the culprit. The presence of gypsum crusts on damaged buildings was very much an indicator of the key role played by sulfur compounds (Sabbioni 2003). It was clear that, in polluted atmospheres, the carbonate surfaces had been almost entirely replaced by sulfate layers, frequently incorporating large amounts of black carbon into the deposits.

From the 1970s, the problem of damage to buildings became linked to the acid rain issue. The massive emissions of sulfur dioxide from coal burning and its long-range transport led to widespread concern about the acidification of rain, particularly as sulfuric acid. This caused the declining pH of lakes and contributed to forest damage in many parts of Europe. Acid rain was formed during the long-range transport of pollutants. Parallel worries arose that acid rain was also damaging building stone, although the damage in cities could be seen as arising from the deposition of sulfur dioxide to building stone.

In many large cities, by the 1970s, sulfur dioxide was already declining in concentration, so there was some confusion about why many regarded the rates of recession to carbonate building stones in cities as much increased in recent years. Some of the confusion arose from misperceptions, e.g. it was not uncommon for the cumulative rather than rate of damage to be the center of public attention. There was also a possibility that high rates of pollutant deposition from earlier periods had initiated rapid rates of decay that continued long after the pollutants had declined. This memory effect was explored by Vleugels et al. (1993), who examined the changes in the rate of loss of material from Massangis stone slabs when they were switched to locations in Belgium with different pollutant loads. After the stone slabs were transferred, the rate of stone loss immediately changed to the value expected in the new environment. This experiment provided no evidence of a memory effect.

Since longer records of recession rates have emerged, it has become clear that, as urban air has become cleaner, the rate of recession has declined. While, in the early parts of the 20th century, sulfur dioxide could have been 100 ppb, by the end of the century, it was more than an order of magnitude lower. The work started by Trudgill's group (Trenhaile 2001) has studied the long-term recession of the rain-washed balustrade of St. Paul's Cathedral and shown the gradual improvement in attack on stone at this site in central London (Fig. 5.5).

### 5.3.1.2 Development of Black Crust

On damp, but not strongly rain-washed surfaces of buildings, substantial black crusts were common manifestations of exposures in great cities. The formation of these crusts has been studied extensively. The key driver is the deposition of sulfur dioxide to the stone. This can take place on wet-to-dry stone, but is more effective when the stone is wet. Hydration reactions at the surface convert the dissolved sulfur dioxide into sulfites or bisulfites. These anions contain sulfur in the IV oxidation state. Subsequent oxidation converts the anions to S(VI) as sulfate. Both sulfites and sulfates are found as calcium salts in building crusts.

**Fig. 5.5** Annual erosion rate on the rain-washed balustrade of St Paul's Cathedral, London (data from Trenhaile 2001)

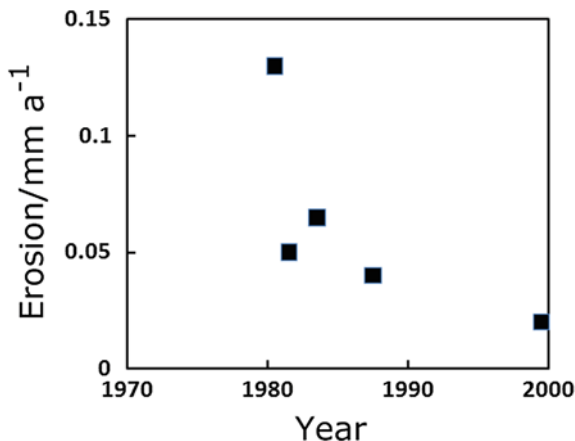
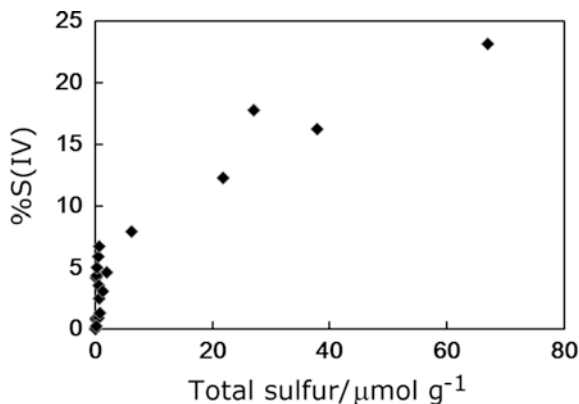


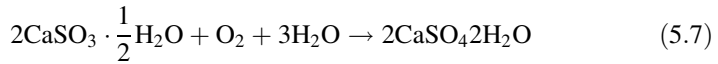
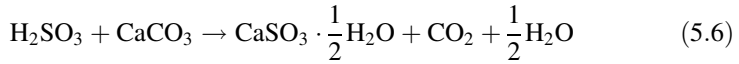
**Fig. 5.6** The fraction of sulfur as sulfite, S(IV), expressed as a percentage of the total for a range of stone and mortars (data from Gobbi et al. 1998)



Sulfite is readily oxidized, so analysis of sulfite from building surfaces requires care. Despite the relative ease with which sulfite is converted to sulfate, it can still be found in significant proportions on building surfaces (Gobbi et al. 1998), as illustrated in Fig. 5.6. Here, we see the amount of sulfur as sulfite and sulfate, i.e. S(IV) and S(VI), from a range of stone and mortars: Ancona, Carrara, Travertine, Trani, Portland, lime, pozzolan, and cement exposed for a year. In some cases, concentrations reached more than 50  $\mu\text{mol g}^{-1}$ . It has also been noticed that, although there is a relationship between the amount of S(IV) and S(VI), this is not linear. As S(IV) concentrations increase, so does its proportion. This is probably the result of depletion of likely catalysts and oxidizing agents in the surface of the stone.

The general view is that the creation of gypsum (sulfate) crusts on stone proceeds as such:





The oxidation of S(IV) shown above uses oxygen as the oxidant. Ozone and hydrogen peroxide in the atmosphere can also promote this process. Where oxygen is involved, the transformation is slow in the absence of catalysts such as iron or manganese. These metals may be present in the stone or deposited dust which can act as an important sink for pollutants, and reactions may continue to take place during much longer time periods than in the atmosphere (McAlister et al. 2008).

Damage to materials by pollutants can be described in terms of damage or dose response functions. A range of these are available and may have been done for limestone, particularly Portland limestone (Brimblecombe and Grossi 2009). A widely known example is the Lipfert function, which quantifies annual surface recession ( $-dx/dt$ ) as the sum of (i) the karst effect (ii) acid rain, and (iii) the dry deposition of pollutants:

$$-\frac{dx}{dt} = LvRn + 0.16H^+Rn + 0.18V_{ds}\text{SO}_{2(g)} + V_{dN}\text{HNO}_{3(g)} \quad (5.8)$$

where  $dx/dt$  is the rate of recession as  $\mu\text{m a}^{-1}$ ;  $Rn$  is rainfall as  $\text{m a}^{-1}$ ;  $V_{ds}$  and  $V_{dN}$  are deposition velocities taken as 0.38 and 0.32  $\text{cm s}^{-1}$  (Sabbioni 2003);  $\text{SO}_{2(g)}$  and  $\text{HNO}_{3(g)}$  are concentrations as  $\mu\text{g m}^{-3}$  and  $[\text{H}^+]$  is the concentration as  $\mu\text{mol l}^{-1}$ . The term  $Lv$  is the Lipfert value, which is typically set at 18.8  $\mu\text{m}$  (recession) per  $\text{m}^{-1}$  (precipitation). There are functions for Portland limestone from the International Cooperative Programs (ICP) and MULTI-ASSESS (Kucera 2005). The non-linear nature of these functions can be problematic when we extrapolate. The ICP damage function is (Kucera et al. 2007):

$$\Delta x(\mu\text{m}) = 2.7 \text{SO}_{2(g)}^{0.48} \exp(0.018T)t^{0.96} + 0.019 Rn[\text{H}^+]t^{0.96} \quad (5.9)$$

where  $T$  is temperature ( $^{\circ}\text{C}$ ). It should be noted that the amount of recession  $\Delta x$  varies with the length of exposure  $t$  in years (a). The MULTI-ASSESS function is:

$$\begin{aligned} \Delta x = & 3.1 + (0.85 + 0.0059\text{SO}_{2(g)}RH_{60} + 0.054 Rn[\text{H}^+] \\ & + 0.078 \text{HNO}_{3(g)}RH_{60} + 0.0258 \text{PM}_{10})t \end{aligned} \quad (5.10)$$

Note that this equation has a fixed value of 3.1  $\mu\text{m}$  independent of time, but the rest of the equation is linear with exposure. The novel symbols in this equation are  $RH_{60}$ , where  $RH_{60} = RH - 60$ , where  $RH > 60$  and zero elsewhere, and  $\text{PM}_{10}$  is the concentration of particulate matter less than 10  $\mu\text{m}$  in diameter expressed as  $\mu\text{g m}^{-3}$ .



Direct production of gypsum is also possible from the reaction of sulfuric acid produced in water layers on monuments or the arrival of acid rain at the surface:



The transformation of calcium carbonate minerals in the stone to gypsum causes some dramatic changes. Gypsum is more soluble than the carbonates, so, in rain-washed areas, it can be removed via dissolution. This often means facades appear white and black as the soot-laden gypsum crusts are removed. The pronounced rain streaking often leaves undesirable patterns over the building. Additionally gypsum has a much higher molecular volume than the carbonate mineral. This induces mechanical stresses in the stone, and the resultant expansion of the corroding black surface layers can be seen as an efflorescence that peels outward from damaged facades.

### 5.3.2 Nitrogen Oxides, Nitric Acid, and Ozone

The role of nitrogen oxides in the weathering of building stone is far less clear than that of sulfate. These oxides occur at concentrations in urban areas at 100 ppb or even 1000 ppb in very polluted areas. The oxidation of these oxides to nitric acid would seem an inevitable process likely to lead to stone damage. However, calcium nitrate is extremely soluble, so, when it forms on the surface of a building, it is soon removed by rainfall. This nitrate would be expected in the drainage waters rather than as the distinct crusts that characterize sulfur deposits on buildings.

Although a number of studies have examined the role played by the nitrogen oxides in damage to stone (Massey 1999), the situation remains complex. Although there is a lot of evidence that  $\text{NO}_x$  ( $\text{NO}_2 + \text{NO}$ ) is able to enhance the rate of oxidation of sulfite to sulfate, it is not clear how effective this is in comparison to other oxidants that are present in the modern urban atmosphere. In fact, it appears that  $\text{NO}_2$  is less efficient than ozone in oxidizing the sulfite on surfaces since it requires moisture to be present, while ozone will induce the transformation under dry conditions. There is a noticeable increase in the amount of deterioration when stone is exposed to a combination of  $\text{SO}_2$ ,  $\text{NO}_x$ , and  $\text{O}_3$ .

There is a direct impact of atmospheric nitrogen on stone when present as nitric acid. This acid is found at low concentrations (1 ppb) in urban areas and is formed via photochemical mechanisms (Cadle et al. 1982). Sikiotis and Kirkitsos (1995) found that stone is a better absorber of  $\text{HNO}_3$  than  $\text{NO}_2$ . Under the active photochemistry in Athens, they argue that nitric acid could play an important role in degradation of the Pentilic marble of the Acropolis. The surface density of nitrates in the Parthenon at the end of the dry season has been found to be  $6.9 \mu\text{g cm}^{-2}$ . However, this represents only nanometers of recession in the marble.

### 5.3.3 Particulate Material and Crusts

Fine particulate material deposited onto buildings affects their appearance. Fine particles, from a health perspective, are often thought to be less 2.5  $\mu\text{m}$  in diameter, but, in the case of building surfaces, it may be even larger in size and include most of the suspended matter, perhaps up to 10  $\mu\text{m}$ . Particulate materials remain a major issue in urban areas even today when coal smoke is no longer found. It is now diesel soot that proves to be a pernicious pollutant. Concern over the blackening process is a result of the perceptible damage to architecture value and its appreciation. Verhoef (1988) considered that soiling could reach a serious extent after 10 years and that an interested observer would notice the soiling patterns after a year or so.

Although many forms of equations have been used to describe the soiling process, data are often collected over a period that is too short to distinguish which is most appropriate. Longer data sets seem to confirm the usefulness of a properly bounded exponential function of the form (Brimblecombe and Grossi 2004)

$$R_t = (R_0 - R_\infty) \exp(-kt) + R_\infty \quad (5.12)$$

where  $R_t$ ,  $R_0$  are the reflectance at time  $t$  and the initial reflectance, while  $R_\infty$  (the final color of the surface). This equation has some physical justification and offers useful parameters, such as the rate parameter, which is likely to be a function of the concentration of depositing particles. Many authors reduce the equation to (Watt et al. 2008):

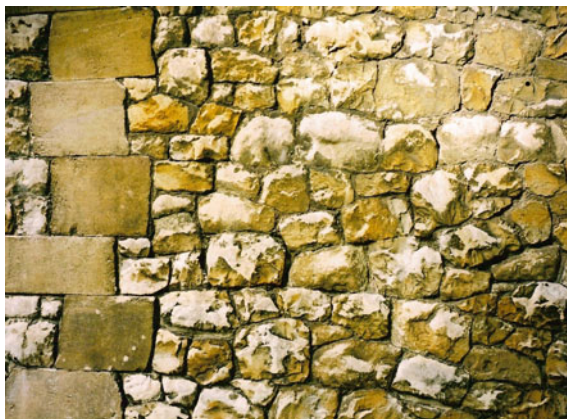
$$R_t = R_0 \cdot \exp(-kt) \quad (5.13)$$

which is valid if  $R_\infty$  is close to zero. However, this is not often true because blackened building surfaces still reflect as much as 30 %.

It is the elemental carbon (EC) or black carbon within particulate material that contributes most strongly to the blackening of urban facades. Depending on the source of the suspended particles in air, elemental carbon can range from a few percentage points to perhaps 50 % of the total mass. This can change dramatically over time in modern cities, because diesel and residential coal burning produce particles with a high proportion of elemental carbon, while emissions from furnaces running on pulverized coal can be less than a percent (Streets et al. 2001). Measurements of aerosol composition in central London at background sites since the late 1990s show particulate EC as about 2.6  $\mu\text{g m}^{-3}$ , and, at roadsides, quite naturally given the diesel source, it was higher—9.2  $\mu\text{g m}^{-3}$  (see Bonazza et al. 2007).

In the contemporary atmosphere, the elemental carbon is associated with a wide range of organic carbon. In London in the late 1990s, this amounted to 5.2–7.6  $\mu\text{g m}^{-3}$ , with an OC/EC from 2.0 to 2.9, but, again, it is usually higher at the roadside. High proportional amounts of OC derive from gasoline with smaller emissions from diesel, such that typical OC/EC ratios are 2.2 and 0.8 for light-duty gasoline and heavy-duty diesel vehicles, respectively. The OC contributions from wood, biomass, and some types of coal burning are often more significant than that of EC.

**Fig. 5.7** Yellow coloration of polluted stone surfaces at the Tower of London (photograph by Carlota Grossi)



So far, we have focused on the blackening of urban surfaces by soot. However, there is an increasing awareness, especially since buildings are cleaner, of a color change in stone surfaces. There is a range of potential sources of these color changes, which is typically reflected in warmer tones (Grossi et al. 2007a). These can arise through the oxidation of metals in the stone or cleaning processes. It is also possible for the deposited organic material to be oxidized in the modern urban atmosphere with secondary pollutants such as ozone. Gaviño et al. (2004) found both aliphatic and aromatic carboxylic acids and phenols in black crusts, and they are able to migrate and form a yellow layer at the crust/stone interface. These color changes are particularly evident at the Tower of London (Fig. 5.7), where yellowing may become of concern, especially as the central keep is called the White Tower (Grossi and Brimblecombe 2005).

The organic materials likely to cause color changes are high-weight substances, but they are accompanied by low molecular weight compounds such as oxalic acid. This is found in particles in urban air, where it forms as an oxidation product of hydrocarbons in photochemically active atmospheres. It is accompanied by smaller, higher molecular weight dicarboxylic acids (e.g. malonic and succinic acid). Calcium oxalate is not very soluble, so it is a frequent component of the building crusts where it is present as the minerals whewellite and wheddelite (Sabbioni 2003). However, it is likely that the atmosphere is not the dominant source, since oxalic acid is also produced from biological activity on the stone surface. There are simple carboxylic acids, such as formic and acetic acid, in contemporary polluted urban air (e.g. formate 7.3 ppb and acetate 3.9 ppb in Yokohama). The calcium salts of these acids are soluble and typically more mobile in crusts (Bonazza et al. 2007).

White crusts are also known. While, typically, the white areas of stone facades arise from the area washed clean by rain, it is possible for white deposits to form. These can derive from materials applied to buildings, which can ultimately appear as carbonate-rich white streaks (Alves 2010).

Coarse materials can also be found in the crusts deposited on buildings along with traces of treatments that reveal their presence in the layers within the crust (Sgobbi et al. 2010). The coarse fragments in these layers contain small pieces of wind-blown sand and dust that become cemented to the surfaces. The dust particles deliver a range of calcium and transition metals to facades (McAlister et al. 2008; Sulaiman et al. 2009).

## 5.4 Long-term Change

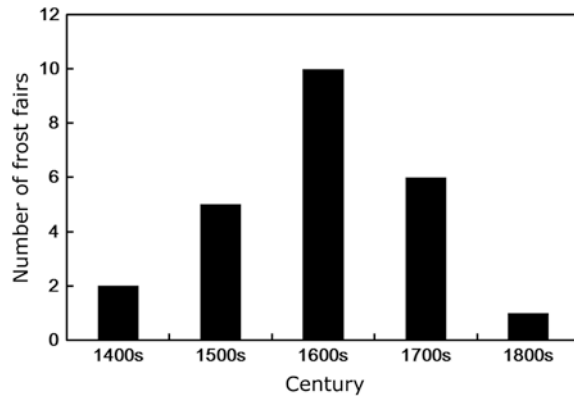
### 5.4.1 *Historic Changes in Pressures on Architectural Stone*

The changing environments of cities and the buildings from which they are formed have made themselves evident. Ruins of cities now appear in the desert, and once-thriving ports seem kilometers inland. It is hardly surprising that the weather to which great buildings are exposed can change significantly over their lifetime. Best known, perhaps, is the changing climate of the Sahara, which has alternated between wet and dry over time. This is often described by stories of Egypt, renown as the production center for wheat in Roman times. Pliny the Younger suggested that Rome could not survive without Egyptian wheat.

The changing climate of Europe has exhibited some key patterns over the last millennium. The climatologist Hubert Lamb promoted the notion of a Little Ice Age in Europe in the middle of the second millennium and the possibility of an early Medieval Warm Period (Lamb 1997). Although these generalizations are doubtful on a global basis, there remains some evidence of these cooler and warmer periods in the climate of northwestern Europe. Camuffo (1987) has examined changes in the Mediterranean region using records of freezing in the Venetian Lagoon since the 9th century AD. This suggests that the Little Ice Age was broken by a milder interval in the Mediterranean. In England, the years when the River Thames froze in London are also taken as an indicator of low temperatures (Fig. 5.8), although other factors such as a slower-flowing and broader river could be important. It may well be that frost shattering was a more important process in the weathering of building stones in the past, especially as the impact of air pollutants was much lower in the Middle Ages. Records of daily temperatures available for central England from the 1700s suggest that the number of freeze-thaw events has decreased substantially (Brimblecombe and Camuffo 2003; Grossi et al. 2007b). There may have been more storms in the Little Ice Age which could have driven rain onto buildings, and, where storms were especially intense, sea salt incorporated into the rain was driven far inland.

As we have seen, there were no doubt changes in Europe other than temperature over the last millennium. Some important parameters for building materials, such as relative humidity, are more difficult to derive from non-instrumental observations in old diaries and other documents (Brimblecombe 2003). There is also a

**Fig. 5.8** Frequency of frost fairs held on the river Thames in London



lengthy instrumental record that can span a number of centuries at a limited number of locations. The problem with these records is that they are often difficult to calibrate.

Since most buildings are in cities, it is important to consider that cities create their own climates as they become more populous. Urban climates are a few degrees hotter than those of the surrounding countryside because of the way the urban fabric intercepts incoming solar radiation. Heat generation within cities can also contribute, most importantly, in winter. The paved surfaces of cities mean less evaporation, so the climate can be drier. Wind and rainfall patterns can also be altered by densely built areas (Oke 1988).

### 5.4.2 Future Climate Impacts

Some changes in climate can be subtle or merely cyclic. In recent decades, climate change has largely been interpreted as being the result of greenhouse warming induced by increasing concentrations of radiatively active gases, such as carbon dioxide, methane, etc. The consequences of rising temperatures and changing precipitation for the future are unpalatable and these have triggered a public debate that has been more charged than is typical of many scientific forecasts.

The “IPCC Fourth Assessment Report: Climate Change 2007” (AR4) suggested that, over the next two decades, global temperatures would increase by about 0.2 °C per decade independent of the emission scenarios chosen. Best estimates for the temperature increases by the final decade of the 21st century compared with the period 1980–1999 are 1.8–4.0 °C, dependent on the scenarios chosen. Regionally, these increases in temperature may differ significantly, with some of the largest predicted increases for northern latitudes. Precipitation is typically predicted to increase in tropical high-rainfall areas, with general decreases in the subtropics. Rainfall may, nevertheless, be more intense, even

where total annual amounts decline. This has meant that some historical buildings have been renovated to increase the capacity of drain pipes and guttering.

The IPCC reports do not consider impact on building materials and cultural heritage, although, within Europe, the European Commission has funded research on this topic. Initial summary maps have appeared in “The Atlas of Climate Change Impact on European Cultural Heritage” (Sabbioni et al. 2010).

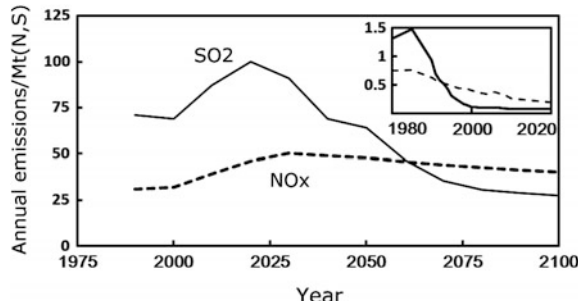
The increases in temperature are just a few degrees in Europe, and, although it might be important for human comfort, this would not, in itself, lead to a significant change in the rate of deterioration of materials. However, as noted earlier, there are mechanisms that enhance the impact of small temperature increases. Some metal corrosion decreases at temperatures above 9–11 °C as surfaces remain drier. In the case of porous stone, the number of freeze–thaw cycles should continue to decrease in all but the coldest polar and mountain areas of Europe. This should further reduce the incidence frost shattering.

The seasonal patterns of relative humidity are likely to change across much of Europe where the climate is currently fully humid with warm to hot summers (Köppen-Geiger type Cfab). The climate may often be drier, which means that many materials would see a decrease in deterioration rate, as moisture so often serves to increase the rate of material damage. However, stone is especially vulnerable to damage from hygroscopic salts. This occurs when the humidity oscillates between high and low values and causes crystals to form from brines in pores. The frequency of such phase changes could increase in the future along with changes in the seasonality of salt weathering they induce (Benavente et al. 2008). This may be pronounced in the areas of Europe with Cfab climate, and it is relevant that this region is rich in highly detailed Gothic architecture. This is usually carved from porous stone and vulnerable to attack from salt weathering.

Change of precipitation can alter the rate of damage by wet deposition and the dissolution of surface layers. Bonazza et al. (2009a) have modeled the impact of climate change on the surface recession of carbonate building stone in Europe for the 21st century. They have used the Lipfert function, which gives weathering by rainwater a major role. However, the changes in rainfall amounts have only a slight effect on altering recession rates, although recession is enhanced by a decrease in the proportion of precipitation arriving as snow. Most of the increase in rates of recession in the future seems to arise through enhanced CO<sub>2</sub> concentrations that make rainwater better at dissolving calcium carbonate. Much of the enhanced surface recession by the end of the 21st century will occur in northern Russia, where recession has typically been low. In the fully humid warmer parts of Europe (Köppen-Geiger type Cfab), recession remains at 20 μm a<sup>-1</sup> with little change from contemporary values.

It is not very easy to be certain of future changes in wind speed and direction because wind varies over spatial scales that are smaller than those of climate prediction models. Change in the wind velocity can alter the eddies around historical buildings, affecting the deposition rates of gases and particles to surfaces, change the strength of driving rain, and redistribute soot over building facades such that rain streaking makes them less appealing (Grossi and Brimblecombe 2004).

**Fig. 5.9** Global emissions of  $\text{SO}_2$  and  $\text{NO}_x$  taken from the A1 scenario of emissions (SRES) and assembled for the IPCC third assessment report. The inset shows the emissions for the former German Democratic Republic as used in EMEP Models from the CEIP database



Biodeterioration is an important mode of attack on stone (see Sect. 4.5). Climate has the potential to alter the types of organisms found on stone and the potential damage they cause.

### 5.4.3 Future Changes in Air Pollution

Models for future climate are well developed. These models rely on a range of inputs that include greenhouse gas emission scenarios, which are later coupled into global climate predictions. This means that the input contains estimates of the likely change in pollutant emissions. However, the emission scenarios are based on likely future pathways for human development through to the end of the 21st century.

Offering such a range of scenarios is seen as a sensible approach, although deciding which we are likely to follow over the next 90 years is far from easy. Even if we accept a given scenario, there are still difficulties about the estimates of pollutant emissions at a local level, as these could readily be affected by national or regional air pollution control policies. Furthermore, a number of pollutant gases, ozone being the striking example, are produced by reactions in the atmosphere, so it is necessary to consider the impact of a changing atmospheric chemistry.

The increasing concentrations of carbon dioxide are best understood, and this increase will enhance the ability of rainwater to dissolve carbonate stone. This could mean dissolution will increase, perhaps as much as 30 % over the natural rate from the Karst effect. However, this is likely to be overwhelmed by the decrease in attack by the pollutant sulfur dioxide. Globally, sulfur dioxide emissions are predicted to decline in the latter half of the 21st century (Fig. 5.9). In Europe, they have been in decline for a number of decades (e.g. Fig. 5.9 inset), and, in urban areas, the concentrations are often an order of magnitude or more lower than in the past. This is largely due to changes in fuel use in cities. There are also declines in emissions from large plants in the countryside, where flue gas desulfurization in the case of coal-burning power plants also has an effect. It seems likely that legislative pressures will keep future urban  $\text{SO}_2$  concentrations at low levels. This is important for architectural stone, which has been so damaged by this pollutant in the past.



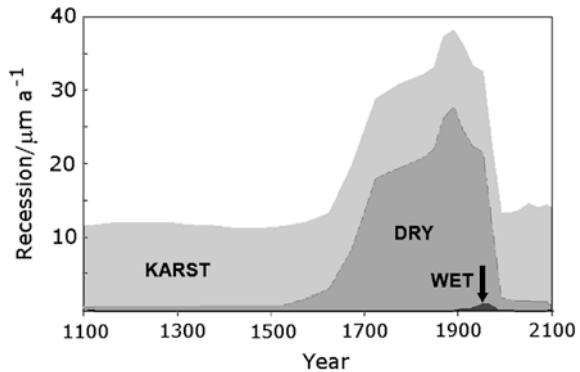
The changes in nitrogen dioxide concentrations in urban air have not been as dramatic as for sulfur dioxide. This is partly due to the increased use of gas and oil as energy sources in cities. Even though there is a strong desire to decrease the emission of the nitrogen oxides (e.g. Fig. 5.9), this does not always mean that the nitrogen dioxide level declines, because its concentration is sensitive to the amount of oxidant in the air. Significant reductions in total nitrogen oxide emissions sometimes lead to only modest improvements in nitrogen dioxide.

The situation is even more uncertain in the case of future levels of ozone. There is a wide variation in predictions of future ozone concentrations in Europe and North America. These vary from predictions of an increase through to a decrease. This means it is important to explore the reasoning behind these diverse opinions. Some models allow climate to change, but assume emissions to remain at current levels (Meleux et al. 2007). This is a legitimate exercise as it isolates the impact of climate change, but it will not give a realistic prediction in a changing world. The emissions of some pollutants that are tightly regulated will continue to decrease, but some predictions argue that increased numbers of emission sources, such as increased automobile numbers, will overwhelm improvements derived from new engine technology and catalytic converters. Even with such improvements, it is likely that higher temperatures in the future could lead to more evaporated fuel and biological volatiles, so warmer climates will mean more ozone precursors. Future climates may be more stagnant and low wind-speeds could lead to the accumulation of pollutants. To counterbalance these possibilities, higher temperatures also reduce particle concentrations by preventing the condensation of “semi-volatile” compounds (ammonium nitrate and some organic materials), while more frequent summer rains in some areas can reduce pollutant concentrations.

This complex situation for ozone might not be critical for stone decay, as it is only an indirect contributor to acids that induce stone decay. However, as the rate of decay by traditional aggressive pollutants such as sulfur dioxide decline, the effect of ozone and nitrogen oxides on the remaining amount of sulfur dioxide may have a proportionally stronger role to play. The major problem with regard to buildings is that they are mostly found in cities, and much of the modeling work on future air pollution represents regional pollutant concentrations under changed climates. Changing wind speeds, rainfall amounts, irradiation, and temperature are all factors that need to be considered, although it is likely that administrative pressures will limit emissions in cities. Thus, these are likely to have the greatest impact on future concentrations; certainly that is the hope of regulators.

It is also important to consider not only quantitative issues here and to account for qualitative changes that surround pollutant emissions. This is especially true in the case of particles. It may well be that changes in color, stickiness, or composition will be especially relevant to future damage to architectural stone. It is already evident that the black crusts found on urban facades are very different from those that characterized the days when coal smoke was the dominant pollutant in urban air. These modern crusts are often rich in organic materials, not so coarse, and thinner than those of the past.

**Fig. 5.10** Long-term changes in recession rates in London from various processes estimated using the Lipfert function (details in Brimblecombe and Grossi 2009)



#### 5.4.4 Future Environment and Architectural Stone

Stone has remained a major building material for many thousands of years. Although modern architects have a wide variety of building materials to choose from, stone remains a durable and attractive material that represents a good choice for public buildings. Although stone has suffered greatly from the impacts of air pollutants over the past few centuries, this was to a large extent the result of burning coal. In London, the changes have been especially dramatic (Fig 5.10). It is difficult to tell if these trends, typical of many European cities, will continue into the future, but these inverted U type patterns of change, often called in environmental economics “Kuznets curves”, are not uncommon. They can be typical of pollutants which are generated locally and have clear local impacts (Brimblecombe and Grossi 2009).

The economic argument, in terms of environment, is that industrialization initially occurs with little concern for environmental quality, but society eventually reaches a point where environment can no longer be sacrificed. There are no a priori reasons why air quality should follow the Kuznets relationship, but the patterns lend support to the way pollution problems come and go, often being replaced by newer problems over time. It appears that we are unlikely to see a return high levels of aggressive pollutants and so reduced stone decay is a likely consequence of regulatory control.

We will probably enter a period when climate will change more in a century than it has in a millennium. This makes it likely that climate will become a more important factor in the weathering of stone. Although facades could well be cleaner, architectural surfaces could change more rapidly via new weathering and soiling patterns along with different forms of biological growth and color, providing us with new problems. Those interested in the conservation of our heritage built from stone will face novel challenges.

## References

- Alves C (2010) White crusts on recent buildings. *Mater Sci Forum* 636–637:1300–1305
- Benavente D, Brimblecombe P, Grossi CM (2008) Salt weathering and climate change: In: Colombini MP, Tassi L (eds) *Trends in analytical, environmental and cultural heritage chemistry*. TSN, Trivandrum
- Blocken B, Carmeliet J (2004) A review of wind-driven rain research in building science. *J Wind Eng Ind Aerod* 92:1079–1130
- Blocken B, Dezsö G, van Beeck J, Carmeliet J (2010) Comparison of calculation models for wind-driven rain deposition on building facades. *Atmosph Environ* 44:1714–1725
- Bonazza A, Brimblecombe P, Grossi CM, Sabbioni C (2007) Carbon in black layers at the tower of London. *Environ Sci Tech* 41:4199–4204
- Bonazza A, Brimblecombe P, Grossi CM, Messina P, Sabbioni C (2009a) Mapping the impact of climate change on surface recession of carbonate buildings in Europe. *Sci Total Environ* 407:2039–2050
- Bonazza A, Sabbioni C, Messina P, Guaraldi C, De Nuntiis P (2009b) Climate change impact: mapping thermal stress on carrara marble in Europe. *Sci Total Environ* 407(15):4506–4512
- Bowler C, Brimblecombe P (1990) The difficulties of abating smoke in late Victorian York. *Atmos Environ* 24B:49–55
- Brimblecombe P (1978) Interest in air pollution among early members of the royal society. *Notes Rec R Soc Lond* 32:123–129
- Brimblecombe P, Bowler C, Doktor P (1992) Air pollution and the cost of repairs to English cathedrals since 1700. *Patrimonio Historico artistico y Contaminacion*. Consorcio para la Organizacion de Madrid Capital Europea de la Cultura, Madrid
- Brimblecombe P (1996) *Air composition and chemistry*, Cambridge University Press, Cambridge
- Brimblecombe P (1987) *The big smoke*. Methuen, London
- Brimblecombe P (2003) Documentary records. In: Mackay A, Battarbee R, Birks J, Oldfield F (eds) *Global change in the Holocene*. Arnold, London
- Brimblecombe P (2010a) Heritage climatology. In: Lefevre RA, Sabbioni C (eds) *Climate change and cultural heritage*. Edipuglia, Bari—Italy
- Brimblecombe P (2010b) Mapping heritage climatologies In: Bunnik T, de Clercq H, van Hees R, Schellen H, Schueremans L (eds) *Effect of climate change on built heritage*. WTA-Publications, Pfaffenhofen, 34, pp 18–30
- Brimblecombe P, Camuffo D (2003) Long term damage to the built environment. In: Brimblecombe P (ed) *The effects of air pollution on the built environment*. Imperial College Press, London, pp 1–30
- Brimblecombe P, Grossi CM (2004) The rate of darkening of material surfaces. In: Saiz-Jimenez C (ed) *Air pollution and cultural heritage*. A. A. Balkema, Rotterdam, pp 193–198
- Brimblecombe P, Grossi CM (2005) Aesthetic thresholds and blackening of stone buildings. *Sci Total Environ* 349:175–189
- Brimblecombe P, Grossi CM, Harris I (2006) Climate change critical to cultural heritage. In: Fort R, Alvarez de Buergo, M, Gomez-Heras M, Vazquez-Calvo C (eds) *Heritage, weathering and conservation*. Taylor and Francis, London. pp 387–393
- Brimblecombe P, Grossi CM (2009) Millennium-long damage to building materials in London. *Sci Total Environ* 407:1354–1361
- Brischke C, Rapp AO, Bayerbach R, Morsing N, Fynholm P, Welzbacher CR (2008) Monitoring the material climate of wood to predict the potential for decay: results from in situ measurements on buildings. *Build Environ* 43:1575–1582
- Cadle SH, Countess RJ, Kelly NA (1982) Nitric acid and ammonia in urban and rural locations. *Atmos Environ* 16:2501–2506
- Camuffo D, Del Monte M, Sabbioni C, Vittori O (1982) Wetting, deterioration and visual features of stone surfaces in an urban area. *Atmos Environ* 16:2253–2259

- Camuffo D (1987) Freezing of the Venetian lagoon since the 9th century A.D. in comparison to the climate of western Europe and England. *Clim Change* 10:43–66
- Davidson CI, Tang W, Finger S, Etyemezian V, Striegel MF, Sherwood SI (2000) Soiling patterns on a tall limestone building: changes over 60 years. *Environ Sci Technol* 34(4):560–565
- Drake F (1736) *Eboracium*. London
- Gaviño M, Hermosin B, Vergès-Belmin V, Nowik W, Saiz-Jimenez C (2004) Composition of the black crusts from the saint Denis Basilica, France, as revealed by gas chromatography-mass spectrometry. *J Sep Sci* 27:513–523
- Gobbi G, Zappia G, Sabbioni C (1998) Sulphite quantification on damaged stones and mortars. *Atmos Environ* 32:783–789
- Grossi CM, Brimblecombe P (2004) Aesthetics of simulated soiling patterns on architecture. *Environ Sci Technol* 38:3971–3976
- Grossi CM, Brimblecombe P, Harris I (2007a) Climate change and frost impact on the built heritage. *Sci Total Environ* 377:273–281
- Grossi CM, Brimblecombe P (2005) The white tower and the perception of blackening. *J Archit Conserv* 1:34–44
- Grossi CM, Brimblecombe P, Esbert RM, Alonso FJ (2007b) Color changes in architectural limestones from pollution and cleaning. *Color Res Appl* 32:320–331
- Grossi CM, Brimblecombe P et al (2011) Climatology of salt damage on stone buildings (submitted *Science of Total Environment*)
- Hall K, André M-F (2003) Rock thermal data at the grain scale: applicability to granular disintegration in cold environments. *Earth Surf Proc Land* 28(8):823–836
- Hawksmoor N (1934) Letters to the dean. *Wren Soc* 11:32–34
- Hussein AS, El-Shishiny H (2009) Wind flow modeling and simulation over the Giza plateau cultural heritage site in Egypt. *J Comput Cult Heritage* 2(6):1–22
- Keepe H (1682) *Monumenta Westmonasteriensa*, London
- Kottek M, Grieser J, Beck C, Rudolf B, Rubel F (2006) World map of the köppen-geiger climate classification updated. *Meteorol Z* 15:259–263
- Krier JE, Ursin E (1977) *Pollution and policy*. University of California Press, Berkeley
- Kucera V (2005) Model for multipollutant impact and assessment of threshold levels for cultural heritage. Swedish corrosion Institute, Stockholm
- Kucera V, Tidblad J, Kreislova K, Knotkova D, Faller M, Reiss D, Sneath R, Yates T, Henriksen J, Schreiner M, Melcher M, Ferm M, Lefevre R-A, Kobus J (2007) UN/ECE ICP materials dose-response functions for the multi-pollutant situation. *Water Air Soil Pollut Focus* 7:249–258
- Lamb H (1997) *Through all the changing scenes of life—a Meteorologist's tale*. Taverne Publications, East Harling
- Lamschus C (1993) Die Holzversorgung der luneburger saline. In *mittelalter und frer neuzeit*. In: Urbanski S, Lamschus C, Ellermeyer J (eds) *Recht und alltag im hanseraum*. Frederkreis Industriedenkmal Saline, Luneburg, pp 321–333
- Lipfert FW (1989) Atmospheric damage to calcareous stones: comparison and reconciliation of recent experimental findings. *Atmos Environ* 23:415–429
- Massey SW (1999) The effects of ozone and NO(x) on the deterioration of calcareous stone. *Sci Total Environ* 227:109–121
- Matsuoka N (2008) Frost weathering and rock wall erosion in the southeastern Swiss Alps: long-term (1994–2006) observations. *Geomorphology* 99:353–368
- McAlister MM, Smith BJ, Torok A (2008) Transition metals and water soluble ions on a building and their potential catalysis of stone decay. *Atmos Environ* 42:7657–7668
- Meleux F, Solmon F, Giorgi F (2007) Increase in summer European ozone amounts due to climate change. *Atmos Environ* 41:7577–7587
- Oke TR (1988) *Boundary layer climates*. Routledge, London
- Sabbioni C (2003) Mechanisms of air pollution damage to stone. In: Brimblecombe P (ed) *The effects of air pollution on the built environment*. Imperial College Press, London, pp 63–106

- Sabbioni C, Brimblecombe P, Cassar M (eds) (2010) The atlas of climate change impact on European cultural heritage. Anthem Press, London
- Schaffer RJ (1932) The natural weathering of building stones. Building research special report No. 18. HMSO, London
- Sgobbi M, Brimblecombe P, Grossi C, Biscontin G, Zendri E (2010) Surface stratigraphy on limestone of Venetian palaces. *J Arch Conserv* 16:52–70
- Sikiotis D, Kirkitsos P (1995) The adverse effects of nitrates on stone monuments. *Sci Total Environ* 171:173–182
- Streets DG, Gupta S, Waldhoff ST, Wang MQ, Bond TC, Yiyun B (2001) Black carbon emissions in China. *Atmos Environ* 35:4281–4296
- Sulaiman FR, Brimblecombe P, Grossi CM (2009) Mobilization and loss of elements from roofing tiles. *Environ Geol* 58:795–801
- Tang W, Davidson CI, Finger S, Vance K (2004) Erosion of limestone building surfaces caused by wind-driven rain: 1. Field measurements. *Atmos Environ* 38:5589–5599
- Tang W, Davidson CI (2004) Erosion of limestone building surfaces caused by wind-driven rain: 2. Numerical modeling. *Atmos Environ* 38:5601–5609
- Trenhaile AS (2001) Twenty-year weathering re-measurements at St Paul's cathedral, London. *Earth Surf Proc Land* 26:1129–1142
- Verhoef LGW (1988) Soiling and cleaning of building facades. RILEM report. Chapman and Hall, New York
- Vleugels G, Dewolfs R, Van Grieken R (1993) On the memory effect of limestone for air pollution. *Atmos Environ* 27A:1931–1934
- Watt J, Jarrett D, Hamilton R (2008) Dose-response functions for the soiling of heritage materials due to air pollution exposure. *Sci Total Environ* 400:415–424
- Wren C (1713) Report on Westminster abbey to Francis atterburg, dean. In: Soo LM (ed) Wren's tracts on architecture and other writings (1998). Cambridge University Press, Cambridge. pp 79–92

# Chapter 6

## Characterization of Stone Deterioration on Buildings

Heiner Siedel and Siegfried Siegesmund

**Abstract** In this chapter the main methods applied to the characterization of stone deterioration on buildings and art objects are presented. The text begins with the classification of weathering forms. A short, illustrated glossary following the recent proposal of the ICOMOS (International Council on Monuments and Sites) is given, and the techniques and problems of mapping are discussed. On-site evaluation tests (non- and less-destructive) as well as laboratory investigations on material samples are explained. Their main goals, preconditions, side-effects and tools are demonstrated and illustrated with results from selected case studies. The focus is on routine methods such as moisture and salt analysis, and determination of mechanical, structural and hydric properties (drilling resistance, ultrasonic wave measurements, Karsten tube measurements etc.). Additional methods are briefly discussed and linked with the recent literature. A separate part is dedicated to classical biological methods of investigation as well as modern molecular techniques.

### 6.1 Introduction

Weathering and deterioration of rocks is a natural occurrence (Fig. 6.1). The description and explanation of weathering forms on bedrock and the driving forces behind them has been the subject of geosciences like geomorphology and physical

---

Sect. 6.4.4 by Katja Sterflinger

---

H. Siedel (✉)

Institut für Geotechnik, TU Dresden, George-Bähr-Str. 1, 01069 Dresden, Germany  
e-mail: Heiner.Siedel@tu-dresden.de

S. Siegesmund

Geoscience Centre, University of Göttingen, Goldschmidtstrasse 3, 37077 Göttingen, Germany  
e-mail: ssieges@gwdg.de

**Fig. 6.1** The creation of cone karst formations is an extensive phenomenon in warm and humid regions, e.g. Thailand, where they essentially define much of the landscape



geography for many years (Robinson and Williams 1994; Turkington and Paradise 2005). Some peculiar weathering forms have especially attracted the interest of science, e.g. tafoni on granite (Migon 2006), alveolar or honeycomb weathering on different rock types (e.g. Mustoe 1982; Siedel 2010, and many others; Fig. 6.2), earth pillars (Poesen et al. 1994, Fig. 6.3), or the formation of big arches in sandstone (Fig. 6.4, Cruikshank and Aydin 1994; Zvelebil et al. 2002).

The interest in natural weathering is mainly scientific, aiming at the general understanding of geological and geomorphological processes. Within the last several decades, however, weathering research has focused on building stones as well. The understanding of weathering processes, and of the contribution of various intrinsic and extrinsic factors to it, is a crucial precondition for both the choice of appropriate building stones and the conservation and restoration of deteriorated stone objects. Some lessons can be learned from natural weathering. As can be seen from Fig. 6.5, dense, highly cemented sandstone layers are obviously more resistant to weathering than porous, weak sandstone strata.

To face the problems arising with the practical application of scientific knowledge about rock weathering in the field of stone construction and restoration of buildings, however, weathering processes and their causes have to be elucidated in more detail. The scope often has to be modified from the macro to the micro scale and from description to quantification.



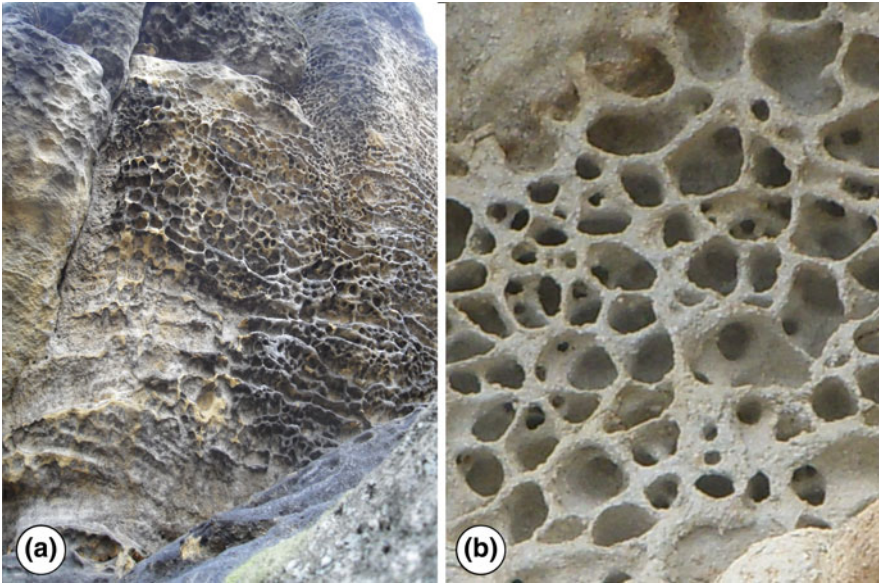


**Fig. 6.2** Alveolar weathering of sandstones in the **a** sandstone area south of Dresden (Germany), called Sächsische Schweiz. This feature is also well-known in **b** igneous rocks for example from the Elba Island (Italy)

**Fig. 6.3** Earth pyramids near Bozen represent an interesting erosional form, which formed by differential weathering (Figure by B. Lammerer)



Bedrock and building facades generally undergo the same natural processes as freeze–thaw, moistening–drying, warming up–cooling, etc. There are some additional factors, however, that might modify “natural” weathering on buildings. Many buildings have been exposed to aggressive environmental conditions in the urban atmosphere (Fig. 6.6) for decades and even centuries (Klemm and Siedel 2002; Hüpers et al. 2005; Török et al. 2007; Siegesmund et al. 2007). Constructions are “mixtures” of different materials like stone, joint mortar, plaster, paint etc. (Wedekind et al. 2013).

Building stones may therefore chemically and physically interact with other construction materials. Since most historical buildings are still being used,



**Fig. 6.4** Landscape arch is a bridge-like rock formation with a span of 92 m in Arches National Park (U.S.A.)

**Fig. 6.5** The Devils Wall by Neinstedt consists of siliceous Cretaceous sandstone, which is visible over a large extent. In the immediate vicinity the non-siliceous equivalents are quarried as sand



the climate in the interior differs greatly from that of the exterior, thus causing heat and moisture movements through the building stones. Moreover, the shape and exposure of different construction elements on facades might cause specific moisture load and microclimatic situations.

Nowadays weathering research on building stones has become a special scientific field with its own methodology including measurements on facades and laboratory tests. There is some overlap with the classical testing of construction materials and with the methodology of mineralogy and petrography as well. In the last several years, a number of non-destructive geophysical methods of rock

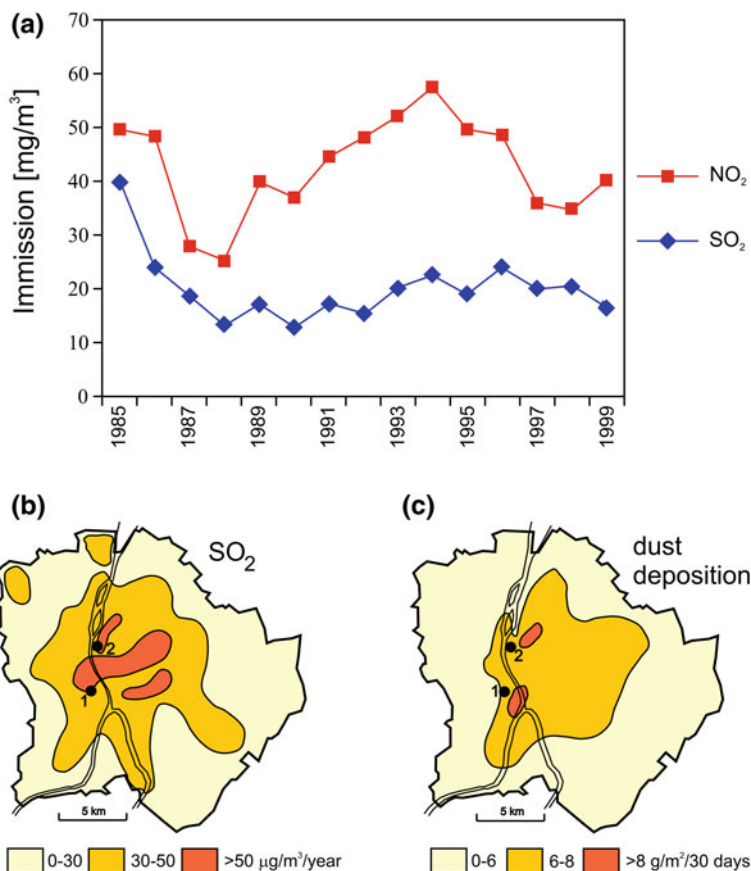


**Fig. 6.6** Environmental conditions: **a** development of the SO<sub>2</sub> and NO<sub>2</sub> immissions in Budapest from 1985 to 1999, **b** distribution diagram of the average SO<sub>2</sub> immissions and **c** dust immissions in Budapest from 1987 to 1990. The location of the Citadella fortress and the Parliament in Budapest are labeled with numbers (1, 2) (after Hüpers et al. 2005)

investigation have been tested with some success. Moreover, appropriate low-destructive techniques have been especially developed for weathering research on buildings.

In this chapter, the main methods applied to the characterization of stone deterioration on buildings and art objects shall be presented. Some of them have been used as routine methods for many years, whereas others have only recently been developed but seem to be promising, even though more experience still has to be collected. There are some other methods that will not be presented here or only shortly mentioned in the text because they require very expensive, sophisticated special equipment and are only applicable in a few certain cases. Technical aspects of routine methods from other disciplines like building climatics (measurements of climate) or environmental monitoring (immission measurements) are not discussed

in detail, although such measurements may provide valuable information in some cases. The methods presented here can be used in practical, routine deterioration diagnostics as well as in weathering research.

## 6.2 Classification of Weathering Forms

Different weathering forms are a result of environmental interaction on dissimilar stone structures (each one determined by its geological origin). The changes on the rock surface produced by weathering processes can be described with the aid of specific terminology utilizing morphological and geometrical criteria.

Various systems were established in the past (e.g. Arnold et al. 1979; Grimmer 1984; Beeger 1988; Raccomandazione Normal 1990; Fitzner et al. 1995), and a lot of problems have arisen with the use of these different terms. Some of the terms used had already been created in the first half of the 20th century (Hirschwald 1908, Kieslinger 1932, De Quervain 1945).

The classification scheme after Fitzner et al. (1995) created a clear characterization of damage phenomena and developed criteria for describing the phenomena. They developed a system of four basic groups of weathering forms: group 1—loss of stone material, group 2—discoloration/deposits, group 3—detachment, and group 4—fissures/deformation. In the second classification layer 25 main weathering forms can be differentiated, whereas in the third layer 75 individual weathering forms can be ascertained. Fitzner and Heinrichs (2001) introduced a more updated version, a fourth layer (see e.g. [www.stone.rwth-aachen.de](http://www.stone.rwth-aachen.de)), which contains a further differentiation of the individual weathering forms based on suitable intensity criteria. Such parameters could be the depth of back-weathering, the volume of a breakout, and the thickness of a contour scaling as well as the length or opening width of cracks (fissures).

Many terminologies can be a source of misunderstanding. To overcome these problems and to harmonize all the existing classification approaches, the ICOMOS International Scientific Committee for Stone (ISCS) has recently constructed a website, that includes an illustrated glossary on stone deterioration ([http://www.international.icomos.org/publications/monuments\\_and\\_sites/15/pdf/Monuments\\_and\\_Sites\\_15\\_ISCS\\_Glossary\\_Stone.pdf](http://www.international.icomos.org/publications/monuments_and_sites/15/pdf/Monuments_and_Sites_15_ISCS_Glossary_Stone.pdf)).

The committee has already screened seven existing glossaries or classification systems, gathering terms and definitions in English and French (printed version: ICOMOS-ISCS 2008), and re-defining some of them more clearly. A German version was released in 2010; Spanish, Czech, Japanese and Korean versions are also available, and further translations shall follow. The work of these 36 international experts from 19 different countries provides a good, scientifically based classification system for use in cataloguing weathering forms. Although discussions about single terms and details will undoubtedly continue, the further growth in knowledge concerning weathering processes will lead to modifications in the future. Thus, the ISCS Glossary can be recommended as the latest national and



**Table 6.1** Survey of terms used for characterization of stone deterioration (according to ICOS-MOS-ISCS 2008)

Alteration—damage—decay—degradation—deterioration—weathering				
Crack and deformation	Detachment	Features induced by material loss	Discoloration and deposit	Biological colonization
Crack (Fracture; star crack; hair crack; craquelé; splitting)	Blistering	Alveolization	Crust (Black crust; salt crust)	Lichen
	Bursting	(Coving)		Moss
Deformation	Delamination	Erosion	Deposit	Mold
	Disintegration	(Differential erosion; loss of components or of matrix; rounding; roughening)	Discoloration (Coloration, bleaching, moist area; staining)	Plants
	(Crumbling; granular disintegration like powdering, chalking, sanding, sugaring)	Mechanical damage (Impact damage; cut; scratch; abrasion; keying)	Efflorescence	
	Fragmentation (Splintering; chipping)		Encrustation film	
	Peeling	Microkarst	Glossy aspect	
Scaling (Flaking; contour scaling)	Missing part (Gap) Perforation pitting	Graffiti Patina Soiling Subflorescence		
See Fig. 6.7	See Figs. 6.8 and 6.9	See Figs. 6.10 and 6.11	See Figs. 6.12 and 6.13	See Fig. 6.14

international standard system for use in science and applied practice. The use of specific terms in science, planning, and restoration work will simplify cooperation and scientific understanding. Therefore, the terms presented in the following text refer to the system and definitions used in the ISCS glossary (Table 6.1).

The glossary is arranged into six categories: general terms, crack and deformation, detachment, features induced by material loss, discoloration and deposit, and biological colonization. The general terms include a definition of alteration, damage, decay, degradation, deterioration, and weathering. In many cases, deterioration is also referred to as “decay” or “degradation” and sometimes even as weathering or alteration (see discussion in Charola 2004). Part of the reason for the richness in the use of various terms originates from the different disciplines that first coined those terms. Weathering is defined as a natural process in the decay of rocks, while alteration has different connotations for geologists and for other scientists.

Decay and degradation can be considered as two more general terms equivalent to deterioration. However, the definition given by the new glossary is still a matter of discussion. Decay is defined as “any chemical or physical modification of the intrinsic stone properties leading to a loss of value or to the impairment of use”, while weathering is used as “any chemical or mechanical process by which stone exposed to the weather undergoes changes in character and deteriorates.”

The other five categories are comparable with the groups defined by Fitzner and Heinrichs (2001) except for biological colonization. For a further explanation, the reader should refer to Table 6.1 and to Figs. 6.7, 6.8, 6.9, 6.10, 6.11, 6.12, 6.13, and 6.14. Category two comprises “cracks and deformation”. Cracks are defined as individual fissures, clearly visible to the naked eye, resulting from the separation of one part from another (Fig. 6.7). They can cause detachment patterns, like bursting or fragmentation (see below). This category is subdivided into fractures, star cracks, hair cracks, craquelé, and splitting, while “deformation” refers to a change in shape without loss of integrity, leading to the bending, buckling or twisting of a stone. In the latter case deformation mainly affects crystalline marble slabs (e.g. tombstones or marble cladding). Grimm (1999) and Siegesmund et al. (2008a, b) reported that slabs made from granite, Nagelfluh (a conglomerate), or limestones may also show a bending.

The category “detachment” (Figs. 6.8 and 6.9) includes all weathering forms showing disintegration of stone structures at the macroscopic and microscopic scale, such as blistering, bursting, delamination (exfoliation), disintegration (crumbling, granular disintegration), fragmentation (splintering, chipping), peeling, and scaling (flaking or contour scaling). When referring to granular disintegration, three individual weathering forms can be distinguished, i.e. powdering (chalking), sanding, and sugaring, which are related to the grain size of the stones. Granular disintegration into sand or detritus show transitional forms both to flaking and to crumbling (Fitzner et al. 1995). Crumbling and splintering as a detachment of larger compact stone elements are not further subdivided.

Features induced by “material loss” include all forms describing a loss of stone material (Figs. 6.10 and 6.11). These are subdivided into alveolization (coving), erosion (differential erosion and loss of components, loss of matrix, rounding, and roughening), mechanical damage (impact damage, cut, scratch, abrasion, keying), microkarst, missing part (gap), perforation, and pitting.

The category “discoloration and deposit” includes all forms characterizing a modification of stone color and deposit on the stone surface or near the stone surface (Figs. 6.12 and 6.13). These include crusts (black crust, salt crust), deposit, discoloration (coloration, bleaching, moist area, staining), efflorescence, encrustation (concretion), film, glossy aspect, graffiti, patina (iron-rich, oxalate patina), soiling, and subfluorescence (e.g. Török et al. 2011, Graue et al. 2013).

“Biological colonization” refers to a colonization of the stone by plants and micro-organisms such as bacteria, cyanobacteria, algae, fungi, and lichen (Fig. 6.14). Biological colonization also includes influences by other organisms such as animals nesting on and in stone (see Sect. 4.3).

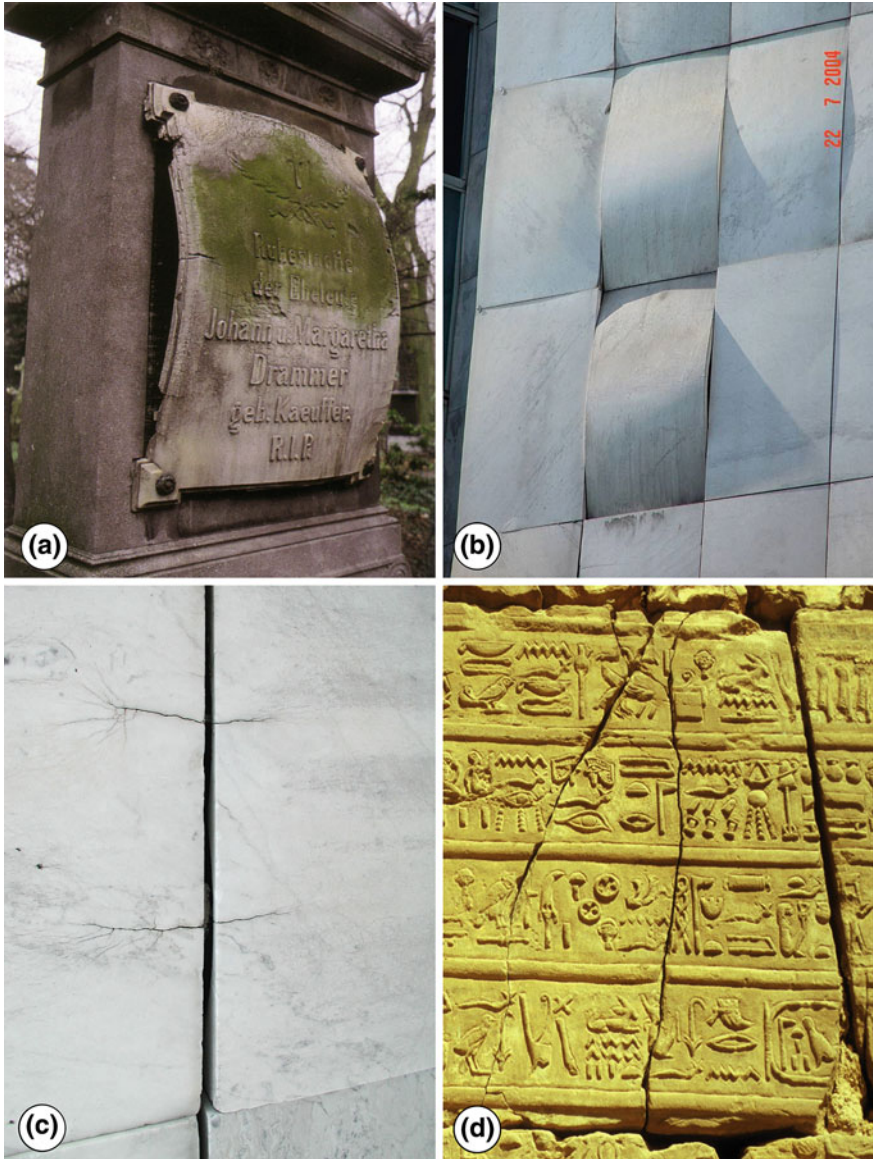


**Fig. 6.7** Crack and deformation: **a** marble bowing (gravestone at the Old Cemetery in Bonn, Germany), **b** marble bowing (facade in Zagreb, Croatia) (Figure by the TEAM-Project taken by J. Brundin), **c** crack due to iron corrosion (marble, Lower Saxony State and University Library, Göttingen, Germany), and **d** crack (sandstone, Karnak Temple, Luxor, Egypt) (Figure by B. Fitzner)



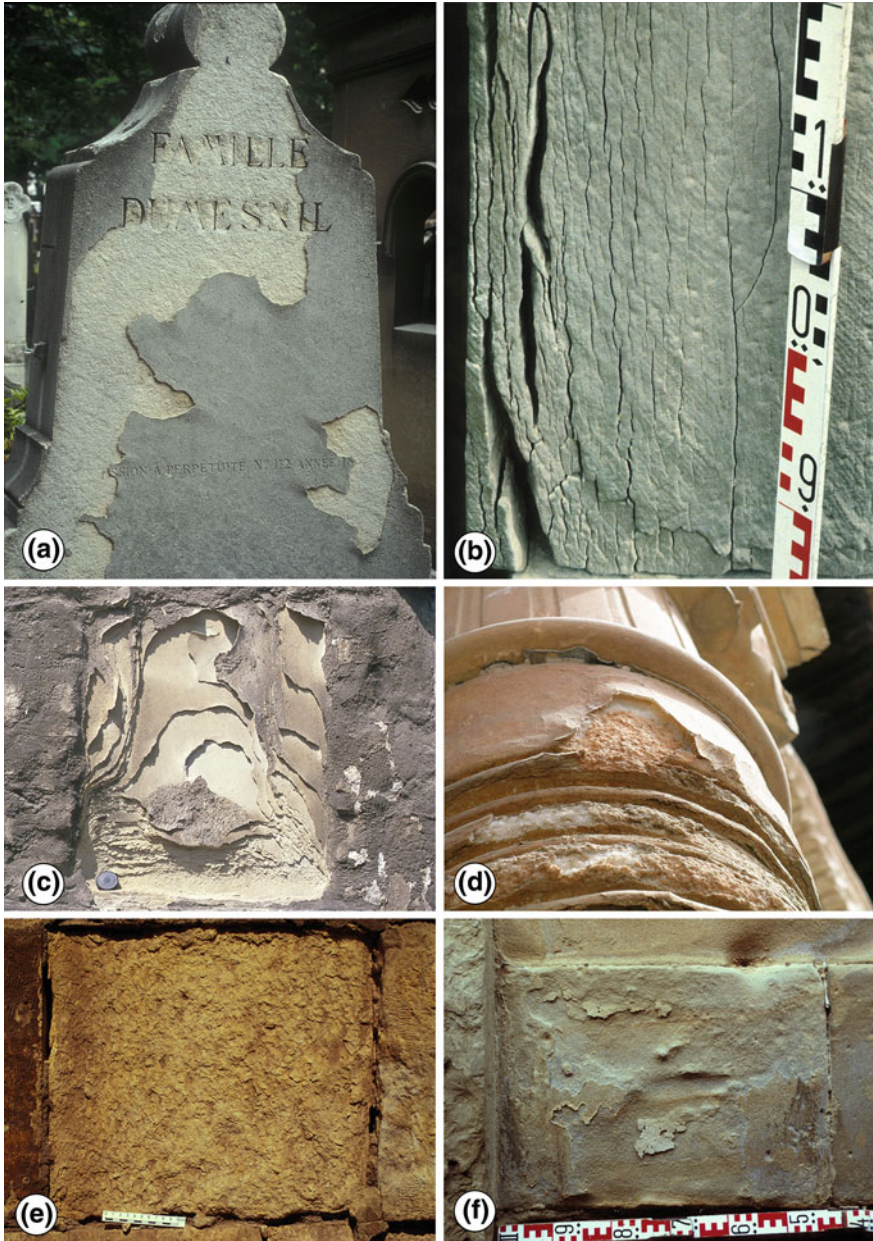


**Fig. 6.8** Detachment 1: **a** peeling (limestone, Cemetery Montmartre, Paris, France), **b** delamination (sandstone, church in Iphofen, Germany), **c** exfoliation (sandstone, church in Zeitz, Germany), **d** granular disintegration (Alhambra in Granada, Spain), **e** multiple flaking (limestone, mosque in Cairo, Egypt) (Figure by B. Fitzner), and **f** single flaking (sandstone, Castle of Ludwigsburg, Germany) (Figure by B. Fitzner)



**Fig. 6.9** Detachment 2: **a** disintegration—sugaring of marble (Old Southern Cemetery, Munich, Germany), **b** disintegration—crumbling (limestone, mosque in Cairo, Egypt) (Figure by B. Fitzner), **c** blistering (granite, Church of Christ, Dresden, Germany), **d** fragmentation—splintering (limestone, Sanctuary of Demeter, Eleusis, Greece) (Figure by B. Fitzner), **e** contour scaling (limestone, masonry, Cairo, Egypt) (Figure by B. Fitzner), and **f** bursting (sandstone, Luxor Temple, Luxor, Egypt) (Figure by B. Fitzner)



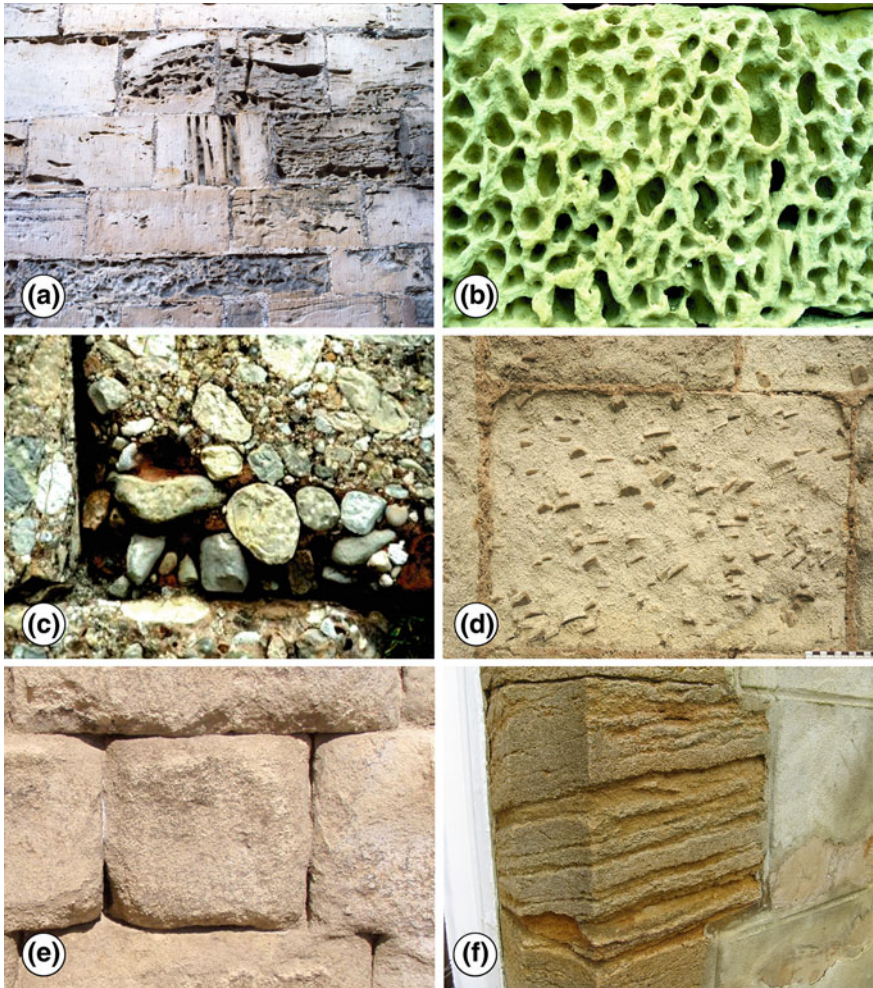


**Fig. 6.10** Material loss I: **a** alveolization (sandstone, Kronborg Castle, Denmark), **b** alveolization—honeycombing (limestone, Rabat—Gozo, Citadel, Malta), **c** erosion—loss of components (conglomerate, monastery, Montserrat, Spain) (Figure by B. Fitzner), **d** erosion:—loss of matrix (trachyte, church in Cologne, Germany), **e** erosion:—rounding (Bad-Sooden-Allendorf in Germany), and **f** differential erosion (limestone, Sherborne, U.K.)



**Fig. 6.11** Material loss 2: **a** microkarst (Munich in Germany) (Figure by W.-D. Grimm), **b** microkarst (limestone, Nemrud Dag, Turkey) (Figure by B. Fitzner), **c** pitting (marble, Rialto Bridge, Venice, Italy) (Figure by B. Fitzner), **d** cut (Quedlinburg in Germany), **e** missing part (Budapest), and **f** mechanical damage (sandstone, Banteay Chmar Temple, Cambodia)





**Fig. 6.12** Discoloration and deposit 1: **a** encrustation (slate, Bad Steeben in Germany), **b** deposit of pigeon droppings (limestone, Wells Cathedral, U.K.), **c** gypsum crust (limestone, Halle, Germany), **d** gypsum crust (limestone, Naumburg Cathedral, Germany) (Figure by B. Fitzner), **e** bleaching and glossy aspect (limestone, Piazza San Marco, Venice, Italy), and **f** film: old oil paint on sandstone (Dresden, Germany)

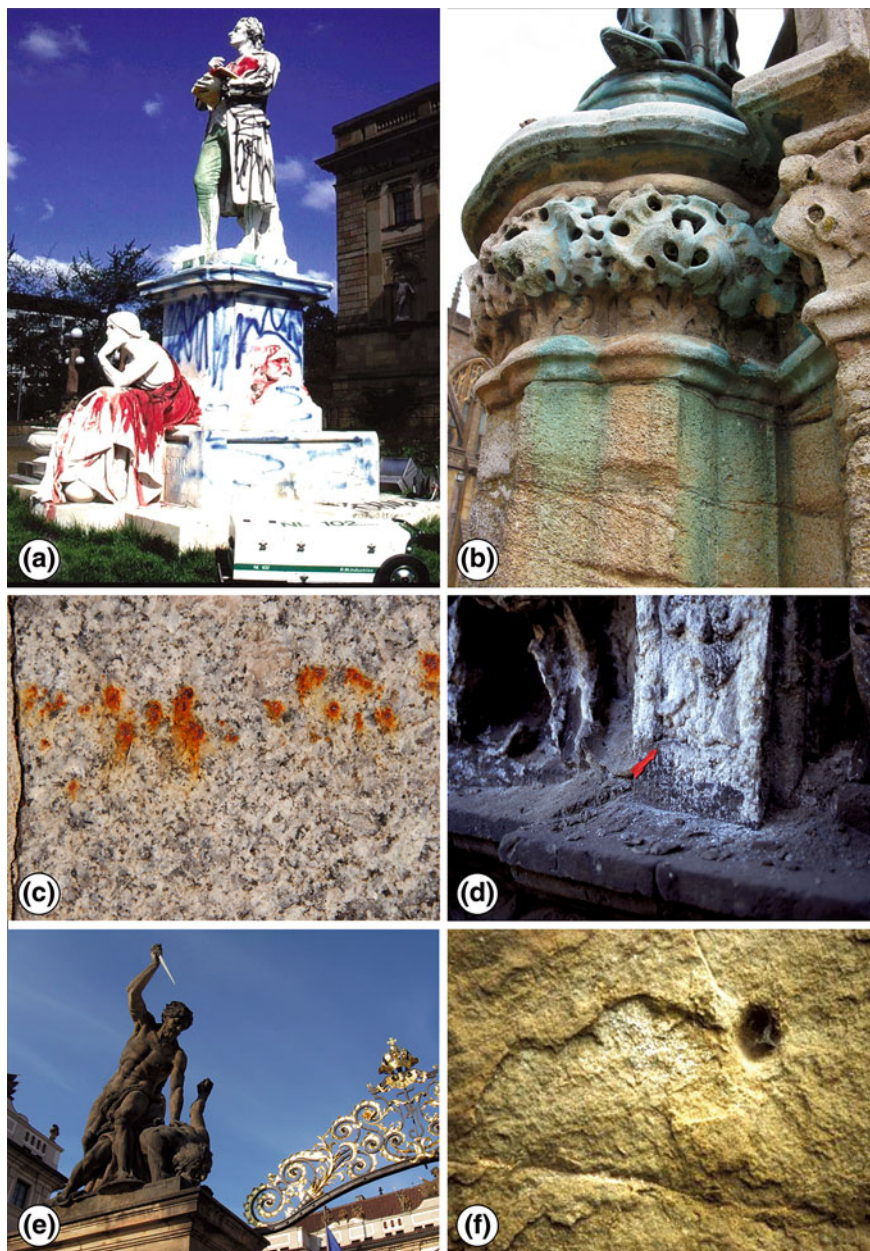


**Fig. 6.13** Discoloration and deposit 2: **a** graffiti (marble, Wiesbaden, Germany) (Figure by M. Auras), **b** discoloration: staining (limestone, Sherborne, U.K.), **c** discoloration: staining (granodiorite Bad Steeben, Germany), **d** salt efflorescence (sandstone, Hartenfels Castle, Torgau, Germany), **e** patina (sandstone, Prague Castle, Czech Republic), and **f** subflorescence (sandstone, St. Stephan's Chapel, Egersheim, Germany) (Figure by B. Fitzner)



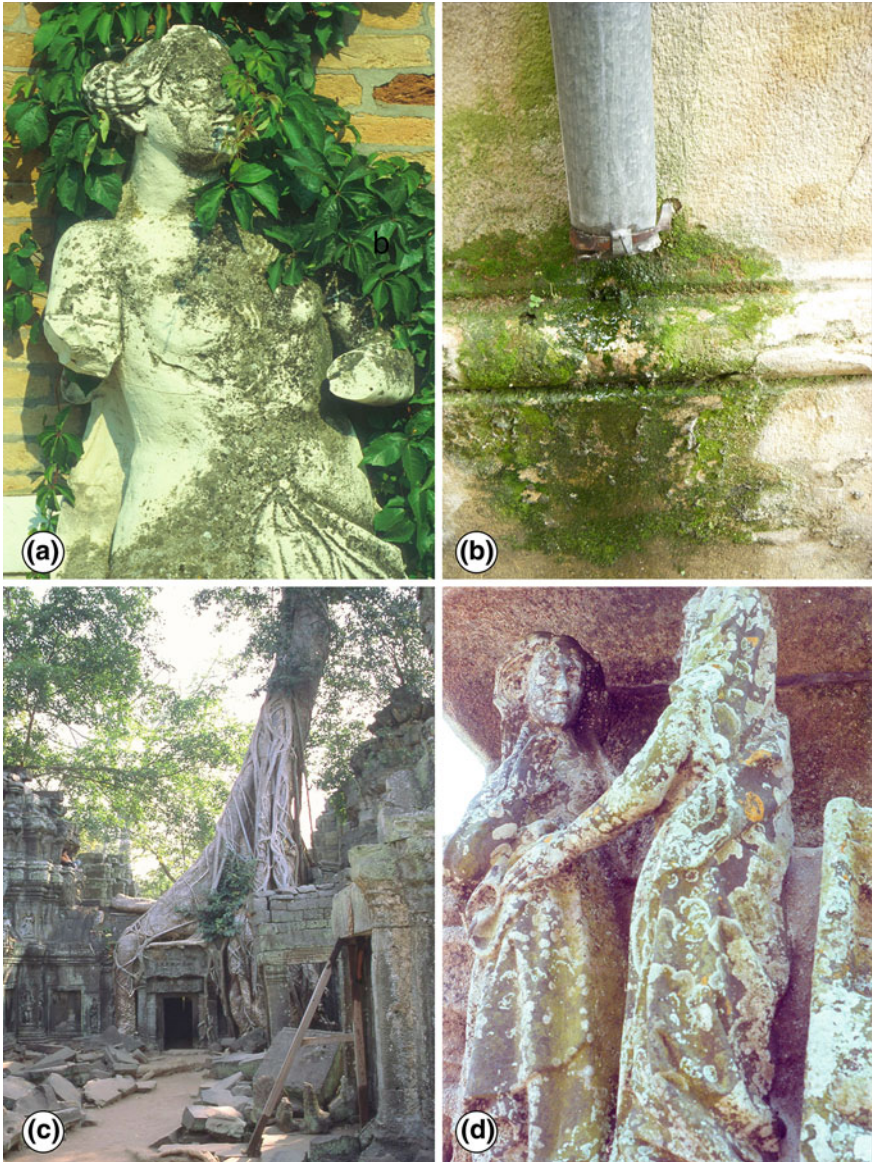


**Fig. 6.14** Biological colonization: **a** Colonization of a statue with lichen, moss and higher plants (Figure by B. Fitzner), **b** development of biofilms as a result of constant moisture exposure, **c** secondary diameter growth of the roots of a gigantic strangler fig, which has led to considerable damage to the temples of Preah Khan in Angkor, Cambodia and for conservation purposes have been partly removed, and **d** the weather-oriented east side, where lichen has colonized the granite figures from the Calvary near Concarneau in Brittany



### 6.3 Condition Survey: Mapping of Weathering Forms

Different weathering forms can coexist or superimpose each other on various types of constructions that use natural building stones. The intensity of the weathering can also be dissimilar on different building sections or even on individual building stones. After the weathering forms have been analyzed and recorded, a map of the type and intensity of weathering should be recommended where applicable. The systematic mapping of weathering forms and the intensities of deterioration on a stone object (like a sculpture, a relief, a tombstone, etc.) or on a whole building facade provides a survey of distinct weathering forms and their frequency of appearance. This includes their distribution and the different intensities in various places. The following goals can be attained within the scope of a damage analysis:

*Recording the present state of deterioration.* This might be valuable for scientific purposes (e.g. recording the weathering progress, the dependence on environmental influences) as well as documenting the starting point for conservation or restoration measures.

*Acquiring information about the distribution of deterioration on the object and localization of the most deteriorated areas.* The results may give an indication of the causes and mechanisms of weathering. For example, stone deterioration and salt efflorescence mainly concentrated at the bottom of a building might be caused by rising dampness. This hypothesis should be verified by selective sampling for moisture and salt investigations in the affected area (see [Sect. 6.4.3](#)).

*Extent and intensity of deterioration* recorded by systematic mapping are the basis for detailed planning of restoration measures and assessment of costs (cf. [Sect. 7.3](#)).

The prerequisite for mapping a building facade is the availability of a drawn-to-scale plan or a photogrammetric survey, which exactly depicts the size and form of the building stones as well as the grouting pattern. For smaller objects like gravestones or sculptures, good photos are also adequate as a mapping base. These should show little distortion when possible. Sculptures require a complete survey of all damages from many points of view.

Since photogrammetric surveys and photos are available in digital form today, the map data can be directly transferred into the digital template. Digital processing requires a portable computer (laptop) at the location of the survey site. For the data processing, corresponding computer programs are available, whereby the data collected from well-defined stone surfaces (e.g. individual stone blocks) can be arranged and defined by a chosen color. The simultaneous acquisition of data collected per stone surface (e.g. multiple weathering forms, the natural stone type or variety) is possible in different layers. These can either be represented individually or combined on the map. The combining of the analytical results is also possible, in principle, for those areas of concern where analyses have been obtained.

Mapping by hand on a printed plan or photo is still an alternative method today. As a rule this requires digital post-processing at the office, but it also has the advantage that expensive and sensitive instruments do not need to be employed

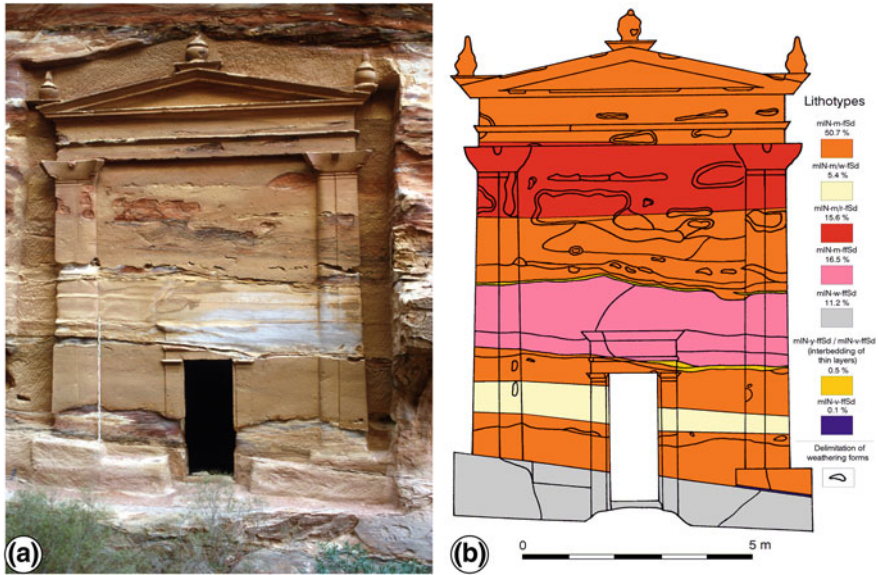


**Fig. 6.15** Lithological map of Tomb No. 455 (Wadi Kharrouba) in Petra, Jordanien (Heinrichs 2008)

under construction site conditions. This can be advantageous, especially when the weather conditions are not favorable. Moreover, digital on-site processing entails a greater expenditure of time. Because the timeframe for mapping is usually tight and the costs for scaffolding and elevated work platforms on facades need to be taken into consideration, creating map plans by hand can, on occasion, be a practical replacement for direct digital processing.

Ideally, mapping should be done in as close proximity to the object as possible. Detailed recordings and the spatial differentiation of the damages are easily constructed. Haptic and visual tests can be conducted, such as tapping on concave peelings, checking the stone surface with respect to sanding effects etc. In some situations, no scaffolding or elevated work platform is placed at the worker's disposal for cost-saving reasons. For people experienced with mapping, the analysis of damage forms at higher elevations can be done by using binoculars when the areas on the facade are not directly accessible. In such cases, the accuracy of the mapping is appreciatively restricted, since false assessments of the situation can occur.

The following information can be mapped:

*Type of building stones* (Fig. 6.15). If different stone types or significantly dissimilar varieties of the same stone type are present in a facade, mapping of their distribution might be appropriate, because their different structures and properties may cause different weathering forms or weathering intensities, respectively. Moreover, the appearance of different stone types in certain construction periods may provide valuable information for investigations into the history of construction (Graue et al. 2011, Siedel 2013). For sedimentary rocks, cases of unusual

orientation of bedding planes (parallel to the surface) should be recorded, because they might cause delamination.

*Replaced parts of the stone surfaces.* Historic conservation measures (replacement with stone pieces or restoration mortars) may indicate what the long-term weathering behavior of certain stone types or their varieties are. Replacements indicate past weathering. Even the replaced parts of the surface may undergo deterioration again.

*Type of weathering/weathering forms.* Weathering forms should be recorded according to the glossary presented in Sect. 6.2. Parts of stone surfaces or the whole stone block on the map are marked with different colors or signatures to visualize type and extent of deterioration. There are different systems suggested by various authors (e.g. Eickelberg et al. 1990; Fitzner et al. 1995). A system of colors or signatures accepted world-wide does not exist yet. The intensity of weathering can be displayed by darker or lighter colors or by special signatures (Fitzner et al. 1995).

Mapping is labor intensive, requires well-trained personnel, and is, thus, an expensive undertaking. Not every case requires the compiling of a detailed, time-consuming analysis of the damages in order to subdivide the main individual weathering form into further subforms or to make a differentiated evaluation of the damage intensity. Whether all the observed data have to be recorded in detail, or the analysis is sufficient even though less information has been collected, depends upon each individual case and the specific tasks at hand. Before an object is mapped, the goal of data acquisition should always be defined, and then the corresponding accuracy can be adapted accordingly.

Small stone objects and those with artistic cultural significance like statues or epitaphs have to be restored and protected at much expense. Detailed analyses of the damage forms and their distribution are necessary and sensible, because the restoration work has to proceed in a differentiated way. Therefore, the costs can be kept relatively manageable since only small areas are being restored.

The mapping of large-scale facades that have simple stone surfaces, like the effort made for sculptures with the same accuracy and maintenance, are neither required nor affordable. Research projects have also been carried out on large objects wherein they have been mapped in detail (Fitzner et al. 2003, 2004; Hüpers et al. 2005; Heinrichs 2008). Scientific knowledge is gained from such research with regards to the relationship between the material properties, exposure, weathering forms, weathering intensity, and how weathering advances. From these maps, damage categories have been derived based on a weighted assessment of individual damage forms. These can be used to delimit and highlight the focal point of weathering on an object. This type of representation highlights vulnerable areas in a section of a facade, which also appear at risk in a simple overview photo (see e.g. Fig. 6.16).

From the detailed maps, a linear damage index can be derived, in which the proportion of the planes are appraised with specific damage classes over the entire surface (Fitzner and Heinrichs 2001). These indexes, however, have little relevance for practical construction questions. Attempts to quantify and increase the objectivity of qualitative assessments from the mapping should be viewed with appropriate caution. Results are subjectively influenced because the mapping utilizes

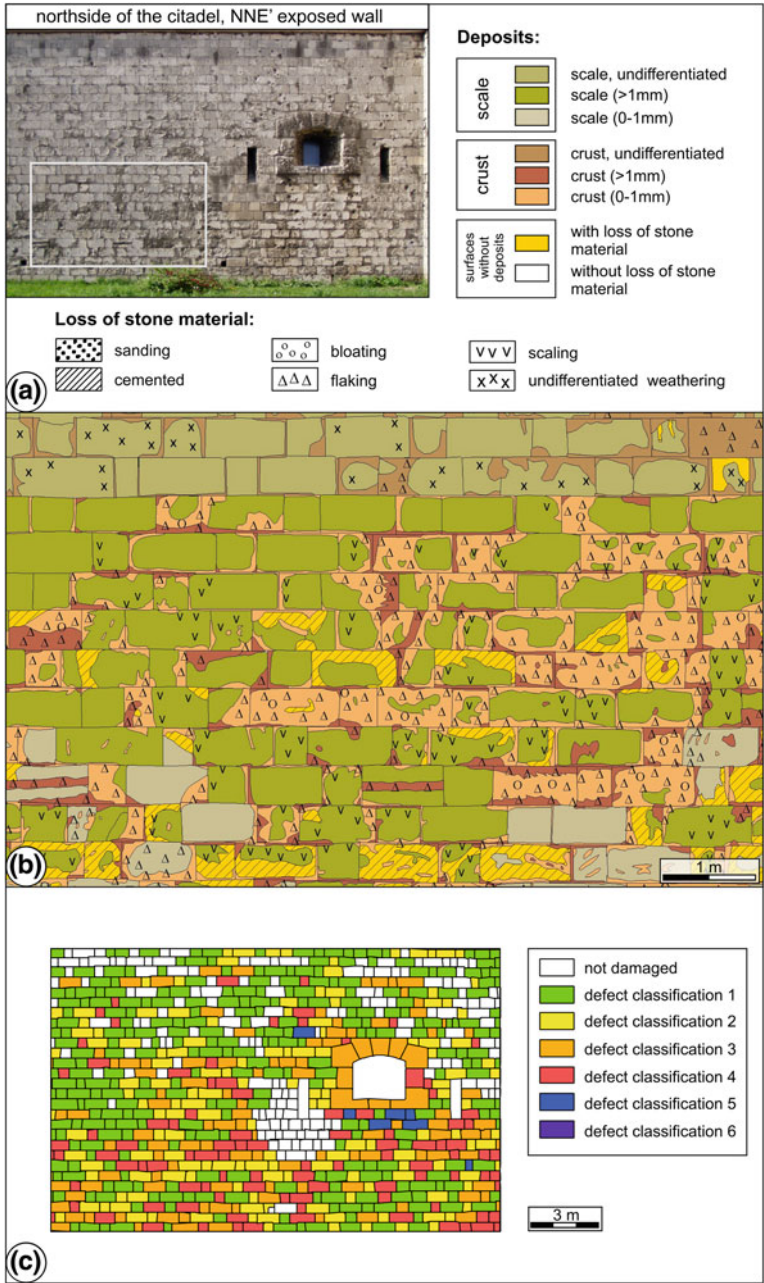


**Fig. 6.16** Mapping of the north side of the Budapest Fortress. **a** Overview of the mapped wall, **b** diagram of the material crustations and peelings in a representative study area, and **c** determination of the damage class for rock loss. After Hüpers et al. (2005)





**Fig. 6.17** Gravestone from Eberbach Monastery (Germany) with minimal map (*left*) and maximal map (*right*) of damages recorded by different workers. After Eickelberg et al. (1990), for explanation see text (Figure by the Zollern-Institut, Deutsches Bergbaumuseum)

descriptive criteria to determine the condition of the surface. The same phenomenon can be classified by different people in their own way and intensity, because this is dependent on the experience of the person doing the mapping and their individual point of view. Within the framework of a German project on damage documentation, damaged gravestones were mapped by different people (Eickelberg et al. 1990). Subsequently, all the damage data collected by all the workers was incorporated into a minimal map, whereas the sum of all the determined damages analyzed by the workers was registered on a maximal map. The minimal maps only show about 60–80 % of all the recorded damages (Fig. 6.17). However, it could be shown that the essential damages were recorded by all the workers.

The results show that even a time-consuming, extremely detailed analysis of all damages, including only weak zones and locally restricted individual phenomena, does not improve the objectivity of the maps. The large number of signatures and colors on the map complicates the assessment of the object's condition, because important and less important information becomes difficult to visually separate and to evaluate. Instead, a weathering phenomenon needs to be analyzed under practical conditions that represent significant damages to the stone surface. In other words, it is characterized by a strong loss of material or a noticeable deterioration of the stone's surface properties. When damage mapping is carried out with the goal of planning the maintenance measures, specific damage phenomena can be summarized with regard to the planning measures, and thus, the large number of colors and signatures can be reduced. This is exemplified by the tympanum in St. Lukas Church in Zwickau, Germany (Fig. 6.18). In this example, individual and different



**Fig. 6.18** Mapping of damages on the tympanum (St. Lukas Church, Zwickau, Germany) for the planning of appropriate restoration measures



weathering forms have been classified into groups that require specific measures. Despite the reduction of the mapped information to a few relevant damage phenomena and its summarized analysis, the strongly stressed areas become visible at a glance without having to do any post-processing work (e.g. division into individual damage classes). The overall picture shows the concentration of heavy damages along the gable boards, where the moisture stress is especially high. The focus is in the southwest corner of the gable where frequent wet-dry changes take place (right part of the image). The map serves as a document of the status quo with satisfactory accuracy and as a practical basis for estimating the necessary peripheral work and costs. Mapping in this way requires experienced workers who are not only able to describe and record the weathering forms but are also able to evaluate the damage relevancy and suggest adequate maintenance measures.

## **6.4 Material Testing, Scientific Investigations**

### ***6.4.1 General Remarks***

The results acquired from mapping create an overview of the type, intensity, and distribution of the damages. To evaluate the causes of the damages as well as develop plans for restoration, detailed information is necessary for the rocks and their technical properties, the changes that occurred during weathering and what type of pollutants are involved. By comparing restored surfaces with those before treatment (Auras et al. 2011), assessments for preservation measures and long-term monitoring can only be successful when material investigations are undertaken.

Material investigations should basically be performed on surfaces that are typical for the entire object or specific areas on the object, which are representative of the stone variety and the damage condition. These places can be determined from the mapping and defined according to the technical and financial possibilities for the specific object (e.g. accessibility for follow-up studies, the number of investigations financially possible, etc.).

In most cases, the objects that display damages caused by weathering are monuments. Special conditions are required for the investigation and sampling, since the historical surface needs to be preserved as much as possible, while at the same time, the precise nature of the damage, depth and intensity needs to be determined. This is especially true for sculptures, ornaments, tombstones, etc. or, in other words, highly-valued, artistic natural stone objects. In comparison to facade surfaces that only involve simple surface machining, the latter objects require special treatment in regards to the application of specific testing methods. Non-destructive or less destructive investigation methods have to be the rule for such artistic objects. In this case, non-destructive testing might be the only possibility for conducting a scientifically-based analysis of the object's condition if destructive measurements or samplings are restricted or not possible.

Non-destructive methods are also important for building facades, since comparative investigations can easily be performed at many different points on the

object. Non-destructive methods allow a regular and comprehensive measuring point grid which cannot be realized the same way as by drill core sampling with regards to cost and extent of destructive intervention. In addition, non-destructive and less-destructive investigation methods measure the same surface areas exactly before and after successful treatment, and can be used for the long-term study of natural stone conservation measures.

The results of non-destructive methods, however, might be less powerful because the signals or data obtained have to be interpreted on the basis of theoretical models built upon a number of assumptions. Moreover, the measurements are often affected by several material conditions like moisture content, salt load, or temperature. The conclusions reached can be improved case by case when a minimum amount of sample material is removed in terms of a calibration from the areas where non-destructive measurements have been performed.

The basic definition of how many samples and measurements should be taken from a specific object is not only justifiably a technical and financial one for monuments, but also a decision made for preservation purposes. In the process, the expected recommendations from the investigation and its necessity need to be evaluated in advance and carefully considered against any interference with the original material. In terms of the preservation of cultural monuments, sensible compromises need to be found. These should not only be supported by the monument conservators on the project but also by the participating scientists.

Measurements for characterizing the exterior and interior climate (e.g. temperature, humidity, dew point) have long been a part of the instrumental means used in building inspections, especially from the viewpoint of building climates. Not only are they routinely used in measuring natural stone objects, but also for masonry constructed from bricks and cultural objects made of wood or ceramics. Therefore, they will not be dealt with in detail here, even though the results from such measurements should be included on a case-by-case basis in the investigation of stone objects when it is deemed necessary. The climate influences the moisture state of the material and the reactions of structure-damaging salt in the pore spaces.

#### ***6.4.2 On-Site Evaluation Tests (Non-Destructive and Less-Destructive)***

When different non-destructive and less-destructive testing methods are used, specific considerations are required, such as:

The results collected with different testing methods are often influenced by the fabric of the object being investigated. Furthermore, temperature, moisture, and salt concentration are parameters which are not homogeneously distributed but, in numerous cases, show distinct gradients in space and time. This means that a clear acquisition of individual parameters is not possible with regards to making a prediction based on classical material properties. The significance of repeated measurements can be severely limited, since temperature, moisture, and salt

concentration can change. The comparison between many objects or building elements is only possible to a certain degree.

Direct contact between the measuring device/testing head and the object can be problematic on sensitive surfaces. Thus, the deployment of a coupling medium for improving the signal transmission between the object and testing head/sensor can lead to the introduction of foreign substances into the surface of the object being investigated. Mechanical damage may occur when the testing sensor is pressed to the surface. Especially desirable are measurements that produce variables independent of the device, which serve as a basis for long-term observations and the comparison of different objects.

Furthermore, a high resolution in different spatial directions is preferable, since most of the weathering damages occur in the surface zone. In many cases, the evaluation of stonework is only accessible from one side. This circumstance requires appropriate equipment and corresponding measuring procedures. When investigating sculptures and ornaments, complex geometries have to be taken into consideration. At the same time, the material strength can vary to a large degree even in the smallest space. In these situations, the resolutions at the millimeter scale are essential. Testing procedures need to be suitable for such fragile and complex geometries. Then objects like sculptures, vases, columns, etc., which are accessible all-around, can be measured from different sides by the method of tomography. Of course, the amount of time and labor involved in measurement and analysis increases considerably. The limitations noticeable in this case are that the effects are not self-explanatory and that they demand an interpretation. These need to be accounted for by the material, pollutant, and climatic influences mentioned above. The inhomogeneities and anisotropies of building stones need to be recognized and numerically ascertained, so that their influence can be computed from the measuring results on a case-by-case basis. Without question, anisotropies most probably play a key role and are a catalyst for the weathering or alteration processes.

In the last several years, various non-destructive investigation methods have been successfully tested for the maintenance and preservation of buildings and historical monuments (e.g. Binda et al. 2007). Systematic and comparative investigations utilizing various methods have so far only been done within the framework of scientific projects on a few structures and ideal test walls. Some of these applied methods show a fundamental potential for being used for building stone investigations but are still far from being implemented in a routine way. Comparative measurements utilizing different non-destructive methods can be found in Patitz et al. (1999), Ruedrich et al. (2004, 2013), Yates et al. (2004), Weise and Patitz (2005).

Other methods have been used exclusively in research projects in order to determine the material effects at a high resolution in the dynamics of weathering. This is especially true for optical laser methods with interferometric precision, which play an important role in non-invasive testing techniques (e.g. Jones and Wykes 1983; Castellini et al. 1996; Paoletti and Schirripa Spagnolo 1996; Rastogi and Inaudi 2000; Tornari et al. 2000). Using holographic interferometry, even objects with rough surfaces can be measured, wherein the method is sensitive down to the

sub-microscopic level. The deployment of video and computer image processing software allows the direct transference of measurements of objects in the laboratory (e.g. video holography in connection with sonic scanning). At the forefront is the determination of climate-caused deformation of natural stones and plastered surfaces as well as the detection of cavities behind walls (Gülker et al. 1991, 1993, 1996, 2000; Fricke-Begemann et al. 1999, 2000). Presently, the application of this method on a routine basis is still plagued with problems and is labor intensive. In the following section only those methods will be discussed in detail which have often been applied successfully to monuments over a long time period.

#### 6.4.2.1 Moisture Content

The purpose of measuring the moisture content is to determine the causes of the moisture penetration based on a distribution of the moisture on the stone surface (e.g. determination of rising, uncontrolled water addition due to defective drainage systems, etc. see Stück et al. (2013)). Non-destructive measurements of moisture on building surfaces are often used for construction investigations of masonry built from bricks or natural stones. A large number of commercial moisture testing devices are available that essentially measure the electrical conductivity or perform capacitive measurements. The latter device uses the differences in the dielectrical constant between the water and the dry building material. In these measurements, exact numerical values using a non-calibrated scale are depicted on the measuring apparatus, which measures a “high” or “low” moisture content in the material.

Such measurements can only be used in terms of a qualitative summary assessment for a rough delimitation of areas exhibiting strong moisture content and a high salt concentration. Only the surface area is measured whose moisture content is strongly dependent on the surrounding climate, and the field of measurement only reaches a maximum depth of a few centimeters. Furthermore, electrical conductivity measurements are strongly influenced by the salt content in the pore solution so that the measurement value only represents information on the combined salt-moisture content. Values not obtained directly on the specific material from non-calibrated measurements should not be considered reliable. When exact determinations of the moisture content are required, only then can destructive methods be applied (see Sect. 6.4.3).

Microwave measurements can be used as an alternative because integral moisture values can be delivered over a larger cross section of a stone construction (Blum et al. 1996). However, no extensive practical experience which has used this method is available.

#### 6.4.2.2 Analysis of Efflorescing Salts

Efflorescing salts or salt crusts can be carefully taken from the surface without affecting the stone substrate in some cases. For a quick survey of the occurring salts,

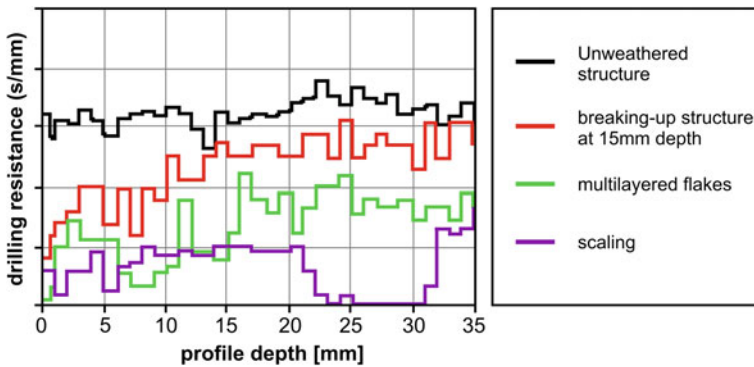


**Fig. 6.19** Different DR-graphs depicting different weathering forms with drilling resistance profiles. After Pfefferkorn (2005)

the material can be dissolved in distilled water, and the solution is then analyzed with test strips for water testing (similar to those used for pH testing and produced, for example by MERCK, Germany). These show characteristic color reactions and are available for sulfates, nitrates, chlorides and other salts. The results only allow a rough, qualitative evaluation of the occurrence of the most frequent salt anions. If possible, efflorescence should be analyzed by X-ray diffraction in a laboratory with respect to the salt minerals present. In this case, the information is more useful because a thorough analysis of the chemical compounds forming the salts can be obtained. Efflorescing salts, however, are only part of the whole system of soluble salt ions in a porous building stone. Even if some of them crystallize at the surface, forming salts, others might still be in solution in the stone pores, since their solubility is higher.

### 6.4.2.3 Drilling Resistance

Hirschwald (1908) used a drilling machine under dry and wet conditions to measure the drilling resistance. Based on this data he defined the so-called “softening coefficient”.

The drilling resistance (DR) test represents a less-destructive method (producing drill holes with a diameter of 3–5 mm only), whereby the weathering profile (DR profile) can be qualitatively and quantitatively recorded by the forward rate of speed of the drill in the near-surface areas. The result of the measurements is a DR profile from surface to depth. DR profiles offer an excellent spatial resolution (at millimeter scale) of changes in strength due to weathering (Fig. 6.19) or consolidation (Fig. 6.20) which cannot be obtained by other methods (e.g. bending strength tests on drill core slices). The values from DR measurements, however, are dimensionless and undefined in terms of “classical” mechanical strength and, therefore, cannot be directly compared to uniaxial compressive strength or bending strength. Nevertheless, DR is controlled by the rock strength, as clearly shown by

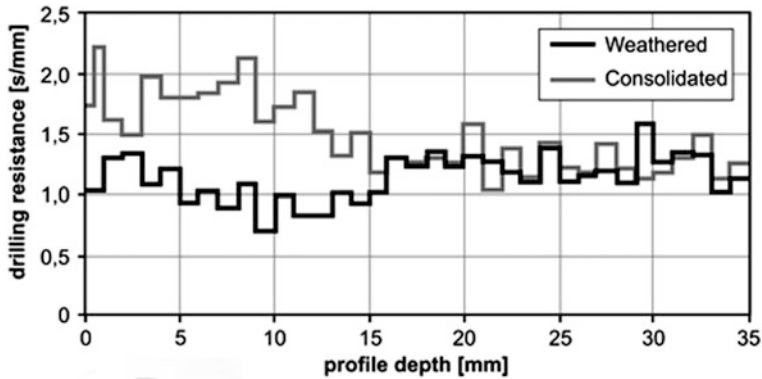


**Fig. 6.20** DR-graphs of a weathered sandstone surface before and after consolidation with ethyl silicate (after Pfefferkorn 2005)

correlations between DR and bending strength (Wendler and Sattler 1996) as well as uniaxial compressive strength (Pamplona et al. 2007) for different types of building stones.

Several drilling machines are available on the international market (Pamplona et al. 2007). The drilling resistance apparatus DURABO (see Fig. 6.21) and TERSIS from Geotron-Elektronik (Germany) are in widespread use. The Drilling Resistance Measurement System (DRMS) is a new but more expensive drilling machine produced and marketed by Sint Technology in Italy. DRMS is electronically operated.

The device uses a pressure load cell with constant device parameters such as drill speed rate and the drill revolutions per minute of the drill, thus allowing a direct measurement of the drilling force in N in time intervals of 1/10 s to be recorded. The analysis takes place directly using special software, with whose help average drill hardness values are calculated over the whole depth profile or specific sections. The apparatus has the advantage that measured physical quantities are provided that correlated better to the strength than the measurement of drilling speed. In contrast, DURABO is a mechanical drilling machine, wherein the drill has a constant weight of 1–3 kg for advancement into the investigated material. Results are recorded on paper, diagramming a drilling advance curve in units of millimeters per minute. Wendler and Sattler (1996) and Pfefferkorn (1998, 2005) indicate that, in order to obtain comparative and reproducible results, specific boundary conditions need to be kept constant. These conditions are: (1) the contact pressure of the drill on the stone surface (regulated by a weight of one, two, or three kilograms), (2) the advancement speed of the recorder, (3) the type of drill bit (diameter, tip design, and performance of the drill bit including a fixed cutting angle), (4) the contact pressure as well as the position of the testing machine on the stone surface, and (5) the mechanical capacity of the drilling machine.

DR for an arbitrary part of the distance drilled can be calculated with the following equation:



**Fig. 6.21** The DURABO drilling machine being applied (Figure by S. Pfefferkorn)



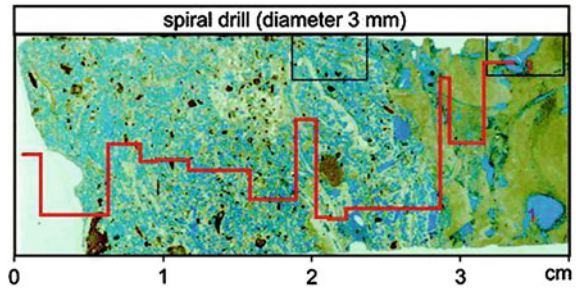
$$B'_i(\Delta s) = \Delta p / \Delta s \cdot v_s \quad (6.1)$$

where  $B'_i$  = the DR in s/mm for a depth profile section,  $\Delta p$  (mm) = the recording paper advancement,  $\Delta s$  (mm) = drilling depth section, and  $v_s$  (mm/s) = the recording speed. During drilling, the abrasive property of the drill cuttings from the investigated stone can cause wear and tear at the drill bit tip, which leads to inaccuracies in the determination of the drilling resistance. The wear and tear at the drill bit tip is dependent upon the mineral constituents of the stone and upon the drilling time. It can be corrected with the following equation (Pfefferkorn 1998):

$$B_i = B'_i - \alpha \cdot \sqrt{t_i} \quad (6.2)$$

where  $B_i$  = the corrected value of the DR in s/mm,  $B'_i$  = the DR in s/mm,  $\alpha$  = the abrasion value in  $s/mm \cdot s^{-0.5}$ , and  $t_i$  = the cumulative drilling time in s. The mechanical wear on the drill bit tip is mostly dependent on the mineralogical composition of the stone (Wendler and Sattler 1996; Pfefferkorn 2005). According to Hofestädt et al. (2002), the results of drilling resistance measurements in

**Fig. 6.22** Thin section of a limestone with a truncated canal from a DR-measurement. The *red curve* depicts the drilling resistance profile. *Blue areas* show the portions of the fabric containing *pores* (after Schlütter and Juling 2002) (Figure by F. Schlütter)



limestones with a low quartz content are less affected by abrasion and can give an abrasion value of  $0.001 \text{ s/mm} \cdot \text{s}^{-0.5}$ . Investigations conducted at buildings on-site are exposed to normal climatic fluctuations like temperature and humidity. These fluctuations lead to different moisture contents in the stone and can influence the results of the DR measurements (Pfefferkorn and Siedel 1999). This effect is ascribed to the impediment of the drill cutting transport, which means high moisture content changes the consistency of the drilling powder and sticks to the spiral rod of the drill. The drilling advance is considerably reduced in moist and clay-rich rocks, which, at the practical level, can lead to a complete cessation of the drilling investigation. With the help of systematic measurements, Pfefferkorn (2000) established a correction function considering both the abrasion on the drill bit tip and the influence of the drill cutting transport. Moreover, a continuous calibration against a standard material is necessary, because drill cuttings are not constant over time but are generated faster in the initial drilling stage than in the later stage. Pamplona et al. (2007) reported on a self-manufactured, very fine-grained ceramic material with an average DR which has proved to be a very good means of calibrating unused drill bits and describing the abrasion.

Pfefferkorn (2000) indicated that the hindrance of drill cuttings increases with drilling depth until 18 mm, after which an increasing slope becomes evident. The constant zone (<18 mm) should be used to calculate the average drilling force value in order to avoid the drill cutting transport effect.

The influence of stone fabric on DR is demonstrated in Fig. 6.22 (Schlütter and Juling 2002). Variations in DR obtained from a Triassic limestone drilled perpendicular to the bedding can be explained by the high amount of fossiliferous shell fragments that creates a vuggy limestone fabric. In contrast, the dense microsparitic limestone fabric shows high DR values. Thus, it becomes evident that DR measurements are best for homogeneous, fine to medium-grained, and dense building stones like sandstones and some types of limestones or pyroclastic rocks.

#### 6.4.2.4 Schmidt Hammer and Duroscope

The Schmidt hammer is a device for non-destructive testing that can be easily applied in situ for estimating rock strength. Originally, it was developed for measuring the strength of hardened concrete (Schmidt 1951). Recently, it has been

**Fig. 6.23** **a** Digi-Schmid and  
**b** Duroscope being used in  
the field



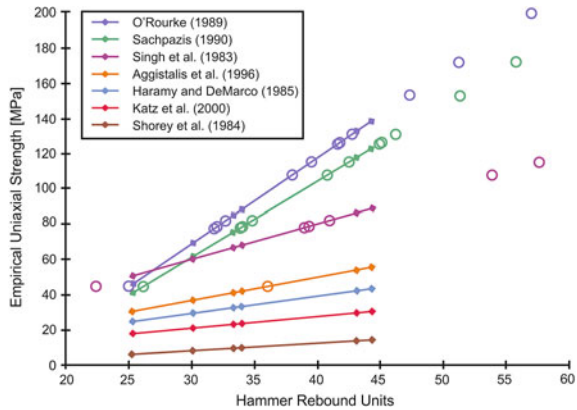
applied occasionally to building stone surfaces (e.g. Queisser 1986; Schneider et al. 2008). The advantage of using the Schmidt hammer is its cost-effectiveness and easy handling, and therefore, it seems to be a promising tool at first sight for testing weathered stone surfaces as well. On the other hand, sensitive surfaces or weathered surfaces with scales, flakes, etc. might be mechanically destroyed by applying too much energy. Because of this, it should only be used on rough stonework (e.g. fortress walls), not on sculptures or ornaments. Furthermore, the values obtained summarily indicate changes in strength (compared to fresh quarried stone, for example) without any specific information about weathering depth, type of weathering profile, etc.

The operating mechanism of the instrument is rather simple. When a Schmidt hammer is pressed onto the rock surface, a spring-loaded mass is released against a plunger. The plunger impacts the surface, and the mass recoils. The rebound distance is proportional to the total energy absorbed by the impact surface. The distance traveled by the piston after it rebounds is called the rebound value (see Aydin and Basu 2005; Buyuksagis and Goktan 2007).

Different types of Schmidt hammers are available, e.g. the Digi-Schmidt (Fig. 6.23a, L-type, N-type and P-type), and the Duroscope, which provides comparative test results on stone surfaces. The N-type can be used for a larger range of rock types with compressive strengths ranging from 20 to 250 MPa. The L-type hammer has a much lower impact and can be employed on softer rocks, while the P-type is for testing materials of very low strength. The Duroscope (Fig. 6.23b) differs in its power of impact, and thus, only near-surface areas up to a depth of 3 cm can be measured. This also allows the determination of the strength differences of individual weathering forms.

The correlation of the rebound values with the rock's compressive strength is the most important value that has been studied (e.g. Queisser 1986; Singh et al. 1983; Sachpazis 1990, etc.). One of the key questions concerns the difficulty of converting rebound values into strength values and that such formulas are available for concrete but need further elaboration for building stones. Vellone and Merguerian (2007) summarized well known empirical relationships between the

**Fig. 6.24** Relationship of uniaxial unconfined compressive strength to Schmidt hammer rebound units. Modified after Vellone and Merguerian (2007)

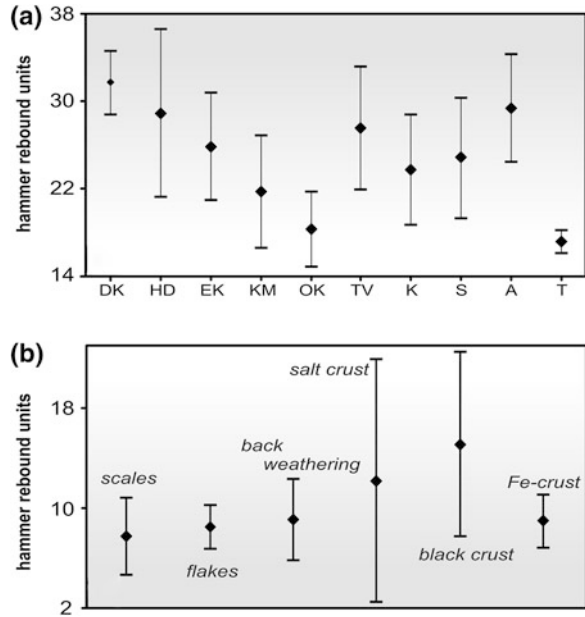


uniaxial compressive strength and the rebound values (Fig. 6.24) given by previous authors for different rocks. To test the hitherto existing relationships, they used rocks like amphibolites, marbles, gneisses, calc-silicates, schists, etc. from the New York City region displaying a wide range of rebound values (25.2–44.3). These rebound values are used to calculate the uniaxial compressive strength (UCS) and are plotted as solid lines. On the other hand, experimental UCS data published by Baskerville (1987) were used to calculate the corresponding rebound numbers. They found that many of the existing correlations significantly underestimated the UCS. Only the empirical relationships developed by Singh et al. (1983), O'Rourke (1989), and Sachpazis (1990) provide reasonable correlations.

Applying the Schmidt hammer and Duroscope in assessing grades of weathering might be a useful tool, but the limitations of the method need to be understood. These measurements also point out the detectable differences in the rates of weathering in polluted urban environments and in rural areas. Schneider et al. (2008) investigated the rebound values of different weathering forms and lithotypes (see Fig. 6.25). The Duroscope rebound values for scaling, flaking, back-weathering, salt crusts, black crusts and iron crusts cover a broad range from 7.7 to 15.1, and, in general, show a high standard deviation. The reason for this lies in the contact plane between the stone surface and the respective weathering phenomenon. Low values for scaling and flaking are attributed to the marginal contact between the stone surface and the detaching fragments. A near-surface compaction of the stone in the area of crust formation may explain the relatively high rebound values. The examples show that the Schmidt hammer and Duroscope might be useful to a certain extent as “assisting tools” for mapping different lithotypes. Assessing the “grade of weathering” on the basis of data measured on different weathering forms is not possible, because the range of values for severe damages like scales or flakes overlaps with those for deterioration limited to the surface, like salt crusts or black crusts.

Goudie (2006) summarized a larger data set including weathering phenomena on the effect of rock strength. Test results show that there are significant differences in rebound values of the same surface when different Schmidt hammer types

**Fig. 6.25** **a** Schmidt hammer rebound values of different lithotypes from the wall of the Buda Castle (*DK* Dachstein limestone, *HD* Main dolomite, *EK* Eocene limestone, *KM* marl, *OK* oolitic limestone, *TV* travertine, *K* conglomerate, *S* sandstone, *A* andesite, *T* tuff) and **b** Duroscope rebound values of the various weathering forms. The range of the values is marked by error bars. After Schneider et al. (2008)



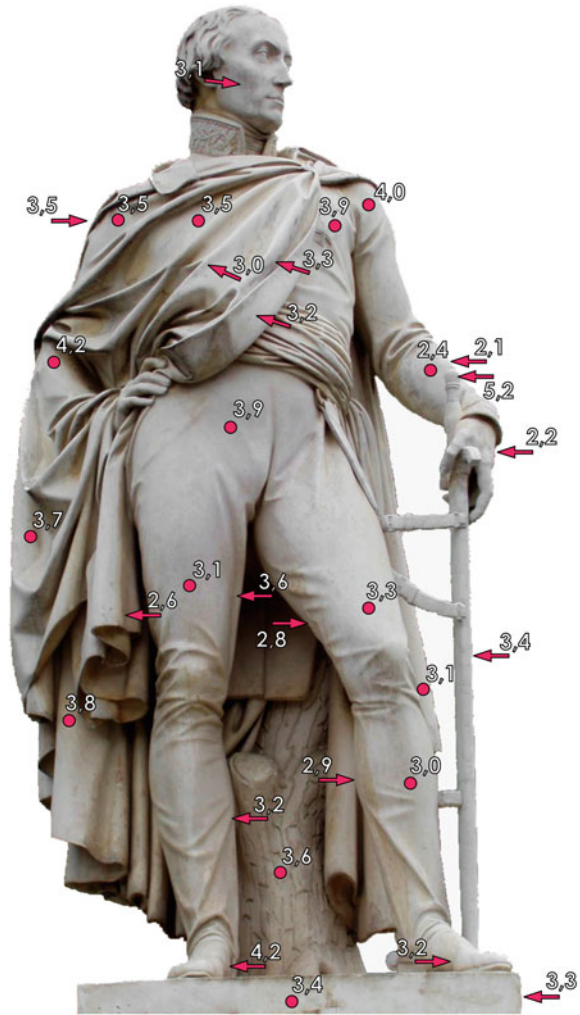
are used. The number of measurements also influences the reliability of test results together with the surface roughness.

### 6.4.2.5 Ultrasonic Wave Measurements, Other Geophysical Methods

Damage diagnosis by means of sonic wave measurements has been increasingly applied in the last several years (Fig. 6.26). Average P-wave velocities ( $V_p$ ) of 6 km/s for marbles are reduced to about 1 km/s because of disintegration due to microcrack formation (see discussion in Weiss et al. 2000; Dürrast et al. 1999). The disintegration associated with porosities of less than 3 % clearly shows that extreme elastic decoupling of the crystallites occurs simultaneously with a more or less intact rock mass. P-wave and possibly even S-wave measurements are an important tool for the volumetric characterization and early detection of disintegration processes (e.g. Köhler 1988, 1991, 1993; Dürrast et al. 1999; Lindner et al. 1999; Sneathage et al. 1999; Weiss et al. 2002a,b; Siegesmund et al. 2004). Ultrasonic tomography investigations have also been successfully applied (Mayer et al. 1990; Potts and Santamarina 1993; Jalinos et al. 1994; Cardarelli 1995; Schickert 1995; Dines and Lytle 1996; Schechter et al. 1996; Tewary and Fortunko 1996; Bernabini and Cardarelli 1997; Cardarelli and De Nardis 1999; Lindner et al. 1999; Siegesmund et al. 2000; Ruedrich et al. 2001; Siegesmund et al. 2009; Ruedrich et al. 2010; Ruedrich et al. 2013). Ultrasonic measurements used for determining the integral velocities are a routine method, whereas the tomographic approach is occasionally deployed predominantly for 2-dimensional



**Fig. 6.26** Single ultrasonic measurements of the sculptural group “Nike Teaches the Young History” (Group 1 from Emil Wolff 1874) on the Schlossbrücke in Berlin, Germany (after Ruedrich et al. 2010). *Dots* refer to a vertical ray path while *arrows* characterize a diagonal ray path (Figure by J. Ruedrich)



analysis of material and structural heterogeneities. Weathered stone monuments have physical and geometric material properties that are not often adequately measured with the routine techniques available. There are especially strong heterogeneities in the elastic parameters and a strong anisotropy as a result of the rock fabric, cracks, or zones of loosening. In contrast, the tomographic approach presupposes a weak heterogeneity and a weak anisotropy. The consequences of applying an inadequate technology are diffuse and partly generate misleading false tomograms. In order to improve the imaging quality and the reconstruction of the mechanical parameters, adequate 3D tomographic approaches need to be formulated and tested for anisotropic mediums. The recording equipment has to be enhanced and optimized while taking into consideration the three-dimensionality



of the investigated object. A high-energy broadband signal stimulus is also very important. High resolution methods for analyzing the surfaces of natural stones are largely missing in the literature.

Ultrasonic methods are very well established in material testing, for example, in analyzing the state of deterioration of building and ornamental stones. For approximately the last 15 years, the degree of environmentally influenced natural stone weathering on buildings and sculptures has been determined by using ultrasonic measurements in several cases. The advantage of this method is that it can be applied in a non-destructive way, thus allowing in situ analyses of the condition of damaged free-standing natural stones or those used for construction. With the help of a velocity scale, conservation measures that need to be implemented can be reassessed. This is generally the case for marble when the sonic velocity at different measuring points falls below 3 km/s (see Snethlage et al. 1999). Furthermore, conservation measures and their long-term effectiveness can be evaluated very well with this method.

Köhler (1993) measured the ultrasonic velocity of the tomb monuments by the sculptor Michael von Wagnmüller (see Sect. 3.7 and Fig. 3.87). Considering the  $V_p$  measurements, the monument seems to be in a pretty good condition. The average ultrasonic speeds of 4.8 km/s seem to prove that the monument, in general, will last for about 100 more years until its accelerated decay (Grimm 1999). However, in more filigree parts of the monument, the ultrasonic study yields speeds of only 3.0 km/s, a strong hint of reduced density and probably earlier decay for these parts of the monument. Since the ultrasonic velocities of an outdoor marble sculpture are, in part, different from test point to test point, a sufficient number of measurements are required in order to gain an overview of the condition of the sculpture (see Fig. 3.87).

As discussed in Sect. 3.7, ultrasonic measurements applied in situ utilize the principles of the ultrasonic method (Fig. 3.80). In this method, the transmitter and receiver are positioned at opposite sides on a surface, e.g. on a sculpture. One can assume the weathering initiates at the surface and penetrates deeper into the stone, which means the weathering is greatest at the surface and decreases with depth. From the interrelationships discussed in Sect. 3.7, it follows that the degree of weathering is coupled with the velocities of the P-waves (see Fig. 6.27a), or, in other words, the higher the degree of weathering, the lower the velocity. When the ultrasonic velocity is measured from the transmitter to the receiver, the waves travel through the weathered zone first, then through the intact core, and then through the weathered zone again on the opposite side. When the weathering depth is assumed to be similar, the P-wave travel time increases disproportionately with the total thickness of the sonically scanned object as well as the average velocity. Blum and Rahm (1998) determined the weathering depth by means of ultrasonic measurements on sculptures made from the Baumberg calcareous sandstone to a depth of 2.5 cm, where velocities of 3.5 km/s were measured in the intact core up to around 1.0 km/s near the surface. An examination of the loosened material at the surface edge could be verified by extracting an additional drill core. The pronounced strength variation was also confirmed by comparative drilling resistance measurements (Stadlbauer and Wendler 1998).

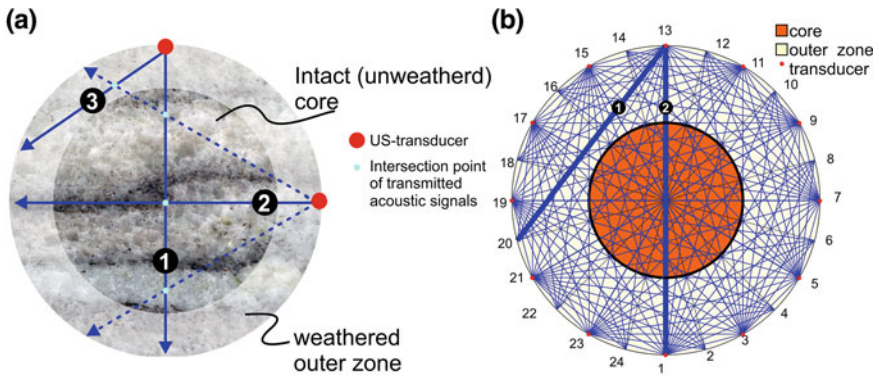
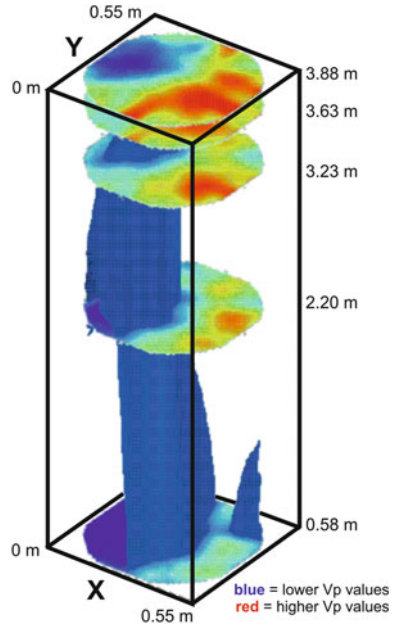


**Fig. 6.27** The basic principle of tomography: **a** Dependent on the position of the transmitter and receiver, only one weathering crust (3) or a mixture including the crust and the intact core (1, 2) is sonically scanned. In the process, the rays can continue parallel to (2) or perpendicular to (1) the observed bedding. **b** The spatial resolution of the ultrasonic velocities can be determined from the corresponding intersection of two or more rays. Under some circumstances, the rays only pass through the edge zone (1) or through the core and the edge zone (2)

Longitudinal wave velocities can be determined from the time of the ultrasonic impulses and the transmission distance. They depend initially on the elastic properties and the density of the stone being subjected to ultrasonic transmission. Material inhomogeneities along the sonic path influence the determined velocities. Structural inhomogeneities as well as the porosity lower the velocity similarly to an increase in weathering. Applying the tomographic approach, ultrasonic velocities can further constrain the damage classification. By means of tomographic analysis, the spatial resolution can be further localized. In this case, the cross section has a fixed transmitter position, where the sonic transmission radiates in a fan-shaped manner (Fig. 6.27b). An array of one transmitter and seven receivers can be oriented along the horizontal circumference of a sculpture, etc. During each measuring cycle, a sector of  $67^\circ$  can be covered. Almost complete coverage can be obtained by moving the transmitter and receiver array. This allows very dense coverage of the cross section with sonic runtimes, which is achieved because the different angles overlap. From these results, local velocity contrasts can be selectively evaluated for a chosen measuring grid. The 2D-velocity distribution can, for example, be computed by a tomographic wave front migration (see Jackson and Tweeton 1994; Lindner et al. 1999; Ruedrich et al. 2001; Siegesmund et al. 2009). This measuring concept is only possible on a limited scale, since this requires a considerable amount of measuring time and digital equipment as well as the corresponding evaluation software.

The ultrasonic tomography will be explained for a column of Prieborn Marble from the Marmorpalais in Potsdam (Germany). Damages on the column are easily visible and have been the subject of much discussion for a long time (see also Ruedrich et al. 2001). The columns display a weathering appearance that extends deep into the stone. The columns have a diameter of 0.55 m and were sonically

**Fig. 6.28** Tomogram of a column of Prieborn Marble. Different horizontal layers were scanned. A 3D connection in the area of lower velocities shows a low-velocity tunnel, which permeates from the base of the column to the upper edge of the column (*red*: high damage, *blue*: low damage) (after Siegesmund et al. 2004)



scanned at different sections (Fig. 6.27b). To prevent measuring errors from occurring near the edge of the circle-like cross section, every shot point (transmitter frequency of 46 kHz) was carried out with seven receivers spanning a sector of  $67^\circ$ . This results in a total of 56 different receiver positions per measuring section.

Calculations for the 2D velocity distribution in the Prieborn Marble were carried out at different heights on the column (Fig. 6.28). The velocity distribution in the column at 3.23 m is subdivided into two partitions: in one part, velocities reached a value of 4.8 km/s, whereas in the opposite sector, lower velocities of 3.4 km/s were observed. Similar velocity distributions were also observed at different cross sections of the columns, i.e. at heights of 0.58, 2.20, 3.23, 3.63, and 3.88 m, respectively.

A quasi three-dimensional reconstruction shows a low velocity canal that passes locally and slightly through the column center (Fig. 6.28). However, to explain the velocity structure additional investigations were performed. The macroscopically visible structural features of the Prieborn column are schematically illustrated with respect to the geographic coordinates in Fig. 6.29. The foliation strikes N–S and plunges steeply to the W. Two fracture populations were discriminated: C1 (open fractures) dipping steeply to the SE, while C2 (predominantly sealed) shows an intermediate plunge to the NW. Based on the cross sectional area at 3.23 m, the disintegration of the fabric should result in a reduction of  $V_p$  along the north–south-oriented part, which means the tomograms cannot be explained by macroscopic cracks. Comparative measurements of rock samples under dry and water-saturated conditions on a reference sample of weathered Prieborn Marble

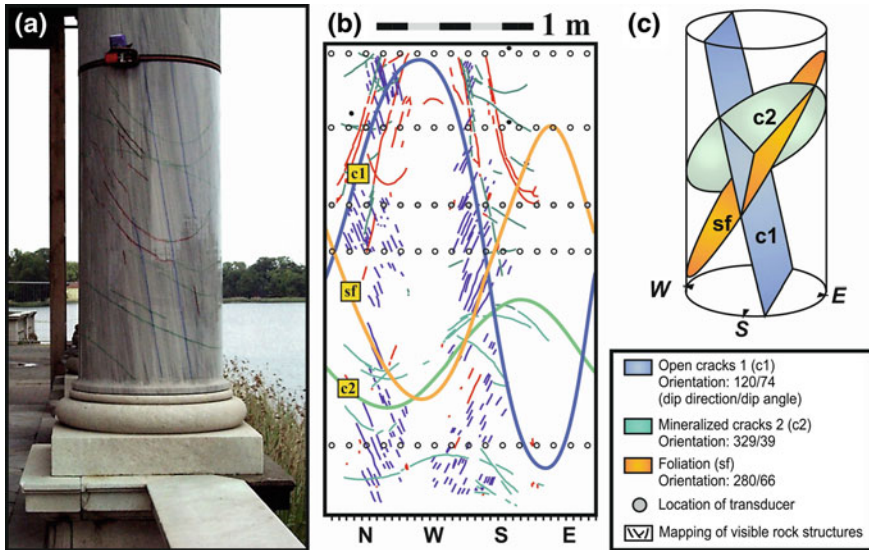
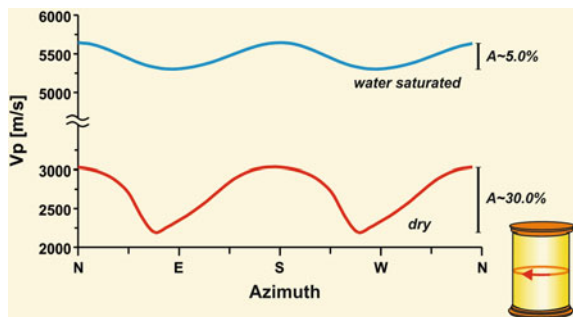


**Fig. 6.29** Fabric map of a column of Prieborn Marble. **a** Transparent foil wrapped around the column allows the mapping of fabric characteristics [see legend in **c**]; **b** from the unwound foil, the main dip directions can be reconstructed and **c** schematic representation of a column diagram showing the values of the amount and direction of dip. After Ruedrich et al. (2001)

**Fig. 6.30** Ultrasonic velocities on a reference sample of Prieborn Marble. Depending on the type of conditions (dry or water-saturated),  $V_p$  directional dependencies between 5 % and 30 % can be expected (after Siegesmund et al. 2004)



show that the anisotropy has a distinct influence on the observed velocity distribution, i.e. it cannot be explained exclusively by the state of weathering (see Fig. 6.30). Therefore, Ruedrich et al. (2001) introduced a modeling approach by using synthetic tomograms based on experimental and field data. Synthetic tomograms were calculated using the velocity data from the laboratory in order to investigate whether anisotropy can be considered. Due to the observed directional dependence of the velocities presented in Fig. 6.31, the anisotropy was also incorporated into the tomographic inversion of the field measurements (for details, see Jackson and Tweeton 1994). By introducing anisotropy of around 20 %, a distinct low-velocity channel along the N–S direction was achieved. Thus, the effect of open macrocracks which strike N–S can be monitored.

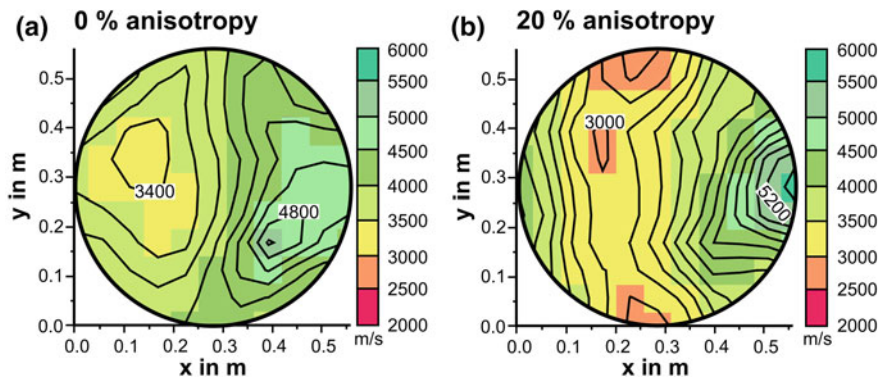


**Fig. 6.31** Ultrasonic tomography on an example of Prieborn Marble (layer at 3.23 m). Without considering the anisotropy, two diffuse fields of high and low velocities can be seen. If rock anisotropy of 20 % is considered for the calculation of the tomogram, then the tomogram changes significantly (for explanation see text; see also Ruedrich et al. (2001) or Siegesmund et al. 2004)

In some cases, the ultrasonic measurements are combined with other geophysical methods. Köhler (2009) discussed the advantage of a combination of various methods. For example, ultrasonic and georadar measurements can be combined because both methods use different boundary criteria and are able to collect different information. Cracks, inhomogeneities, and cavities behave differently when they are analyzed by ultrasonic and radar measurements. According to Köhler (2009), a crack can be localized and its course can be described when utilizing georadar, whereas the quality of the crack can be characterized if the ultrasonic method is applied. On columns in the palace gardens of Sanssouci in Potsdam (Germany), the extent of the obviously visible crack formation and the condition of the limestone was inspected with regards to structural integrity. The results of the ultrasonic and radar measurements were directly compared with the damage mapping (see Köhler 2009). The columns of the Adnet nodular limestone show a very intensive damage pattern, such as complex crack patterns, breakouts, delaminations, and scaling formation. Conspicuously visible are further opened cracks that are parallel to the bedding and traced by fossils. These cracks are clearly visible with the georadar method. Ultrasonic velocities vary between ca. 1.3 km/s and 3.6 km.

Ruedrich et al. (2004) conducted a comprehensive study of high resolution geophysical methods (combining ultrasonic findings with georadar or electrical resistivity measurements) on the Market Gate of Miletus at the Pergamon Museum in Berlin. The Market Gate was reconstructed from fragments of the original marble material mounted on a steel skeleton and partially replaced by substitute material copies. Non-destructive methods of ultrasonic tomography, electrical resistivity tomography, and ground-penetrating radar have been applied to evaluate the ability to render the internal structure of the reconstructed marble columns, the state of preservation and characterization of the original and different types of substitute materials. The investigations have shown that the weathering condition of the marble can be easily detected. This is an important factor for



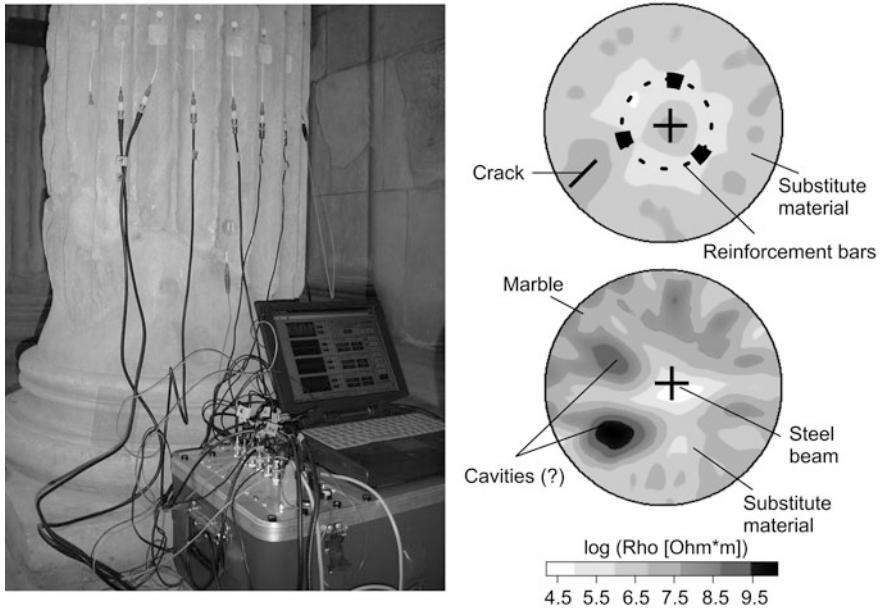


**Fig. 6.32** Measurement configuration at the column. Resistivity tomograms (frequency 1.46 Hz) in two planes of the column. *Top*: replacement material with suspected additional reinforcement. *Bottom*: original marble at the outer areas, replacement material in the inner areas. A steel beam exists at the center of the column, which causes a resistivity minimum in the lower measuring plane but is blocked from sight in the upper plane by the additional reinforcement (after Ruedrich et al. 2004)

subsequent restoration work at the Market Gate. Lower ultrasonic velocities characterized the parts made of mortar and brick. Thus, different materials can also be detected with ultrasonic tomography. The steel in the central part of the column is not reflected in the tomographic inversion. This can be attributed to a nonexistent cohesion between the steel and the concrete.

The electrical resistivity tomography provided a detailed image of the internal structure of the investigated column in a non-destructive way (Fig. 6.32). The different materials (original marble and substitute material) emerge as clear resistivity contrasts. Whereas the steel core in the lower measuring plane causes a significant resistivity minimum, additional reinforcements were found in the upper plane, which admittedly shield the steel core. However, the anomalous sizes do not match the real geometrical structures minutely because of the limited resolution of potential tomography.

The ground-penetrating radar technique (GPR) provides sufficient resolution for reliably rendering the internal structure of the investigated marble columns (Fig. 6.33). Not only the location and orientation of the steel core was detected, but also additional reinforcements have been found in the substituted section of the column. The transition between the original material and substitute materials was



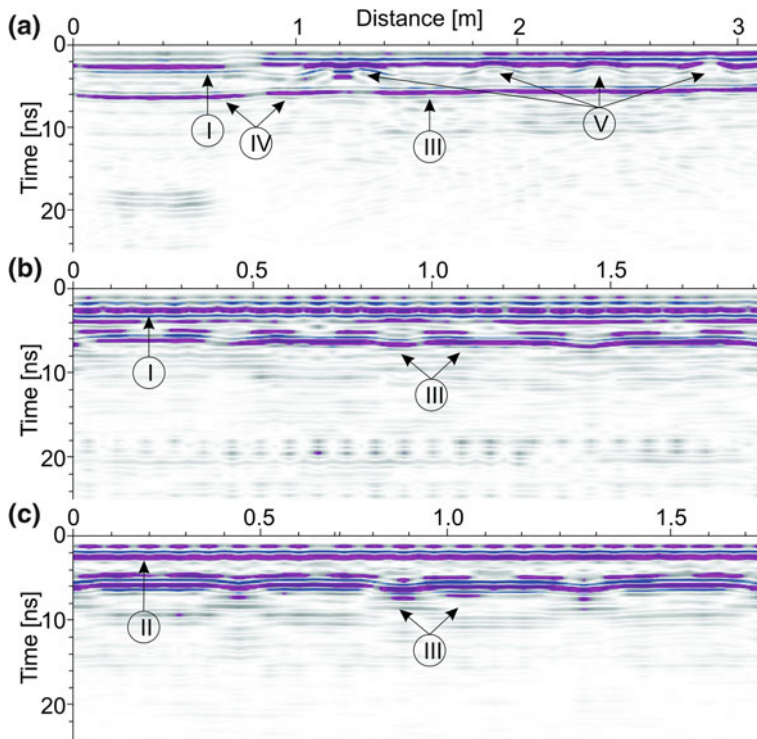


**Fig. 6.33** Radar sections at the marble column. **a** In vertical direction from *bottom to top* and in *horizontal* sections around the column, **b** at around 0.6 m, and **c** at around 1.60 m (after Ruedrich et al. 2004)

found by analyzing the amplitude and shape of the wavelet of the direct wave. This fits well with the visual observations. The high data quality and surprisingly high resolution of this method as applied to such a complex structure requires a tomographic investigation of the columns. Since the contrast of the dielectrical permittivity inside the columns is obviously more significant than electric and acoustic contrasts, a reconstruction of the internal geometry with GPR-tomography is promising.

#### 6.4.2.6 Capillary Water Uptake: Karsten Tube Measurements

Characterization of the capillary water uptake of stone surfaces is crucial for the assessment of their weathering behavior (fresh stone), weathering state (deteriorated stone), and the decision of whether a stone surface can be treated with fluids for conservation at all. Moreover, measurements of changes in capillary suction before and after restoration measures (cleaning, hydrophobic treatment, consolidation) allow for an assessment of the effectiveness of the applied treatments.

**Fig. 6.34** Setup of the Karsten tube measurement on a facade



The capillary water uptake of building stones can be determined in the laboratory according to the EN 1925 (1999) or RILEM test no. II. 6 (Commission 25-PEM Protection et érosion des monuments 1980). The test provides a quantitative value, the “water absorption coefficient”  $A$  (RILEM) or  $C$  (EN 1925) in  $\text{kg}/\text{m}^2 \cdot \text{s}^{0.5}$ . It provides information on how much water (in kg) is suctioned by capillary action up into the stone by a certain area of the stone surface (in  $\text{m}^2$ ) per unit of time ( $\text{s}^{0.5}$ ), thus describing the dynamics of capillary water uptake. To determine this value according to the test method above, drill cores with a diameter of at least 5 cm are needed. Since core drilling is not possible on monuments like sculptures or on building ornaments and, in principle, is limited in the number of cores taken from building facades, non-invasive methods of testing water uptake are preferred.

Karsten tube measurements (Karsten 1983) can be applied alternatively on even surfaces (RILEM test no. II. 4, Commission 25-PEM Protection et érosion des monuments 1980). In practice, Karsten tubes with diameters between 1.2 cm and 6 cm have been used, depending on the shape and state of the stone surface. The pipe-like glass tube is attached to the stone surface with removable putty (Fig. 6.34). Afterwards, the tube is filled with distilled water. As soon as it is filled

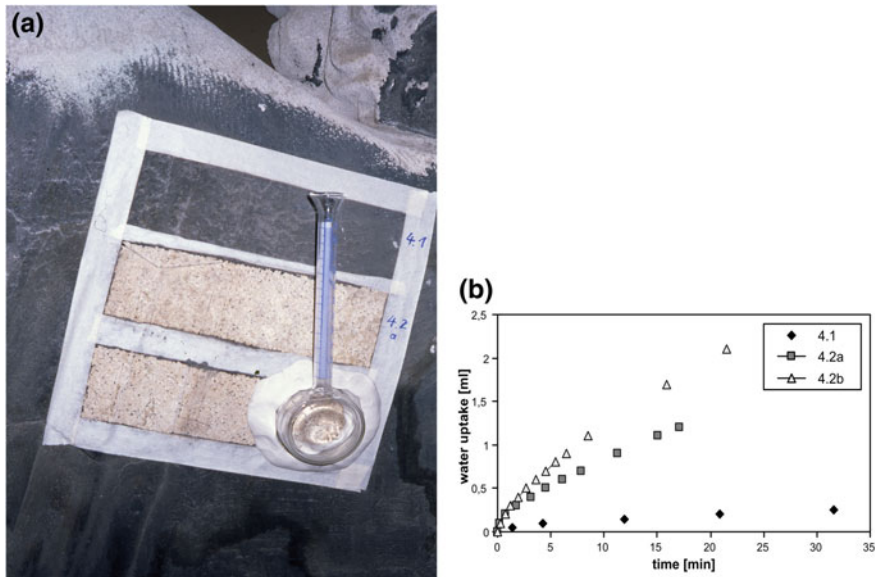
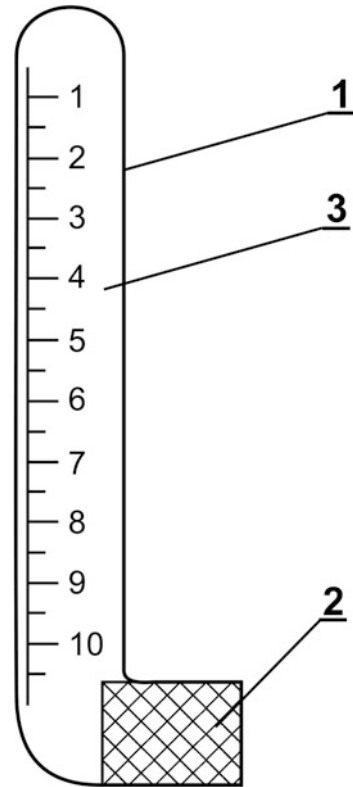


**Fig. 6.35** Results of Karsten tube **a** measurements on a surface of a limestone angel sculpture from the Cologne Cathedral **b** before and after cleaning (4.1 on black gypsum crust; 4.2a laser-cleaned surface, energy density 1.9 J/mm<sup>2</sup>; 4.2b laser-cleaned surface, energy density 7.2 J/mm<sup>2</sup>)

up to a benchmark, a stopwatch is switched on, and the volume of water taken up by the stone after a certain time interval can be recorded on the scale. Since the capillary water uptake of the surface is dependent on pressure, the tube has to be refilled when about 1 ml of water has penetrated the surface. Time-dependent water uptake on different parts of the surface or at the same place before and after a treatment can be graphically displayed and directly compared to each other (Fig. 6.35). Snethlage and Wendler (1989) suggested a method of calculation to obtain the A- and C-values, comparable to those determined from the EN or RILEM laboratory tests, directly from Karsten tube measurements. This calculation, however, will only work in the case of regular, capillary-controlled water uptake. In the case of uncontrolled horizontal movement of water behind the surface (due to cracks, scale formation, impregnation with chemicals, etc.) as well as in the case of soaking due to cracks or bigger pores, the calculation should not be used. Figure 6.35 shows the results of Karsten tube measurements before and after cleaning a soiled stone surface.

Domasowski (2003) suggested another tube (after a patent of R. Mirowski) for non-invasive, in-situ measurements (Fig. 6.36). Because of its small diameter, it can be well applied on small areas. Contact without putty allows application to more deteriorated surfaces. However, moving the water through a sponge-like, porous plug might be problematic because water transport into the stone might be additionally influenced by the pore structure of the plug in relation to that of the stone, i.e. by the difference in moisture tension between the two materials.

**Fig. 6.36** Principle sketch of the Mirowski tube (after Domasłowski 2003); (1) transparent tube (2) porous plug, and (3) volume scale in  $\text{cm}^3$



For more details on the tube methods and a detailed discussion of advantages and disadvantages (Karsten vs. Mirowski tube) see also D'ham et al. (2011).

#### 6.4.2.7 Color Measurements

Color measurements may help to assess any changes due to conservation measures such as consolidation or cleaning (e.g. Siedel et al. 2000, 2003). Besides subjective visual interpretations, quantitative values for color changes can be determined and direct comparisons between the surface being treated and its pre-state condition are possible.

For color measurements light illuminates the stone surface at a specific incidence angle or diffusely, and then the reflected part is evaluated with regards to brightness and pigmentation. Various portable devices exist for practical applications which can be deployed for evaluation directly at the object's surface with a circumference of up to several square centimeters. Investigations by Vergès-Belmin et al. (2008) demonstrated the influence of moisture on the measurement of color.

The principle will be demonstrated here on sample surfaces, for example, that were created for an optimal investigation of the conditions required to laser clean

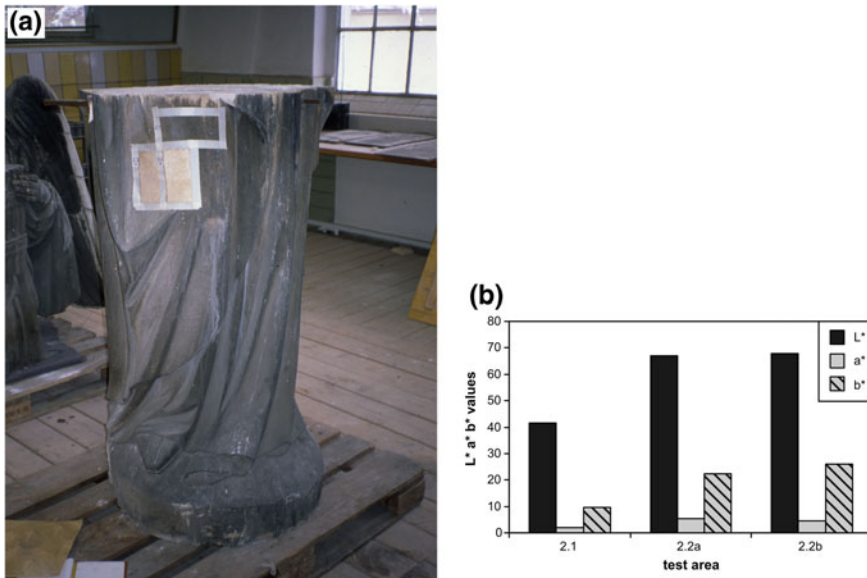


**Fig. 6.37** Results of color measurements on (a) an angel sculpture from the Cologne Cathedral before and after laser cleaning (b) (2.1 on black gypsum crust; 2.2a laser-cleaned surface, energy density  $1.9 \text{ J/mm}^2$ ; 2.2b laser-cleaned surface, energy density  $7.2 \text{ J/mm}^2$ )

limestone sculptures (Fig. 6.37). The measurements were performed with a Minolta Chromameter CR 300 (Fig. 6.38) using a xenon flash-lamp (measured spot 8 mm in diameter). The results are presented as  $L^*a^*b^*$  values according to the CIE (Commission Internationale de l'Eclairage = International Commission on Illumination) system.  $L^*$  describes the brightness within a range of values between 0 (black) and 100. The  $a^*$  parameter corresponds to a green/red axis (with a range between  $-60$ : green and  $+60$ : red) and  $b^*$  to a blue/yellow axis (with a range between  $-60$  and  $+60$ ). The results demonstrate an increase in lightness ( $L^*$ ) due to cleaning. Higher energy density of the laser does not influence the result significantly in this case. The color of the surface tends towards “warmer” red (increase in  $a^*$ ) and yellow (increase in  $b^*$ ) shades after cleaning.

### 6.4.3 Laboratory Investigations

Laboratory investigations can only be carried out on material samples taken from the object. This is connected with material loss or even with active destruction of the original surface. Therefore, number and size of samples should be limited to a minimum, which is unavoidably necessary for the measurements and appropriate interpretation. In contrast to most of the in-situ measurements, however, tests on



**Fig. 6.38** Color measurements with chromameter at the Freiburg Minster, Germany



**Fig. 6.39** Sampling of drill cores ( $d = 5$  cm) on weathered parts of a facade



stone samples provide direct, more reliable information about material properties and their changes due to weathering.

In most cases, core drilling is the appropriate technique for acquiring samples from stone objects (Fig. 6.39). This technique allows subsequent division of the



core into well-defined sections (slices) from the surface to specific depths, each representing part of the weathering profile or the fresh, unaltered stone behind the surface, respectively. Information about the intensity of weathering, the weathering profile, and the depth of the altered zone can be obtained in this way. The cores should be divided into profile sections as soon as possible after extraction to avoid moisture and salt movements within the core under changed climatic conditions. In some cases, broken fragments of the weathered surface can also be used for laboratory investigations (e.g. thin-section microscopy).

The necessary diameter of the drill cores depends on which investigations shall be carried out. Petrographic thin sections or salt analysis can be made on 2 cm drill cores. For measurements like bending strength or water vapor diffusion, cores have to be 5 cm in diameter. Since some of the tests are not destructive to the core section used for measurement, sections can be used again for other tests afterwards. The principle is to obtain as much information as possible from one and the same core or core section, because sample material might be rare. A possible scheme of investigation is given in Table 6.2.

Physical properties like bending strength, modulus of elasticity, total water uptake, water vapor diffusion, etc. are measured according to laboratory standards for material testing (cf. Chap. 3). Since sample sizes are smaller than the recommended standards for routine testing in most cases, some of the procedures and machines have to be slightly modified. This has been demonstrated, for example, by Wittmann (1983) for bending strength. More details and experiences with other testing methods are given in Sneathlaga and Wendler (1995).

Beside the “classical”, mainly standardized methods of construction material testing, there are special destructive investigations that have been qualified for damage analysis on stone objects. In the following section, the most important ones will be discussed briefly.

Petrographic characterization of rocks with microscopy of thin sections in polarized light is a common method in geology (Adams et al. 1984; Jones 1987; McKenzie and Adams 1994). It is also useful for the characterization of the weathered surfaces of building stones, which might be compared with the unaltered stone. Features like microcracks, new formation of minerals, dissolution patterns, loss of the binding agent, structure of crusts and surface layers, etc. can be studied in detail (Figs. 6.40 and 6.41), providing mineralogical and structural arguments for the discussion of changes in physical properties measured with other methods. If necessary, the distribution of single chemical elements (like sulfur, calcium, etc.) in microscopic profiles of uncovered thin sections can be displayed under the scanning electron microscope (SEM) coupled with energy dispersive element analysis (EDX). Furthermore, small pieces (mm to cm) of stone or broken slabs of drill core sections can be directly investigated under the SEM, where three-dimensional pictures with high resolution (magnification by a factor of some 1,000) are possible (Fig. 6.42).

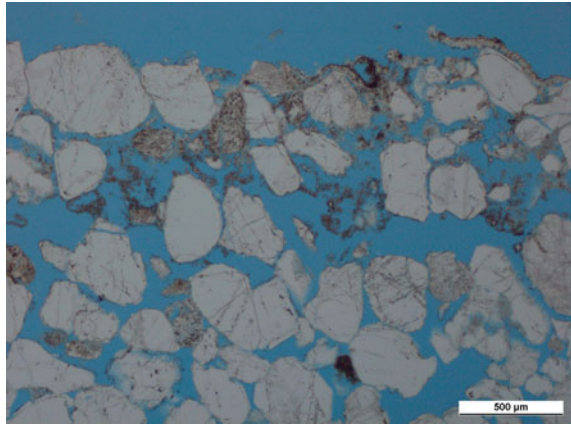
Salt load and salt distribution are crucial factors for many deterioration patterns on building stones (cf. Chaps. 4 and 5, see also Fig. 6.43). To assess their contribution to stone weathering on certain objects, the type and quantity of salts as

**Table 6.2** Type and order of possible investigations on one and the same drill core section

Order of investigation	Core with d = 2 cm	Core with d = 5 cm	Type of investigation	Remarks
1	+	+	Actual moisture content	Weighing; drying and weighing again (soon after taking the sample from the object!)
2	+	+	Hygroscopic moisture ( $\pm$ hygric dilatation)	Exposing dry sample to high relative humidity (RH), determining the mass difference to dry sample. Hygric dilatation due to high RH might be determined in the same course, if necessary
3	–	+	Water vapor diffusion	According to EN ISO 12572
4	–	+	Bending strength	On air dry sample; destructive; cf. Wittmann (1983)
5	+	+	Content of soluble salts	From crushed pieces of the broken core section obtained after investigation 4. The 2 cm core might be sawed (dry!) lengthwise into two pieces; one half is used for 5
6	(+)	(+)	SEM investigations	On pieces of the broken core section obtained after investigation 4. On the second half of the 2 cm core (if necessary); sample material can be used again
7	+	+	Total water uptake	According to EN 13755. On pieces of the broken core section obtained after investigation 4. On the second half of the 2 cm core
8	+	+	Thin section for optical microscopy	Destructive. From piece of the broken core section obtained after investigation 4. On the second half of the 2 cm core used for 6 (if soluble parts are of interest, total water uptake should not be measured before)
9	(+)	+	Mercury intrusion porosimetry	Destructive. On pieces of the broken core section obtained after investigation 4. On the second half of the 2 cm core (alternatively to thin section)

well as their spatial distribution have to be taken into account. The best way to acquire information about this is to drill profiles (dry!) at several (at least three) heights above the ground. The same cores can be used for analysis of moisture content if they are wrapped immediately after drilling and investigated soon after taking them to the laboratory. Drill cores should be cut into sections as described above. Since the concentration of soluble salts near the surface is much higher than

**Fig. 6.40** Deteriorated Ummendorf Sandstone from the Potsdam Castle (Germany) in petrographic thin section (parallel Nicols, voids impregnated with blue resin). The surface and the upper grain layers are affected by gypsum crust. The quartz grains have lost contact and a crack parallel to the surface has developed (Figure by F. Schlütter)



below in many cases, the slices should be thinner near the surface (1 cm maximum) to distinguish differences in concentration more clearly, whereas thicker profile sections (up to several cm thickness) can be used after the first two centimeters. Alternatively, smaller boreholes (10 mm in diameter) can be drilled with a twist drill, separately collecting the drill powder obtained from different depth sections of the borehole for analysis. Several hundred milligrams of stone powder are enough for analysis.

The content of soluble salt ions in every slice or in the powder samples can be analyzed after elution with demineralized water (immersion of a crushed piece of the slice or the powder with defined weight, stirring for several hours). Since some of the salts are less soluble than others, the excess of water should be high enough to avoid saturation of the solution in case of less soluble salts like gypsum (solubility about 2.4 g/l at room temperature), which would lead to underestimation of high gypsum contents.

Ion contents in the solution can be measured with analytical methods such as ion chromatography (for the anions sulfate, nitrate, chloride, and sometimes also phosphate or oxalate), or with emission spectroscopy (ICP-AES) and atomic absorption spectrometry (AAS) for the cations. They are normally related to the dry mass of the sample (weight %) and can be converted to equivalent concentrations (mEq/kg) using the atomic or the molaric mass and the charge number. This allows a direct comparison of the amounts of anions and cations.

The analysis of only anions of the most frequent salts, i.e. sulfates, nitrates, and chlorides, is of limited value, even if this is a common practice for economic reasons. Destructive activity and damage potential of salts and salt mixtures are dependent on the system including anions and cations as well. This is described in detail in Sect. 4.4. Sulfate, nitrate, and chloride contents, which are often the only ions analyzed, can only give a rough idea of the salts acting in the deterioration process and do not allow a thorough analysis of the deterioration mechanisms and assessment of the salt load. For example, it mainly depends on the cations occurring with a low-to-medium sulfate content, whether the sulfate salts will be

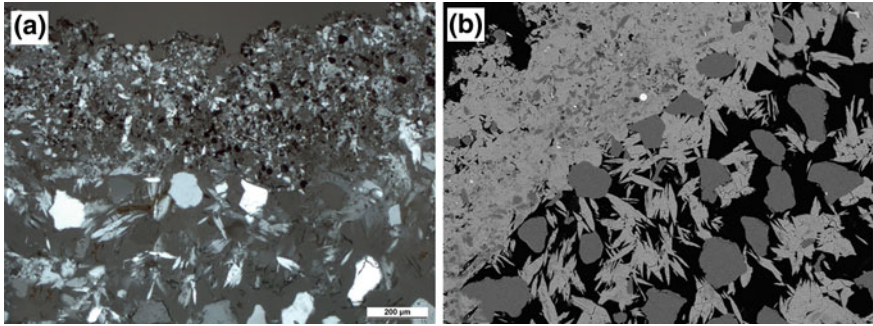


**Fig. 6.41** Ummendorf Sandstone from the Potsdam Castle (Germany) with dense gypsum crust on the surface and needles of gypsum crystallized in the voids. **a** Thin section under the petrographic microscope, crossed Nicols and **b** same thin section under the scanning electron microscope (back scattered electron image) (Figure by F. Schlütter)

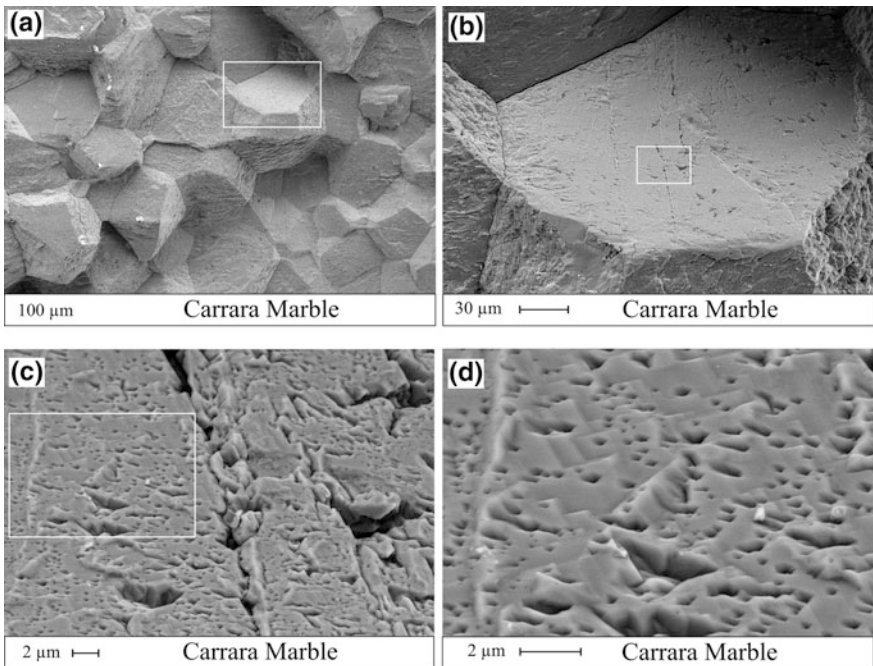


**Fig. 6.42** Fractographic illustration of the sub-microfabric of weathered Carrara Marble (same sample area, increasing magnification, the sections for the following images are indicated). **a** The morphology of the microcrack planes is dominated by open grain boundaries **b–d** especially along crystallographic preferred planes, but there are also structures recognizable along the grain boundaries that can be interpreted as being dissolution phenomena (Weiss et al. 1999, 2001)

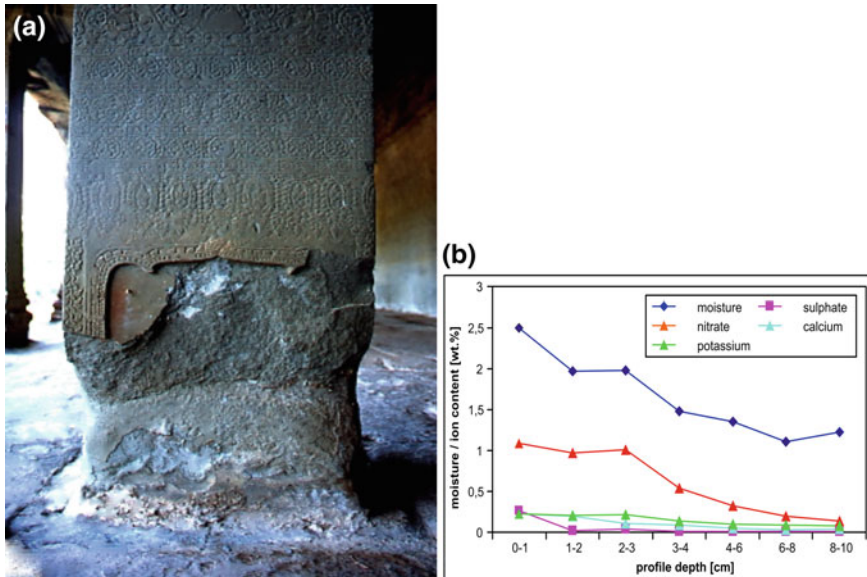


**Fig. 6.43** Moisture and salt profiles analyzed from drill powder from a pillar of the temple Angkor Wat, Cambodia (height 45 cm above the floor). Ions with very low contents such as chloride, magnesium and sodium are neglected

harmful to the stone or not: If only calcium occurs, the salt is gypsum, which is less dangerous with regard to its solubility, deliquescence behavior, or hydration-dehydration activity, compared to very “aggressive” salts such as magnesium or sodium sulfate.

Actual moisture content and hygroscopic moisture of the stone material are important for the assessment of the paths the water took into the object. In many cases, investigations of moisture distribution in a wall are the basis for decisions on how to deal with the object further: Is it necessary to isolate the wall from the ground, e.g. by sawing a slot and inserting a dense foil or by chemical impregnation? Or is there no more active rising dampness and is moisture only kept in the stone by hygroscopic salts? Information about the spatial distribution of moisture can be obtained in a way similar to the one described above for salt investigations. It is important to know that results only give a momentary image (similar to those for salt distribution). Moisture content in porous construction materials like stone is dependent on the ambient climate (insolation, temperature, and relative humidity, RH, of the air). Therefore, the results have to be discussed carefully, with respect to the season and actual climatic conditions.

The most reliable way to determine moisture content in building stones is dry-core drilling with a subsequent Darr test. The sample has to be weighed as soon as possible after it has been taken from the object. If weighing is not possible at the site, it has to be wrapped carefully to avoid water loss from evaporation. If different sections of a core are to be investigated separately to get a profile from surface to



depth, they best be cut on-site and then weighed or wrapped. The first value, obtained from this procedure (mass 1), can be used to calculate the actual water content of the sample. In the laboratory, the samples are dried and then weighed again (mass 2). The difference between mass 1 and 2, related to the dry mass (2), provides the actual moisture content of the sample (in %) at the time of sampling.

To get additional information about hygroscopic behavior, the dry sample has to be exposed to a high RH environment again (e.g. in a desiccator with constantly high RH inside, generated by a bowl with saturated salt solution at the bottom). The sample is weighed from time to time until mass changes are negligible (this might take several weeks, depending on the size and shape of the sample). The difference between the mass of the sample after this procedure (mass 3) and the dry mass (2) can again be related to the mass in dry state (2), providing the maximum moisture content is caused by hygroscopic salts. Eventually, the sample is saturated by immersion in distilled water and weighed again afterwards (mass 4). The mass difference of the saturated (4) and the dry sample (2) provides the maximum moisture content, allowing a quantitative assessment of actual and hygroscopic moisture in relation to the saturated state.

The actual moisture content measured in drill cores might be affected by the heat generated from drilling (especially in drill cores with small diameters). In principle, determination of actual moisture content can also be carried out on stone powder samples for salt analysis. Although the latter investigations do not allow one to get the “true” moisture content of the stone, because side effects due to sample heating and evaporation of water are much stronger, they may provide qualitative information about moisture distribution in cases where bigger drill cores are not available.

Indirect on-site measurements of moisture content by gamma-ray spectrometer (Kumaran and Bomberg 1985) or neutron radiation techniques (Tveit 1966) also need boreholes for the introduction of the measuring heads (Krus et al. 1995). They might, therefore, be calibrated with the drill cores obtained and can be measured repeatedly on-site in the same holes under changed climatic or seasonal conditions. These measurements, however, are still far from being routine tests and need expensive equipment as well as special care for safety while dealing with radiation.

## ***6.4.4 Biological Methods***

### **6.4.4.1 Phenomenological Analysis and Microscopy**

Many sophisticated techniques exist today to study the interaction of microbes and materials. However, concerning the practice of conservation, consolidation, and prevention of biodeterioration, the phenomenological analysis of the objects under consideration is also the first and most important step for microbiological analysis. Careful observation of the physical, environmental, and architectural parameters that influence a building or statue is necessary in order to find the explanations for



microbial growth and to develop appropriate solutions. Thus, before extensive laboratory analysis is carried out, the phenomenology has to be analyzed directly on site. The photographic and schematic documentation—mapping of deterioration phenomena—should be carried out as a basis for further chemical, biological, and physical analysis and for the development of appropriate treatment measures. Based on a detailed phenomenological analysis, the number of representative samples for further analysis can be restricted to the minimum. A set of methods for assessing bio-receptivity, abrasion, bulk density, and a quantitative method of comparing phenomenological observations of surface biogenic color changes on stone were published by Albertano (2003) and Prieto et al. (2006).

Several microscopy techniques have been used to study the interaction of microorganisms with the substrate. The first investigations of the relationship between microorganisms and stone using non-destructive techniques were carried out with light microscopy and light microscopy combined with scanning electron microscopy. In the early 1990s, a detailed study of the interactions between microorganisms and rock lithic substrates was made possible by the development of scanning electron microscopy utilizing back-scattered electrons (SEM-BSE). This technique allows the joint analysis of organic and mineral phases (in-situ) with good resolution. In SEM-BSE, fixed rock fragments containing biological material are embedded in resin, polished, and then analyzed. As with light microscopy, the SEM-BSE technique allows the examination of an area of several square centimeters, but with a higher resolution, more similar to that of transmission electron microscopy (TEM). The increased resolution allows epilithic and endolithic microorganisms as well as nearby minerals to be simultaneously visualized (De los Rios and Ascaso 2005).

Recently, the SEM-BSE technique was complemented with other in-situ microscopy methods, such as low-temperature SEM (LTSEM) and confocal scanning laser microscopy (CSLM), which allows the compilation of a complete picture showing all aspects of the colonizing microbial communities involved in biodeterioration processes. Fluorescence signals can be measured by the digital image analysis system, which semi-automatically counts the microorganisms in the stone materials. Staining by means of acridine orange (AO) has been shown to be suitable for visualizing microorganisms on and in natural stone. After dye application, the green fluorescing microorganisms can be easily distinguished from the red fluorescing mineral components. However, with AO staining, it is not possible to distinguish between active and inactive microorganisms. The depth of the biofilm, including EPS layers inside of a stone, can be visualized using the Perjud-Schiffs reagent staining technique (PAS), which results in a bright red staining of the bacteria biofilm as well as fungal hyphae and colonies.

Assessing and monitoring the risk of biodeterioration in a stone monument, it may be necessary to know the in-situ activity of microorganisms. Tetrazolium salts have been used to analyze the activity of natural populations. They act as artificial electron acceptors within a functional electron transport system (e.g. respiratory) or for certain active dehydrogenases. The tetrazolium salts 2,3,5-triphenyltetrazolium chloride (TTC) and 2-(p-iodophenyl)-3-(p-nitrophenyl)-5-phenyltetrazolium

chloride (INT) (Taylor and May 2000) have been used to investigate microbial activity in stone materials. A recent work reported on the use of tetrazolium salt 5-cyano-2,3-ditolyltetrazolium chloride (CTC) to visualize and quantify the actively respiring microorganisms in natural stones in situ. In contrast to TTC and INT, the formazan crystals formed by CTC reduction (CTF) show red fluorescence. CTC is, therefore, more suitable for the visualization of microorganisms in stone by using confocal laser scanning microscopy (Bartosch et al. 2003).

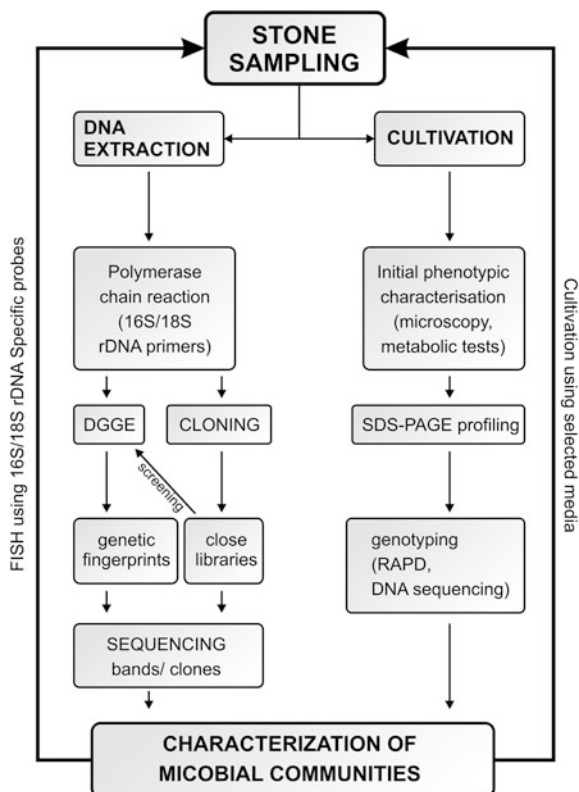
#### 6.4.4.2 Classical Microbiological Methods

Traditionally, microbiology research carried out in the field of microbial biodeterioration of stone and other building materials has mainly been based on classical cultivation methods. To evaluate the danger to historical buildings, monuments, or statues from biodeterioration, it is essential to identify and, if possible, to quantify these microorganisms. Enumeration is usually done by plate count and most probable number (MPN) techniques, which are based on the cultivation of microorganisms on selective media. Culture-based approaches, while extremely useful for understanding the physiological potential of isolated organisms, do not necessarily provide comprehensive information on the composition of microbial communities. It is generally accepted that cultivation methods recover less than 1 % of the total microorganisms present in environmental samples. In addition, cultivation strategies require a relatively high amount of sample material and are quite time consuming requiring 1–6 weeks of incubation. Due to suboptimal culture conditions and methodological limitations, the cell numbers are usually underestimated. An overview of destructive and non-destructive methods used to study the stone-inhabiting microflora in rocks and building stones was reported by Hirsch et al. (1995). Nevertheless, the use of conventional culture techniques and the developing of new culture media are encouraged due to the advantages of having pure isolates to perform physiological and metabolic studies. Combining both molecular analysis and enrichment culture techniques, it is possible to characterize the microbial diversity and culture characteristics of the isolated microorganisms in different environments, allowing a more complete picture. The phylogenetic information obtained by using molecular techniques on the identity of the microorganism to be cultivated can be a very useful tool for the specific design of appropriate culture media.

#### 6.4.4.3 State of the Art Molecular Techniques

Generally, the first step in the molecular detection of microorganisms consists of the extraction of nucleic acids from collected samples. Most studies dealing with molecular strategies applied in this field have followed the basic protocol described by Schabereiter-Gurtner et al. (2001), which is shown with some modifications in Fig. 6.44. Thereafter, the detection of microorganisms is mainly

**Fig. 6.44** Flow sheet for molecular analysis of microorganisms in stone samples (Figure by K. Sterflinger)



based on the sequences of the small subunit (16S for prokaryotes and 18S for eukaryotes) ribosomal RNA (rRNA) genes. This is a universal gene present in every living organism. Recently, the Internal Transcribed Spacers (ITS regions), which are nested in the nuclear rDNA repeat, have been selected for the investigation of the fungal diversity of fungi on building materials (Sterflinger and Prillinger 2001). The ITS regions possess a high variation between taxonomically distinct fungal species and even within the species. Different primers have been published to analyze these regions. The existence of complete DNA databases for rRNA genes guarantees optimal identification of the microorganisms detected through their sequences and the possibility of carrying out phylogenetic analysis with their closest relatives. rRNA genes are highly conserved and contain a level of divergence that allows microorganisms to be differentiated.

In the basic molecular protocol, specific target genes are PCR-amplified in order to obtain a large number of copies of these DNA fragments. The PCR technique requires two gene-specific primers and is carried out through 25–35 thermal cycles consisting of a denaturation step, annealing of the primers, and extension of the newly synthesized DNA fragment. In the current literature, there are available primers which are able to target any class of microorganism within a

microbial community, such as bacteria, archaea, or eukarya. Furthermore, the range of microorganisms to be detected can be restricted to group-specific amplifications, e.g. sulfate-reducing bacteria, nitrate-reducing bacteria, and even to a unique and specific microorganism.

PCR amplification products can be processed to obtain a microbial community fingerprint. This allows the analysis of the microbial diversity of a specific sample, its comparison with the fingerprint from other samples, and the evaluation and/or monitoring of sites, or temporal series (Gonzalez and Saiz-Jimenez 2004). The community fingerprint or profile can be obtained from a variety of available techniques, such as Denaturing Gradient Gel Electrophoresis (DGGE), Temperature Gradient Gel Electrophoresis (TGGE), terminal-restriction fragment length polymorphisms (t-RFLP), single-strand conformational polymorphisms (SSCP), and others. An ideal fingerprinting technique should be able to differentiate highly similar DNA fragments even if they show minimal differences. Sequences with single nucleotide differences can be discriminated by using some of these methodologies.

Separation of DNA fragments in DGGE and TGGE is based on differences in migration of the molecules with different sequences that have a different melting behavior in polyacrylamide gel containing a linear gradient of DNA denaturants or a linear temperature gradient. For studies of microbial communities colonizing building materials and artworks, DGGE is the technique most often used (Schabereiter-Gurtner et al. 2001; Portillo et al. 2008).

Terminal restriction fragment length polymorphism (t-RFLP) is a method that has been used frequently to survey the microbial diversity of environmental samples and to monitor changes in microbial communities. T-RFLP is a highly sensitive and reproducible procedure that combines a PCR with a labeled primer, restriction digestion of the amplified DNA, and separation of the terminal restriction fragment (t-RF). The reliable identification of t-RF requires the information of nucleotide sequences as well as the size of t-RF.

Single Strand Conformation Polymorphism (SSCP) is an electrophoretic technique which was developed, like others, for detection of mutations. Under non-denaturing conditions, single-stranded DNAs will fold into a secondary structure or specific conformations, depending on their nucleotide sequences and physico-chemical conditions such as temperature and ionic strength. The electrophoretic mobility of the DNA in a gel is dependent not only on its length and molecular weight, but also on its shape. Due to the differential electrophoresis mobility of these structures, these conformations can be separated by non-denaturing polyacrylamide gel electrophoresis, producing a fingerprint. This technique has been applied for the analysis of microbial communities on natural environments (Lee et al. 1996), and attempts have been made with this method for screening the clone libraries of samples obtained from building materials.

Microorganisms forming a microbial community must be phylogenetically identified further. Cloning and sequencing can complement the information obtained from a community fingerprint of the investigated sample by allowing a precise identification of the microorganisms corresponding to the detected target

DNA sequences. This is done by constructing a 16S rDNA library and then following a generally time-consuming screening, using an electrophoretic analysis (e.g. DGGE) process for the analysis of individual clones to select different clones while avoiding replicated copies.

The information contained in any 16S rRNA gene sequence is enough to obtain an unambiguous identification of a microorganism at the genus level. A homology search of the sequence against DNA databases provides information on the taxonomic and phylogenetic lineage of the microorganism corresponding to that sequence. The most commonly used homology search algorithm is Blast, which is available online at the US National Center for Biotechnology Information [<http://www.ncbi.nlm.nih.gov/BLAST/>].

Fluorescence in-situ hybridization (FISH) is a rapid and highly valuable tool for the cultivation and independent identification of individual microbial cells from environmental samples using rRNA-targeted oligonucleotide probes. Since then, a series of oligonucleotide probes for rapid determination of organisms, which are difficult either to differentiate by traditional criteria or to be grown in pure cultures, have been published in the literature (Amann et al. 2001). Design of new probes for specific taxa of microorganisms thus permits the application of a top-to-bottom approach to the characterization of the microbial community structure.

In recent years, FISH has also been applied in the field of building materials and historical monuments to study bacteria, archaea, and fungi involved in the biodeterioration of surfaces (Urzi et al. 2003). Furthermore, the application of FISH directly on adhesive tape strips has added another advantage to this non-destructive sampling method: the “in-situ” identification of the microorganisms present on a given area without the destruction of the valuable surfaces and with little biofilm disturbance.

Because DNA probes used for FISH are often not able to penetrate the cell due to a rigid fungal cell wall, only recently have peptide nucleic acid-probes (PNA) been applied for fluorescent in-situ detection of filamentous fungi. PNA probes are synthetic DNA mimics, where the negatively charged DNA backbone is replaced by a neutral polyamid backbone (Stender et al. 2002). Due to this property, PNA probes have better binding features to complementary targets and penetrate fungal cell walls more easily. This method may be a promising tool for specific detection and visualization of fungi on and in building materials.

Recent improvements in molecular studies have shown the advantages of RNA-based molecular analyses. In an RNA-based approach, called reverse transcriptase qPCR, not only the presence of a species of microorganism but also its metabolic activity can be determined, since the levels of RNA in a cell are proportional to the need of that cell for synthesizing proteins required for metabolism. This type of microbial community survey provides information on the fraction of the microbial community actually involved in the metabolic activity of a given sample. Consequently, microorganisms comprising that community are the ones directly responsible for any biodeterioration processes occurring on the artwork under study. Although RT qPCR is nowadays a routine tool for scientific questions, it is still only rarely used for routine monitoring in samples of cultural heritage

(Portillo et al. 2008; Martin Sanchez et al. 2013). This is due to the fact that the costs for molecular analysis are still high in relation to the overall costs that are usually available for the restoration and conservation of an object. Recent genomics and transcriptomics technology, called Next Generation Sequencing (NGS), opens up more possibilities for understanding the activity and function of whole microbial communities: sequencing of meta-transcriptomes—meaning the whole RNA in a sample—and metagenomes—meaning the whole DNA in a sample. Furthermore, the use of NGS technology can help in the understanding of how stones and monuments attacked by microbes and how the microbes interact with the material and with each other. For example in biofilm or to monitor specifically the effect of biocide treatments on the viability, the function and possible community shifts (Simon and Daniel 2011).

## 6.5 Synthesis: Discussion of Results, Recommendations for Restoration

The main aim of all the investigations presented above is to find out the causes of deterioration and to provide a scientific basis for decisions about appropriate restoration measures. The latter should change the conditions that are harmful as far as it is possible and stabilize or improve the current state of the object.

Therefore, all information obtained about moisture, salt load, hygroscopic effects, and stone properties and their changes in deteriorated zones have to be put together and discussed. The weathering forms recorded at the object might be caused by the interaction of different, more or less important weathering mechanisms and influential factors. The most important ones have to be found out via systematic treatment of all data. This has been demonstrated on numerous buildings and stone objects (e.g. Bayer et al. 2004; Laue 2005; Graue et al. 2007, 2008; Meinhardt-Degen and Sneathlage 2008; Weber and Burszan 2008; Siedel et al. 2010; Wedekind et al. 2010; Stück et al. 2011). If possible, specialists from all relevant fields (building climatics, salts, material testing, restoration, and architecture) should be involved.

The results should provide information that can be used in the practice of restoration, such as:

- sources of damaging salts and their transport paths through the object,
- depth of weathering; type of weathering profile,
- assessment of changed material properties in the deteriorated zone (is there any chance for conservation, or does the material need to be replaced?),
- assessment of climatic conditions with respect to salt activity and material behavior (proposals for changes, if necessary),
- recommendations for replacement materials (stone, mortar), etc.



## References

- Adams AE, McKenzie WS, Guilford C (1984) Atlas of sedimentary rocks under the microscope. Wiley, Chichester
- Albertano P (2003) Methodological approaches to the study of stone alteration caused by cyanobacterial biofilms in hypogean environments. In: Koestler RJ, Koestler VH, Charola AE et al (eds) Art biology and conservation: biodeterioration of works of art. The Metropolitan Museum of Art, New York, pp 302–315
- Amann R, Fuchs BM, Behrens S (2001) The identification of microorganisms by fluorescence in situ hybridisation. *Curr Opin Microbiol* 12:231–236
- Arnold A, Jeanette D, Zehnder K (1979) Proposal for a terminology of weathering phenomena on building stones. International Council of Monuments and Sites (ICOMOS) Group Petrography, unpublished
- Auras M, Meinhardt J, Sneath R (2011) Leitfaden Naturstein-Monitoring, Fraunhofer IRB Verlag Stuttgart, 301 pp
- Aydın A, Basu A (2005) The Schmidt hammer in rock material characterization. EngineeringGeo ASTM D 5873, “Standard Test Method for Determination of Rock Hardness by Rebound Hammer,” ASTM International, Annual Book of ASTM Standards, Vol. 4.09
- Bartosch S, Mansch R, Knötzsch K et al (2003) CTC staining and counting of actively respiring bacteria in natural stone using confocal laser scanning microscopy. *J Microbiol Methods* 52:75–84
- Baskerville CA (1987) Unconfined compressive strength on rock samples representative of the types found in Bronx county. U.S. Geological Survey Open-file report 87–136, New York, 5 pp
- Bayer K, Justa P, Kacer J et al (2004) Scientific examination and the restoration of tombs of princes Borivoj II and Bretislav II in the Chapel of St. John the Baptist in the Cathedral of St. Vitus in Pague. In: Kwiatkowski D, Löfvendahl R (eds) Proceedings of the 10th International Congress on Deterioration and Conservation of Stone, Vol 2. Stockholm, pp 907–914
- Beeger D (1988) Zur Dokumentation der in Architektur und Plastik verwendeten Gesteinsarten und der auftretenden Verwitterungsformen. *Abh Staatl Museum Mineral Geol Dresden* 35:129–137
- Bernabini M, Cardarelli E (1997) Variable damping factors in travel time tomography. *J Appl Geophys* 38:131–141
- Binda L, Drdácý M, Kasal B (eds) (2007) In-situ evaluation and non-destructive testing of historic wood and masonry structures. Institute of Theoretical and Applied Mechanics of the Academy of Science of the Czech Republic. Prague, 253 pp
- Blum R, Nägelsbach E, Rahm U (1996) Non-destructive physical methods in preservation of monuments: results in Tours and Meissen (in German with English abstract). In: Filtz J-F (ed) *Gemeinsames Erbe gemeinsam erhalten, 2. Statuskolloquium des Deutsch-Französischen Forschungsprogramms für die Erhaltung von Baudenkmälern*, Bonn, pp 159–165
- Blum R, Rahm U (1998) Ultraschall- und Bohrwiderstandsmessungen. *Arbeitshefte zur Denkmalpflege in Niedersachsen* 15:83–86
- Buyuksagis IS, Goktan RM (2007) The effect of Schmidt hammer type on uniaxial compressive strength prediction of rock. *Int J Rock Mech Min Sci* 44:299–307
- Cardarelli E (1995) 3D tomography of some pillars of the Coliseum. *Boll Geof Teor Appl* 37:257–265
- Cardarelli E, De Nardis R (1999) An application of 3D and 2D seismic tomography of some sample of building panels. *Eur J Environ Eng Geophys* 3(2):131–142
- Castellini P, Paone N, Tomasini EP (1996) The laser Doppler vibrometer as an instrument for nonintrusive diagnostic work of art: application to fresco paintings. *Opt Lasers Eng* 25:227–246

- Charola AE (2004) Stone deterioration in historic buildings and monuments. In: Kwiatkowski D, Löfvendahl R (eds) *Proceedings of the 10th International Congress on Deterioration and Conservation of Stone*, Vol 1. Stockholm, pp 3–14
- Commission 25-PEM Protection et érosion des monuments (1980) Recommended tests to measure the deterioration of stone and to assess the effectiveness of treatment methods. *Mater Constr* 13(75):175–253
- Cruikshank KM, Aydin A (1994) Role of fracture localization in arch formation, Arches National Park, Utah. *Geol Soc Am Bull* 106:879–891
- D'ham G, Meinhardt J, Niemeyer R (2011) Bestimmung der kapillaren Wasseraufnahme mit Messröhrchen nach Karsten und Mirowski. In: Auras M, Meinhardt J, Snelthage R (eds) *Leitfaden Naturstein-Monitoring*, Fraunhofer IRB Verlag Stuttgart, pp 82–92
- De los Rios A, Ascaso C (2005) Contributions of in situ microscopy to the current understanding of stone biodeterioration. *Int Microbiol* 8:181–188
- De Quervain F (1945) Verhalten der Bausteine gegen Witterungseinflüsse in der Schweiz. *Beitr Geol Schweiz, Geotech Ser* vol 23, Kümmerly & Frey, Bern
- Dines KA, Lytle RJ (1996) Computerized geophysical tomography. *Proc IEEE* 67:1065–1073
- Domasłowski W (ed) (2003) Preventive conservation of stone objects. *Wydawnictwo Uniwersytetu Mikołaja Kopernika*, Torun, pp 93–95
- Dürrast H, Siegesmund S, Prasad M (1999) Die Schadensanalyse von Naturwerksteinen mittels Ultraschalldiagnostik: Möglichkeiten und Grenzen. *Z dtsh geol Ges* 150:359–374
- Eickelberg U, Herppich S, Zallmanzig J (1990) Die Dokumentation in der Bestandsaufnahme–Untersuchung, Bewertung und Restaurierung denkmalpflegerischer Objekte. *Bautenschutz und Bausanierung*, Special Issue, 42 pp
- EN 1925 (1999) Natural stone test methods–Determination of water absorption coefficient capillarity
- Fitzner B, Heinrichs K (2001) Damage diagnosis at stone monuments–weathering forms, damage categories and damage indices. In: Prikryl R, Viles H (eds) *Understanding and managing stone decay*. The Karolinum Press, Prague, pp 11–56
- Fitzner B, Heinrichs K, La Bouchardiere D (2003) Weathering damage on Pharaonic sandstone monuments in Luxor, Egypt. *Build Environ* 38:1089–1103
- Fitzner B, Heinrichs K, Kownatzki R (1995) Weathering forms–classification and mapping. In: Snelthage R (ed) *Denkmalpflege und Naturwissenschaft*. Natursteinkonservierung I. Ernst und Sohn, Berlin, pp 41–88
- Fitzner B, Heinrichs K, La Bouchardiere D (2004) The Bangudae Petroglyph in Ulsan, Korea: studies on weathering damage and risk prognosis. *Environ Geol* 46:504–526
- Fricke-Begemann T, Gülker G, Hinsch KD et al (1999) Analyse dynamischer Vorgänge an technischen Oberflächen mit Speckle-Korrelation. *Tech Mess* 66:463–469
- Fricke-Begemann T, Gülker G, Hinsch KD et al (2000) Mural inspection by vibration measurement with TV-holography. *Opt Lasers Eng* 32:537–548
- Gonzalez JM, Saiz-Jimenez C (2004) Microbial activity in biodeteriorated monuments as studied by denaturing gradient gel electrophoresis. *J Separ Sci* 27:174–180
- Goudie AS (2006) The Schmidt hammer in geomorphological research. *Progr Phys Geogr* 30(6):703–718
- Graue B, Kordilla J, Siegesmund S (2007) Natursteinverwitterung und -konservierung der altägyptischen Grabanlage des Neferhotep (TT49) in Theben (Ägypten). *Z dt Ges Geowiss* 158(3):593–615
- Graue B, Kordilla J, Siegesmund S (2008) Stone deterioration and conservation of the ancient Egyptian tomb of Neferhotep (TT 49) in Thebes (Egypt). In: Lukaszewicz JW, Niemcewicz P (eds) *Proceedings of the 11th international congress on deterioration and conservation of stone*, Vol 2. Torun, pp 1231–1238
- Graue B, Siegesmund S, Middendorf B (2011) Quality assessment of replacement stones for the Cologne Cathedral: mineralogical and petrophysical requirements. *Environ Earth Sci* 63:1799–1822

- Graue B, Siegesmund S, Simon K, Licha T, Oyhantcabal P, Naumann R (2013) The effect of air pollution on stone decay: the decay of the Drachen fels trachyte in industrial, urban and rural environments—a case study of the Cologne, Altenberg and Xanten cathedral. *Environ Earth Sci* 69:1095–1124
- Grimm W-D (1999) Betrachtungen und Überlegungen zur Verformung von Marmormorobjekten durch Gefügeflockungen. *Z dt geol Ges* 150:195–235
- Grimmer AE (ed) (1984) A glossary of historic masonry deterioration problems and preservation treatments. National Park Service Preservation Assistance Division, Washington, DC
- Gülker G, Helmers H, Hinsch KD et al (1996) Deformation mapping and surface inspection of historical monuments. *Opt Lasers Eng* 24:183–213
- Gülker G, Hinsch K, Hölscher C et al (1991) Laseroptische Messungen feuchtebedingter Prozesse an Natursteinen. *Jahresberichte Steinzerfall-Steinkonservierung* 1:223–237
- Gülker G, Hinsch KD, Hölscher C et al (1993) Untersuchung der Dynamik von Salzausblühungen an steinernen Baudenkmalern durch laseroptische Verformungsmessung. *Jahresberichte Steinzerfall-Steinkonservierung* 3:107–115
- Gülker G, Hinsch KD, Kraft A (2000) TV-Holography on a microscopic scale: deformation monitoring on polychrome terracotta warriors. In: Jacquot P, Fournier JM (eds) *Interferometry in speckle light*. Springer, Berlin, pp 337–344
- Heinrichs K (2008) Diagnosis of weathering damage on rock-cut monuments in Petra, Jordan. *Environ Geol* 56:643–675
- Hirsch P, Eckhardt FEW, Palmer RJ (1995) Methods for the study of rock-inhabiting microorganisms—a mini review. *J Microbiol Methods* 23:143–167
- Hirschwald J (1908) *Die Prüfung der natürlichen Bausteine auf ihre Wetterbeständigkeit*. Wilhelm Ernst and Sohn, Berlin
- Hofestädt B, Kalisch U, Pfefferkorn S (2002) Forschungsberichte der Kooperationspartner. In: Schmuhl B (ed) *Kalksteinkonservierung am Westportal des Halberstädter Domes St. Stephan und St. Sixtus*. Domstiftung Sachsen-Anhalt, Leitzkau, pp 11–41
- Hüpers A, Müller C, Siegesmund S et al (2005) Kalksteinverwitterung: Die Zitadelle und das Parlament von Budapest. In: Siegesmund S, Snethlage R, Auras M (eds) *Stein-Zerfall und Konservierung*. Edition, Leipzig, pp 201–209
- ICOMOS-ISCS (2008) *Illustrated glossary on stone deterioration patterns*. English-French version. ICOMOS Documentation Centre, Paris, 78 pp (Monuments and Sites, vol. XV). English-German version, Michael Imhof Verlag Petersberg 2010
- Jackson MJ, Tweeton DR (1994) *Migratom-geophysical tomography using wavefront-migration and fuzzy constraints*. Report of Investigations, U.S.B.M., 35 pp
- Jalinos F, Olson LD, Aouad MF et al (1994) Acoustic tomography for QNDE of structural concrete. In: *Proceedings quantitative non-destructive evaluation (QNDE) 14*, Iowa State University
- Jones MP (1987) *Applied mineralogy*. Graham and Trotman Ltd., London
- Jones R, Wykes C (1983) *Holographic and speckle interferometry*. Cambridge University Press, Cambridge
- Karsten R (1983) *Bauchemie für Studium und Praxis*, 7th edn. Lüdiche Verlagsgesellschaft, Haslach, pp. 498–500
- Kieslinger A (1932) *Zerstörung an Steinbauten*. Deuticke, Leipzig
- Klemm W, Siedel H (2002) Evaluation of the origin of sulphate compounds in building stone by sulphur isotope ratio. In: Siegesmund S, Weiss T, Vollbrecht A (eds) *Natural stone, weathering phenomena, conservation strategies and case studies*. Geological Society, London, *Special* 205:419–430
- Köhler W (1988) Preservation problems of Carrara marble sculptures, Potsdam Sanssouci. In: *Proceedings of the 6th international congress on deterioration and conservation of stone*, Vol 1. Torun, pp 653–662
- Köhler W (1991) Untersuchungen zu Verwitterungsvorgängen an Carrara-Marmor in Potsdam-Sanssouci. *Berichte zu Forschung und Praxis der Denkmalpflege in Deutschland* 2:50–54

- Köhler W (1993) Ultrasonic investigations on four marble tombs in the Old Northern and the Old Southern Cemetery in Munich. *Forsch.-Ber.* 11/1993 (Eurocare-Euomarble EU 496):95–107, München (Bayer. Landesamt für Denkmalpflege)
- Köhler W (2009) Riss- und Verwitterungsanalytik mit zerstörungsfreien Verfahren. In: Venzmer H (ed) *EU-Sanierungskalender 2009*. Beuth, Berlin, pp 259–278
- Krus M, Künzel HM, Kießl K (1995) Feuchtemessung und Feuchteverteilung in Stein und Mauerwerk. In: Snethlage R (ed) *Denkmalpflege und Naturwissenschaft. Natursteinkonservierung I*. Ernst and Sohn, Berlin, pp 93–118
- Kumaran MK, Bomberg M (1985) A gamma-spectrometer for determination of density distribution and moisture distribution in building materials. In: *Proceedings of the international symposium on moisture and humidity*, Washington DC, pp 485–490
- Laue S (2005) Salt weathering of porous structures related to climate changes. *Restor Build Monum* 11(6):381–390
- Lee DH, Zo YG, Kim SJ (1996) Non-radioactive method to study genetic profiles of natural bacterial communities by PCR-single strand-conformation polymorphism. *Appl Environ Microbiol* 62:3112–3120
- Lindner H, Pretschner C, Rost C (1999) Ultraschallmessungen an Bauwerken. *Z dt geol Ges* 150:375–386
- Martin-Sanchez M, Alabouvette C, Bastian F, Saiz-Jimenez C (2013) Real-time PCR detection of *Ochroconis lascauxensis* involved in the formation of black stains in the Lascaux Cave, France. *Sci Tot Environ* 443:478–484
- Mayer K, Marklein R, Langenberg KJ et al (1990) Three-dimensional imaging system based on fourier transform synthetic aperture focusing technique. *Ultrasonics* 28:241–255
- McKenzie WS, Adams AE (1994) *A colour atlas of rocks and minerals in thin section*. Manson Publishing, London
- Meinhardt-Degen J, Snethlage R (2008) Materialtechnische Untersuchungen zur Risikoabschätzung von Folgekonservierungen bei Sandsteinen am Beispiel von Regensburger Grünsandstein und Grünem Mainsandstein. *Z dt Ges Geowiss* 158(4):921–930
- Migon P (2006) *Granite landscapes of the world*. Oxford University Press, Oxford
- Mustoe GE (1982) The origin of honeycomb weathering. *Geol Soc Am Bull* 93:108–115
- O'Rourke JE (1989) Rock index properties for geo-engineering in underground development. *Min Eng* 1989(2):106–110
- Pamplona M, Kocher M, Snethlage R et al (2007) Drilling resistance: overview and outlook. *Z dt Ges Geowiss* 158:665–676
- Paoletti D, Schirripa Spagnolo G (1996) Interferometric methods for artwork diagnostics. *Prog Opt* 35:197–255
- Patitz G, Illich B, Wenzel F (1999) Zerstörungsarme Voruntersuchungen an der Steinernen Brücke Regensburg—Vortrag und Bericht. In: Wittmann FH, Gerdes A (eds) *Proceedings of the 5th international colloquium material science and restoration*. Aedificatio Publishers, Freiburg, Unterengstringen, pp 1069–1084
- Pfefferkorn S (1998) Untersuchung des Einflusses des Bohrverschleißes auf das Ergebnis von Bohrwiderstandsmessungen. *Restor Build Monum* 4:467–478
- Pfefferkorn S (2000) Correction functions for eliminating drill bit abrasion and blocked drill dust transport. In: Tiano P (ed) *Proceedings of the workshop DRILLMORE*, Firenze, pp 67–74
- Pfefferkorn S (2005) Beurteilung von Verwitterungserscheinungen an Natursteinoberflächen mit dem Bohrwiderstand-Messverfahren. In: Siegesmund S, Auras M, Snethlage R (eds) *Stein: Zerfall und Konservierung*. Edition, Leipzig, pp 155–159
- Pfefferkorn S, Siedel H (1999) Einfluss der Materialfeuchte auf die Ergebnisse des Bohrwiderstand-Messverfahrens an Sandsteinen verschiedener Gefügetypen. In: Wittmann FH, Gerdes A (eds) *Proceedings of the 5th international colloquium material science and restoration*, Aedificatio Publishers, Freiburg, Unterengstringen, pp 1559–1568
- Poesen JW, Torri D, Bunte K (1994) Effects of rock fragments on soil erosion by water at different spatial scales: a review. *Catena* 23:141–166
- Potts BD, Santamarina JC (1993) Geotechnical tomography. *ASTU* 16:510–517

- Portillo MC, Gonzalez JM, Saiz-Jimenez C (2008) Metabolically active microbial communities of yellow and grey colonizations on the walls of Altamira Cave, Spain. *J Appl Microbiol* 104:681–691
- Prieto B, Silva B, Aira N et al (2006) Towards a definition of a bioreceptivity index for granitic rocks. Perception of the change in appearance of the rock. *Int Biodeterior Biodegrad* 58:150–154
- Queisser A (1986) Geotechnische und mineralogische Bewertung von Naturwerksteinen aus dem Raum Bamberg. PhD thesis, unpublished, 153 pp., University of Mainz
- Raccomandazione Normal 1/88 (1990) Alterazioni Macroscopiche dei Materiali Lapidei: Lessico (Macroscopic alterations of stone materials: glossary). CNR-ICR, Comas Graphica, Rome, 36 pp
- Rastogi P, Inaudi D (eds) (2000) Trends in optical nondestructive testing and inspection. Elsevier, Amsterdam
- Robinson DA, Williams RBG (1994) Sandstone weathering and landforms in Britain and Europe. In: Robinson DA, Williams RBG (eds) Rock weathering and landform evolution. Wiley, Chichester, pp 371–391
- Ruedrich J, Hettrich M, Just A et al (2004) Construction physics of the market gate of miletus discovered by non-destructive tools. In: Kwiatkowski D, Löfvendahl R (eds) Proceedings of the 10th international congress on deterioration and conservation of stone, Vol 2. Stockholm, pp 745–752
- Ruedrich J, Rieffel Y, Pirsakewitz S et al (2010) Development and assessment of protective winter covers for marble statues of the Schlossbrücke, Unter den Linden, Berlin, Germany. *Environ Earth Sci* 69:1451–1469
- Ruedrich J, Siegesmund S, Richter D (2001) Marble columns and its state of weathering: structural evidences and US-tomography. *Zt dt Geol Ges* 152:665–680
- Ruedrich J, Knell C, Enseleit J, Rieffel Y, Siegesmund S (2013) Stability assessment of marble statues of the Schlossbrücke (Berlin, Germany) based on rock strength measurements and ultrasonic wave velocities. *Environ Earth Sci* 69:1451–1469
- Sachpazis CI (1990) Correlating Schmidt hardness with compressive strength and Young's modulus of carbonate rocks. *Bull Int Assoc Eng Geol* 42:75–83
- Schabereiter-Gurtner C, Piñar G, Lubitz W et al (2001) An advanced strategy to identify bacterial communities on art objects. *J Microbiol Methods* 45:77–87
- Schechter RS, Mignogna DB, Delsano PP (1996) Ultrasonic tomography using curved ray paths obtained by wave propagation simulations on a massively parallel computer. *J Acoust Soc Am* 100(4):2103–2121
- Schickert M (1995) Einfluss der frequenzabhängigen Schallschwächung auf die Ultraschall-Laufzeitmessung an mineralischen Stoffen. In: Proceedings of the DGZfP-Jahrestagung Zerstörungsfreie Materialprüfung 1994. DGZfP, Berlin, pp 479–485
- Schlütter F, Juling H (2002) Mikroskopische Untersuchungen an Testflächen. In: Schmuhl B (ed) Kalksteinkonservierung am Westportal des Halberstädter Domes St. Stephan und St. Sixtus, Domstiftung Sachsen-Anhalt, Leitzkau, pp 129–162
- Schmidt E (1951) A non-destructive concrete tester. *Concrete* 59:34–35
- Schneider C, Ziesch J, Bauer A et al (2008) Bauwerkskartierung zur Analyse des Verwitterungsstatus an den Außenmauern des Schlosses von Buda (Budapest, Ungarn). In: Siegesmund S, Sneath R (eds) Denkmalgesteine–W.-D. Grimm-Festband. Schriftenreihe der Deutschen Gesellschaft für Geowissenschaften 59:219–235
- Siedel H (2010) Alveolar weathering of Cretaceous building sandstones on monuments in Saxony, Germany. In: Prikryl R, Török A (eds) Natural Stone Resources for Historical Monuments. Geological Society, London, Special Publications 333:11–23
- Siedel H (2013) Recording natural stones on facades as a tool to assess their utilization and functional aspects over time. *Quart J Eng Geol Hydrogeol* 46:439–448
- Siedel H, Hubrich K, Kusch HG et al (2000) Results of laser cleaning on encrusted oolithic limestone of angel sculptures from the Cologne Cathedral. In: Fassina V (ed) Proceedings of

- the 9th International Congress on Deterioration and Conservation of Stone, Vol 2. Venice, pp 583–590
- Siedel H, Neumeister K, Sobott RG (2003) Laser cleaning as a part of the restoration process: removal of aged oil paints from a Renaissance sandstone portal in Dresden, Germany. *J Cult Heritage* 4, Issue Supplement 1:11–16
- Siedel H, Pfefferkorn S, von Plehwe-Leisen E et al (2010) Sandstone weathering in tropical climate: results of low-destructive investigations at the temple of Angkor Wat, Cambodia. *Eng Geol* 115:182–192
- Siegesmund S, Kracke T, Ruedrich J et al (2009) Jewish cemetery in Hamburg Altona (Germany). State of marble deterioration and provenance. *Eng Geol* 115(3–4):200–208
- Siegesmund S, Nikolayev D, Mosch S et al (2008a) Bowing potential of granites. *Environ Geol* 55:1437–1448
- Siegesmund S, Pretzschner C, Ruedrich J et al (2000) Deterioration characteristics of columns from the Marmorpalais Potsdam (Germany) by US-tomography. In: Fassina V (ed) Proceedings of the 9th international congress on deterioration and conservation of stone, Vol 1. Venice, pp 145–153
- Siegesmund S, Ruedrich J, Koch A (2008b) Marble bowing: comparative studies of different public building facades. *Environ Geol* 56:473–494
- Siegesmund S, Török A, Hüpers A, Müller Chr, Klemm W (2007) Mineralogical, geochemical and microfabric evidences of gypsum crusts: a case study from Budapest. *Environ Geol* 52: 385–397
- Siegesmund S, Weiss T, Ruedrich J (2004) Schadensmonitoring mittels Ultraschalldiagnostik. *Restauro* 2:98–105
- Simon C, Daniel R (2011) Metagenomic analysis: past and future trends. *Appl Environ Microbiol* 77:1153–1161
- Singh RN, Hassani FP, Elkington PAS (1983) The application of strength and deformation index testing to the stability assessment of coal measures excavations. In: Proceedings of the 24th US symposium on rock mechanics, Texas A and M University, pp 599–609
- Sneath R, Ettl H, Sattler L (1999) Ultraschallmessungen an PMMA-getränkten Skulpturen. *Z dt geol Ges* 150:387–396
- Sneath R, Wendler E (1989) Der Wassereindringprüfer nach Karsten-Anwendung und Interpretation der Messwerte. *Bautenschutz und Bausanierung* 12:110–115
- Sneath R, Wendler E (1995) Methoden der Steinkonservierung—Anforderungen und Bewertungskriterien. Anhang: Zusammenstellung der in der Steinkonservierung häufig verwendeten Prüfmethode. In: Sneath R (ed) *Denkmalpflege und Naturwissenschaft. Natursteinkonservierung I*. Ernst und Sohn, Berlin, pp 22–40
- Stadlbauer E, Wendler E (1998) Messung der kapillaren Wasseraufnahme und des Bohrwiderstandes. *Arbeitsheft Denkmalpf Nieders* 15:79–82
- Stender H, Fiandaca M, Hyldig-Nielsen JJ et al (2002) PNA for rapid microbiology. *J Microbiol Methods* 48(1):1–17
- Sterflinger K, Prillinger H (2001) Molecular taxonomy and biodiversity of rock fungal communities in an urban environment (Vienna, Austria). *Antonie Van Leeuwenhoek* 80:275–286
- Stück H, Siegesmund S, Ruedrich J (2011) Weathering behaviour and construction suitability of dimension stones from the Drei Gleichen area (Thuringia, Germany). *Environ Earth Sci* 63(7–8):1763–1786
- Stück H, Plagye R, Siegesmund S (2013) Numerical modeling of moisture transport in sandstone: the influence of pore space, fabric and clay content. *Environ Earth Sci* 69:1161–1188
- Taylor S, May E (2000) Investigations of the localisation of bacterial activity on sandstone from ancient monuments. *Int Biodeterior Biodegrad* 46:327–333
- Tewary VK, Fortunko CM (1996) Theory of elastic waves in three dimensional anisotropic plates. *J Acoust Soc Am* 100:2964–2968
- Tornari V, Zafropoulos V, Vainos NA et al (2000) Discrimination of photomechanical effects in the laser cleaning of artworks by means of holographic interferometry. In: Fotakis C,



- Papazoglou T, Kalpouzas C (eds) Optics and lasers in biomedicine and culture. Springer, Berlin
- Török A, Licha T, Simon K, Siegesmund S (2011) Urban and rural limestone weathering; the contribution of dust to black crust formation. *Environ Earth Sci* 63:675–693
- Török A, Müller C, Hüpers A et al (2007) Differences in texture, physical properties and microbiology of weathering crust and host rock: a case study of the porous limestone of Budapest (Hungary). In: Prikryl R, Smith BJ (eds) *Building Stone Decay: From Diagnosis to Conservation*. Geological Society, London, Special Publications 271:261–276
- Turkington AV, Paradise TR (2005) Sandstone weathering: a century of research and innovation. *Geomorphology* 67:229–253
- Tveit A (1966) Measurements of moisture sorption and moisture permeability of porous materials. Rapport 45. Norwegian Building Research Institute, Oslo
- Urzi C, La Cono V, De Leo F et al (2003) Fluorescent in situ hybridization (FISH) to study biodeterioration. In: Saiz-Jimenez C (ed) *Molecular biology and cultural heritage*. Lisse, the Netherlands, Balkema Publishers, pp 55–60
- Vellone DA, Merguerian C (2007) Measuring engineering properties of NYC rocks using a Schmidt rebound hammer-preliminary results. In: Hanson GN (ed) *Proceedings of the 14th annual conference on geology of Long Island and metropolitan New York*, State University of New York at Stony Brook, NY, Long Island Geologists Program with Abstracts, 7 pp
- Vergès-Belmin V, Rolland O, Leroux L (2008) Can we be confident in colour measurements performed outdoors? In: Lukaszewicz JW, Niemcewicz P (eds) *Proceedings of the 11th international congress on deterioration and conservation of stone*, Vol 1. Torun, pp 267–274
- Weber J, Burszan R (2008) Salt-induced decay of interior walls and climate control. The case study of Virgil's Chapel, Vienna. In: *Proceedings of the international conference on salt weathering on buildings and stone sculptures*, Copenhagen, Technical University of Denmark, pp 257–267
- Wedekind W, Middendorf B, Siegesmund S (2010) Denkmalgerechte Ruinensicherung. In: Siegesmund S, Hoppert M (eds.) *Die Drei Gleichen: Baudenkmäler und Naturraum*. Edition Leipzig, pp 160–201
- Wedekind W, López-Doncel R, Dohrmann R, Kocher M, Siegesmund S (2013) Weathering of volcanic tuff rocks caused by moisture expansion. *Environ Earth Sci* 69:1203–1224
- Weise F, Patitz G (2005) *Moderne Methoden der Bauwerksdiagnostik in der Praxisanwendung*. In: Siegesmund S, Auras M, Snethlage R (eds) *Stein-Zerfall und Konservierung*. Edition, Leipzig, pp 140–149
- Weiss T, Fuller EH, Jr, Siegesmund S (2002a) Thermal expansion and its control on the durability of marbles. In: Siegesmund S, Weiss T, Vollbrecht A (eds) *Natural stone, weathering phenomena, conservation strategies and case studies*. Geological Society, London, Special Publication 205:57–72
- Weiss T, Leiss B, Oppermann H et al (1999) Microfabric of fresh and weathered marbles: implications and consequences for the reconstruction of the Marmorpalais Potsdam. *Z dt geol Ges* 150:313–332
- Weiss T, Rasolofosaon PNJ, Siegesmund S (2001) Thermal microcracking in Carrara marble. *Z dt geol Ges* 152(2–4):621–636
- Weiss T, Rasolofosaon PNJ, Siegesmund S (2002b) Ultrasonic velocities as a diagnostic tool for the quality assessment of marble. In: Siegesmund S, Weiss T, Vollbrecht A (eds) *Natural stone, weathering phenomena, conservation strategies and case studies*. Geological Society, London, Special Publications 205:148–164
- Weiss T, Siegesmund S, Rasolofosaon P (2000) The deterioration-velocity-porosity-relation constraint. In: Fassina V (ed) *Proceedings of the 9th international congress on deterioration and conservation of stone*, Vol 1. Venice, pp 215–223
- Wendler E, Sattler L (1996) Bohrwiderstandsmessung als zerstörungsarmes Prüfverfahren. In: Wittmann FH, Gerdes A (eds) *Proceedings of the 4th international colloquium material science and restoration*, Aedificatio Publishers, Freiburg, Unterengstringen, pp 145–160

- Wittmann FH (1983) Mesures de l'effet consolidant d'un produit traitement. *Materiaux Construction* 16:235–342
- Yates T, Brundin JA, Goltermann P et al (2004) Observations from the inspection of marble cladding in Europe. In: Prikryl R (ed) *Dimension stones*. AA Balkema Publishers, Leiden, pp 267–276
- Zvelebil J, Cilek V, Stemberk J (2002) Partial results of monitoring of stability deterioration on Pravičice Rock Arch, NW Bohemia. In: Prikryl R, Viles HA (eds) *Understanding and managing stone decay*. The Karolinum Press, Prague, pp 243–261

# Chapter 7

## Stone Conservation

Rolf Sneathlage

**Abstract** Since antiquity, replacement and repair of damaged stone has been practised to delay the deterioration of buildings and monuments. Today, the aim of stone conservation is the preservation of these historic and/or artistic objects for future generations in the state in which we have received them. The approach that has been taken to address this challenge has direct links to the emergence of chemistry in the 19th century. Chemicals such as water glass, fluorosilicates and ethyl silicate were tested as consolidants for stone shortly after their synthesis in the laboratory. After World War II, organic compounds, such as acrylic and epoxy resins found their way into conservation practice. This chapter deals with all the steps required in a conservation intervention, such as the problems presented by cleaning as well as those of desalination. It includes a review of conservation materials, such as consolidants, water repellents and biocides. Silicon organic compounds are given special attention since they are the main chemicals used in the formulation of both consolidants and water repellents. The requirements for the various mortars that may be needed, including renders, as well as that of other finishes such as paints and antigrffiti coatings are also discussed.

### 7.1 Introduction

The Athens Charter for the Restoration of Historic Monuments, adopted by the First International Congress of Architects and Technicians of Historic Monuments in Athens in 1931 (ICOMOS 1996), is the first international document formulating

---

Sect. 7.11 by Katja Sterflinger.

---

R. Sneathlage (✉)

Natural Stone, Building Chemistry and Building Physics for the Conservation of Monuments, Wetzelstraße 24, 96047 Bamberg, Germany  
e-mail: rolf@sneathlage.net

general principles for the maintenance and restoration of historic monuments. The conference experts stated that “monuments throughout the world were being threatened to an ever increasing degree by atmospheric agents”. To delay their further decay they recommend “... the judicious use of all resources at disposal of modern technique and more especially of reinforced concrete”, further recommending that this work of consolidation should be concealed in order not to impair the aesthetic integrity of the monument.

It took no less than 33 years for this organization to re-examine the principles of the Athens Charter during the 2nd International Congress held at Venice in 1964. The revised guidelines were summarized in the Venice Charter (ICOMOS 1966). Concerning the use of modern materials in restoration and conservation the Venice Charter in its article 10 states that “... where traditional techniques prove inadequate, the consolidation of a monument can be achieved by the use of any modern technique for conservation and construction, the efficacy of which has been proven by scientific data and experience.” It has been often argued that reversibility of any measure undertaken on a monument is one of the basic demands of Venice Charter and should apply to chemical as well as mechanical methods. This is not the case. The Venice Charter does not exclude innovative methods to be used on historic buildings; rather, its main intention is the careful and considerate use of those materials whose long term behavior has not been yet proven. Reversibility also has been misattributed to Brandi, a well-known art historian with a large amount of practical experience. In fact, the concept behind reversibility can be traced to Plenderleith, the first director of ICCROM, who stated during the 1972 North American International Regional Conference “In conservation work, there is a dictum that nothing should be done that cannot, if necessary, be undone easily in the future” (Plenderleith 1976). It took many years until this concept was re-elaborated into what Brandi had called the third principle in his book “Theory of Restoration” (Brandi 1963) that each restoration treatment should not impede but rather facilitate any future treatment.

The scientific community began to reflect whether reversibility could be a feasible objective at all and after another 30 years, it was suggested that the word “reversibility” be replaced by “retreatability” (Petzet 1993; Teutonico et al. 1997). The question was further discussed at several conferences held in London, Torino and Bressanone between the years 1999 and 2003, as analyzed by Giusti (2006). The outcome of these discussions and considerations finally resulted in the consent to replace the ideal, and therefore unattainable, reversibility by the more practical demand for retreatability and to highlight the importance of compatibility.

The concept of retreatability and that of compatibility provide the framework for a strictly scientific approach to the problems of conservation and restoration. They require the selection of parameters relevant to assess the state of a material before and after treatment and to evaluate the effectiveness of a conservation agent in comparison to other chemicals tested. They also require the documentation of the undertaken measures and an on-going, regular monitoring of the monument in order to obtain the necessary knowledge regarding the long-term durability of

treatments. Since the theoretically ideal treatment is never achievable in practice, the best that can be done is to introduce tolerance limits. These, in turn, have to be derived from laboratory measurements and practical observation on buildings.

“Conservation—restoration—renovation” are the three essential concepts in the field of preservation of historic/artistic objects. They differ with respect to goals pursued with the measures undertaken on an object. Definitions of the terms are given for instance by Petzet (1993).

“Conservation” aims to preserve the monument in its present state and within the historic setting we have received it. It avoids, wherever possible, any additions to complete missing parts, except those which are absolutely necessary for its future preservation, for instance, to prevent water penetration. Existing deterioration is repaired and the long-term preservation may be improved by strengthening the material. “Remedial Conservation” does not address active deterioration factors that affect the object. On the other hand, “Preventive Conservation” addresses environmental factors that are the cause for deterioration. Under outdoor conditions, this could mean the erection of a shelter, under indoor conditions the installation of climate control to stabilize the temperature and relative humidity of the air.

“Restoration” aims at the sustainable preservation of a monument. In cases where deterioration is widely advanced, the concept of “Restoration” accepts the addition of missing parts or the filling of lacunae with new stone or with repair mortars. Similarly, the restoration of irritating aesthetic damage of religious objects, for example, a destroyed face, is acceptable in order to present the object of veneration in a suitable condition to its function.

“Renovation” aims to recreate the “original appearance” by either totally overworking the surface or by completing all missing parts. Renovation can also refer to the replacement of the original by a new copy. Therefore, renovation cannot be considered in the spirit of conservation. Furthermore, the replaced originals are stored away, in many cases, under inappropriate conditions. There are innumerable repositories worldwide where valuable originals fade away. They can be visited, but they are not readily found.

This chapter mainly deals with those methods that are in use within the conservation definition but are also applicable when considering restorations. The sequence of the sections follows the steps necessary when a conservation intervention is carried out in practice.

## 7.2 Historic and Actual Stone Conservation Compounds

Since antiquity, replacement of deteriorated stone has been a well-known problem in the conservation of architectural heritage. Buildings were mostly erected with stones from nearby quarries. Some may have been of good quality, but many had poor weathering resistance. Probably the earliest example of stone restoration is the Great Sphinx in Giza (2700–2600 BC). Buried under sand for centuries, it had

**Fig. 7.1** Great Sphinx in Gizah. Replacement stone from the first restoration under Pharaoh Thutmose IV



been excavated and restored for the first time by Pharaoh Thutmose IV (1400 BC). The square stones then put in place for re-shaping the decayed surface of the Sphinx can still be seen today (Fig. 7.1).

Further excavation followed in Roman times under Marc Aurelius and Septimius Severus. In 1925/1926 Émile Baraize repaired the Sphinx with new limestone and mortar. The relatively perfect shape of the back head of the Sphinx is the result of this restoration campaign, clearly documented by the imprints of the plank lining used to apply the restoration mortar.

The complexity of preserving large historic stone structures, such as cathedrals, demonstrates the necessity of regular maintenance and repair. It is for this reason that cathedrals undergo regular inspection by the so-called cathedral architects and the required repairs are then carried out by specially qualified stone masons. Several cathedrals have their own stone workshops, keeping up a long tradition, like York, Cologne, Bale, Vienna and many others. The stone mason workshop of Strasbourg Cathedral has existed since the erection of the building. In these cases, the preferred restoration method is the replacement of damaged stone, which can be justified by the complication posed by scaffolding needed to do the work. Thus,



a replacement that can be expected to last for at least another 50 years is justified when compared to a conservation treatment that could probably only last 30 years and especially considering that this would require regular monitoring.

For centuries, the only conservation materials available for repairing small defects or applying preventive conservation layers were lime, plaster of Paris, linseed oil, wax, animal and vegetable glues. Lime with casein admixtures as well as mixtures of animal and vegetable glue were used to produce mortars for filling lacunae. Broken parts were glued together with bone glue or shellac, and if heavy pieces were involved, they were fixed with bronze or iron clamps or pins. The repair of indoor sculptures made of marble or limestone was carried out using a mixture consisting of finely ground gypsum and animal glue. This mixture is practically identical to that used for making artificial marble “stucco lustrum” and can be colored and polished in whatever desired manner.

For outdoor location, bees wax provided shiny gloss and water repellency to limestone and marble tombstones. Bees wax is by far the most frequently used wax, available in different grades with increased refinement, i.e., through bleaching. Its acidity is an important parameter because the fatty acids contained in it can attack susceptible surfaces. Bees wax has the advantage of not becoming brittle even after decades, but has the disadvantage of remaining sticky so that dust deposition is increased (Fig. 7.2). It can be applied either heated to a liquid state or dissolved in turpentine or spirit. Because it does not crosslink, it can be easily removed by hot water or steam together with a little detergent, even after long time. Modern waxes for stone care are based on a mixture of microcrystalline paraffin waxes obtained from petroleum distillation. They have a higher melting temperature than beeswax so that they are not sticky at normal temperatures.

In former times, paints were used with the double purpose of decorating and protecting monument surfaces. The binding media of historic paints was lime by itself or in combination with casein, protein and oil, e.g., linseed oil. The latter paints are more stable under outdoor conditions since they provide some water repellency. The linseed oil formulation with lead white, a basic lead carbonate, has been extensively used for painting park sculptures. More information about paints will be given in [Sect. 7.8](#).

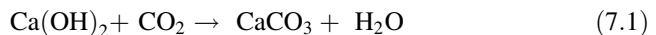
Scientific investigations into deterioration and conservation of building stone began in the 19th century. Its development reflects the general progress in chemical research. The products were primarily synthesized for industrial applications but soon recommended for conservation to open new sales as is still the practice nowadays. Initially, conservation was focused in the preservation of the many works of art that entered European museums after having been excavated in the Mediterranean countries. Rathgen (1915) published the first scientific research report about conservation of archaeological finds that has remained exemplary for many decades. Comprehensive bibliographies on historic sources of stone conservation were compiled by Lewin (1966), Riederer (1973), and Wheeler (2005). A rather complete compilation of commercially available stone conservation products from 1840 to 1940 can be found in Herm et al. (1998).

**Fig. 7.2** Red nodular limestone epitaph from outside wall of the parish church in Wasserburg Germany. *Dark areas* correspond to bees wax layers *blackened* by soot deposition. The *light areas* are those where the rain water runs over the surface removing both the soot and the bees wax



### 7.2.1 Limewater, Lime Wash and Barita Water

Limewater is a saturated solution of  $\text{Ca(OH)}_2$ , which contains 0.18 g  $\text{Ca(OH)}_2$  per liter of water. To consolidate a deteriorated and poorly cohesive stone it has to be soaked with limewater several times, a procedure that takes weeks or month because between the applications the stone must dry out completely. The idea is to reinforce the poor binding material by new calcium carbonate deposited inside the pores according to the reaction



Given the low solubility of  $\text{Ca(OH)}_2$  the total amount of deposited  $\text{CaCO}_3$  is consequently very small and measurable strength increase has never been proven (Price 1984). Furthermore, the crystals are mainly formed near the surface where the  $\text{Ca(OH)}_2$  can most quickly react with the  $\text{CO}_2$  from the ambient air. A critical review of this method has been made by Hansen et al. (2003). The method has serious negative effects due to the enormous quantities of water applied to the stone,

which may mobilize and precipitate salts from inside the stone. The fine calcite crystals may also lead to whitish discolorations. An even more negative effect is the high alkalinity of limewater ( $\text{pH} = 11$ ). The high pH will moreover mobilize soluble iron compounds, which may cause brownish discolorations. In addition, the alkaline pH increases the deposition rate of acidic air pollutants like  $\text{NO}_x$  and  $\text{SO}_2$  so that all of the newly formed  $\text{CaCO}_3$  will be dissolved again in very short time.

Lime washes are thin layers of very fine lime mortar with a thickness of a few millimeters and not exceeding 5 mm. They can be considered to fall between lime paints and renderings. Their main function is to serve as a sacrificial layer and thus to protect limestone surfaces from rain and air pollutants. Because it is a thin sacrificial layer it wears down in a relatively short time, but it can be renewed by a new layer as has been done traditionally thus providing regular protection to the surface. In recent years, the method has received increasing attention in several European countries, based on the criteria of compatibility and retreatability. It is to be stressed that while it is a simple method to apply it requires permanent monitoring and frequent reapplication, in a word, regular maintenance.

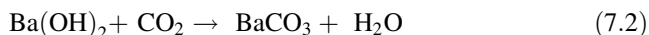
During the decades of the 1970s and 1980s, lime wash applications were very popular in United Kingdom following the traditions from south and middle England. These developed there since most of the historic buildings and cathedrals were built of a porous oolitic limestone (Portland limestone) eminently more compatible to lime washes than any other natural stones. It is to be highlighted that the English approach, the “lime method” relies on a three part operation beginning with limewatering, followed by mortar repairs and ending in the application of the lime wash, usually referred to as a shelter coat. This is rubbed into surface cracks and delaminating flakes with soft brushes thus stabilizing the sensitive surface parts. The most famous example in UK is the treatment of the sculptures and traceries of the west façade of Wells Cathedral during the restoration of the whole façade in the 1980s, which is reported and evaluated in many publications (Caroe 1985; Ashurst and Dimes 1990; Butlin et al. 1991; Martin 2000b; Woolfitt 2002). Besides some aesthetical constraints the authors come to positive results of the lime method with respect to the protection of the façade against driving rain.

Following the English example, a campaign was launched in Austria to protect valuable historic facades with lime based sacrificial layers (Nimmrichter and Koller 2000; Nimmrichter et al. 2000). It was found that the pure lime sacrificial layer was washed away in direct rain exposed areas within 1 year. A better durability was achieved with a modified lime wash added with a few percent of an organic polymer dispersion.

Good experiences were obtained with the application of sacrificial layers made of silicone emulsion paint to the flying buttresses, in Krenshheimer Shell Limestone, of the Cologne Cathedral (Wolff 1996, 1997, 1998; Schock-Werner 1999). This modern paint system contains very fine particle filler, mainly calcite and some talc, in acrylic and silicone resin dispersion as binder. While pure lime washes were worn down within a short time, the recent applications made with this silicone emulsion lime paint have performed better. Its water repellency does not significantly reduce water vapor diffusion or the drying rate of the stone.

Because of its high filler to binder ratio much of the fine calcite aggregates are exposed. Therefore, they may be partly dissolved by rain, acting as a sacrificial layer similarly to pure lime washes, but their overall durability is extended by the high weathering stability of the binder that protects the rest of the filler.

Dissolved barium hydroxide has also been used to consolidate stone but to much lesser extent than limewater. The basic concept is similar to that of lime-water. The reaction with  $\text{CO}_2$  from the air forms the stable and insoluble mineral witherite,  $\text{BaCO}_3$ , is formed:



The solubility of  $\text{Ba(OH)}_2$  in water is much higher than that of  $\text{Ca(OH)}_2$ , however, strongly temperature dependent. Related to water-free  $\text{Ba(OH)}_2$  the solubility ranges from 27.3 g/L in cold water to 462 g/L in hot water. Theoretically, the application of a barium hydroxide solution could be successful because there is a sufficient concentration in the liquid to produce a strengthening deposit in the pores. In practice, however, in most cases gray-whitish surface deposits form on the treated monuments because the rather slow reaction with  $\text{CO}_2$  will occur first on the surface. Consolidation reaching greater depth therefore cannot be expected. Hansen et al. (2003) also discuss this approach in detail. Again, the high alkalinity of the solution (pH 12) may result in the mobilization of iron compounds with the consequent discoloration.

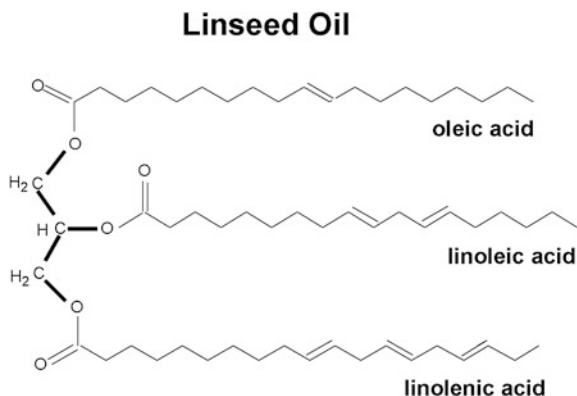
## 7.2.2 *Linseed Oil*

Linseed oil belongs to the group of unsaturated drying oils. It is obtained by pressing dried ripe seeds of the flax plant. Chemically, it is an ester of tri-basic glycerin and unsaturated fatty acids such as oleic acid (single unsaturated), linoleic acid (twofold unsaturated) and linolenic acid (threefold unsaturated) with minor amounts of saturated fatty acids such as palmitic and stearic acid. The average concentration of these acids is: 20 % (oleic); 24 % (linoleic); 47 % (linolenic); 6 % (palmitic) and 2.5 % (stearic). The backbone of the structure is formed by the three-basic alcohol glycerin. A structure of linseed oil is shown in Fig. 7.3.

Linseed oil is commercially available in different grades depending on the degree of refining. Stand oil is obtained by heating raw linseed oil in closed vessels, in the absence of air, up to 250 °C. By this process, the double bonds react with each other, thus forming larger molecular units. Stand oil is therefore more viscous than raw linseed oil. The drying process of linseed oil is enhanced by lead compounds, such as lead white, and for this reason it is the typical constituent of the so-called lead white paints (for further information see Sect. 7.8).

For centuries, probably even since antiquity, linseed oil has been used for stone preservation mainly to turn surfaces water repellent. From 1850 to 1950 it was the main constituent in many commercial products partly as pure linseed oil, partly

**Fig. 7.3** Chemical structure of linseed oil



with admixtures like paraffin (Herm et al. 1998) and was applied to sandstone as well as limestone. To improve penetration, linseed oil has been heated to lower viscosity. Stois (1935) underlines both its water repellent as well as consolidating effect. With time the dried linseed oil is subject to increasing resinification causing a decrease of hydrophobicity and increasing brittleness. However, yellow and brown discolorations make linseed oil unacceptable to stone.

### 7.2.3 Fluosilicates

Fluosilicates are salts of fluosilicic acid  $\text{H}_2\text{SiF}_6$  and they were first synthesized by Kessler in 1883. Different salts can form depending on the cations, e.g., Mg, Zn, Pb, Al,  $\text{NH}_4$  and others. The most common ones are those of Mg and Zn. By the 1930s several patents had been granted to various formulations of fluosilicates, mostly in combination with water repellent compounds (Lewin 1966; Herm et al. 1998; Wheeler 2005). These products were applied to many objects in various countries, such as the UK (Schaffer 1931) and Germany (Hörmann 1913). A very famous example of fluosilicate treatment is the consolidation of the figure pairs of the Fürstenportal of Bamberg Cathedral in 1903/1904.

Still today fluosilicates are applied to improve the density of pores and the chemical resistance of concrete surfaces. This is called “fluatation” or fluosilicate sealing. The strengthening effect is based on the formation of amorphous silica gel. As its application on concrete indicates, fluosilicates need calcium or other alkalis to react. Two different chemical equations describing the reaction with concrete and calcite containing sedimentary stones can be found in literature:

In concrete, the reaction is preferential with the portlandite,  $\text{Ca}(\text{OH})_2$ :



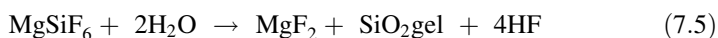
For limestone and calcareous sandstone, the reaction is preferential with the calcite,  $\text{CaCO}_3$ :



The sealing or consolidation occurs by the formation of the silica gel. The formation of  $\text{CaF}_2$  is a consequence of the etching of the calcite crystals, as is the case for teeth with fluoride treatments. The  $\text{MgF}_2$  by product has never been clearly identified and is probably included within the silica gel formed.

Practical experience shows that the silica gel is precipitated mostly on the very surface thus leading to a high strength increase in the uppermost 1 or 2 mm. Therefore, fluosilicates can be harmful to stones with weakened surface zones because the brittle consolidated surface layer is likely to delaminate from the weaker subsurface. The high acidity of fluosilicate solutions can also discolor iron oxide containing stone.

In the presence of water  $\text{Mg}_2\text{SiF}_6$  decomposes:



In this case, the highly aggressive hydrofluoric acid HF is formed. This acid, used to etch glass, will react with any siliceous material with the formation of the volatile  $\text{SiF}_4$ . Therefore it will readily attack sandstones and granites, etching quartz and feldspars, as well as the silicates present in the concrete. However, for this last material, the overall reaction is one of densifying the surface. While this may be a desirable effect for concrete structures, this is not the case for historic stone structures.

The aggressiveness of the fluosilicates in general and the toxicity of the HF in particular do not make this a user-friendly method. Consequently, fluosilicates have no longer a practical application in stone conservation, since the consolidation obtained by the silica gel deposition can be obtained in a far better way with the silicate esters discussed in [Sect. 7.2.9](#).

## 7.2.4 Waterglass

The synthesis of water glass can be summarized by the following steps:

- 1818: synthesis of sodium waterglass by Fuchs.
- 1847: synthesis of potassium waterglass by Kuhlmann.
- 1878: invention of “Stereochromy” by A W Keim.

Waterglass is produced by melting pure quartz sand with alkali carbonates such as sodium or potassium carbonate at temperatures around 1,300 °C. The molten alkali silicate has a structure similar to glass with randomly distributed  $\text{SiO}_4$  tetrahedra. The quenched solid waterglass is then ground and dissolved in water at a temperature between 120 and 150 °C and a pressure of 2–5 bars. In commercial waterglass the  $\text{SiO}_2/\text{M}_2\text{O}$  molar ratio (where  $\text{M} = \text{Na}$  or  $\text{K}$  or both) is about 4:1. In aqueous solution the silicate anion is polymerized to nearly spherical particles, which consist of ca. 90  $\text{SiO}_2$  units linked by oxygen bridges (Osswald and Snethlage 1996).



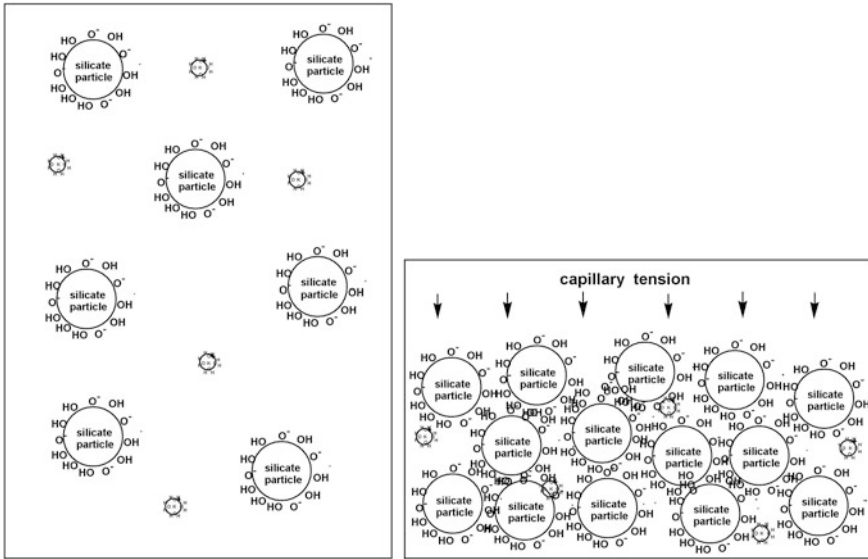
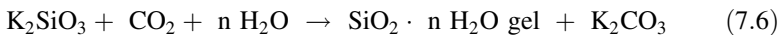


**Fig. 7.4** Schematic representation of the inner structure of a water glass solution (Figure by Osswald)

On the surface of each particle, which has a size of 2–3 nm, the oxygen atoms are hydroxylized so that each Si atom at the surface of a spherical particle is linked to one OH group. The potassium or sodium cations, which stabilize the solution, are hydrated with a water shell. Waterglass solutions have a very high pH of 12 (see Fig. 7.4).

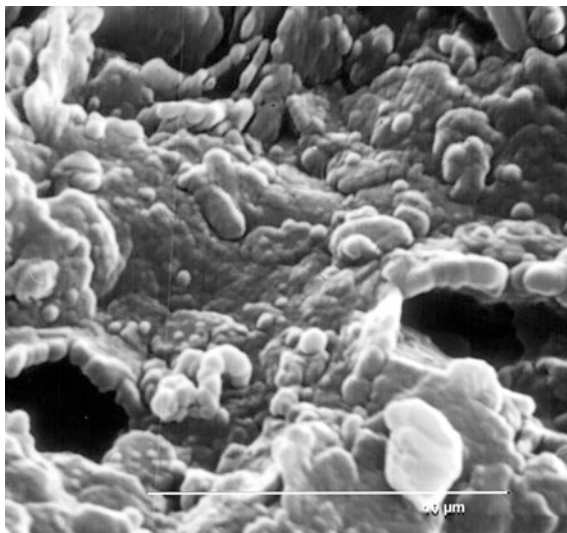
In recent years lithium waterglass attracted some interest as an alternative product for stone consolidation because the lithium carbonate formed by reaction with CO<sub>2</sub> from the atmosphere is by far less soluble than potassium and sodium carbonate formed when using regular sodium potassium waterglass. The product, however, did not pass laboratory testing phase most likely because of its far higher price.

In practice the aqueous water glass solutions are applied either ready made or diluted. The reaction to form amorphous silica gel can be explained by the presence of atmospheric CO<sub>2</sub> according to the equation:



In principle, this reaction should be very slow because of the low concentration of CO<sub>2</sub> in the air. In practice however, the silica gel precipitates spontaneously when the water glass solution gets in contact with the surface of a porous material as water is withdrawn from the solution and the relatively big silicate particles coalesce. Consequently, the solution is increasingly concentrated until the negatively charged solid silicate particles come into such close contact that the

**Fig. 7.5** Aggregates of silica gel formed from waterglass. SEM photo



Si–OH-groups on their surfaces condense to Si–O–Si siloxane bonds. Thus resultant macro particles immediately precipitate out of the solution (Osswald and Snethlage 1996). The process is depicted in Fig. 7.4.

A SEM picture of the silica gel formed from waterglass is shown in Fig. 7.5. Unlike the gel formed from tetraethoxysilane (TEOS. See Sect. 7.6) the gel is composed of irregularly formed spheres, which are compacted to a solid layer. The shape of the gel still resembles the spheric silica particles in the waterglass solution.

This fast reaction also explains why waterglass is not appropriate for consolidation of stones. Since the silica compound is retained on the surface the penetration depth is extremely low and a brittle surface layer is formed. Only water and the alkali ions penetrate deeper into the pore space. The strongly consolidated zone hardly exceeds 1 or 2 mm and risks spalling off from the underlying softer unconsolidated layer. Another reason for excluding waterglass as a consolidant for stone is its high alkali ion content that will form hygroscopic salts, such as sodium or potassium carbonate in the course of time. The use of waterglass can be accepted for the consolidation of brittle renders or wall painting layers because the pores of those materials are coarser than those of stone and allow waterglass to penetrate deeper into the material.

At the turn of the 20th century, numerous stone conservation products were based on waterglass. One of the most famous ones may have been Szerelmey, because it was applied on a sample area at Houses of Parliament (Lewin 1966). The Szerelmey process included consolidation of the stone with sodium waterglass with the subsequent application of a bituminous lacquer to making the surface water repellent.

### 7.2.5 Silica Sols

In recent years silica sols gained increasing importance for preparing repair mortars or for consolidating flaking surfaces. Their composition is similar to waterglass. The main difference is the content of alkali metal ions, mostly sodium, which reaches 0.5 weight% at most. Silica sols are produced from sodium silicate solutions by reducing the sodium content by ion exchange with  $H^+$  ions. Alkaline as well as acidic silica sols are available on the market.

Silica sols are colloidal silica dispersions with 15–50 weight% total silica. Depending on the silica content the solutions are slightly cloudy to milky (see Table 7.1). The colloidal particles range in size from 7 nm to 125 nm and are larger than those in waterglass solutions (2–3 nm).

As in the case of waterglass the precipitation of the silica gel is caused by the loss of water when the solution comes in contact with the surface of a porous material. Through the condensation of the hydroxyl groups larger particles form that precipitate out of the solution. Although some formulations of silica sols have quite small particle sizes they are not appropriate for consolidating stone. The reason is that the silica particles formed are still retained on the surface in much the same way as those from waterglass, densifying the surface layer.

The main field of application for silica sols is the preparation of repair mortars for filling small cracks or for reshaping missing edges. Thin silica sol washes are also used to consolidate flaking surfaces. Detailed recipes for producing silica sol mortars and washes are described in Ettl et al. (1996).

### 7.2.6 Acrylates

Acrylates are very important in the conservation of building materials. They are applied either as macromolecules dissolved in organic solvents or as aqueous dispersions, in the latter case mainly as additives for mortars or repair mortars. Their general formula ( $CXY = CH_2$ ) can be derived from that of the acrylic acid ( $CH_2 = CH-COOH$ ). The letters X and Y stand for various organic groups that determine the chemical and mechanical properties of the polymeric acrylic resin (see Fig. 7.6). Chemically all acrylic compounds are esters from acrylic acid and an alcohol.

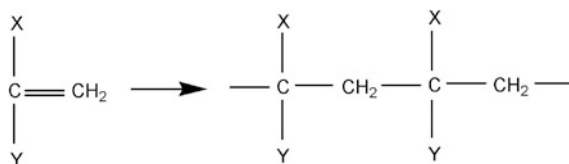
The most important acrylic monomers are listed in Table 7.2 (Merrill 1997). The polymer formation results through the splitting of the  $C=C$  double bonds with the formation of long  $C-C$  chains. These form the backbone of the polymer molecule (see Fig. 7.6).

As mentioned above, acrylates are esters from acrylic acid and an alcohol. The names listed in the above table are therefore simplifications of the correct chemical names. So the correct name of methyl methacrylate would be methyl ester of the methacrylic acid.

The most widely known product among acrylates is polymethyl methacrylate (PMMA) that is obtained through the polymerization of methyl methacrylate. This

**Table 7.1** Properties of different types of silica sol

SiO <sub>2</sub> Weight (%)	Na <sub>2</sub> O Weight (%)	pH	Particle size (nm)	Specific surface (m <sup>2</sup> /g)	Viscosity (cP)	Visual appearance
30	0.44	10.1	7	300	7	Barely opalescent
30	0.30	9.9	25	250	6	Slightly opalescent
40	0.20	10.0	40	165	15	Opalescent
40	0.16	10.2	125	70	5	Highly opalescent
50	0.20	10.2	125	70	9	Highly opalescent
15	0.06	10.2	125	70	2	Highly opalescent
20	–	6	40	80	–	Opalescent
40	–	6	40	80	–	Opalescent
30	–		15	220	–	Opalescent

**Fig. 7.6** Principal reaction scheme of the formation of an acrylic polymer

is the material known as Plexiglas. It was synthesized for the first time by O. Röhm and W. Bauer in 1932. The formation reaction of PMMA is depicted in Fig. 7.7.

The yellowing of acrylates is low because most acrylate compounds are polymerized by peroxides, which decompose during reaction. There are, however, acrylates that are prone to yellowing because they are polymerized by amines.

The glass transition temperature,  $T_g$ , largely determines the suitability of an acrylic polymer for conservation purposes. The mechanical properties change when the temperature increases above the  $T_g$ . Below the  $T_g$ , the polymer is hard and glassy, above this temperature it turns flexible and soft. The  $T_g$  of an acrylate should be above the temperature range to which the treated object is exposed so that the consolidation effectiveness is not lost. According to Table 7.2 the products MMA and EMA would be the most suitable ones for conservation.

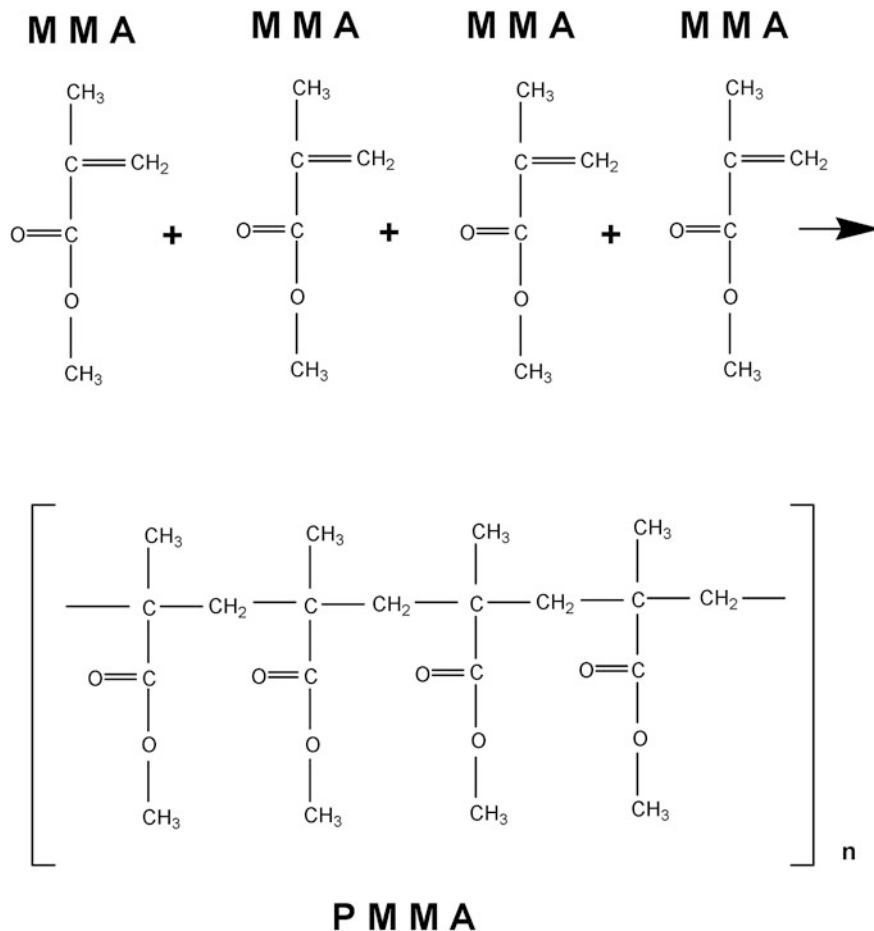
Among acrylates, the most frequently used by far is the Paraloid B 72 from Roehm and Haas. Chemically it is a copolymer of three parts of EMA (ethyl methacrylate) and 7 parts of MA (methyl acrylate) with a  $T_g$  of 35–40 °C (Koller and Baumer 2000). Its chemical structure is shown in Fig. 7.8.

Paraloid B 72 is used for consolidating disintegrating stone surfaces, ceramic and metallic archaeological finds, wall paintings and many other objects. It is mainly applied in concentrations of about 2–10 % by weight in organic solvents such as acetone, butyl acetate and toluene. The volatility of the solvent determines the area and method of application. When deeper penetration is needed the solvent should be slower to evaporate, i.e., it should have a higher boiling point. The effectiveness is based on the formation of a thin polymer layer that covers the internal surfaces and binds loose particles together. However, acrylic polymers

**Table 7.2** General formula of principal acrylic monomers

Name	Abbreviation	X Group	Y Group	T <sub>g</sub> (°C)
Methyl-methacrylate	MMA	-CH <sub>3</sub>	-C(=O)-O-CH <sub>3</sub>	100
Ethyl-methacrylate	EMA	-CH <sub>3</sub>	-C(=O)-O-CH <sub>2</sub> -CH <sub>3</sub>	65
n-Propyl-methacrylate	nPMA	-CH <sub>3</sub>	-C(=O)-O-CH <sub>2</sub> -CH <sub>2</sub> -CH <sub>3</sub>	35
Methyl-acrylate	MA	-H	-C(=O)-O-CH <sub>3</sub>	10
Ethyl-acrylate	EA	-H	-C(=O)-O-CH <sub>2</sub> -CH <sub>3</sub>	-24
Acrylic acid	AA	-H	-C(=O)-OH	-

T<sub>g</sub> glass transition temperature

**Fig. 7.7** Polymerization reaction scheme for MMA to PMMA

cannot penetrate deeply into porous materials. Therefore they only can be used for coarse porous materials. The maximum penetration depth that has been assessed is about 5 mm, as in the case of strongly weathered marble or sandstone. If the

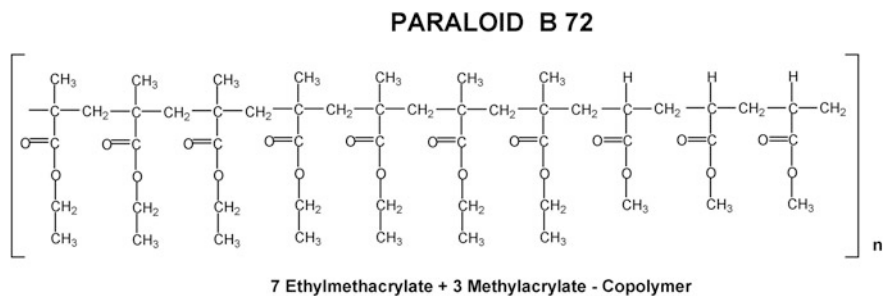


**Fig. 7.8** Schematic chemical structure of Paraloid B 72. In the real structure the components are randomly distributed

thickness of the weathered zone is higher, the application of acrylic polymers can be dangerous because the risk of delamination of the treated surface increases.

Several attempts have been made to combine the consolidating effect of acrylates with a hydrophobic effect. Besides numerous private recipes, which circulate among restorers, a formulation based on a mixture of Paraloid B 72 and Dri-Film 104 (General Electric product based on methyl trimethoxysilane) diluted with a mixture of solvents became very popular. The product is well known as the “Bologna Cocktail” because it was developed, tested, and applied in Bologna by the Italian restorer Nonfarmale (1976) and the chemist Rossi-Manaresi (1976).

The polymer structure of acrylic resin becomes evident when viewed in the SEM. The pore surfaces are covered by a coherent viscous film of the resin (see Fig. 7.9). As can be seen the film blocks finer pores just leaving the coarse pores open. For this reason there is a risk of reducing the water vapor diffusion when acrylic resins are applied on porous materials. Better results are obtained when acrylic resins in a dilution of 5–10 % in organic solvent are used for consolidating narrow surface zones situated over dense stone structures with low water capacity. Examples of this are the disintegrated sugary surface layers that form on marble. In this case a sufficient penetration depth can be reached without problems.

### 7.2.7 Polyester and Alkyd Resins

Another organic polymer very frequently encountered where older restorations were carried out is polyester resin and alkyd resin. Unsaturated polyester resins (UP resins) consist of multibasic unsaturated carboxylic acid (phthalic acid, maleic acid, fumaric acid) and dihydric alcohols such as ethyleneglycol, propanediol, butanediol. As shown in Fig. 7.10 the acid and the alcohol condense by releasing intermolecular  $H_2O$  to form a polyester chain.



**Fig. 7.9** Viscous film of acrylic resin covering pore space. SEM photo

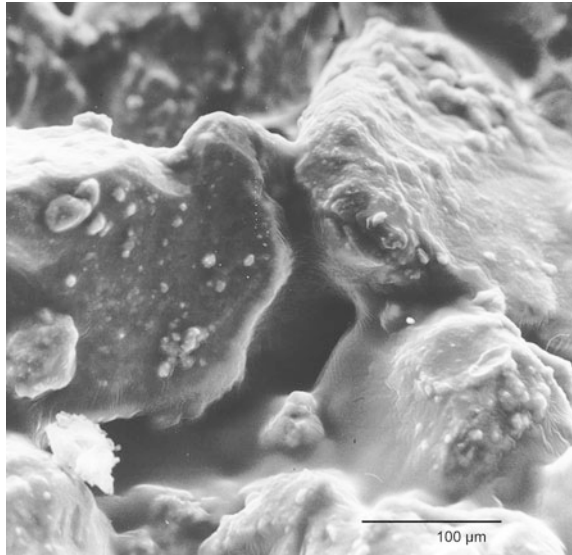
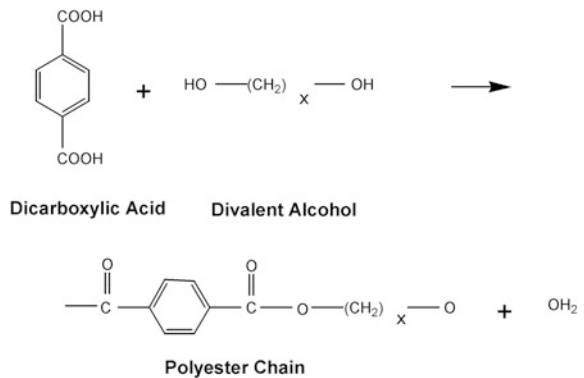


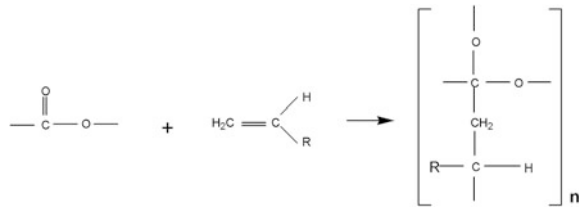
**Fig. 7.10** Formation of polyester chain by dicarboxylic acid and divalent alcohol



As can be seen from the figure above, polyester resins contain the periodically occurring group  $-\text{C}(=\text{O})-\text{O}-$  onto which other reactive groups, such as a vinyl group, can link to form a three-dimensional network (Fig. 7.11).

In stone conservation, polyesters have been used as binders for stone repair mortars, applied mainly in the 1960s and 1970s on limestone and marble. However, these repairs did not prove durable because their thermal expansion is very different from that of stone. Moreover, because of the ongoing crosslinking the patch becomes increasingly brittle and tends to detach from the stone. Today, most of the old repairs have already fallen out or are so loose that they have to be removed. However, polyester repair mortars are still used for filling defects in pavements or

**Fig. 7.11** Three dimensional crosslinking of polyester chain with vinyl groups



façade tiles, mainly because they are easy to work. If the patching is carried out appropriately it is hardly distinguished from the surrounding stone. Nevertheless, polyester bound repair mortars cannot be recommended for outdoor use when the patching is exposed to strong temperatures, humidity cycles and UV light.

Alkyd resins are similar to polyester resins. They derive from a mixture of the same or similar dihydric alcohols, the anhydride of phthalic or maleic acid and additional polyunsaturated fatty acids (e.g. linseed oil, sunflower oil, soybean oil). The content of the latter may range from 15 to 75 % so that alkyd resins can be regarded as a link between drying oils and polyesters. Alkyd resins are the dominant binders in commercial alkyd paints, which were frequently applied to facades in the past. Alkyd paints show typical damage like crack formation and subsequent peeling off from the substrate.

In Germany, “Lemisan”, was a popular product applied to many monuments between 1960 and 1970. It was based on an unsaturated polyester (Leguval W 16) dissolved in styrene (Degussa Evonik) and diluted to a concentration of 10–15 % with dichloroethane to adapt its properties to the needs of stone conservation.

### 7.2.8 Epoxy Resins

Most epoxy resins are based on the bisphenol-A epoxy resin, which is the reaction product of bisphenol-A (a divalent alcohol) and epichlorhydrin (Fig. 7.12).

The bisphenol-A epoxy resin needs to be crosslinked to form a solid resin. This is achieved through the use of a curing agent such as an amine. These hardeners can be primary, secondary and tertiary amines that induce different types of crosslinking bonds that will influence the properties of the cured epoxy. The common terminology for epoxy resins is a bit confusing because the starting resin component, bisphenol-A, as well as the hardened final product are referred as “epoxy resin”. To avoid this issue, only the bisphenol-A is called an epoxy resin, while the cured product is referred to simply as an epoxy.

In stone restoration, epoxies are used because of their strong adhesive force. Depending on the type of resin, adhesive strength of up to 30 MPa or even more may be obtained. This property makes epoxies appropriate for glueing broken pieces together or to fix dowels or anchors. The adhesive strength of epoxies is such that the bond does not fail in the joint but in the adjacent stone.

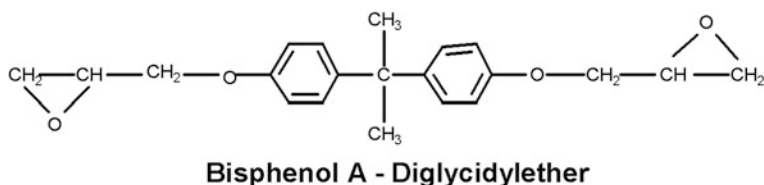


**Fig. 7.12** Bisphenol-A epoxy resin

Another application of epoxies is the preparation of repair mortars. Mixed with fine sand and stone powder, epoxy repair mortars are suitable for application to and repair of limestone or marble because their adhesive strength is very good even to dense stone surfaces. Because in the long term the amine hardeners always cause some yellowing, epoxy repair mortars should be used preferentially for dark colored stone. If necessary, the surface of epoxy repair mortars can even be polished if the appropriate mixing ratio is observed. Polishable repair mortars can also be made from white cement mortars, which are modified with aqueous epoxy resin emulsions.

On the other hand by mixing an epoxy resin in a 1:15 ratio with an appropriate aggregate, repair mortars with high porosity and an appearance similar to natural stone can be produced because the epoxy resin is colorless and clear. In contrast, casts made from white cement or Portland cement look either too whitish or gray because of the color of the cement matrix. For this reason, the famous original sandstone sculptures of the Fürstenportal of Bamberg Cathedral were replaced by epoxy replicas in 200 (Fig. 7.13).

Several attempts have also been made to adapt epoxy resins to the needs of stone consolidation (Littmann et al. 1998; Wagener et al. 1992; Stark and Dimmig 1997). Low viscous epoxy resins have been diluted in organic solvents to improve the penetration into porous materials. In practice, epoxy resins have been applied in particular in Poland and the former DDR, and in some instances in the USA. An obvious drawback of epoxy resins is that the two components may separate during penetration through the chromatographic effect. As a consequence the resin will not or insufficiently harden without having the desired effect (Wagener et al. 1993).

### 7.2.9 Silicate Esters

The tetra ethyl ester of the orthosilicic acid (TEOS) is by far the most widely used chemical compound for consolidating natural stone, mainly sandstone but also granite or historic renderings. This compound is also referred to as silicic acid ester, ethyl silicate, tetra ethyl silicate or tetraethoxysilane.

Its synthesis can be traced back to the 19th century when several chemists investigated the links between inorganic silicon and organic carbon chemistry.

**Fig. 7.13** The first epoxy bound replica (*light color*) of a pair of sculptures of the Fürstenportal at Bamberg Cathedral



In 1823 Berzelius synthesized silicon tetrachloride  $\text{Si}(\text{Cl})_4$  the substance that is still used for the production of TEOS. Noll (1968) reports the historic developments of silicon organic chemistry in the efforts to synthesize compounds containing the Si–C bonds that do not exist in nature. This is achieved by substituting the Cl atoms by organic C chains in a process similar to the Friedel–Crafts synthesis. The first synthesis of TEOS  $\text{Si}(\text{OC}_2\text{H}_5)_4$  is attributed to Ladenburg in 1872 (see Noll 1968).

In 1861, the German chemist August Wilhelm von Hofmann during a meeting of the Royal Institute of British Architects in London came up with the idea to test the newly prepared compound “silicic ether” for stone conservation at Houses of Parliament (see Lewin 1966). The synthesis and composition of silicic ether is described in Regnault (1853). Its synthesis also starts from  $\text{Si}(\text{Cl})_4$  to which pure ethanol is added resulting in a product which was called an ether and consisted of three molecular units of ether and one of silicic acid. The term ether corresponds to the old nomenclature where the  $-\text{C}-\text{O}-\text{Si}-$  group had been considered an ether group. The chemical formula of the ether can be assumed to be  $(\text{C}_2\text{H}_5\text{O})_3\text{SiOH}$ .

In 1926 A. P. Laurie (see Lewin 1966) obtained the first patent for stone consolidation with tetraethyl silicate. His product contained 10 %  $\text{H}_2\text{O}$  to ensure the hydrolysis to the intermediate silanol compound. In his survey about the effectiveness of various stone conservation products in England and after several samplings of areas that had been treated with the new product, Schaffer (1931) states that no significant effect was detectable, neither good nor bad. This negative assessment may be have been due to the fact that a difference between treated and non treated areas cannot be observed on the basis of visual inspection alone but only by thorough strength measurements. These had not been carried out by Schaffer.

The deposition of amorphous silica gel by TEOS occurs via a two step process where the reactions run concurrently. The first one is the hydrolysis of the alkoxy groups splitting off ethanol molecules. This step can be enhanced either by acidic or alkaline catalysis or with a tin-organic catalyst already admixed to the majority of the ready commercial products presently available on the market. The second

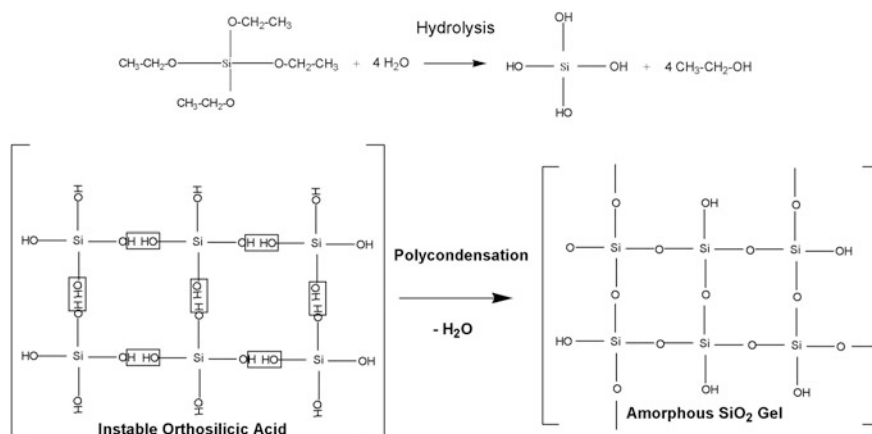


**Fig. 7.14** Hydrolysis and condensation of TEOS to silica gel

one is the condensation of the unstable intermediate silanols  $\text{-Si-OH}$  to amorphous silica gel. The chemical reaction formula is shown in Fig. 7.14.

The gel is the strengthening substance that makes TEOS useful as a stone consolidant. One of the great advantages of this product is that no deleterious by-products are formed and that the resulting ethanol evaporates completely.

Depending on the industrial way of production there are two kinds of TEOS available on the market: monomer and oligomer TEOS. Their reaction path of both to form silica gel is identical. The only difference is the presence of oligomer molecules in the liquid (see Fig. 7.15).

Depending on the catalyst, temperature and humidity, the gel structure formed may be harder or softer. Microscopically the gel deposited within the pore space consists of spherical particles of several nanometers in diameter forming an open structure with cavities filled with water, ethanol and TEOS molecules. The rigidity of the structure and the distance between silanol groups prevent the latter from a complete condensation. Thus, the gel will always retain some water and condensation will remain incomplete.

On the other hand, silanol groups of the TEOS molecule and of the surface of the gel may react with OH-groups that cover the surface of quartz or feldspar minerals, i.e., they are hydroxylated, or form hydrogen bonds with them. Thus a strong adhesion of the gel especially to the inner surface of sandstone is obtained.

$\text{SiO}_2$  gel from TEOS forms plaques separated by typical shrinkage cracks. An example is shown in a SEM photograph (Fig. 7.16). It can be seen that the gel plaques preferably deposit in narrow interstices forming new bridges between the grains and strengthening the entire structure.

The precondensed oligomer TEOS shown in Fig. 7.15 is available on the market. In this product, a small amount of water is added during the manufacturing

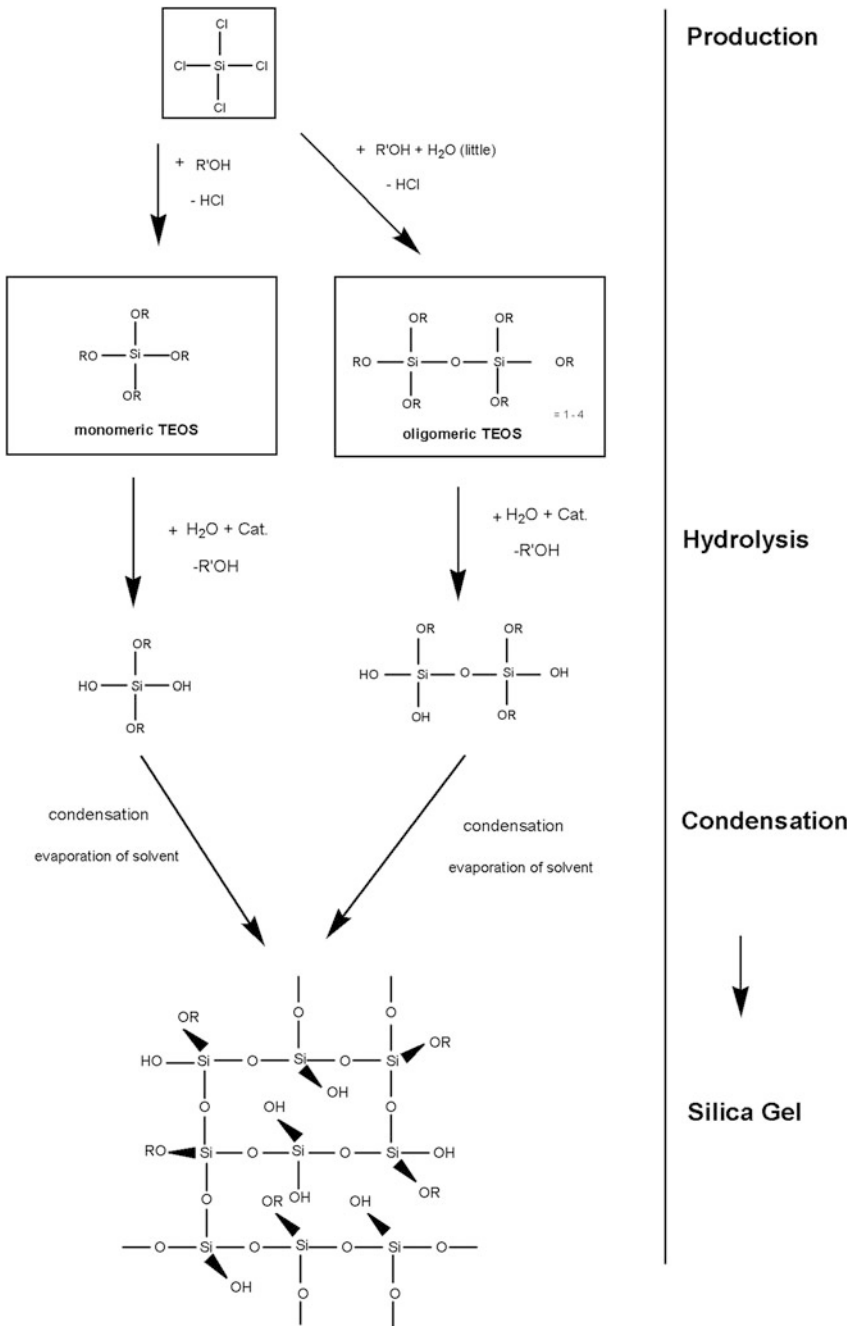
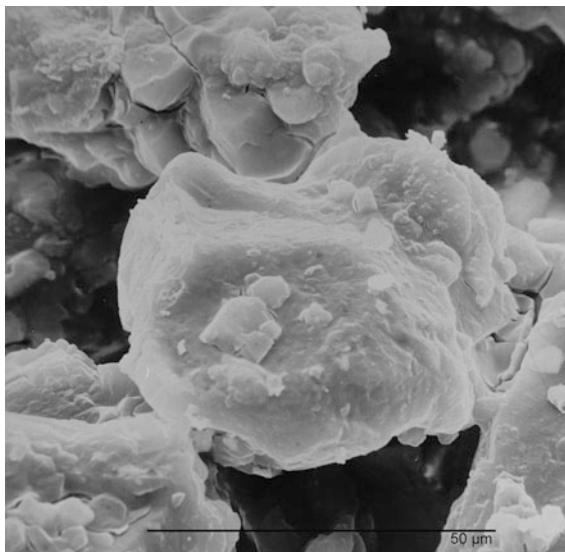


**Fig. 7.15** Formation of TEOS from  $\text{SiCl}_4$ . Gel formation by hydrolysis and subsequent condensation. The gel still contains some uncondensed silanol groups



**Fig. 7.16** Plaques of  $\text{SiO}_2$  gel formed from TEOS. SEM photo



process so that hydrolysis is initiated. Therefore the product already contains some precondensed units of 4–6 molecules.

The reaction scheme depicted in Fig. 7.15 also indicates that water is essential for the reaction of TEOS and the formation of silica gel. Therefore care has to be taken that the porous materials that are to be treated contain some absorbed water within the pore space to initiate hydrolysis. In arid climates, TEOS often is not effective because of the lack of moisture in the pore space so that the applied TEOS evaporates without having the opportunity of forming a gel.

As will be described later in Sect. 7.7 specific formulations of TEOS can be used to make repair mortars, injection grouts and washes. It should be also mentioned that in the 1960s and 1970s tetramethoxysilane, available from several producers, was frequently used as a stone consolidant because of its fast reaction. These were subsequently withdrawn from the market because they release toxic methanol.

### 7.2.10 Alkyl-triethoxysilane

Alkyl-triethoxysilanes are similar to tetraethoxysilanes except they have one direct Si–C bond by which an organic C-chain is linked to the central silicon atom. This Si–C bond is referred to as a silane bond, by extension of the real silane bond Si–H. Their general formula therefore is  $\text{R-Si}(-\text{OC}_2\text{H}_5)_3$ . The production starts from alkyl-trichlorosilane  $\text{R-SiCl}_3$  (see Fig. 7.17), which is mixed with ethanol plus some water to produce oligomer siloxanes. The –Si–O–Si– bonds are called a siloxane and this name is also given to the whole molecule. The alkyl group confers hydrophobic properties to these compounds.

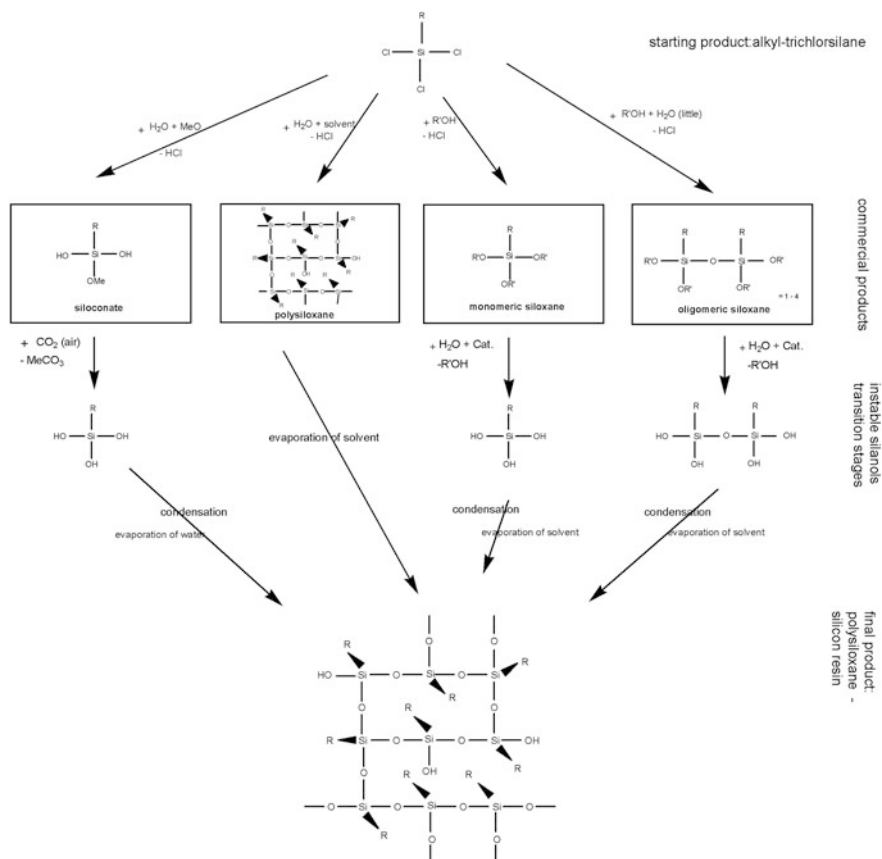


**Fig. 7.17** Production of different hydrophobic agents from alkyl-trichlorosilane

Siliconates represent a special group of hydrophobic agents. They differ from the alkyl trialkoxy silanes, in that they have two silanol groups  $-\text{Si}-\text{OH}$  and an additional alkali cation  $\text{K}^+$  or  $\text{Na}^+$  replacing the  $\text{H}^+$  in the third silanol group. For that reason siliconate molecules can be dissolved in water and thus admixed to mortars or waterglass.

Alkyl-trialkoxysilanes are used for hydrophobizing porous materials. The purpose is to greatly reduce the amount of liquid water taken up by capillarity without significantly reducing water vapor transport. As can be seen from Fig. 7.17 the final result of all commercial hydrophobic products is a silicone resin or polysiloxane, a macromolecule with simultaneous hydrophilic and hydrophobic properties. The process is the same as in case of TEOS. The catalyst together with moisture in the pore space starts hydrolysis of the  $-\text{Si}-\text{O}-\text{C}-$  bond. The subsequent condensation by intermolecular release of  $\text{H}_2\text{O}$  leads to the reticulation to a macromolecule which is named polysiloxane.

The first products on the market were polysiloxanes or silicone resins. These are practically completely crosslinked siloxane macromolecules. They are produced by adding sufficient water and solvent to the alkyl-trichlorosilane so that the hydrolysis and condensation to the polysiloxane network occurs during manufacture. Those products are diluted in organic solvent in concentrations of around 6–8 % vol of polysiloxane in the solution. While the solvent completely evaporates the polysiloxane macromolecules deposit on the pore walls and make them hydrophobic.

The hydrolyzed alkyl-trialkoxysilanol exhibits opposing properties: the carbon chain linked to the central Si-atom is hydrophobic while the OH-groups are strongly hydrophilic. Therefore the molecules arrange themselves with their hydrophilic part towards the polar pore surfaces and the non-polar, hydrophobic carbon chains point away from the pore surface providing the hydrophobic effect. This way the former polar and hydrophilic pore surface is coated with a thin non-polar layer and becomes hydrophobic. As a consequence liquid water cannot penetrate into the hydrophobized pore space. The diffusion of water vapour, however, is only slightly reduced. The mechanism of orientation of the polysiloxane and the transformation of the surface from a hydrophilic to a hydrophobic one is shown in Fig. 7.18.

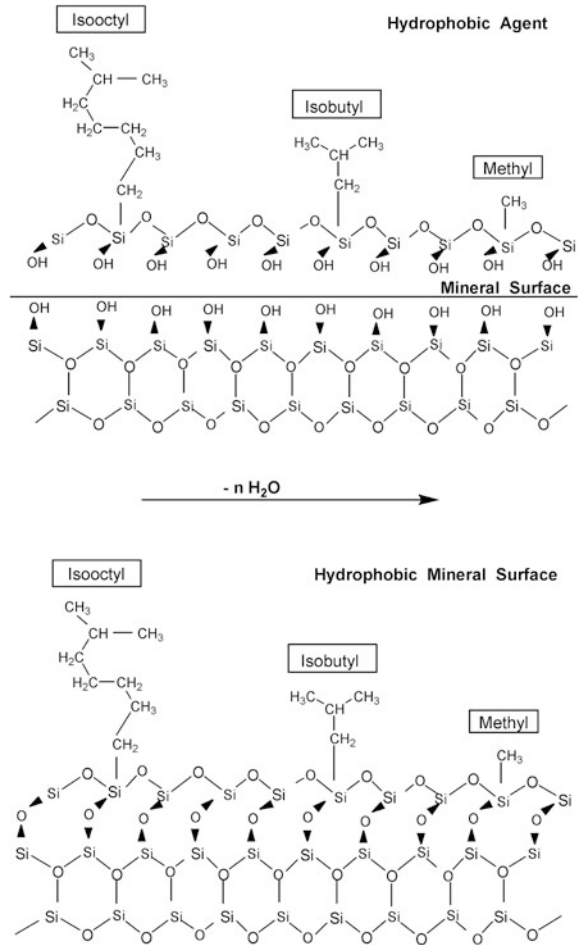
As can be seen from Fig. 7.18 the mechanism of adhesion between the polar mineral surface and the polysiloxane is the same as in case of TEOS adhesion on mineral surfaces. The OH-groups of the silanol namely can condense among each other thus forming a three-dimensional polysiloxane network but also with OH-groups on mineral surfaces. In particular the free surfaces of silicate minerals such as quartz and feldspar are hydroxylated so that the silanols of the hydrophobic agent can react with them. The connection either happens by formation of a strong  $\text{-Si-O-Si-}$  bond formed by intermolecular release of  $\text{H}_2\text{O}$  or by hydrogen bond where the two H atoms of the neighboring OH groups belong to both oxygen atoms simultaneously.

A further characteristic of hydrophobic alkyl-trialkoxysilanes can be seen from Fig. 7.18. The alkyl groups attached to the siloxane backbone can be very different. In the simplest example it is the methyl group that, since it is very small, does not provide good protection to the siloxane bonds from attack of acids or bases. On the other hand, the long isooctyl chain provides good steric protection against acid or alkaline attack; however, the long chain is a drawback for good reticulation of the polysiloxane.

The optical appearance of a polysiloxane film is shown in Fig. 7.19. Normally, a polysiloxane film only needs to have a one molecular layer thickness to be effective. For this reason, it is difficult to detect polysiloxane films in treated stones as can be seen in Fig. 7.19. The polysiloxane in this picture can only be recognized by the small cracks occurring on the edge of the coated mineral grain.

Another example is shown in Fig. 7.20 where the polysiloxane film, shaped like a thin sail, is suspended between the edges of clay platelets. In this case, because of the clay platelets displacement caused by hygric and thermal influences, the film shows some cracks.

**Fig. 7.18** Adhesion of polysiloxane layer on a polar surface



More information about the practical issues of stone hydrophobation will be presented in [Sect. 7.9](#).

### 7.3 Mapping of Conservation Interventions as a Planning Tool

Restoration and conservation interventions need thorough planning and documentation. Restorers and conservation scientists point out that more than half of interventions undertaken today are due to damages caused by inappropriate conservation measures taken in the past. Therefore, good documentation about what had been done in previous conservation interventions and which materials had been used would help a lot in solving the conservation problems being faced currently.

**Fig. 7.19** Polysiloxane film coating a mineral grain. SEM photo

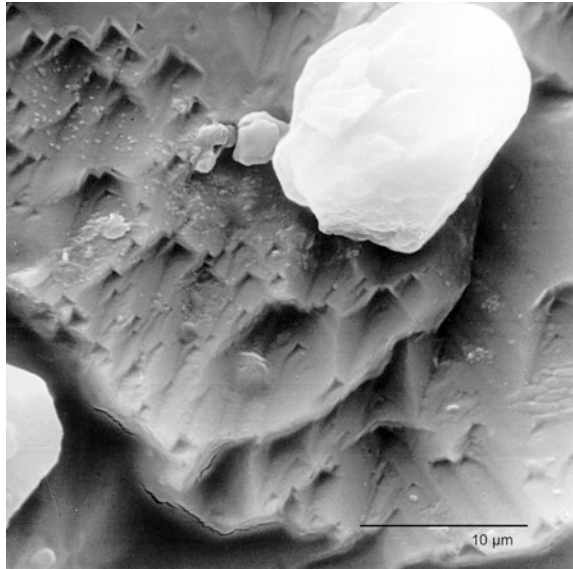
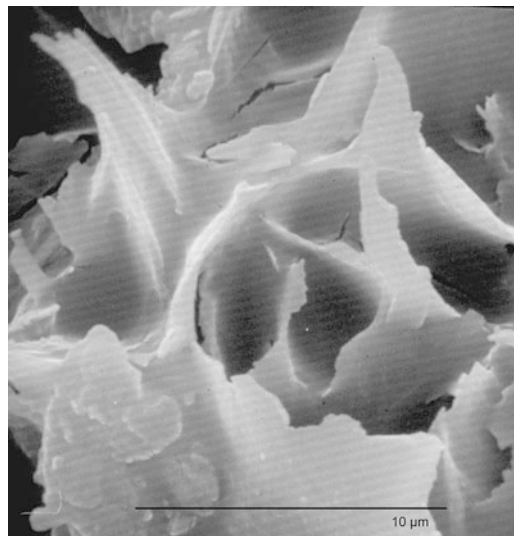


**Fig. 7.20** Polysiloxane film suspended between the edges of clay plates. SEM photo



A conservation project should always start with a thorough investigation of the archives with respect to previous conservation and renovation measures. Information of the past is a prerequisite to arrive at conclusive project aims and planning since conservation today means to undertake all measures necessary to preserve the monument in the state it presently is. Therefore, any information about previous stone replacements, additions or traces of polychromy is essential to understand the history of the object so as to preserve it as a historic document.

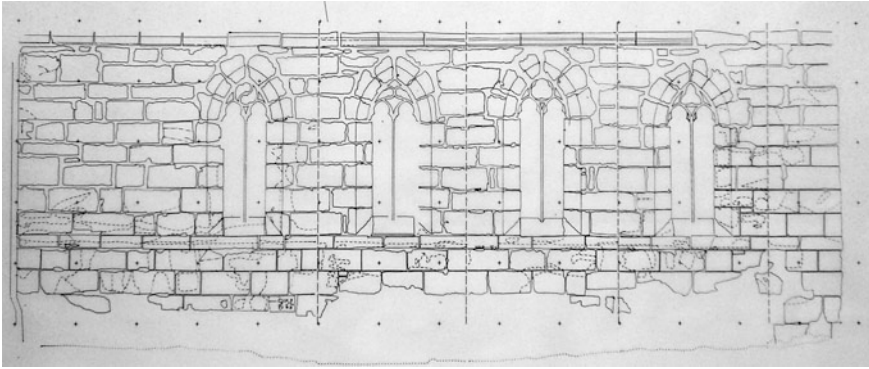


**Fig. 7.21** Photogrammetric plan of the apses of St. Stephen's church in Ergersheim, Bavaria. Scale 1:25. Deutsche Bergbaumuseum Bochum und Geologisches Institut RWTH Aachen 1987

It is important to remember that the object is the most reliable witness of its past. Only through archival investigation can the areas of particular historic importance be identified so as to conserve them with the special care they require. These areas include delicate stone decorations, ornaments and sculptures, as well as stone mason tool and cutter marks.

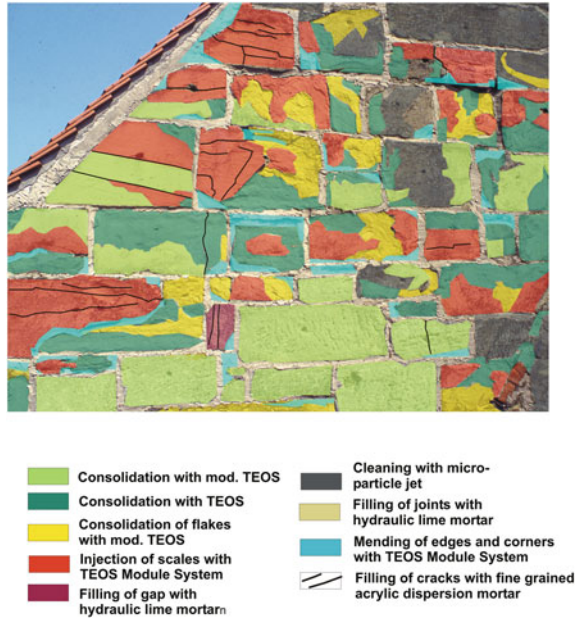
Planning stone conservation begins with the preparation of exact façade plans. These plans have to show the current state and not just schematic representations of an ideal situation. They must be true to the size and shape of ashlar blocks and joints in the façade. Previously, façade plans were drawn from the object by fixing horizontal and vertical threads. Later they have been done by photogrammetry using pairs of stereo photographs. A façade plan drawn from stereo photographs is depicted in Fig. 7.21. It shows the ashlars with the correct shape so that the stone type, its deterioration phenomena and the measures planned for conservation can be mapped on it.

Today drawing photogrammetric plans is practically obsolete. CAD based mapping software uses rectified digital photography onto which the perimeters of the ashlars can be traced out. With precise distance measurements on the façade itself, the mapping software can calculate length and area of the elements of interest. This allows fundamental data to be obtained that simplify the setting up the list of bid items and quantities. Figure 7.22 shows a simple example of the measures undertaken for conserving the gable of the Birkenfeld Monastery located in Bavaria. The ashlar stones on the gable showed severe damage, mostly contour scaling and subsequent flaking due to wind and rain exposure. As can be seen, the different measures are precisely mapped so that they can be read easily. They also include information of what is to be done on each single stone. Mappings of this kind are good documents for the future.

Complex restoration and conservation interventions very often require several procedures to be undertaken on the same ashlar. In this case, the 2-dimensional true mapping of every procedure on one map is impossible. One solution to the



**Fig. 7.22** Mapping of conservation measures for west gable of the church of Monastery Birkenfeld, Bavaria



problem is to map each required procedure separately. For example, one map shows the stone replacements, another cleaning, or stone repair, consolidation etc. However, this leads to a large number of maps that would be difficult to handle.

A more practical solution is shown on Fig. 7.23. It can be seen that a separate rectangle is assigned to each stone block. The rectangle is composed of several small columns, each one representing a different procedure. If the particular column, for instance the one for desalination, is colored, desalination has to be carried out on this stone. If it is blank, no desalination is needed. With this simplification it is possible to map all measures on one map so that the practical work is far easier to interpret than when handling several maps. This kind of compiled mapping, however, requires experienced conservators-restorers because even though they know the kind of measure to do on the respective block, they have to decide whether the measure has to be done on the whole stone or just on a part of it. And the order in which they have to be carried out.

Equally important to the visual part is the written report that every contractor has to deliver at the end of his work. This should contain information about the time it took to complete the job, the methods and the materials applied as well as extensive photographic documentation taken before, during and after the intervention. The Table 7.3, shows an example of the information to be included in the report for the specific case of a consolidation intervention.

For each type of procedure a separate sheet has to be delivered because their specifications would be different. Of special interest is the precise information about the exact name of the product and its chemical composition. In past years,



**Fig. 7.23** Nuremberg Maxtormauer. Mapping of complex conservation projects with the help of simplified indication of measures (Wendler 1997)

usually only the trade name of the product was indicated. This is insufficient because the real chemical composition cannot be derived from this name, and product formulations vary over time, or are discontinued. The precise specification of the chemical compound(s) involved in the formulation is far more important. Moreover, trade names and companies may change or disappear with time so that this information will no longer be available in the future.

In recent years 3-D laser or visual light scanning has become more popular. Thanks to enhanced computer capacity and to improved software precise 3-D models of all kind of objects can be produced, rendered more realistically by introducing photographs from the original, and their surface can be calculated accurately. An example of 3-D visual light scanning of a portal is shown in Fig. 7.24. It can be seen that the scan is carried out with a simple scanning head that automatically registers the 3-D coordinates of the scanned object. The number of individual scans required increases with the complexity of the surface. The software compounds the various scans to produce a complete 3-D image of the object. The operator has to check the computer model and will eliminate mistakes the software probably has made to create the final 3-D model.

The method is of particular interest in the conservation of sculpture or other 3-dimensional works of art such as vases or columns. It can be predicted that in a few years mapping of state of conservation and mapping of conservation measures will be conducted mostly with this new technique.

**Table 7.3** Documentation sheet for stone consolidation

No	Designation	Description	Example
1	Company		Name and address of company. Names and number of workers on the site. Responsible worker
2	Execution		Time of execution of the work
3	Climate		Weather conditions during the execution of the work. Average, maximum and minimum temperature, average, maximum and minimum relative humidity. Days, duration and intensity of rainfall. Other specific climatic events
4	Protective measures		Protection of the worksite with nets or plastic sheets. Protection of windows, wooden and plastic elements
5	Technique of application		Name and type of device used, e.g. washing bottle, airless spray. Application of poultices
6	Name of product(s)		Name and composition of product. Producer. Chemical composition
7	Method of application		Type of application: spraying/brushing “wet on wet” until saturation. Number of applications. Waiting time between applications
8	Consumption		Consumed product L/m <sup>2</sup>
9	Extraordinary events		Surface gloss, “bloom” or gray depositions on the surface
10	Documentation		Date of documentation delivery. Content of documentation: written report, documentary photographs, façade plans with mapping treated areas

**Fig. 7.24** 3-D laser scanning of a stone portal in Bamberg (Figure by Bellendorf)



## 7.4 Cleaning Methods

When considering the cleaning of stone the first question that inevitably comes up is: Why is it necessary? Even if the most gentle method is chosen cleaning always causes some slight damage to the surface. Therefore, can't this repeatedly induced

damage be reduced by extending the cleaning intervals? And furthermore, people in general tend to believe that dark encrustations serve to protect the surface from air pollutants and that for this reason they should not be removed. And the darkened appearance has been considered a patina conveying particular age value to the object.

These opinions, however, do not withstand scientific analysis because black crusts and discolorations should first of all be regarded as indicators for severe neglect. To begin with, the black crusts are formed by the reaction of the air pollutants with calcareous materials. If these are not in the stone, then they may be found in the mortar around them. Thus, their composition is essentially gypsum with quartz and other siliceous minerals embedded in them plus soiling, carbon particles and fly ash. They do not have a protecting effect because their specific surface is several times bigger than that of the stone and therefore they strongly absorb moisture that allows gypsum to migrate from the crust into the stone and by successive crystallization cycles reduce its subsurface to a powdery condition. In the course of time the crust will detach from the surface and will lay open the powdery skin of the stone, a process that is frequently observed on buildings (Fig. 7.25). Therefore, a stone covered by a black crust is far more endangered than a clean one (Snethlage 2008).

In general, there are two overall reasons for cleaning stone: aesthetic and technical reasons concerning preservation. Ashurst and Dimes (1990) as well as Martin (2000a) point out that soiling mostly consists of two kinds of material:

- Foreign matter—such as soot, grease and dust particles deposited from air or rain and fixed to the original material.
- Reaction products of the original material from acidic pollutants deposition that result in the formation of gypsum or other salts.

In addition, living and dead biological matter plays an important role in the blackening of surfaces; especially for black films growing on rain exposed surfaces (see Sect. 7.11). Removal of those alterations aims at the following objectives.

The aesthetic reasons for enhancing the appearance would include:

- Removal of disfigurements (Fig. 7.26).
- Revealing the nature, color or details of buildings or sculptures.
- Unifying the appearance of a building or sculpture that has been altered or repaired.

The technical reasons for regular maintenance or conservation would include:

- Removal of harmful or undesirable deposits in order to reduce the deterioration rate of the substrate.
- Exposure of concealed defects in order to establish the nature and extent of necessary repair.
- Preparation of the surface for additional treatments (improving uptake of liquid conservation agents).

**Fig. 7.25** White limestone surface lay open after detachment of black crusts. Romanesque portal of St. Jacob church Regensburg, Bavaria

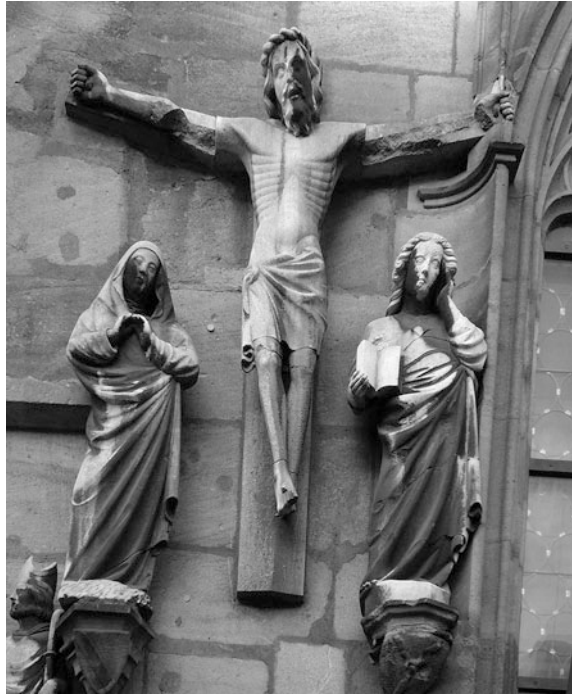


From a preservation point of view, cleaning to remove harmful deposits is by far most important because it improves the long term protection of the work of art.

However, in many cases cleaning is not as simple as the removal of dirt and harmful substances. Especially in the case of limestone, gypsum crusts may not only cover the surface but the subsurface may have also been transformed into gypsum, so that the original surface is lost within it. Consequently, removing the crust would result in the loss of the original surface and the formation of a new surface that may have no relation to the original one (see Fig. 7.27).

Therefore, cleaning sculptures may be a particularly difficult undertaking when the original polychrome layer has been included within the gypsum crust as has been the case for sculptures at the Naumburg and Halberstadt Cathedrals (Domstiftung Leitzkau 2002). In such cases, the aim of the cleaning should be to preserve part of the gypsum crust even though it may be harmful for the stone. Furthermore, it should be considered that in many cases the first ground layer of

**Fig. 7.26** Disfigurement of faces by black encrustations. St. Sebaldus Church Nuremberg, Germany



polychrome stratigraphy on stone consists of a gypsum-calcite layer bound with animal glue and other organic matter to provide a smooth surface for the application of the paint layers (Drewello and Herkner 2009). Therefore, a distinction has to be made as to the original gypsum layer, a primary document of the painting technique, which should be preserved under all circumstances, and the gypsum layer resulting from air pollution attack, which should be removed insofar as possible, but without destroying the polychromy layers.

### ***7.4.1 Water Based Cleaning Techniques***

Water based cleaning techniques are still very frequently used. These methods vary widely, ranging from cold water spray to pressurized steam. The effect of water on soiling is to soften the dirt by partly, dissolve the gypsum present and then wash it away. Detergents may help to dissolve soot components, which are not water soluble. Pressurized cold water improves the cleaning effect only through enhancing the mechanical action of the water jet. The risk of damaging the monument increases with an increase of the applied pressure. With extreme pressure a whole sound surface can be totally eroded.



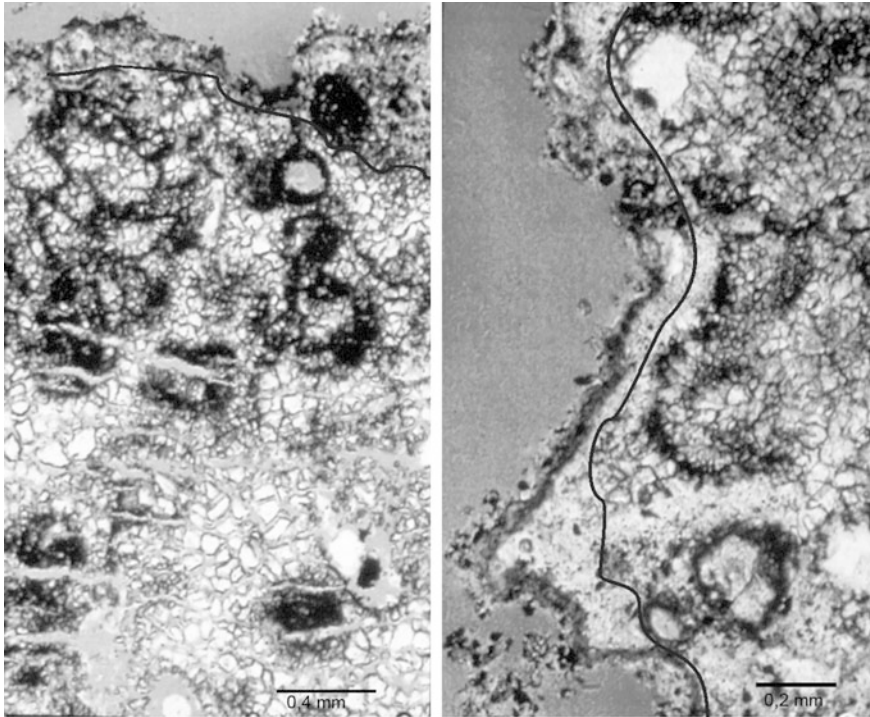


**Fig. 7.27** Alteration of original surface by gypsum formation, frost damage and accumulation of crust. For the position of the presumable original surface see black line. Limestone from Naumburg Cathedral. With permission by Neumann (1994)

A relatively softer method is the application of a mild water spray. The surface is sprayed with a fine mist of water for days or even weeks until the dirt layer is washed away. An arrangement of three water sprays cleaning blackened marble is shown on Fig. 7.28. The method can be only effective if the crust is composed mainly of gypsum or other materials that are softened by water. Therefore, for many kinds of incrustations cold water spray is not successful. A particular risk of water cleaning methods is the moistening of the masonry. Specifically, when defective joints are present, water may penetrate into the building with the consequent damage to its interior. This problem should be particularly avoided for the case of galleries or museums given the valuable interior content. The effect of mild water spray is similar to the effect rain has over exposed stone surfaces, and that originates the white-black patterns on buildings depending on the prevailing wind directions that will tend to have one side washed white and the other one dirty.

Warm or hot water increases the dispersion of soiling components in the water jet. So the cleaning effect is enhanced and less water has to be used. However, using hot water does not remarkably improve the cleaning effect compared to cold water.

**Fig. 7.28** Wet mist cleaning of Gustav Adolf monument in Gothenburgh (Lindborg 1995)



Among water cleaning techniques steam jet offers the best efficiency. The steam is generated by heating water in a closed vessel up to 140–180 °C so that the pressure increases to 20–40 bars (2–4 MPa). When the operator opens the nozzle, the steam jet consisting of small over-heated liquid water droplets comes out of the vessel. The speed of the steam jet is so high that most of the liquid water droplets burst into water vapor when they impinge upon the building surface. This process exerts a mechanical impact on the surface because of the one thousand fold volume expansion resulting from the change of liquid water to water vapor at that temperature. Therefore, steam cleaning has good dissolving power as well as relatively mild mechanical effect. It is therefore most frequently used for cleaning monuments and buildings in general. It also consumes far less water than any other water based method. Nevertheless, water steam is not effective for many severe encrustations, which can only be removed by particle or micro particle cleaning methods. For short information about cleaning techniques see Table 7.4.

Until around 1980s acidic cleaners were extensively used for removing persistent encrustations, mainly on quartzitic sandstone or granite where plain water did not have sufficient cleaning effect because the gypsum crusts were full of soot and oily compounds. Hydrofluoric acid (HF) has been the favorite agent but even hydrochloric acid (HCl) and sulfuric acid (H<sub>2</sub>SO<sub>4</sub>) and mixtures of them have been used. Very often the concentrations of these acids were so high that not only carbonates dissolved but also feldspars and clays transformed into amorphous silica species. In addition, strong acids can cause ugly discolorations because they mobilize iron oxide hydroxide compounds contained in colored sandstone or granite.

In case of hydrofluoric acid, it has been even argued that for instance stable fluorite (CaF<sub>2</sub>) would be formed instead of the more soluble calcite with the consequence that the acid was even advertised as kind of conservation agent for limestone. It is to be considered that all strong acids release highly aggressive

**Table 7.4** Selection of main cleaning methods. Note that some of the cleaning methods in general are not appropriate for historic monuments because they can cause severe damage like highly pressurized water or particle jet cleaning with coarse grains

Method	Parameter	Application	Risks
Cold water	Spraying without pressure optional detergents	Gypsum crusts, dense stones	Moistening of masonry
Pressurized water	Cold/warm/hot 10–20/60–90 °C Up to 150 bars (15 MPa)	Gypsum crusts, dense stones	Water penetration through open joints Material loss from friable surfaces
Water steam	140–180 °C 20–40 bars (2–4 MPa)	Gypsum crusts, dense and porous stones	Material loss from sanding and flaking surfaces
Cleaning poultices	Active agents: EDTA, (NH <sub>4</sub> ) <sub>2</sub> CO <sub>3</sub> poultice Ionic exchanger poultice with CO <sub>3</sub> <sup>2-</sup> and OH <sup>-</sup> Poultice materials: clay mixtures of attapulgite, sepiolite, bentonite, methyl cellulose, cellulose, highly dispersed silica, etc.	Gypsum crusts, especially on limestone and marble. Transformation of gypsum to calcite Testing and observing correct application time	Full adherence of the poultice to the surface Formation and migration of salts: (NH <sub>4</sub> ) <sub>2</sub> SO <sub>4</sub> Dissolution of calcite by EDTA Difficult removal of thin gray clay remains
Particle jet	Particle materials: glass slag, natural sand, quartz sand, hollow glass spheres	All kind of soiling Dense and hard materials Dry or wet	Dust development Loss of flakes and loose material Risk for loose paint layers
Micro particle jet	Particle size: 0.1–0.5 mm Particle materials: calcite, corundum, quartz powder, hollow glass spheres, fine sand	All kind of soiling and stones Dry or wet	Dust development Risk for loose paint layers possible
Laser	Particle size 0.05–0.1 mm Nd YAG laser Adjustment of pulse frequency, pulse duration and beam focus	All kind of soiling Especially on light stones like marble and limestone	Discoloration of pigments Color change of stone through removal of coloring clay layers

vapors to which the workers will be exposed with the consequent health risk. Still today, however, milder acids such as formic, acetic, and sulfamic (amidodisulfonic) acid are in use for removing calcitic incrustations from places where seepage water extrudes to the surface.

The experience obtained in Scotland with acidic cleaners for heritage buildings mainly constructed with sandstone, or granite in some areas, has been carefully documented and studied by the Masonry Conservation Research Group of The Robert Gordon Institute of Technology from 1989 to 1991. It was found that the re-soiling rate of buildings cleaned with acidic cleaners is much higher than that one after cleaning with water or steam jet (RGIT 1991). The study comes to the conclusion that initially acidic cleaning appears to be very effective as reflected by the clean appearance of the façades, however, in the long term it does more damage. Another important recommendation of the report is that when row houses are to be cleaned, it is important to do them sequentially, since it is very hard to achieve the same degree of “cleanliness” on a particular building to match those around it.

The application of alkaline cleaners, that require their subsequent neutralization with an acid, has decreased during the past decades although it is still in use in many countries. In most cases the alkaline cleaner is based on a sodium hydroxide (NaOH) solution thickened to a pasty consistency ready for application with a brush. Though the alkaline cleaner itself is not damaging the stone, it is the neutralization of the excess of the applied alkaline cleaner by an acid that results in the formation of soluble salts. The most frequently used acids for neutralizing the base is hydrofluoric or hydrochloric acid, so that alkaline cleaning ends up with an acidic treatment as in the case of acidic cleaners. Because the amount of remaining alkaline cleaner can never be accurately assessed, the neutralization will be incomplete if too little acid is applied or, if too much acid is applied, some acid will remain that will immediately be neutralized by reacting with the calcareous components in the stone or the mortar, and in both cases, soluble salts will form. As explained in a previous chapter, soluble salts are one of the main damaging factors for stone. Taking into account the possibilities of water based, micro particle jet or laser cleaning with the help of which all kind of crusts can be carefully removed there is no reason why acidic or alkaline cleaners should be used at all.

### ***7.4.2 Cleaning Poultices***

In many cases cleaning poultices are an alternative to water cleaning methods or particle jet cleaning. They are preferred to other methods when cleaning has to combine with transformation of gypsum back into calcite. In essence, a poultice is constituted by an inert support mixed with an active ingredient. Two of the most important poultices used for the removal of black crusts, shall be described.

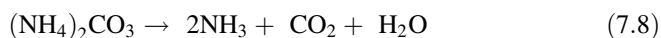
The first one employs the sodium salt of the ethylenediamine-tetraacetic acid, abbreviated as (Na-EDTA) as active ingredient and has been in use since the

1970s. They are particularly appropriate for gypsum crusts because EDTA forms a stable complex with  $\text{Ca}^{2+}$  ions. Thus gypsum is transformed into soluble sodium sulfate ( $\text{Na}_2\text{SO}_4$ ) that is mobilized into the poultice as well as into the stone. Though the main reaction is restricted to the interface between poultice and stone, mobilization of sodium sulfate into the stone cannot be excluded. In practice, the extraction of the produced sodium sulfate with neutral aqueous compresses remains difficult and will not be completely successful in most cases. It is therefore questionable whether the exchange of little soluble gypsum with the risk to leaving highly soluble sodium sulfate in the stone is really advantageous. To be effective the active agent Na-EDTA has to be applied in a mildly alkaline solution with controlled pH (approx. 8.5), i.e., a buffer solution, to avoid any discoloration that may happen to the stone by an alkaline pH. It should also be taken in mind that Na-EDTA cannot distinguish a calcium ion incorporated into gypsum from one incorporated in the calcite of the substrate. For this reason there is a risk that Na-EDTA when applied in excess will also dissolve calcite from the stone resulting in an undesired etching of the stone surface.

The second kind of poultice, developed in the late 1960s after the great flood in Florence, uses ammonium carbonate as the active ingredient. The research was undertaken mainly by Matteini and his co-workers (Matteini 1987). For more than 30 years it has been applied on thousands of monument worldwide. The poultice acts by transforming the relatively soluble gypsum into the less soluble calcite as shown by the chemical reaction equation below.



Because ammonium carbonate is alkaline with a  $\text{pH} = 9.5$  the application of the poultice is accompanied by a strong cleaning effect that in many cases is also required. Excess ammonium carbonate is not harmful because it decomposes into volatiles compounds, i.e., ammonia and carbon dioxide, according to the reaction equation below:



The problem of applying ammonium carbonate for gypsum transformation is the formation of the highly soluble ammonium sulfate that, as any other salt, may cause damage. Unlike ammonium carbonate it only decomposes at temperatures above  $235^\circ\text{C}$  and therefore it must be extracted from the substrate with the help of neutral aqueous poultices. As mentioned above, and discussed in more detail in another section, removal of soluble salts with poultices is a difficult and often incomplete process. Therefore especially among German scientists it is still under discussion whether all ammonium sulfate can effectively be removed from the pore space at all. To resolve this problem, Matteini suggests the application of a barite water poultice in order to transform soluble ammonium sulfate into highly insoluble barium sulfate:



From the equation it can be seen that only the stable barium sulfate remains while the gaseous ammonia evaporates. The effectiveness of this treatment is controversially discussed among scientists, especially in Germany. SEM investigations by the author demonstrate that the reaction of barium hydroxide with ammonium sulfate is restricted to the surface probably because the former's strongly temperature dependent solubility prevents it to reach the ammonium sulfate in the pore space of deeper layers.

More recently poultices based on ion-exchange resins with exchangeable carbonate or hydroxide ions ( $\text{CO}_3^{2-}$  or  $\text{OH}^-$ ) have been tested. The ion exchange resin consists of a porous synthetic resin into which the exchangeable anions are embedded. Depending on their nature, they are applicable in slightly acidic or alkaline conditions. For each sulfate anion the ion exchanger resin releases one  $\text{CO}_3^{2-}$ , or two  $\text{OH}^-$  anions. Thus, as the sulfate is extracted from the gypsum, either calcite,  $\text{CaCO}_3$ , or calcium hydroxide,  $\text{Ca}(\text{OH})_2$ , is formed. The latter will slowly react with  $\text{CO}_2$  from the atmosphere to turn into calcite as well.

The application of cleaning poultices may be less critical in case of unpainted masonry stones. However, if paint layers are present, it has to be taken into account that an acidic or alkaline pH will destroy any organic binding media of historic paint layers and thus, destroy a valuable document of historic painting technology.

The inert support material of poultices is made from substances that guarantee a high specific surface such as clay minerals (attapulgite, sepiolite, bentonite), methyl cellulose and highly dispersed silica. To be fully effective, the poultice has to have a perfect contact with the stone surface to allow the diffusion of ions from the poultice to the stone surface layers and back. However, such close contact may hamper the complete removal of the poultice, in particular from rough surfaces. For this purpose, restorers use Japanese paper as contact medium between poultice and stone in many cases so as to avoid leaving grayish or whitish traces of the poultice on the surface.

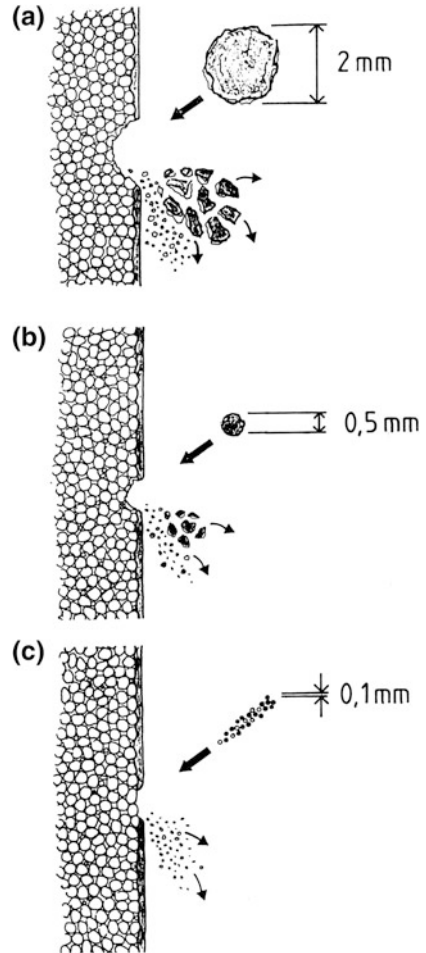
Recently natural latex for cleaning has seen a revival. The latex emulsion is sprayed or brushed onto the surface to clean and, after hardening to a plastic coating, it is stripped off. Any dust and dirt particles that are not strongly adhered to the surface are peeled off together with the entire coating. It is evident that latex cleaning can only be recommended for hard and sound surfaces.

### ***7.4.3 Particle Jet and Micro Particle Jet***

Currently, particle jet or micro-particle jet cleaning is the most frequently used technique. The technique has been developed to such an extent that it is no longer comparable to the harsh sand blasting technique used originally, as when Paris was sand blasted in the 1950s. In principle, particle and micro particle jet cleaning are equivalent because both use solid particle jets to remove dirt from the surface.



**Fig. 7.29** Damage risk of different particle sizes.  
**a** Sandblasting, **b** particle jet,  
**c** micro particle jet (Prickartz and Heuser 1991b)



However, particle jet is more appropriate for large facades, while micro particle jet is the appropriate for cleaning decorative elements or sculptures.

The size of particle jet powder ranges from 0.1 to 0.5 mm with an average of around 0.2 mm, the one of micro particle jet from 0.05 to 0.1 mm. The nature of the particles can be very different: blast furnace glass slag, natural sand with mica or with calcite, quartz sand with rounded or broken grains, hollow glass spheres. Depending on the pressure and on the particle material the method is more or less abrasive. Figure 7.29 presents a schematic drawing of the impact of different particles onto a stone surface. It is evident that the coarse sand blasting particles with sizes up to 2 mm put the highest risk while micro particles with sizes up to 0.1 mm bear only little risk.

**Fig. 7.30** Nozzle for particle jet cleaning



Large buildings can be cleaned within reasonable times and costs using nozzles such as shown in Fig. 7.30. The whole particle jet device consists of a compressor for pressurized air and a separate reservoir for the particles. The particle reservoir is kept either under pressure (pressure particle jet) or is left open under normal air pressure (injector particle jet). In the latter technique the fast air stream picks up the particles from the reservoir by the vacuum generated in the tube between reservoir and nozzle. As evident from Fig. 7.30, the operator can only vary the amount of particles admixed to the air jet to increase or reduce the cleaning effectiveness. The variation of the air pressure can only be regulated at the compressor that stands on the ground, not on the scaffolding. To avoid the formation of dust some water in variable quantities can be admixed to the air jet from a separate reservoir.

In the 1980s, the JOS method was developed in Germany by Josef Szücz. It proved of interest not only in Germany but in other European countries as well as in North American countries (Martin 2000a). The JOS method differentiates itself from others by the special nozzle that produces a rotating, whirling jet that requires less pressure to be effective. In Fig. 7.31 the Justice Building in Munich is shown after cleaning by the JOS method in the 1980s.

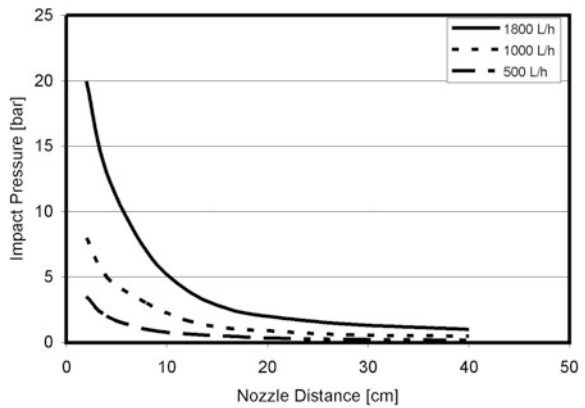
Particle jets work with pressure between 1 and 20 bars (1–2 MPa). The method should therefore only be applied on sound and stable surfaces. Flaking or disintegrating surfaces would certainly be heavily eroded. However, it should always be taken into account that mere figures of the pressure prevailing at the nozzle tip are not very informative. Prickartz and Heuser (1991a) found that the impact of the particle jet to the wall surface strongly reduces with the distance to the nozzle. Figure 7.32 shows that a pressure of 20 bars (2 MPa) measured at the surface when the distance between nozzle and surface is 2 cm drops down to about 2.5 bars (0.25 MPa) when the distance increases to 20 cm. It is also evident that the pressure depends on the volume of the air stream. Logically it drops from the highest values for 1,800 L/h to low values for 500 L/h.

Furthermore, the particle impact also depends on the angle between nozzle and surface. The nozzle should not be pointed directly towards the surface because the



**Fig. 7.31** Justice building in Munich before and after cleaning with JOS technique

**Fig. 7.32** Dependence of impact pressure from the nozzle distance from the surface. Note the strong decrease of pressure between 5 and 20 cm distances. Jet angle 25°. Compressor vessel pressure 200 bars. After Prickartz and Heuser (1991a)



rebounded particle cloud deviates the jet from its target, with the consequence that the pressure has to be increased to obtain the same cleaning effect. On the other hand, an angle below 45° between nozzle and stone surface creates a cloudy appearance of the cleaned area because the jet hits the surface sideways. In practice, an angle of 65° and a distance of 20–30 cm should be maintained.

For the case of micro-particle jet cleaning, dust can be a serious problem. It is therefore compulsory to encase the building site carefully. First of all, however, the operators who work inside the shelter case must be protected from inhaling dust particles. Often, it is necessary for the workers to wear dust proof protective overalls with a separate supply of fresh breathing air from outside.

If the dust clouds formed inside the shelter case are too thick the workers would not be able to clearly see the areas to be cleaned. And work will have to be interrupted to allow extracting the floating dust via strong vacuum cleaners. Therefore, it becomes evident that working with micro particle jets on a large scale building facade requires the addition of water to the micro/particle jet to prevent dust formation.

The situation is, however, different for micro scale devices that have been developed for micro-particle jet application on delicate ornaments or sculptures on the object or in the restoration workshop. For such tasks, a series of particle materials of a size of 0.05–0.1 mm is available: calcite, corundum, quartz, garnet, fine sand, hollow glass micro-spheres, plastic granulate, cork. No general recommendation can be given for the best particle to use because this will depend upon the nature of the soiling to be removed and the substrate itself. Therefore, tests should be carried out to determine which material yields the best results. As a general rule, however, it can be stated that soft powders like cork, plastic granulate or sometimes calcite powder are not appropriate to remove even mild incrustations because they may have a polishing effect only. In many cases, broken grains with sharp edges remove the dirt better with lower pressure than grains with round shapes at higher pressures. Cleaning polychrome ornaments or sculptures requires particular care and the results should be evaluated by microscope observation, and, in some cases, with an SEM, so as to select the best method. Figure 7.33 shows a restorer cleaning a polychrome sculpture with a micro-particle jet. The small area under treatment at the tip of the small nozzle indicates that the area that can be cleaned within 1 h may be only  $5 \times 5$  cm in size. So cleaning a whole sculpture may become an undertaking of several weeks. Such careful cleaning procedure, however, is always justified when dealing with unique and irrecoverable works of art. Figure 7.33 illustrates that it is necessary to work with a dust mask that covers both mouth and nose for health reasons, and with magnifying glasses to allow seeing the results obtained in detail, so as to achieve good results. The dust created by the micro particle jet should be soaked away by a vacuum cleaner.

A special method is the use of dry ice particles for cleaning. This uses frozen carbon dioxide particles at a temperature of  $-40$  °C so that the cleaning effect is a combined effect of temperature and mechanical impact. An obvious advantage is the volatility of the carbon dioxide. The dry ice evaporates without leaving residues behind. But a clear disadvantage is the necessity to keeping the dry ice reservoir at the appropriate temperature to prevent the ice particles from coalescing into a big lump. Dry ice cleaning is mostly applied for removing old coatings from metal surfaces, such as airplanes, or from wooden floors. Yet it does not have a ready application in stone conservation.

**Fig. 7.33** Restorer working with a micro particle jet cleaner



#### ***7.4.4 Laser Cleaning***

The first tests that employed a laser in the field of conservation had other goals than cleaning of the stone. It was in 1972 when Asmus, Lazzarini and other researches tested pulsed ruby laser to produce archival laser holograms of crumbling Venetian sculptures in order to demonstrate an innovative means of virtual preservation of endangered work of arts (Asmus et al. 1973). This cooperation finally led to the discovery that pulsed laser could also be used to remove black incrustations from decaying marble sculptures (Lazzarini and Asmus 1973; Cooper 1998).

From these first and thorough investigations concerning the removal threshold of various kinds of incrustations on marble and other materials over 20 years went by before the laser could be applied in the field. The main reason for that delay has certainly been that the first lasers were very heavy, large sized and of complicated handling. Not until the 1990s, were transportable lasers for on-site use available on

**Fig. 7.34** Nd:YAG Laser with articulated arm in practical employment (Figure by Bauer-Bornemann)



the market. Currently there are several companies in USA, Italy, France, Germany and other countries selling laser equipment for cleaning artworks.

Before 1990, lasers were far less efficient and therefore were mainly used for indoor work in museums for materials such as stone, wood, ceramics, ivory and others. The progress achieved by many comparative investigations testing different laser types on materials, such as terracotta, textiles, paper, polychrome surfaces, stained glass and others, are mainly due to Martin Cooper, John Larsen, Costas Fotakis and Vassilis Zafiroopoulos (see Cooper 1998).

Worthy of mention are the projects carried out in Germany and funded over a 12 years period by the German Environmental Foundation (DBU) that dealt with stone, bronze and stained glass windows cleaning. The results obtained for stone cleaning are compiled in Siedel and Wiedemann (2002). Nowadays national and international expert groups of scientists and restorers meet regularly to discuss questions of laser cleaning in the forum of the biannual LACONA conferences, the first one having been organized by FORTH in Heraklion, Crete, in 1995.

Though other lasers like carbon dioxide (laser wavelength 10.6  $\mu\text{m}$ ), dye (590  $\mu\text{m}$ ) or Excimer laser (248 nm) could also be employed for cleaning, the most commonly used laser in practice is of the Nd:YAG laser in its Q-switched option. The core of this kind of laser is an Yttrium Aluminum Garnet doped with Neodymium. The Q-switching is achieved by putting a type of variable attenuator into the laser's optical system. This allows the generation of laser light pulses with extremely high peak power, much higher than would be produced by continuous wave mode.

The Nd:YAG laser produces light with a wavelength of 1,064 nm (Fig. 7.34). The efficiency of the laser can be adapted to the task through adjustment of such variables as energy threshold level, pulse duration, pulse frequency and the focus and/or distance of the laser beam to the surface. The pulse duration can be varied in the ns to several  $\mu\text{s}$  range, while the pulse frequency varies from single pulse to some hundred Hz. With increasing pulse duration the energy density transferred to the surface increases significantly, for example, from 0.8  $\text{J}/\text{cm}^2$  at 8 ns pulse duration to 2.8  $\text{J}/\text{cm}^2$  at 20  $\mu\text{s}$  pulse duration (Giamello et al. 2004). With the help of a lens that is located within the laser hand piece the width of the focus of the



laser beam can be varied from narrow focus less than 1 mm spot to several square centimeters. By varying these three parameters the best appropriate working conditions for the object under consideration can be found.

The transportable laser equipment consists of the generator and the cooling unit. Attached to the generator is either an articulated arm or a flexible glass fiber tube through which the laser beam is conducted to the hand piece. The latter produces what is called a “top hat” energy distribution, while the former has a Gaussian energy distribution because the laser beam is directed by highly reflective mirrors. So this equipment provides more efficiency than that one with glass fiber tube but is more sensitive because the mirrors may deviate from precise adjustment with time.

Because laser light has the same properties as visible light, it is absorbed by dark colored materials and reflected by light colored ones. Laser cleaning for this reason is most appropriate for removing dark incrustations from light colored material such as marble or limestone. Because laser light is reflected from the light surface the process of ablation is automatically stopped when the dark crust is removed and the light surface appears. Therefore, with appropriate use laser will not damage the stone even if it is directed to the surface. Experiments carried out by many scientists yielded congruent results for the energy thresholds of different blackening on marble surfaces:

- Vaporization of black crust:  $6.8 \text{ J/cm}^2$
- Vaporization of black fungi:  $0.3\text{--}0.5 \text{ J/cm}^2$
- Vaporization of mould:  $0.1\text{--}0.2 \text{ J/cm}^2$
- Vaporization of marble:  $17 \text{ J/cm}^2$ .

These data show that the threshold beyond which marble is damaged by laser light is much higher than the one required for the vaporization of black crusts. Damaging marble surfaces is in principle excluded if the correct adjustments are followed. For further information to this subject see Cooper (1998), Siedel et al. (2000), Frantzikinaki et al. (2004), Sliwinski et al. (2006), and Koss and Marezak (2008).

The restoration department of the Prussian Castles and Gardens Foundation regularly uses laser cleaning for the marble sculptures and vases in the parks under their responsibility, for example, those of the Sanssouci and Charlottenburg Palace. The sharp contrast between the black crust cover and the light white surface after cleaning is evident (Fig. 7.35). Because of the high energy of the laser beam, it is compulsory to wear special laser goggles to protect the eyes of the restorer and any person standing nearby, as well as to cordon off the working site for non authorized people.

For the cleaning of the light colored limestone of the huge choir of St. Stephan’s cathedral in Vienna, a private company employed various laser systems (Laserblast, Thales, Artlight, ArtLaser, Palladis, Lambda Scientific). The costs of the entire measure of 30,000 working hours over 7 years, was turned out not more expensive than for traditional cleaning methods.

**Fig. 7.35** Marble sculpture in Sanssouci garden after laser cleaning



Recently, lightweight laser equipment has come to the market. Clean Laser 20 Q, a diode laser, weighs only 12 kg and can be carried on the back directly to the site. For example, the equipment has been tested in the tombs of Neferhotep and Meret Re in Thebes in Egypt. Recent tests on the cathedral of Bamberg yielded such good results so that it has been decided to clean the ornamental parts of the towers with

this technique. Unlike the laser systems mentioned above, Clean Laser 20 Q has a line focus which can be extended or contracted so that the power impact of the laser can be adapted to the desired cleaning effect. Also its power is in the same range as that one of the Nd:YAG lasers.

Meanwhile Nd:YAG laser has been successfully tested for cleaning a great variety of very delicate materials: wood, plaster, ivory, paper, textile, metal, stained glass and many others. As laser light is totally reflected by metallic surfaces it is not applicable for reflecting surfaces. Dark layers on metallic surfaces, however, can be removed. Removing layers from surfaces is based on several effects:

- The strong absorption of laser light of high energy density of several  $\text{J}/\text{cm}^2$  leads to a sudden temperature increase of several hundred degrees of the dark particles.
- Rapid heating is combined with expansion and resultant forcing away from the surface.
- The thermo elastic stresses in combination with the frequency of laser light causes the heated layer to vibrate and repulse any particles adhering to the surface.
- The ablation rate of black layers may be enhanced by moistening the surface with water. The rapid heating causes water to instantly evaporate and the consequent volume expansion exerts a mechanical action sweeping the black crusts particles away.
- The heat wave induced by the laser only penetrates a few microns into the surface. Therefore ablation can be specifically controlled and limited to the black layers to be removed.

The bursting of the crust layer makes a snapping sound that can be used by the restorer to establish the best appropriate power density for the dirt removal. Another possibility, and a very sophisticated one, is the online registration of chemical elemental spectra by Laser Induced Breakdown Spectroscopy (LIBS) with the help of which the ablation of successive layers can be monitored and stopped at the desired level (Zafirooulos and Fotakis 1998).

At low temperature ranges, solid particles of a few microns size burst from the surface. With increasing power density of the beam a plasma cloud is generated consisting of free atoms and radicals. Both plasma and particles pose a health hazard since they may penetrate into the lungs of the operator, therefore the wearing of dust masks is compulsory and it is important to vacuum them off as soon as they are generated.

Amount and composition of emitted matter have been investigated for example by Siedel et al. (2000) and Sliwinski et al. (2006). For some years discussions were held among scientists whether the yellow-brownish layer that often was visible after the removal of black crusts could have been caused by the laser (Fig. 7.36). Such layers have been found especially on sculptures or columns in the Mediterranean area. They are resistant to the energy density used for removing the crust above them. Detailed investigations have resulted in different interpretations of their origin. In some cases, it may simply be the very thin undermost layer of the black crust consisting of gypsum and yellow-brownish soot components.

**Fig. 7.36** Laser cleaning sample on the town hall in Munich. Under the *black crust* appears the *brownish layer*, in this example a *thin colored gypsum layer*, the undermost part of the *black crust*



Pouli et al. (2008) confirm that the yellowish coloring is not induced by the laser treatment itself but represents an already existing discoloration, which is uncovered by the laser cleaning. The discoloration is caused by a multitude of hydrocarbons, which are typically present in black discolorations and may migrate into the stone surface. These discolorations can be removed by IR and UV laser radiation in sequential as well as synchronic mode.

In other cases, the discoloration may indicate former treatment with linseed oil that turns brown by oxidation processes under environmental influences. Such findings often go together with an oxalate layer that may have been produced by microbial activity. Finally, a third interpretation attributes them to the presence of scialbature, a protective layer, 100–300  $\mu\text{m}$  thick, consisting of fine inert aggregate and micritic calcite if not converted to gypsum. Because the undermost yellowish–brownish layer may provide important witness of previous treatments it should never be removed before its nature is thoroughly identified. Interesting work concerning this topic has been made by Vergès-Belmin et al. (1993) and Giamello et al. (2004).

The main objection to laser cleaning is the risk of pigment discoloration. The rapid heat increase causes many natural pigments to release water thus changing their crystallographic structure and color. Thorough investigations on this topic have been made by Sobott (2000) who found that many pigments of importance for cultural heritage are indeed at risk of being destroyed by a laser beam. Among them are the frequently used lead white, azurite, malachite, ochre and other natural pigments that contain hydroxyl groups, as well as all organic pigments. On the other hand smalt, cobalt blue, hematite and green earth are very stable pigments. However, the effect of laser on them depends strongly on the binding medium the paint. Colored stone also can be discolored, in particular if the coloring substance is due to the presence of thin clay layers with iron oxide-hydroxide minerals. Nevertheless, in practice, the soiling over paint layers can be cleaned without any damaging the coloring. For these reasons it is absolutely necessary to determine the best conditions for the laser application by carrying out sample tests on these areas. A promising possibility to circumvent discoloration by Nd:YAG laser may be the use of UV excimer laser with wavelength 248 nm or a combination of different laser wavelength by employing the 2nd and 3rd harmonic vibration of Nd:YAG laser with their wavelength of 532 and 355 nm. Fundamental work in this direction has been undertaken by Frantzikinaki et al. (2004) and Pouli et al. (2004). Equipment using this technology is, however, not yet available on the market because of its technical complexity and cost. Task group CEN/TC 346-WG 3 is currently elaborating a guideline for laser cleaning techniques for cultural heritage.

Practical tests of laser in comparison with other techniques reveal advantages as well as disadvantages. Great advantages are selectivity, avoidance of dust and water and its harmless application to brittle surfaces. Because laser photons have no mass they do not induce stresses to the surface such as even the lightest grains of micro particle jets may do. For this reason, incredibly delicate and fragile details and thinnest scales can be preserved. On the other hand, there is the risk of pigment discoloration, high costs of the equipment, high energy consumption and difficult protection measures to be taken at the building site. Therefore practitioners recommend a combination of different techniques to arrive to the best and most economically satisfying solutions (Bromblet 2000; Endemann 2000; Martin 2000b; Pallot-Frossard 2004; Koss and Marezak 2008).

Unfortunately, cleaning interventions are short lived, particularly in urban environments due to increasing dust emissions. An elucidating example is the Romanesque portal on the south side of St. Ulrich church in Regensburg/Germany. The portal had been cleaned by micro particle jet using corundum in 1985. Figure 7.37 shows the state during cleaning intervention. The spotty appearance is due to discolored remains of oil paint layers. After 10 years, the portal was again substantially covered in dust, especially on the upwards facing areas. Moreover, the amount and size of surface detachments had increased dramatically. Though the portal is partly protected by a wooden shelter case during winter, the water, salt and dust that cars and city buses spray onto the surface during the summer months is apparently sufficient to cause this severe damage increase.



**Fig. 7.37** View of Romanesque portal of St. Ulrich church in Regensburg/Germany. State 1985 during cleaning intervention (*left*) and 10 years later (*right*)

Quality control of cleaning measures can be undertaken by several methods. If cleaning aims at opening the pore space for better absorbing conservation agents the result can be evaluated with water uptake measurements using the RILEM pipe (or Karsten tube) (Wendler and Snethlage 1989). By using this simple device and the evaluation program CALCAROW that is supplied by Dr. Eberhard Wendler, Labor für Konservierungsfragen (e.wendler@t-online.de) the possibility of correlating the measurements made to the water uptake coefficient  $W$ .

Visual inspection yields a qualitative analysis that is only based on a subjective impression of the observer. Detailed surface examination by a loupe will determine more accurately if damage has been inflicted. For a more profound analysis, sample examination by SEM is necessary to determine whether methods are harmful to the surface, for example by breaking mineral grains (Siedel et al. 2000).

Quantitative data for comparing cleaning methods can be obtained by color measurements.  $L^* a^* b^*$  values of cleaned sample areas show the tendency of color shift from black surface to original stone color and are appropriate to define the desired degree of cleaning (Siedel et al. 2000).

Surface roughness measurements as well provide quantitative data for the surface alteration (Rousset et al. 2004). The problem, however, is that these measurements are pointless if the surface is completely covered with a black dirt layer so that the roughness of this layer would be measured and not the roughness of the underlying surface. Therefore, this method is only useful for comparing areas that are not so dirty so that the properties of the stone surface can still be recognized. It is important, that the exactly same areas be measured before and after the cleaning.

The most frequently used instruments for surface roughness measurements are mechanical instruments (profilometer) that register a single roughness profile along a fixed line. Average roughness  $R_a$  as well as maximum surface roughness  $R_{max}$  of the registered profile can be used to evaluate the cleaning result. The problem of the roughness parameters  $R_a$  and  $R_{max}$  is that they do not correlate with the visual impression of the viewer because they reflect roughness dimensions which can not be seen with the naked eye.

Better results are obtained by laser scan roughness measurements or confocal imagery technique. Both of them provide 3-D representations of the measured



surface area together with automatic calculations of the indicative roughness parameters. The stationary instruments, however, can not be employed directly on the object and therefore imprint moulds of the surface using dental products have to be used.

An optical roughness measurement method, which can be applied on buildings, is now available on the market (Weinhold et al. 2008). The technique combines documentation of the visual impression and surface topography. It is based on the intensity of shading, which is directly correlated with roughness. The software calculates the well-known parameters  $R_a$  and  $R_{max}$  as well as the roughness of the visual impression which is decisive for the viewer. The measurement head, however, which has an opening of 2.5 cm needs a planar surface because side light would disturb the measurement.

Roughness measurements are most appropriate for monitoring roughness increase of polished surfaces upon exposure to environmental influences. For all roughness measurements it has to be taken into account that the roughness values do not necessarily correspond to the visual impression. The roughness identified by the instruments is much finer than what can be seen with the naked eye but it can be assessed by touch (Grissom et al. 2000). Moreover roughness values cannot be correlated with an absolute scale but have to be interpreted in relation to the stone type, i.e., marble, sandstone, granite. Furthermore, it should be noticed that cleaning mostly results in higher roughness values since it removes the dirt that sits in the pores and smoothens the surface. Analyzing cleaning effects by surface roughness measurements is still in the beginning and much work has to be done to develop a standard methodology.

## 7.5 Desalination of Masonry

As described in Chap. 5, salts in combination with moisture are the main factors for stone deterioration. Before undertaking conservation measures such as consolidation or hydrophobation, desalination should be carried out. This is part of the necessary preventive conservation in order to enhance the durability of the total intervention. In Fig. 7.38 salts can be seen to creep upwards even through massive stone blocks. It has been found that nitrates migrate highest (due to their high solubility) while sulfates reach minor heights. In most cases, sulfates concentrate in few millimeters depth near the surface while nitrates tend to disseminate over the whole width of masonry. Extraction of sulfates from sculptures or masonry therefore is easier and has yielded greater success than that of nitrates.

The salts contaminating stone can originate from very different sources. Archaeological objects from desert areas like Egypt are normally contaminated with sodium chloride NaCl. In European countries and North America chlorides mostly derive from de-icing salt. Sulfates, as gypsum, sodium sulfate or magnesium sulfate may arise from reaction of the calcite bearing stones or lime mortars with environmental pollution, or from other materials, such as bricks and Portland

**Fig. 7.38** “Rising damp” and salt crystallization horizon on pillars of Royal Mint Building in Munich



cement, from burning them with sulfur rich coal. Nitrates have their origin in manure from animal stables. Methods for reducing salt content will differ depending whether this is a single object, e.g., a tombstone, or an entire masonry.

Movable objects, e.g., sculptures or vases, can be transported to restoration workshops and desalinated in water baths. Franzen et al. (2008) did a complete desalination of a Cotta type sandstone vase from the Dresden Zwinger. Keeping the vase in a water bath for 65 days, 340 g salt, mainly sulfates, could be extracted. By drying the object covered by a poultice, another 108 g salt could be extracted. The authors recommend regular exchange of the water because the driving force for salt extraction from stone pores is the concentration gradient. If the water is not exchanged, the concentration gradient decreases over time until equilibrium is reached between the salt concentration in the water and in the stone. The change in salt concentration can be easily monitored by measuring the conductivity of the water bath.

Wedekind et al. (2008) compared desalination in water bath with desalination of two objects—an obelisk and a tombstone—in the Göttingen Bartholomew

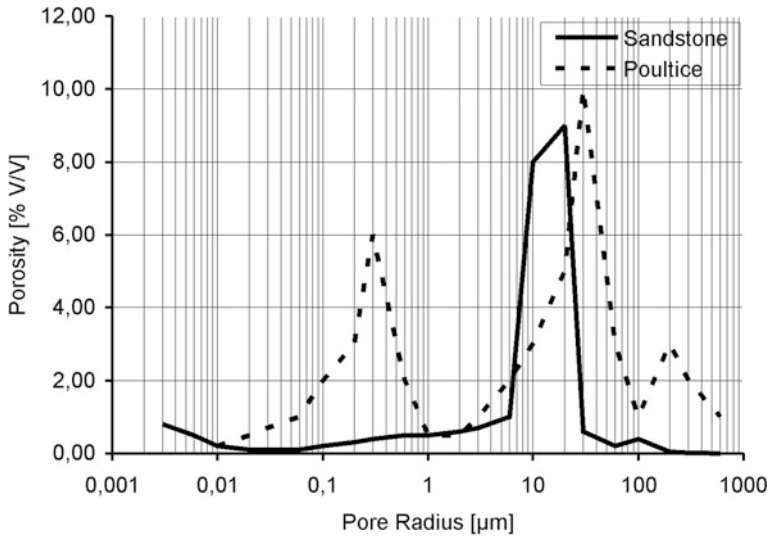


**Fig. 7.39** Pore size distribution of a poultice able to extract salt from the sandstone given in this example (IUAV 2006, 2007) (Figure by van Hees)

cemetery. The two in situ methods tested were periodical wetting of the surface and an injection system where water was introduced into the interior of the stone via drill holes of 10 cm depth. To ensure one-dimensional drying the tombstone was sealed on three faces with a plastic foil and a cellulose poultice was applied to the fourth surface. In the first case, i.e., surface wetting, a total of 16 g per square meter could be extracted. In the second one, the injection system, a total of 38 g per square meter was extracted, proving it to be more efficient. Both methods, however, proved less effective than water bath desalination of a third sandstone tomb of 1 m<sup>3</sup> size, out of which in total 1,500 g salts could be extracted. Only by the first bath, the salt content was lowered by half while the subsequent cycles progressed in smaller steps (Ruedrich et al. 2008).

Desalination of stone and stone or brick masonry depends on the moisture transport properties of both the substrate and the poultice. Since the pore size distribution of the substrate cannot be changed, it is important to vary that of the applied poultice, including its suction capacity to adapt it to that of the stone. The basic requirements the poultice must fulfill to be effective is shown in Fig. 7.39.

As can be seen in Fig. 7.39 the poultice shows two pore size maxima, one of it in the pore range above and another one in the pore range below the pore maximum of the sandstone. The function of the two pore size maxima is different. In the wetting process, the stone suctions water from the poultice because its pores (10–20 µm radiuses) are finer than the second pore size maximum of the poultice (around 30 µm radius). During the drying phase, the fine micro pores (0.3 µm radius) of the poultice suction out the salt loaded liquid from the stone. As the water evaporates the salt burden is concentrated in the poultice. It is essential to

tailor poultices so that their pores are able to withdraw liquid from the stone pores because otherwise the migration of salt into the poultice will not be efficient.

Lombardo and Simon (2004) investigated the effectiveness of different poultice mixtures on bricks contaminated with sodium chloride. The various poultices were composed of cellulose, sand (+ glass micro-sphere) and mineral component (kaolinite, bentonite or Na-zeolite). They found bentonite rich poultices more efficient initially, while Na-zeolite and kaolinite rich mixtures required more time to reach saturation. It is important to find the right ratio between the components to control the drying behavior, reduce shrinkage and increase the efficiency of salt extraction. A mixing ratio of cellulose:mineral component:aggregate of 1:1:4 proved quite suitable for most applications. The use of Japanese paper in the interface between stone surface and poultice did not negatively affect the efficiency of the poultices while serving to facilitate complete removal of the poultice.

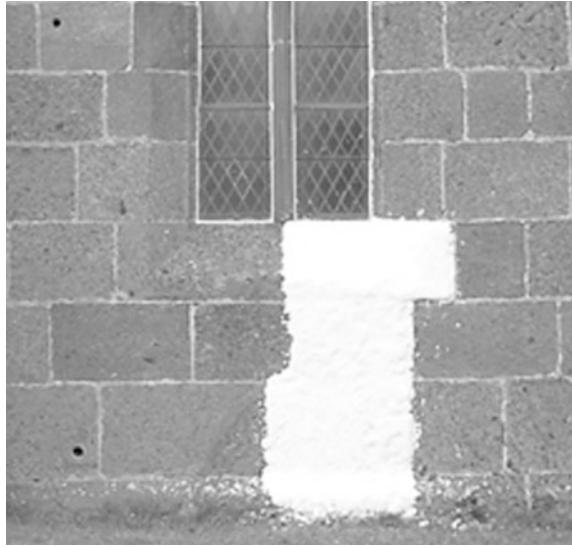
Bourguignon et al. (2008) studied the drying process of stone and poultice attached by means of Nuclear Magnetic Resonance Imaging (NMR Imaging). The poultices consisted of cellulose, sand or glass spheres and kaolinite in different proportions and confirmed that the stone dried faster than the poultice when the latter had a higher capillary suction as previously described.

It is a big step from desalinating a single object to the desalination of an entire masonry wall. In the latter case, long application times -up to month- are necessary to obtain a satisfactory efficiency. Ensuring low shrinkage of the poultice and perfect adhesion to the stone surface are difficult to achieve for such a length of time. Nevertheless poultice technology has advanced so far that large masonry walls can now be treated with success. For large scale desalination the poultice mixture is applied by spraying machines, such as used for shotcrete. An example of a desalination poultice on a church wall is presented in Fig. 7.40.

Within the frame of EU project "Desalination" Doehne et al. (2008) have been treating sample areas on historic brick and timber houses in New Orleans. The humid climate combined with low drying rates turned out to be helpful when leaving the poultices for a month on the wall. Thus a desalination efficiency of 90 % could be achieved. Under normal conditions, poultices can be left applied for at most 6–8 weeks. At this point, the entire poultice has dried out and no further extraction can occur. High advection increases drying rate and causes poultices to dry fast and detach from the surface. It is therefore necessary to protect the poultice from direct wind and sun. However, a moderate circulation of wind is necessary to dry the poultice slowly.

Since some 20 years ago, electro-osmotic methods are periodically being proposed for desalination and moisture reduction of masonry. In case of active electro-osmotic methods an electric field is imposed to the masonry in an opposite direction to the fluid flow potential in the material. Theoretically, this way reduction of moisture and salt in the masonry can be obtained. The complex interactions between the different materials within the masonry as well as the complicated physical background of the zeta-potential cannot be discussed here in detail (Wittmann 1981, 1983). IDK (2001) reports that the zeta potential may change in course of the drying process thus leading to re-moistening of the

**Fig. 7.40** Desalination poultice on a church wall (Belk 2005)



masonry. In practice, electro osmotic installations never appear to work effectively, mainly because of the complete corrosion of the electrodes after short time. Conclusive investigations about effectiveness and long term performance are missing. Nonetheless, electro-osmotic systems are still being sold in several countries. In general, all electro-osmotic methods are not sufficiently investigated and because of their questionable effectiveness they should not be applied.

## 7.6 Consolidation of Stone

Presently, most stone consolidation interventions are carried out with the tetra ethyl ester of orthosilicic acid (TEOS) and its modifications. Previously it only had been used for sandstone consolidation but over the years it has been adapted to others types of stone, such as limestone and granite. Therefore this section will mainly deal with the TEOS group of chemicals. Detailed information about inorganic and organic stone consolidating materials may be found in the previous [Sect. 7.2](#) or in [Clifton \(1980\)](#).

Deterioration always causes a decrease in strength starting from the surface and progressing into the interior of stone. Consolidating stone therefore aims at equalizing this strength deficiency. [Figure 7.41](#) shows three different hypothetical strength profiles of weathered stone. Curve a shows a steady strength decrease towards the surface; in terms of the deterioration glossary ([Chap. 5](#)) it may be referred to “granular disintegration”. Curve b describes an in-between-step during the formation of a surface scale, which still adheres to the stone. The interior and the surface are bridged by a transition zone with reduced strength that, however, still maintains capillary conductivity. When the transition zone is further

**Fig. 7.41** Three schematic strength profiles of a stone. Curve (a) granular disintegration. Curve (b) contour scale in process of formation. Curve (c) detached contour scale

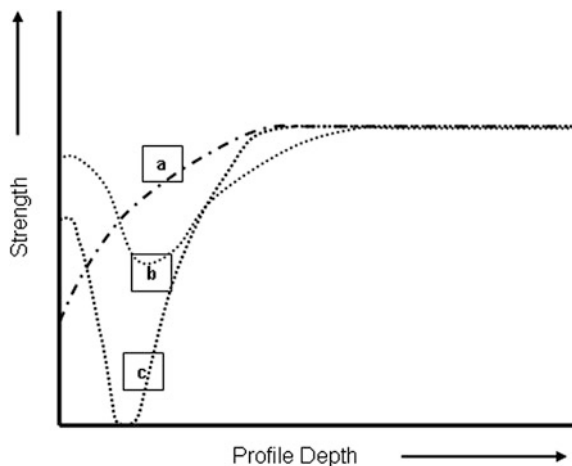


**Table 7.5** SiO<sub>2</sub> content and SiO<sub>2</sub> gel formation per unit consolidant volume of common consolidants

Compound	Concentration W/W (%)	SiO <sub>2</sub> W/W (%)	SiO <sub>2</sub> gel formation (g/l)
Sodium hexafluoro silicate	30	10	15
Potassium waterglass	25	18	25
TEOS monomeric	75	21	300
TEOS monomeric	100	28	400
TEOS precondensed	100	40	500

weakened, the scale will eventually detach as shown by curve c. In this case the strength of the transition zone has dropped to zero and no capillary conductivity is possible. Consolidation with TEOS (and other consolidants as well) is only possible for deterioration corresponding to curves a and b, because the capillary conductivity allows the liquid consolidant to penetrate into the stone. In the case of curve c, however, consolidation would be counterproductive leading to a strengthening of the scale with the consequent enhanced risk of immediate detachment.

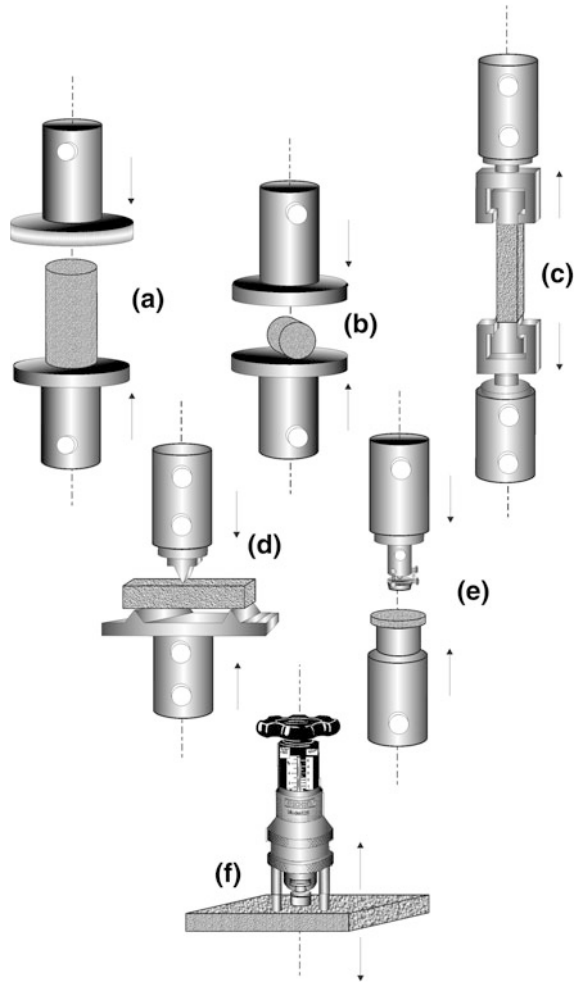
Among other advantages, such as not producing undesired by-products, TEOS products are preferred to other consolidants because of their high SiO<sub>2</sub> content and SiO<sub>2</sub> gel formation per unit consolidant volume. Table 7.5 presents an overview of the most common products including inorganic SiO<sub>2</sub> gel forming consolidants.

It is evident that a gel formation of 500 g/l is extremely efficient for strengthening weakened stone in comparison to other agents, such as the fluosilicates. TEOS is applied to the stone with a brush, a laboratory spray bottle or an airless device. It is important not to disperse the liquid to fine droplets but to provide a coherent liquid stream running down the treatment area. The liquid is soaked up by the capillary forces of the material. Therefore, the application time will depend on the type and degree of damage as well as on the material substrate



**Fig. 7.42** The most frequent methods for measuring material strength.

**a** Compressive strength,  
**b** cleaving strength (Brazilian Test),  
**c** tensile strength,  
**d** uniaxial bending (flexural) strength,  
**e** biaxial bending (flexural) strength,  
**f** surface pull-off strength (Kocher 2005)



properties. Investigations into application techniques are very rare and date back to the former German research project “Steinzerfall—Steinkonservierung”. The prototypes developed by the Institute of Construction Machinery and Organization of RWTH Aachen unfortunately never developed commercially (Prickarts and Schoonbrod 1993, 1998a, b). Consequently, the technical standard in this field is quite poor and completely inadequate with regards to the importance that good applications have in providing an effective consolidation treatment.

A compilation of the most frequent methods for testing material strength is presented in Fig. 7.42. Among them compressive strength, bending strength or biaxial flexural strength of drill core slices are most frequently used for determining consolidation effectiveness. The first two tests require rather large sample sizes so they are mostly appropriate for laboratory testing. But biaxial flexural

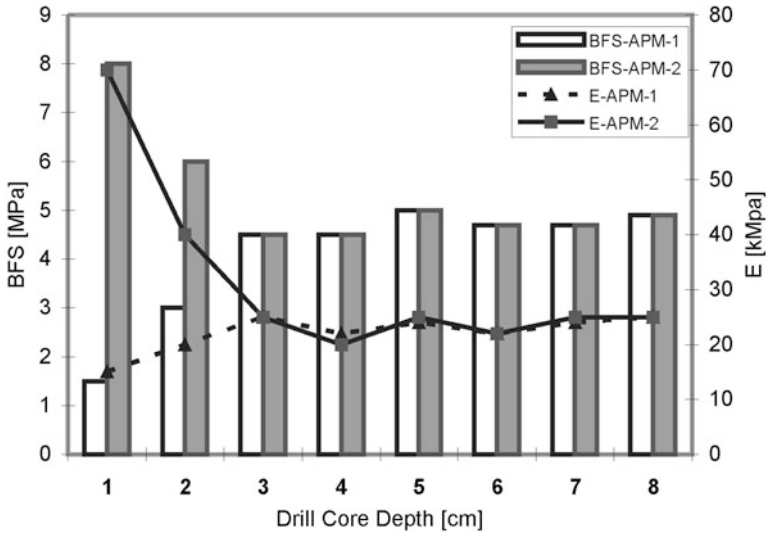


**Fig. 7.43** Bi-axial flexural strength and E-modulus profiles before and after consolidation with TEOS. BFS before *light bars*, after *dark bars*. E-modulus before *dashed line*, after *full line*. Greensandstone from Alte Pinakothek Munich (Sattler 1992)

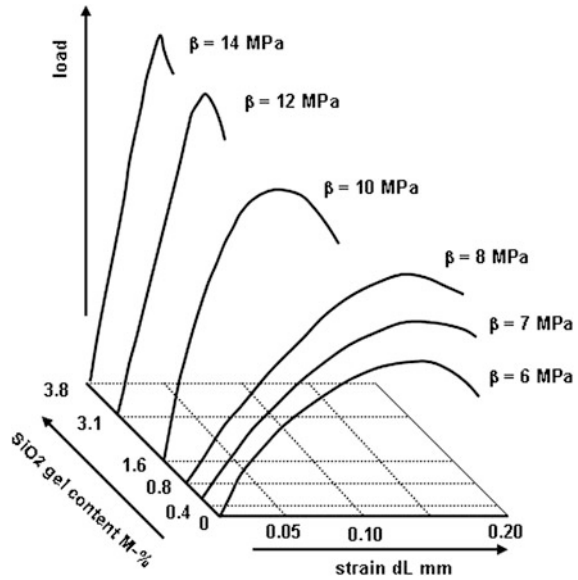
strength is especially appropriate for measurements of treated large objects because it only requires drill cores with a moderate diameter that can be cut into slices for testing.

The great advantage of measuring biaxial flexural strength with the described methodology is that by compiling all measured values a strength profile is obtained that goes from the surface into the interior of the treated stone. With the help of such strength profiles the penetration of the consolidant into the stone and the effectiveness of the treatment can be evaluated. Moreover, the modulus of elasticity, E-modulus, can also be determined at the same time. An example of a strength profile is depicted in Fig. 7.43.

As shown in Fig. 7.43, strength decreases towards surface before treatment. After treatment there is a clear increase of strength within the first two slices. The penetration depth of the consolidant can be estimated at two centimeters. Likewise it is important to notice that together with the strength, the E-modulus increases as well (solid lines in Fig. 7.43). As strength and E-modulus increase far above the level of the unconsolidated and unweathered stone (indicated by the rear part of the drill core) the question arises whether the increase bears a risk of delamination by over-strengthening the surface layer. This topic will be discussed later in detail.

The effect of strengthening with TEOS becomes even more evident in Fig. 7.44. The tested Maulbronner sandstone shows a strength increase of a two-fold factor with increasing  $\text{SiO}_2$  gel content and mechanical properties change gradually from viscous-elastic to elastic behavior as indicated by the steeper stress-strain lines.

**Fig. 7.44** Stress strain lines of Maulbronner sandstone with increasing content of SiO<sub>2</sub> gel deposited in pore space by multiple treatments with TEOS. The mechanical behavior changes from viscous to elastic (Sattler 1992)



That change of mechanical behavior can be very dangerous when a surface layer with high E-modulus (strongly elastic) lies on an inner stone layer with low E-modulus (viscous-elastic). If the two layers are exposed to severe wetting and drying, the stresses generated at the interface between treated and untreated inner part could rise to such a level that the treated zone may detach from the inner part. In Fig. 7.45 an example is shown how far E-modulus of treated zone may deviate from untreated zone.

The diagram is based on stress–strain lines simply calculated for assumed E-modulus differences  $\Delta E$ . Into this diagram the measured tensile strength values for untreated Schilfsandstone variety from Schloss Schillingsfürst (SSF) and Greensandstone variety from Alte Pinakothek Munich (APM) are introduced. Furthermore, the difference of hydric dilatation between TEOS consolidated and untreated samples of both stone varieties have to be measured and introduced into the diagram. From Fig. 7.45 the following results can be read.

In case of the Schilfsandstone with low tensile strength (2 MPa) but high difference of hydric swelling (1.2 mm/m) the E-modulus between treated and non-treated zone may only differ by 2 GPa. It is necessary to select fully appropriate consolidants and to prove their efficiency before application on the object. In case of the much stronger Greensandstone from Alte Pinakothek Munich (tensile strength 6 MPa) the situation is less critical. Because the hydric swelling difference is only around 0.3 mm/m the E-modulus difference between treated and non-treated zone may reach almost 20 GPa, a very high a value but that can occur as shown in Fig. 7.43 where the E-modulus rises from 25 to roughly 70 GPa.

The values referred to in Fig. 7.45 need further discussion because they only represent a rough estimate of the real situation. First of all, it has to be taken into

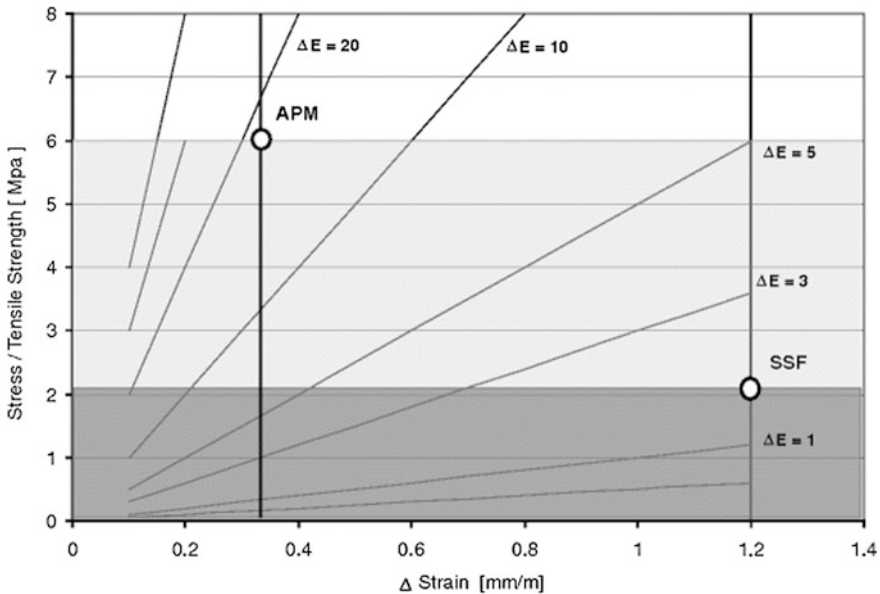


**Fig. 7.45** Maximum acceptable difference of E-Modulus between consolidated and non consolidated zone. *APM* Greensandstone variety from Alte Pinakothek Munich. *SSF* Schilfsandstone variety from Castle Schillingsfürst. For more information see text

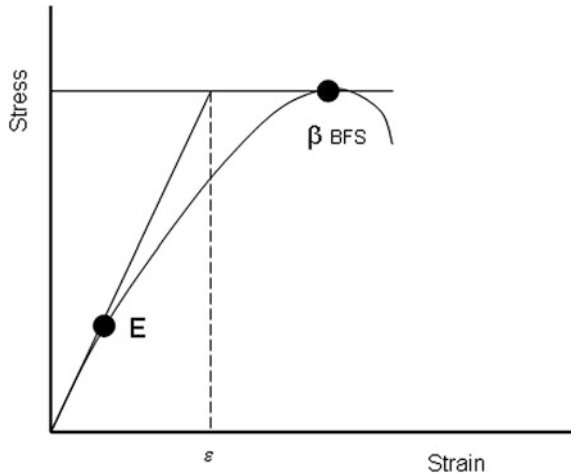
account that all strength and E-modulus values that are reported in the literature relate to internationally standardized testing conditions, a load rate of 0.5–1.5 MPa/s and moisture content conditioned to 20 °C and 65 % RH. This load increase rate is very high and far higher than in nature. In the latter, environmental stress on the stone surface layers is generated by moisture and temperature cycles. These cycles change at a slower rate than those in the standard test conditions and, consequently, the stress increase rate is also far slower.

With slowly increasing stress, the breaking strength of any material will be lower than when subjected to a fast stress increase. Moreover, the strength of wet stone is lower than that of dry stone, in particular in case of clay-rich sandstone for which the strength decrease may drop to less than of the half of dry stone. Given these premises the values derived from Fig. 7.45 would be too high and not applicable to predict behavior in nature.

Furthermore, under low loading rate the stone material is able to reduce stress by creep (creep is a very slow deformation process within the grain structure without the formation of cracks). Likewise for slow processes and increased moisture content, the E-modulus is much lower thus reducing the stress at the interface between treated and non-treated zone.

Thus, it can be concluded that both parameters work into opposite directions and therefore may balance each other. Investigations into this issue to clarify the conditions under which a risk for surface detachment exists would be very welcome; however, data about creep and fatigue under moisture and temperature cycles are not yet available.

**Fig. 7.46** Schematic stress–strain curve and calculation of maximum strength and E-modulus

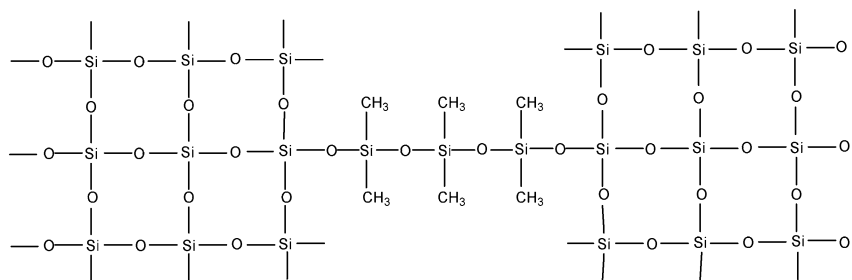


It is important to note that strength and E-modulus values used for risk assessment are calculated from different points of the stress–strain curve (Fig. 7.46). Strength is calculated at the maximum breaking force at the top of the curve whereas, by convention, E-modulus is calculated at one-third of the curve. It can be seen from Fig. 7.46 that the strain calculated from strength and E-modulus (dashed line) is much lower than the real breaking strain measured at the top of the stress–strain curve. Also the E-modulus is much lower towards the breaking point of the stress–strain curve (it must be noticed that in the flat part of the stress–strain curve a real E-modulus is not defined because strain is not reversible. It is, however, a fact that the elasticity is decreasing).

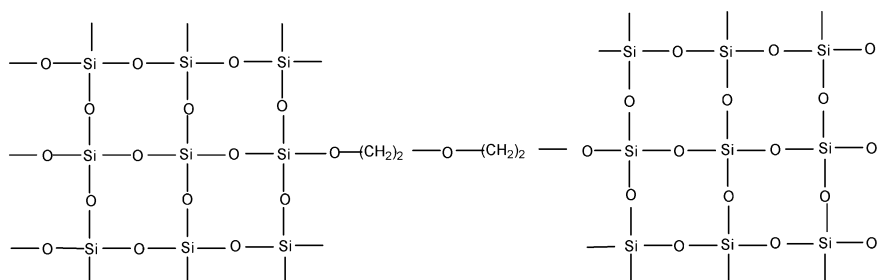
For the above reasons the values depicted in Fig. 7.45 refer to severe testing conditions and represent worst conditions for evaluating the damage risk at the treated–untreated interface. The data in Fig. 7.45 do not represent exact data but are sufficient for rough but useful assessment. For further information see Sneathlge and Meinhardt-Degen (2004) and Sneathlge (2008).

SiO<sub>2</sub> gel formed by pure TEOS is a brittle material often leading to high strength but also undesired E-modulus increase. Therefore several attempts have been made to lower the brittleness of the gel by introducing flexible segments into the gel structure. For example this can be done by either introducing dimethylsiloxane or polyether both with various chain lengths (Fig. 7.47).

The dimethylsiloxane or polyether chains break the rigid network of SiO<sub>4</sub> tetrahedrons making the entire gel more flexible. Because dimethylsiloxane is hydrophobic (due to the attached methyl groups) the modified gel is also slightly water repellent. On the other hand, the polyether modified gel is as hydrophilic as the unmodified gel. The latter product is marketable by REMMERS under the brand name Funcosil 300 E. The other one can be made in laboratory by mixing the components in an appropriate ratio. In effect the E-modulus of the gel is lowered



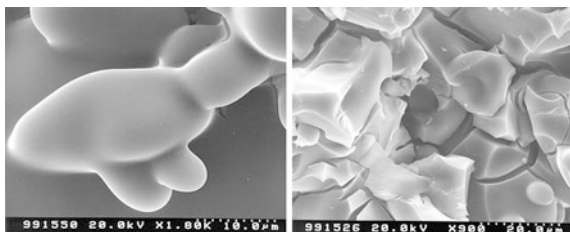
Flexible hydrophobic silica gel with soft segment of dimethyl siloxane



Flexible hydrophilic silica gel with soft segment of polyether

Fig. 7.47  $\text{SiO}_2$  gel with soft segments of dimethylsiloxane or polyether chains

Fig. 7.48 Funcosil 300 E gel on fritted glass (*left*) and Funcosil OH gel on fritted glass (*right*). The flexible Funcosil 300 E gel exhibits almost no cracks. SEM photos (Remmers Chemistry) (Figure by Wheeler)



and consequently, also that of the treated stone. Because of this, the cracking of the gel upon drying is strongly reduced. Figure 7.48 shows the modified Funcosil 300 E gel in comparison with  $\text{SiO}_2$  gel formed from regular TEOS Funcosil OH. It can be seen that the modified gel shows almost no cracks whereas the regular one is completely cracked and disintegrated into single gel plates.

As pointed out in Sect. 7.2, TEOS and the gel formed from it have a special affinity to siliceous stones, such as sandstones containing mainly quartz and feldspar minerals. This can be attributed to hydroxyl groups covering these mineral surfaces to which the gel can tightly link. In limestone, marble and in



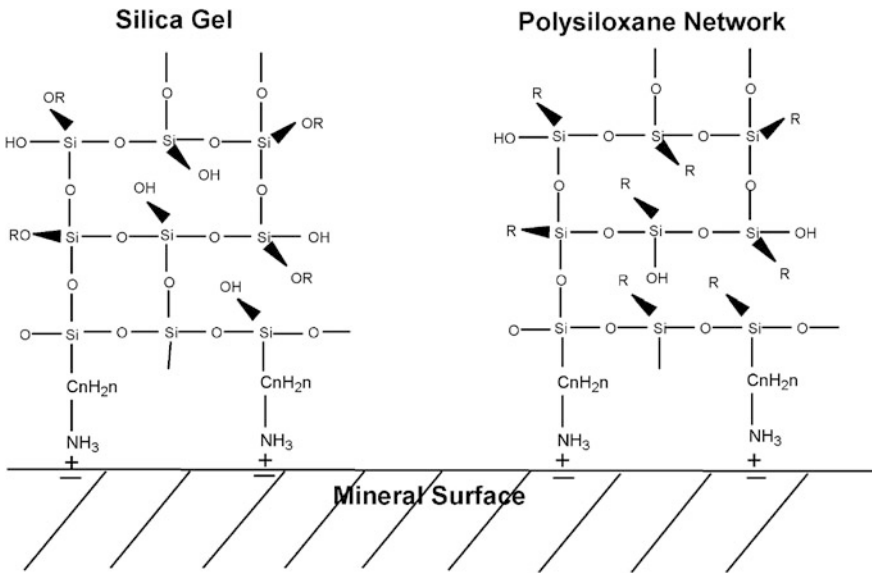


**Fig. 7.49** Amino-functional silane coupling agent bridging silica gel and polysiloxane to mineral surface with negatively charged surface

calcareous sandstones, there are far fewer hydroxyl groups attached to the calcite mineral because its crystal lattice is very different from that of the mentioned silicates. For this reason consolidation of limestone, marble and calcareous sandstone is by far less efficient than for sandstone (Wheeler et al. 1992; Goins et al. 1996a, b). It has been observed that  $\text{SiO}_2$  gel very quickly detaches from the calcite surface during the course of the drying process that occurs within a few months (Elfving and Jäglid 1992). The detached gel grains do not strengthen the stone any more but can be compared to loose sand grains filling the pore space.

Several attempts have been made in the past to overcome this difficulty. Weiss et al. (2000) demonstrate the possibility of forming a hydroxylated conversion layer on calcitic crystal surfaces by applying dilute tartaric acid solution. The conversion layer adheres very well to the substrate and permits reaction with TEOS based consolidants and hydrophobic silanes. Tests on dolomitic limestone treated with Conservare OH proved a strength increase of 25–50 %.

Another approach is based on the admixture of coupling agent to TEOS. Snethlage et al. (1996b) and Snethlage and Wendler (2001) proposed various coupling agents based on silanes for improving the adhesion between  $\text{SiO}_2$  gel and calcareous and clay-rich substrate. Figure 7.49 shows the chemical mechanism of how an aminosilane coupling agent acts as a bridge between the gel and the substrate. The silanol part of the aminosilane is connected with the tetrahedron network of the  $\text{SiO}_2$  gel (or with a polysiloxane) while the positively charged amino functional group at the other end of the molecule is connected to negatively charged positions on the calcitic substrate surface.

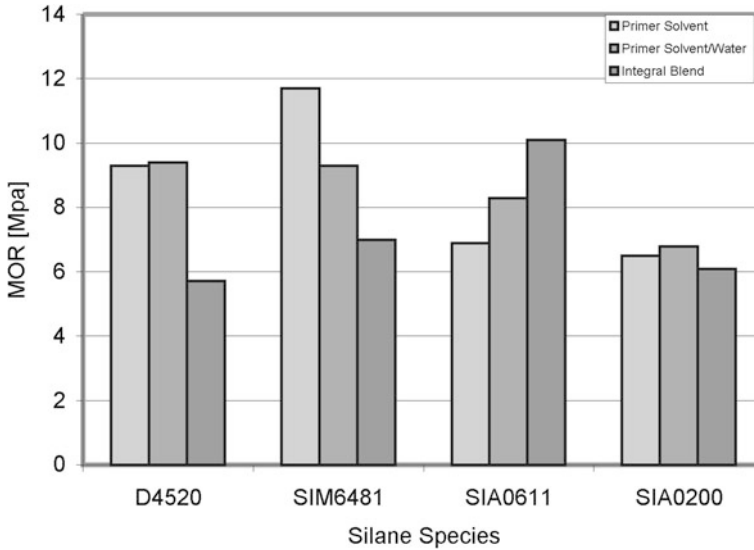


**Fig. 7.50** Improvement of the modulus of rupture MOR of limestone by various silane-based coupling agents. *Solid line* is MOR of untreated limestone. *Dashed line* is MOR of limestone treated with TEOS alone (from Wheeler et al. 2000)

The effect of a coupling agent on the strengthening of limestone with TEOS products has been shown by Wheeler et al. (2000) through measuring the modulus of rupture (MOR) (three-point-bending test ASTM C 674-88). By testing several silane-based coupling agents the enhanced consolidating effect of TEOS was clearly established. The actual agents tested are not listed here since the chemistry is not essential for understanding the results. What is important is that the obtained result depends not only on the nature of the coupling agent but also on the application methodology (Fig. 7.50). In general, the result proved better when the coupling agent was applied as a primer and not admixed with the TEOS. Furthermore, in one example no improvement was found at all in comparison with pure TEOS.

Wheeler's results have been confirmed by Steinhäuser et al. (2006) by testing various adhesive couplings and primer pretreatments on limestone and artificial silica gel bound mortars.

Impregnation with TEOS is only effective for porous limestone having sufficient capillarity. Laurenzi-Tabasso (2000) therefore differentiates three main Italian limestone categories requiring different conservation treatments:

- Very compact homogeneous limestone, such as Istrian stone, Travertine, Carrara and alpine marble.
- Compact but heterogeneous, veined limestone, such as Verona Red and Assisi limestone.
- Very porous and marly limestone and calcarenites, such as Vicenza stone, Lecce limestone and calcarenites from Sicily, e.g., Agrigento or Noto.

Sufficient capillarity can only be expected for the very porous stones of the last category and therefore effective treatments with TEOS are possible. The dense stone varieties require other conservation products with a more adhesive effect than the  $\text{SiO}_2$  gel, since the latter effectiveness is mainly based on large internal surface of the treated stone where the gel can spread and penetrate into interstices. However, calcite grains with flat surfaces must be bound together. Therefore, regular TEOS is mostly ineffective because the internal surface of marble is too low. Also its water content is too low to initiate the hydrolysis of TEOS, even in deteriorated marble, and finally, a silane coupling agent would be needed to address this problem.

Mainly in Italy, but also in most countries worldwide Paraloid B 72 and mixtures with methyl-trimethoxysilane (MTMOS) have been used to conserve dense and compact limestone or marble by impregnating veins or small cracks. The products have also been used as protective surface varnishes against environmental air pollution and acid rain (Nonfarmale 1976; Laurenzi-Tabasso 2000; Haake and Simon 2004).

Finally, some preliminary tests with fluorinated polymers carried out in Italy should be mentioned (Aglietto et al. 2000; Chiantore et al. 2000; Fassina 2004). Fluorinated polymers exhibit a better resistance against acidic environmental attack and are more stable against UV radiation. They can be applied as pure agents or in combination with common acrylic polymers. The products are still in experimental phase and have as yet not experienced wider application.

Strengthening of Ança and Lecce stone with inorganic consolidants, i.e., barium hydroxide  $\text{Ba}(\text{OH})_2$  and ammonium oxalate  $(\text{NH}_4)_2\text{C}_2\text{O}_4$ , has been tried by Ferreira Pinto and Delgado Rodrigues (2008). The results obtained by microdrilling measurement (Tiano et al. 2000a, b) revealed them to be less effective than TEOS treatments of the same stone.

Criteria for evaluating consolidation treatments have been established by Snethlage and Wendler (1996), Sasse and Snethlage (1997), Laurenzi-Tabasso and Simon (2006), Snethlage (2008). Whereas Snethlage, Sasse and Wendler define numerical evaluation criteria, Tabasso and Simon just present descriptive criteria assessments (“moderate increase”, “homogeneous profile”).

In the following paragraphs the most important evaluation criteria for stone consolidation are described:

### 1. Visual Appearance

Consolidation with TEOS normally causes a slight surface darkening and intensification of color due to the enhanced absorption of light by the deposited gel. Normally, this change disappears after few days or weeks. If not, persisting darkening and color change may be a criterion to exclude a given consolidation product. Surface gloss is mostly consequence of an inappropriately carried out application. If the moisture content was too high when the treatment was applied,  $\text{SiO}_2$  gel precipitates directly on the surface thus producing gloss and later gray deposits that can not only be removed by micro particle jet blasting.

**Table 7.6** Required penetration (s) depth depending on water uptake coefficient W

$W \text{ kg/m}^2 * \text{h}^{0.5}$	s (cm)
0.1–0.5	$\geq 1$
0.5–3.0	$\geq 3$
$>3.0$	$\geq 6$

## 2. Capillarity (Water Uptake Coefficient W and Water Penetration Coefficient B)

The units of the water uptake coefficient W are  $[\text{kg/m}^2\text{h}^{1/2}]$ . The water penetration coefficient B  $[\text{cm/h}^{1/2}]$  is directly related to the water uptake coefficient (the units are chosen for practical reasons, since SI standard units result in very small numbers difficult to compare). Given the same magnitude of water uptake coefficient the water penetration coefficient will be higher for a lower total porosity and vice versa. The assessment criterion is that both parameters should not increase by treatment ( $t = \text{treated}$ ,  $ut = \text{untreated}$ ), with  $W_t \leq W_{ut}$  and  $B_t \leq B_{ut}$ .

## 3. Penetration Depth

Penetration depth can be obtained by measuring the strength profile from the surface to the interior of the sample. This can be done either by microdrilling or with the help of a drill core taken from the monument. Penetration depth should be equal to the depth of decreased strength, in normal cases ranging from a few millimeters to few centimeters. In many cases, for example in case of valuable historic monuments or sculptures, neither microdrilling nor taking a drill core is acceptable. Then, the necessary penetration depth can be estimated by means of the extension of the zone of maximum average moisture content (Sneathlge and Wendler 1997). This can be understood in the following way. Moisture taken up during rain penetrates into stone depending on its capillarity. During drying, the surface will dry out very quickly; however, moisture is retained longer at a certain depth of the stone and takes more time to evaporate. During the course of a year, moisture content on the surface changes rapidly between saturation and absolute dryness. Some millimeters or centimeters below the surface, there is higher moisture content than at the surface or further in the interior of the stone. The location of that moisture maximum depends on the capillarity and on the climatic conditions in the immediate vicinity (rain intensity, wind ventilation, sunshine). The required penetration depth of the consolidant should go beyond that maximum value. As for most stones the water uptake coefficient W is known the required penetration depth can be estimated from it. Sneathlge (2008) recommends the following values (see Table 7.6).

The required penetration depth should be achieved within five minutes of application of the consolidant by brushing or spraying. If this is not possible, the application should be carried out with long term spraying or poultices. The author is aware the difficulty to reach such penetration depth in practice, however, under the premise of best practice and to ensure quality these values should be aimed at.

#### 4. Hydric Dilatation

The dilatation ( $\mu\text{m}/\text{m}$ ) of the treated stone should not deviate from the untreated state.

#### 5. Water Vapor Diffusion Resistance ( $\mu$ )

The water vapor diffusion resistance ( $\mu$ ) should not increase by more than 20 %.

#### 6. Biaxial Flexural Strength ( $\beta_{\text{BFS}}$ )

As pointed out before,  $\beta_{\text{BFS}}$  provides the possibility of determining the strength profile and weathering penetration depth. In an ideal case, the consolidation should just cancel out the strength deficiency thus creating a homogeneous strength profile on the level of fresh un-weathered untreated stone,  $\beta_{\text{BFS}, t} = \beta_{\text{BFS}, ut}$ .

In practice, however, the strength near the surface will increase above that of the unweathered stone. For this reason, and to prevent the risk of scaling, the question arises how to establish acceptable tolerance limits. Moreover, transition from treated zone to untreated zone should not be abrupt but gradual. Snethlage and Wendler (1996), Sasse and Snethlage (1997) and Snethlage (2008) established the following boundary conditions:

$$[\beta_{\text{BFS}, t} - \beta_{\text{BFS}, ut}] / \beta_{\text{BFS}, ut} \leq 50 \% \quad (7.10)$$

$$\Delta\beta_{\text{BFS}, t} / \Delta x \leq 0.2 \text{ MPa}/\text{mm} \quad (7.11)$$

The first equation fixes a limit of a 50 % increase above the strength of untreated stone. This limit is based on experience, since it was found that within a specific stone type (not “sandstone” in general), strength deviations of  $\pm 50$  % may occur. Therefore, it is not meaningful to set narrower limits. On the other hand, deviations higher than 50 % already define a new variety of the same stone type.

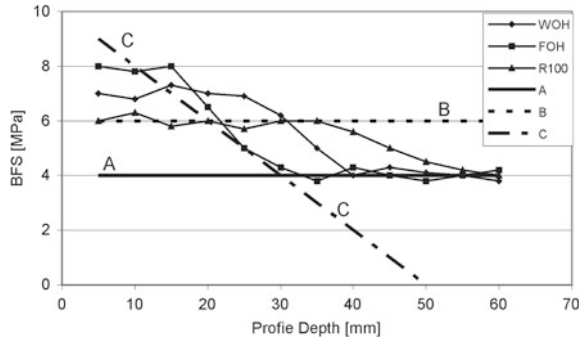
The slope of strength decreases with the distance  $\Delta x$  from treated zone seems sufficiently low to ensure that the stress between treated and untreated zone cannot increase high enough to produce scaling.

The same rules can be applied to compressive or bending strength measurements.

Figure 7.51 presents an example of how these boundary values can be used to choose the most appropriate product for a given consolidation project. In Fig. 7.51 line a represents the strength level of the fresh unweathered stone, dashed line b the boundary limit of 50 % increase and line c the slope of 0.2 MPa/mm. Furthermore three measured strength profiles of three different strengtheners are depicted.

It can be seen that product FOH should be excluded because it breaks the <50 % rule and the slope from treated to non-treated zone is steeper than allowed

**Fig. 7.51** Boundary limits for strength profiles illustrated by an actual example. Products FOH and WHO exceed boundary limit of 50 % strength increase and the slope to the level of the unweathered stone is too steep. Product R100 fulfils all requirements



by the rule. Product WOH also violates the <50 % rule, however, fulfils the slope rule. Product R100 is the only one of the three, which fulfils both rules and should therefore be chosen for application.

**7. Modulus of Elasticity (E)**

Two kinds of modulus of elasticity E can be considered, the one derived from strength measurements E[static] in a testing machine, the other one derived from ultrasonic measurement E[dynamic]. Both moduli are proportional to each other, the ratio between them, however, differs from stone type to stone type. In many examples E[dyn] is higher than E[static]. For the E-Modulus the authors previously mentioned (Snethlage and Wendler 1996; Sasse and Snethlage 1997; Snethlage 2008) have established similar limits as for biaxial flexural strength  $\beta_{BFS}$ :

$$[E_t - E_{ut}]/E_{ut} \leq 50 \% \tag{7.12}$$

$$\Delta E_t/\Delta x < 1 \text{ GPa/mm} \tag{7.13}$$

The rules for the modulus of elasticity E have the same meaning as for strength  $\beta$ . They are derived from experimental experience and are mainly meant to prevent the risk of scale formation and detachment.

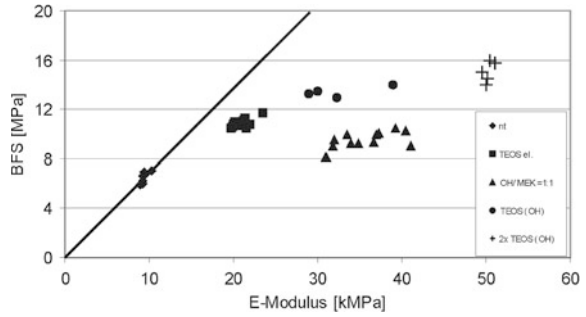
The most important rule is derived from the consideration that the ratio between the biaxial flexural strength  $\beta$  and the E-modulus is characteristic for every stone. According to Hooke’s law, this ratio defines the strain that a given material undergoes when externally loaded. Therefore it is important that this ratio is not changed by strengthening or any other treatment. Expressed in an equation the rule is written as:

$$\beta_t/E_t \leq \beta_{ut}/E_{ut} \tag{7.14}$$

In other words, the ratio E/ $\beta$  for the treated zone should be more or less the same or lower than for the fresh, unweathered stone. Plotting measured strength and E-modulus values for a non-treated material into a diagram  $\beta$  versus E results in a narrow field of points as shown in Fig. 7.52.



**Fig. 7.52** Biaxial flexural strength versus E Modulus plot for Maulbronn Sandstone. The measurement values for elastified TEOS plot next to the line of constant ratio  $\beta_{ut}/E_{ut}$



A straight line beginning at the zero point of the diagram and running through the field of the untreated stone represents the constant ratio of  $\beta/E$ . The areas of the consolidated stone samples that maintain the constant  $\beta/E$  ratio should therefore plot as closely as possible to this line. It can be seen from Fig. 7.52 that the area of elastified TEOS lies next to the line thus almost perfectly fulfilling the requirement. The other products lie more or less far away and should therefore not be used. In particular, it should be pointed that double treatment with TEOS OH raises the E-modulus by a factor of nearly 5, a value far too high to be acceptable. In such cases the risk of scaling cannot be excluded.

Further methods to be used for consolidation assessment are pull-off strength, drilling resistance and ultrasonic velocity. Pull-off strength mainly relates to the surface and is a method for measuring mortar adhesion. However, by cutting a drill core into separate slices a strength profile can be obtained by measuring this property on each single slice. Pull-off devices are not very expensive, however, they are less precise and do not provide measurement of E-modulus.

Measurement of micro drilling resistance (Tiano et al. 2000a, b) is an alternative for strength measurements because it is minimally destructive. The hole drilled into the stone is only 5 mm diameter and up to 50 mm deep. The evaluation, however, is not so easy because abrasion of the drill tip and sticking drill dust in the drill hole may influence the result. Investigations to correlate drilling resistance with compressive strength and other mechanical parameters of stone are in progress (Pamplona et al. 2008).

Ultrasonic velocity of the compressive wave (km/s) is also a promising tool to assess consolidation measures. The velocity of the ultrasonic wave mainly depends on the porosity and the E-modulus of the material. The ultrasonic velocity after treatment should be equal to the value of that of the unweathered stone. Ultrasonic velocity measurements are less appropriate for sandstone than for marble and limestone because compressive wave velocity does not change so much during weathering. Marble, however, is particularly appropriate because ultrasonic velocity may drop from 5 to 7 km/s for fresh marble to as low as 1 km/s for very decayed marble.

Furthermore, it is recommended not to use instruments with just digital display because for obtaining reliable results it is necessary to observe the shape of the

**Fig. 7.53** Bad and good workmanship of repair mortar. *Left* discolored repair mortar at Castle Veitshöchheim Bavaria (Germany). *Right* nicely adapted repair mortar at colonnades of Royal Mint Building Munich (Germany)



signal on an oscilloscope. The shape of the signal is far more indicative of defects than the velocity value alone.

It has been demonstrated in this paragraph that sufficient and well developed tools are available for evaluating consolidation measures in situ at the object or in the restoration workshop. The transfer of this information into practice, however, is stagnating because of lack of funding for the necessary investigations.

## 7.7 Repair and Joint Mortar

Repair and joint mortars are used to fill open masonry joints or to repair smaller missing parts of dimension stones, ornaments and sculptures. They consist of identical materials, based on the same manufacturing technology and do not differ with respect to application requirements. Therefore they will be addressed together in this section.

In principle, mortars are composed from an inorganic or organic binder and sand or gravel aggregate with or without pigments. Inorganic binders may be lime, cement, silica gel or gypsum, while organic binders can be animal glue, polyester, acrylic or epoxy resins. The kind of binder depends on the area where it is to be applied, the climatic impact and especially from the moisture transport and mechanical properties of stone. Mortars often may contain inorganic or organic additives to adapt properties to the stone and to improve their workability and durability.

Mixing mortars requires skill and a great deal of experience in predicting the final properties of a moist mortar mixture after hardening. Changing one component necessarily requires the amount of all other components to be changed as well to obtain the same result. Therefore, most craftsmen prefer pre-fabricated mixtures that only have to be mixed with the prescribed amount of water. Figure 7.53 demonstrates an example of good and bad stone repair.

As will be seen later in more detail, the mixing ratio of inorganic binders and aggregate is surprisingly constant ranging around 1 V/V% binder and 3–4 V/V% aggregate. Mixing ratios of mortars are still specified in V/V% because the parts are put together by counting the number of scoopful. Because mortars based on lime and cement make up the great majority of mortars used in building and

sculpture repair, mainly this class of mortars will be described here. The production and technology of working with mortar is, however, so extraordinarily vast that it is impossible to address all areas related to them. Therefore, the chapter will limit itself to the basic principles so that mortars and their properties can be understood. Of particular interest will be the compatibility of mortar and stone.

As has been pointed out above mortars consist of aggregate and binder. Both of them have an influence on the moisture transport and mechanical properties of mortar. However, before tailoring mortar recipes the first step should be to carefully investigate the historic mortars on the building of interest and to determine aggregate, binder and additives. Knowledge about the original mortar in most cases can provide good recipes for preparing a repair mortar, which is compatible to the stone as well as to the historic mortar. In their comprehensive book for practitioners Ashurst and Dimes (1990) provide many practical examples and advises for correctly tailoring and working mortars.

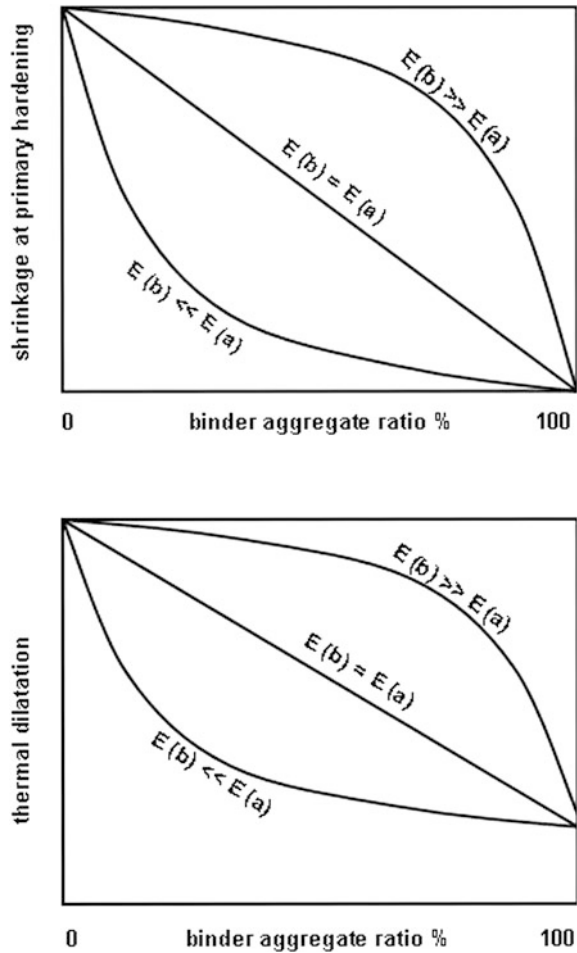
### *7.7.1 Aggregates and Pigments*

The aggregate in a mortar can be natural or ready mixed factory sand of variable grain size and grain size distribution. The grains mainly consist of quartz, feldspar and/or calcite, and should be round shaped. In some cases, for example when an especially resistant mortar is required, also broken sand with edged grains are used. The grain size of sand should normally vary between 0.125 and 4 mm, for joints wider than 20 mm the maximum grain size should amount 8 mm. As a general rule, the maximum grain size of the aggregate should amount to one-third of the joint width. The sand should have a gradual grain size distribution to ensure the densest packing of grains thus minimizing the amount of required binder. The optimal grain size distribution can be derived from the Fuller curve that describes the ideal densest possible packing of spherical grains. The sand to be used should be washed and have no fine clay components, which would soften the ready mortar. The influence of various grain size distributions on porosity, capillary coefficient, compressive strength and E-Modulus of lime mortar has been extensively investigated by Henriques et al. (2004).

There are, however, exceptions from the ideal mixing ratios. The aggregate of historic mortar may be found well sorted, therefore having a bad grain size distribution with one distinct grain size maximum, or the sand used for the historic mortar has been colored with natural clay bearing iron oxide pigment. In such cases compromises have to be made so as to retain the original appearance of repairs or joints with the new mortar.

Figure 7.54 demonstrates why mortar properties can be significantly influenced by the binder—aggregate mixing ratio. Since the binder is responsible for shrinkage and thermal dilatation of the set mortar, its content should be minimized. If the E-modulus of both binder and aggregate are similar, then shrinkage and thermal dilatation will depend linearly from the mixing ratio. If the E-modulus of

**Fig. 7.54** Dependence of primary hardening shrinkage and temperature dilatation on mortar mixing ratio



the binder is higher than of the aggregate (as for the case of a cement binder with a calcitic aggregate) shrinkage and dilatation will only be reduced with a high aggregate content. On the other hand, a binder of low E-modulus with an aggregate of high E-modulus (as for the case of a lime binder with a quartz sand) shrinkage and dilatation rapidly change with a small increase of the aggregate content. It has to be taken into account that air bubbles formed by air-entraining agents significantly reduce the E-modulus of the aggregate.

Shrinkage with primary setting is especially important because failures of mortars mainly happen within the first weeks or months after application. Enhanced shrinkage causes repair mortars to crack and eventually to detach from the substrate. Respecting the mixing rules is therefore an important prerequisite for producing durable mortars.

Coloring mortar with pigments is a crucial issue. Because pigments are effectively fine aggregate grains, their percentage in the mortar must not be too high so that the binder-aggregate ratio is not affected. Furthermore, it is extremely difficult, requiring a lot of practical experience, to judge the correct color of a mortar in wet state. In most cases natural pigments like umber, ochre and green earth should be preferred to industrial pigments because the latter ones are too fine and too intense to produce natural looking coloring to the mortar. The negative example of the pink repair mortar in Fig. 7.53 is caused by the use of modern iron oxide pigment. Therefore, ground stone as main aggregate can be recommended to achieve the closest adaptation to the original stone color. Coloring of mortars is also complicated by the color of the binder. The light color of lime and white cement as well as the gray color of cement may often preclude achieving the desired coloring.

### 7.7.2 Water

Water is necessary for producing mortars but the amount added should not be too high. A workable mortar should be moist like earth but not liquid (excepting injection mortars). Hydraulic binders like cement and pozzolans need a certain amount of water for their setting reaction that is why the correct water/cement ratio is precisely prescribed in concrete technology. The reason for this is easily understood. Every excess of water not consumed by the reaction of the binder will evaporate leaving an air bubble in its place. Thus water absorption of mortar increases but strength and frost resistance decrease. Pavia and Caro (2006) found that the compressive strength of magnesium lime mortars mixed with an excess of water was reduced by one half as compared to mortars with the correct water/binder ratio. That is why mortars prepared with too high an amount of water are not resistant and will quickly deteriorate.

On the other hand care has to be taken to moisten sufficiently the underlying stone and the joint faces to avoid water withdrawal from the mortar during setting. Mortar can not harden without water and if too much water is lost a weak and powdery mortar will result that can be easily scratched away with a knife or spatula. It is important that the water should be free of salts and this should be checked before preparing the mortar. In desert areas, the halite (sodium chloride, NaCl) content of the water can be a serious problem, and in regions with underground gypsum beds, this mineral ( $\text{CaSO}_4 \cdot \text{H}_2\text{O}$ ) can also be problematic.

### 7.7.3 Gypsum

For interior application gypsum may be used to produce repair or joint mortars filled with an appropriate amount of sand or even finer aggregate. The  $\text{CaSO}_4$

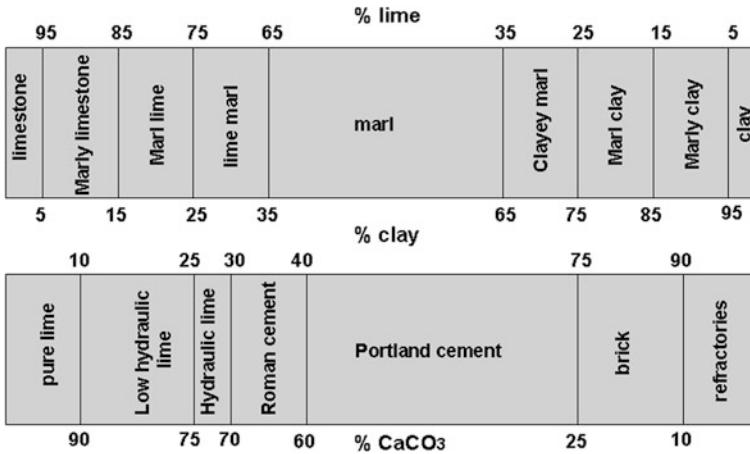


Fig. 7.55 Natural raw materials and related technical products. A gradual transition exists from pure lime to cement

modifications to be considered are the hemihydrate and the anhydrite III modification as well as mixtures of lime and anhydrite II. Those mortars are not meant to be exposed in outdoor environments because they are not stable against water. However, for interiors they may be preferred to lime and cement mortars in several cases, in particular as repair material for marble. Ground pure gypsum blended with animal glue is a perfect mixture to repair defects in marble sculptures. The mortar can be polished to a fineness and gloss that closely resembles the original marble. Stucco lustro is another kind of pigmented gypsum plaster bound with glue for replacing real marble. It used to be very popular in the Baroque for the rich decorations in the interior of churches and castles.

### 7.7.4 Lime and Cement

Lime and cement are the most frequently used materials for producing mortar. They are made from related raw materials as can be seen in Fig. 7.55. In nature, a steady gradual transition exists from pure limestone over marl to pure clay. Likewise, there is a gradual transition from pure lime over cement to fired brick and various fire resistant ceramic products. The difference in composition and properties of these technical products is due to the increasing clay to SiO<sub>2</sub> content and the burning temperature.

The different firing temperatures of lime and cement products are explained in Fig. 7.56. From pure limestone burnt at temperatures below 1,000 °C, quick lime, CaO, is formed through the release of CO<sub>2</sub> from the calcite lattice. Quick lime has to be slaked with water to transform it into slaked lime, Ca(OH)<sub>2</sub>. In historic times,



	Burning Temperature °C			CaO content [M/M %]	
	90	80	70	60	40
< 1000	CL 90	CL 80	CL70		
< 1200		NHL 2	NHL 2/3,5	NHL 2/3,5/5	NHL 5 Roman cement
> 1200				cement	special cements
< 1000		DL 85 DL 80			

**Fig. 7.56** CaO content and burning temperature of different types of lime and cement. *CL* calcium lime, *DL* dolomitic lime, *NHL* natural hydraulic lime

slaking of quick lime was carried out in vessels directly before mixing the mortar or in special pits where the lime putty was kept under coverage of water for long term storage over several years. Lime putty consists of especially fine  $\text{Ca(OH)}_2$  particles obtained from pure white raw materials of high quality, therefore more expensive and preferentially used for painting interior walls of churches and castles.

Nowadays quick lime is directly slaked in the factory by adding the equivalent amount of water necessary to transform all  $\text{CaO}$  into  $\text{Ca(OH)}_2$ . The product is a dry powder (hydrated lime) that is packaged in paper bags.

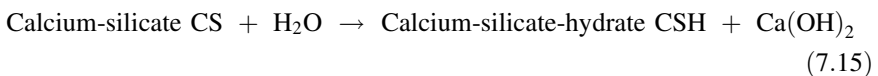
A variation of the slaking procedure with a long tradition is to put into a basin, or in a conical pile, layers of quick lime lumps alternating with layers of sand. By adding an appropriate amount of water the slaking reaction is initiated. After some waiting time the quick lime lumps will crack and the lime and sand layers can be mixed to obtain the ready mortar (Fig. 7.57). The mortar is immediately worked when it is still warm. The mortar produced this way is not very homogeneous; however, when marly lime has been used as a raw product it may even develop higher strength than pure lime mortar. The higher strength is the result of hydraulic components, which are formed during the burning process from the clay component in the marly lime.

Cement production requires much higher temperatures of 1,400 °C. Cement requires water to set, and therefore it is called a hydraulic binder, in opposition to lime that sets with  $\text{CO}_2$  from the ambient air to re-convert into  $\text{CaCO}_3$  (carbonation). The reaction of water with cement is called a hydraulic reaction. It can take place even when immersed totally in water. From a mineralogical aspect, cement is a mixture of different calcium silicates and calcium aluminates, the so-called cement clinker minerals: tri-calcium silicate  $\text{C}_3\text{S}$ , di-calcium silicate  $\text{C}_2\text{S}$ , tri-calcium aluminate  $\text{C}_3\text{A}$ , and tetra-calcium aluminate ferrite  $\text{C}_4\text{AF}$ . Together with water the cement clinker minerals transform into so-called calcium-silicate-hydrate phases, very fine grained, half-amorphous minerals with chemically and physically

**Fig. 7.57** Producing of on-site mortar by direct mixing quick lime and sand



adsorbed water layers and complex crystallographical properties. The agglomerates of these calcium-silicate-hydrate phases are also called “cement gel”.



Portlandite  $\text{Ca(OH)}_2$  is responsible for the alkaline conditions prevailing in cement mortars as well as in concrete. The standard normal cement product Portland cement was produced and patented for the first time in England in 1838. Its color is gray to slightly gray-green due to its iron content, the  $\text{C}_4\text{AF}$  compound. For special purposes, i.e., restoration, purely white cement is available, which is made from very pure raw materials and contains almost only tri-calcium silicate.

As shown in Figs. 7.55 and 7.56 there is a continuous series of products between the end members, lime and cement. With increasing cement content the hydraulic character of hardening becomes prevalent. Lime of quality CL 90 does not harden under water but only in air. Lime of quality CL 80 and CL 70 may partially harden with water but not to complete hardness. Both materials also need  $\text{CO}_2$  from air to consolidate. Hydraulic lime HL and high hydraulic lime HHL are mechanical

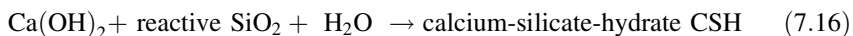
mixtures of cement and lime powder. They require both water and  $\text{CO}_2$  from the air with the hydraulic reaction being responsible for the initial hardness development. As mentioned, cement only needs water to harden. The hardness of the ready mortars increases from pure lime mortar to pure cement mortar.

Unlike hydraulic lime, the natural hydraulic lime NHL is burnt directly from natural marl or marly limestone at temperatures between 1,000 and 1,200 °C. It differs from Portland cement in that its main clinker mineral is di-calcium silicate  $\text{C}_2\text{S}$ . This compound reacts slower with water and develops less strength than the tri-calcium silicate  $\text{C}_3\text{S}$  found in Portland cement. The hydraulic character of the setting as well as the final strength of the mortar increases from NHL 2 to NHL 5 (Fig. 7.56). The last one is also known as “Roman Cement”. It is able to harden under water and its origin has been attributed to the Romans, although it actually is a product of the 19th century.

Romans, however, were capable to erect bridges and aqueducts that required water resistant hydraulic mortars. It is their undisputable merit to having discovered the hydraulic effect of the so-called latent hydraulic or pozzolanic additives that were already described by Pliny. The “original Roman cement” therefore is not a specially produced material but a mixture of lime and latent hydraulic additives. In the course of history, and still today, plenty of pozzolanic additives are known:

- Pozzolana: Terra di Pozzuoli, volcanic ash from near Pozzuoli (Italy)
- Thera (Santorine): volcanic ash from the island Thera (Greece)
- Trass: volcanic ash from Rhine valley near Andernach (Germany)
- Bavarian Trass: Ground impact rock (Suevit) from Ries Crater (Germany)
- Brick: brick powder of low temperature fired brick (not over 900 °C)
- Diatomaceous earth: sediments of siliceous skeleton of diatoms
- Blast furnace slag: by-product of steel production
- Fly ash: dust filtered from the exhausts of power plants
- Metakaolinite: kaolinite fired to 400–600 °C.

Common to all latent hydraulic additives is the content of very reactive amorphous silica. Latent hydraulic compounds do not react directly with water but need an initiation by the alkaline condition of  $\text{Ca}(\text{OH})_2$ :



As can be seen from the chemical reaction, latent hydraulic additives can be added to cement too, because the reaction product of cement hydration (portlandite  $\text{Ca}(\text{OH})_2$ ), is also able to initiate the reaction of pozzolanic additives. Thus the reaction product of pozzolanic additives with  $\text{Ca}(\text{OH})_2$  corresponds to the same CSH phases as that of the hydration of cement clinker phases.

The formation of CSH gel therefore raises the strength of lime as well as of cement mortars. Over time, a lime Trass mortar finally is as strong as a hydraulic lime mortar mixed from lime and cement. The strongest mortar that can be produced is cement Trass mortar because the weaker portlandite is replaced by the

stronger CSH gel. Domaslawski (2000) measured strength increases of lime mortars by pozzolanic additives up to 400 %.

This section has only outlined the basic principles of lime and cement mortar technology. Cement chemistry and research on historic lime technologies are distinct scientific areas of enormous size and complexity. The interested reader may find further information in related literature (Eitel 1966; Keil 1971; Krenkler 1980; Taylor 1990; Ashurst and Dimes 1990; Henning and Knöfel 1997).

### 7.7.5 *Historic and Modern Additives*

Since antiquity it has been common usage to improve workability and properties of mortars by organic additives. The identification of the historic admixtures used by craftsmen and artists in former times is an interesting research field. Some of the admixtures aim to increase plasticity while others improve the internal cohesion in order to reduce cracking. The most common additives and their function are listed below:

- Historic additives
  - Casein: milk protein. Plasticizer
  - Whey protein: milk protein. Plasticizer
  - Collagen: animal protein. Plasticizer
  - Charcoal: water retention. Weight reduction.
  - Fibers: calf hair, straw or linen fiber. Crack prevention
  - Cellulose: polysaccharide. Water retention

Modern additives are dispersions in water of plastic micro particles of a few microns in size. Some examples of the most common additives are listed here:

- PA Polyacrylate
- PVAc Polyvinylacetate (to differentiate it from PVA alcohol)
- PVP Polyvinylpropionate
- PU Polyurethane dispersion
- EP Epoxide emulsion
- AS Acrylate Styrol Copolymer

Very detailed investigations concerning the influence of organic additives to low hydraulic lime mortar have been undertaken by Knöfel and assistants (Table 7.7). For simplicity sake, the various modern plastic dispersions which have been used are not differentiated.

It is evident that the additives have different effects on strength, elasticity and water uptake. As the arrows indicate compressive strength  $\beta_{cs}$  is reduced by all additives. Bending strength is reduced by casein, whey protein and collagen, however increased by dispersion which also enhances tensile strength  $\beta_{ts}$ . Especially enhanced tensile strength  $\beta_{ts}$  is very desirable for repair and joint mortars. Except

**Table 7.7** Effect of organic additives to low hydraulic mortars

Additive	$\beta_{ts}$	$\beta_{cs}$	$\beta_{bs}$	E	W	WR
Casein	↓	↓	↓	↓	↑	nd
Whey protein	↑	↓	↓	↑	↓	nd
Collagen	↑	↓	↓	↑	↓	nd
Charcoal	↑	↓	↑	↓	nd	↑
Fibers	nd	↓	nd	↓	↑	nd
Cellulose	nd	nd	nd	↓	↓	↑
Dispersion	↑	↓	↑	↓	↓	nd

Source Compiled from Knöfel and Winnefeld (1995), Degenkolb and Knöfel (1998), Winnefeld and Knöfel (1998a, b), Hafezi et al. (1998)

$\beta_{ts}$  tensile strength,  $\beta_{cs}$  compressive strength,  $\beta_{bs}$  bending strength,  $E$  Modulus of elasticity,  $W$  Capillary water uptake coefficient,  $\epsilon_o$  primary shrinkage during hardening,  $WR$  water retention, *nd* not determined

whey protein and collagen which have a different effect, all additives lower E-modulus of elasticity so that the strain arising from temperature dilatation is reduced. An interesting result of these investigations is the unpredictable effect of charcoal and cellulose on water retention capacity. Although both products are especially mixed into mortars to improve water retention and reduce drying rate, they do so uniformly. In some cases the effect is positive, in other cases negative. However, it has to be mentioned that the arrows indicate increase or decrease of the respective material property parameter, not an improvement or worsening of the mortar.

A disappointing result for supporters of historic technologies may be the fact that modern organic dispersions are superior to historic additives with respect to all material properties investigated. The reason may be that the reaction of natural protein with alkaline medium inside the mortar is not controllable while modern alkali stable plastic dispersions behave like inert substances inside the mortar mixture.

A comprehensive study on additives admixed to cement mortar has been carried out by Domaslowski (2000). He confirmed the positive effect of acrylic dispersion on shrinkage and compressive strength  $\beta_{cs}$ . Modifying 1:1 lime cement mortar with metakaolinite, however, revealed a failure. Although the compressive strength  $\beta_{cs}$  was increased, the linear shrinkage and capillary water suction were much higher than without metakaolinite admixture. Also mixed with cement mortars, metakaolinite did not have positive effects. From the results reported here it becomes obvious that the effect of additives cannot simply be predicted but has to be experimentally proven for every kind of binder, aggregate and binder/aggregate ratio. Therefore, it cannot be advised to tailor mixtures of mortar and additives unless the necessary testing equipment is available to confirm the actual results.

**Table 7.8** Physical and mechanical properties of lime cement mortar mixtures

Type of cement	C:L:S Ratio	Shrinkage (%)	Water absorption V/V (%)	Compressive strength $\beta_{cs}$ (MPa)
45	0.5:1.5:4	0.30	22.5	1.9
45	1:1:4	0.19	17.0	8.3
45	1:1:6	0.05	16.0	6.4
45	1:1:8	0.01	14.6	4.6
45	1.25:0.75:6	0.03	12.9	11.2
45	1.25:0.75:7	0.07	12.6	10.7
45	1.5:0.5:8	0.01	10.3	13.8
35	1:1:4	0.56	18.7	6.6
35	1:1:6	0.35	15.4	6.0
35	1:1:8	0.12	13.7	4.5

C cement, L lime, S sand (Domaslowski 2000)

**Table 7.9** Minimum compressive strength  $\beta_{cs}$  requirements for mortar groups 1–25. EN 998-2 standard

Mortar group	M 1	M 2.5	M 5	M 10	M 15	M 20	M d
Compressive strength $\beta_{cs}$	1	2.5	5	10	15	20	>25

### 7.7.6 Compressive Strength $\beta_{cs}$ of Lime and Cement Mortars

It has been mentioned that mortar strength increases with increasing cement content. To give an idea about the range of strength values, the results obtained by Domaslowski (2000) are briefly reported (see Table 7.8).

It can be seen that shrinkage is highest for lime rich mortar and mortar with low cement quality 35. Compressive strength  $\beta_{cs}$  is in a range of 1.9 up to 13.8 MPa thus covering a wide range of properties. Water absorption also varies in a wide range from 10 V/V% to 22 V/V%. As the mortar compositions cover a wide range of properties it should be possible to find an appropriate mortar for nearly any kind of stone.

Joint mortars within masonry have to fulfill certain requirements concerning compressive strength  $\beta_{cs}$  because they have to withstand the load of the above masonry. For this reason the compressive strength  $\beta_{cs}$  requirement is fixed in national standards. The new standard EN 998-2 requires the following minimum values (Table 7.9).

For a long time it has been known that cement nearly reaches its maximum hardness after 28 days of storage in appropriate climate of 20 °C and 65 % RH. The subsequent strength increase is only minor. It is therefore justified to relate strength measurements carried out on cement or cement containing mortars to storage time of 28 days. Given these premises strength requirements for cement containing mortars can be established and fixed in national standards like EN 98-2.



There are, however, exceptions for pure lime mortars and mortars with pozzolanic additives. Pure lime mortars harden through evaporation of the water admixed for mortar preparation and subsequent carbonation. The latter process is slow and may take years within a thick masonry. For this reason, strength requirements for pure lime mortars do not exist, however, as a compromise curing time of 90 days has been proposed.

Similar difficulties are found for the case of latent hydraulic additives, i.e., pozzolans. The hydration reaction of the reactive silica within the additive with the  $\text{Ca}(\text{OH})_2$  is also very slow and may take weeks or months. It will even cease when the mortar dries too quickly, without reaching the final and desired strength. It is therefore recommended to test cement mortars containing latent hydraulic additives only after a curing time of 90 days. The workability of mortars containing latent hydraulic additives under practical building conditions is often very problematic. Many failures have been produced because curing time and curing conditions (regular wetting of the mortar) have not been carefully observed.

### ***7.7.7 Mortars Bound with Silica Gel***

TEOS and silica sols can also be used as binders for mortars. Producing casting moulds with silica sols like SYTON X30 has a long tradition in metal industry. However, for restoration purposes application of silica gel bound mortars remained quite rare and reserved to small repairs. For example, in Germany they have been applied for small repairs on the sculptures at the Fürstenportal of Bamberg Cathedral (1974); the south gate of Augsburg cathedral (1985); and, the north gate of Schwäbisch-Gmünd Minster (1987). At that time, systematic investigations into the properties of those mortars had not been carried out so that it depended on the skill of the restorer to find the optimal mixture.

Fundamental investigations of silica gel repair mortars were undertaken by Ettl (1987) and Ettl et al. (1996). It was found that silica gel bound mortars can be adapted to a great variety of properties with respect to moisture transport and mechanical properties. Precise instructions are given with regards to how the components of such mortars should be mixed to obtain the desired properties. The topic is too broad to be addressed in detail so for further information the reader may obtain information from the referred literature.

In 2000, REMMERS put on the market a modular system for producing various kinds of mortars based on TEOS. This development was made possible when the highly concentrated precondensed TEOS, with a gel formation of 500 g/l, was obtainable as it imparted sufficient strength to the mortar types produced. The basic components and the various mortars which can be mixed within the REMMERS Module System are shown in Fig. 7.58.

The center of the Module System is the binder TEOS 500 STE. This is actually the 500 E product enriched with highly dispersed silica. Around it six further components are grouped: coarse and fine sand, quartz and clay powder, pigments,

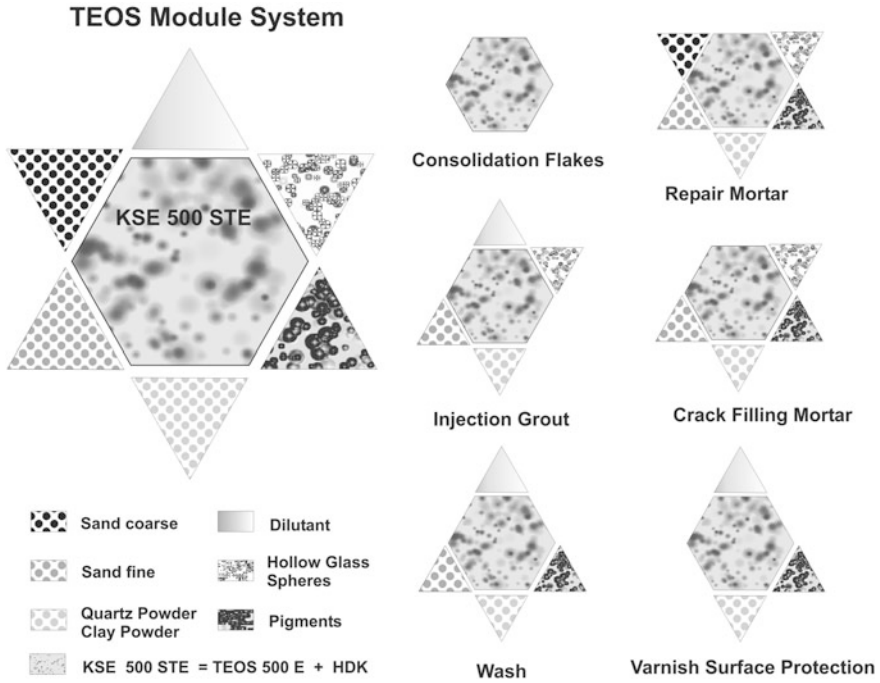


**Fig. 7.58** REMMERS Module System for producing silica gel bound mortars (Figure by Remmers)

hollow glass spheres and thinner. The pure TEOS 500 STE binder can be used for fixing loose surface flakes and for preparing a stable underground for further treatments. The mortars can be mixed in different formulations depending on the requirements of their application. To fill fine cracks a pigmented mortar containing fine sand is prepared. To repair bigger lacunae a similar mortar is used with the addition of coarse sand. A low viscous injection grout can be mixed with fine sand, hollow glass spheres and a sufficient amount of thinner. Pigments are not needed because the mortar is not visible. Fine surface washes can be prepared with fine sand, mineral powder and pigments while a thin varnish for protecting the surface against environmental attack can be mixed with mineral powder, pigments and thinner.

The great advantage of the Module System is that all products are built up with the same binder. Moreover, it is possible to consolidate silica gel repairs with regular TEOS after application so that a gradual transition from the repair to the stone underneath is obtained. This option differs from lime or cement repair mortars that always exhibit a sharp boundary at the stone-repair interface.

Figure 7.59 shows a view on an ashlar situated in the west gable of former Kloster Birkenfeld in Bavaria. The heavy destruction due to contour scaling, crack formation and rounded edges is easy to recognize. The right photograph shows the same ashlar after restoration with silica gel bound repairs. A surface wash for

**Fig. 7.59** Ashlar on the west gable of former Kloster Birkenfeld before (*left*) and after restoration (*right*)

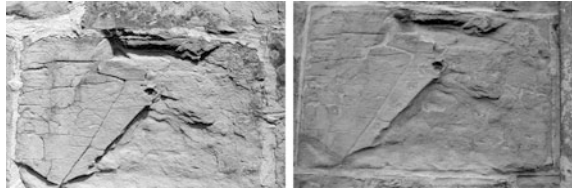


**Fig. 7.60** Discolored stone repair mortars on Greensandstone ashlars at Residenz Munich, Germany



protecting the surface, repairs on the damaged edges and crack fillings can be seen. Moreover the hollow space underneath the scale has been filled with an injection grout. The thin holes for injecting the grout are still visible. The restoration has been undertaken in 1993 and, as of the writing, is still in good shape.

### ***7.7.8 Assessment Criteria for Compatibility of Repair and Joint Mortars and Stone***

The questions of tailoring and testing mortars for conservation are discussed in detail by Henriques (2004). The concept of compatibility is based on the similarity of essential parameters so that the long-term behavior of repair and joint mortars in relation to the masonry stone can be predicted. Moisture transport and mechanical properties that are not compatible will lead to ugly discolorations and the eventual detachment of repairs (Fig. 7.60). Furthermore, the preferential deterioration of the repair instead the stone if damage should occur, is also considered within the compatibility principle.

Based on the compatibility principle, Sasse and Snethlage (1997) and Snethlage (2008) recommend a system of quality control measurements to adapt repair and joint mortars to the stone properties.

**Table 7.10** Requirements for joint and repair mortar related to stone property based on compatibility concept (Sasse and Snethlage 1997)

Material property	Symbol	Joint mortar	Repair mortar
E-Modulus dynamic	E	20–60 %	≤80 %
Compressive strength	$\beta_{CS}$	20–60 %	≤60 %
Hydric dilatation	$\alpha_{hydric}$	50–100 %	50–100 %
Thermal dilatation	$\alpha_{thermal}$	50–150 %	50–150 %
Capillary water uptake coefficient	W	50–100 %	50–100 %
Number of water vapor diffusion resistance	$\mu$	50–150 %	50–100 %
Pull-off strength	$\beta_{POS}$	0.5–1.0	0.5–0.8

The requirements formulated in Table 7.10 are related to the corresponding stone properties. The most important ones refer to strength and E-modulus of the repair and/or joint mortar. The values of both properties should be lower than that ones of the stone to which the mortar is applied in order to ensure that the deterioration occurs in the mortar and not in the stone. Hydric and thermal dilatation, capillary water uptake coefficient and water vapor diffusion resistance should be close to the stone. However, thermal dilatation is allowed to deviate between 50 % and up to 150 % in some cases. However, in general a lower thermal dilatation than that of the stone is favorable for better mortar adhesion. The pull-off strength requirement is of major importance for the performance of the composite system stone-mortar. The pull of strength of the mortar should never exceed the pull-off strength of the stone surface to guarantee that if adhesion fails, it should be within the mortar thus leaving a thin mortar layer on the stone surface. In cases where the pull-off strength of mortar is higher than that of the stone, the detaching mortar pulls off part of the stone surface with the consequent loss of original material.

The mortar—stone combination is a composite system where thermal and hydric dilatations cause stress at the boundary plane when their values are significantly different. The stress exerted to the adjacent materials is higher the higher these strains are and—especially important—the higher the E-modulus difference is. This can be easily understood by the following equation, which is a simple approximation to the real problem but sufficiently precise for making an approximation. According to Hooke's Law stress  $\sigma$  is proportional to E-modulus and strain  $\epsilon$ . In the boundary plane the stress due to thermal and hydric strain is then proportional the differences of the E-moduli and strains  $\epsilon$ . Therefore the following simple formula regarding materials 1 and 2 can be written:

$$\sigma_1 = E_1 \cdot (\epsilon_{1, thermal} + \epsilon_{1, hydric}) \quad (7.17)$$

$$\sigma_2 = E_2 \cdot (\epsilon_{2, thermal} + \epsilon_{2, hydric}) \quad (7.18)$$

$$\sigma = \sigma_1 - \sigma_2 = \Delta E \cdot \Delta \epsilon \quad (7.19)$$

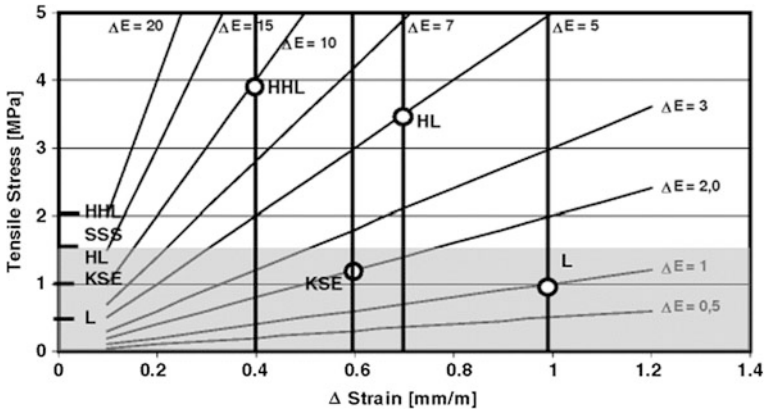


**Fig. 7.61** Evaluation of repair mortars appropriate for Schilfsandstone Castle Schillingsfürst Bavaria. *L* lime mortar, *HL* hydraulic lime mortar, *KSE* silica gel bound mortar, *HHL* high hydraulic mortar, *SSS* Schilfsandstone. Vertical lines represent the measured differences of hydric dilation between the Schilfsandstone and the respective mortars

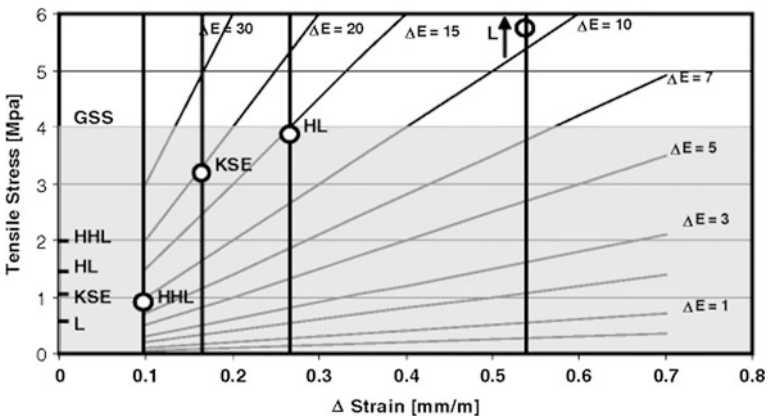


**Fig. 7.62** Valuation of repair mortars appropriate for Greensandstone from Alte Pinakothek Munich, Germany. *L* lime mortar, *HL* hydraulic lime mortar, *KSE* silica gel bound mortar, *HHL* high hydraulic mortar, *GSS* Greensandstone. Vertical lines represent the measured differences of hydric dilation between the Schilfsandstone and the respective mortars

If the thermal and hydric strain differences are known from experimental data as well as the tensile strength of each material, then an appraisal can be made with regards to which extent E-modulus of repair or joint mortar may be different from that one of stone. The result is shown in Figs. 7.61 and 7.62.

As for Fig. 7.45, Fig. 7.61 is based on a theoretically calculated stress–strain diagram assuming certain E-modulus differences  $\Delta E$ . The vertical lines represent the measured differences of hydric dilatation between the Schilfsandstone and the respective mortars. To derive, for example, the compatibility of lime mortar with

Schilfsandstone from Castle Schillingsfürst it is necessary to measure in advance the difference of the E-modulus and that of the hydric dilatation. These were found to be  $\Delta E = 1 \text{ kMPa}$  and  $\Delta \varepsilon = 1 \text{ mm/m}$ . The intersection of the lines  $\Delta E = 1 \text{ kMPa}$  and  $\Delta \varepsilon = 1 \text{ mm/m}$  lies within the gray field that marks the maximum tensile strength  $\beta_{ts}$  of Schilfsandstone, i.e.,  $1.5 \text{ MPa}$ . With the same procedure it is possible to derive the appropriateness of the other repair mortars. It is found that silica gel bound mortar is also appropriate for this variety of the Schilfsandstone. On the other hand, hydraulic and high hydraulic mortars are not suitable because the difference in E-Modulus is too high. From this figure it can also be deduced that if failure occurs for the case of lime and KSE mortar, this would occur within the mortar, while for the case of HL and HHL mortar, this would happen within the stone because its tensile strength  $\beta_{ts}$  is lower than that of the mortars.

It can be shown by the example of the Alte Pinakothek in Munich that the tensile strength of the Greensandstone is much higher than that of the Schilfsandstone and therefore is compatible with harder repair mortars. Figure 7.62 shows this example.

On the other hand, lime mortar is not appropriate in combination with this particular Greensandstone variety because the difference in E-modulus is too high even though the hydric dilatation difference is smaller than in the previous example. However, KSE, HL and even HHL mortar are appropriate because the intersections of the lines representing the difference of hydric strain with the lines representing the difference of E-modulus plot inside the gray area that corresponds to the maximum tensile strength  $\beta_{ts}$  of the Greensandstone. Unlike the previous example, the strongest mortar, HHL, yields the best result especially since the hydric strain difference with the Greensandstone is very small.

From the above examples it can be concluded that mortars with high strength and E-modulus are not necessarily excluded a priori for stone repair. The decisive factor is the behavior of the composite mortar—stone system characterized by the different material properties. It is also evident that general recommendations for repair and joint mortars can not be given. The most appropriate mortar for each stone variety has to be determined by laboratory and practical experiments on a case by case basis.

As already mentioned in Sect. 7.6, it is emphasized that the calculation on the basis of Hooke's Law is just an approximation. The risk of cracking and detachment depends, besides strain and E-modulus difference, also on the rate of dilatation and the influence of moisture on the mechanical properties. Moisture decreases the strength and E-modulus of materials, therefore the calculated values may be too high. In nature, the rate of strain development is much slower than in laboratory experiments that are the basis for these calculations. Under slowly increasing stress mortar and stone may creep thus reducing the stress exerted at the boundary plane. Hooke's Law for calculating the stress should therefore be adjusted by the so-called relaxation or creeping number  $\psi$ :

$$\sigma = E(\epsilon_{\text{thermal}} + \epsilon_{\text{hydric}})\psi \quad (7.20)$$



Relaxation number  $\psi$  is always smaller than one and has to be obtained experimentally. To date, however, no research dealing with this important topic has been published. From this it is evident that far more research in stone repair and joint mortars is necessary to avoid future failures.

### 7.7.9 Repair with Natural Stone

Heavily damaged stone that can no longer be repaired with a mortar should be replaced by new stone. For centuries repair with natural stone is the most common practice by cathedral workshops in all countries in the world. Even though the method contradicts the aim of preserving the original substance as long as possible in case of churches and cathedrals different arguments should apply. Cathedral workshops have to consider the long term perspectives of every measure they are undertaking today because it may take 50 years or even longer before scaffolding is erected again for that part of the building.

Nevertheless, choosing the right repair stone needs serious considerations because in many cases the original quarries are closed. Inappropriate new stone may cause damage to the original stone, in particular in case of strongly deviating mineralogical composition and porosity.

Besides color, the new stone should fulfill certain properties to be compatible with the original stone. Some criteria that should be observed have been compiled by Snethlage (2008):

- *Structure* Coarse—medium—fine grained
- *Texture* Parallel layering, cross bedding
- *Mineral composition* Special attention should be put to the binding cement (carbonatic, clayey, siliceous)
- *Porosity* Similar porosity of the new stone.
  - High porosity:  $P > 20 \text{ V/V}$ .
  - Medium porosity:  $P = 20 - 10 \text{ V/V}$ .
  - Low porosity:  $P < 10 \text{ V/V}$ .
- *Pore size distribution*: The maximum of the pore size distribution is in the area
  - Coarse pore size  $> 50 \mu\text{m}$
  - Medium pore size  $50 - 1 \mu\text{m}$
  - Micro pore size  $< 1 \mu\text{m}$
- *Water absorption coefficient*  $W$ :  
 $W$  of new stone should be in the same class as original stone:
  - Low water absorption coefficient  $w < 0.5 \text{ kg/m}^2 \cdot \text{h}^{1/2}$
  - Medium water absorption coefficient  $w = 0.5\text{--}3.0 \text{ kg/m}^2 \cdot \text{h}^{1/2}$
  - High water absorption coefficient  $w > 3.0 \text{ kg/m}^2 \cdot \text{h}^{1/2}$

- *S-value*:
  - The saturation coefficient should be below 70 %
- *Water vapor diffusion resistance*:  $\mu$ -value should be in the order of the  $\mu$  value of the original stone  $\pm 10$  units
- Compressive strength and modulus of elasticity:
  - New stone should be in the range of 80–120 % of  $\beta_{\text{cps}}$  (original stone) and  $E$  (original stone)

These criteria are considered useful to avoid unsightly deviating “patination” of the new stone with regards to the original stone. It is, however, not possible to establish definite limits for the difference in properties of the two materials. Therefore, it is recommended to select new stone not on the basis of strict figures but on the bases of property ranges as described above.

## 7.8 Paints on Stone

Polychrome sculptures and buildings have not always had the same appreciation over time. In particular, classicism highly appreciated the pure and unaltered surface of marble sculptures as an ideal representation of the human skin. Winkelmann (1764) praised “Stille Einfalt und edle Größe” (quiet simplicity and noble greatness) of the antique white marble sculptures as the ideal of beauty; he strictly declined “die barbarische Sitte des Bemalens von Marmor und Stein” (the barbaric custom of painting marble and stone). Still the famous Prussian architect Semper (1834) polemicized against painting sculptures from an aesthetical point of view because paints would disturb the clear artistic design of sculptures. However, by looking closer at antique temples and excavated sculptures more and more traces of polychromy have been detected. Towards the end of the 19th century, the first attempts were made to recreate the painting technique of antique Greek sculptures. In 2004, the exhibition “Bunte Götter. Die Farbigekeit antiker Skulptur.” (Colorful Gods. The Polychromy of Antique Sculpture) proved the rich polychromy of classical temples and sculptures in the antique world (Brinkmann and Wünsche 2004). Also in other cultures, painting was used extensively, as illustrated by the colorfully painted Qin Shihuangdi’s Terracotta Warriors from China (Blänsdorf 2007; Horn 2007; Fig. 7.63).

In mediaeval time cathedral gateways and castle doorways were colorfully decorated (Sauerländer 2000). The color design of tympana and gateway figures obeyed a fixed color iconography and was not chosen simply by taste (Fig. 7.64). In Christian symbolism yellow and gold symbolize the divine light, red the blood of Jesus Christ or the fire of burning love, blue the color of heaven or faith, and green the making power of God or the sprouting green nature. Thus the color program followed a precise prescription so that it could be understood by all Christian people.

**Fig. 7.63** The so-called “Kneeling Archer with Green Face”. *Left* original state after excavation. *Right* virtual 3D reconstruction. Photo Felix Horn (2006) (Figure by Horn and Blänsdorf)



**Fig. 7.64** Tympanum of Last Judgment Portal Saint Sebaldus Nuremberg, Germany. The rich mediaeval polychromy is faded away or covered by soot layers (Figure by Beckett)



The iconographic meaning of colors is of course known for all cultural areas. In China, for example, gold and red color is reserved for the emperor as can be observed from the red columns and yellow glazed roof tiles on the buildings of the Imperial Palace in Beijing, while green roof tiles indicate the buildings where his sons lived.

**Fig. 7.65** Putto with original Baroque lead white Linseed oil paint (second half 18th century) excavated in the park of Castle Seehof near Bamberg, Germany



During the Baroque period, linseed oil-lead white paints were used to embellish garden sculptures made from sandstone, following the double aim of protecting the surface against rain as well mimicking a more precious material, e.g., marble or porcelain (Fig. 7.65). This white paint was also used extensively for building facades, a good practice for several centuries such as the Netherlands and Switzerland. On the sandstone areas of the Lübeck Town hall erected in 1650 (Herm 1997) some 20 layers of paint were found that allowed to estimate that the façade had been painted every 20–25 years.

The example of the Lübeck Townhall proves that the linseed oil-lead white paints need regular repair or renewal. For this reason no severe damage happened to garden sculptures because they were regularly maintained and repainted. As of the 20th century, damage increased due to lack of maintenance. If the paint is not renewed, the fine crazele widens to real cracks and water can penetrate into the underlying stone. Given the high water vapor diffusion resistance of the linseed oil-lead white paint, the moisture content in the stone substrate increases steadily and induces its deterioration. The damage caused by this process is larger than if the stone had not been painted. Analyzing these damages Kieslinger (1932) considered the linseed oil-lead white paints as artificial deleterious crusts that resulted in so many damages and costly repair.

**Fig. 7.66** Rape of Proserpina in park of Castle Seehof near Bamberg, Germany. Figure group freshly painted in original leadwhite linseed oil technique



Nevertheless, some 20 years ago the Bavarian State Department of Historic Monuments decided to repaint two original sandstone figure groups in the park of Castle Seehof next to Bamberg with historic linseed oil-lead white paint. After little more than 10 years the paint had to be renewed because of cracking and delaminating. The new paint shows already similar damage and it should be renewed again and will continue to require regular maintenance (Fig. 7.66).

According to present international conservation principles restoration of polychrome objects is aimed at preserving all remains of original polychromy as valuable documents of the history. Retouching gaps in the paint layer is an accepted means to create a coherent visual appearance, however, without inventing new “original” polychromy. In a few cases it has been decided to completely renovate the historic polychromy of objects by a total repainting as has been the case for the main portals of the Bern Minster in Switzerland and Freiburg Minster in Germany.

### ***7.8.1 Binding Materials of Paints***

Lime, linseed oil and watrglass are the most important binding materials of paints for stone buildings, both for the interior and exterior. Schramm and Hering (1988)

**Table 7.11** Most important paint systems and their composition

Paint system	Binding medium	Additives	Filling materials
Lime paint	Ca(OH) <sub>2</sub>	Historic: casein, oil, protein ("Lime Tempera") Modern: modern synthetics	Fine sand, chalk, marble powder
Oil paint	Linseed oil Poppy oil	Siccative: leadwhite, hematite	Barite, chalk, marble powder
Silicate paint 2 components	Waterglass	Working additives: natural resin, protein ("Oil tempera")	Quartz powder, fluorite, other
Dispersion silicate paint 1 component	Waterglass	Stabilizer Acrylic dispersion stabilizer Admixtures for improving workability	Quartz powder, fluorite, other
Silicone resin emulsion paint	Silicone resin Acrylic dispersion	Stabilizer Admixtures for improving workability	Chalk, talc, quartz powder, other
Acrylic dispersion paint	Acrylic dispersion	Admixtures for improving workability	Chalk, marble powder, titanium white



report the earliest use of linseed oil paint in Mesopotamia around 3000 BC. In Europe it appears by the 12th century AD and is used for painting objects exposed outdoors (Kühn 1988). The earliest use of lime paint is very hard to determine and may be as old as burnt lime for mortar production, around 7000 BC. On the other hand, silicate paints, based on waterglass have been patented only in 1878 by AW Keim who describes this new painting method “Stereochromy” in the scientific series “Chemisch-technische Bibliothek” in 1881 (Keim 1881a, b).

To produce good paints additives are as or even more important than the binding material itself (Table 7.11). The purpose of additives is to improve workability as well as to enhance stability and opacity. Pure lime paint without additives does not really cover the substrate, remains chalky and is therefore of limited applicability on stone. The most frequent additives for lime paint are small quantities of linseed oil and or various kind of protein like casein, animal glue, egg yolk and egg white. Using one or more of these additives in various compositions the so-called lime tempera is produced that is appropriate for making detailed and delicate paintings. Lime paint should not be confused with fresco wall painting because in the latter technique the pigments are fixed within the hardening mortar substrate layer. Modern additives derive mainly from acrylic dispersion. Neutral or white material is used as filling material like fine sand, ground marble or light limestone.

While lime paint is mainly appropriate for indoor use linseed oil paint can be applied both in interiors and exteriors (Hotz 2006). The drying of linseed oil is enhanced by so-called siccatives, in most cases heavy metal elements like Fe and Pb. For this reason linseed oil paint is mostly found in combination with lead white or hematite pigments, as both improve the drying of this paint. For centuries the well known historic additives of so-called oil tempera have been egg yolk or egg white protein as well as resins from conifers (turpentine) and broad-leaved trees (dammar, gummy arabicum, mastic). Oil paints are filled with white or slightly gray aggregates like chalk, ground marble or barite.

The original silicate paint from the 19th century is two-component silicate paint. To date the paint is still worked according to the prescriptions by Keim (1881a, b). One component of the paint system is the binding material consisting of a waterglass solution; the other one is a mixture of alkali stable pigments, “ripened” for 12 h in waterglass that corresponds to the paint itself. The waterglass solution serves as a primer for making a homogeneous underground and as fixative for the application of the paint. The hardening process of waterglass is extensively described in Sect. 7.2.

Preparing two component silicate paints is quite difficult and needs at least 12 h time to produce the paint mixture. When this has “ripened” then there are only a few hours left for working since the paint will become too stiff for safe application. On the other hand, the modern silicate paints are easy to work. They are single component paints and due to the admixture of dispersants the paint is stable and can be stored over months without losing workability. Even the pigments can be immediately mixed into the paint so that it can be used immediately. The very fine ground filling materials are mostly quartz powder, fluorite, and barite among others.

The most modern paint system is the silicone resin emulsion paint that is in fact a mixture of acrylic resin dispersion and a silicone resin dispersed in water. Admixtures of acrylic dispersions are necessary to secure the cohesion of the paint because the low binding capacity of the silicone resin. The price is directly proportional to the formulation ratio between acrylic dispersion and silicone resin. Low quality silicone resin emulsion paint contains more acrylic dispersion since this is cheaper than the silicone resin (Erfurth 1992). Unlike the other silicate paints silicone resin emulsion paint is hydrophobic due to the presence of the silicone resin. A high content of filling material is necessary to ensure sufficient water vapor conductivity because otherwise the paint would be film forming and not water vapor permeable.

Acrylic dispersions alone are also used for the production of paints. If the dispersion content of this paint is too high, their properties resemble those of the old latex paints that are typically known for peeling off from the substrate surfaces. It is therefore of high importance that the filling material content (chalk, marble powder, quartz powder, titanium oxide) is high enough to break the film forming properties of acrylic dispersions.

### ***7.8.2 Painting Techniques***

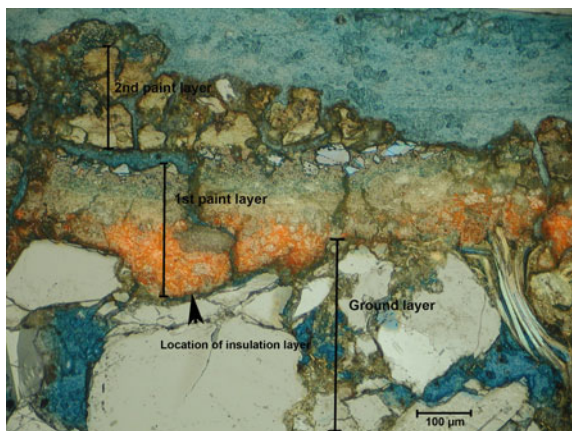
Painting on stone requires pre-treatment of the surface in order to even out surface heterogeneities and prevent uncontrolled penetration of the paint binder into the pores resulting in a spotty appearance. The way the pre-treatment is done depends on the structure of the stone. For fine-grained and dense stones pre-treatment can be done with the diluted pure binding material. In the case of lime paint, the pre-treatment can be done with lime water or diluted lime-casein mixtures, while for oil paint, diluted linseed oil is used. Silicate paints require pre-treatment with pure waterglass solution (so-called “Fixative”) to homogenize the absorption of the stone surface and the silicone resin emulsion paint needs pretreatment with the acrylic-silicone resin binder alone. An example of a thin lime tempera painting having been directly applied to the pre-treated stone surface is shown in Fig. 7.67. It can be recognized that the coarse grain structure of the stone is visible through the thin paint layer.

Coarse grained stone structures, however, need more complicated pre-treatment with one or two ground layers. An illustrative example of mediaeval painting technique is presented by Drewello and Herkner (2009) using the results obtained from investigations of the Weltgerichtsportal (Last Judgement Portal) from the St. Sebaldus church in Nuremberg (Fig. 7.68). With the help of cross sections and IR analysis they found two layers of gypsum ground (Bologna chalk) containing animal glue and oil. The application of two ground layers had been necessary to fill the gaps between the coarse grains of the stone. Then a pigmented insulating layer made of egg tempera was applied. This consisted of egg, linseed oil varnish and tree resin mixed with some filling material such as chalk, lead white and bone

**Fig. 7.67** Late mediaeval lime tempera painting directly applied to stone surface after pre-treatment. Former Cistercian monastery Himmelkron Bavaria, Germany



**Fig. 7.68** Cross section of paint layer from St. Sebaldus Weltgerichtportal (Last Judgement Portal) in Nuremberg showing ground layer, insulation layer and sequel of mediaeval paint layers (Drewello and Herkner 2009)



white. The purpose of this white insulating layer was to prepare a stable substrate on which the painting could be carried out.

Concerning investigation of paint layers in general it should be taken into account that the insulation layer is extremely thin so that it may be easily overlooked. For technical reasons such insulation layer is, however, absolutely necessary because otherwise the first paint layer could well be soaked into the ground layer.

Regarding the mechanical properties such paint layer stratigraphy has, the principal risk is that of detachment because the gypsum and glue ground layer is weaker than the paint layers above it bound with oil. The fatty insulation layer exhibits much more affinity to the oil paint layers above it than to the gypsum glue layer below and is therefore prone to detach from the underground layer. On the other hand, it is interesting to see that painting technique on stone is very similar to panel and easel painting. For a introduction into the investigation of paints and pigments see Wulfert (1989).

### 7.8.3 Moisture Transport Properties of Paint Layers

Andersson and von Haslingen (2000) have been pointing out painting stone as a means to protect and to decorate stone elements exposed outdoors. However, to fulfill all requirements with respect to protection and durability only those paint systems may be selected that are compatible with the underlying stone. In this context the moisture and water vapor transport parameters of paints in comparison to the stone are of essential importance. Basically, two general types of paint systems can be distinguished, film forming paints that block water vapor transport, and permeable paint layers that are open to water vapor transport. Water vapor diffusion through paint layers is therefore an essential parameter to assess the compatibility between paint and stone.

Water vapor diffusion through any material is described with the help of water vapor diffusion resistance coefficient  $\mu$ , a dimensionless figure. It describes the diffusion resistance of the material under concern in comparison to that one of air. A  $\mu$  value of 10 therefore means that this material has a ten times greater water vapor diffusion resistance than an air layer of the same thickness. On a material the real water vapor resistance, however, depends on the thickness of the paint layer, and therefore the  $\mu$  value should be replaced by the sd-value, the water vapor conductivity or diffusion equivalent air layer thickness, which is the product of the thickness of the paint layer  $s$  (m) and the  $\mu$ -value:

$$sd = \mu \cdot s \text{ [m]} \quad (7.21)$$

As can be seen from Table 7.12 the water vapor conductivity, sd, depends on both the paint system and the substrate (Herm 1991; Herm and Snethlage 1992). Although  $\mu$ -values can be sometimes high, the sd-values are generally quite low because the paint layer thickness is usually in the order of 50–250  $\mu\text{m}$ .

**Table 7.12** The sd-values and  $\mu$ -values of historic and modern paint systems (Herm 1991, Herm and Sneathlge 1992). Note that sd—value is given in cm

Paint system	Stone substrate	sd (cm)	$\mu$
Silicate paint 2 components	FRG	1.9–2.7	120
	SAN	2.0–3.6	258
	OBK	10.1–12.8	854
	GL	4.7–5.2	nd
Dispersion silicate paint 1 component	FRG	0.1–0.3	9.5
	SAN	1.0–2.3	241
	OBK	2.9–4.2	563
	GL	1.7–2.4	nd
Silicone resin emulsion paint	FRG	2.5–2.8	132
	SAN	3.8–5.9	239
	OBK	7.9–8.0	479
Acrylic dispersion paint	FRG	10.2–12.7	806
	SAN	22.5–25.0	2,191
	OBK	30.7–33.6	2,598
Linseed oil	FRG	506–592	30,242
Lead white paint	SAN	22.7–44.2	1,615
	OBK	216–276	12,269
	GL	177–214	nd
Lime paint	FRG	0.7–1.1	132
Pure	GL	0.9–1.5	131
Lime + casein paint	FRG	0.8–1.4	90
	GL	0.9–1.3	103
Lime paint + acrylic dispersion	FRG	2.4–8.8	462
	GL	0.9–3.0	212

FRG fritted glass, SAN Sander Schilfsandstone, OBK Obernkirchen sandstone, GL Gotland sandstone, nd not determined

It is evident from Table U that the linseed oil—lead white paint has by far the highest water vapor diffusion resistance and the highest sd-value, even higher than the acrylic dispersion paint. The lowest sd-value and water vapor resistance corresponds to lime paints and silicone resin emulsion paints. Pure silicate and dispersion silicate paints show also low water vapor resistance and sd-values. However, the results may differ from the general rule depending on the stone substrate and vary with formulation within the different paint types. Therefore the values will differ from case to case.

The German European Standard DIN EN 1062 and DIN 52615 establish certain values for capillary water absorption  $W$  and water vapor conductivity  $sd$  with the objective to assess properties of paint systems. The requirements refer to paint systems alone without substrate. The capillary absorption is divided into three classes:

- High capillary absorption:  $W \geq 0.5$  [ $\text{kg}/\text{m}^2 \text{h}^{1/2}$ ]
- Medium capillary absorption:  $W = 0.1 \dots 0.5$  [ $\text{kg}/\text{m}^2 \text{h}^{1/2}$ ]
- Low capillary absorption:  $W \leq 0.1$  [ $\text{kg}/\text{m}^2 \text{h}^{1/2}$ ]

The water vapor permeability  $s_d$  is also classified into three classes:

- High water vapor permeability:  $s_d \leq 0.14$  [m]
- Medium water vapor permeability:  $s_d = 0.14 \dots 1.4$  [m]
- Low water vapor permeability:  $s_d \geq 1.4$  [m]

The suitability of any paint system is best assessed by evaluating whether the water taken up by the paint and the underlying stone by capillary absorption during rainfall is able to evaporate during the drying periods between rainfalls. The length of the drying periods is not the same in all regions but is of course shorter in climatically highly exposed areas. In any case, capillary water uptake  $W$  and water vapor permeability should be correlated to each other such way that the higher the  $W$  value the lower the  $s_d$ -value must be. On the other hand, the lower the  $W$  value then a higher  $s_d$ -value can be acceptable. In experiments carried out on painted façade renderings Künzel (1969) found out that if the product  $W \cdot s_d$ , also known as “Künzel Number”:

$$W * s_d \leq 0.1 \left[ \text{kg/m h}^{1/2} \right] \tag{7.22}$$

is lower than  $0.1 \text{ kg/m h}^{1/2}$ , any façade is able to completely dry out after rainfall even in harsh climatic conditions with heavy rainfall, as is the case in areas close to the Alps. The correlation described above is presented in graphic form in Fig. 7.69. All points that plot within the shaded area fulfill the requirement of the above formula. Theoretically, the requirement would be also fulfilled for a paint system with infinite high water vapor diffusion resistance but infinitely low capillary water uptake. However, because such boundary conditions would not be realistic, the Künzel number is limited to  $W \leq 0.5$  and  $s_d \leq 2.0$  as can be seen in Fig. 7.69.

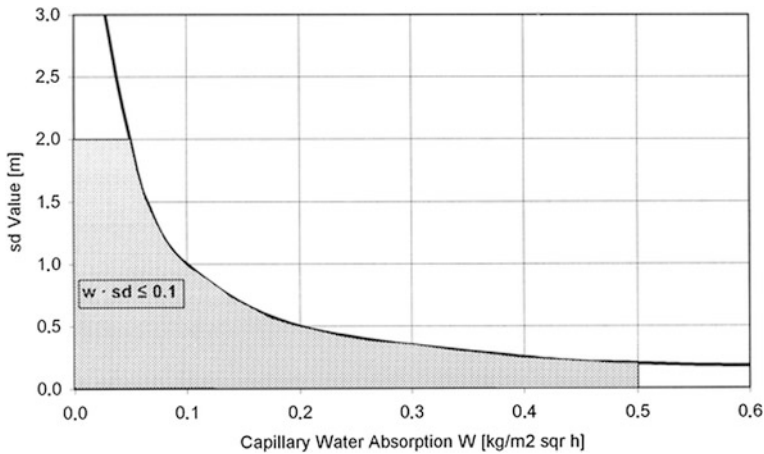


Fig. 7.69 Graphic depiction of Künzel Number  $w \cdot s_d$  (Figure by Künzel)



### 7.8.4 *Aspects of Conservation*

In former times worn down paint layers were simply removed mechanically or were painted over. If the number of paint layers, however, had grown too high, removal became necessary to prevent damage to the stone. Whereas lime based paint is not stable and mostly weathers away in rain exposed areas, linseed oil paint has to be removed either with a scalpel or using alkaline paint removal pastes that are not to be recommended for paint removal from stone.

According to the new EU law any use of lead white is forbidden because of its toxicity. However, in the field of cultural heritage preservation lead white may still be applied in special cases where historic evidence requires the use of lead white containing paint. It is to be remembered that in the case of linseed oil—lead white paint, regular maintenance is essential for its durability. In former times, the common practice was to refresh the paint every 2 or 3 years by applying a new paint layer, which closed the cracks that had formed in the old paint layer thus preventing water penetration into the substrate and renewing water repellency.

Pure lime paint is not resistant exposed to the environment and is washed away by rain. Tests carried out to lighten the black color of the putti at the Dresden Zwinger with lime paint failed after one winter. However, lime paint with an acrylic dispersion or silicone resin emulsion paint proved stable over several years. Similar to lime paint, the silicone resin emulsion paint is not film forming and has good water vapor conductivity. This can be attributed to the high pigment/volume concentration, PVC, within paint. Acrylic dispersion and silicone resin emulsion paints are unable to form a coherent plastic film if they have high PVC. The plastic components cover the aggregate surfaces as a thin film thus leaving sufficient pore space for water vapor transport. With long term exposure silicone resin emulsion paints will also be worn down because as water repellency is reduced over time, the calcitic aggregate will dissolve in rain water thus slowly reducing the paint thickness layer by layer.

The most stable paint system for outdoor use is pure silicate paint. However, its application has to be carefully evaluated because if removal becomes desirable it can only be done mechanically by grit blasting and with a high risk of damage to the substrate.

If possible, flaking paint layers may be softened with solvents and fixed to the surface with PVAc or PVA or acrylic glue. Brittle paint layers of silicate paint can be consolidated with ethyl silicate or similar products. But the case of old linseed oil—lead white paint is the most difficult (Siedel 2000). In some cases, application of PVAc, PVA and acrylic resin may be successful. These products, however, are not specifically designed for the purpose of fixing those paints and can therefore only be regarded as a first aid remedy with short term perspectives. Taking into account the small efficiency of these products, Wendler et al. (2009) has recently tested various reactive silanes in combination with ethyl silicate for consolidating and re-attaching linseed oil—lead white paint layers onto the stone substrate with apparently better results.

Darkened paint layers can be cleaned in most cases with micro particle jet methods. However, before any cleaning is carried out, the stratigraphy of the paint layers has to be investigated to avoid the removal of any of the uppermost darkened paint layer.

## 7.9 Hydrophobic Treatment

The purpose of treating natural stone facades or sculptures with hydrophobic agents is to make the surface water repellent, or in other words, impermeable to liquid water. The effect of such treatment is commonly known from the spraying of a silicone on shoes or clothes. Rainwater will then no longer wet the surface but run down in droplets as is shown in Fig. 7.70.

The idea behind a hydrophobic treatment of stones is that all weathering processes are driven or enhanced by the presence of water. Reducing the ingress of liquid water would then reduce the rate of weathering and protect monuments in the open from environmental attack. The treatment can be considered a preventive measure because it effectively alters the surface of the stone. However, despite its misleadingly simple definition, it is a measure that requires careful evaluation before its application. The main reason for this is that a water repellent surface may prevent repair, renewal of joint mortars, and other conservation treatments that may become necessary in the future. Furthermore, in some cases, such as the presence of soluble salts, the presence of a water repellent may lead to severe deterioration. Finally, too little is known about the interaction of these products with the substrate and their long-term stability. In any case, investigations in Germany covering 40 years of experience do not indicate extraordinary durability (Wendler and Snethlage 1988; Wendler et al. 1992).

One of the reasons why many people still oppose hydrophobization is the erroneous idea that the treatment seals the surface and therefore causes similar

**Fig. 7.70** Water droplet on a water repellent stone surface (Figure by Leisen)



damage to the older formulations of dispersion paints. In fact, however, hydrophobization only prevents penetration of liquid water while diffusion of water vapor is practically not influenced because the hydrophobic polysiloxane films are so thin that they do not diminish the diameter of the coarse pores that are responsible for the major part of water vapor transport.

Many laboratory and outdoor exposure site studies of hydrophobic products belonging to different chemical classes such as silanes, siloxanes, siliconates, epoxy resins, acrylates, waxes, mixtures of various products, have been carried out in the past. These have confirmed that mainly silanes and siloxanes are the best products for application in building restoration or even for new buildings. Therefore, only these types of water repellents will be addressed.

### 7.9.1 Effectiveness of Hydrophobic Agents

As has been mentioned in Sect. 7.2, the historic treatments with waxes or linseed oil had the aim of protecting the surface stones by making it water repellent. To date, however, hydrophobic treatments are exclusively carried out with alkyl-trialkoxysilanes. These compounds are far more durable and do not block the pores. The effect of a hydrophobic treatment on a surface is schematically depicted in Fig. 7.71.

On hydrophilic surfaces a water droplet will spread as shown in Fig. 7.71 and then absorbed by the stone. The contact angle between water droplet and stone surface will be zero when the water droplet is completely spread out. On a hydrophobic surface, however, the water droplet cannot spread because the attractive forces acting between the water molecules and the stone surface are blocked by the hydrophobic polysiloxane. In this case, the contact angle between the droplet and the surface will be above  $90^\circ$ , in an ideal case close to  $180^\circ$ . The water droplet will stay on the surface until complete evaporation. Measuring the contact angle can therefore be used to determine the degree of hydrophobization (RILEM 25 PEM 1980; Ferreira Pinto and Delgado Rodrigues 2000). It yields, however, only information about the state of the very surface. However, in many cases the water repellent effect of the surface disappears after some time thus allowing the water drop to spread. Nonetheless, the subsurface, maybe only 1 or 2 mm deep, the hydrophobization may still be effective preventing further

**Fig. 7.71** Shape of water droplet on hydrophilic (*left*) and hydrophobic surface (*right*)

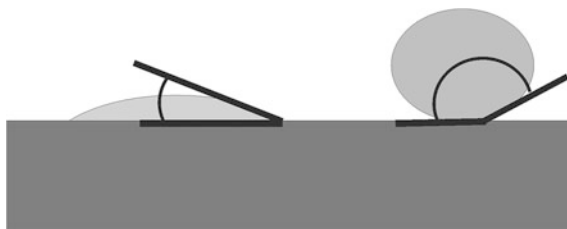


**Fig. 7.72** Karsten tube fixed on a façade *square* stone



penetration of water. Those effects can only be detected by measuring capillary rise on drill core samples or with the help of the Karsten tube.

The Karsten tube, or RILEM pipe (Fig. 7.72), is a practical and reliable tool for measuring water uptake on facades or sculptures. It permits to undertake measurements on as many numbers of points as necessary on a façade. Therefore these measurements yield far better information about the condition of a façade than would be possible through drill core sampling. Furthermore, the Karsten tube allows to measure water uptake as a function of time. In the most simple case, the water uptake, measured in milliliters per unit time, is compared between the different points of measurement, but this can be repeated after some time thus allowing to draw conclusions as to whether the state of hydrophobation is still sufficient or not.

The great advantage of the Karsten tube is that it is a non-destructive test because the tube can be simply fixed to the surface with sanitary putty (“Plastic Fermit”) without damaging the object surface. Such broad information could never be obtained by drill cores because such excessive sampling would never be permitted.

In Fig. 7.72, it can be seen that a moist circle formed around the Karsten tube. This phenomenon indicates that water repellency of the very surface has already disappeared while hydrophobization underneath is still intact. In these cases, water can only spread in the thin surface layer extending beyond the perimeter of the Karsten tube after some time. Given the fact that the penetrating water front has the shape of a half sphere, Wendler and Snethlage (1989) derived a formula to calculate the water uptake coefficient  $W$  ( $\text{kg}/\text{m}^2 \cdot \text{h}^{1/2}$ ) from the data obtained with the Karsten tube. Thus, it is possible to compare every Karsten tube measurement directly with the capillary water uptake measurement on drill cores or even prisms carried out in the laboratory according to standard conditions. Although the

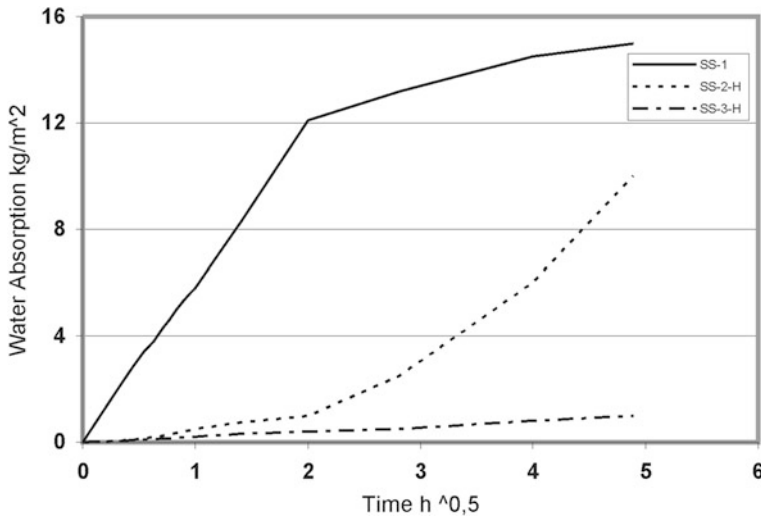


**Fig. 7.73** Effect of two hydrophobic agents on Schilfsandstone (SS). *SS-1* non-treated, *SS-2-H* agent 2, *SS-3-H* agent 3

Karsten tube measurements are precise and reproducible, Wendler and Sneath (1989) recommend the supporting information from capillary uptake measurements with drill cores.

The effectiveness of hydrophobic agents is different on different stones. Therefore, laboratory tests are needed before any product can be applied. These require testing with identical stone or at least one with similar composition and moisture transport properties. An example of different effectiveness of products is shown in Fig. 7.73.

In the curve *SS-1* for the untreated stone sample three steps can be distinguished. An initial steep slope corresponds to the filling with water of the coarse pores and this is broken when the moisture level reaches the upper side of the sample. In the 2nd phase, the remaining smaller pores are filled, since the water penetration rate into small pores is slower. In the 3rd phase, the water absorption is again lowered as the smallest micropores are filled with water. Product 2 (curve *SS-2-H*) loses effectiveness after 2 h. The hydrophobic effect starts to diminish and nearly disappears by the end of the test. Product 3 (curve *SS-3-H*) exhibits good effectiveness as the water absorption is strongly reduced. From this result it is evident that product 2 is not durable and only product 3 can be recommended for application.

Under repeated contact with water effectiveness of hydrophobic agents is very often reduced, in particular on carbonate stones because siloxanes do not bind so tightly to carbonate surfaces as onto siliceous surfaces. In these cases the effectiveness, however, may be improved by pretreatment with adhesive coupling agents to the product (see Sect. 7.2).

According to Snethlage and Wendler (1996), Sasse and Snethlage (1997), and Snethlage (2008) an effective hydrophobic treatment should reduce the capillary water absorption coefficient to  $0.1 \text{ kg/m}^2 \cdot \text{h}^{1/2}$ . Whether this effectiveness is obtained in practice can only be proven by the application of various hydrophobic products on test areas on the building considered and measuring the capillary absorption coefficient  $W$ , either by drill cores, or preferably, via the Karsten tube.

As mentioned in Sect. 7.8, the decisive parameter to assess the compatibility of a product with the stone is the Künzel number, the product of the capillary water absorption coefficient  $W$  and the water vapor permeability  $sd$ :

$$W \cdot sd \leq 0.1 \left[ \text{kg/m h}^{1/2} \right] \quad (7.23)$$

The Künzel number should be lower than  $0.1 \text{ kg/m}^2 \cdot \text{h}^{1/2}$  to ensure complete drying of a façade even under harsh climatic conditions. For the specific case of water repellents, the thickness of the hydrophobic layer  $s$  has to be introduced for calculating  $sd$ :

$$sd = \mu \times s[\text{m}] \quad (7.24)$$

The water vapor diffusion resistance  $\mu$  has to be measured separately in the laboratory.

Similarly to other conservation measures, Snethlage and Wendler (1996) and Sasse and Snethlage (1997) also established requirements for assessing effectiveness of hydrophobic treatments. The most important ones are presented in Table 7.13, and the requirement for capillary water uptake coefficient  $W$  being the most important one. It is required that after treatment  $W$  should not exceed the value of  $0.1 \text{ kg/m}^2 \cdot \text{h}^{1/2}$ , a value small enough to provide sufficient protection against driving rain. The requirement, on the other hand, is not too strict because it can be fulfilled by every product that is effective on the specific substrate considered.

Though it is likely that the treatment may cause some darkening of the stone it should not be excessive. The appearance of gloss is an indication that the treatment was carried out on a wet surface. As mentioned, water vapor diffusion resistance is only slightly changed because of the extremely small thickness of the polysiloxane films formed by polycondensation of the hydrophobic agent. The requirement, therefore, can be fixed to a 20 % increase above that of the untreated stone.

The requirement concerning hydric dilatation  $\alpha$  deserves a more detailed discussion. Snethlage and Wendler (1996, 2001) and Mertz and Jeanette (2004) found that hydrophobic treatment may enhance hygric and hydric dilatation, especially in case of clay rich sandstones. The increase may be explained by the polysiloxane films stretching between clay plates of the matrix. Thus, single clay plates may no longer move individually but react as a bulk to changing moisture content so that the total hygric and hydric dilatation are enhanced. It should be noted that hygric dilatation of hydrophobic stone, (dilatation in the range of changing RH in the air) may be even bigger than hydric dilatation of non treated stone, (dilatation under immersion of water). Since changes of relative humidity in ambient air are much



**Table 7.13** Quality requirements for hydrophobic treatment

Symbol	Property	Units	Testing method	Requirements
–	Visual appearance	–	Color chart CIE-LAB coordinates	No or minor color change or darkening No gloss
W	Capillary water uptake coefficient	$\text{kg/m}^2 \cdot \text{h}^{1/2}$	Standard test on drill cores	$W \leq 0.1$
W	Capillary water uptake coefficient	$\text{kg/m}^2 \cdot \text{h}^{1/2}$	Karsten tube measurement	$W \leq 0.1$
s	Penetration depth	mm	Capillary soaking during 5 min	$W \leq 2$ ; $s = 7$ $W \geq 2$ : see Fig. 7.74
$\alpha$ (hygric and hydric)	Hygric and hydric dilatation	$\mu\text{m/m}$	Dilatometer	No increase compared with untreated stone
$\mu$	Water vapor diffusion resistance	–	Dry and wet cup	Increase $\leq 20$ % untreated stone

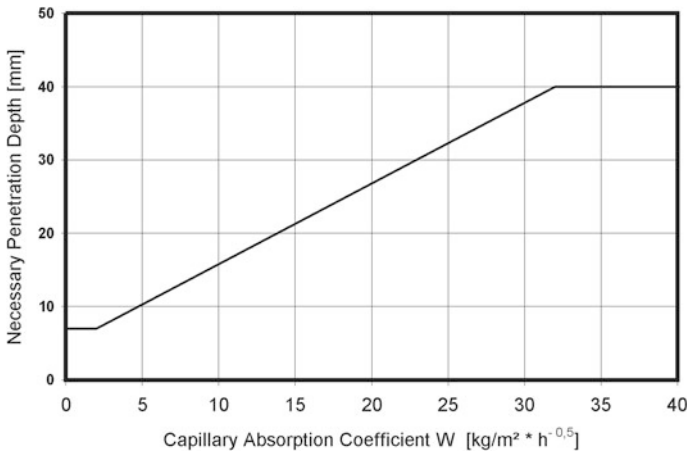


**Fig. 7.74** Penetration depth requirements for hydrophobic agents depending on capillary water uptake coefficient  $W$  (WTA 2010)

more frequent than rain events, enhanced hygric dilatation may be a serious source for deterioration of hydrophobic stone. Testing hygric and hydric dilatation of stone before and after hydrophobic treatment is therefore an important part of the testing procedure.

### 7.9.2 Practical Advises

Necessary penetration depth of hydrophobic agents has been the objective of Wissenschaftlich Technischer Arbeitskreis (WTA) working group 3.14 (WTA 2010). The working group defined a minimum penetration depth of 7 mm for all stones with a capillary water uptake coefficient of  $W \leq 2 \text{ kg/m}^2 \cdot \text{h}^{1/2}$ . With higher  $W$  values the necessary penetration depth should increase as shown in Fig. 7.74. The abscissa covers the whole range of capillary water uptake coefficients occurring in nature. Finally, a penetration depth higher than 40 mm is considered unnecessary.

For quality control in practice the question arises whether the required penetration depth can be achieved on the building taking into account that spraying time of hydrophobic agents onto the façade may not exceed a few minutes. The WTA 3.17 working group, based on practical building site experience, therefore established a limit of 200 s, i.e., some 3 min, for applying liquid hydrophobic products. If it is possible to achieve the required penetration depth within 200 s hydrophobic treatment can be carried out with liquid hydrophobic agent. If more time is necessary to achieve the required penetration depth a hydrophobation cream should be applied. This has a gel like consistency and can be brushed on.

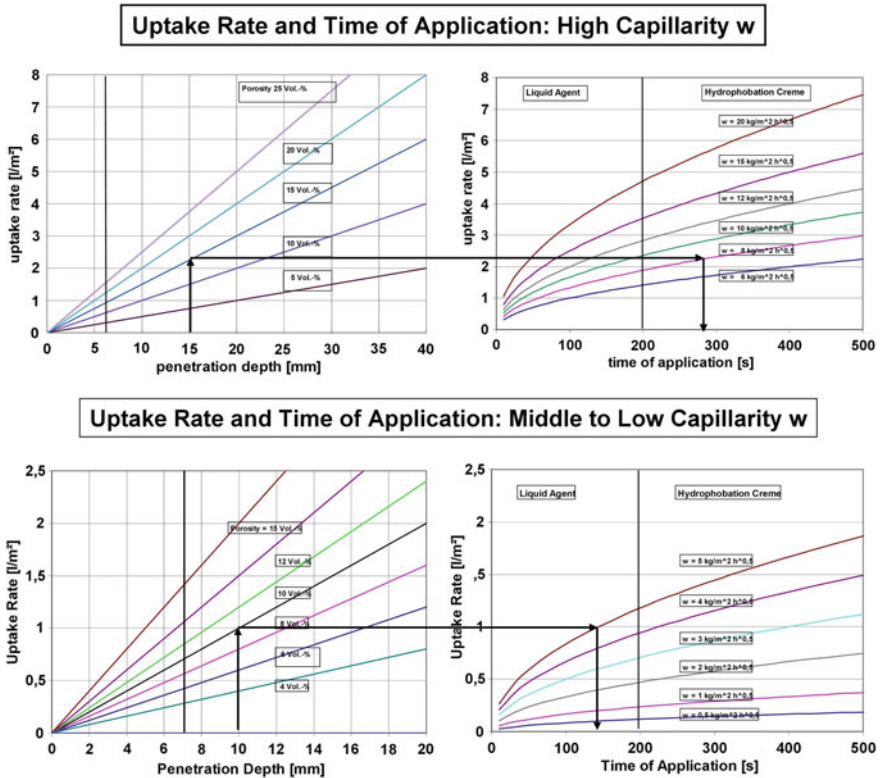


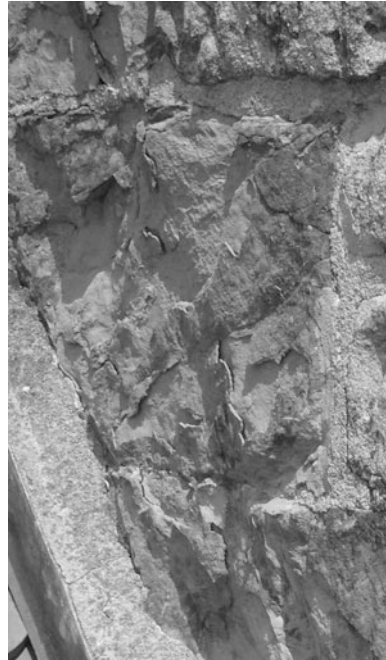
**Fig. 7.75** Uptake rate and time of application for hydrophobic treatment of stone with high capillarity water uptake coefficient  $W$ . In the left diagram, penetration depths below the 7 mm minimum are highlighted (Figure by WTA)

The crème stays on the surface and will be completely absorbed by the surface with time. Detailed information about time and application methodology can be found in Sneathlge (2008).

An example for deriving the necessary penetration depth and application time is given in Fig. 7.75. The left part shows the uptake rate of the agent depending on the penetration depth, assuming materials with different porosity from 5 to 25 v/v%. The right part also presents the uptake rate but depending on application time, assuming different  $W$ -values from 6 to 20  $\text{kg/m}^2 \cdot \text{h}^{1/2}$ . Therefore, a direct correlation exists for the two diagrams and starting from the necessary penetration depth found in Fig. 7.74 the corresponding application time can be derived.

For instance, given a model stone with a porosity of 15 % v/v and a  $W = 8 \text{ kg/m}^2 \cdot \text{h}^{1/2}$ , from Fig. 7.74 the required penetration of 15 mm can be read. This value is used to enter into the left part of Fig. 7.75 and to find that the uptake of 2.3  $\text{l/m}^2$  is necessary to reach this 15 mm penetration depth. By projecting the value of 2.3  $\text{l/m}^2$  to the curve labeled with  $W$ -value = 8  $\text{kg/m}^2 \cdot \text{h}^{1/2}$  in the right diagram it

**Fig. 7.76** Formation of contour scales on Schilfsandstone after hydrophobation with silanes. Former Monastery Birkenfeld, Germany



is found that this uptake of agent can only be achieved with a 280 s application time. This application time cannot be achieved by a liquid hydrophobic agent but requires hydrophobic crème instead. For clarity reasons, in Fig. 7.75 the curves for  $W$ -values lower than  $6 \text{ kg/m}^2 \cdot \text{h}^{1/2}$  are omitted. Those who want more information are requested to look up in Snethlage (2008) or WTA (2010).

Hydrophobic treatments only prevent liquid water absorption, but will not reduce the absorption of water vapor of the material. Therefore, the presence of hygroscopic salts represents a high risk factor for masonry even if treated with hydrophobic agents. Depending on the relative humidity in the ambient air hygroscopic salts absorb or release water, thus going into solution or being precipitated. Therefore, a salt contaminated masonry is under risk of being strongly wetted behind the hydrophobic surface layer and salts will tend to accumulate at this boundary. With time, the repeated dissolution—crystallization—cycles the hydrophobic surface layer may detach from the stone, in particular if the penetration depth is too low. The damage caused by the hydrophobic treatment of salt contaminated masonry may be worse than the treatment had not been applied. Hydrophobation of salt contaminated masonry should therefore be avoided. An example of delaminating contour scales some years after a hydrophobic treatment had been carried out is shown in Fig. 7.76.

When hydrophobic products were introduced into restoration practice some 30 years ago, partial hydrophobization of sculptures or facades had sometimes been favored. This was the result of the erroneous idea that hydrophobization might

**Fig. 7.77** Heavily wetted foundation of façade of Pommersfelden Castle Bavaria, Germany, after hydrophobic treatment of the façade's *upper part*



**Fig. 7.78** Dark vestiges of rinsing rain drops on the hydrophobic surface. Lion on the Gate to Pranner Street Munich, Germany



significantly reduce water vapor diffusion. At the façade of the Pommersfelden Castle near Bamberg, this consideration led to the decision to treat the façade but to spare the foundation in order to allow drying of the basement wet masonry. The consequences of this treatment are shown in Fig. 7.77. The greater flow of rain water down the hydrophobic façade leads to an increased wetting of the foundation, probably some 20 times more than before. Therefore, generally for practical work either the entire object is treated or no treatment at all should be applied.

In the past hydrophobic treatment has been often recommended to reduce the soiling of the treated object. This argument, however, did not always prove true as Fig. 7.78 shows (see also Moreau et al. 2008b). Nowadays, many hydrophobic facades show ugly dark vestiges because dust deposited on horizontal surfaces is washed away by the rain drops which run down the hydrophobic surface. Observing such patterns is a clear proof that a hydrophobization treatment was applied to the object in the past.

### 7.9.3 Durability of Hydrophobic Treatment

Karsten tube and contact angle are suitable methods to assess the durability of hydrophobic treatments. Because they are non-destructive they are preferred to drill core measurements.

Ferreira Pinto and Delgado Rodrigues (2000) used water drop contact angle and microdrop absorption time to evaluate durability of silane water repellents applied on four Portuguese limestones. The samples had been exposed to the open air in Lisbon and near the sea coast for 3 years. After exposure the authors found that the products had lost their superficial water repellent effect on most of the tested stones although the efficiency might still prevail in the interior.

This result highlights the difference between the water repellent properties of the surface and the interior pore space. Spreading of water drops on façade stones does not automatically mean that the hydrophobic effect has been lost. Concentric rings forming around the Karsten tube are an indicator for the reduced hydrophobic effect of the surface zone of a façade stone (Fig. 7.79).

In the example depicted in Fig. 7.79, water spreads along a moisture permeable superficial zone of around 1 mm thickness. Deeper penetration into the stone, however, is prevented by the retained hydrophobicity of the pores inside. Therefore by capillarity water migrates also upwards in vertical direction so that the wetted zone will have a round shape. This case must not be confused with a leak in the sealing of the Karsten tube because in case of a leak the water would just rinse down the façade and no wet zone would form above the Karsten tube.

Comprehensive studies have been carried out in France evaluating treatments after 20–30 years after application (Bromblet 2000). The investigation illustrates the difficulties in evaluating results because the different environmental conditions and the variability of stone material on the treated buildings limit the comparisons

**Fig. 7.79** Wet halo around Karsten tube due to superficial capillary water transport

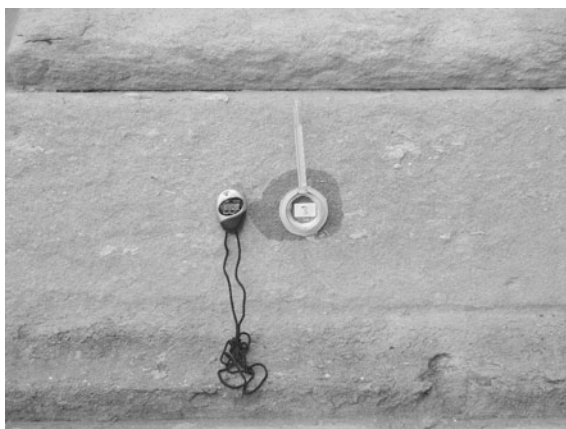


**Fig. 7.80** View of the south façade of Alte Pinakothek Munich, Germany



that can be made between the obtained results. Therefore, only some generalized but nevertheless important conclusions could be drawn:

- A key parameter for good durability is a good penetration depth.
- Efficiency and durability depend on the substrate; therefore, preliminary tests on the effectiveness of any product under concern have to be carried out.
- Effectiveness may persist for 20 or 30 years, in particular with polysiloxane based water repellents.

The most comprehensive investigation about durability of hydrophobic treatment was carried out by Wendler and Sneathlague (1988), Sneathlague et al. (1996a) and Meinhardt-Degen and Sneathlague (2004) on the Alte Pinakothek in Munich. Figure 7.80 presents a partial view of the south façade of the 150 m long building. The building had been heavily damaged in World War II. After re-erection (1952–1957) the brick facades including different varieties of Regensburg greensandstone were re-installed in a 5-year campaign (1984–1989).

The stone elements of the facades were cleaned with steam jet and micro particle jet, consolidated with TEOS Wacker OH and finally with Wacker H, a hydrophobic mixture of TEOS and silane. Measurements of the hydrophobic efficiency using the Karsten tube was carried out immediately after application, and then repeated in 1991, 2001 and 2009. The four measurement campaigns served to show the water repellency condition around the whole building. For clarity and to simplify the evaluation, the facades are separated into different measurement areas that are compared separately. Figure 7.81 shows the results of the last campaign in 2009.

The results obtained from 120 single measurements are presented in a box and whisker diagram. The rectangle of each box and whisker represents 50 % of the measured values. The cross in the middle of the box represents the average of the measured values, the length of the line the minimum and maximum value. It can



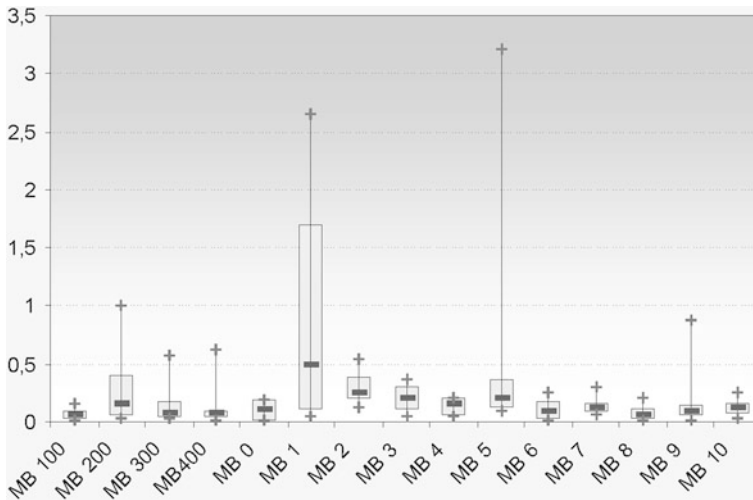


**Fig. 7.81** Variation of capillary water absorption  $W$  on different façade areas of the Alte Pinakothek Munich, Germany, measured in 2009

be seen from Fig. 7.81 that in most of the measurement areas the average  $W$  value is still close to the optimum value of  $0.1 \text{ kg/m}^2 \cdot \text{h}^{1/2}$ . In areas MB 2, MB 3, MB 4 and MB 200 the  $W$  value has reached more than  $0.2 \text{ kg/m}^2 \cdot \text{h}^{1/2}$ . MB 1 yields the worst average value with  $0.5 \text{ kg/m}^2 \cdot \text{h}^{1/2}$ .

The narrow width of the boxes themselves indicates the good hydrophobic state of the facades because the critical limit of  $0.5 \text{ kg/m}^2 \cdot \text{h}^{1/2}$  that has been established by Künzel (1969) as the upper limit for an effective façade protection against rain has not been exceeded. The only exception is represented by MB 1. In this area, the average value, the width of the box and the maximum value lie far above the critical limit. Water repellency of the façade in MB 1 is no longer sufficient and therefore re-treatment should therefore be carried out soon.

In spite of the available information, there remain doubts as to whether one or more hydrophobic re-treatments could block the pores and impede water vapor diffusion by an increased water vapor diffusion resistance  $\mu$ . To answer this point it should first be considered that if capillary water uptake is effectively reduced then only a small amount of water vapor needs to diffuse through the hydrophobic zone to let the stone dry. Moreover, re-treating sample areas at the Alte Pinakothek in Munich with FUNCOSIL SN and SNL Meinhardt-Degen and Snethlage (2004) found that re-treating did not cause the Künzel number to exceed  $0.1 \text{ kg/m}^2 \cdot \text{h}^{1/2}$ . The risk of forming water vapor impermeable surface zones by multiple hydrophobic treatments is negligible if not non-existing, at least for silanes and siloxane based water repellents. In case of film forming products like resins or plastic dispersion, however, the risk is well existing.

### ***7.9.4 General Aspects About Hydrophobation***

Hydrophobic treatment of buildings or sculptures has raised more debates than any other restoration measures. Some support it because of its preventive effect. Others completely object to it because they consider hydrophobation irreversibly confining future treatment options. Investigations on buildings, especially in Germany, demonstrate that the surface water repellency disappears very fast. Therefore the surface will turn hydrophilic and water based joint and repair mortars can be applied without risk of detaching immediately after application.

On the other hand, the decrease in the soiling of facades has not been fulfilled as expected with different soiling patterns developing.

From our present knowledge the effectiveness of hydrophobization with silanes or siloxanes may last over 20 years if the treatment is properly applied. Similarly to ethyl silicate consolidation, the treatment of limestones is difficult, in particular for the case of dense limestone. This kind of stone weathers away only from the surface because calcite is dissolved by acids, i.e., carbonic or sulfuric acids, and washed away. Therefore, preventing surface wetting will reduce the dissolution of calcite. However, if the surface repellency has disappeared, in most cases by UV radiation, the dissolution of the calcite on the surface will continue. Thus, application of water repellents to dense limestones will protect them for a short time only.

Hydrophobization serves to protect building parts that are exposed to frequent and heavy rain. Therefore, in practice, it should be taken into account whether the building to be treated really suffers from exposure to strong rain. Only if this is the case hydrophobation should be carried out. Facades surrounded by other buildings and protected against driving rain normally do not require this treatment.

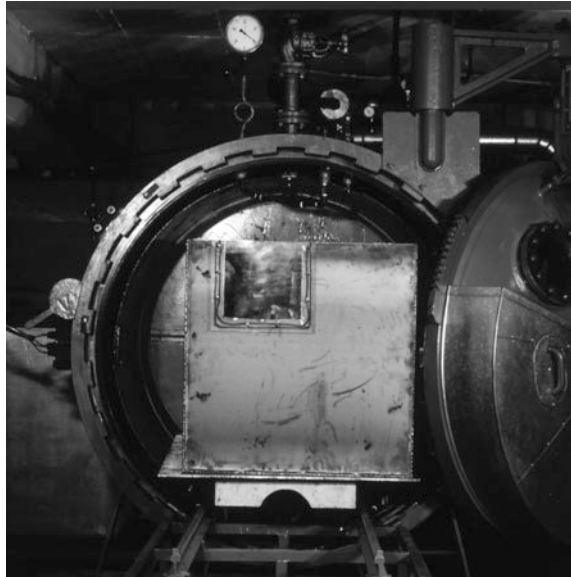
## **7.10 Acrylic Resin Full Impregnation**

The acrylic resin full impregnation (in German “Acrylharzvolltränkung” AVT) is also known as the Ibach Method named after “Ibach Stone Conservation” company, which developed the method 30 years ago and runs the only facilities to carry out full impregnation worldwide.

The idea of AVT is to completely fill the pores of the deteriorated stone by polymerization of methylmethacrylate (MMA) monomer into the polymethylmethacrylate (PMMA) polymer within the pore system. After the treatment all pores are blocked to gaseous and liquid water transport and deterioration may virtually come to a complete stop so that the object is preserved in the condition it was at the time of the treatment. From the point of view of material sciences the object is no longer a stone but a composite material.

The polymerization process, in principle similar to the production of “Plexiglass”, is not easy to conduct. The AVT therefore can only be carried out in a

**Fig. 7.82** Vacuum-pressure-vessel for acrylic resin full impregnation (Figure by Ibach)



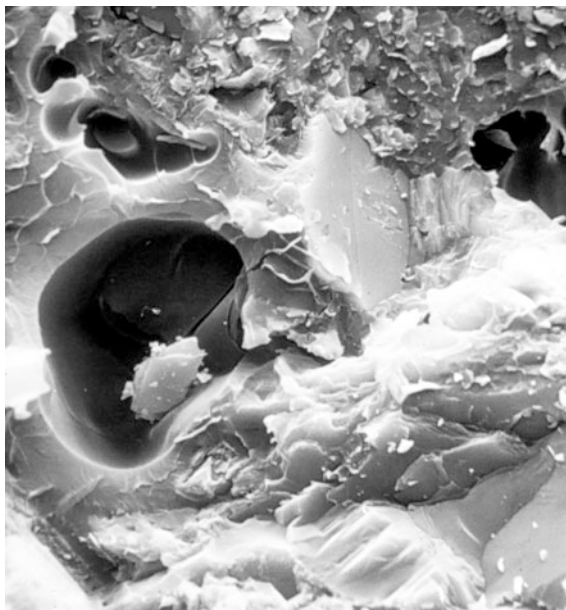
special vessel and not on the site. Objects under question to be treated with AVT have to be demountable and transportable.

First, the object has to be dried very carefully at a temperature of 50–70 °C in a drying chamber in order to remove all the moisture. Depending on its size, drying may take several weeks. Then, the object has to cool back to room temperature, which may also take weeks to months. Both drying and cooling are recorded with the help of temperature measurements inside small drill holes which have to be drilled into the centre of the stone from the bottom of the base or from other hidden places. As soon as room temperature is reached the object is placed into a metal case that is then introduced into the vacuum-pressure-vessel (Fig. 7.82).

The closed vessel is then evacuated to a technical vacuum of 0.1 bars to extract all air from the pores. This process may also take several days to one week, depending on the size of the object. Once the necessary vacuum is reached the metal case inside the vessel is slowly filled with the liquid MMA monomer until the object is completely immersed in it. Then the pressure inside the vessel is raised to 10 bars by pumping nitrogen into the vessel. The sequence of vacuum and pressure is repeated several times because the aim of impregnation is to fill all pores through to the core of the object. It has to be emphasized that only pressure, not vacuum, enhances penetration of the impregnation liquid into pores smaller than 10 µm.

Once the object is fully impregnated with the monomer, the surplus impregnation liquid is pumped back into the reservoir. The object is now no longer in contact with the liquid. Under prevailing pressure the temperature inside the vessel is raised stepwise to 60–70 °C to start the polymerization reaction. Polymerization also may take 2 weeks or sometimes more because the entire object must be

**Fig. 7.83** Shrinkage bubble inside polymethylmethacrylate



heated to the desired temperature. After completion of the polymerization the whole vessel is slowly cooled down to room temperature and the object can be removed from the vessel.

The impregnation liquid of AVT is composed of over 90 % monomer methylmethacrylate MMA, with some other monomer acrylates to reduce stiffness of the PMMA as well as some dissolved polymeric polymethylmethacrylate PMMA. Through polymerization to solid PMMA the volume will shrink by around 12 v/v% thus creating new pore space water could penetrate into the stone. For this reason the impregnation liquid contains a few percent of coupling agents that ensure that no shrinkage bubbles develop at the pore surface—PMMA boundary but only inside the PMMA itself (Fig. 7.83). Because the shrinkage bubbles are not interconnected but isolated they cannot serve for liquid and gaseous moisture transport.

Very often it is argued objects treated with AVT could attain glossy or greasy appearance; however, this has not been the case with all objects treated so far. The objects look totally natural and even stone conservation experts can hardly recognize whether an object is treated or not by AVT. The reason for this is that when the temperature inside the vessel is slowly raised to start the polymerization, some of the monomer MMA will evaporate from the surface so that it keeps its natural look (Fig. 7.84). Therefore limestones or marble may still suffer a slow surface recession of around 20  $\mu\text{m}/\text{year}$  due to environmental influences. The essential aim of the treatment, the stabilization of the whole stone structure is not endangered by this process.

AVT completely changes the mechanical properties of treated stone. Strength and E-modulus may rise by a factor of 5 or even more. It is therefore absolutely

**Fig. 7.84** Balustrade in park of Castle Seehof near Bamberg Bavaria, Germany



necessary that the impregnation liquid reaches the core of the object and the stone is homogeneously hardened throughout its full diameter. If total impregnation fails to reach all parts of the stone because of insufficient drying the core area of the stone the AVT treated outer part will break apart after short time, in most cases after one or two winters already. Careful drying and cooling are therefore essential for a successful and durable treatment. During the first years of application of AVT, the time for complete drying and cooling were sometimes underestimated so that the objects suffered severe cracking. Meanwhile, however, improved know-how and save conducting of the process have prevented further failures.

Which kind of objects come into consideration for AVT? First of all the object should not have an extraordinary artistic or historic value and it must be moveable. Secondly, its state of preservation should be such that normal conservation with consolidant and repair mortars could not result in a significant increase of durability. Therefore AVT is primarily appropriate for serial stone mason work like balusters, steps, tombstones, ornamental pieces on buildings, field memorial stones and other works that are of value in their present location but do not have the value to be displayed in a museum.

Applying repair mortars to AVT impregnated stones are not a problem. Preferably, cement-bound commercial products should be used to fill cracks and missing parts before the AVT process because the repairs will be then also impregnated with PMMA and adhere tightly to the bulk stone. Repairs after AVT treatment should be done with acrylic or epoxy bound mortars but cement-bound mortars with underlying dispersion primer layer are also possible.

AVT is mainly carried out in Bavaria and other parts of Germany as well as in the Netherlands. Since 1979 more than 3,000 objects have been treated. AVT therefore can be regarded an approved method. In particular it is appropriate for preserving marble sculptures and vases, which are sometimes completely disintegrated down to the very core.

Nevertheless, the AVT method has been rejected by many as compared to any other conservation method. Reasons range from ethical to partly economic reasons

or just out of prejudice and lack of knowledge. Furthermore, the economic interests of stone masons who may consider that increased AVT treatments could endanger the stone mason tradition and education to good carving skill. In most cases, however, it is the ethical argument that the AVT treated stone can no longer be considered a stone but a composite, which has lost “authenticity”. These arguments, relating to the more profound cultural aspects of conservation, are beyond the objectives of this book.

## 7.11 Antimicrobial Treatments and Preventive Measures

### **Katja Sterflinger-Gleixner**

*Institute of Applied Microbiology, University of Natural Resources and Life Sciences, Muthgasse 18, A-1190, Vienna, Austria*

As described in [Sect. 4.5](#), fungi, bacteria, algae and even some plants have a considerable impact on the aesthetical appearance and the weathering of stone. Since biological colonization may be detrimental to stone and other building materials, the inactivation or removal of any biogenic layer is often necessary. However, architects, restorers, stone cutters and conservators that consider applying an antimicrobial treatment have to keep in mind that the structure and function of microbial communities are far from being fully understood. Microbes interact with each other, they compete for nutrients and space and they have an enormous adaptive potential to fill any and all ecological niches offered by the stone and its environment. Because of the complexity of microbial communities, it is nearly impossible to predict the consequences of a biocide treatment or of a severe change of environmental conditions, such as climate control inside a cave, church or catacomb.

A selective removal of one or several groups of the micro-biota may give rise to others that may prove even more detrimental (Piñar and Sterflinger 2009). For this reason, there are no general anti-microbial treatments but object specific solutions that have to be developed on a case by case basis. This requires a careful analysis of the microbial community and the physico-chemical parameters. An anti-microbial treatment should always be accompanied by a sound scientific analysis monitoring program.

### ***7.11.1 Climate, Humidity and Exposure***

To a large extent, the species diversity present and the absolute amount of organisms growing on and in stone are determined by the environmental conditions. As mentioned in the deterioration chapter, water is the most important factor controlling life on and in stone. Sunlight is essential for algae, plants and

cyanobacteria but on the other hand, high UV-radiation damages the DNA of all organisms on earth and thus can be a lethal factor for some microbes on stone. Micro-organisms differ widely in their need for water and sunlight but as a general rule it can be said that the diversity of a microbial community and the absolute biomass produced in a certain time decreases with extreme environmental conditions. Low water availability, good ventilation for a fast drying of surfaces after a rain event, direct sun exposure and avoiding the presence of water, be it from condensation, infiltrations or resulting from the presence of surrounding trees, are the best measures to prevent the biocolonization of stone. Water trickling from roofs or plants transports organic material—sugars and waxes from plants, particulate organic matter from dust—and thus can supply nutrients to the micro-organisms. For this reason controlling the amount of water that reaches the surface of a building by good design and construction is the most important factor to prevent and inhibit biocolonization.

Trees and other plants can influence the object by water dripping from the leaves but also by providing shade to them, thus retarding the drying of a wet surface. In some cases—especially if objects of high cultural value are concerned—the trimming or even complete removal of plants may be indicated.

Hoods of transparent acrylic have been used frequently to shelter free standing sculptures or structures against freezing weather or even to protect them. However, they can enhance biofilm development by creating a warm and humid hothouse climate. Wooden laggings, albeit being less aesthetical and hindering the view of the object during winter time are far more suitable because they allow good ventilation.

In some cases, extending a roof or installing a rain gutter, as well as repairing broken down spouts, cornices, roof overhangings, roof tiles and window sills can have an enormous effect in reducing the amount of moisture in a building and thus the development of biofilms on its surfaces.

### ***7.11.2 Cleaning and Biocidal Treatments***

In the field of preservation, cleaning, i.e., the removal of soiling, patinas and crusts is among the first steps of a restoration intervention. In most instances the appropriate cleaning method is determined by the chemical composition and strength of the material itself and by the nature of the soiling to be removed.

When a building suffers from strong biological contamination, the following considerations should be taken into account for cleaning. Algal and cyanobacterial layers and crusts should be completely dry before cleaning, since dry crusts detach from the material more readily and can be removed mechanically using brushes or microparticle jet. In contrast, damp layers of algae or cyanobacteria are strongly attached to the material and trying to remove them mechanically results in a mucilaginous smear that will press them even deeper into porous material. Likewise this treatment may cause damage to fragile surfaces.



In general, cleaning stone with pressurized or superheated steam should be avoided because it pushes both water and organisms deep into the material. As a consequence, microbial growth will not only be faster afterward the cleaning but colonization will also take place deeper in the material (Warscheid and Braams 2000).

Before the application of a biocide it is important to activate a dry biofilm because in the dry state microorganisms might be inactive and a biocide will not even penetrate the cells. In contrast, an active metabolism is more sensitive to biocide attack. In order to activate the metabolism of the microbes, the stone can be treated by a soft water spray, which only influences the uppermost layer of the stone but does not penetrate into the material.

Care has to be taken with the use of laser-cleaning on darkly pigmented lichen or fungal crusts since laser is known to cause certain pigments to discolor. Melanins and carotenes are bio-pigments produced by many micro-organisms. These natural pigments can be burnt into the crystal matrix of a calcareous stone by the heat of the laser and the resulting black, brown or reddish stain is even more difficult to remove. Here, cleaning with microparticle jet can be a suitable alternative. Only recently, the surface cleaning of stone by ionized gas (plasma) was tested for its application on sandstone and marble and was shown to be a promising and environment-friendly procedure to remove surface crusts and to eliminate the microorganisms in one step.

The use of a high intensity, pulsed Xenon flash lamp was suggested as a promising tool for the removal of lichens from monuments (Leavengood et al. 2000). Monochromatic light was successfully used as a non-destructive methodological approach for the control and prevention of cyanobacterial biofilms growth on stone (Albertano et al. 2005).

Having thoroughly removed all macroscopically visible micro-flora from an object, a biocide treatment can be considered. In order to minimize the amount of biocide needed—which is important for both environmental and financial reasons—biofilms and crusts should be removed before applying the biocide. The remaining biomass, especially inside the stone, can then be treated with the biocide. Since biogenic layers or colonies are often located inside the material as organisms penetrate pores, fissures and grow under exfoliating crusts or between paint layers, they cannot be reached mechanically. Therefore, the application of a biocide is required in these cases, as any residues in form of single viable cells or whole colonies are a source for rapid recurrence of fouling-processes. Especially if a superficially cleaned stone surface is to be coated with a lime wash or paint, such a layer will be detached within a period of only 2–5 years if residues of lichen or fungi in the interior start growing out again (Fig. 7.85).

If restorers or architects decide upon a biocide treatment, the choice for the appropriate active component should best be based on preliminary micro-biological studies that focus on the object-specific micro-flora and conditions. These studies should be carried out by a micro-biologist and should include the analysis of the microorganisms present, counts of viable microbial cells and analysis of microbial activity before and after the biocide treatment. The choice of the toxic

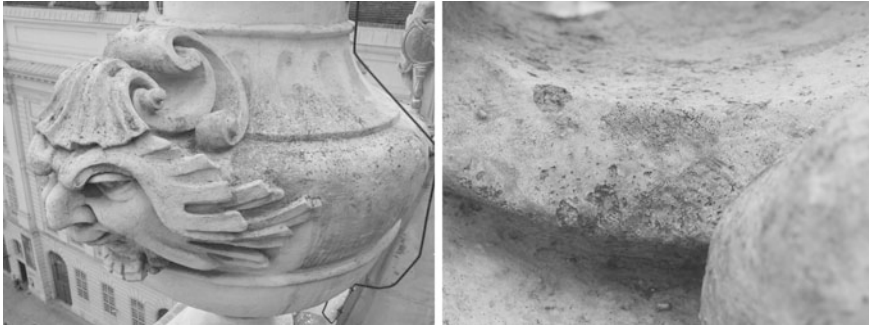


**Fig. 7.85** Lime wash detachment by recurrent lichen and fungal growth (Figure by Sterflinger)

agent is restricted and regulated in Europe by the European Biocide Directive (<http://ec.europa.eu/environment/biocides/index.htm>). For this reason highly toxic organo-tin or -mercury and other heavy-metal components can no longer be used in restoration. Albeit a variety of biocides that are effective on different groups of organisms are available on the market (Bagda 2000), in restoration practice substances effective against a broad spectrum of organisms are needed. In addition to its effectiveness, a biocide should have low viscosity to allow good penetration, be UV-resistant, stable in a broad pH range, have no interaction with the stone material nor cause precipitation of salts or induce color changes. It should also be relatively environment friendly and, if possible, cost effective.

All products used in the field of conservation should have their chemical composition fully described by the producer and/or marketing firm. This is particularly critical for biocides, since the ready to use products contain small amounts of additives, e.g., detergents, anti foaming agents, or just fragrances. The benefit of some of these is dubious and their long term effects unknown. Some producers try to enhance the biocidal activity by the addition of organic acids, such as formic acid, to enhance access to the cells. However, these can corrode calcareous stones and materials. While these may be useful in the case of some stones or ceramics on private homes' terraces and monuments of little architectural or cultural value, they can be disastrous when applied to polished stone surfaces or world heritage monuments.

Three substance groups are approved that are effective against fungi, bacteria, algae, moss and lichen because they affect the general cellular processes. The first one corresponds to products containing formaldehyde releasers; the second one, to products containing quaternary ammonium salts, such as benzalkonium chloride (e.g., Metatin 5810-101, Neo Desogen, Dimanin, Antimoos); and the third one, to dithiocarbamates (Ziram, Thiram). These have a broad spectrum but are only stable in a pH range from pH 7–10, that can be problematic when applied to or mixed with highly alkaline materials, such as lime-slurries, plaster or mortar.

The quaternary ammonium salts have good biocidal effects. For example, on facades good results were obtained by a product containing 1 %



**Fig. 7.86** Cyanobacterial and fungal growth on water runnels caused by water repellent (Sterzinger Marble, Schönbrunn, Vienna, Austria) (Figure by Sterflinger)

benzalkoniumchloride and 0.045 % isothiazolon (Remmers BFA) and by a more recent product based on 2,3,5,6-tetrachloro-4 (methyl suphonyl) pyridine. The latter product is available under the name Algophase<sup>®</sup> as a formula miscible in organic solvents and Algophase PH025/d as a water compatible formulation (Urží and de Leo 2007). Quaternary ammonium-salts mixed with borates, such as Remmers Adolit M, are used to combat the most destructive indoor fungus *Serpula lacrymans*, which degrades wood in indoor environments but is able to grow and to penetrate into porous stone, plaster and mortar. Also triazoles are used but they have a selective spectrum within the fungi and are not effective against algae.

Koretrel© contains alkyleneoxide (97.6 %), alkylaminotriazine (0.98 %), N-(3,4-dichlorophenyl)-N,N dimethyl urea (0.98 %) and denaturated alkyltrihydroxybenzene polyoxide (0.58 %). The biocide is designed to clean stone from cyanobacteria, lichen and algae in open-air condition and has been shown to be highly effective on siliceous substrates such as granites and basalt. It is not subject to the UN hazard classification and numbering rules. Since 1998, it has been used widely in Japan and Thailand, e.g., for treatment of the Angkor Wat monuments. The biocide shows a good activity against lichens but it decreases the capillary water absorption of the stone, similarly to a water repellent. Moreover a significant chromatic effect on light colored calcitic stones was observed even after drastic washing of the surface (Tretiach et al. 2007).

Hydrophobic treatments applied to a new or cleaned stone surface can considerably retard the primary or secondary colonization by micro-organisms since the water availability is reduced to a minimum. No significant differences on the microbial colonization was observed among different types of hydrophobic compounds (Hydrophase Superfici, Rhodorsil RC80 and Hydrophase Malte) tested by Urží and de Leo (2007). Nevertheless the water repellent effect, depending on the shape of the object, may cause runners or stripes on the surface that are readily colonized by algae and cyanobacteria due to the high water availability in them (Fig. 7.86).

To enhance the anti-microbial effect of a hydrophobic treatment the combined application of biocides and water repellents can be considered. However, the use

of quaternary ammonium compounds in combination with hydrophobic treatments is problematic since the surfactant effect of the biocide decreases the hydrophobic effect. A removal of the biocide by poultices is recommended before application of the hydrophobic treatments (Moreau et al. 2008a). Good anti-microbial results were obtained on mortar when the water repellent (Hydropahse Superfici, Rhodorsil RC80 or Hydrophase Malte) and the biocide (Algophase) were applied combined in a single application. Case studies and long term results for such a combined application on stone are still missing.

The choice of the biocide has to be complemented by an appropriate application. Field studies carried out on stone facades and statues have shown that biocides have to be applied in at least two coats in order to be effective. In case of lichens, three applications on a physiologically active lichen thallus are necessary. Several authors have shown that the effect of different biocides on a lichen thallus was faster and stronger when these were applied during a rain period as the thalli were in a fully hydrated state.

As mentioned previously, a physiologically active biofilm is far more vulnerable to biocides than dried or dormant cells. Therefore, it is recommended to keep surfaces humid several hours before the biocide is applied. This can be done by a mild water spray. For a superficial biogenic crust or a biofilm, the biocide is best applied in a poultice because it increases exposure time. For an in-depth colonization, flooding of the stone is appropriate. In case the biocide is applied to a humid surface, it has to be taken into account that the biocide will be diluted to a certain amount and that penetration into pores may be hampered by the water layer coating them. In each case the pros and cons of application on the humid or dry surface have to be discussed based on the individual conditions of the object and of the micro-biota.

It is important to keep in mind that none of the biocides currently available on the market have a long-term effect on re-colonization. Thus, controlling the humidity, temperature, light, nutrients and combinations of these environmental parameters is the only way to reduce microbiological contamination and prevent re-infection. In case those parameters cannot be controlled, regular maintenance including monitoring, cleaning, etc., is required. These must be agreed upon between authorities/sponsors and conservators. Restorers should put into writing in their contracts that they cannot guarantee the long term re-colonization of the object in case the owner/sponsor does not agree with architectural, building physics and climatic measures necessary to prevent microbial growth.

### ***7.11.3 Bioremediation***

Specific metabolic activities have been employed to develop new bioremediation methods based on the use of microbial cells and enzymatic activity to remove organic material (Antonioli et al. 2005) or bioinduced calcite precipitation using specific bacteria for monumental stone consolidation (Jimenez-Lopez et al. 2007).

Bioremediation of artworks is also based on the use of sulphate-reducing bacteria, which reduce sulphate ions to gaseous hydrogen sulphide (Cappitelli et al. 2007); and nitrate-reducing bacteria, which reduce nitrates to gaseous nitrogen and nitrous oxide (Saiz-Jimenez 1997).

Bacteria-induced carbonate mineralization has been proposed as an environmentally friendly method to protect and consolidate ornamental stone, in particular, porous limestone, either decayed or just quarried to replace seriously altered one (Jimenez-Lopez et al. 2007). The process of biomineralization is started by first spraying the surface to be consolidated with a bacterial suspension culture. Afterwards the culture is fed in situ with a suitable medium containing proteins and sufficient  $\text{Ca}^+$  ions by spraying. Biocalcification results in a thin (several micrometers) hydrophobic layer on the surface of the stone, the so-called “biocalcin”. A real consolidation by this method is not possible because of the low depth of penetration of the bacterial culture. In tests carried out on baroque plaster, the spraying of the nutrient solution onto the plaster surface gave rise to the colonization by other microorganisms causing a serious aesthetical damage. The biocalcite method is still being developed and has to be optimized. Some research has been done in this regard by using different microorganisms—mainly *Bacillus cereus* and *Myxococcus xanthus*—that are able to induce the extracellular formation of calcium carbonate. Although further research is necessary for the “in situ” application of a *M. xanthus*-inoculated culture medium, it seems that the use of these organisms could be more effective in consolidating ornamental stone than the use of *B. cereus*, due to its ability to consolidate the stones without pore plugging.

## 7.12 Concluding Remarks

Science applied to the conservation of outdoor monuments is a relatively new area of research. Already in the 19th century there were some efforts in developing chemical products for protecting monuments from environmental attack, however, the following scientific approach that dealt with these questions revealed itself as inappropriate because products testing was mainly limited to treating sample areas. This strategy did not yield clear results, mainly because the idea that the differences between the treated and the untreated areas would become visible in a reasonable time. i.e., a few years, did not prove to be true. In fact, weathering processes are not fast enough to make differences evident in such a short period of time. Therefore, the many sample areas on monuments and endless number of test sites all over the world are of no use for conservation science unless they are accompanied by a precise monitoring plan including measurements of visual appearance, moisture transport and mechanical properties.

Conservation is a multi-disciplinary field, where historic research, scientific disciplines such as geosciences, chemistry, material science and biology and practical restoration have to contribute to develop really scientifically based

conservation strategies. The scope of each discipline alone is too narrow to consider all aspects that have to be taken into account when conservation research and practical conservation have to be brought into accord to decide the best possible preservation program for a monument.

In spite of all the efforts undertaken so far, both in science and practice, it has to be recognized available conservation methods cannot stop further decay but only decrease the rate of future deterioration. Achieving really long-term effective results needs accompanying preventive measures, e.g., the improvement of structural deficiencies of the original object (e.g., installation of a functional water drainage system, protection of moldings and other protruding building parts with metal shelters) or the change of deleterious environmental conditions (e.g., exposure to strong rain or heavy traffic).

As has been shown in the previous chapters, there are appropriate physical and chemical parameters available to help assess the deterioration of stone over time and the effectiveness of conservation products applied to diminish it. Thus, monitoring programs could be designed to determine declining effectiveness of former treatments and to define the appropriate time for re-treatment. However, monitoring conservation treatments requires steady interest and a regular budget for financing the necessary investigations, a situation that seldomly is realized. As a consequence, the information that could be gained from previous treatments if regular monitoring were carried out is not available for predicting the effectiveness of products and durability of the treatments. Still governmental building administration prefers intermittent extensive and expensive intervention instead of steady maintenance with a low but permanent budget.

At present the scientific methods we have available for evaluating effectiveness and durability of treatments yield the necessary results only in retrospect. Therefore, the predictions that can be made only cover a length of time similar to that where the performance of a product has been controlled, generally some 20–30 years. To be able to look into future performance of conservation products numerical modeling of climatic impact and ageing processes of these products would be needed.

However, because at present this important area of science practically does not exist there is all the more need for it in the field of conservation. In order to avoid irreparable damage to our cultural heritage, possibly even caused by the methods we have applied, we should be able to foresee the future performance of all measures we are going to apply as long as the time the monuments exist since their erection. Therefore, all measures we recommend for treating monuments should be well considered and seen in the timeframe of several 100 years during which they must not turn deleterious. The problems incorporated into these aims are very intricate and include the aspects of historic values, institutions and economic preferences of the society which is responsible for the care of the monuments. In 21 different papers these important questions were discussed in a Dahlem workshop on “Rational Decision-making in the Preservation of Cultural Heritage” (Baer and Snickars 2000).

We are aware that these demands for long-term prognosis of conservation measures are extremely challenging and new. Nevertheless, we should not reduce our efforts to consequently further conservation science and best restoration practice because both they are the best prerequisites for preserving our cultural heritage for future generations.

## References

- Aglietto M, Castelvetro V, Ciardelli F, Matteoli U, Botteghi C, Chiantore O, Lazzari M, Alessandrini G, Peruzzi R, Toniolo L, Fassina V (2000) An integrated approach to design Fluoro substituted 'smart' polymers for protection of monumental buildings. In: Fassina V (ed) Proceedings of the 9th international congress on deterioration and conservation of stone, Venice, 19–24 June. Elsevier, Amsterdam, pp 209–214
- Albertano P, Bruno L, Bellezza AO (2005) New strategies for the monitoring and control of cyanobacterial films on valuable lithic faces. *Plant Biosyst* 139(3 SI):311–322
- Andersson T, von Haslingen B (2000) Painted sandstone as protection and as an architectural and historical concept. In: Fassina V (ed) Proceedings of the 9th international congress on deterioration and conservation of stone, Venice, 19–24 June. Elsevier Amsterdam, pp 731–738
- Antonoli P, Zapparoli G, Abbruscato P, Sorlini C, Ranalli G, Rigetti PG (2005) Art-loving bugs: the resurrection of Spinello Aretino from Pisa's cemetery. *Proteomics* 5:2453–2459
- Ashurst J, Dimes FG (1990) Conservation of buildings and decorative stone, vol 2. Butterworth Heinemann, London, pp 174–184, 229
- Asmus JF, Guattari G, Lazzarini L (1973) Holography in the conservation of statuary. *Stud Conserv* 18:49–63
- Baer NS, Snickars F (eds) (2000) Rational decision-making in the preservation of cultural property. Report of the 86th Dahlem workshop, Berlin, 26–31 March. Dahlem University Press, Berlin
- Bagda E (2000) Biozide in Bautenbeschichtungen. Expert Verlag, Renningen, p 136
- Belk G (2005) Erproben von arbeitstechnischen Möglichkeiten für die verschiedenen Sicherungs-, Konservierungs- und Restaurierungsarbeiten von Tuffsteinflächen. In: Evangelische Kirche Kurhessen Waldeck (ed) Innovative Konzepte zur Konservierung und zum Schutz umweltgeschädigter historischer Tuffsteinflächen am Beispiel von drei nordhessischen Kirchen. DBU Projekt 18981-45, p 88
- Blänsdorf C (2007) Die farbige Armee, Eindruck des Lebendigen—Teil 1: Maltechnik und Farbrekonstruktion der Terracottaarmee des Qin Shihuangdi. In: Kunst- und Ausstellungshalle der Bundesrepublik Deutschland (ed) Unter der gelben Erde. Die deutsch-chinesische Zusammenarbeit im Kulturgüterschutz—Kongressbeiträge. Philipp von Zabern, Mainz, pp 71–76
- Bourguignon E, Bertrand F, Moreau C, Coussot P, Shahidzadeh-Bonn N (2008) Desalination of model stones by poulticing. In: Lukaszewicz JW, Niemcewicz P (eds) Proceedings of the 11th international congress on deterioration and conservation of stone, Torun, 15–20 Sept. Uniwersytetu Mikolaya Kopernika, Torun, pp 803–810
- Brandi C (1963) *Teoria del restauro*. Einaudi, Roma (Theory of restoration. English translation 2005. ICR, Rome)
- Brinkmann V, Wünsche R (2004) *Bunte Götter. Die Farbigekeit antiker Skulptur*. Katalog Sonderausstellung Glyptothek München. Biering, München
- Bromblet P (2000) Conservation of limestone in France. What do we know about the long-term performance of treatments. In: Domstiftung Regensburg Turm Fassade Portal, Regensburg, 27–30 Sept. Schnell & Steiner, Regensburg, pp 127–130



- Butlin RN, Coote AT, Ross KD, Yates TJS (1991) Weathering and conservation studies at Wells Cathedral, England. In: Baer NS, Sabbioni C, Sors AI (eds) Proceedings European symposium science technology and European cultural heritage, Bologna, Italy, 13–16 June 1989. Butterworth Heinemann, Oxford, pp 306–309
- Cappitelli F, Toniolo L, Sansonetti A, Gulotta D, Ranalli G, Zanardini E, Sorlini C (2007) Advantages of using microbial technology over traditional chemical technology in removal of black crusts from stone surfaces of historical monuments. *Appl Environ Microbiol* 73:5671–5675
- Caroe MB (1985) Wells Cathedral: conservation of figure sculptures 1975–1984. *Assoc Preserv Technol Bull* XVII:2–13
- Chiantore O, Poli T, Aglietto M, Castelvetro V, Peruzzi R, Colombo C, Toniolo L (2000) Effect of fluorinated groups on photooxidative stability of polymeric protectives applied on calcareous stone. In: Fassina V (ed) Proceedings of the 9th international congress on deterioration and conservation of stone, Venice, 19–24 June. Elsevier, Amsterdam, pp 215–223
- Clifton JR (1980) Stone consolidating materials a status report. National bureau of standards technical note 1118. Washington, DC
- Cooper M (1998) Laser cleaning in conservation. Butterworth Heinemann, Oxford
- Degenkolb M, Knöfel D (1998) Untersuchungen zum Einfluß von Holzkohle-Zusatz zu Kalkmörteln. In: Snethlage R (ed) Jahresberichte Steinerfall—Steinkonservierung, Band 6, 1994–1996. Fraunhofer IRB Verlag, Stuttgart, pp 237–245
- Doehne E, Schiro M, Roby Th, Chiari G (2008) Evaluation of poultice desalination process at Madame John's Legacy New Orleans. In: Lukaszewicz JW, Niemcewicz P (eds) Proceedings of the 11th international congress on deterioration and conservation of stone, Torun, 15–20 Sept. Uniwersytetu Nikolaya Kopernika, Torun, pp 857–864
- Domaslowski W (2000) Investigations on technology of joint mortars in brick. In: Fassina V (ed) Proceedings of the 9th international congress on deterioration and conservation of stone, Venice, 19–24 June. Elsevier, Amsterdam, pp 843–852
- Domstiftung Leitzkau (2002) Kalksteinkonservierung am Westportal des Halberstädter Doms St. Stephan und St. Sixtus. Domstiftung Sachsen-Anhalt, Leitzkau
- Drewello R, Herkner S (2009) Zwischen Diagnose und Therapie: Der Wandel historischer Anstrichsysteme am Weltgerichtportal und Optionen der Erhaltung. In: Bauhütte St. Sebald eV (ed) Das Weltgerichtportal der Sebalduskirche in Nürnberg. Konservierung kalkund ölgebundener Malschichten auf frei bewitterten Natursteinoberflächen. Fraunhofer IRB Verlag, Stuttgart, pp 25–45
- Eitel W (1966) Silicate science vol 5: ceramics and hydraulic binders. Academic Press, New York
- Elfving P, Jäglid U (1992) Silane bonding to various mineral surfaces. Department of Inorganic Chemistry Chalmers University Gothenburg Report OOK 92:01
- Endemann S (2000) Cleaning samples at Regensburg Cathedral—what are the long-term perspectives to re-soiling and gypsum formation. In: Domstiftung Regensburg Turm Fassade Portal, Regensburg, 27–30 Sept. Schnell & Steiner, Regensburg, pp 95–98
- Erfurth W (1992) Siliconharzfarbe—Dichtung und Wahrheit. *Deutsche Malerzeitschrift*, Ausgabe 4/1992, p 5
- Ettl H (1987) Kieselsäureestergebundene Steinersatzmassen. *Münchner Geowissenschaftliche Abhandlungen*, Reihe B, Heft 5, München
- Ettl H, Sattler L, Schuh H (1996) Konservierung von Sandstein mit Kieselgel-gebundenen Steinersatzstoffen. In: Snethlage R (ed) Denkmalpflege und Naturwissenschaft Natursteinkonservierung I. Ernst & Sohn, Berlin, pp 105–126
- Fassina V (2004) Evaluation of multifunctional Fluoropolymers ad hoc designed for stone protection of monuments. In: Kwiatkowski D, Löfvendahl R (eds) Proceedings of the 10th international congress on deterioration and conservation of stone, Stockholm, 27 June–2 July. ICOMOS, Sweden, pp 503–510

- Ferreira Pinto A, Delgado Rodrigues J (2000) Assessment of the durability of water repellents by means of exposure tests. In: Fassina V (ed) Proceedings of the 9th international congress on deterioration and conservation of stone, vol 2, Venice, 19–24 June. Elsevier, Amsterdam, pp 273–285
- Ferreira Pinto A, Delgado Rodrigues J (2008) The action of inorganic consolidants on limestone. In: Lukaszewicz JW, Niemcewicz P (eds) Proceedings of the 11th international congress on deterioration and conservation of stone, Torun, 15–20 Sept. Uniwersytetu Nikolaya Kopernika, Torun, pp 873–880
- Frantzikinaki K, Panou A, Vassiliadis C, Papakonstantinou E, Pouli P, Ditsa T, Zafropoulos V, Fotakis C (2004) The cleaning of the Parthenon west frieze: an innovative laser methodology. In: Kwiatkowski D, Löfvendahl R (eds) Proceedings of the 10th international congress on deterioration and conservation of stone, Stockholm, 27 June–2 July. ICOMOS, Sweden, pp 801–807
- Franzen C, Hoferik F, Laue S, Siedel H (2008) Water bath desalination of sandstone objects. In: Lukaszewicz JW, Niemcewicz P (eds) Proceedings of the 11th international congress on deterioration and conservation of stone, Torun, 15–20 Sept. Uniwersytetu Nikolaya Kopernika, Torun, pp 881–888
- Giamello M, Pinna D, Porcinai S, Sabatini G, Siano S (2004) Multidisciplinary study and laser cleaning tests of marble surfaces of Porta della Mandorla Florence. In: Kwiatkowski D, Löfvendahl R (eds) Proceedings of the 10th international congress on deterioration and conservation of stone, Stockholm, 27 June–2 July. ICOMOS, Sweden, pp 841–848
- Giusti A (2006) Brandi's "Reversibility" forty years later. In: Delgado Rodrigues J, Mimoso JM (eds) Proceedings of the international seminar theory and practice in conservation, Lisbon, 4–5 May. LNEC, Lisbon, pp 139–144
- Goins ES, Wheeler G, Fleming SA (1996a) The influence of reaction parameters on the effectiveness of tetraethoxysilane-based stone consolidants: solvent effects. Methods of evaluating products for the conservation of porous building materials in monuments. In: ICCROM (ed) Proceedings of the international colloquium science and technology for cultural heritage, May 1995. Rome, pp 259–274
- Goins ES, Wheeler G, Wypyski MT (1996b) Alkoxysilane film formation on quartz and calcite crystal surfaces. In: Riederer J (ed) Proceedings of the 8th international congress on deterioration and conservation of stone, Berlin, 30 Sept–4 Nov. Möller Druck, Berlin, pp 1255–1264
- Grissom CA, Charola AE, Wachowiak MJ (2000) Measuring surface roughness: back to basics. *Stud Conserv* 45(2):73–84
- Haake S, Simon S (2004) The Bologna cocktail—evaluation of consolidation treatments on monuments in France and Italy after 20 years of natural aging. In: Kwiatkowski D, Löfvendahl R (eds) Proceedings 10th international congress on deterioration and conservation of stone, Stockholm, 27 June–2 July. ICOMOS, Sweden, pp 423–430
- Hafezi M, Pfeiffer M, Knöfel D (1998) Leichtkalkmörtel für den Einsatz im Fachwerkbau. In: Sneath R (ed) Jahresberichte Steinzerfall—Steinkonservierung, Band 6, 1994–1996. Fraunhofer IRB Verlag, Stuttgart, pp 247–259
- Hansen E, Doehne E, Fidler J, Larson J, Martin B, Matteini M, Rodriguez-Navarro C, Pardo ES, Price C, de Tagle A, Teutonico JM, Weiss N (2003) A review of selected inorganic consolidants and protective treatments for porous calcareous materials. *Rev Conserv* 4:13–25
- Henning O, Knöfel D (1997) *Baustoffchemie. Eine Einführung für Bauingenieure und Architekten*. Gabler Wissenschaftsverlag, Wiesbaden
- Henriques FMA (2004) Replacement mortars in conservation: an overview. In: Kwiatkowski D, Löfvendahl R (eds) Proceedings of the 10th international congress on deterioration and conservation of stone, Stockholm, 27 June–2 July. ICOMOS, Sweden, pp 973–983
- Henriques FMA, Moreira Rato V, Charola AE (2004) The influence of grain size distribution on the performance of mortars. In: Kwiatkowski D, Löfvendahl R (eds) Proceedings of the 10th international congress on deterioration and conservation of stone, Stockholm, 27 June–2 July. ICOMOS, Sweden, pp 1001–1008

- Herm C (1991) Die Wasserdampfdurchlässigkeit von Anstrichen auf Naturstein. Arbeitsblätter für Restauratoren, Heft, Feb, pp 238–246
- Herm C (1997) Anstriche auf Naturstein—Untersuchungen zur Zusammensetzung historischer Fassungen, Kolloidchemie von Kalkfarben und Bauphysik. Dissertation, Ludwig-Maximilians-Universität München
- Herm C, Pfefferkorn S, Snethlage R (1998) Historische Verfahren und Handelsmarken in der Steinkonservierung 1840 bis 1940. In: Snethlage R (ed) Naturwissenschaft und Denkmalpflege Natursteinkonservierung II. Fraunhofer IRB Verlag, Stuttgart, pp 9–26
- Herm C, Snethlage R (1992) Water vapour permeability of painted stone. In: Delgado Rodrigues J, Henriques F, Telmo Jeremias F (eds) Proceedings of the 7th international congress on deterioration and conservation of stone, 15–18 June. LNEC, Lisboa, Portugal, pp 677–686
- Hörmann H (1913) Kessler'sche Fluat. Bewährte Mittel zur Härtung und Erhaltung von weichen Kalksteinen, Sandsteinen, Mörteln, Zementwaren, Kunststeinen und Gips. Verlag Tonindustrie—Zeitung Seger & Kramer, Berlin
- Horn F (2007) Die farbige Armee, Eindruck des Lebendigen—Teil 2: Virtuelle Farbrekonstruktion an 3D-Modellen von Terracottakriegern. In: Kunst- und Ausstellungshalle der Bundesrepublik Deutschland (ed) Unter der gelben Erde. Die deutsch-chinesische Zusammenarbeit im Kulturgüterschutz. Kongressbeiträge. Philipp von Zabern, Mainz, pp 77–79
- Hotz T (2006) Ölen von Sandstein als Witterungsschutz am Berner Münster. Diplomarbeit Hochschule der Künste, Bern
- ICOMOS (1966) The Venice Charter International Charter for the conservation and restoration of monuments and sites. Approved by the 2nd international congress of architects and technicians of historic monuments. Venice, 1964
- ICOMOS (1996) The Athens Charter for the restoration of historic monuments. Adopted at the first congress of architects and technicians of historic monuments. Athens, 1931
- IDK (Institut für Diagnostik und Konservierung von Denkmalen) (2001) Beseitigung von Feuchte und Salzsäuren an verputztem Mauerwerk erzgebirgischer Kirchen. Bericht DD, Dresden, Dec
- IUAV (University of Venice—Faculty of Architecture) (2006) Assessment of desalination mortars and poultices for historic masonry. Zezza F (coordinator) EU contract 022714 Newsletter 1/2006. IUAV, Venice, p 17
- IUAV (University of Venice—Faculty of Architecture) (2007) Assessment of desalination mortars and poultices for historic masonry. Zezza F (coordinator) EU contract 022714 Newsletter 3/2007. tudelft.nl
- Jimenez-Lopez C, Rodriguez-Navarro C, Piñar G, Carrillo-Rosua FJ, Rodriguez-Gallego M, Gonzalez-Muñoz MT (2007) Consolidation of degraded ornamental porous limestone stone by calcium carbonate precipitation induced by the microbiota inhabiting the stone. *Chemosphere* 68:1929–1936
- Keil F (1971) Zement, Herstellung und Eigenschaften. Springer, Berlin
- Keim AW (1881a) Die Mineral-Malerei. Neues Verfahren zur Herstellung witterungsbeständiger Wandgemälde. Technisch-wissenschaftliche Anleitung, Wien (Reprint Thomas Hoppe, Stuttgart, 1995)
- Keim AW (1881b) Die Mineralmalerei. Neues Verfahren zur Herstellung witterungsbeständiger Wandgemälde. Chemisch-Technische Bibliothek, Band 78. A Hartleben, Wien, Leipzig
- Kieslinger A (1932) Zerstörungen an Steinbauten. Deuticke, Leipzig und Wien
- Pouli P, Zafropoulos V, Fotakis C (2004) Novel laser cleaning. In: Kwiatkowski D, Löfvendahl R (ed) Proceedings of 10th international congress on deterioration and conservation of stone, Stockholm, 27 June–2 July 2004. ICOMOS, Sweden, pp 315–321
- Knöfel D, Winnefeld F (1995) Anpassung von Fugendeckmörteln an Ziegelmauerwerk. In: Snethlage R (ed) Jahresberichte Steinzerfall—Steinkonservierung, Band 5, 1993. Ernst & Sohn, Berlin, pp 147–157
- Kocher M (2005) Quelldruckmessungen und thermische Druckmessungen an ausgewählten Sandsteinen. Dissertation, Fakultät Geo- und Umweltwissenschaften Universität München

- Koller J, Baumer U (2000): Kunstharzfirnisse Teil II. Mechanische Eigenschaften, Alterungsverhalten und Löslichkeiten von polymeren Kunstharzfirnissen. *Restauro* Nr. 8/2000, pp 616–625
- Koss A, Marezak J (2008) Implementation of laser technology in conservation in last decade. In: Lukaszewicz JW, Niemcewicz P (eds) *Proceedings of the 11th international congress on deterioration and conservation of stone*, Torun, 15–20 Sept. Uniwersytetu Nikolaya Kopernika, Torun, pp 939–946
- Krenkler K (1980) *Chemie des Bauwesens*. Band 1: Anorganische Chemie. Springer, Berlin
- Kühn H (1988) *Farbmaterialien. Pigmente und Bindemittel*. Reclams Handbuch der künstlerischen Techniken Band 1. Reclam, Stuttgart
- Künzel H (1969) Anforderungen an Außenanstriche und Beschichtungen aus Kunstharzdispersion. *Kunststoffe im Bau* 12:6–32
- Leavengood P, Twilley J, Asmus JF (2000) Lichen removal from Chinese spirit path figures of marble. *J Cult Herit* S1:71–74
- Laurenzi-Tabasso M (2000) The conservation of limestone in Italy in the last decades—evolution and trends. In: Domstiftung Regensburg Turm Fassade Portal, Regensburg, 27–30 Sept. Schnell & Steiner, Regensburg, pp 117–120
- Laurenzi-Tabasso M, Simon S (2006) Testing methods and criteria for the selection/evaluation of products for the conservation of porous building materials. *Rev Conserv* 7:67–82
- Lazzarini L, Asmus JF (1973) The application of laser radiation to the cleaning of statuary. *Bull AIC* 13:39–49
- Lewin SZ (1966) The preservation of natural stone 1839–1965. An annotated bibliography. *Art Archaeol Tech Abstr* 6(1):185–277
- Lindborg U (1995) Acoustic measurement and conservation of the Gustav Adolf monument in Göteborg. In: *Proceedings of the 5th workshop EUROCARE EUROMABLE EU 496*, Innsbruck, 10–15 Oct 1994. Bayerisches Landesamt für Denkmalpflege—Zentrallabor Forschungsbericht 15/1995, München, pp 1–6
- Littmann K, Riecken B, Sasse HR (1998) Steinschutzstoffe nach dem Aachener Konzept. In: Sneath R (ed) *Denkmalpflege und Naturwissenschaft Natursteinkonservierung II*. Fraunhofer IRB Verlag, Stuttgart, pp 207–226
- Lombardo T, Simon S (2004) Desalination by poulticing. Laboratory study on controlling parameters. In: Kwiatkowski D, Löfvendahl R (ed) *Proceedings of the 10th international congress on deterioration and conservation of stone*, Stockholm, 27 June–2 July. ICOMOS, Sweden, pp 323–330
- Martin B (2000a) Cleaning British limestone—what are the methods to arrive at optimal solutions. In: Domstiftung Regensburg Turm Fassade Portal, Regensburg, 27–30 Sept. Schnell & Steiner, Regensburg, pp 99–103
- Martin B (2000b) Lime shelter and lime poultice—two methods with a narrow relationship to limestone? In: Domstiftung Regensburg Turm Fassade Portal, Regensburg, 27–30 Sept. Schnell & Steiner, Regensburg, pp 111–115
- Matteini M (1987) In review: an assessment of florentine methods of wall painting conservation based on the use of mineral treatment. In: Cather S (ed) *The conservation of wall paintings, proceedings of a symposium organized by the Courtauld Institute of Art and the Getty Conservation Institute*, 13–16 July. London, pp 137–148
- Meinhardt-Degen J, Sneath R (2004) Durability of hydrophobic treatment on sandstone facades—investigations of the necessity and effects of retreatment. In: Kwiatkowski D, Löfvendahl R (eds) *Proceedings of the 10th international congress on deterioration and conservation of stone*, Stockholm, 27 June–2 July. ICOMOS, Sweden, pp 347–354
- Merrill EW (1997) Polymers in preservation and restoration: two examples. In: Vandiver PB, Druzik JR, Merkel JF, Stewart J (eds) *Materials issues in art and archaeology V. Materials research society symposium proceedings*, vol 462. Pittsburgh, pp 353–358
- Mertz JD, Jeanette D (2004) Effect of water repellent treatments on the hydric dilatation of sandstone during water capillary absorption and drying stages. In: Kwiatkowski D,

- Löfvendahl R (eds) Proceedings of the 10th international congress on deterioration and conservation of stone, Stockholm, 27 June–2 July. ICOMOS, Sweden, pp 355–362
- Moreau C, Vergès-Belmin V, Leroux L, Oriol G, Fronteau G, Barbin V (2008a) Water-repellent and biocide treatments: assessment of the potential combinations. *J Cult Herit* 9:394–400
- Moreau C, Vergès-Belmin V, Leroux A, Kisselinskaia A, Oriol G, Barbin V (2008b) The influence of protective treatments on limestone soiling, sulphation and cleaning. Results after ten years of outdoor exposure. In: Lukaszewicz JW, Niemcewicz P (eds) Proceedings of the 11th international congress on deterioration and conservation of stone, Torun, 15–20 Sept. Uniwersytetu Nikolaya Kopernika, Torun, pp 983–991
- Neumann HH (1994) Aufbau, Ausbildung und Verbreitung schwarzer Gipskrusten, dünner schwarzer Schichten und Schalen sowie damit zusammenhängender Gefügeschäden an Bauwerken aus Naturstein. Institut für Anorganische und Angewandte Chemie der Universität Hamburg, Schriftenreihe Angewandte Analytik Nr. 24
- Nimmrichter J, Koller M (2000) Opferschichten auf Kalksandstein und Kalkstein—Langzeitperspektiven einer präventiven Konservierungsmethode. In: Domstiftung Regensburg Turm Fassade Portal, Regensburg, 27–30 Sept. Schnell & Steiner, Regensburg, pp 121–126
- Nimmrichter J, Koller M, Paschinger H, Richard H (2000) Sacrificial layers for conservation of calcareous stones in Austria—theory, practice and evaluation. In: Fassina V (ed) Proceedings of the 9th international congress on deterioration and conservation of stone, Venice, 19–24 June. Elsevier, Amsterdam, pp 903–912
- Noll W (1968) Chemie und Technologie der Silicone: 16. Verlag Chemie, Weinheim
- Nonfarmale O (1976) A method of consolidation and restoration for decayed sandstone. In: Rossi-Manaresi R (ed) The conservation of stone I. Proceedings international symposium, Bologna, 19–21 June 1975. Centro per la Conservazione delle Sculture all'Aperto, Bologna, pp 401–410
- Osswald J, Snethlage R (1996) The hardening process in silicate paints. In: Riederer J (ed) Proceedings of the 8th international congress on deterioration and conservation of stone. Berlin, pp 1265–1275
- Pallot-Frossard I (2004) What is the real impact of new technologies on conservation methodology and deontology? Examples in France. In: Kwiatkowski D, Löfvendahl R (eds) Proceedings of the 10th international congress on deterioration and conservation of stone, Stockholm, 27 June–2 July. ICOMOS, Sweden, pp 763–776
- Pamplona M, Kocher M, Snethlage R, Aires-Barros L (2008) Drilling resistance: state of the art and future developments. In: Lukaszewicz JW, Niemcewicz P (eds) Proceedings of the 11th international congress on deterioration and conservation of stone, Torun, 15–20 Sept. Uniwersytetu Nikolaya Kopernika, Torun, pp 449–456
- Pavia S, Caro C (2006) Lime mortars for masonry repair: analytical science and laboratory testing versus practical experience. In: Delgado Rodrigues J, Mimoso JM (eds) International seminar theory and practice in conservation, Lisbon, 4–5 May. LNEC, Lisbon, pp 493–499
- Petzet M (1993) Denkmalpflege heute. Arbeitsheft 60. Bayerisches Landesamt für Denkmalpflege, München
- Piñar G, Sterflinger K (2009) Microbes and building materials. In: Cornejo DN, Haro JL (eds) Building materials: properties, performance and applications. Nova Science Publishers, Inc., New York, pp 163–188
- Plenderleith HJ (1976) Preservation and conservation: introductory statement. In: Preservation and conservation: principles and practices. Proceedings of the North American international regional conference 1972. The Preservation Press, Washington, DC, pp xvii–xxi
- Pouli P, Fotakis C, Hermosin B, Saiz-Jiminez C, Domingo C, Oujja M, Castillejo M (2008) The laser induced discoloration of stonework; a comparative study on its origin and remedies. *Spectrochim Acta A* 71:932–945
- Pouli P, Zafiroopoulos V, Fotakis C (2004) Novel laser cleaning. In: Kwiatkowski D, Löfvendahl R (ed) Proceedings 10th international congress on deterioration and conservation of stone, Stockholm, 27 June–2 July 2004. ICOMOS, Sweden, pp 315–321

- Price CA (1984) The consolidation of limestone using a lime poultice and limewater. In: Adhesive and consolidants IIC. London, pp 160–162
- Prickartz R, Heuser H (1991a) The low-water injector jet process. A new suitable cleaning process for masonry. Proceedings of the 9th international brick/block Masonry conference DGFM. Berlin, 13–16 Oct
- Prickartz R, Heuser H (1991b) Feinstaubstrahltechnik, ein Verfahren zur Reinigung von Natursteinoberflächen. In: Snethlage R (ed) Jahresberichte Steinzerfall—Steinkonservierung, Band 1, 1989. Ernst & Sohn, Berlin, pp 215–221
- Prickartz R, Schoonbrod J (1993) Applikation von Steinschutzstoffen mit dem Caisson-Verfahren. In: Snethlage R (ed) Jahresberichte Steinzerfall—Steinkonservierung, Band 3, 1991. Ernst & Sohn, Berlin, pp 117–120
- Prickartz R, Schoonbrod J (1998a) Praxisorientierte Steinschutzstoffrängung. In: Snethlage R (ed) Jahresberichte Steinzerfall—Steinkonservierung, Band 6, 1994–1996. Fraunhofer IRB Verlag, Stuttgart, pp 97–100
- Prickartz R, Schoonbrod J (1998b) Entwicklung und Erprobung einer neuen Imprägniertechnik: der Fluid-Applikator III. In: Snethlage R (ed) Jahresberichte Steinzerfall—Steinkonservierung, Band 6, 1994–1996. Fraunhofer IRB Verlag, Stuttgart, pp 101–103
- Rathgen F (1915) Die Konservierung von Altertumsfunden Teil 1: Stein und steinartige Stoffe. Verlag, Berlin
- Regnault MV (1853) Elements of chemistry. Clarke & Hesser, Philadelphia, p 532
- RGIT (Robert Gordon Institute of Technology) (1991) Stone cleaning in Scotland. Research summary, research report 1, 2, 3. Historic Scotland, Edinburgh
- Riederer J (1973) Bibliographie der deutschsprachigen Literatur zur Verwitterung und Konservierung natürlicher Bausteine. Deutsche Kunst und Denkmalpflege, Jahrgang 1973 Heft 1/2. Deutscher Kunstverlag, Berlin, München
- RILEM 25 PEM (1980) Recommendation provisoires, Essais recommandés pour mesurer l'alteration des pierres et évaluer l'efficacité des méthodes de traitement. Matériaux Constr 13(75):175–253
- Rossi-Manaresi R (1976) Treatments for sandstone consolidation. In: Rossi-Manaresi R (ed) The conservation of stone I. Proceedings international symposium, Bologna, 19–21 June 1975. Centro per la Conservazione delle Sculture all'Aperto, Bologna, pp 547–571
- Rousset B, Gal G, Giradet F, Constantine J, Cornet A, Guinchard D (2004) Roughness measurements before and after cleaning. In: Kwiatkowski D, Löfvendahl R (eds) Proceedings 10th International congress on deterioration and conservation of stone, Stockholm, 27 June–2 July. ICOMOS, Sweden, pp 603–610
- Ruedrich J, Wedekind W, Kracke T, Siegesmund S (2008) Präventive Natursteinkonservierung. Modellhafte Salzreduzierung an Buntsandstein-Grabmälern des Bartholomäus-Friedhofs in Göttingen. Restauro 114. Jg. 2008 Heft 7:444
- Saiz-Jimenez C (1997) Biodeterioration vs. biodegradation: the role of microorganisms in the removal of pollutants deposited on historic buildings. Int Biodet Biodeg 24:225–232
- Sasse HR, Snethlage R (1997) The methods for the evaluation of stone conservation treatments. In: Baer N, Snethlage R (eds) Saving our cultural heritage: the conservation of historic stone structures. Dahlem workshop reports ES20. Wiley, Chichester, New York, pp 223–243
- Sattler L (1992) Sandsteinfestigungen mit Kieselsäureester. Dissertation, Universität München. Bayerisches Landesamt für Denkmalpflege, Zentrallabor, Forschungsbericht 9/1992: 156 S mit Anhang
- Sauerländer W (2000) Quand les statues étaient blanches. Discussion au sujet de la polychromie. In: Verret D, Steyaert D (eds) La couleur et la pierre. Polychromie des portails gothiques Actes du Colloque. Amiens, 12–14 Oct. A et J Picard, Paris, pp 27–34
- Schaffer RJ (1931) The weathering of natural building stones. Building research establishment spec. report 18 (reprint 1972). Garston-Watford
- Schock-Werner B (1999) Schutzanstrich Chorstrebewerk. 40. Dombaubericht Okt 1998–Sept 1999, p 19

- Schramm HP, Hering B (1988) Historische Malmaterialien und ihre Identifizierung. Akad. Druck und Verlagsanstalt, Graz
- Semper G (1834): Vorläufige Bemerkungen über bemalte Architektur und Plastik bei den Alten. In: Semper G Kleine Schriften. Berlin Stuttgart, p 239
- Siedel H (2000) Zur Problematik alter Ölfarbenanstriche auf Sandstein. In: Boué A (ed) Farbe in der Steinrestaurierung. Fassung und Schutz. Fraunhofer IRB Verlag, Stuttgart
- Siedel H, Hubrich K, Kusch HG, Wiedemann G, Neumeister K, Sobott R (2000) Results of laser cleaning on encrusted oolithic limestone of angel sculptures from the Cologne Cathedral. In: Fassina V (ed) Proceedings of the 9th international congress on deterioration and conservation of stone, Venice, 19–24 June. Elsevier, Amsterdam, pp 583–590
- Siedel H, Wiedemann G (2002) Laserstrahlreinigen von Naturstein. Fraunhofer IRB Verlag, Stuttgart
- Sliwinski G, Bredal-Jørgensen J, Jankowska M, Sawczak M (2006) Laser techniques for the conservation practice. Case study on Gotlandic sandstone. In: Delgado Rodrigues J, Mimoso JM (eds) International seminar theory and practice in conservation, Lisbon, 4–5 May. LNEC, Lisbon, pp 473–482
- Snethlage R (2008) Leitfaden Steinkonservierung. Fraunhofer IRB Verlag, Stuttgart
- Snethlage R, Auras M, Leisen H, Sattler L, Wendler E (1996a) Alte Pinakothek München. In: Snethlage R (ed) Denkmalpflege und Naturwissenschaft Natursteinkonservierung I. Ernst & Sohn, Berlin, pp 153–194
- Snethlage R, Meinhardt-Degen J (2004) Re-treating sandstone with ethyl silicates—is there a risk of over-strengthening the surface. In: Kwiatkowski D, Löfvendahl R (eds) Proceedings of the 10th international congress on deterioration and conservation of stone, Stockholm, 27 June–2 July. ICOMOS, Sweden, pp 283–289
- Snethlage R, Wendler E (1996) Methoden der Steinkonservierung Anforderungen und Bewertungskriterien. In: Snethlage R (ed) Denkmalpflege und Naturwissenschaft Natursteinkonservierung I. Ernst & Sohn, Berlin, pp 3–40
- Snethlage R, Wendler E (1997) Moisture cycles and sandstone degradation. In: Baer NS, Snethlage R (eds) Saving our architectural heritage. The conservation of historic stone structures. Report of Dahlem workshop, Berlin, 3–8 March 1996. Wiley, Chichester, New York, pp 7–24
- Snethlage R, Wendler E (2001) Chemical conservation of stone structures. Ullmann's encyclopedia of industrial chemistry electronic release 2001. Wiley-VCH, Weinheim
- Snethlage R, Wendler E, Klemm DD (1996b) Tenside im Gesteinsschutz—bisherige Resultate mit einem neuen Konzept zum Schutz von Denkmälern aus Naturstein. In: Snethlage R (ed) Denkmalpflege und Naturwissenschaft Natursteinkonservierung I. Ernst & Sohn, Berlin, pp 127–146
- Sobott R (2000) Investigations on the effects of laser cleaning on pigments and polychromed workstones. In: Domstiftung Regensburg Turm Fassade Portal. Regensburg, 27–30 Sept. Schnell & Steiner, Regensburg, pp 87–90
- Stark U, Dimmig A (1997) Über das Stein-Eindringverhalten wäßriger Epoxidharz-Emulsionen. Bautenschutz & Bausanierung 3/1997, pp 8–11
- Steinhäuser U, Snethlage R, Wendler E (2006) Conservation of architectural ceramics by a new process using modified consolidants. In: Delgado Rodrigues J, Mimoso JM (ed) International seminar theory and practice in conservation, Lisbon, 4–5 May 2006. LNEC, Lisbon, pp 501–508
- Stois U (1935) Verwitterung und Steinschutz. In: Reis OM (ed) Die Gesteine der Münchner Bauten und Denkmäler. Gesellschaft für Bayerische Landeskunde. Heft, 7–12. München, pp 199–224
- Taylor HFW (1990) Cement chemistry. Academic, London
- Teutonico JM, Charola AE, de Witte E, Grassegger G, Koestler RJ, Laurenzi-Tabasso M, Sasse HR, Snethlage R (1997) Group report: how can we ensure the responsible and effective use of treatments (cleaning, consolidation, protection)? In: Baer NS, Snethlage R (eds) Saving our architectural heritage: the conservation of historic stone structures. Wiley, Chichester



- Tiano P, Delgado Rodrigues J, De Witte E, Vergès-Belmin V, Massey S, Snethlage R, Costa Doria D, Cadot-Leroux L, Garrod E, Singer B (2000a) The conservation of monuments: a new method to evaluate consolidating treatments. *Int J Restor Build Monum* 6(2):133–150
- Tiano P, Filareto C, Ponticelli S, Ferrari M, Valentini E (2000b) Drilling force measurement system, a new standardisable methodology to determine the “superficial hardness” of monumental stones: prototype design and validation. *Int J Restor Build Monum* 6(2):115–132
- Tretiaich M, Crisafulli P, Imai N, Kashiwadani H, Moon KH, Wada H, Salvadori O (2007) Efficacy of a biocide tested on selected lichens and its effects on their substrata. *Int Biodet Biodeg* 59:44–54
- Urzí C, de Leo F (2007) Evaluation of the efficiency of water repellent and biocide compounds against microbial colonization of mortars. *Int Biodet Biodeg* 60:25–34
- Vergès-Belmin V, Pichot C, Oriol G (1993) Elimination de croûtes noires marbre et craie: à quel niveau arrêter le nettoyage? In: Proceedings of the UNESCO-RILEM international congress on the conservation of stone and other materials. Paris, pp 534–541
- Wagener S, Hessland A, Höcker H (1992) Schein oder Sein...Steinschutzsysteme auf dem Prüfstand. In: Snethlage R (ed) *Jahresberichte Steinzerfall—Steinkonservierung*, Band 2, 1990. Ernst & Sohn, Berlin, pp 139–151
- Wagener S, Schneider U, Höcker H (1993) Der Chromatographieeffekt: in der Analytik erwünscht—in der Praxis der Natursteinimprägnierung gefürchtet. In: Snethlage R (ed) *Jahresberichte Steinzerfall—Steinkonservierung*, Band 3, 1991. Ernst & Sohn, Berlin, pp 73–84
- Warscheid T, Braams J (2000) Biodeterioration of stone: a review. *Int Biodet Biodeg* 46:343–368
- Wedekind W, Ruedrich J, Kracke T, Licha T, Siegesmund S (2008) Object-specific desalination of tomb monuments. In: Lukaszewicz JW, Niemcewicz P (eds) Proceedings of the 11th international congress on deterioration and conservation of stone, Torun, 15–20 Sept. Uniwersytetu Nikolaya Kopernika, Torun, pp 1339–1347
- Weinhold WP, Diegelmann C, Tiano P, Pummer E, Goretzki L (2008) Mobile measuring and documentation of visual impression and surface topography. In: Castillejo M, Moreno P, Oujja M, Rad van R, Ruiz J (eds) *Laser in the conservation of artworks*. Proceedings of the international conference LACONA VII, 17–21 Sept 2007. T&F Group, London, p 3
- Weiss NR, Slavid I, Wheeler G (2000) Development and assessment of a conversion treatment for calcareous stone. In: Fassina V (ed) Proceedings of the 9th international congress on deterioration and conservation of stone, vol 2, Venice, 19–24 June. Elsevier, Amsterdam, pp 533–540
- Wendler E (1997) Maxtormauer Nürnberg Zustandserfassung, Erstellung eines Konservierungskonzepts. Bericht für die Stadt Nürnberg Berichtszeitraum 11/1996–12/1997: 119 S. München
- Wendler E, Snethlage R (1988) Durability of hydrophobing treatments of natural stone buildings. In: Marinos PG, Koukis G (eds) *The engineering geology of ancient works, monuments and historical sites*, 19–23 Sept. Balkema, Rotterdam, Brookfield, pp 945–952
- Wendler E, Snethlage R (1989) Der Wassereindringprüfer nach Karsten—Anwendung und Interpretation der Messwerte. *Bautenschutz & Bausanierung* 12-1989 H. 6, pp 110–115
- Wendler E, Rückert-Thümling R, Klemm DD, Snethlage R (1992) Zur Dauerhaftigkeit von Hydrophobierungsmaßnahmen auf Naturstein. Vergleichende Fallbeispiele am Kölner Dom und am Ulmer Münster. In: Snethlage R (ed) *Jahresbericht Steinzerfall—Steinkonservierung*, Band 4, 1992. Ernst & Sohn, Berlin, pp 197–204
- Wendler E, Steinhäuffer U, Herkner S, Schütte K, Holter E, Snethlage R, Gruber C (2009) Nachstellung objekttypischer Schäden an Laborprüfkörpern: Auswahlverfahren und Optimierung von Konsolidierungsstoffen zur Stabilisierung ölgebundener Malschichten auf gipshaltigen Untergründen im Tympanonbereich. In: Bauhütte Sankt Sebald und Bayerisches Landesamt für Denkmalpflege (eds) *Das Weltgerichtportal der Sebalduskirche in Nürnberg*. Konservierung kalk- und ölgebundener Malschichten auf frei bewitterten Natursteinoberflächen. Fraunhofer IRB Verlag, Stuttgart, pp 59–66
- Wheeler G (2005) Alkoxysilanes and the consolidation of stone (with annotated bibliography by E S Goins). The Getty Conservation Institute, Los Angeles

- Wheeler G, Fleming SA, Ebersole S (1992) Evaluation of some current treatments for marble. In: Decrouez D, Chamay J, Zezza F (eds) Proceedings of the 2nd international symposium on the conservation of monuments in the mediterranean basin. Genève, pp 439–444
- Wheeler G, Méndez-Vivar J, Goins ES, Fleming SA, Brinker CJ (2000) Evaluation of Alkoxysilane coupling agents in the consolidation of limestone. In: Fassina V (ed) Proceedings of 9th international congress on deterioration and conservation of stone, Venice, 19–24 June 2000. Elsevier, Amsterdam, pp 541–545
- Winckelmann JJ (1764) Geschichte der Kunst des Altertums. In: Wissenschaftliche Buchgemeinschaft 1972. Darmstadt, p 148
- Winnefeld F, Knöfel D (1998a) Modifizierung von Kalkmörteln zur Fugenreparatur von Ziegelmauerwerk. In: Snethlage R (ed) Jahresberichte Steinzerfall—Steinkonservierung, Band 6, 1994–1996. Fraunhofer IRB Verlag, Stuttgart, pp 227–236
- Winnefeld F, Knöfel D (1998b) Entwicklung eines Kalkputzmörtels für Ziegelmauerwerk am Beispiel der Orangeriesäle im Schloß Schwerin. In: Snethlage R (ed) Jahresberichte Steinzerfall—Steinkonservierung, Band 6, 1994–1996. Fraunhofer IRB Verlag, Stuttgart, pp 261–268
- Wittmann FH (1981) Kann das Prinzip der Elektrosmose zur Trockenlegung von Mauerwerk angewendet werden. Bautenschutz Bausanierung 4–81:126–132
- Wittmann FH (1983) Zeta-Potential und Feuchtigkeitstransport durch poröse Werkstoffe. In: Wittmann FH (ed) Kolloquium Werkstoffwissenschaften und Bausanierung. Edition Lack & Chemie, Filderstadt, pp 47–50
- Wolff A (1996) Schutzanstrich Chorstrebewerk. 37. Dombaubericht Okt 1995–Sept 1996, p 16
- Wolff A (1997) Schutzanstrich Chorstrebewerk. 38. Dombaubericht Okt 1996–Sept 1997, p 18
- Wolff A (1998) Schutzanstrich Chorstrebewerk. 39. Dombaubericht Okt 1997–Sept 1998, p 30
- Woolfitt C (2002) Lime method evaluation. In: Fidler J (ed) Stone, vol 2. English Heritage, James & James, London, pp 29–44
- WTA Merkblatt AG 3.17 (2010) Hydrophobierende Imprägnierung von mineralischen Baustoffen. WTA Publications 3–17. Ausgabe 06.2010
- Wulfert S (1989) Blick ins Bild. Lichtmikroskopische Methoden zur Untersuchung von Bildaufbau, Fasern und Pigmenten. Bücherei des Restaurators, Band 4. Otto Maier Verlag, Ravensburg
- Zafropoulos V, Fotakis C (1998) Lasers in conservation of painted artworks. In: Cooper M (ed) Laser cleaning in conservation. Butterworth Heinemann, Oxford, pp 79–90